

**The Development of PVP-based Solid Dispersions
using Hot Melt Extrusion for the Preparation of
Immediate Release Formulations**



Chan Siok Yee

School of Pharmacy

University of East Anglia

Thesis Submitted for the Degree of Doctor Philosophy 2013

唯心所现，唯识所变

*“All things are preceded by the mind,
led by the mind, and
created by the mind”*

Acknowledgement

My gratitude to the following people who have helped me with this project and writing cannot be adequately expressed.

First of all, I would like to thank my supervisors, Professor Duncan Craig and Dr Sheng Qi who have given a lot of ideas, their precious time and patience for the discussion sessions and assistance in the research as well as the writing process. Besides, I am very grateful for the help from Dr Mike Ridout from Institute of Food Research (IFR) Norwich who has helped me out in some of the experimental procedures. I am also thankful for the support from the members of the research group, especially Miss Maria De Fatima Gomes Pina who has been the “main actress” throughout my PhD research life. Thanks for her spirited intellectual companionship.

In regard to this thesis writing, there are a few people who deserve a special appreciation, Dr Lorina Bisharat, Mr Kai-Hui Leong, Dr Min Zhao, Dr Jin Heppel, Dr Kate Bowman, Dr Bahijja Raimi Abraham, Dr Susan Baker, Dr Laszlo Fabian, Dr Jonathan Moffat, Professor Yan Hong Wang, and Professor Gam Lay Harn. Many thanks to their thoughtful questioning and careful editing that clarified my fuzzy thoughts. My thanks are also extended to my fellow best friends in Norwich and Malaysia for their treasured encouragement and thoughtful comments, Miss Doroty Codoni, Miss Claudia Pigliacelli, Dr Giulia Pergolizzi, Dr Annalisa Mercuri, Dr Sarah Otun, Mr Alberto Berardi, Mr Ziyi Yang, Miss Isra’a, Mrs Germeen Girgis, Mr Wei Guo Wang and wife, Mrs Laili Che Rose, Mr Abdulrahman Saeed, Mr Dereck Xolani Gondongwe, Miss Aqilah Adnan, Mr Awis Sabere, Mr Goh Choon Fu, Mr Pratchaya Tipduangta, Miss Shirley Tan, Miss Noor Armylisa, Mr Jacob Bouman, Mr Hao Pan, Miss Liu Yang, Mr Lim Ming Teng, Mr Long Chiau Ming, Professor Yuen Kah Hay, Dr Nurzalina Abdul Karim Khan, Encik Azman Che Hussain, Cik Hajar Zituakmar Mohd Fauzi, Encik Nadzrull, “brothers” and “sisters” from Malaysia. Financial support from my lovely country, specifically University Sains Malaysia is greatly acknowledged.

Last but not least, I would like to pay my deep gratitude to my lovely parents, Mr Chan Kim Bock and Mrs Mak Yin Moy, my fiancé, Mr Kenny Dang Chee Chean and his family members. Thanks to my beloved siblings, Chan Beng Chin, Chan Siok Pei, Chan Beng Loong, Chan Siok Yin, Chan Siok Sin, Chan Beng Zhong, Dede, Dodo, Yy, Oo and relatives, particularly the big “Mak’s family” whom have given me outstanding support and love, without them I would not have the motivation to start off this project and finish the work of this research.

I appreciate the existence of the inevitable flaws and errors that arose throughout the research route which has contributed to my personal and professional development.

Abstract

Bioavailability and clinical effectiveness of a poorly soluble drug can be highly affected by its formulation design. In this respect, research on solid dispersion of hydrophilic carrier has commenced a decade ago to resolve the problem of poorly soluble drug. However, the availability of solid dispersion is commercially limited due to the concerns of its physical instability, unpredictability and inconsistency formulation performance. This is attributed to the lack of fundamental understanding on the processing method, physicochemical properties of the obtained solid dispersion. Therefore, better understanding on the processing methods and factors underlying the performance of solid dispersion may be required to maximize the use of solid dispersion.

Hot melt extrusion (HME) method was introduced in formulating solid dispersion. The use of this production method offers many advantages such as environmental friendly, cost sparing and readily scalable production as compared to conventional methods. On the other hand, the hydrophilic polyvinylpyrrolidone (PVP) polymer with its good stabilising ability in the solid dispersion is less applied in HME process due to its possible degradation at high temperature. However, rejection on the use of PVP without thorough understanding of its potential might lead to underuse of this polymer in HME solid dispersion.

This project explores the feasibility of using PVP and its derivative in HME manufacturing method. It offers an in-depth study on the hot melt processing, physical stability and dissolution behaviour of HME PVP-based solid dispersion. Factors affecting the production of fully amorphous solid dispersion and its physical stability are discussed, taking into account the influence of the composition and characteristic of the drug, drug-polymer interaction and the molecular weight of the polymer. In parallel, HME poorly soluble drug in PVP based solid dispersion were produced and investigated for their dissolution performances in order to understand the mechanism underlying the dissolution process of the HME PVP-based solid dispersion system.

Table of Content

Acknowledgement.....	i
Abstract	ii
Table of Content.....	iii
List of Figures.....	xii
List of Tables	xx
List of Abbreviation	xxiii
Chapter 1. Introduction	
1.1. General Introduction.....	1
1.2. Amorphous pharmaceutical and its advantages.....	2
1.2.1. Behavioural features of amorphous materials.....	3
1.2.1.1. Glass transition temperature.....	3
1.2.1.2. Fragility.....	6
1.2.1.3. Structural relaxation and molecular mobility.....	7
1.2.1.4. Plasticization	9
1.3. Solid dispersion	10
1.3.1. Preparation of solid dispersion.....	12
1.3.1.1. Traditional melting methods	12
1.3.1.2. Milling/cryogrinding	13
1.3.1.3. Solvent method : co-evaporation / co-precipitation	14
1.3.1.4. Spray drying.....	15
1.3.1.5. Freeze drying	16
1.4. Pharmaceutical hot melt extruded solid dispersions.....	17
1.4.1. Principles of HME	18
1.4.1.1. Feeding zone: feeding raw material	19
1.4.1.2. Transition Zone.....	20

1.4.1.2.1.	Melting / plasticization	20
1.4.1.2.2.	Mixing/ dispersion	20
1.4.1.3.	Metering zone	21
1.4.1.4.	Die pressurization	21
1.4.2.	Materials used in HME solid dispersions.....	21
1.4.2.1.	Active pharmaceutical ingredient	21
1.4.2.2.	Carriers used in HME formulations	26
1.4.2.2.1.	Polymers	27
1.4.2.2.2.	Plasticizers used in HME systems	28
1.4.2.2.3.	Surfactant.....	32
1.4.2.2.4.	Other additives used in HME processing.....	32
1.5.	Stability issues.....	33
1.5.1.	Physical stability of HME solid dispersions	34
1.5.1.1.	Post-extrusion stability.....	37
1.5.1.1.1.	Short term stability.....	37
1.5.1.1.2.	Long term stability.....	37
1.6.	Dissolution performance of solid dispersions	41
1.6.1.	Anomalous dissolution of solid dispersions.....	43
1.6.1.1.	Crystallinity.....	44
1.6.1.2.	API / polymer loading.....	44
1.6.1.3.	Molecular weight of carriers	45
1.6.1.4.	Structure of carriers.....	46
1.6.1.5.	Particle size influences.....	48
1.6.1.6.	Addition of surfactant	49
1.6.1.7.	Processing methods.....	49
1.6.1.8.	Extreme storage conditions	50
1.7.	Objective of this study.....	51

Chapter 2. Material and Methods

2.1.	Introduction	53
2.2.	Materials	53
2.2.1.	Model drugs	53
2.2.1.1.	Paracetamol.....	54
2.2.1.2.	Caffeine.....	55
2.2.1.3.	Naproxen.....	56

Table of content

2.2.1.4.	Ketoprofen	57
2.2.1.5.	Indomethacin.....	58
2.2.1.6.	Olanzapine	59
2.2.2.	Carriers.....	60
2.2.2.1.	Homopolymer PVP	60
2.2.2.2.	Co-polymer PVPVA 6:4	63
2.2.3.	Raw Material Sourcing	65
2.2.4.	Summary of the properties of raw materials	66
2.3.	Preparation of solid dispersion : Hot Melt extrusion.....	67
2.3.1.	Extrusion temperature	68
2.3.2.	Screw Speed.....	69
2.3.3.	Torque	70
2.4.	Characterization techniques.....	73
2.4.1.	Differential scanning calorimetry	73
2.4.2.	Thermogravimetric Analysis.....	74
2.4.3.	Attenuated total reflectance-Fourier transfer Infrared	75
2.4.4.	Hot stage microscopy.....	76
2.4.5.	X-ray Powder Diffraction	76
2.4.6.	Scanning electron microscopy	77
2.4.7.	Laser diffraction for particle size analysis	78
2.4.8.	Contact angle measurement	79
2.4.9.	Atomic Force Microscopy	81
2.5.	Dissolution studies.....	81
2.5.1.	The theory of dissolution	82
2.5.2.	Factors Affecting the Dissolution Rate	83
2.5.2.1.	Surface area of un-dissolved solid	84
2.5.2.2.	Solubility of solid in the dissolution medium (C_s).....	84
2.5.2.3.	Concentration of solute in the bulk solution at time t (C_b).....	84
2.5.2.4.	Thickness of diffusion layer (h)	84
2.5.2.5.	Diffusion coefficient of solute in the dissolution medium (D)	85
2.5.3.	Preparation of Dissolution Media	85
2.5.4.	Dissolution method	85
2.5.5.	Ultraviolet-Visible Spectrophotometer (UV-VIS).....	86

Chapter 3. Theoretical miscibility estimation and basic characterization of hot melt extruded solid dispersions

3.1.	Introduction	89
3.2.	Materials and methods.....	90
3.2.1.	Preparation of physical mixtures.....	90
3.2.2.	Estimation of drug-polymer miscibility	90
3.2.2.1.	Solubility parameter approach	91
3.2.2.2.	Melting point depression approach	92
3.2.3.	Preparation of hot melt extruded solid dispersions	92
3.2.4.	Hot stage microscopy.....	93
3.2.5.	Thermogravimetric analysis.....	93
3.2.6.	Modulated temperature differential scanning calorimetry	93
3.2.7.	Attenuated total reflectance -Fourier transform infrared spectroscopy	93
3.2.8.	Powder X-ray diffraction	94
3.2.9.	Scanning electron microscopy	94
3.3.	Results	94
3.3.1.	Estimation of drug-polymer miscibility	94
3.3.1.1.	Solubility parameter approach	94
3.3.1.2.	Melting point depression approach	97
3.3.2.	Preparation of HME PVP-based SDs.....	104
3.3.2.1.	HME parameter investigation: Extrusion temperature.....	104
3.3.2.2.	HME parameter investigation: Torque.....	107
3.3.3.	Characterization of HME solid dispersions	111
3.3.3.1.	Water content of physical mixtures and hot melt extrudates	111
3.3.3.2.	MTDSC of HME PVP-based SD.....	112
3.3.3.2.1.	MTDSC of HME PCM in PVP K29-32 and PVPVA 6:4.....	112
3.3.3.2.2.	MTDSC of HME CAF PVP K29-32 and PVPVA 6:4	118
3.3.3.3.	ATR-FTIR studies of HME preparation	123
3.3.3.3.1.	ATR-FTIR studies of HME PCM - PVP K29-32.....	123
3.3.3.3.2.	ATR-FTIR studies of HME PCM in PVPVA 6:4.....	126
3.3.3.3.3.	ATR-FTIR studies of HME CAF-PVP K29-32 and PVPVA 6:4.....	126
3.3.3.4.	X-ray Powder Diffraction of HME solid dispersions	128
3.3.3.4.1.	XRPD of HME PCM in PVP K 29-32.....	128
3.3.3.4.2.	XRPD of HME PCM in PVPVA 6:4.....	129
3.3.3.4.3.	XRPD of HME CAF in PVP K29-32 and PVPVA 6:4	130

3.3.3.5.	Scanning Electron Microscopy	132
3.3.3.5.1.	SEM of HME PCM in PVPK29-32 and PVPVA 6:4	132
3.3.3.5.2.	SEM of HME CAF in PVP K29-32 and PVPVA 6:4.....	133
3.4.	Discussion	134
3.4.1.	Theoretical estimation of miscibility	134
3.4.2.	Production of amorphous solid dispersion	135
3.4.3.	Extrudate properties	136
3.5.	Conclusion.....	136

Chapter 4. An investigation into the recrystallization of paracetamol in HME PCM PVP-based solid dispersions

4.1.	Introduction	138
4.2.	Material and methods	139
4.2.1.	Establishment of quantification methods for crystalline PCM	139
4.2.1.1.	Preparation of amorphous and Form II of PCM	139
4.2.1.2.	The detection of crystalline PCM by using ATR-FTIR and high speed DSC	139
4.2.2.	Preparation of amorphous HME solid dispersions.....	140
4.2.2.1.	Basic characterisation of HME solid dispersions.....	140
4.2.2.2.	Fragility calculation of the HME solid dispersions.....	140
4.2.3.	Recrystallization studies of HME PCM-polymers system.....	141
4.2.3.1.	DSC studies.....	142
4.2.3.2.	TGA studies	142
4.2.3.3.	ATR-FTIR.....	142
4.2.3.4.	XRPD.....	142
4.2.3.5.	SEM	142
4.3.	Results	143
4.3.1.	Development of ATR-FTIR method as a quantification method for crystalline PCM	143
4.3.1.1.	Identification of different polymorphs of PCM in ATR-FTIR	143
4.3.1.2.	Tracking of the relative intensity of 807 cm ⁻¹ in QC PCM by using ATR-FTIR.....	144
4.3.1.3.	Quantification of the recrystallized PCM using DSC	146
4.3.2.	Fully amorphous HME solid dispersions.....	149
4.3.3.	Recrystallization profile of aged HME PCM-PVPs on storage at elevated humidities	152
4.3.3.1.	Recrystallization of HME 40% PCM PVPVA 6:4 at different humidity conditions	152

4.3.3.2.	Recrystallization of HME 40% PCM with different PVPs carriers	156
4.3.3.3.	Effect of PCM loading on the recrystallization behaviour of HME different PVPs carrier system.....	161
4.3.3.3.1.	Recrystallization profile of aged HME 50% PCM-carriers at 75% RH	161
4.3.3.3.2.	HME 30% PCM-carriers on storage at 75% RH	166
4.3.4.	Influence of storage temperature on the stability of HME PVP-based SD.....	169
4.3.4.1.	Annealed sample of HME 40% PCM with different polymers	169
4.4.	Discussion	171
4.4.1.	Establishment of quantification methods for crystalline PCM	171
4.4.2.	The influence of humidity on HME PCM in PVP-based polymers.....	171
4.4.3.	Hydrogen bonding between drug and polymer: a key for physical stability?.....	172
4.4.4.	The effect of molecular weight of PVP on physical stability of HME formulations..	174
4.4.5.	The influence of temperature on physical stability of HME PCM-PVPs	175
4.5.	Conclusion.....	176

Chapter 5. An investigation into factors governing the drug release mechanism of PVP-based hot melt extrusion formulations Part I: Dissolution performances of HME of poorly soluble drugs with PVPVA 6:4

5.1.	Introduction	178
5.2.	Material and methods	179
5.2.1.	Estimation of the amorphous solubility advantage	179
5.2.2.	Solubility testing	180
5.2.3.	Preparation of PM.....	180
5.2.4.	Hot melt extruded products.....	180
5.2.5.	Characterization of the amorphous solid dispersions.....	181
5.2.5.1.	Differential scanning calorimetry	181
5.2.5.2.	Attenuated total reflectance-fourier transform infrared	181
5.2.5.3.	X-ray diffraction	181
5.2.6.	Dissolution studies of PM and HME of APIs – PVPVA 6:4.....	181
5.2.6.1.	Light microscopy observation.....	182
5.2.6.2.	Particle size analysis	182
5.2.6.3.	Scanning electron microscope	183
5.2.6.4.	Contact angle measurement	183
5.3.	Results	185

5.3.1.	Estimation of amorphous solubility advantages ratio of APIs	185
5.3.2.	Equilibrium phase solubility studies of APIs in the presence of PVPVA 6:4	186
5.3.3.	Basic characterization of HME products: XRPD and DSC	187
5.3.4.	Interaction between APIs and PVPVA 6:4	188
5.3.5.	Comparison of dissolution profiles of PM and HME products.....	190
5.3.6.	Investigation of factor governing dissolution performance of HME API-PVPVA 6:4 system	192
5.3.6.1.	Wetting properties of the solid system.....	192
5.3.6.1.1.	Wetting properties of PM APIs-PVPVA 6:4 in comparison to their APIs	193
5.3.6.1.2.	Wetting properties of the HME and PM system.....	196
5.3.6.2.	Agglomeration of the dissolving solid	198
5.3.6.3.	Recrystallization of APIs during dissolution	200
5.4.	Discussion	203
5.4.1	Dissolution performance of APIs in comparison their PM API-PVPVA 6:4	203
5.4.2	Dissolution performance of HME APIs-PVPVA 6:4 in comparison to PM.....	204
5.5.	Conclusion.....	207

Chapter 6. An investigation into factors governing the drug release mechanism of PVP-based hot melt extrusion formulations Part II: Dissolution performance of hot melt extruded naproxen-carrier systems

6.1.	Introduction	208
6.2.	Materials and Methods	209
6.2.1.	Preparation of PM	209
6.2.2.	Dissolution studies of pure NAP and its PMs	209
6.2.2.1.	Phase solubility of PVP and NAP.....	210
6.2.2.2.	Surface tension of PVPs solutions	210
6.2.3.	Production of HME NAP PVP-based SDs.....	211
6.2.4.	Basic characterisation of HME NAP PVPs SD systems.....	211
6.2.4.1.	Differential scanning calorimetry	211
6.2.4.2.	Attenuated total reflectance-fourier transform infrared	211
6.2.4.3.	X-ray diffraction	211
6.2.5.	Dissolution studies of HME NAP PVP-based SD	212
6.2.5.1.	SEM	212
6.2.5.2.	Hot stage microscope	212

6.2.5.3.	Particle size of residue	212
6.2.6.	Contact angle measurement	212
6.3.	Results	214
6.3.1.	Investigation of dissolution behaviour of PM formulations.....	214
6.3.1.1.	Dissolution behaviour of PM NAP in different carriers system: PVP K12, PVP K17, PVP K29-32, PVPVA 6:4.....	216
6.3.1.2.	Solubility tests of NAP in PVP solutions.....	218
6.3.1.3.	Surface tension properties	219
6.3.2.	Dissolution performances of amorphous HME PVP-based SDs	220
6.3.2.1.	Dissolution studies of different NAP loading on HME NAP PVPVA 6:4 SDs ..	223
6.3.2.1.1.	Agglomeration	224
6.3.2.1.2.	Recrystallization	226
6.3.2.2.	Dissolution study of HME 30% NAP using different MW of PVPs carriers	228
6.3.2.2.1.	Surface properties of HME and PM of NAP in different PVP polymers	229
6.3.2.2.2.	Agglomeration	231
6.3.2.2.3.	Recrystallization	232
6.3.2.3.	Dissolution studies of HME 30% NAP-PVPVA 6:4-2% and 10% Tween 80....	233
6.3.2.3.1.	Agglomeration	234
6.3.2.3.2.	Recrystallization	235
6.3.3.	Dissolution study of partially crystalline NAP-PVPVA 6:4 system.....	236
6.4.	Discussion	237
6.4.1.	Dissolution process of PM	238
6.4.2.	Different drug loadings of HME NAP PVPVA 6:4.....	238
6.4.3.	Different carriers	239
6.4.4.	The effect of Tween 80 in the HME extrudates on dissolution behaviour of HME NAP-PVPVA 6:4-surfactant system	240
6.4.5.	Pathway of dissolution mechanisms in a physical mixture and HME solid dispersion	241
6.5.	Conclusion.....	242

Chapter 7. Concluding Remarks and Recommendations for Future Work

7.1.	Conclusion.....	243
7.2.	Recommendations for future works	254

References	256
Appendices	282
Appendix I: Calibration curve of PCM crystallinity based on diffracted peak of XRPD.....	282
Appendix II: Validation of ATR-FTIR method in tracking crystalline content of PCM in HME PCM PVPs-based solid dispersions	282
Appendix III : Dissolution of crystalline PCM during heating scan of DSC.....	287
Appendix IV: Analysis of surface of HME API-PVPVA systems for contact angle measurement 289	
Appendix V : Amorphous nature of HME NAP-PVPVA-Tween 80 systems.....	290
Publications.....	291

List of Figures

Figure 1.1: The change in volume or enthalpy with temperature for a material undergoing crystallization or glass transition. T_m is melting temperature of the crystalline material. T_{g1} is the point at which there is a discontinuity in volume and enthalpy. The dashed line between T_{g1} and T_k representing the profile of volume and enthalpy change when a melt is slow-cooled. T_{g2} is the glass transition temperature when the slow cooling is performed. T_k is Kauzman temperature (Craig et al., 1999, Pinal, 2008).	4
Figure 1.2: Measurement of T_g using DSC thermogram. T_b is the beginning of the transition and the extrapolated onset of the transition point is T_1 . T_g is taken as half height of the transition event. Similarly the extrapolated end point is T_2 and the transition process end at T_e	5
Figure 1.3: The simplified schematic of Angell Fragility concept (Angell, 1995).....	6
Figure 1.4: Substitutional crystalline or interstitial crystalline solid dispersion (Leuner and Dressman, 2000).....	11
Figure 1.5: Solid dispersion of amorphous polymeric carrier (Kolter et al., 2012).....	11
Figure 1.6: Schematic diagram of a hot melt extrusion system (Radl et al., 2010).....	18
Figure 1.7: Diagram of a screw extruder (Crowley et al., 2007).....	19
Figure 1.8: The evolvement of solid dispersion which gives rise to the different generations of the formulations (Vasconcelos et al., 2007).....	26
Figure 1.9: Stability influences of HME extrudate.....	34
Figure 1.10: Summary of contributing factors in dissolution enhancement of poorly soluble API via the formation of an SD.....	43
Figure 1.11: The dissolution profiles of amorphous felodipine at 37°C in the presence of various polymers pre-dissolved at 500 µg/mL concentration of; PVP (Δ), HPMC (●) and HPMC-AS (■). Dissolution of crystalline felodipine at 37 °C is included as a reference (▲) (Figure reproduced from Alonzo et al., 2010).....	47
Figure 1.12: Flow chart of the development of HME PVP-based system.....	52
Figure 2.1: Chemical structure PCM.....	54
Figure 2.2: Chemical structure CAF.....	55
Figure 2.3: Chemical structure NAP.....	56
Figure 2.4: Chemical structure KTP.....	57
Figure 2.5: Chemical structure of INDO.....	58
Figure 2.6: Chemical structure of OZP.....	59

Figure 2.7: Chemical structure of soluble polyvinylpyrrolidone (Kibbe, 2002).....	60
Figure 2.8: Chemical structure of the repeating unit of PVPVA (Bühler, 2005).....	63
Figure 2.9: Hot Melt Extruder of Thermo Scientific HAAKE MiniLab II Micro Compounder	67
Figure 2.10: The changes of molten residence time as a result from process modulations during HME of binary hydrocortisone and Kinetisol®, i.e. screw speed and extrusion temperature (adopted from reference DiNunzio et al. 2009)	69
Figure 2.11: The changes of torque as a result from process modulations during HME of binary hydrocortisone and Kinetisol®, i.e. screw speed and extrusion temperature (adopted from reference DiNunzio, et al. 2009).....	70
Figure 2.12: Conveyer belt used to collect the extruded material from the HME die	71
Figure 2.13: example of scattering off a spherical particle (HORIBA Scientific, 2013).....	78
Figure 2.14: Schematic of a sessile drop, contact angle (θ), and the three components of interfacial tensions, i.e. γ_{lv} : liquid-vapor, γ_{sv} : solid-vapor and γ_{sl} : solid-liquid.....	79
Figure 2.15: : Possible mechanism as proposed by Craig 2002 (a) Carrier-controlled dissolution, whereby the drug dissolves into the concentrated carrier layer prior to release and (b) drug-controlled dissolution whereby the drug is released effectively intact into the dissolution medium. Large spheres represent un-dissolved drug particles, small spheres partially dissolved drug particles, and shaded regions correspond to hydrated material (Figure adopted from Craig 2002).	83
Figure 2.16: Calibration curve of NAP in 0.1M HCl pH 1.2 at 272 nm.....	87
Figure 2.17: Calibration curve of KTP in 0.1M HCl pH 1.2 at 259 nm	87
Figure 2.18: Calibration curve of INDO in distilled water at 265 nm	88
Figure 2.19: Calibration curve of OZP in distilled water at 254 nm.....	88
Figure 3.1: DSC thermograms of PM of PCM-PVP K29-32 (from 70% w/w to 90% w/w drug loading) measured at 2 °C/min. Onset melting point of the DSC thermograms was taken as the melting temperature of the systems.	98
Figure 3.2: Change in onset of T _m of PM PCM and CAF in PVP K29-32 as a function of percentage API loading.....	98
Figure 3.3: Plot used to determine the interaction parameter of PCM-PVP K29-32 and CAF-PVP K 29-32	100
Figure 3.4: The changes in free energy of mixing as a function of volume fraction of polymer as predicted using interaction parameter of Flory-Huggins lattice theory	101
Figure 3.5: HSM screens of PM of 50% API-polymers. I) Fusion of PCM- PVP K29-32 at T ≈ 140 °C, II) Fusion of PCM- PVPVA 6:4 at T ≈ 130 °C, III) Fusion of CAF- PVP K29-32 at T ≈ 180 °C, and IV) Fusion of CAF- PVPVA 6:4 at T ≈ 175 °C. Figures on the left which is denoted as (a) are	

screens captured before the apparent fusion was noted and figures on the right which is denoted as (b) are screens captured when the fusion event was clearly seen.105

Figure 3.6: Appearance of extrudates of HME 20 - 70% PCM-PVP K29-32 prepared at 120 °C..107

Figure 3.7: Torque value recorded during the processing of HME 20-70% w/w at 120 °C after approximately 5 minutes of molten circulation107

Figure 3.8: The comparison of torque profiles of a) HME 20% PCM-PVP K29-32 and b) HME 20% CAF-PVP K29-32. The peak at beginning of the profiles indicated the manual pressure applied to the raw material upon loading. The profile of torque was thus considered after this peak.108

Figure 3.9: Torque of the HME twin-screw during hot melt extrusion at 120 °C as a function of processing time, a) HME 40% PCM PVP K29-32, b) HME 40% PCM PVPVA 6:4. The peak at beginning of the profiles indicated the manual pressure applied to the raw material upon loading. The profile of torque was considered after this peak.110

Figure 3.10: Water content determination of HME 40% PCM-PVP K29-32 system by performing isothermal analysis on the samples at 100 °C for 30 minutes. The marked value (1.232%) is the water content of this SD.....111

Figure 3.11: MTDSC thermograms of HME 20% - 70% PCM-PVP K29-32 using aluminum pin-hole pans113

Figure 3.12: MTDSC thermograms of HME 20% - 70% w/w PCM-PVP VA 6:4113

Figure 3.13: Comparison of experimental Tg(s) to calculated Tg(s) based on Gordon Taylor equation a) HME PCM PVP K29-32, b) HME PCM PVPVA 6:4: binary PCM-PVPs polymer theoretical value based (Δ), ternary PCM-PVPs polymer-water theoretical value (+) and experimental glass transition values (\diamond).....115

Figure 3.14: MTDSC thermograms of HME 20% PCM PVP K29-32 a) intact extrudates of circa 4 mm, b) ground extrudates from the same sample by using aluminium pin-hole pan117

Figure 3.15: MTDSC thermograms of HME 10% CAF-PVP K29-32 by using pin-holed pan.....118

Figure 3.16: MTDSC thermogram of HME 20% CAF - PVP K29-32 by using pin-holed pan119

Figure 3.17: MTDSC thermogram of HME 10% w/w CAF in PVPVA 6:4 by using pin-holed pan120

Figure 3.18: HSM investigation of HME 10% CAF-PVPVA 6:4 at a heating rate of 10 °C per minute. The marked temperatures at left bottom corner of each screen indicates the temperature of sample121

Figure 3.19: MTDSC thermogram of HME 20% CAF PVPVA 6:4 by using pin-holed pan.....122

Figure 3.20: ATR-FTIR spectra of PM and HME PCM-PVP K29-32 a) Form I PCM, b) raw PVP K29-32, c) PM 50% PCM and PVP K29-32, d) HME 20% PCM-PVP K29-32, e) HME 30% PCM-

PVP K29-32, f) HME 40% PCM-PVP K29-32, g) HME 50% PCM-PVP K29-32, h) HME 60% PCM-PVP K 29-32, i) HME 70% PCM-PVP K29-32	123
Figure 3.21: ATR-FTIR spectra of PCM, PVPVA 6:4 and HME PCM-PVPVA 6:4 systems.....	126
Figure 3.22: FTIR spectra for a) CAF, b) PVP K29-32, c) PM 10% CAF-PVP K 29-32, d) HME 10% CAF-PVP K29-32, e) HME 20% CAF-PVP K29-32.....	127
Figure 3.23: ATR-FTIR spectra for a) CAF, b) PVP VA 6:4, c) PM 10% CAF-PVPVA 6:4, d) HME 10% CAF-PVPVA 6:4 e) HME 20% CAF-PVPVA 6:4.....	127
Figure 3.24: X-ray Diffraction patterns of PCM and PVP K29-32, a) HME 20% PCM, b) HME 30% PCM , c) HME 40% PCM, d) HME 50% PCM, e) HME 60% PCM, f) HME 70% PCM, g) PM 20% PCM and h) Pure PCM	128
Figure 3.25: X-ray diffraction patterns of PCM with PVPVA 6:4, a) HME 20% PCM, b) HME 30% PCM , c) HME 40% PCM, d) HME 50% PCM, e) PM of 20 % PCM-PVPVA 6:4.....	129
Figure 3.26: X-ray diffraction patterns of CAF and PVP K29-32, a) HME 10% CAF, b) HME 20% CAF, c) PM of 10% CAF d) commercial CAF as received.....	130
Figure 3.27: X-ray diffraction patterns of CAF and PVPVA 6:4, a) CAF, b) PM of 10% c) HME 30%, d) HME 20%, e) HME 10%	131
Figure 3.28: SEM image of a)PM of PCM-PVP K29-32, b) fresh extrudate of HME 40% PCM-PVP K29-32 surface, c) fresh extrudate of HME 40% PCM-PVPVA 6:4, d) Cross section of extrudates of HME 60% PCM-PVP K29-32	132
Figure 3.29: a) raw CAF (Form II), b) heated CAF (Form I was prepared by heating the From II in a covered petri-dish condition. The sublimated product were Form I as confirmed by XRPD), c) HME 10% CAF-PVPVA 6:4 and d) c) HME 10% CAF-PVP K29-32	133
Figure 4.1: ATR-FTIR spectra of different solid-state forms of PCM. (a) Form I was scanned as received (raw), (b) Form II was prepared by slow cooling as described in the method section, (c) ATR-FTIR spectra of amorphous PCM which was obtained by immediately scanning after the quenched-cooling of the molten PCM.	144
Figure 4.2: Multiple ATR-FTIR spectra of quench-cooled PCM that were taken every 2 minutes. Growing of the diagnostic 807 cm^{-1} band was started from the grey line (lowest absorbance), in which its IR absorbance was found to increase with time.	145
Figure 4.3: Examples of DSC profile of QC PCM run at $100\text{ }^{\circ}\text{C}$ / minute with pin-holed pans at the specified time points	146
Figure 4.4: a) Exponential recrystallization profile of PCM as a function of time predicted by DSC b) Exponential profile of relative peak intensity $807\text{ cm}^{-1} / 797\text{ cm}^{-1}$ as a function of time predicted by ATR-FTIR.....	148

Figure 4.5: Correlation curves between the relative peak intensity of $807\text{ cm}^{-1} / 797\text{ cm}^{-1}$ as obtained of ATR-FTIR spectra of QC PCM and the crystal percentage of QC PCM as approximated from DSC thermograms.....	148
Figure 4.6: An example of heating rate dependence of the glass transition temperature of extrudates (HME 40% PCM-PVPVA 6:4). Error bars indicate the standard deviation, $n = 3$	150
Figure 4.7: DSC curves for HME 40% PCM-PVPVA 6:4 system after 3 months storage under different humidity conditions a) 0% RH, b) 22% RH, c) 33% RH, d) 53% RH and e) 75% RH...	153
Figure 4.8: Moisture contents and Tg values of aged HME 40% PCM PVPVA 6:4 after 1 month storage in different humidity conditions. Bar chart in red indicated the early water content of the aged HME 40% PCM PVPVA 6:4 after 9 days and 3 days storage in 53% and 75% RH, respectively	154
Figure 4.9: Recrystallization profiles of HME 40% PCM-PVPVA 6:4 under different humidities condition at room temperature detected by scanning the aged samples overtime using the developed ATR-FTIR quantification method. Dotted lines shown in the Figure is just a guide in following the data points	155
Figure 4.10: DSC thermograms of the freshly prepared HME 40% PCM -carriers, (a) PVP K12, (b) PVP K17, (c) PVP K29-32 and (d) PVPVA 6:4.....	157
Figure 4.11: DSC curve for HME 40% PCM-carriers at 75%RH after 3 months storage.....	157
Figure 4.12: Recrystallization of 40% loading of PCM in different carriers at 75% RH calculated based on characteristic peak of $807\text{ cm}^{-1} / 797\text{ cm}^{-1}$ in ATR-FTIR spectra of the aged sample using Equation 4.6. Dotted lines shown in the Figure is just a guide in following the data points	158
Figure 4.13: Surface morphology of HME 40% PCM-PVPs after 1 month storage in 75% RH a) PVP K12, b) PVP K17, c) PVP K29-32 and d) PVPVA 6:4. Right (ii) images are the corresponding magnification of the left (i) images.....	160
Figure 4.14: Recrystallization of HME 50% PCM in different polymer systems at 75% RH measured by using ATR-FTIR. Dotted lines shown in the Figure is just a guide in following the data points	162
Figure 4.15: The comparison of crystallinity on surface and bulk extrudates after 4 days in 75 % RH measured by using ATR-FTIR	164
Figure 4.16: Surface images after 4 hours in 75% RH HME 50% PCM-PVPs a) PVP K12, b) PVP K17, c) PVP K29-32, and d) PVPVA 6:4.....	165
Figure 4.17: SEM images of HME of 50% PCM PVPs (a) PVP K12, (b) PVP K17, (c) PVP K29-32 and (d) PVPVA 6:4 after 1 week in 75% RH	166
Figure 4.18: Recrystallization profile of HME 30% PCM PVPs system at 75%RH over 120 days produced by using the data from ATR-FTIR.....	167

Figure 4.19: SEM images of HME of 30% PCM different PVPs carriers (a) PVP K12, (b) PVP K17, (c) PVP K29-32 and (d) PVPVA 6:4 after 2 weeks in 75% RH.....168

Figure 4.20: The summary of recrystallization rate of HME 30 to 50% PCM-carriers system. The rate of the recrystallization was obtained from the slope of initial (first 5 days) crystallization profile of each formulations detected from ATR-FTIR method.....168

Figure 4.21: DSC thermograms of HME 40% PCM PVPs after 3 months storage at 0RH 40°C...169

Figure 4.22: SEM images of HME of 40% PCM in polymer for different carriers (a) PVP K12, (b) PVP K17, (c) PVP K29-32 and (d) PVPVA 6:4 after 3months in 40°C.....170

Figure 5.1: Apparent solubility of APIs in the presence of PVPVA 6:4 after 48 hours at 37 °C ..186

Figure 5.2: XRPD profiles of HME 30% APIs-PVPVA 6:4187

Figure 5.3: MTDSC thermograms of HME 30% APIs-PVPVA 6:4. Blue lines present the reversing heat flow signal, whereas the green lines present the total heat flow of the corresponding samples188

Figure 5.4: Theoretical FTIR-ATR spectra of PVPVA 6:4 from different HME-drugs-PVPVA 6:4 systems.....189

Figure 5.5: Dissolution profiles of pure API (orange dotted line), HME 30% API-PVPVA (in red) and their corresponding PM (blue dotted line) in their respective dissolution media: a) KTP, b) NAP, c) INDO and d) OZP. The similarity factors, f_2 indicated the comparison of dissolution profile between PM and HME formulations.....190

Figure 5.6: Contact angles between the pure APIs and their dissolution media. 0.1 M HCl was used as the liquid phase in contact angle measurement of KTP and NAP, whereas distilled water was used as a liquid phase in the measurement for the surfaces of INDO and OZP.193

Figure 5.7: Contact angles of the compacts PMAPIs-PVPVA 6:4 to its corresponding dissolution medium. 0.1 M HCl was used as the liquid phase in contact angle measurement of KTP and NAP, whereas distilled water was used as a liquid phase in the measurement for the surfaces of INDO and OZP194

Figure 5.8: The differences of contact angles profiles between ‘APIs-dissolution medium’ and ‘APIs -1% w/v PVPVA in dissolution medium’195

Figure 5.9: Comparison of contact angle profiles between PM and HME API-PVPVA 6:4 solid dispersions using corresponding dissolution medium a) KTP, b) NAP, c) INDO, and d) OZP196

Figure 5.10: Observation during dissolution process of HME 30% NAP-PVPVA 6:4.....198

Figure 5.11: Examples of particle size analysis of HME 30% KTP-PVPVA in dissolution medium after 2 minutes of the dissolution experiment.....199

Figure 5.12: Particle size analysis: 90% of the cumulative undersize distribution of HME 30% APIs-PVPVA 6:4 in dissolution medium199

Figure 5.13: Images captured upon addition of dissolution media to HME 30% APIs-PVPVA 6:4. From top to bottom of the images a) KTP, b) NAP, c) INDO, d) OZP and from left to right:(i) t=0, (ii) t=1, (iii) t=30, (iv) t=60 minutes	200
Figure 5.14: SEM images of particle collected from dissolution of HME 30% APIs-PVPVA after 1 minute of dissolution process a) KTP, b) NAP, c) INDO and d) OZP	202
Figure 6.1: Schematic to illustrate the dissolution experiment performed with addition of two components at different ends of the dissolution vessel, 'Exp S'	210
Figure 6.2: Dissolution profiles of NAP in the presence of PVPVA 6:4 at various ways as presented in Table 6.1.	215
Figure 6.3: Comparison of the dissolution profiles for PM (blue \diamond) and 'Exp S' (pink \square) of binary NAP PVPs systems a) PVP K12, b) PVP K17, c) PVP K29-32 and d) PVPVA 6:4.	217
Figure 6.4: Phase solubility relationships between different polymer concentrations and solubility of naproxen after stirring for 48 hours at 37 °C	218
Figure 6.5: MTDSC thermograms of HME NAP PVPVA 6:4 with different NAP loading (a) 10% NAP, (b) 20% NAP, (c) 30% NAP and (d) 40% NAP. Green lines of the thermograms are total heat flow profile whereas blue line represents reversing heat flow of the DSC thermograms.	221
Figure 6.6: MTDSC profiles of HME 30% NAP-PVPs different carriers system, i.e. (a) PVPVA 6:4, (b) PVP K12, (c) PVP K17 and (d) PVP K29-32. Green lines of the thermograms are total heat flow profile whereas blue line represents reversing heat flow of the DSC thermograms.	222
Figure 6.7: Dissolution of HME formulations of NAP PVPVA 6:4 in 0.1M HCl pH 1.2.	223
Figure 6.8: The effect of NAP-PVPVA 6:4 compositions in HME and PM products on the initial dissolution rate (at first 5 minutes) of solid dispersion	224
Figure 6.9: Particle size distribution of particles collected from the dissolution vessel at 2 minutes of dissolution of HME 10-40% NAP PVPVA 6:4 systems	225
Figure 6.10: SEM images of residues collected from a dissolution experiment of HME 40% NAP PVPVA 6:4 system at a) 1minute, b) high magnification for particles at 1 minutes, c) 2 minutes, and d) 1 hour	226
Figure 6.11: Hot stage microscopy examination of HME a) 10%, b) 20%, c) 30% and d) 40% of NAP PVPVA 6:4 upon contact with 0.1M HCl at room temperature. Left to right of each row shows the change in appearance of the ground extrudates upon contact with dissolution medium at various time point, a) i =96s, a) ii=118s, a) iii = 3min, a) iv = 5 min, b) i =60s, b) ii=79s, b) iii = 3min, b) iv = 5 min, c) i =45s, c) ii=48s, c) iii = 3min, c) iv = 5 min, d) i =10s, d) ii=55s, d) iii = 3min, d) iv = 5 min. All the captured images are under magnification of 20x (the white scale bar at right bottom corner indicates 150 μ m).....	227
Figure 6.12: Dissolution profiles of HME 30% NAP with different PVPs carriers (PVP K12, PVP K17, PVP K29-32, PVPVA 6:4) in 0.1M HCl at 37 °C.....	228

Figure 6.13: The comparison of initial dissolution rate (at linear release of NAP in the first 10 minutes) between HME and PM system of NAP in different PVPs carriers system.....229

Figure 6.14: Particle size changes of formulation during dissolution experiment.231

Figure 6.15: Microscopic images of HME 30%NAP with a) PVP K12, b) PVP K17, c) PVP K29-32, and d) PVPVA 6:4 after addition of 0.1M HCl at 48 seconds. All the captured images are under magnification of 20x (white horizontal line at right bottom corner indicated 150 μ m).....232

Figure 6.16: Dissolution profiles of PM NAP PVPVA 6:4, PM NAP PVPVA 6:4-Tween 80, HME NAP-PVPVA 6:4, and HME NAP-PVPVA 6:4 -Tween 80 in 0.1M HCl at 37 °C.....233

Figure 6.17: Cumulative curves of particle size analysis of PM and HME SD of NAP PVPVA 6:4 and HME NAP-PVPVA 6:4 –Tween 80 systems after 2 minutes of dissolution234

Figure 6.18: Hot stage microscopic observations of a) HME 30%NAP PVPVA +2% Tween 80 , b) HME 30%NAP PVPVA +10% Tween 80 upon contact with 2 drops of 0.1M HCl. Images in the corresponding row from left to right indicated the time increase of the sample contact with 0.1 M HCl up to 5 minutes. All the captured images are under magnification of 20x (white horizontal line at right bottom corner indicated 150 μ m)235

Figure 6.19: Dissolution profiles of the freshly prepared fully amorphous HME NAP PVPVA 6:4, partially amorphous NAP PVPVA 6:4 systems and the corresponding PM systems in 0.1 M HCl at 37 °C.....237

Figure 6.20: Dissolution mechanisms of PM and HME of PVP-based poorly soluble APIs241

Figure 7.1: Schematic of a wetted particle of HME poorly soluble drug PVP-based solid dispersion when it is in contact with dissolution medium.....250

Figure 7.2: A schematic of the proposed dissolution mechanism of HME PVP-based solid dispersion system based on this study. The spheres represent drug domains and the curved lines represent the polymer. Pathway (a) on the left indicates dissolution process of a system with low ‘solubility advantages’ of its amorphous API: 2a shows the occurrence of agglomeration or phase separation, 3a shows the decrease in the effective surface area for dissolution as a result of agglomeration and 4a shows a new barrier formed as a result of continuous recrystallization and agglomeration process which give rise to a hydrophobic layer at the dissolving front of the solid dispersion. Pathway (b) on the right illustrates the dissolution process of a system with high ‘solubility advantage’ of its amorphous API: 2b shows that the drug domains are ready to dissolve once the carrier is dissolved, 3b shows the stable drug molecule in the midst of medium and polymer without agglomeration or crystallization and at 4b, system has completely dissolved. ...251

List of Tables

Table 1.1: Biopharmaceutical classification system of API adapted from Kolter 2012	1
Table 1.2: Types of Solid dispersion based on physical state of API and carrier matrix (Kolter et al., 2012)	10
Table 1.3: APIs used in HME production and characterization of HME process.....	23
Table 1.4: different types of plasticizer used in HME pharmaceutical application	30
Table 1.5: Example of surfactants used in HME process	32
Table 1.6: The effects of processing parameters and excipients the physical stability of extrudates	35
Table 2.1: Physicochemical properties PCM.....	54
Table 2.2: Physicochemical properties CAF.....	55
Table 2.3: Physicochemical properties NAP	56
Table 2.4: Physicochemical properties KTP.....	57
Table 2.5: Physicochemical properties INDO	58
Table 2.6: Physicochemical properties of OZP	59
Table 2.7: Grades of PVP available on the market (Kibbe 2002).....	61
Table 2.8: Average molecular weight (M _v) of various grades of PVP polymer which are calculated from the K-value, i.e. viscosity of 1 % polymer solution (Kibbe 2002).....	61
Table 2.9: Physicochemical properties polyvinylpyrrolidone vinyl acetate (PVPVA 6:4)	64
Table 2.10: Sources of materials employed in this study.....	65
Table 2.11: Melting and glass transition temperatures of model APIs and carriers employed in this study.....	66
Table 2.12: Parameter used in the production of HME systems.....	72
Table 3.1: Solubility parameter calculations for PCM using the Hoftyzer and Van Krevelen methods. Column 1 represents the chemical group contribution of PCM. Columns 2 to 4 represent the respective forces attributed by each of the chemical group. The last column represents the molar volume of the contributed groups (Van Krevelen and Te Nijenhuis, 2009).	95
Table 3.2: Solubility parameter calculations for PCM using the Hoy methods. Column 1 represents the chemical group contribution of PCM. Columns 2 and 3 represent the molar attraction function and polar component, respectively attributed by each of the chemical group. Column 4 represents	

the molar volume of the contributed groups and the last column is the Lydersen correction for non-ideality of each chemical group (Van Krevelen and Te Nijenhuis, 2009).	96
Table 3.3: Solubility parameters of APIs and PVP polymers	97
Table 3.4: Flory-Huggins interaction parameters based on melting point depression.....	101
Table 3.5: Theoretical solid solubility of APIs in PVP carriers at their corresponding extrusion temperatures predicted by using melting point depression approach	103
Table 3.6: Thermal properties of raw materials from DSC and TGA analysis.....	104
Table 3.7: Water content (% w/w) of freshly prepared extrudates as a function of composition ...	112
Table 3.8: Values used to calculate the theoretical Tg of the mixture of Ternary PCM-Polymer-Water system.....	115
Table 3.9: Infrared bands of hot melt extrudate of PCM PVP in comparison to the corresponding PM.....	125
Table 3.10: Percentage crystalline PCM in HME PCM- PVP K29-32.....	129
Table 3.11: Percentage of crystal based on Bragg reflection peak from XRPD	129
Table 4.1: Glass transition temperature/ activation energy/ fragility for different HME PCM-PVP systems.....	150
Table 4.2: The predicted trend of product stability based in fragility and Tg prediction	151
Table 4.3: Ratio of PCM to polymer in different composition (hydrogen bonding limit of PCM-PVP polymers are highlighted in pink).....	173
Table 5.1: Medium and UV wavelength used for the solubility measurement of pure API and PM API-PVPVA.....	180
Table 5.2: Experiments of contact angles between the solid phase and the liquid phase	184
Table 5.3: Experimental solubility of APIs, free energy difference between the crystalline APIs and their amorphous form, solubility ratio and theoretical amorphous of amorphous form to their crystalline counterpart in the selected media	185
Table 5.4: Summary of the dissolution performances among pure APIs, PMs and HME PVPVA systems.....	191
Table 6.1: Dissolution experiments of NAP with the presence of PVPVA 6:4 in various conditions	209
Table 6.2: HME formulations that were prepared and investigated in this study. All the HME formulations were prepared at 150 °C, 100rpm with a residence time of 10 minutes.	211
Table 6.3: Experiments of contact angle measurement between the solid phase and liquid phase.	213

Table 6.4: Values used for the calculation of interfacial energy by using Fowkes Equation (6.1) to (6.4).....	214
Table 6.5: Average surface tensions and average volume of drops during the 120 seconds of the experiment time frame. All the solutions were saturated with NAP which was denoted as ‘sat NAP’.....	219
Table 6.6: onset time of birefringence upon contact with dissolution medium as recorded via HSM	228
Table 6.7: Interfacial tensions of different HME NAP PVPs system between their solid phase and 0.1 M HCl	230
Table 6.8: Onset time of birefringence base on HSM studies of HME 30% NAP-PVPs systems .	232
Table 6.9: Particle size distribution of formulation after 2 minutes of dissolution experiment.....	234

List of Abbreviation

AFM	Atomic force microscopy
API	Active Pharmaceutical Ingredient
ATR-FTIR	Attenuated total reflectance- Fourier Transform Infrared
CA	Contact angle
CAF	Caffeine
CMC	Critical micelle concentration
CP	Co-precipitated
C_p	Heat capacity
DSC	Differential Scanning Calorimetry
Ea	Activation Energy
FH	Flory-Huggins model
G-T	Gordon-Taylor
HCl	Hydrochloride acid
HME	Hot Melt Extrusion
HPMC	Hydroxypropyl methylcellulose
HSM	Hot stage Microscopy
INDO	Indomethacin
KTP	Ketoprofen
m	Fragility Index
MTDSC	Modulated mode DSC
MW	Molecular weight
NAP	Naproxen
NSAID	Non-steroidal anti-inflammatory drug
OZP	Olanzapine
PCM	Paracetamol
PEG	Propylene glycol
PM	Physical Mixtures
PVP	Polyvinylpyrrolidone
PVPVA 6:4	Polyvinylpyrrolidone : vinyl acetate in ratio of 6:4
RH	Relative Humidity
rpm	Rotation per minutes
SD	Solid dispersion
SEM	Scanning Electron Microscope
STDEV	Standard deviation
Tg	Glass transition temperature
TGA	Thermogravimetry Analysis
Tm	Melting temperature
UV	Ultraviolet
UV-VIS	Ultraviolet-visible light
XRPD	X-ray Powder Diffraction
γ	Surface tension
χ_{12}	Flory-Huggins interaction parameter

Chapter 1. Introduction

1.1. General Introduction

For any oral administered product, absorption of the active pharmaceutical ingredients (API) is depending on its aqueous solubility and gastrointestinal permeability (Abrahamsson and Lennernäs, 2009). In this context, Biopharmaceutics Classification System (BCS) provided by U.S. Food and Drug Administration has classified APIs into 4 classes according to their aqueous solubility and gastrointestinal permeability (Kasim et al., 2003). Table 1.1 illustrated the 4 different classes of BCS classification system. This system is a guide in understanding the intestinal absorption of an API.

Table 1.1: Biopharmaceutical classification system of API adapted from Kolter 2012

	High solubility	Low solubility
High permeability	Class I	Class II
Low permeability	Class III	Class IV

Low membrane permeability of class III and IV substances will usually revert to its structural optimization phase to obtain the desired physicochemical properties. High solubility properties of class I is not a concern in the therapeutic achievement as sufficient doses of these API will be obtained after oral administration. In contrary, low solubility of class II substances is often deemed to be a concern in inadequate drug absorption. This is due to the limited drug release (of BCS class II substance) in the gastrointestinal area despite its high permeability.

Today, formulation scientists are facing significant challenges due to the increasing number of poorly soluble API. It has been reported that more than 40% of the newly discovered APIs are poorly soluble (Fahr and Liu, 2007). These APIs are often classified as BCS class II or IV, based on their solubility and permeability properties. Poor solubility characteristic of BCS class II API during the dissolution process is the rate limiting step to drug absorption into the bloodstream. Thus, the key to establish successful oral formulation for BCS class II API is through proper formulation which is the main interest of this thesis.

The common strategies in the formulation of BCS class II APIs are the physical addition of hydrophilic or surface active excipients, micronisation of drug particles, formation of inclusion complexes, emulsion/ micro emulsion and production of amorphous solid dispersion (SD). Amongst the aforementioned strategies, amorphous solid dispersions (SDs) have been one of the most promising dosage forms due to their promising dissolution enhancement of BCS class II APIs. However, this type of dosage form is not widely commercialized due to their inherent thermodynamic instability that might alter the therapeutic effect of the API upon long-term storage. Therefore, there is a great need to improve amorphous SD system in order to bring about the maximum benefit of this formulation approach.

The subsequent section of this chapter will cover the basic nature of a typical amorphous pharmaceutical system with emphasis on the application of SD systems as a means of overcoming the difficulties associated with formulating an amorphous API. In addition, various processing methods of SD will be introduced with the emphasis on the use of hot melt extrusion (HME) as this is the main manufacturing method employed in this study. Subsequently, a review on the stability and dissolution performance of SD is presented.

1.2. Amorphous pharmaceutical and its advantages

Amorphous pharmaceutical can be obtained under three main sets of circumstances (Craig et al., 1999, Hancock and Zografi, 1997). Firstly, some materials exist naturally as an amorphous form which is stable at room temperature. These materials include polymers such as polyvinylpyrrolidone, polyethylene glycol and D/L polylactic acid. Secondly, amorphous materials can be generated unintentionally during manufacturing processes such as milling, drying or compression. Thirdly, amorphous material may be prepared deliberately for its high apparent solubility or dissolution rate. The conversion of crystalline APIs into their amorphous form has been shown to increase the dissolution rate of API by enhancing apparent solubility of the compound; hence, amorphous APIs have gained considerable attention in the field of pharmaceuticals for dosage form design.

Amorphous materials have excess free energy, enthalpy, entropy, higher specific volume, lower density and higher molecular mobility as compared to the crystalline structure. This has led to mechanical properties (viscosity and elastic modulus) that resemble those of a liquid rather than those of a solid and hence these systems can be visualized as supercooled liquids (Hancock et al., 2002, Hancock and Zografi, 1997). The absence of long range order and crystalline bonds in the structure of amorphous systems has resulted in ready dissolution as less activation energy is needed for dissolution in relation to the structurally ordered crystalline form (Elamin et al., 1994). This has

also given rise to several fold solubility enhancement (Hancock and Parks, 2000, Hancock and Zografi, 1997) and subsequently enhanced bioavailability of the compound (Craig et al., 1999, Graeser et al., 2009a). Therefore amorphous systems have been seen as a means of overcoming the issue of poorly soluble APIs.

Although amorphous systems are reported to be a reliable way of solving the problem of poorly soluble APIs, there are only limited amorphous products in the market such as Kaletra® (ritonavir and lopinavir), a sustained release formulation of verapamil (Isoptin SRE), Sporanox® (itraconazole) and Prograf® (tacrolimus) (Graeser et al., 2009a). This is mainly due to the inherent physical instability of the amorphous state that could lead to reversion to its crystalline counterpart over a period of time, causing sub-therapeutic effects of the amorphous product due to lowered dissolution and hence absorption. Thus, the behaviour of an amorphous system should be well understood before one can effectively design a successful pharmaceutical dosage form with consistent product performance and desired therapeutic effect.

1.2.1. Behavioural features of amorphous materials

The most significant features of amorphous material include the glass transition temperature (T_g), fragility, molecular mobility and relaxation, plasticization, annealing and aging. These features are discussed in detail with accompanying theoretical background in the subsequent sections.

1.2.1.1. Glass transition temperature

The glass transition temperature (T_g) is a temperature at which a material transforms from its liquid / rubbery state to its corresponding glassy state. It is associated with a change in molecular mobility rather than a change of state as such, as there is no significant change in ordering through this temperature. Figure 1.1 illustrates the pathway of generating an amorphous material begins from the cooling of a melt and the correlation to the glass transition temperature of the material (Craig et al., 1999).

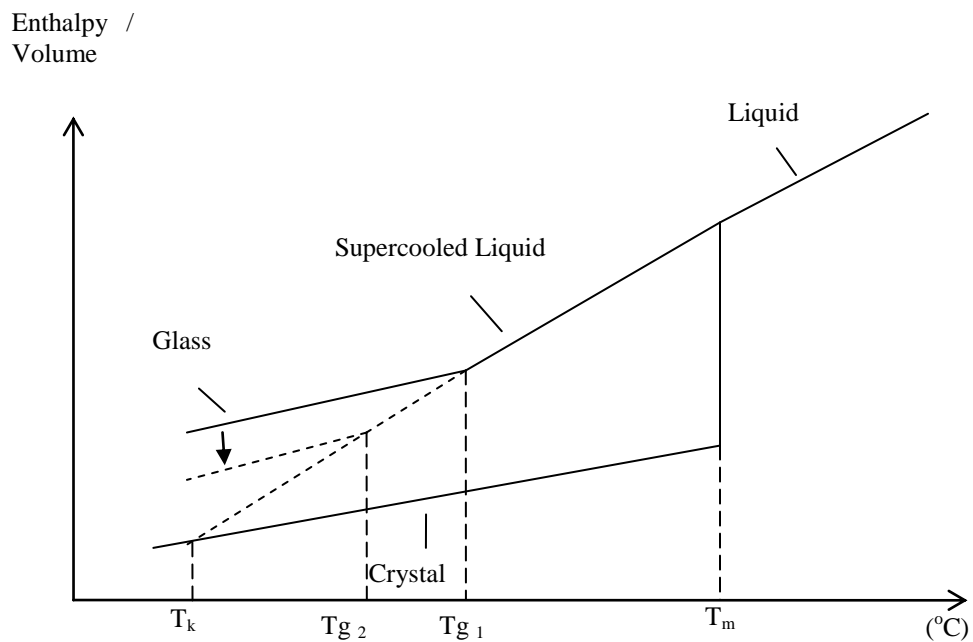


Figure 1.1: The change in volume or enthalpy with temperature for a material undergoing crystallization or glass transition. T_m is melting temperature of the crystalline material. T_{g1} is the point at which there is a discontinuity in volume and enthalpy. The dashed line between T_{g1} and T_k representing the profile of volume and enthalpy change when a melt is slow-cooled. T_{g2} is the glass transition temperature when the slow cooling is performed. T_k is Kauzmann temperature (Craig et al., 1999, Pinal, 2008).

From Figure 1.1, an API will exist in the liquid state at temperatures above the melting temperature (T_m). Decreasing the temperature of the melted API to a temperature lower than its melting point will result in the transition of the melt to its crystalline form via a recrystallization process. It is an exothermic process that leads to sudden contraction of the system (shown by the long downward arrow in Figure 1.1) which is caused by the decrease in its free volume (a volume in which the molecules are free to move) at T_m . Consequently, both enthalpy and volume of the system decrease at T_m . The solid line at the bottom of the graph represents the crystalline state, as shown in Figure 1.1.

When the decrease in temperature of the API is too fast for the crystallization process to take place, an amorphous material may be obtained. This is because the fast cooling process may cause unfavourable molecular shape, size and configuration that is important for a crystallization process. In the fast cooling process, no discontinuity in enthalpy of the melted API is seen at temperature below T_m . At this point, a super-cooled liquid is formed and it exists in “rubbery state” (Figure 1.1). In this state, the average time range for its molecular motion is approximately 100 seconds with a typical viscosity of between 10^{-3} and 10^{12} Pa.s (Hancock and Zografi, 1997).

Upon continual cooling, the material is unable to attain its equilibrium kinetically in the time scale of the cooling rate and then it reaches a frozen state at T_{g1} . In this state (at T_{g1}), the translational and rotational motions of the molecules are dramatically reduced. Finally, glassy material is formed at temperature lower than T_{g1} whereby only molecular vibrations are taking place. The T_g value of an amorphous material is highly dependent on the cooling rate of the melt. Slower cooling rates resulted a lower T_g value that is represented by the dashed line in Figure 1.1 with a value of T_{g2} , where T_{g2} is $< T_{g1}$.

The glass transition temperature of a material can be obtained using various methods as outlined in the literature (Hancock and Zografis, 1997, Craig et al., 1999). Commonly, it is detected by using Differential Scanning Calorimetry (DSC) (Craig et al., 1999, Hancock and Zografis, 1994). The detail of the DSC instrument is presented in Chapter 2. In brief, the sample is heated or cooled alongside a reference whereby the differential heat flow between the sample and reference as a function of temperature is measured. This provides the data regarding the heat capacity of the sample and reference. Figure 1.2 shows the measurement of T_g using DSC method.

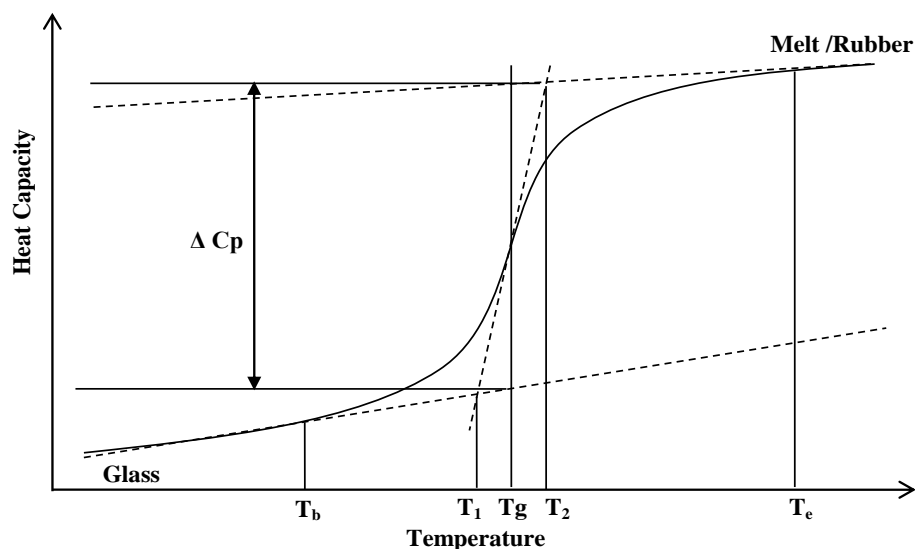


Figure 1.2: Measurement of T_g using DSC thermogram. T_b is the beginning of the transition and the extrapolated onset of the transition point is T_1 . T_g is taken as half height of the transition event. Similarly the extrapolated end point is T_2 and the transition process end at T_e .

T_g is specified by the half height of the transition event on cooling, i.e. the temperature at which the heat capacity is in the middle of that of glassy and rubbery state. It is a kinetic event and therefore the detected value is highly constrained by the timescale of the experiments i.e. heating or cooling rate during manufacturing as measured with DSC. At T_g , a transition of heat capacity, ΔC_p , is noted due to the change of molecular mobility before and after the glass transition temperature. Viscosity of the material at T_g temperature is in the region of 10^{12} - 10^{14} Pa.s which is the main parameter used in deriving the fragility concept of an amorphous system that will be covered in the next section.

1.2.1.2. Fragility

Temperature dependency of the viscosity of a melt may be described by the well-known Arrhenius Equation (1.1).

$$\eta = K e^{\frac{-Ea}{RT}} \quad (1.1)$$

where η is viscosity, K is a constant, Ea is the activation energy of melt flow, R is universal gas constant and T is temperature (DiNunzio et al., 2009). According to Equation (1.1), higher temperature of the melt will give rise to low viscosity of the melt.

In defining Fragility, Angell plotted the relationship of melt viscosity and the melt temperature scaling with T_g by taking the natural logarithm of Arrhenius Equation (1.1), i.e. plotting $\log(\eta)$ versus (T_g/T) (Angell, 1995). Based on the plot of variety of liquids, it was found that some liquid exhibited a linear relationship and some deviated from linearity of Arrhenius equation (Angell, 1995). Angell (1995) suggested that system that showed linear relation in the Arrhenius plot is designated as a strong melt and those that deviated from linearity of the Arrhenius plot could be designated as fragile liquids (Angell, 1995). Figure 1.3 shows the Arrhenius plot of fragility of strong and fragile glass former which is also known as Angell plot.

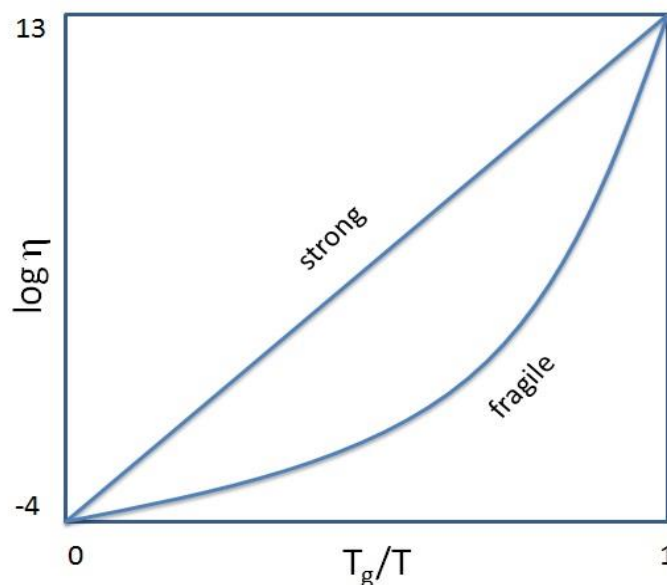


Figure 1.3: The simplified schematic of Angell Fragility concept (Angell, 1995)

According to Figure 1.3, the fragility index of a material is described by the degree of non-Arrhenius behaviour of the material. A fragile system possesses higher density of configurationally state which leads to rapid thermal excitations and a higher increase in heat capacity (Ojovan and Lee, 2005). Thus, the activation energy of a fragile system would be greatly influenced by the temperature. Conversely, strong glasses like SiO_2 , GeO_2 , B_2O_3 are structured with covalent bond, in which their activation energies are slightly influenced by the change of temperature.

The fragility of an amorphous material is usually described by the fragility index, m . This parameter, m is evaluated from the Tg values from different heating/cooling rate of DSC scan by using Equations (1.2) & (1.3),

$$m = \frac{\delta \log \tau}{\delta (T_g - T)} \quad (1.2)$$

$$m = \frac{\Delta E_{T_g}}{2.303 * RT_g} \quad (1.3)$$

where δ indicates derivative function of Equation (1.2), ΔE_{T_g} is the activation energy for structural relaxation at Tg, τ is relaxation time and R is universal gas constant. ΔE_{T_g} can be obtained from heating/cooling rate dependent of calorimetric Tg as described in Equation (1.4) (Moynihan et al., 1976),

$$\frac{d(\ln q)}{d\left(\frac{1}{T_g}\right)} = \frac{-\Delta E_{T_g}}{R} \quad (1.4)$$

By obtaining the magnitude of the fragility index, an amorphous material could be classified into strong liquid when $m < 40$, and fragile liquid when $m > 75$, and those lie in between this range is known as intermediate fragile liquid (Yu, 2001). With that, the value of fragility index, m can be used to reflect the physical stability of an amorphous system upon annealing (described in more detail in Chapter 4.3.2).

1.2.1.3. Structural relaxation and molecular mobility

Despite the use of Tg in representing a sudden decrease in mobility, molecular mobility of an amorphous system at temperatures well below Tg has been reported (Hancock and Zografi, 1997, Nagapudi and Jona, 2008). Thus, together with Tg, molecular mobility has also been correlated to the structural relaxation time, whereby the structural relaxation time of an amorphous system is the time taken for the relaxation of the amorphous structure toward the thermodynamic equilibrium that originally exists in its non-equilibrium state. This parameter could be evaluated by noticing the loss of enthalpy accompanied by the relaxation event of the amorphous structure overtime.

The lost enthalpy value can be obtained from DSC measurement where the enthalpy is inferred by the endothermic relaxation peaks which accompany the glass transition events. These relaxation events and T_g could be separated by using modulated mode of DSC which is further presented in Chapter 2. With the recovery of the enthalpy, the relaxation time, τ could be estimated by using the enthalpy of recovery over time using the empirical Kohlrausch-William-Watts (KWW) Equation (1.5).

$$\phi_{(T,t)} = \exp \left[- \left(\frac{t}{\tau} \right)^\beta \right] = 1 - \frac{\Delta H_{relax}}{\Delta H_\infty} \quad (1.5)$$

where β is the stretch parameter which could be obtained by fitting the value of enthalpy recovery to Equation (1.5). ΔH_{relax} is the measured endotherm peak accompanied the T_g event and ΔH_∞ represents the maximum enthalpy that could be recovered, this value could be obtained by using Equation (1.6) with the values of heat capacity changes between the liquid and glassy state of the sample, ΔC_p ,

$$\Delta H_\infty = \Delta C_p (T_g - T) \quad (1.6)$$

where T is the intended storage temperature. The main assumption of this model is that the relaxation time did not change during the experiment time scale (Graeser et al., 2009a). Due to the limitations of KWW approach, Adam-Gibbs Equation (1.7) has been suggested as another prediction of the relaxation time,

$$\tau = \tau_0 \exp \left[\frac{DT_0}{T(1 - T_0/T_f)} \right] \quad (1.7)$$

where τ_0 is a constant which is taken as the lifetime of atomic vibration, 10^{-14} s. T_f is fictive temperature which can be obtained by extrapolation of the linear part of the enthalpy line above and below the T_g of a system as shown by T₁ in in Figure 1.2 (Lacey et al., 2006). D is Angell's strength parameter and T₀ is the temperature where no structural mobility occurred. Both D and the T₀ can be obtained by solving Equation (1.8) and Equation (1.9), respectively.

$$D = \frac{\ln 10 \times m_{min}^2}{m - m_{min}} \quad (1.8)$$

$$T_0 = T_g \left(1 - \frac{m_{min}}{m}\right) \quad (1.9)$$

In Equation (1.9), m is predefined in Equation (1.2) or (1.3) and m_{min} is the minimum possible fragility value which has been calculated as 16 (Aso et al., 2004, Graeser et al., 2009a).

Besides the relaxation associated with the glass transition temperature (alpha relaxation), beta relaxation has also been reported (Nagapudi and Jona, 2008). Beta relaxation is related to the molecular motions in small length-scale such as rotations of methyl group and ring flips in benzene group (Van Krevelen and Te Nijenhuis, 2009). These minor motions are thought to promote the spontaneous formation of small nuclei thereby causes physical instability of the amorphous phase. It was suggested that at temperature < 40 °C of T_g , the beta relaxation is the dominant relaxation process which would be the main factor for physical stability at $T < T_g - 40$ °C (Nagapudi and Jona, 2008).

1.2.1.4. Plasticization

Amorphous materials are highly affected by the presence of moisture and additive materials. This is because the small molecule size of the additive materials may introduce a considerable excess free volume in the system which will cause plasticization of the system (Hancock and Zografi, 1997). Due to the hygroscopic nature of amorphous systems (Hancock and Zografi, 1994, Hancock and Zografi, 1997), amorphous materials tends to absorb considerable amounts of water which can potentially cause plasticization of the amorphous system. The presence of water could change T_g of the system significantly due to the difference in the size of water molecule and drug molecule. Since T_g is an important parameter for consideration in physical stability of an amorphous API, it is imperative to understand the influence of water molecules on the amorphous API which often causes plasticization. In this case, the Gordon – Taylor (1952) equation may be employed to predict the final T_g of the blend system. Detail calculation of this approach will be presented in Chapter 3.3.3.2.1.

In the pharmaceutical field, blended systems are commonly used, where the addition of excipients to an amorphous API might plasticize or anti-plasticize (raise the T_g of the amorphous API) the system. In consideration of physical stability, anti-plasticizing agents are often preferred depending on the manufacturing process.

1.3. Solid dispersion

The use of SDs in pharmaceutical formulation was first discovered by Sekiguchi and Obi in 1961, whereby the authors found that an eutectics mixture could dramatically improve drug release rate, and hence bioavailability of the active ingredients (Sekiguchi and Obi, 1961).

Literally, SD refers to the dispersion of one or more ingredients in a solid form of continuous matrix/carrier. SD could be classified based on physical state. These include eutectics, amorphous precipitates in crystalline matrix, solid solutions, glass suspension and glass solution. Table 1.2 provides the definition of different types of solid dispersion based on physical state of the drug and carrier matrix adopted from Kolter et al. (2012).

Table 1.2: Types of Solid dispersion based on physical state of API and carrier matrix (Kolter et al., 2012)

Types of solid dispersion	Matrix	API	Phases
I. Eutectics	C	C	2
II. Amorphous precipitates in crystalline matrix	C	A	2
III. Solid solution • Continuous vs discontinuous • Substitutional vs interstitial	C	M	1 or 2
IV. Glass suspension	A	C	2
V. Glass suspension	A	A	2
VI. Glass solution	A	M	1

C= crystalline, A= amorphous and M= molecularly dispersed

For eutectic solid dispersion, two crystalline solids co-crystallized at their eutectics composition and temperature. Deviation from the eutectic composition will lead to crystallization of one of the two components before the other. In eutectics solid dispersion, dissolution rate enhancement is mainly attributed to the dispersion of drug as fine crystal which increases its surface area of dissolution process (Janssens and Van den Mooter, 2009). Amorphous precipitate is another possible physical state of a solid dispersion. However, there are limited reports regarding solid dispersion of this physical state. In solid solution, carrier matrix exist in crystalline state, whereas the drug is predominantly in molecularly dispersed state. Solid dispersion in this group could be further classified into continuous solid solution or discontinuous solid solution (Leuner and Dressman, 2000). In continuous SD, both the solute and the carrier are miscible in all proportions. Ideally, the bonding strength between the solute and carrier is greater than the bonding strength of individual molecule of each phase. In a discontinuous SD, distribution of the solute may be substitutional crystalline or interstitial crystalline as shown in Figure 1.4.

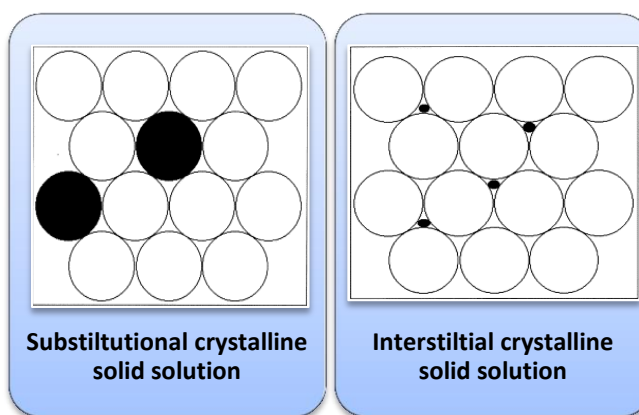


Figure 1.4: Substitutional crystalline or interstitial crystalline solid dispersion (Leuner and Dressman, 2000)

Based on Table 1.2, type IV SD is categorised as crystalline glass suspension whereby the drug remains in its crystalline form but dispersed in the amorphous polymeric matrix. Whereas type V is amorphous glass suspension and type VI SD is referred to as solid glassy solution. Figure 1.5 illustrates the main three types of solid dispersion that cover types IV, V and VI. These three types of solid dispersion are the commonly obtained forms of solid dispersion.

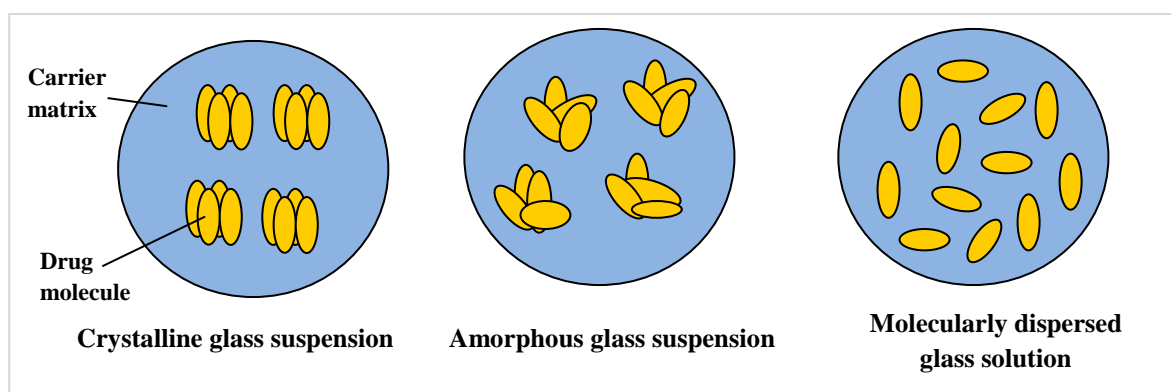


Figure 1.5: Solid dispersion of amorphous polymeric carrier (Kolter et al., 2012)

Based on Figure 1.5 crystalline and amorphous glass suspension are two-phase solid dispersions. Between the glass suspensions, crystalline glass suspension is relatively more stable as the drugs exist in their stable crystalline forms. In this system, the melting point of the drug shall be detected in analytical methods such as differential scanning calorimetry (DSC) and X-ray powder diffraction (XRPD). On the other hand, the amorphous domain in the amorphous glass suspension is only kinetically stabilized and tends to revert to its crystalline state over time. Detection of the amorphous domain in this system is feasible by using DSC measurement which may reveal the T_g values of the drug. Among the three systems shown in Figure 1.5, molecularly dispersed glass solution is the most desired form of SD as molecular dispersion of the drug in the carrier matrix is a one-phase system which renders its good stability alongside with significant dissolution rate enhancement of the dispersed drug.

SDs offer promising effects in bioavailability enhancement of poorly soluble drugs as evidenced by several publications (Six et al., 2005, Zheng et al., 2007b). It is postulated that SD formulation increases the surface area available for dissolution process via particle size reduction, and improves wetting of compounds surfaces. In amorphous SDs, further advantages are assumed to be due to the removal of crystalline drug structure (Chawla and Bansal, 2008). However, during the dissolution process of amorphous APIs, the API is often present in the supersaturation state in the medium. In such case, careful selection of carrier is essential whereby it should help to modulate the properties of the solvent (Craig, 2002) and to inhibit precipitation of the drug from the supersaturated solution. Moreover, it is postulated that if the drug does precipitate, it will precipitate into metastable polymorphs which have higher solubility properties than the original form (Vasconcelos et al., 2007).

1.3.1. Preparation of solid dispersion

SD can be prepared via several methods. These include melt quenching, milling or cryo-grinding, freeze drying, co-evaporation or co-precipitation and by the means of spray drying. The principle of each method will be introduced briefly in the subsequent sections. In particular, more detail will be given on the use of HME methods which is the main manufacturing method used in this study.

1.3.1.1. Traditional melting methods

Amongst the aforementioned methods, melting is one of the most conventional. This method involves the mixing of components at molten state and the cooling of mixture into a solid form (Nagapudi and Jona, 2008). The cooling of the melt could be performed through slow cooling at room temperature or fast / quench cooling by using ice or liquid nitrogen. The cooling rate is shown to be the crucial factor that determines the formation of thermodynamically unstable solid dispersion. This method is useful for the preparation of small quantity of sample.

The melting method can only be applied to compounds which are thermally stable upon melting (Patterson et al., 2005, Forster et al., 2001a). For example, piroxicam starts to degrade upon melting, thus the use of melting methods might not be suitable for this compound (Forster et al., 2001a). Besides, the time and temperature pause for complete melting determines the outcome of the generated amorphous system (Van den Brande et al., 2004, Wojnarowska et al., 2010). For example, Van den Brande et al. (2004) reported a significant degradation of loviride processed at slow cooling (Van den Brande et al., 2004). However, a stable amorphous form of loviride could be obtained by using fast cooling of its melt. This is attributed to the long residence time of the

loviride molten at high temperature condition with their preparation at a slow cooling rate which promotes degradation of drug.

To avoid potential degradation via the melting method, an alternative melting carrier method may be performed. This alternative method involves the use of carrier with low melting or glass transition temperature. The carrier is first melted or softened. Then the API is mixed on top of the molten carrier. This alternative method entails high compatibility between the API and carrier or a high solid solubility of the API at a lower softening temperature of the carrier (Schachter et al., 2004).

1.3.1.2. Milling/cryogrinding

The possibility of generating an amorphous pharmaceutical product through milling or cryogrinding has been reported (Balani et al., 2010, Descamps et al., 2007, Elamin et al., 1994, Nagapudi and Jona, 2008). Three mechanisms were proposed for the possible conversion of a crystalline material into its amorphous phase through milling or cryogrinding. Firstly is the local thermal melting and rapid quenching of the API during the milling process. Secondly, the amorphous form of the API is obtained from the intermediate state formed during polymorph conversion while milling. For instance, the milling of form IV fananserine could lead to its intermediate amorphous state which precedes the transformation of the metastable Form I polymorphs (Willart and Descamps, 2008). The third mechanism in amorphization of a crystalline API is the accumulation of defects or structural disordering of the API through milling (Descamps et al., 2007, Elamin et al., 1994). The huge accumulation defects in the crystal resulted in an increase in the Gibbs free enthalpy of the solid which will then be amorphized spontaneously at the milling temperature. This is reported in Elamin et al. (1994) whereby an increase of free energy of griseofulvin upon milling process was observed which lead to its reduction in molar heat of solution (Elamin et al., 1994).

The amorphicity of a product prepared by milling is highly dependent on the milling temperature and its relation to the T_g and crystalline strength of the API. A few reports have shown that high proportion of amorphous content could be obtained in the condition where the milling temperature is below the T_g of the API. When milling is performed at a temperature slightly below the T_g, the milling intensity was reported to be crucial in determining the nature of the transformation. For instance, milling the γ form of indomethacin at room temperature (which is approximately 20 °C, a temperature lower than the T_g of amorphous indomethacin) induces the production of amorphous at high milling intensity. However, polymorphic conversion occurs at a lower milling intensity

(Descamps et al., 2007). On the other hand, milling above T_g can cause crystal-crystal polymorphic transformation (Descamps et al., 2007).

The milling method was shown to produce SDs with reduced physical stability as compared to the SD prepared from other methods such as spray drying and melt quenching methods (Graeser et al., 2009a, Ke et al., 2012, Wojnarowska et al., 2010). According to Ke et al.,(2012) this is due to the heterogeneous relaxation of the milled sample at molecular level as indicated by its lower value of the relaxation distribution (β) in comparison to the same sample system prepared through spray drying and melt-quenching. This may be explained by the high proportion of nuclei available to undergo recrystallization as compared to the complete dissolution and melting of API in the other preparation methods such as solvent method or melting method.

1.3.1.3. Solvent method : co-evaporation / co-precipitation

The solvent method was described in 1965 by Tchibani and Nakumara who obtained a co-precipitated solid dispersion by drying a mixture of lipophilic β -carotene in a water soluble PVP which were previously dissolved in a common solvent. Since then many workers have taken up this method for preparation of solid dispersion (Sekikawa et al., 1978, Wegiel et al., 2013, Biswal et al., 2009, Mura et al., 2003).

Principally, the solvent method requires a common solvent such as ethanol or chloroform to completely dissolve both the API and carrier. The mixture is then allowed to mix at solution state. Subsequently the common solvent of the mixture is evaporating at reduced pressure and elevated temperature. During the evaporation of the solvent, the viscosity of the sample increases very rapidly leading to reduction in drug mobility. At the same time, concentration of the drug increases and reaches its solubility in the carrier; eventually, it exceeds this solubility which forms the precipitate. Thus, the formation and maintenance of an amorphous solid dispersion in co-precipitation method is the result of crystallization inhibition attributed to drug-polymer interaction or the entrapment of the drug in the polymeric matrix during the evaporation process (Biswal et al., 2009).

The solvent method is useful to formulate a SD of thermolabile APIs which may not be prepared by the melting method due to the concern of degradation upon melting. However, the solvent method can cause environmental hazards due to the use of large amount of solvent use. Products obtained from this method have been shown to be less homogeneous as compared to the co-ground material of the same composition (Corti et al., 2008).

1.3.1.4. Spray drying

Spray drying is another type of solvent method which is used for isolating dry compound from a solution or suspension. It is a well-established technology for the formation of solid particle whereby the yield of solid particle produced from this method is relatively high (Nagapudi and Jona, 2008, Thybo et al., 2008b).

Similar to the first step of co-evaporation, spray drying manufacturing method of SD requires a common solvent to prepare a solution of API and carrier. Generally, aqueous solutions are used. However, organic volatiles are also frequently used as common solvent due to the wide range of their solubilisation capacity on most of the poor soluble drugs. Alternatively, solvent mixtures such as mixes of aqueous and organic solvent may be used.

In the process of spray drying, the mixture of API and carrier in the common solvent is pumped by a peristaltic pump and sprayed via an orifice atomizer through an inlet whereby the temperature is pre-set for the drying process. Upon spraying, the mixture is atomized into the micrometer range and the droplets undergo solidification in milliseconds to form fine solid particles (Guns et al., 2011). Guns et al. (2011) suggested that pre-treating the solution before spraying, such as preheating the mixture, could reduce the de-mixing tendency between API and carrier upon spraying.

To achieve an effective drying process, an overall drying procedure is equipped in the spray drying machine apart from the inlet temperature drying. This drying process is mainly performed using nitrogen as a drying gas in a closed-cycle spray drying plant to dry off the residues of organic solvent, where the residues of solvent is condensed out of the exhaust gas and collected as waste. Close-cycle spray drying plant is used mainly for environmental reasons (Thybo et al., 2008a). This method will create a more homogeneous product when compared to the co-precipitated or co-evaporated methods (Janssens et al., 2009). Similar to the co-precipitated or co-evaporated methods, major disadvantage of spray drying method is the concern on using non-environmental friendly solvent. Besides, the use of organic solvent in this case could limit the rise of inlet temperature in order to avoid explosion of organic vapour.

1.3.1.5. Freeze drying

Freeze drying is also known as 'lyophilisation' which implies 'to make solvent loving' (Zhao, 2010). It is a well-developed process that is frequently used for stabilization of labile substances or processing of pharmaceutical with biological origin such as protein, serum, vaccines, peptide drugs and liposomes (Tang and Pikal, 2004, Craig et al., 1999).

The freeze drying process can be divided into three stages i.e. freezing stage, primary drying and secondary drying. In the freezing step, solvent, typically water, is separated from the solute to form ice. As the freezing step progresses, the concentration of the sample will increase. This concentrated sample is termed 'freeze concentrate' (Tang and Pikal, 2004). At the end of the freezing point, the 'freeze concentrate' would have around 20% of water content, or less than 1 % of water content from the initial solution.

The next step is the primary drying process. This process involves the ice sublimation under vacuum with elevated shelf temperature in order to supply the heat required for ice sublimation. The sublimated ice is then condensed on a cooled plate / coils ($< -50^{\circ}\text{C}$) in the condenser (Craig et al., 1999, Tang and Pikal, 2004). This particular step is time consuming. Thus, the optimization of this step is crucial to make the method cost effective (Tang and Pikal, 2004).

The final stage of freeze drying is the secondary drying phase. The main objective of this step is to remove any residual moisture content to an optimal level in order to maintain the stability of the product. The sample is further dried by absorbing the 'unfrozen' water from the 'freeze concentrate' via low pressure at elevated temperature. The secondary drying will occur spontaneously near the end of primary drying in the region of the sample where ice sublimation has completed (Craig et al., 1999). This secondary drying step takes relatively shorter time i.e. a few hours. Temperatures used at this stage are usually much higher (i.e. $25 - 60^{\circ}\text{C}$) than the temperature employed in primary step (Craig et al., 1999). Thus, the product temperature is increased in the secondary drying step (Tang and Pikal, 2004).

The resultant solid form of a freeze dried sample is highly porous. This is considered as an advantage for rapid reconstitution / dissolution besides the formation of amorphous solid dispersion system (Craig et al., 1999). This method has been shown to be superior than co-evaporation method in dissolution performance and amorphization of meloxicam in the production of solid dispersion (El-Badry and Fathy, 2006). However, the powder obtained from this method may be presented with poor flowability which might potentially affect the downstream processes of tableting or capsule filling (Zhao, 2010).

1.4. Pharmaceutical hot melt extruded solid dispersions

Besides the aforementioned preparation methods, recently HME has appeared as a robust method for SD preparation. This is the main method of SD preparation applied in this study; therefore, the basic principles of this instrument and its application in the pharmaceutical formulation field will be discussed.

The first use of HME was reported in 1930's for plastic manufacturing as well as in food industry. It was invented at the end of the eighteenth century by Joseph Brama for the production of lead pipe (McGinity et al., 2006). This technique was then extensively practiced in the plastics industry at mid of nineteenth century for preparation of polymeric insulation in wires (Crowley et al., 2007). More recently HME has found its place in the pharmaceutical field whereby many researchers have adopted this technique in producing SD system with promising formulations performances (Crowley et al., 2007, McGinity et al., 2006).

The main process of this technology is to mix raw materials at the molecular level to produce an intimately mixed extrudate. The extrusion process involves different manufacturing steps, i.e. mixing, melting, homogenizing, and shaping. These processes are carried out in a single continuous step which could potentially give rise to overall cost sparing production (Breitenbach, 2002). This has attracted attention of applying HME manufacturing method in the pharmaceutical industry (Keleb et al., 2001).

There are many potential formulations that could be produced by using HME manufacturing method. These include immediate release SD, targeted release dosage form (Andrews et al., 2008, Bruce et al., 2005, Mehuys et al., 2005a, Cassidy et al., 2011), multiple unit dosage forms (Brabander et al., 2004, Verhoeven et al., 2009a, Verhoeven et al., 2009b), floating dosage forms (Fukuda et al., 2006a, Nakamichi et al., 2001, Whitehead et al., 1998), implants (Cheng et al., 2010, Ghalanbor et al., 2010, Rothen-Weinhold et al., 1999, Witt et al., 2000), transdermal and transmucosal delivery systems (Prodduturi et al., 2007, Repka et al., 1999, Repka and McGinity, 2000, Repka et al., 2003, Trey et al., 2007), controlled release dosage form (Fukuda et al., 2006a, Fukuda et al., 2006b, De Brabander et al., 2003, Özgüney et al., 2009) as well as retarded release dosage form by the formation of nanocomposite (Campbell et al., 2010, Campbell et al., 2008, Campbell et al., 2009). In this study, immediate release SD dosage form is the main product of interest in formulation for its ability to overcome the problem of poorly soluble APIs, particularly BCS class II compounds.

1.4.1. Principles of HME

From the regulatory standpoint, melt extrusion technology is a mature engineering technology. It allows the monitoring of various parameters (temperature, die pressure and torque which will be covered in Chapter 2.3) via typical readout information or load cell outputs. This contributes to comprehensive data documentation, good quality control and quality production (Breitenbach and Mägerlein, 2007). Figure 1.6 depicts the HME processes range from feeding to extruding, which will be discussed in detail in next few sections.

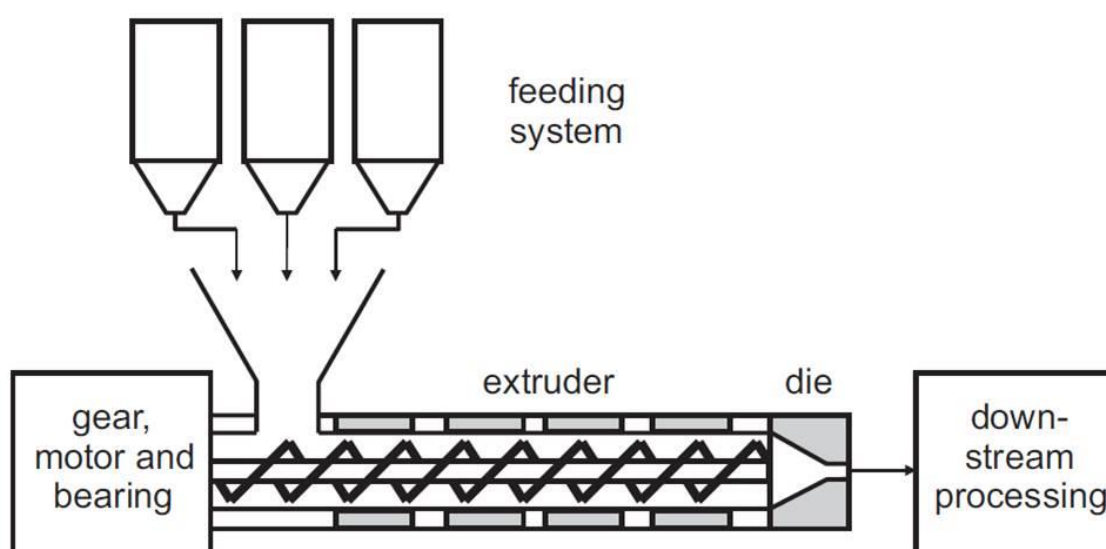


Figure 1.6: Schematic diagram of a hot melt extrusion system (Radl et al., 2010)

As the name implies, HME process operates under elevated temperature (at least 30-60 °C above T_g of feedstock) in order to soften the processing compound (McGinity et al., 2006). Mixtures of materials, namely polymers as API carriers, the API itself and additives are passed through the feeding system and extruded in the extruder as shown in Figure 1.6. Processes within the closed barrel encompass solubilising of API in the polymeric matrix, intense mixing of additive and dispersion of materials within the molten. At the end of barrel, high pressure imparted within the metering zone will force the molten mass extrudes through an orifice to produce a product of high density and uniformity (Mollan, 2007, Andrews et al., 2008). Subsequently, molten material is transported to the downstream equipment for final dosage designation such as melt pelletization, milling, tableting and calendaring.

The extrusion process in the extruder could be divided into three typical zones, i.e. feeding zone, melting or compression zone, and metering zone. Each of the zones has different geometrical screw design that dictates the advance of the process (McGinity and Zhang, 2007).

1.4.1.1. Feeding zone: feeding raw material

The process of feeding is highly dependent on the flow properties of the feedstock. The angle between the wall of hopper and horizontal line must exceed angle of repose of the feedstock (McGinity et al., 2006, Crowley et al., 2007). This is to ascertain consistent feed rate and avoid throat bridging (feeding problem when feeding material are stuck at the throat of hopper) that potentially occurs in cohesive material or fine powder that might cause erratic flow in the hopper.

In order to get easy flow and good conveying of feedstock, a wide pitch and deep flight of the screw is designed in the feeding zone (Rina Chokshi, 2004 , Breitenbach, 2002). Figure 1.7 shows the definition of different parts of the screw extruder.

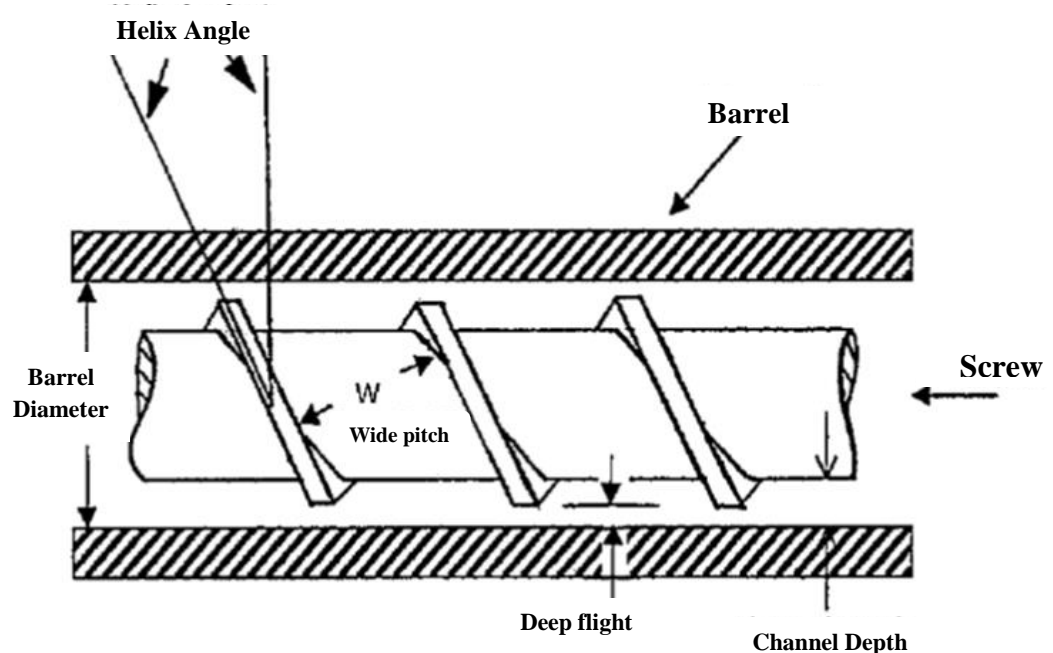


Figure 1.7: Diagram of a screw extruder (Crowley et al., 2007)

Efficiency of pumping in this zone depends on friction coefficient between the feed material and barrel or screw which allows heat dissipation from the shearing process (McGinity et al., 2006). The feeding process generates high pressure for subsequent transportation of feedstock to the transition or compression zone by rotating screw. For bulk solid that is prone to bridging, a driven agitator could be used as a discharge aid in feeding the raw material into the extruder (Doetsch, 2007).

1.4.1.2. Transition Zone

In the transition zone, the reduction of screw pitches and flight depth form progressively narrower spacing between turning and impart a high compression pressure to the material. The materials move along the circulation in helix path of the thread. Transverse flows, drag flow, pressure flow that were generated by the increase pressure following the shallower flight depth as well as leakage are the transporting mechanisms along the barrel (Breitenbach, 2002, McGinity et al., 2006, Rina Chokshi, 2004 , Crowley et al., 2007). In this zone, feedstock is compressed, melted, plasticized and mixed which will be further discussed in the subsequent sections.

1.4.1.2.1. Melting / plasticization

Melting and plasticization processes take place in the transition zone or also known as compression zone. The heating energy is obtained from the electrical heat band that was pre-set prior to the extrusion process as well as heat dissipated from the shearing effect between the screw and material while mixing in the barrel (Breitenbach, 2002, Rina Chokshi, 2004 , McGinity and Zhang, 2007). With the heat energy, small molecule of the drug compound will be melted or diffused in the soften carrier system which causes further plasticization effect to the macromolecule polymer system.

1.4.1.2.2. Mixing/ dispersion

After feeding, the processing material is transported into the mixing or dispersion zone of the hot extruder. The purpose for mixing zone of HME is to produce a highly uniform extrudate. In this zone, the mixing can be further divided into dispersive and distributive mixing (Dreiblatt, 2007a). Dispersive mixing involves the sizing or breaking of the particulate into smaller size while distributive mixing involves the homogenization of particulate within carrier with no interruption on the particle size.

The screw design in the mixing zone may influence quality of the end extrudate. Nakamichi et al. (2003) have successfully demonstrated the important role of kneading paddle (with the twist of 30° and 60°) in mixing nifedipine and an enteric polymer, hydroxypropylmethylcellulose phthalate (HPMCP). In that study, the good uniformity of extrudate was attained from the extrusion with kneading paddle as compared to the extrusion without kneading paddle. This is due the intense mixing of the mixture by kneading paddles (Nakamichi et al., 2003). Similarly, Verhoeven et al. (2008) confirmed the need of kneading paddle for better extrudate quality (smooth extrudates) as compared to the extrusion of the same system without kneading paddles (Verhoeven et al., 2008).

1.4.1.3. Metering zone

The primary function of metering zone is to ensure uniform thickness, consistent flow and steady delivery rate through the die (Breitenbach, 2002, McGinity et al., 2006, Crowley et al., 2007). The output rate of these molten material is dependent on the channel depth and length of meter zone (McGinity et al., 2006). Similar to transition zone, materials in this metering zone are conveyed via drag flow as well as pressure flow.

1.4.1.4. Die pressurization

The process after the metering zone involves pressurizing of the molten material through a die with desired shape (Liu et al., 2001). In some instance, extrudates emerge from the die and undergoes 'die swell'. This phenomena is particularly happen to polymer melt where it attempts to reform from its elastic energy stored within the extrudate while being shear in the die (C.Case, 2007, Schilling et al., 2008, Richardson, 1970). The unintended die swelling of extrudate can be avoided by controlling the drawing force, extrusion temperature and spinning velocity (van Laarhoven et al., 2004). Thus, die pressure should be monitored for desired output to match the geometry of the entangled die (Mollan, 2007).

1.4.2. Materials used in HME solid dispersions

1.4.2.1. Active pharmaceutical ingredient

Intuitively, one may assume it is impossible to process thermally labile drug under HME (Hülsmann et al., 2000, Van den Brande et al., 2004). However, several reports have shown the successful production of pharmaceutical dosage form containing thermo labile API by means of HME. These include production of hydrocortisone films (Repka et al., 1999), delta-9-tetrahydrocannabinol in polyethylene oxide matrices (Thumma et al., 2008b, Thumma et al., 2008c), thermo labile p-amino salicylic acid with assistance of CO₂ as a plasticizer (Verreck et al., 2006a), as well as protein implant, rh-interferon α -2a (IFN- α) (Schulze and Winter, 2009) and somastostatin vapreotide (Rothen-Weinhold et al., 1999). Schulze and Winter (2009) suggested that the solvent free HME is a good processing method for the formulation of proteins (Schulze and Winter, 2009) as biological activity of the proteins could be maintained even at elevated temperature in the dry powder state rather than in aqueous media.

Some APIs appear to plasticize its carrier, such as carvedilol (Lyons et al., 2008, Lyons et al., 2007b), chlorpheniramine maleate (Wu and McGinity, 1999, Albers et al., 2009) and etc. These APIs are good candidates for HME production owing to their better HME processability without additional external plasticizer. More examples of APIs with plasticization behaviours will be provided in section 1.4.2.2.2 as ‘non-traditional’ plasticizer.

Drug loading in the polymeric carrier may also affect the processability of HME. Schilling et al. (2008) confirmed that increase drug loading of diltiazem HCL necessitated higher processing temperature and therefore increased molten flow resistance in the barrel (Schilling et al., 2008). Another study by De brabander et al. (2003) showed that higher percentage of ibuprofen not only eased the HME process but also give rise to a good quality extrudate with an increase in drug release rate (De Brabander et al., 2003). Therefore, thorough understanding of the APIs is indispensable for the processing concern and formulation design of HME system. Table 1.3 summarised the examined APIs from the literature.

Table 1.3: APIs used in HME production and characterization of HME process

	API	Comments	references
1.	17β-estradiol hemihydrate	Solid dispersion of hormone was produced. The dissolution of drug was significantly enhanced.	(Hülsmann et al., 2000)
2.	5-amino salicylic acid (5ASA)	It appeared to create microenvironmental pH that was able to modulate the final release profile. Enteric polymer was used to target the delivery to colon.	(Andrews et al., 2008, Bruce et al., 2005)
3.	Acetohydroxamic acid	Floating dosage form was formed by addition of NaHCO ₃ as porous agent.	(Fukuda et al., 2006a)
4.	Carbamazepine	Immediate release product was processed by HME and it showed an increase in dissolution compared to physical mixture as intimate mixing with hydrophilic polymer efficiently improved wetting.	(Perissutti et al., 2002, Djuris et al., 2013b)
5.	Carvedilol	This drug was investigated in nanocomposite formulation, addition of PCL in the release pattern and impact to the process parameters. The most recent evaluation was done on the addition of CO ₂ in release profile as well as recrystallization.	(Lyons et al., 2007b, Lyons et al., 2007a, Lyons et al., 2008)
6.	Chlorpheniramine maleate	Floating dosage form and retarded release tablet were successfully produced by HME process.	(Crowley and Zografi, 2002, Fukuda et al., 2006a, Fukuda et al., 2006b, Repka et al., 1999)
7.	Chloramphenicol	It was produced by two steps lipid plus PEG base extrusion. The final product revealed a good stability profile in 3 months accelerated studies.	(Windbergs et al., 2010)
8.	Clotrimazole	Transdermal products were developed and exhibited excellent content of uniformity. However degraded products were detected in which necessitate future investigation.	(Repka et al., 2003)
9.	Delta-9 Tetrahydrocannabinol Prodrug	Thermo labile properties justify the use of the component with assistance of excipients in Hot Melt extrusion process. It has been showed that its stability highly dependence on microenvironment pH of formulation.	(Thumma et al., 2008a, Thumma et al., 2008b, Thumma et al., 2008c, Munjal et al., 2006)
10.	Diltiazem HCl	Diltiazem HCL could bind to Eudraggit RSPO that potentially reduces the free drug. Research confirmed it does not possess plasticizing effect.	(Schilling et al., 2008)

(continued)

11.	Dyphilline	A derivative of theophylline. Degradants of the product were detected thus it is at risk for long term stability.	(Dong and Choi, 2008a)
12.	Etonogestrel	Controlled release co-axial fiber was prepared by single screw extruder.	(van Laarhoven et al., 2004)
13.	Guaiazulene Sodium	Water content is an essential key for its stabilization.	(Nakamichi et al., 2003)
14.	Guaifenesin	It possessed plasticizing effect toward Eudragit L100-55. Evaluation of crystal growth inhibitor and recrystallization by nucleating agent was carried out.	(Bruce et al., 2007, Bruce et al., 2010, Crowley et al., 2007)
15.	Hydralazine	HME hydralazine capsule was constructed by extruded hollow pipe and inclusion of drug and additive as a core.	(Mehuys et al., 2005a)
16.	Hydrochlorothiazide	Ampiphilic nature of lipid and water soluble polymer in the formulation enhanced wettability of drug and thus dissolution of the drug	(Mehuys et al., 2004a)
17.	Hydrocortison	A thermal sensitive compound but able to process by HME due to the inclusion of plasticizer and versatility of HME process that enable the drug to process under short residence time frame (about 2 minutes)	(DiNunzio et al., 2009, Repka et al., 1999)
18.	Ibuprofen	Sustained release ibuprofen was fabricated via polymer blends. The drug showed plasticizing effect equivalent to conventional plasticizer DEP/DBS.	(Brabander et al., 2002, Brabander et al., 2004, De Brabander et al., 2000, De Brabander et al., 2003, Verhoeven et al., 2006, Wu and McGinity, 1999, Campbell et al., 2010)
19.	Indomethacin	PVA is not a suitable HME candidate for indomethacin due to immiscibility of both. It possesses good thermal stability	(Forster et al., 2001c, Zhu et al., 2006)
20.	Insoluble microsomal triglyceride transfer protein inhibitor, R103757	It is structurally similar to itraconazole and its HME extrudates (Drug to HPMC ratio, 25:75) possessed fastest in vitro release performance relative to the film coated bead and glass thermoplastic system. No changes detected in 3 months stability test indicated its good stability profile and protection of HPMC.	(Verreck et al., 2004)
21.	Itraconazole	Transdermal sustained release film intended for Onychomycosis and systemic micronized powder coupled with HME process were attempted. Its supersaturated form was found to be stabilized in Methocel E50 (HPMC E50) after pH transition from acid to neutral. It was suggested that formulation of ITZ to be carried out in controlled release manner due to the fact	(Miller et al., 2008b, Miller et al., 2008a, Miller et al., 2007, Shim et al., 2006, Six et al., 2003a, Six et al., 2005, Six et al., 2002, Six et al., 2003, Six et al., 2004, Trey et al., 2007) <i>(continued)</i>

		that rapid precipitation will take place if immediate release of drug occurred in upper GI condition which is acidic.	(continued)
22.	Lysozyme	Implant of this API was produced with biodegradable polymer, polylactide co-glycolide and low MW PEG as release modifying agent.	(Ghalanbor et al., 2010)
23.	Lacidipine	Phase separation was observed by 2 Tg for the thermal analysis and it was further supported by solubility parameter.	(Forster et al., 2001c)
24.	Lopinavir/Ritonavir	HME product of the combination revealed increase in bioavailability, less intra-patient variability and diminished food effect.	(Klein et al., 2007)
25.	Methylparaben	A 'non-traditional plasticizer'	(Wu and McGinity, 1999)
26.	Metoprolol tartrate	HME extruded mini-matrices with release modifying agents and its properties were characterized by groups of researcher.	(Verhoeven et al., 2009a, Verhoeven et al., 2008, Verhoeven et al., 2009b)
27.	Nicardipine	Floating dosage form was developed by incorporating porous agent via HME	(Nakamichi et al., 2001)
28.	Nifedipine	Integration of kneading paddle in HME increases API dispersion.	(Nakamichi et al., 2002)
29.	Nimodipine	Both in vitro and in vivo studies were done with HME product to select the best carrier for bioavailability enhancing effect.	(Zheng et al., 2007a, Zheng et al., 2007b)
30.	Paracetamol	Tablet was prepared with layered silicate polymer to examine the influence in retard release and effect of recrystalline	(Campbell et al., 2009, Qi et al., 2008b)
31.	Phenylpropanolamine HCl	A better particle size distribution was obtained via HME	(Liu et al., 2001)
32.	Propranolol HCl	Extensive first pass metabolism led to complicated analysis for evaluation of factors that may increase bioavailability of HME prepared products.	(Mehuys et al., 2005b, Mehuys et al., 2004b, Mehuys et al., 2004a, Maniruzzaman et al., 2013)
33.	Theophylline	Extensive studies were carried out in formulating mini matrices, sustained release formulation, incorporation of lipid matrix as well as co-extrudate.	(Mehuys et al., 2004a, Özgüney et al., 2009, Quintavalle et al., 2008, Reitz and Kleinebudde, 2007b, Wu and McGinity, 1999, Zhang and McGinity, 2000)

1.4.2.2. Carriers used in HME formulations

Over the past decade, the application of various types of carriers system has been identified. Figure 1.8 shows the different generations of SD based on their carrier systems that has been classified by Vasconcelos et al. (2007).

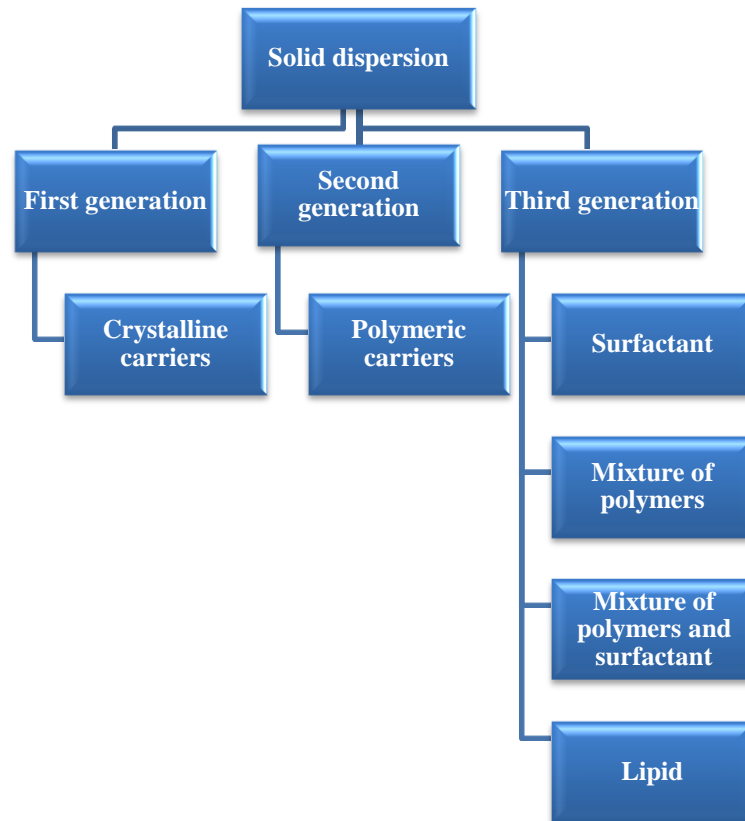


Figure 1.8: The evolvement of solid dispersion which gives rise to the different generations of the formulations (Vasconcelos et al., 2007)

Amongst all carriers, polymeric systems are the most commonly investigated materials in the production of solid dispersion with the inclusion of surfactants, lipids and polymer blends described in some recent studies (Guns et al., 2011, Kalivoda et al., 2012a, Kalivoda et al., 2012b, Mehuys et al., 2004a, Djuris et al., 2013a, Herrmann, 2007, Özgüney et al., 2009, Reitz and Kleinebudde, 2007b, Six et al., 2004). Brief review on the use of these carriers system will be provided in the subsequent sections.

1.4.2.2.1. Polymers

Polymeric carriers are usually used as the dispersing agent in HME solid dispersion systems to stabilize the amorphous API. During the HME process, polymers are subjected to high shear stress, chain scission, chemical de-polymerization as well as thermal degradation (McGinity et al., 2006). Thus, pharmaceutical grade polymer used in HME must be able to process under relatively low temperature. Enteric polymer, pH dependent polymers and hydrophilic polymers are the commonly used polymers in fabricating pharmaceutical dosage forms. Examples of these polymers include acrylic polymer (Eudragit S100, Eudragit L100-55, Eudragit L100, Eudragit RD 100), cellulose polymer (hydroxypropyl methylcellulose), phthalate polymer and polyvinylpyrrolidone (PVP K30, vinylpyrrolidone-vinylacetate copolymer, PVPVA 6:4).

Among these polymers, hydrophilic polymers such as PVP/ PVPVA 6:4 are usually included in numerous HME compositions for immediate release solid dispersion. However, at high polymer concentration, PVP/ PVPVA 64 may result in extruder clogging due to their high glass transition temperature (> 150°C) (Hülsmann et al., 2000). Other hydrophilic polymers, for example polyethylene oxide (PEO) or polyethylene glycol (PEG), xanthan gum, plasdone S-630 and hydroxypropyl methylcellulose could also be added in a formulation to tailor the drug release and to yield desirable sustained release pattern (Verhoeven et al., 2009a, Verhoeven et al., 2008, Ghebremeskel et al., 2007).

Some polymers exhibit a plasticizing effect toward other polymer in a polymers blend system. This is a benefit for HME process as the integrated polymer could aid the material transport in the hot barrel besides tailoring the drug release properties of the system (Repka and McGinity, 2000). For example, PEO 1K appeared to plasticize PEO 1M and enhanced stability of the HME processed polymer (Crowley et al., 2002b). A study performed by Lyons et al (2008) has indicated that the inclusion of poly ϵ -caprolactone in PEO polymer blend can function as a plasticizer in the blend by lowering melt viscosity, torque and head die pressure (Lyons et al., 2008).

1.4.2.2.2. Plasticizers used in HME systems

The conventional role of plasticizer is to reduce brittleness, improve flowability, and impart flexibility, toughness and strength. More specifically, it is used to change certain physical and mechanical properties of a material. In the context of HME, plasticizers are applied to soften the polymer matrix where excessive temperature may be needed to process unplasticized based polymer that could lead to degradation or localized overheating of the polymer (McGinity and Zhang, 2007). By incorporating a plasticizer, the extrusion temperature and thermal degradation of the material may be reduced (Verhoeven et al., 2008, Ghebremeskel et al., 2007). Besides, plasticizer may exert a positive influence on content uniformity of the product by promoting good flowability and mixing of the blend materials (Thumma et al., 2008b). A study carried out by Bruce et al. (2005) has successfully improved the physical properties of Eudragit ®S 100 by incorporating of triethyl citrate as a liquid plasticizer (Bruce et al., 2005).

The interest in investigating solid state plasticizers such as citric acid, PEG 8000 and methylparaben (MP) in HME system is increasing as these solid plasticizer are readily mixed in powder form prior to the extrusion at elevated temperature (Wu and McGinity, 2003). Upon extrusion, the solid state plasticizer is melted and solubilised in carrier in order to exert their plasticization effect (Andrews et al., 2008, Schilling et al., 2010). An example was given by Wu and McGinity, (2003) whom demonstrated that incorporation of methylparaben in the extrudates of Eudragit ® RS PO could reduce its Tg from 55 °C to 32 °C. The authors elucidated that the incorporation of methylparaben within the Eudragit ® RS PO polymer has weakened the cohesive interaction between its polymer chains and subsequently enhance its chain mobility (Wu and McGinity, 2003). Besides, citric acid was shown to alleviate the Tg of HME API-polymer system which indicates its plasticizing properties as a solid state plasticizer (Forster et al., 2001c, Bruce et al., 2005, Andrews et al., 2008).

The combination of both triethyl citrate (liquid state plasticizer) and citric acid (solid state plasticizer) has resulted in the good flowability of a HME API-polymer system and render the used of low processing temperature in the HME manufacturing process (Bruce et al., 2005). Similar attempt was carried out by Andrews et al. (2008) who incorporated the combination of both triethyl citrate (TEC) and citric acid in HME process of Eudragit. The authors elucidated that both TEC and acid citric have improved material flowability in the extruder, reduced Tg, and ultimately aided the extrusion process by lowering screw torque as well as die pressure. This is because TEC and citric acid are able to form hydrogen bonding with Eudragit by occupying 'active site' along the polymer and thus preventing inter-chain association (Andrews et al., 2008).

CO₂ is proposed to be a temporary plasticizer in HME process (Verreck et al., 2005, Verreck et al., 2006b). Verreck and co-workers examined the effect of CO₂ in pharmaceutical polymer such as PVP-VA 64, Eudragit E100 or ethylcellulose. It has shown that CO₂ reduced the processing temperature of HME, increased porosity and specific surface area of extrudate by forming a foam extrudate. The foam like structure of extrudates improved subsequent milling process and caused dissolution rate enhancement of the formulation (Verreck et al., 2005, Verreck et al., 2006b). However, CO₂ was reported to exert a negative impact on physical stability of extrudate where it was shown to induce recrystallization owing to the increase in mobility and realignment of the polymer chains (Verreck et al., 2006b, Lyons et al., 2007a).

Interestingly, some APIs could intrinsically be a plasticizer for polymer. An API has to be dissolved in the polymer system in order to contribute to the plasticizing effect (Verreck et al., 2005). Ibuprofen was shown to possess plasticizer effect toward ethylcellulose and was known as a 'non- traditional plasticizer' (Brabander et al., 2002). Its effect was investigated and compared with other traditional plasticizers such as diethyl phthalate and dibutylsebacate by Brabander et al. (2002). It was elucidated that ibuprofen having equivalent plasticizer efficiency as the traditional plasticizer (diethyl phthalate and dibutylsebacate) toward ethylcellulose. The same effect was also reported in a study where API was found to plasticize Kollidon®SR (polyvinyl acetate: povidone 8:2) (Özgüney et al., 2009). Table 1.4 outlines the different types of plasticizer used in HME pharmaceutical application.

Table 1.4: different types of plasticizer used in HME pharmaceutical application

Types of plasticizer	Polymers	References
Liquid state plasticizer		
Triethyl citrate TEC (Hydrophilic)	Pre-plasticizing step with Eudragit S100 showed better results; Eudragit RD 100, Eudraagit L100-55, Eudragit RSPO, Kollidom SR (8:2), HPC:PEO (50:50, 80:20), Hydroxypropylcellulose (HPC), ethylcellulose. Its plasticizing efficiency was twice as high compared to chlorpheniramine maleate in Eudragit® RSPO.	(Bruce et al., 2005, Andrews et al., 2008, Wu and McGinity, 2003, Mehuys et al., 2005a, Özgüney et al., 2009, Zhu et al., 2006, Repka and McGinity, 2000, Repka et al., 1999, Verhoeven et al., 2008, Zhu et al., 2002)
Triacetin TA (Hydrophilic)	Polyvinyl acetate phthalate, ethylcellulose	(Mehuys et al., 2005a, Verhoeven et al., 2008)
Dibutyl sebacate DBS (Lipophilic)	Eudragit RSPO, ethylcellulose	(Wu and McGinity, 2003, Mehuys et al., 2005b, Mehuys et al., 2004b, Mehuys et al., 2004a, Verhoeven et al., 2008)
Diethylphthalate DEP (Lipophilic)	ethylcellulose	(Verhoeven et al., 2008)
Acetyl Tributyl Citrate(ATBC)	HPC:PEO(50:50, 80:20), Hydroxypropylcellulose (HPC)	(Repka and McGinity, 2000, Repka et al., 1999)
Water content	HPMCP	(Nakamichi et al., 2002)
Solid state plasticizer		
Traditional plasticizer		
Low MW PEO e.g., PEG 400, PEG8000	PEO1000000, HPC:PEO(50:50, 80:20), Hydroxypropylcellulose (HPC)	(Crowley et al., 2002b, Repka and McGinity, 2000, Repka et al., 1999, Repka et al., 2003)
Sorbitol	PVP K30	(Lakshman et al., 2008)
Citric acid/ Citric acid monohydrate (CA MH)	Eudragit S10, Eudragit RSPO, Eudragit L100-55	(Bruce et al., 2005, Schilling et al., 2008, Andrews et al., 2008) <i>(continued)</i>

Non-traditional plasticizer		(continued)
Carvedilol	PEO, PEO/PCL block copolymer	(Lyons et al., 2008, Lyons et al., 2007b)
Chlopheniramine maleate	Eudragit RS PO, Eudragit E PO, Eudragit RS30 D	(Fukuda et al., 2006a, Wu and McGinity, 1999, Zhu et al., 2002)
Vit E TPGS	HPC:PEO (50:50, 80:20)	(Repka and McGinity, 2000)
Guaifenesin	Acryl-EZE/ Eudragit L100-55 , PEO	(Bruce et al., 2007, Crowley et al., 2004a)
Itraconazole	Eudragit L100-55	(Miller et al., 2008a)
Ibuprofen	Kollidom SR (8:2), ethylcellulose, Eudragit RS30 D	(Özgüney et al., 2009, Brabander et al., 2002, De Brabander et al., 2003, Verhoeven et al., 2006, Wu and McGinity, 1999)
Indomethacin	Eudragit RLPO	(Zhu et al., 2006)
Ketoprofen	PEO	(Crowley et al., 2004a)
Lidocaine HCl	Eudragit® E 100	(Aitken-Nichol et al., 1996)
Methylparaben	Eudragit RSPO, Eudragit RS30 D	(Wu and McGinity, 2003, Wu and McGinity, 1999)
Nimodipine	PVP/VA, Eudragit ®PO	(Zheng et al., 2007a, Zheng et al., 2007b)
Paracetamol	Eudragit ®EPO	(Qi et al., 2008b)
Temporary plasticizer		
Carbon Dioxide (CO ₂)	CO ₂ is termed as ‘temporary’ plasticizer due to its absence in the end product of the HME system. The effect of plasticizing appears to be best in ethylcellulose followed by PVP-VA 64 and lastly Eudragit E100.	(Verreck et al., 2005, Verreck et al., 2006a, Verreck et al., 2006b)

1.4.2.2.3. Surfactant

Surfactants such as Tween 80 and docusate sodium are regularly used in the pharmaceutical field as wetting agents and to increase solubilisation of the poorly soluble API. In the production of HME systems, the surfactant could also act as a plasticizer in the extrusion process (Ghebremeskel et al., 2007). Ghebremeskel et al. (2007) has demonstrated the reduction in Tg of the mixture of API and polymer after the addition of surfactant into the composition of extrudate. In that study, the authors suggested that the use of surfactant could aid the extrusion process through an increase in chain mobility of polymer carrier (Ghebremeskel et al., 2007). More specifically, the extrusion torque of binary API-Plasdone was lowered from circa 55-65 Ncm to circa 28-30 Ncm with the addition of Tween 80 (Ghebremeskel et al., 2007). Table 1.5 displays the example of surfactants that have been applied in HME processes.

Table 1.5: Example of surfactants used in HME process

	Surfactant	Polymer system	References
1.	Tween 80	As plasticizer to Plasdone S360, Hydroxypropyl methylcellulose (HPMC) E5, Polyvinylpyrrolidone (PVP) K30	(Ghebremeskel et al., 2006, Ghebremeskel et al., 2007)
2.	Docuste Sodium	As plasticizer to Plasdone S360, Hydroxypropyl methylcellulose (HPMC) E5, Polyvinylpyrrolidone (PVP) K30	
3.	Sodium Lauryl sulfate	As plasticizer to Eugragit L100, Hydroxypropyl methylcellulose (HPMC) E5	
4.	Polyoxyethylene 40 stearate (Myrj-52)	No effect in lowering Tg	
5.	Poloxamer 188NF (Pluronic F68)	No effect in lowering Tg, but showed to enhance drug release.	(Ghebremeskel et al., 2007, Zhu et al., 2006)

1.4.2.2.4. Other additives used in HME processing

Recent investigations of HME were carried out on incorporation of nanoclay within polymeric matrix to tailor the release of API (Campbell et al., 2008, Campbell et al., 2009, Lyons et al., 2007b). Reduction of burst release was attained by addition of polymer layered silicate as carrier for SD of ibuprofen when compared to the same formulation without layered silicate (Campbell et al., 2010). Furthermore, the authors reported a reduction in tensile stress, elongation break and increment in modulus. Thence, mechanical properties of the extrudates by addition of nanoclay may be manipulated accordingly to ease subsequent downstream processes of the extrudates such as milling or compression of the extrudates systems into tablet (Campbell et al., 2010).

Studies have also been described whereby lipids are added to HME formulations to obtain the desired dissolution pattern (Reitz and Kleinebudde, 2007b, Reitz and Kleinebudde, 2007a, Windbergs et al., 2009a, Windbergs et al., 2009b, Schulze and Winter, 2009, Hülsmann et al., 2000). It has been shown that the use of lipid carrier in HME produced a sustained release product with good physical stability as the hydrophobic nature of lipid had reduced the water absorption during storage (Reitz and Kleinebudde, 2007b, Windbergs et al., 2009b). In formulations containing proteins and peptides, the inclusion of lipids in the HME process created a hydrophobic surrounding to the protein, therefore minimizing its denaturation tendency in aqueous conditions (Schulze and Winter, 2009).

Addition of other components such as waxes (Liu et al., 2001, De Brabander et al., 2000), pH modifiers (Thumma et al., 2008c, Thumma et al., 2008b, Thumma et al., 2008a, Munjal et al., 2006, Schilling et al., 2008, Bruce et al., 2005), antioxidants (Repka and McGinity, 2000, Crowley et al., 2002b, Thumma et al., 2008c), lubricants (Verreck et al., 2005, Verreck et al., 2006b) and controlled water content (Nakamichi et al., 2002, Nakamichi et al., 2003) are also possible in formulation of HME extrudates in order to obtain an optimum pharmaceutical dosage form.

1.5. Stability issues

A success pharmaceutical dosage form should exhibit good dissolution profiles, excellent pharmaceutical therapeutic outcome as well as good stability upon storage. Physical stability of SDs is the main concern and hurdle that has restricted commercialization of this type of product. This is due to the high tendency of physical transformation, i.e. recrystallization of the amorphous API into its crystalline counterpart. Besides recrystallization, phase separation has also been identified as physical instabilities in which the resulted formulation might display high variation on drug release and therapeutic result (Lakshman et al., 2008). Hence, in the context of the current study, physical stability of HME SD products will be discussed.

Amongst modes of manufacturing, HME has ostentatiously yielded a relatively stable products as documented in numerous published papers (Dong et al., 2008b, Verreck et al., 2004, De Brabander et al., 2003, Fukuda et al., 2006a). In a 4 month accelerated stability study by Dong et al. (2008b), recrystallization was observed lower in HME extrudates as compared to co-precipitated samples. This is due to the lower surface area of the smooth HME extrudate that was available for water absorption as compared to the co-precipitated products (Dong et al., 2008b). In another study, HME has shown to exhibit a better physical stability profile as compared to film coated beads (Verreck et al., 2004). A consistent drug release of HME product was maintained after 3 months of storage in ambient surrounding as compared to film coated beads, which showed a slight

deterioration in its API release. The stability of HME samples was also proven to be more superior than the direct compression production technique by probing recrystallization of the formulation due to the lower porosity and water sorption of HME moulded tablet compared to compressed tablets (Ndindayino et al., 2002b, Ndindayino et al., 2002a).

1.5.1. Physical stability of HME solid dispersions

Physical stability of extrudates can be categorized into in-process stability, post-extrusion stability and long term storage stability. In-process stability is mainly related to the processing parameters, types of fillers and additives. However, post-extrusion stability and storage stability are mainly influenced by water sorption and storage temperature in a define time frame. Figure 1.9 summarises the factors involved in the stability of HME extrudates.

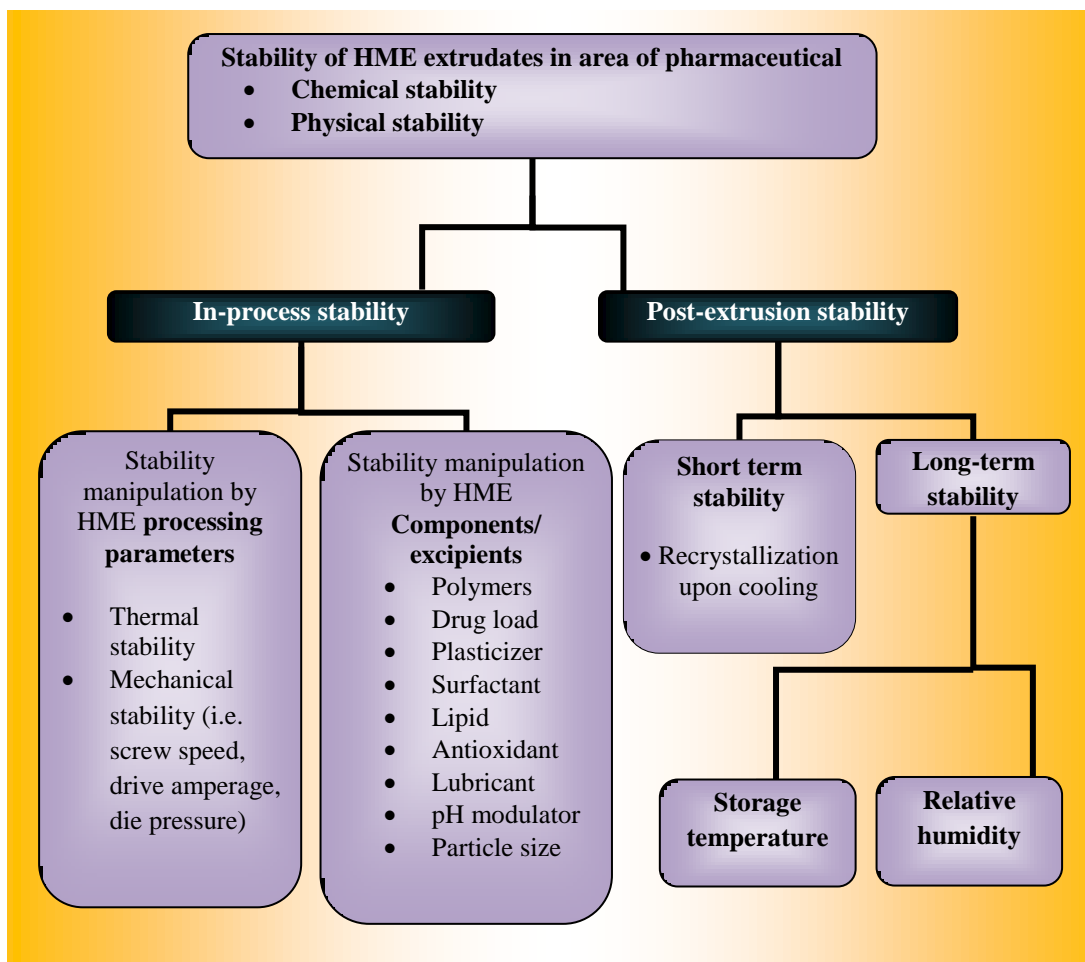


Figure 1.9: Stability influences of HME extrudate

Based on Figure 1.9, the in process stability of extrudates is mainly dependent on the processing parameters and the extruded materials used for extrusion. A high processing temperature has been showed to be advantageous for the production of uniformity in drug content due to reduction of melt viscosity that ease mixing. However, it can cause cumulative heat exposure to the API which results in significant drug degradation. For instance, processing of Δ^9 -tetrahydrocannabinol-hemiglutarate at 90 °C for 7 minute exhibited excellent post processing content with < 5% degradation (Thumma et al., 2008b). However, the same processing parameters with a higher extrusion temperature of 110 °C caused 5.4% degradation in that study. When the residence time was prolonged to 10 minutes and 15 minutes using 110 °C, 9.9% and 16.5% of drug degradation were detected, respectively (Thumma et al., 2008b). Thus the authors suggested that the thermal degradation of drug is dependent on cumulative heating, i.e. longer residence time in heating barrel has caused a higher percentage of degradation (Thumma et al., 2008b, Munjal et al., 2006). Therefore prudent options of processing temperature, additives, and residence time in barrel are essential for the best outcome.

Extrusion temperature could also alter the polymorphism of lipid extrudates. This can be exemplified by the processing of tristearin which is appeared as β -form with its T_m at 65 °C. Tristearin is known to undergo melt crystallization to another polymorphs form (Windbergs et al., 2009b). However, Windbergs et al. (2009b) has reported a polymorphism transformation of tristerin to an α -form endotherm when it was extruded at a temperature lower than its melting, i.e. 55 °C. According to the authors, this is attributed to the temperature and friction of extrusion process that caused a certain degree of lipid melting specifically at the extruded point (Windbergs et al., 2009b).

The effects of other processing parameters and formulation components in influencing the stability of extrudates are briefly explained in Table 1.6.

Table 1.6: The effects of processing parameters and excipients the physical stability of extrudates

Influence of processing parameters		
Factors	Explanation	References
1. Processing temperature	Higher processing temperature causes instability of component. E.g. ethylcellulose degrade at 190 °C but not at a lower temperature.	(Crowley et al., 2004b)
2. Screw speed/ drive amperage	Higher screw speed reduces residence time in barrel, but could cause melt fracture if too high.	(DiNunzio et al., 2009, Crowley et al., 2002b)

(continued)

Influences of excipient/ formulation components		(continued)
Factors	Explanation	References
1. Drug load	Homogeneously dispersed drug can prevent partial crystallization of carrier Percentage of drug load is important for the solubility in carrier system. Surplus of drug act as homogeneous nucleating agent that lead to recrystallization.	(Six et al., 2002, Brabander et al., 2002)
2. polymer	Polymeric interaction in hydrogen bonding give a better stability Hydrophobic nature of aPMMA lead to negligible water uptake hence could hamper the effect of water participation in formulation stability Sterical hindrance avoids crystal formation in extrudates Polymer layered silicate decreases crystallinity compare to pure polymer. It is ascribed to the reduction of chains mobility.	(Forster et al., 2001b, Six et al., 2004, Yang et al., 2010a, Bruce et al., 2007, Miller et al., 2007, Campbell et al., 2008, Campbell et al., 2009)
3. plasticizer	lowering torque, melt viscosity and reduce localized heating of API thus protect API from thermal degradation and increase stability Induce molecular mobility and rearrangement of polymer chains lead to higher crystallinity at post extrusion point. E.g. CO ₂	(Lakshman et al., 2008, Lyons et al., 2007a, Munjal et al., 2006)
4. Surfactant	Serve as a barrier for particle re-aggregation and shield particle from ambient moisture e.g. poloxamer	(Miller et al., 2007)
5. lipid	Lipophilic and hydrophobic nature of carrier impede water uptake and prevent water induce degradation and recrystallization.	(Windbergs et al., 2009b, Reitz and Kleinebudde, 2007b)
6. antioxidant	It stabilizes formulation by reducing radical catalytic decomposition and chain scission.	(Repka and McGinity, 2000, Crowley et al., 2002b)
7. Lubricant	It could act as heterogeneous nucleant which promote nucleation at concentration lower than supersaturation of homogeneous nucleant. E.g. talc	(Bruce et al., 2010)
8. pH modulators	Maintain optimum pH close to maximum stability. Mainly reduce chemical degradation	(Thumma et al., 2008c)
9. Particle size distribution	Wide range of size distribution give rise to phase separation or segregation and influence consistent flow rate which cause “surge” phenomena	(Dreiblatt, 2007a, Luker, 2007)

1.5.1.1. Post-extrusion stability

Post extrusion stability can be further divided into two categories. Firstly, short term stability which is usually correlated with the immediate solid state change upon extrusion and the impact of downstream processes. Secondly is the long term stability which is the main hurdle for product commercialization.

1.5.1.1.1. Short term stability

Mechanical stress such as milling can induce recrystallization of API after extrusion process. Recrystallization of itraconazole (ITZ) was found to be 25% and 14% in the milled and unmilled Eudragit E100 extrudate, respectively at low loading of ITZ (Six et al., 2002). At high loadings of ITZ, the percentage of recrystallization increased dramatically in the milled extrudates as compared to the unmilled extrudates of Eudragit E100 which showed 60% and 20% of ITZ crystalline content, respectively (Six et al., 2002). This is due to the alteration in the kinetics of recrystallization of ITZ by the polymer molecules in the unmilled samples that hinder the conversion of the amorphous API to its more stable crystalline form. Similarly, milling of HME R103757 (water soluble microsomal triglyceride transfer protein inhibitor) – HPMC extrudates causes extensive recrystallization of the R103757 which was originally amorphous after extrusion (Verreck et al., 2004).

Albers et al. (2009) demonstrated that external phase inclusion of polymer (40 mg HPMC) into the milled HME extrudate could delay recrystallization process of the system (Albers et al., 2009). Even though the downstream process of milling might affect the physical stability during the production of extrudate; there are other studies indicated that milling of HME extrudate has no effect on its physical stability (Albers et al., 2009, Forster et al., 2001b).

1.5.1.1.2. Long term stability

As discussed in Chapter 1.5.1, HME products has frequently presented its good physical stability due to the intense mixing, high compression and solubilisation of molten material in HME process (Young et al., 2005). In the subsequent sections, factors dictating the physical stability of HME extrudate will be further discussed.

Steric hindrance / polymer ratio

Addition of polymer to the API has been shown to enhance physicochemical stability of an amorphous API by reducing the interaction among API molecules via steric hindrance and increasing the energy barrier for nucleation (Yang et al., 2010a, Six et al., 2004). Higher molecular weight (MW) of polymer has reported to exert bigger impact by hinder the rearrangement of drug molecule and thus reduce rate of crystallization (Prodduturi et al., 2005). Besides, the ratio of the polymer content is also playing a role in recrystallization inhibition. For instance, Yang et al. (2010a) reported the decrease in recrystallization rate of efavirenz when the ratio of polymer was increased. This is due to the greater number of efavirenz molecules that entrapped in a higher percentage of PVP polymer matrix (Yang et al., 2010a).

In a study, hydrophilic polymers are used as crystallization inhibitor e.g. PVP K-25, Polycarbonil, PEG3350, Poloxamer 188 and Polyethylene oxide (Bruce et al., 2007). The use of these hydrophilic polymers in the composition of extrudate has shown to reduce the recrystallization rate of the API in comparison to the similar formulations without the inhibitors. This is because of the increase of API solubility in the matrix containing both polymer and hydrophilic carrier and which reduces the tendency of recrystallization (Bruce et al., 2007).

Drug-polymer interaction

Interaction between the polymer carrier and drug substance could also impart positive stability to an extrudate. A study conducted by Foster et al. (2001b) suggested the presence of hydrogen bonding between the API and polymer in the investigated extrudate. In that study, the authors proposed that the quantity of these hydrogen bonds is inversely correlated to the ability of water penetration upon storage. With a lower degree of hydrogen bonds between the API and polymer, the proton acceptor sites of the polymer will be exposed and enable its interaction with any absorbed water molecules (Forster et al., 2001b). This causes plasticization of polymer and subsequently promotes recrystallization of API. Hence, the choice of carrier can critically in determine the physical stability of a HME product.

Water content of products

Water content can profoundly affect the physical stability of a product (Forster et al., 2001b). It is particularly important for hygroscopic drugs. For instances, Foster et al. (2001) performed a physical stability tests on HME SD of indomethacin, lacidipine, nifedipine and tolbutamide. The study showed that nifedipine recrystallizes more than indomethacin attributed to the higher water

content of the former drug as compared to the latter (Forster et al., 2001b). Besides, the high water uptake of Δ^9 -tetrahydrocannabinol- hemiglutarate extrudate has caused a high percentage of drug degradation when the product is exposed to humid condition (Thumma et al., 2008a). Similarly, high moisture content of HME ketoconazole films has resulted in high degradation of ketoconazole after 6 months storage in humid condition despite the good stability of the product post extrusion (Mididoddi and Repka, 2007).

Another study carried out by Six et al. (2003) has shown that the water content can cause phase separation and a significant change in Tg of a binary HME system of ITZ-HPMC. The authors suggested that the presence of water in the HME system could impart 2 major effects. Firstly, water acts as a plasticizer to the amorphous system. Secondly, water could interrupt the formation of hydrogen bonds between drug and polymer (Six et al., 2003a).

The water content of a product is highly dependent on the storage humidity. Greater recrystallization of HME guaifenesin (GFN) in Eudragit® L10055 or Acryl-EZE® was seen in higher humidity storage condition (Bruce et al., 2010). In that study, the effect of RH cycling was also tested. The HME GFN guaifenesin Eudragit® L10055 were exposed to two different cycles. The first batch of the sample was stored firstly in a low RH condition (17%) for 6 days, then transferred to a high RH condition (78%) for 12 days and subsequently returned to the low RH condition. The second batch of sample was started with storing in high RH condition (78%) for 6 days followed by low RH condition in the intermediate stage and finally returned to the high RH storage condition. The results indicated that crystallization occurred rapidly when the samples were introduced to the high RH condition, and these crystals remain permanently in the samples to further induce the recrystallization process even though low RH storage conditions were used (Bruce et al., 2010).

Addition of excipient

Addition of excipient such as surfactant, disintegrant or lubricant has shown to benefit the dissolution performance of solid dispersion formulation (Ghebremeskel et al., 2006, Ghebremeskel et al., 2007). However, these excipients could potentially alter the physical stability of the drug product. A study reported that higher percentage of triacetin (TA) in polyvinyl acetate phthalate (PVAP) capsules has led to a higher moisture uptake of the product upon storage as compared to the similar product with a different carrier, hydroxypropylmethylcellulose acetate succinate (HMPC AS) (Mehuys et al., 2005a). Changes of drug release were reported with PVAP capsules after one month storage at 25 °C / 75% RH and 25 °C / 60% RH, respectively.

In contrast, Ghebremeskel et al. (2006) demonstrated that the addition of surfactant did not change the performance of extrudate as indicated by the indiscernible change in drug release profile after 6 month storage in accelerated humidity condition (Ghebremeskel et al., 2006). The authors suggested that recrystallization of the formulations were primarily determined by the polymer carrier rather than other additives, namely surfactant in this case.

Chapter 1.4.2.2.4 describes the possibility of lipid addition to HME products. A more recent investigation has shown that addition of lipid could preserve the physical stability of the solid dispersion product (Unga et al., 2010). This research group demonstrated the influence of lipid in the process of folding and unfolding of polyethylene glycol (PEG 4000), where lipid has shown to form a continuous single phase system with PEG and affect the folding of PEG polymeric chain. In order to effectively retard the unfolding of PEG, Unga et al. (2010) suggested that the lipid molecule should be large, branched and possess a small portion of polar surface. Among the tested lipid systems, tristearin was identified to be the best lipid component in preventing the unfolding process of PEG (Unga et al., 2010). Therefore, a good physical stability of HME product could be obtained by incorporating lipid components.

Storage Temperature

Storage temperature is another important factor in determining physical stability of a SD system. A low storage temperature ($T < T_g$ of the system) could lead to better stability of a SD product due to the reduce molecular mobility of the extrudates (Hancock and Zografi, 1997). On the other hand, storage of formulation at temperature higher than the T_g of product can lead to an increase in polymer ductility and transforms into its rubbery state which unfold the polymeric chain. Eventually, recrystallization occurred due to the rearrangement of drug molecules as a result of the increase in chain ductility of the polymer (Prodduturi et al., 2007).

Besides, the storage temperature has also reported to affect the physical structure of polymeric chain. PEO was reported to be in a meta-stable folded state after treatment of thermal and high shear processing as indicated by the reduction of melting temperature (T_m) (Prodduturi et al., 2005, Prodduturi et al., 2007, Mididoddi and Repka, 2007). However, these meta-stable folded chains can unfold into its stable form at a particular storage temperature of the extrudates. Crowley et al. (2002) demonstrated that storage of PEO (a mixture of amorphous and crystalline polymer) at temperature lower than its T_m can cause degradation of the amorphous fraction of PEO, however, storage at higher temperature than T_m can cause oxidative degradation in both the amorphous and crystallites fractions of PEO (Crowley et al., 2002b).

1.6. Dissolution performance of solid dispersions

The ability of SD in producing formulations with enhanced dissolution rate and bioavailability was widely reported (Fernandez et al., 1989, Tantishaiyakul et al., 1996, Craig, 2002). However, the number of marketed solid dispersion is disappointing despite of many papers published in this field. Besides the inherent physical instability of SD system, poor predictability on the dissolution behaviour of SD in has also been argued as one of the main reasons for the disappointing figures.

Many reports were published on the dissolution enhancement of SD products, but the underlying mechanism of dissolution is still poorly understood. Nevertheless the potential factors to enhance dissolution have been suggested in these publications. These factors are summarised below:

- **The presence of amorphous phase**

During the dissolution process, less energy is required to break the structure of an amorphous API (high energy) as compared to the crystalline API (Corti et al., 2008, El-Badry and Fathy, 2006, Tantishaiyakul et al., 1996). El-Badry et al. (2006) has shown that similar crystallinity of PM and solvent-evaporated of 1:3 Meloxicam PVP K30 gave rise to an overlapped dissolution profile between the two. In the same study, a higher dissolution rate of co-evaporated 1:5 Meloxicam:PVP K30 was attributed to its crystallinity reduction as compared to the formulation of 1:3 Meloxicam:PVP K30.

- **Carrier stabilization**

During the dissolution process, the sustainability of the supersaturation state of an API is highly dependent on the crystallization tendency of the amorphous drug molecules (Alonzo et al., 2010). Thus, the solubility advantages of amorphous API can only be achieved if the carrier possesses a capacity to stabilize the amorphous API against solution mediated recrystallization (Chawla and Bansal, 2008, El-Badry et al., 2009). This stabilization capacity is closely related to the solubilizing effect of the carrier to the API. For instance, greater solubilisation of indomethacin in PEG 4000 than Gelucire 50/13 has led to better amorphization of indomethacin in the former carrier than the latter (El-Badry et al., 2009). Besides, intermolecular interactions between the carrier and API has also been reported to be important in imparting stabilization of the supersaturation state generated by the high degree of apparent solubility of the amorphous molecules (Miller et al., 2008a).

- **Formation of complexes**

The dissolution enhancement of SD can be also ascribed to the formation of soluble complexes. These complexes could be formed via electrostatic forces, hydrogen bonding and hydrophobic interaction between drug and the carrier (Ilevbare et al., 2012a). The formation of soluble complexes is evidenced by the increase in apparent solubility constant of an API in its carrier solution (Verheyen et al., 2002, Biswal et al., 2009)

- **High surface area**

Solid dispersion is claimed to provide large surface area for dissolution process due to the dispersion of API at molecular level (Kapsi and Ayres, 2001, Dong et al., 2008b, Biswal et al., 2009). This effect is found to be highly dependent on the fraction of the hydrophilic carrier (El-Badry and Fathy, 2006). Nokhodchi et al. (2005) revealed that the fraction of molecularly dispersed API in tested lipid-solid compacts is directly proportional to the release rates of indomethacin at 10 minutes point of dissolution experiments (Nokhodchi et al., 2005).

- **Hydrophilicity**

The use of hydrophilic carrier in SD has contributed to the dissolution rate enhancement. This is achieved through fast water penetration and the ability of the hydrophilic polymer in wettability enhancement or solubilisation of the API (Corrigan, 1985, Craig, 2002, Fernandez et al., 1989, Biswal et al., 2009, Chawla and Bansal, 2008).

- **Lowered Interfacial energy**

The interface between API and the dissolution medium has been shown to be an important factor in determining the dissolution performance of SD of a poorly soluble API (Swanepoel et al., 2000, El-Badry and Fathy, 2006). A lower interfacial tension of SD/medium could give rise to a higher wetting effect to the hydrophobic API which can reduce the agglomeration event. In this context, the proportion of the carrier used is critical in lowering the interfacial tension between the poorly soluble API and dissolution medium.

Figure 1.10 presents a summary of the contributing factors in dissolution enhancement of poorly soluble API through the formation of SD.

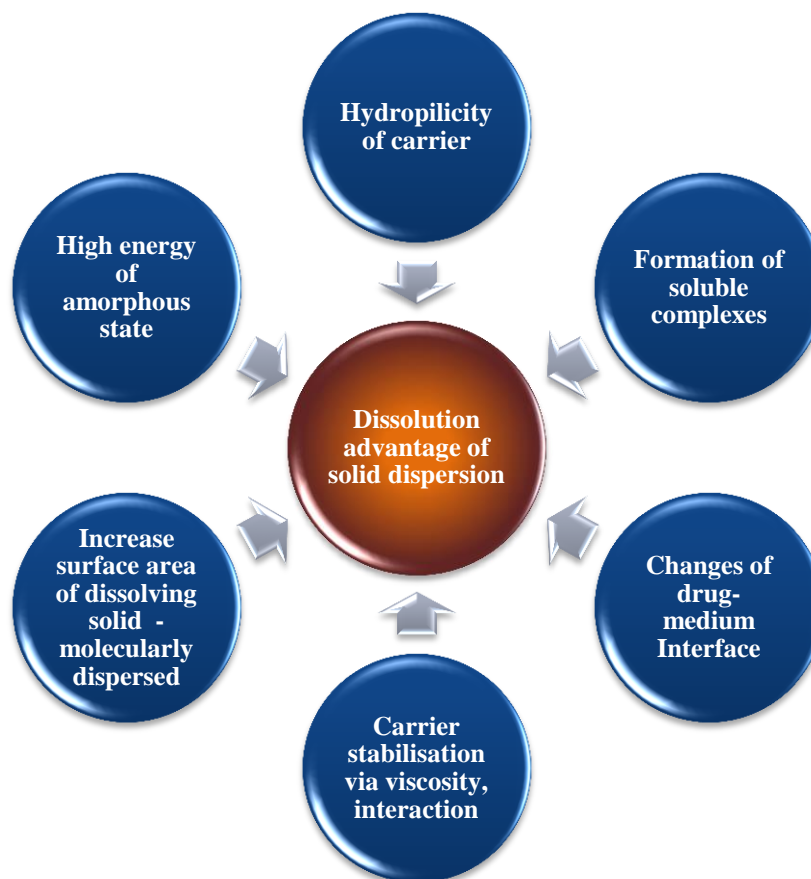


Figure 1.10: Summary of contributing factors in dissolution enhancement of poorly soluble API via the formation of an SD.

1.6.1. Anomalous dissolution of solid dispersions

API in an SD is generally exist in a high energy state, thus there is a risk of API recrystallization. It is difficult to predict the performance of SD in the *in vivo* hydrodynamic condition, as there is a high tendency of recrystallization of the API before drug absorption. A few publications have shed light on the anomalous drug release profiles and potential problems arise in the dissolution process of solid dispersion (van Drooge et al., 2004, Verheyen et al., 2002). In the subsequent sections, the current status of the dissolution performance of SD will be discussed with emphasis given on the different observations disclosed in the reported literature.

1.6.1.1. Crystallinity

Crystallinity is often linked to the dissolution rate limiting step of BCS class II compounds. In general, a product with the lack of crystallinity dissolves faster than a product with fully crystalline structure (Ruan et al., 2005). Unexpectedly, few publications have shown the higher drug release rate (in weight) of the fully crystalline PM drug-polymer system than its corresponding amorphous SD system (Moneghini et al., 1998, Verheyen et al., 2002, van Drooge et al., 2004, Margarit et al., 1994, Tajarobi et al., 2011a). For instance, dissolution of PM ketoprofen-PEG 6000 was faster than the dissolution rate of the corresponding co-evaporated SD system (Margarit et al., 1994). Another example was reported by Tajarobi et al. (2011) where co-evaporated solid dispersion of butyl paraben was revealed with a slower dissolution profile as compared to the corresponding crystalline PM despite the complete amorphization of drug compound in SD system (Tajarobi et al., 2011b). A similar observation was also noted for SD of co-evaporated of atenolol in PVP-CL and in PVPVA, whereby the corresponding PM formulations release faster than the amorphous SD products. In that study, the high viscosity effect exerted by the swellable carrier was claimed to be the main cause of the slow drug release of SD in that study (Moneghini et al., 1998).

Results reported by Yan et al. (2012) revealed a slower API release of the partially amorphized spray dried valsartan-HPMC as compared to the fully crystalline powder of valsartan in alkaline medium (pH 6.8). However, a reverse dissolution performance were seen in acidic medium whereby the release of the spray dried valsartan-HPMC was faster than its PM system (Yan et al., 2012). This is mainly attributed to the ionization of valsartan at the low pH condition. Besides, William et al. (2005) has also concluded that there is no simple relationship between the crystallinity of ibuprofen with its dissolution rate. In that study, higher extent of ibuprofen was released in PM crystalline ibuprofen-PVP-CL as compared to the corresponding amorphous SD formulations (Williams et al., 2005).

1.6.1.2. API / polymer loading

Dissolution performance of a SD is also highly dependent on the proportion of API. There is a critical loading limit of API in a SD system that should not be exceeded in order to ensure good dissolution performance of the SD system when compared with its corresponding PM (Swanepoel et al., 2000, El-Badry and Fathy, 2006, Karavas et al., 2007). For instance, the loading limit for methylparaben and ketoprofen are 10-20% in PEG 6000 and 20% in PEG 6000, respectively (Margarit et al., 1994, Saers and Craig, 1992). Other examples of loading limits of API are 15% of PCM, 10% indomethacin, 5% phenacetin, and 2 % phenylbutazonein, (Fernandez et al., 1989, Verheyen et al., 2002).

In essence, a higher proportion of carrier in a SD system will lead to faster release of the API by increasing its solubilisation. However, Ruan et al. (2005) has demonstrated that the release of ampelopsin is not related to the proportion of PEG 6000 in the studied SD (Ruan et al., 2005). In another study, Tantishaiyakul et al. (1996) revealed that the highest dissolution rate was observed in the SD of 1:4 piroxicam-PVP when compared with SD of 1:1 and 1:6 piroxicam-PVP. The authors suggested that amorphicity of the sample is the main factor that contributed to this unpredicted dissolution profile as a complete amorphous product was obtained in SD 1:4 but not in SD of 1:1 or 1:6 piroxicam-PVP ratio (Tantishaiyakul et al., 1996).

On the other hand, Doherty et al. (1987) has pointed out that high loading of carrier created the high viscosity layer at dissolving front of a system which could potentially retard the dissolution performance of SD, despite the increase wetting and solubilizing effect at high proportion of carrier. In that study, the highest dissolution rate of frusemide achieved an optimum loading of carrier at 60%, higher than this value, drug release of the carrier system reduced (Doherty and York, 1987).

1.6.1.3. Molecular weight of carriers

Molecular weight (MW) of the carrier in a SD system is another important factor that influences the dissolution performance of SD. Studies performed by Bettinetti and Mura (1994) have shown that among a few tested carriers namely PVP K15, PVP K30 and PVP K90, PVP K15 (low MW carrier) is the best carrier to be used in the powdered naproxen-PVP SD, as far as the dissolution rate enhancement is concerned. However when the powder was compacted into disc, PVP K30 has turned out to be the best with the highest dissolution rate followed by PVP K 90, while PVP K15 yielded the poorest dissolution rate among all. The authors suggested that this is attributed to the higher binding ability between the PVP K15 and naproxen while compaction process which lead to its slower dissolution rate (Bettinetti and Mura, 1994).

A few studies have reported the negative impact of high MW polymer carrier on dissolution enhancement of SD (Mura et al., 2003, Körner et al., 2005, Mokarram et al., 2010a). The use of high MW of chitosan as a carrier for naproxen SD resulted in slow release of the API, which was ascribed to the retardation of API diffusion through the high viscosity layer of high MW polymer (Mura et al., 2003). Likewise, Mokarram et al. (2010) demonstrated that the dissolution rate of indomethacin increases with a decrease in MW of PVP due to the ease of drug diffusion into the bulk medium through the non-viscous and short diffusion layer of the low MW carrier (Mokarram et al., 2010a). Similarly, Körner et al. (2005) proposed that a low MW polymer release API at a

faster rate than a high MW polymer which is closely related to the intrinsic viscosity of the polymer carrier (Körner et al., 2005).

In contrast, a few other studies have found the reverse trend whereby the use of high MW carrier contributes positively to dissolution rate enhancement of SD. Chawla and Bansal (2008) suggested that higher Tg of hydrophilic carrier, with their high MW, is advantages in stabilizing amorphous API while dissolution (Chawla and Bansal, 2008). Similarly Kapsi and Ayres (2001) reported that dissolution of an investigated API improves considerably with the increase in MW of its PEG carrier. This is attributed to the higher proportion of oxyethylene molecule that lead to greater interspatial space for trapping of the drug molecule (Kapsi and Ayres, 2001). Likewise, results reported by De Brabander et al. (2003) revealed a faster release rate of API with the use of higher MW HPMC in its SD. The author explain the observation in terms of the presence of ethylcellulose that reduces chains entanglement of HPMC, which subsequently increase the accessibility of the product to the dissolution medium (De Brabander et al., 2003).

Reviewing the available literature, there is no general trend to explain the effect of MW on dissolution performance of SD. On one hand, dissolution rate of a SD is directly proportionally to MW of the polymer carrier. On the other hand, dissolution rate of a SD is inversely proportionally to MW of the polymer carrier due to their high viscosity layer that inhibits drug diffusion during the dissolution process. As well as the aforementioned contradiction, some studies have shown the complex relationship between the MW and dissolution rate of a SD system. Verhoeven et al. (2009) cited that drug release from matrices is inversely correlated to the MW of carrier as confirmed by a slower drug release rate observed in the lower MW carrier system. However, when the concentration of PEO/PEG reached 20% or above, the drug release rate is directly correlated with the MW of PEO/PEG i.e. higher MWs of PEO/PEG caused an increase in gel strength which slows down the drug release (Verhoeven et al., 2009a). In addition, dissolution behaviour of coprecipitated of probucol-PVP indicated that PVP K30 yielded a faster drug release than PVP K90 and PVP K15 (Yagi et al., 1996). The results presented in the review above suggest an urgent need to clarify the effect of molecular weight of carrier in solid dispersion performance (Mokarram et al., 2010a).

1.6.1.4. Structure of carriers

The structure of the carrier is also found to exert an influence on the dissolution performance of SDs. According to Kapsi and Ayres (2001), API release of itraconazole-branched PEG is 2-fold higher than its identical composition but with linear structure PEG 20000. However, the reasons behind this phenomenon remain unknown (Kapsi and Ayres, 2001).

The hydrophilic nature of carrier has been suggested as an important factor to increase dissolution performance of SD of a poorly soluble API. However some researchers have suggested otherwise, whereby a poorer dissolution performance was observed in a relatively more hydrophilic carrier, i.e. PVP system as compared to the HPMC polymer (Alonzo et al., 2010, Callahan et al., 1982). According to study carried out by Alonzo et al. (2010), dissolution of amorphous felodipine at 37 °C has achieved higher supersaturation in the presence of pre-dissolved HPMC 606 and HPMCAS than in the presence of PVP K29-32 despite the same initial dissolution rate of both the systems as shown in Figure 1.11.

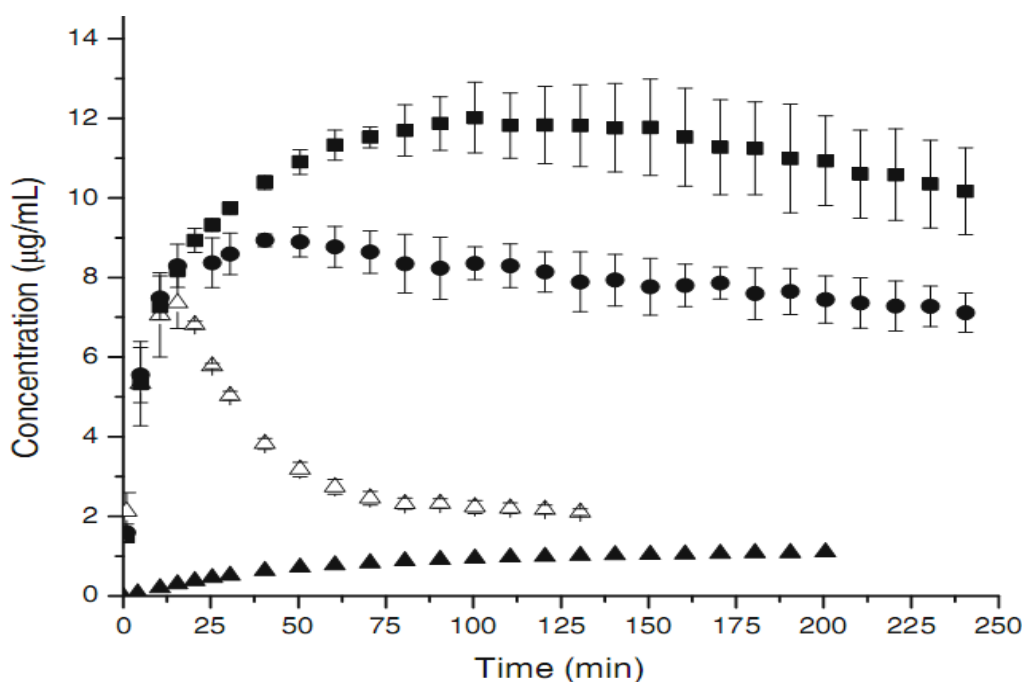


Figure 1.11: The dissolution profiles of amorphous felodipine at 37°C in the presence of various polymers pre-dissolved at 500 µg/mL concentration of; PVP (Δ), HPMC (\bullet) and HPMC-AS (\blacksquare). Dissolution of crystalline felodipine at 37 °C is included as a reference (\blacktriangle) (Figure reproduced from Alonzo et al., 2010).

Furthermore, the achieved supersaturation state is less stable in PVP medium (less than 30 minutes) as compared to a stable concentration of felodipine in HPMC polymer solution for 5 hours. As a result, the less hydrophilic polymers (HPMC 606 and HPMCAS) with their slow dissolving rate has caused a higher degree of protection toward the amorphous molecule of API which consequently generates a better overall dissolution performance of the SD. In the same study, opposite effects of the tested polymers were seen on the release rate of indomethacin. In that case, the presence of PVP has caused a higher drug release rate and sustainability of supersaturation state of amorphous indomethacin as compared to HPMC 606 carrier (Alonzo et al., 2010). This implies the complexity of the dissolution process of amorphous pharmaceuticals.

Recently, Ilevbare et al. (2012) has suggested that there should be an optimal level on hydrophilic/hydrophobic balance to be an effective crystal growth inhibitor (Ilevbare et al., 2012b). This could be achieved by the use of polymers blend carrier system. Miller and co-workers has shown that the use of polymer blend (HPMC and poloxamer) allows more loading of itraconazole for a faster release of drug from the SD system (Miller et al., 2007). Besides, addition of Carbopol® 974P to the itraconazole formulation was also attempted in the same group of researchers. The products obtained exhibited a greater therapeutic drug absorption and gastrointestinal stability in comparison to their previous investigated the SD system (HPMC and poloxamer) due to the better mucoadhesive properties of Carbopol® 974P (Miller et al., 2008b).

1.6.1.5. Particle size influences

In SD, there is no direct relationship between the particle size of the formulations and its dissolution performance as other factors such as agglomeration tendency and precipitation at high energy can occur during dissolution of the SD (Kapsi and Ayres, 2001). Conventionally, small particle size product will lead to greater dissolution performance of the product due to the high effective surface area of the product expose to the dissolution medium (Noyes and Whitney, 1897). Wu et al. (2009) showed that smaller particle size distribution of the piroxicam SD sample prepared via the co-precipitation method gave rise to a higher dissolution rate as compared to the similar sample prepared by spray drying method (Wu et al., 2009).

In other studies, extensive agglomeration was reported upon dissolution of solid dispersion (Karavas et al., 2007, Stewart and Zhao, 2005). A decrease in the release rate of itraconazole was noted in the solid dispersion of small (< 240 µm) and big (381-1400µm) particle size fraction as compared to the intermediate size fraction (240-380 µm) which displayed the highest dissolution rate (Kapsi and Ayres, 2001). According to the authors, this observation is attributed to the higher tendency of recrystallization of smaller particles as compared with the larger fraction sized particles (Kestur et al., 2012). Therefore, the use of product with small particle size may be compromised by the extensive precipitation and higher recrystallization tendency of the product (Kapsi and Ayres, 2001, Kestur et al., 2012, Karavas et al., 2007).

1.6.1.6. Addition of surfactant

Surfactant can be used to increase the dissolution rate of poorly soluble API (Sivert et al., 2009). It acts mainly by increasing the solubilisation of APIs and lowering the interfacial tension between solid particle of SD and dissolution medium which improves wettability of the extrudates (Zhu et al., 2006, Ghebremeskel et al., 2006). SD API/plasdone S630/surfactant undergoes complete drug release in 10 minutes. In comparison, the corresponding sample without surfactant undergoes complete drug release after 45 minutes. In parallel, complete dissolution time of SD API/HPMC was shorten from 120 minutes to 10 minutes after the addition of surfactant into its composition (Ghebremeskel et al., 2006).

It has been suggested that the concentration of surfactant should be kept lower than its critical micelle concentration (CMC) value when incorporating a surfactant into the composition of a SD system (de Waard et al., 2008). For example, a decrease in drug release rate of API/PVP K30/Docusate sodium was noted in the study of Ghebremeskel et al. (2007). According to the author, this is caused by the entrapment of API in the formed micelle as the amount of surfactant used had exceeded its CMC (Ghebremeskel et al., 2007). However, undesired dissolution profiles have also been reported in the SD products despite the used of surfactant below their CMC values (Dabbagh and Taghipour, 2007, Ilevbare et al., 2012a). For instance, addition of Tween 80 (a non-ionic surfactant) (below its CMC) into the composition of SD ibuprofen-Eudragit RLPO has shown to reduce the dissolution rate of ibuprofen (Dabbagh and Taghipour, 2007) as compared to the SD formulation without surfactant. Thus, the role of surfactant in the formulation of SD remains ambiguous.

1.6.1.7. Processing methods

Different processing methods produce formulations with different dissolution performances. According to Dong et al. (2008) SD of co-precipitated (CP) API-HPMCAS revealed a faster dissolution rate than the HME on the same products due to higher specific surface area of the former system. However, intrinsic dissolution experiments have shown different results, whereby the HME system exhibited faster dissolution rate than the CP system due to the higher extent of drug-polymer interaction in CP product compares to the HME product (Dong et al., 2008b).

In contrast, some studies have shown the inferior dissolution performance of HME SD system. HME ibuprofen-PVP-CL was released slower than the same composition prepared by SD (Williams et al., 2005). The authors cited that this is due to the extensive drug-polymer interaction as a result of solvent was used in the preparation of SD. Likewise, a study carried out by Patterson et al. (2008) revealed that the drug release rate of spray dried dipyridamole-PVPVA 3:7 is higher than the drug release rate of the corresponding system prepared by HME (Patterson et al., 2008). Besides, Mura et al. (2003) reported that SD naproxen prepared via co-grinding method had higher dissolution rate than the same samples produced via co-evaporated and kneading processes (Mura et al., 2003).

1.6.1.8. Extreme storage conditions

In contrast to usual expectations, insignificant changes of the dissolution profiles of SD after extreme storage condition such as 75% RH or high storage temperature (40 °C and 60 °C) have been reported (Bruce et al., 2007, Jijun et al., 2010, Gupta et al., 2002, Ghebremeskel et al., 2006). Bruce et al. (2007) reported similar dissolution profiles between the fresh SD and aged SD. According to the authors, this is mainly due to the limited growth of crystal on the surface of the aged tablet, as a result, the total amount of amorphous state inside the matrix remains high in proportion to the content of growth crystal (Bruce et al., 2007).

Unexpectedly, the release rate of diazepam from SD PEG-diazepam after humidity storage (75% RH) was found to be higher than the corresponding sample desiccated at 0% RH (Jørgensen and Torstenson, 2008). Likewise, Gupta et al. (2002) suggested that the increase of drug-polymer interaction after storage is the main factor leading to the increased dissolution rate of naproxen after storage (Gupta et al., 2002). Jijun et al. (2010) has demonstrated that short period of high storage temperature or also known as “post heating” gave rise to low solution mediated recrystallization tendency and therefore it sustains the supersaturation state during dissolution (Jijun et al., 2010). However, the detail of the mechanism of the advantage from this “post heating” effect is still poorly understood. The inconsistent literature reports infer a need to further investigate the role of crystalline material in the dissolution performance of SDs.

1.7. Objective of this study

As stated in Chapter 1.6, hydrophilic carrier has been frequently used in SD of immediate release formulations. In this case, PVP has shown to be a great carrier in dissolution enhancement of solid dispersion (Biswal et al., 2009, Garekani et al., 2003, Tantishaiyakul et al., 1999). Nevertheless, there are limited reports available for the use of PVP in HME procedure (Lakshman et al., 2008, Forster et al., 2001c, Miller et al., 2008a, Miller et al., 2007, Bruce et al., 2007, Andrews et al., 2010, Thybo et al., 2007, Ghebremeskel et al., 2006, Ghebremeskel et al., 2007) due to the potential of its degradation in the thermal processing (Bühler, 2005, Chokshi et al., 2005).

However, PVP has the ability to greatly depress the melting point of API which might enable its usages at lower processing temperature of HME (Marsac et al., 2006, Paudel and Van den Mooter, 2011). Besides, PVP has also been reported with good physical stabilizing effect on SD (Khougaz and Clas, 2000) although its stability enhancing ability could be negated by its hygroscopic nature. This could be resolved using the solvent/aqueous free of HME processing method. Thereby, PVP was investigated as the main carrier in this study. The properties and reviews of PVP polymers will be covered in Chapter 2.2.2 under the section of material.

Previous sections have highlighted the possible factors that may influence the quality of amorphous pharmaceuticals, physical stabilization and dissolution performance (Chapter 1.6.1) of a SD based upon the available literatures. However, by unveiling those factors superficially without having thorough understanding of their impact in the SD performance does not solve the real problem. Therefore, considering the three broad aspects of SD development, i.e. manufacturing, stability issue, and formulations performance, specific objectives of this study are presented as below:

- 1) To understand and explore the possible means in the use of PVP homopolymers and its copolymer derivative in HME application with regards to API-polymer miscibility and processing ability for the production of amorphous SD.
- 2) To understand the stabilization factors of a PVPs-based HME SD product and to determine the critical storage condition that allows a longer shelf life of PVP based HME SD.
- 3) To understand the governing factors in the dissolution performance of PVP-based physical mixture and PVP-based HME amorphous SD across different poor soluble APIs.
- 4) To examine the influence of different APIs, loadings of carrier, MW of carriers and the addition of excipients in modulating the release profile of HME PVP-based SD formulation.
- 5) To further understand the mechanism of release of a HME PVP-based SD for a poor soluble API.

Figure 1.12 outlines the research that will be covered in the latter part of this thesis.

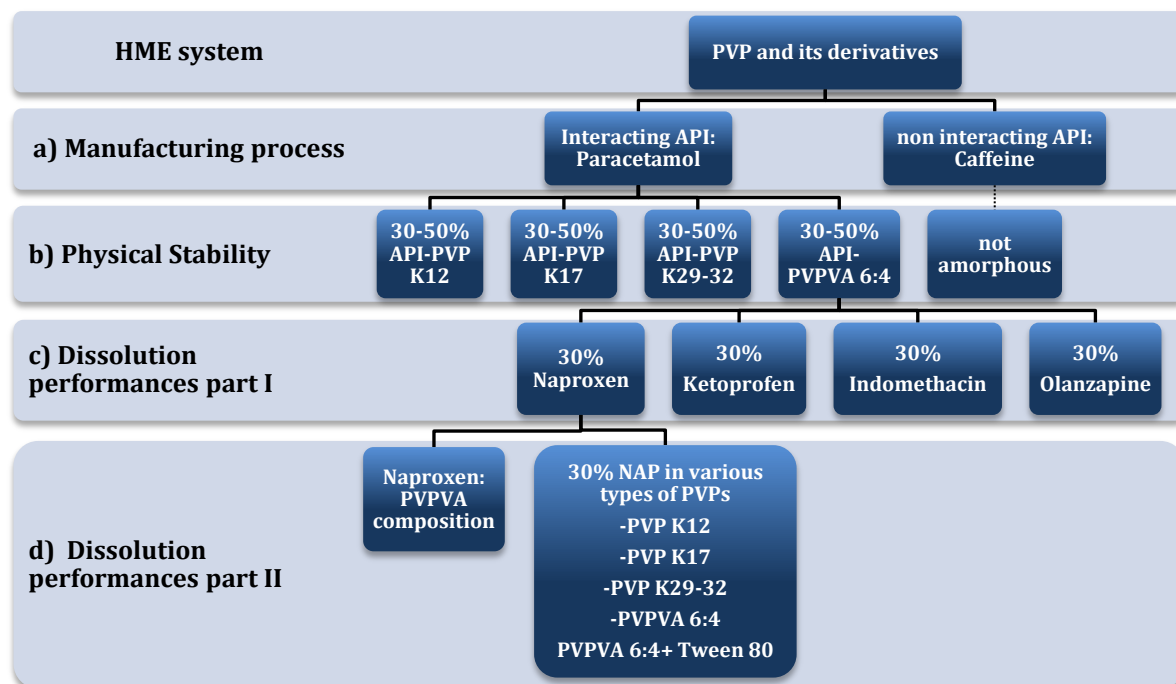


Figure 1.12: Flow chart of the development of HME PVP-based system

As displayed in Figure 1.12, the feasibility of using PVP for HME processing was assessed by characterising the extrudates incorporating both interacting and non-interacting API models. It was found that APIs which do not interact with PVP polymer could not result in fully amorphous dispersions when it was extruded at temperatures lower than T_m of the API (Figure 1.12 (a)). Hence, physical stability studies of the fully amorphous systems with an interactive API (paracetamol) were exclusively carried out (see Figure 1.12 (b)). Then, HME interacting API-PVPVA 6:4 products were subsequently produced and investigated for their dissolution performance in order to identify the possible issues that may occur during the dissolution process (Figure 1.12 (c)). The issues identified were further explored by studying the dissolution performance of HME API prepared using different PVPs carriers in various compositions (Figure 1.12 (d)). By exploring the factors influencing these issues, a dissolution mechanism of HME PVP-based solid dispersion is proposed at the end of this thesis. Experimental details of the investigated areas as shown in Figure 1.12 will be provided in the subsequent chapters.

Chapter 2. Material and Methods

2.1. Introduction

The advent of the hot melt extrusion (HME) process in the pharmaceutical field has led to its potential usage in the formulation of solid dispersions (SDs) (Shah et al., 2012). Based on the knowledge gaps that have been introduced in previous Chapter, fundamental study of the processing and overall performance of the HME formulations is needed. To fill these gaps, a range of active pharmaceutical ingredients (API) and carriers were used in develop an immediate release HME PVP-based formulation. In addition, a laboratory scale of HME equipment was used for the manufacturing of these SDs.

In order to produce a successful HME SD system, it is very important to understand the characteristics and performances of the prepared HME-based systems. Several techniques were used to characterize the thermal and physicochemical properties of the raw materials and the prepared formulations. These techniques include Differential Scanning Calorimetry in standard or modulated mode (DSC or MTDSC), thermogravimetric analysis (TGA), hot stage microscopy (HSM), Fourier Transform Infrared-Attenuated Total Reflectance (ATR-FTIR), X-ray powder diffraction (XRPD) and laser diffraction (LD) particle size analysis. Other techniques such as scanning electron microscopy (SEM), atomic force microscopy (AFM) and contact angle measurements were also used to study surface morphology and surface properties of the prepared formulations.

In this chapter, the general physicochemical characteristics and clinical usages of the applied APIs (Chapter 2.2) will be summarised. In addition, processing parameters of HME (Chapter 2.3) and the operational principles of the aforementioned characterization techniques will be introduced (Chapter 2.4 and 2.5).

2.2. Materials

2.2.1. Model drugs

6 model APIs were employed in this study. Paracetamol (PCM) and caffeine (CAF) were selected to represent interacting and non-interacting APIs, respectively, based on the availability of hydrogen bond interaction with respect to PVP. The other APIs were naproxen (NAP), ketoprofen (KTP), indomethacin (INDO) and olanzapine (OZP); these are BCS class II compounds whereby their clinical therapeutic effect is limited by the dissolution process (please refer to Chapter 1.1 for

details of BCS classification). These APIs were selected based on their poorly water soluble nature in order to access their dissolution enhancement after formulating into the HME SD system. The clinical usages and physicochemical properties of each API model of will be introduced in the following sections.

2.2.1.1. Paracetamol

PCM is an antipyretic compound that is clinically used as an analgesic. Physically, PCM is reported to exist in 3 polymorphic crystalline forms and an amorphous form. The reported crystalline forms include the stable monoclinic crystal (or also known as form I PCM) and its metastable orthorhombic form (or also known as form II PCM) and an as yet poorly defined crystal Form III (Di Martino et al., 1997). Amorphous PCM is found to possess a low glass transition temperature at circa 25 °C which suggests a high tendency for recrystallization under room conditions (Qi et al., 2008a). This has made it as an excellent model of API for studying the stabilization capacity of different polymers carrier in the SD of amorphous PCM. Figure 2.1 and Table 2.1 present the chemical structure and other physicochemical properties of PCM, respectively.

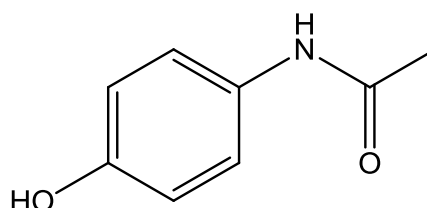


Figure 2.1: Chemical structure PCM

Table 2.1: Physicochemical properties PCM

PCM	Properties	References
IUPAC chemical name	N-(4-hydroxyphenyl) ethanamide	(de Villiers et al., 1998)
Formula	C ₈ H ₉ NO ₂	
Molecular weight	151.16 g / mol	(Baird et al., 2010)
pKa	9.7	(Lemieux et al., 2010)
Melting points	Form I 169-172 °C Monoclinic Form II 158 °C Orthorhombic Form III 123 °C Undefined crystal shape	(Di Martino et al., 1997, Di Martino et al., 1996)
Glass transition temperature	≈ 25 °C	(Qi et al., 2008a, Baird et al., 2010)
Density	1.38 g / cm ³	(Baird et al., 2010)
Solubility	Sparingly soluble in water (14 mg / ml) Freely soluble in alcohol	(British Pharmacopoeia Commission, 2012)

2.2.1.2. Caffeine

CAF is a purine derivative that usually prescribed as a central nervous system stimulant. It is a white crystalline powder with water sparingly soluble properties (British Pharmacopoeia Commission, 2012). Two polymorph forms of CAF were reported where the Form II is a stable form at room temperature while Form I is a metastable form (Lehto and Laine, 1998). However, the metastable Form I was reported to be able to maintain its stability at room temperature for up to up to a month (Lehto and Laine, 1998, Epple et al., 1995). To date, no glassy state of caffeine has been reported although pseudo-glassy state of caffeine was reported by Descamps et.al. (2005). Figure 2.2 and Table 2.2 show the chemical structure and physicochemical properties of CAF, respectively.

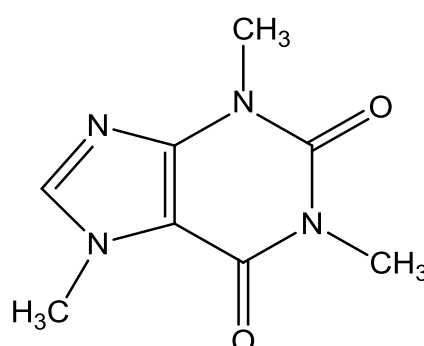


Figure 2.2: Chemical structure CAF

Table 2.2: Physicochemical properties CAF

CAF	Properties	References
IUPAC chemical name	1,3,7-trimethyl-3,7-dihydro-1 <i>H</i> -purine-2,6-dione	(Pinto and Diogo, 2006)
Formula	C ₈ H ₉ N ₃ O ₂	(Derollez et al., 2005)
Molecular weight	194.19 g / mol	(Baird et al., 2010)
pKa	10.4	(Kang et al., 2011)
Melting points	234-239 °C	(Kishi and Matsuoka, 2010)
Pseudo-glass transition temperature	≈-13°C	(Descamps et al., 2005a)
Density	1.35 g/cm ³	(Baird et al., 2010)
Solubility	Sparingly soluble in water (16.7 g/L at 25°C) Slightly soluble in ethanol (96 %)	(British Pharmacopoeia Commission, 2012)

2.2.1.3. Naproxen

NAP is a potent non-steroidal anti-inflammatory drug (NSAID) with analgesic and antipyretic properties. It is clinically used for the treatments of pain, fever, muscle stiffness and inflammation.

NAP is categorized as BCS class II substance, a poorly soluble compound (Kindermann et al., 2011). This has granted its usages as a model API for designing immediate release formulation (Bettinetti and Mura, 1994, Mura et al., 2002, Türk and Bolten, 2010, Zahedi and Lee, 2007).

There is no polymorphism reported for crystalline NAP. In the glassy state, NAP has a low T_g which implies instability of its amorphous form. Thus, NAP is also a suitable API model for the study of its physical stabilization in a SD system (Paudel and Van den Mooter, 2011, Malaj et al., 2010). The chemical structure and physicochemical properties of NAP are presented in Figure 2.3 and Table 2.3 respectively.

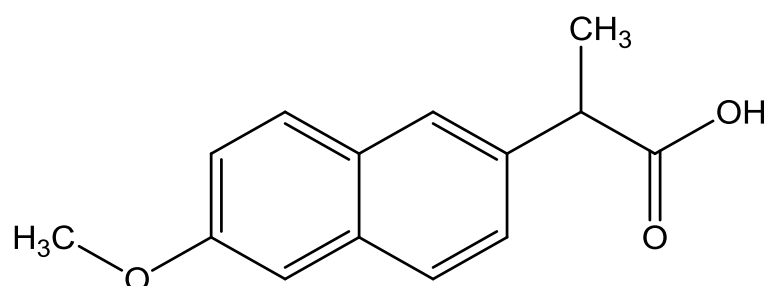


Figure 2.3: Chemical structure NAP

Table 2.3: Physicochemical properties NAP

NAP	Properties	References
IUPAC chemical name	S-2-(6 methoxy-2-naphthyl) propionic acid	(Mura et al., 1995)
Formula	$C_{14}H_{14}O_3$	
Molecular weight	230.26 g / mol	(Malaj et al., 2010)
pKa	4.5	(Corti et al., 2008)
Melting point	155 – 156 °C	(Mura et al., 2003)
Glass transition temperature	-6 to -3 °C	(Gashi et al., 2009, Malaj et al., 2010)
Density	1.268 g / cm ³	(Malaj et al., 2010)
Solubility	Practically insoluble in water (≈ 0.027 mg / ml at 25 °C); sparingly soluble in alcohol	(Mura et al., 1995)

2.2.1.4. Ketoprofen

KTP is a NSAID which possesses both analgesic and antipyretic effects. Clinical applications of KTP include the treatments of arthritis related inflammatory pain, severe pain, musculoskeletal pain and stiffness. Similar to other NSAIDs, the main side effect of KTP is GI irritation. Various attempts were made aiming to reduce the side effect of KTP by formulating into topical formulations such as medicated patches, sustained release dosage forms and solid dispersion formulations (Kulkarni et al., 2010, Jachowicz et al., 2000, Patil et al., 2010, Yang et al., 2008).

KTP is classified as BCS class II compound with no previous report of polymorphic forms. It possess a low Tg value at circa -5 to -6 °C (Malaj et al., 2010). Figure 2.4 and Table 2.4 display both the chemical structure and physicochemical properties of KTP, respectively.

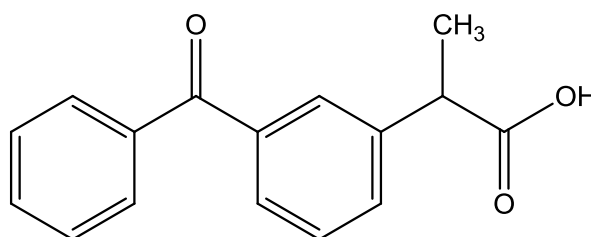


Figure 2.4: Chemical structure KTP

Table 2.4: Physicochemical properties KTP

KTP	Properties	References
IUPAC chemical name	(RS)2-(3-benzoylphenyl)-propionic acid	
Formula	C ₁₆ H ₁₄ O ₃	(Malaj et al., 2010)
Molecular weight	254.28 g / mol	(Baird et al., 2010)
pKa	4.6	(Sheng et al., 2006)
Melting point	94.6-94.9 °C	(Baird et al., 2010)
Glass transition temperature	-5.61 °C	(Malaj et al., 2010)
Density	1.28 g / cm ³	(Baird et al., 2010)
Solubility	Practically insoluble in water Poorly soluble in pH 1.2 at 37 °C (0.17 mg/ml); sparingly soluble in alcohol	(Margarit et al., 1994)

2.2.1.5. Indomethacin

INDO is also a NSAID. It is clinically used to reduce pain as well as to relieve symptoms of muscular stiffness, fever and swelling by inhibiting the production of prostaglandins. INDO is categorized as BCS class II compound (low solubility and high permeability) in which its dissolution process in gastrointestinal tract is the rate limiting process in exerting its therapeutic effect (Nokhodchi et al., 2005). Hence, many studies have been carried out to enhance solubility and dissolution rate of INDO (Nokhodchi et al., 2005, Sivert et al., 2009, Yadav and Yadav, 2009).

Crystalline INDO has been reported to exist in three polymorphic forms, α , γ , δ forms. The γ form is the most stable form in dry state followed by α and δ (Wu and Yu, 2006). In the γ polymorph, INDO exists as a dimer where two molecules of INDO are associated with a hydrogen bond (Taylor and Zografi, 1997). Whereas, amorphous INDO was reported to have a Tg value at circa of 43 °C (Sivert et al., 2009). Its properties as an amorphous pharmaceutical have also been widely studied (Greco and Bogner, 2010, Hilton and Summers, 1986, Liu et al., 2009, Taylor and Zografi, 1997). The chemical structure and physicochemical properties of INDO are presented Figure 2.5 and Table 2.5, respectively.

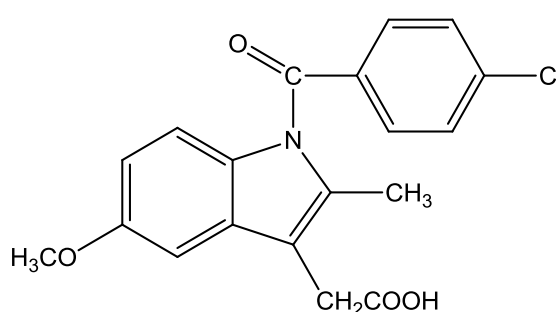


Figure 2.5: Chemical structure of INDO

Table 2.5: Physicochemical properties INDO

INDO	Properties	References
IUPAC chemical name	2-(1-[4-chlorophenyl carbonyl]-5-methyl-1H-indo-3-ly) acetic acid	(Mokarram et al., 2010a)
Formula	C ₁₉ H ₁₆ ClNO ₄	
Molecular weight	357.79 g / mol	(Baird et al., 2010)
pKa	4.5	(Mokarram et al., 2010a)
Melting point	155 °C (α form) 161 °C (γ form) 90 °C (δ form)	(Baird et al., 2010, Crowley and Zografi, 2002)
Glass transition temperature	≈ 43.1 °C	(Sivert et al., 2009)
Density	1.41 g / cm ³	(Baird et al., 2010)
Solubility	Practically insoluble in water (< 1 µg/ml); sparingly soluble in alcohol	(Nokhodchi et al., 2005)

2.2.1.6. Olanzapine

Olanzapine (OZP) is an atypical antipsychotic agent which is clinically applied for schizophrenia and bipolar mania (Odaci et al., 2009). It is categorized as BCS class II compound due to the low water solubility of this API. Thus, many attempts have been made to generate formulations with enhanced dissolution and bioavailability properties of the drug (Freitas et al., 2012, Krishnamoorthy et al., 2012, Krishnamoorthy et al., 2011).

Physically, OZP is reported to exist in 60 distinct solid forms which include 56 non-solvated polymorphs and an amorphous phase (Bhardwaj et al., 2013). Its amorphous form is found to have a T_g higher than the room temperature, i.e. circa 68 °C. This implies that amorphous OZP could be stored at room temperature (25 °C) as the kinetics of converting to its crystalline counterpart would be slow and OZP amorphous phase would be stable during its storage at room temperature. Figure 2.6 and Table 2.6 display the chemical structure and physicochemical properties of OZP, respectively.

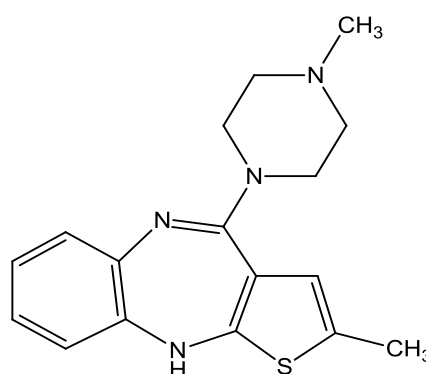


Figure 2.6: Chemical structure of OZP

Table 2.6: Physicochemical properties of OZP

OZP	Properties	References
IUPAC chemical name	2-methyl-4-(4-methyl-1-piperazinyl)-10H-thienol[2,3-b][1.5]benzodiazepine	(Krishnamoorthy et al., 2012)
Formula	C ₁₇ H ₂₀ O ₄ S	
Molecular weight	312.43 g / mol	
pKa (s)	4.69 and 7.37	(Freitas et al., 2012)
Melting point	Form II = 194.47 °C	(Freitas et al., 2012, Krishnamoorthy et al., 2012)
Glass transition temperature	68 °C	
Density	1.32 g / cm ³	
Solubility	Practically insoluble in water (≈5µg/ml); sparingly soluble in alcohol	

2.2.2. Carriers

Polyvinylpyrrolidone (PVP) is a widely investigated hydrophilic carrier for the development of SD formulation of poorly soluble APIs (Leuner and Dressman, 2000). It is a highly hygroscopicity polymer (Callahan et al., 1982), for which the use of aqueous components in the processing of PVP based solid dispersion might be not desirable. This is because the residue of moisture could possibly promote the initiation of a re-crystallization process which causes physical instability of the solid dispersion product (Khougaz and Clas, 2000). Hence, an aqueous or solvent free processing method such as HME process (Khougaz and Clas, 2000) will be favourable for the production of a physically stable PVP-based SD.

As discussed in Chapter 1.5, many studies have highlighted the ability of HME to produce highly stable product. Therefore there is a good potential in coupling the hygroscopic PVP polymers and HME for the production of a physically stable end product.

In this study, PVP polymer and its derivative co-polymer were chosen as the main carriers in the HME processes. The main properties of PVP polymers (including both homopolymer and co-polymer) and its current status in the production of amorphous SD system will be introduced in the next few paragraphs.

2.2.2.1. Homopolymer PVP

PVP, also known as Povidone, is a class of water soluble polymers (Kibbe, 2002) which has been classified into a group of extremely hygroscopic substances by Callahan et al. (1982). Its hygroscopic nature is attributed to the electronegative groups of the carbonyl in the pyrrolidone structure that are able to form hydrogen bond with water. Besides, PVP is frequently incorporated as a hydrophilic carrier in SD formulation due to its ability to increase wetting of poorly soluble API and may eventually increase the bioavailability of the API (Tantishaiyakul et al., 1999, Khougaz and Clas, 2000, Leuner and Dressman, 2000). Figure 2.7 displays the repeating unit of the PVP homopolymer.

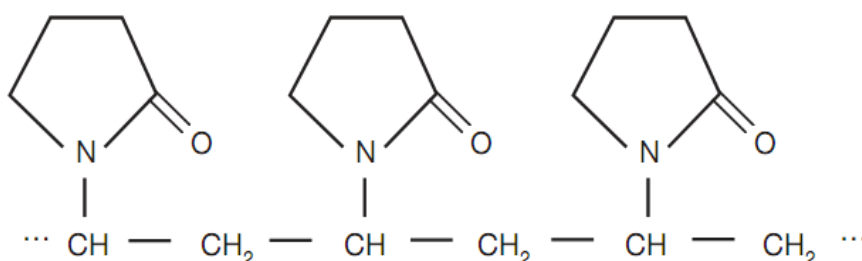


Figure 2.7: Chemical structure of soluble polyvinylpyrrolidone (Kibbe, 2002)

There are different grades of PVP homopolymers which are grouped according to their viscosity in 1% w/v of PVPs solution by K values via Fikentscher's equation (Kibbe, 2002). A higher K value is related to a higher viscosity of the PVP solution. Table 2.7 and Table 2.8 outline the different grades of PVP available commercially and the relationships between their K values and molecular weight of PVP, respectively.

Table 2.7: Grades of PVP available on the market (Kibbe 2002)

Povidone grades	Trade names	Manufacturer
Povidone K12 *	Kollidon ® 12 PF, Plasdone ® K-12	BASF, ISP
Povidone K17 *	Kollidon ® 17 PF, Plasdone ® C-15	BASF, ISP
Povidone K25	Kollidon ® 25, Plasdone ® K-25	BASF, ISP
Povidone K30	Kollidon ® 30, Plasdone ® K-29-32	BASF, ISP
Povidone K90	Kollidon ® 90F, Plasdone ® K-90	BASF, ISP
	Plasdone ® K-90 D**, Plasdone ® K-90 M**	ISP

*endotoxin or pyrogen free grades; **D=densified, M=milled

Kollidone ® is a registered trademark of BASF AG, Ludwigshafen, Germany

Plasdone ® is a registered trademark of ISP Investments Inc., Wilmington, Delaware, USA

Table 2.8: Average molecular weight (M_v) of various grades of PVP polymer which are calculated from the K-value, i.e. viscosity of 1 % polymer solution (Kibbe 2002)

Povidone grades	M _v calculated from the nominal K-value	M _v calculated from the K-value range given in Ph.Eur.
Povidone K 12	3900	2600-5500
Povidone K 17	9300	7100-11000
Povidone K 25	25700	19300-31100
Povidone K 30	42500	31700-51400
Povidone K 90	1100000	790000-1350000

PVP has been reported to have good stabilizing effects on amorphous pharmaceutical API. It acts by inhibiting and retarding the recrystallization process of API via formation of polymer network around the crystal surface or between the drug molecules (Tantishaiyakul et al., 1999) which limits the molecular mobility of the API (Khougaz and Clas, 2000, Sekikawa et al., 1978).

API-PVP interaction such as hydrogen bond and dipole interactions between API and PVP polymer is reported to be another possible stabilizing effect of PVP (Tantishaiyakul et al., 1996). In this context, the proportion of PVP is reported to be important for the optimum hydrogen bond interaction between the API and PVP as orientation of the proton donor and acceptor would assist in the hydrogen bond interaction of API-PVP (Tantishaiyakul et al., 1996, Khougaz and Clas, 2000).

Crystallization inhibition could also be linked to the anti-plasticizing effect of PVP and amorphous API. The incorporation of PVP may increase the overall T_g of the SD system by creating a thermodynamically barrier to retard the recrystallization process or alter the favourable pathway of recrystallization of the API (Hancock and Zografi, 1997), thus reducing the overall recrystallization tendency of API.

To summarise, stabilizing effects of PVP in a SD formulation include:

- Physical hindrance of the polymer chains folded around the API molecule which reduces molecular mobility of API
- The formation of hydrogen bond interaction between the proton donors of API and the proton acceptors of PVP (N and carbonyl site) which reduce both the nucleation rate and crystal growth
- Increase glass transition temperature, T_g and crystallization temperature (T_c^{obs}) of final blend for better storage ability.

Choice of PVP homo-polymer for HME

In the context of HME, different grades of PVP might lead to a different result in processibility, dissolution, API-drug interactions and recrystallization of drug.

In this study, high grades of PVP polymer, e.g. PVP K90, were not employed due to the potential problems in its processing. PVP K90 possess a high T_g values (174 °C) close to its degradation temperature (180 °C), which make it not suitable to be processed in HME process. Besides, PVP K-90 solution was reported to be highly sticky (Tantishaiyakul et al., 1999). This stickiness effect might be worsening under the hot and solvent free process of HME method.

Furthermore, the commercial product of high MW of PVP such as PVP K90 are commercially prepared via roller dried manners which resulted in non-spherical particles (Kibbe, 2002). This leads to the high fraction of the non-spherical particle in high MW of PVP which might affect the flowability of its powder form during the feeding step of HME processes (Kibbe, 2002). In order to get a good flowability through the HME hopper, material with spherical particles is preferred, i.e. PVP K30 and its lower MW polymer which are commercially prepared via spray drying method that give rise to spherical hollow structure (Schilling et al., 2008, S.Craig Dyar, 2007, Luker, 2007).

In terms of physical stabilization, a study carried out by Khougaz and Clas (2000) reported that PVP K90 was not superior to PVP K30 in inhibiting the recrystallization of API (Khougaz and Clas, 2000). According to that study, the stabilization ability of PVP polymer against

recrystallization of API was found to be in the order of, PVP K90 \approx PVP K30 > PVP K17 > PVPVA > PVP K12 (Khougaz and Clas, 2000). Therefore, in this study, the investigated homopolymers were PVP K30, PVP K17 and PVP K12 with the exclusion of PVP K90 based on its limited advantage in a SD system and potential problematic usage in HME process.

2.2.2.2. Co-polymer PVPVA 6:4

PVPVA 6:4 is a derivative of PVP which is fabricated via free radical polymerization with 6 parts of N-pyrrolidone and 4 parts of the lipophilic vinyl-acetate in 2-propanol. Figure 2.8 demonstrates the chemical structure of the repeating unit of PVPVA (Bühler, 2005).

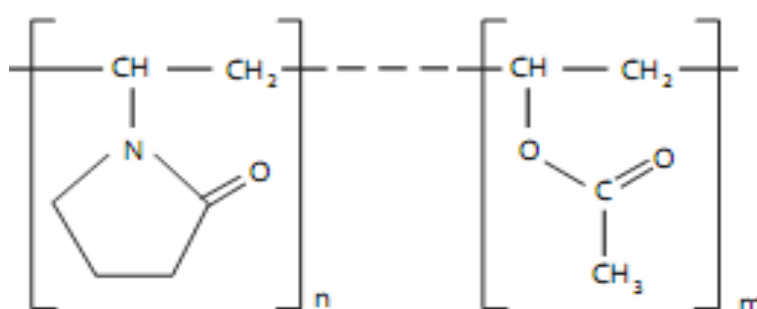


Figure 2.8: Chemical structure of the repeating unit of PVPVA (Bühler, 2005)

As with the PVP homopolymer, PVPVA 6:4 is mainly used as a binder for the production of granules and tablets as well as film forming agent for coating tablets (Kolter et al., 2010). It was produced to address the drawbacks encountered by the homopolymer PVP, namely that the homopolymer may be too viscous and hygroscopic for many applications. The 40% replacement of the lipophilic vinyl-acetate functional group makes this co-polymer to be relatively less hygroscopic and less viscous which has resolved some processing and handling problems of the homopolymer system.

A few researchers have compared the advantages of this newly derived co-polymer (PVPVA 6:4) with the homo-polymers, where PVPVA 6:4 appeared to be not always advantages in the physical stabilization and dissolution enhancement of the SD as compared to the use of homopolymer carrier in a similar system (Matsumoto and Zograf, 1999, Kanaujia et al., 2010, Ghebremeskel et al., 2006, Ghebremeskel et al., 2007).

Matsumoto and Zograf (1999) have found that PVPVA 6:4 did not offer additional advantages in physical stabilization of INDO in its SD system at 30 °C, 0% RH (Matsumoto and Zograf, 1999). Furthermore, *in vitro* dissolution studies carried out by Kanaujia et al. (2010) revealed that PVP 17 is more efficient than PVPVA 6:4 in inhibiting particle growth upon dissolution (Kanaujia et al.,

2010). Conversely, the use of PVPVA 6:4 carrier in a HME API -surfactant SD was found to have a faster dissolution profile than the corresponding formulation using the homo-polymer as its carrier, i.e. PVP K 30 (Ghebremeskel et al., 2007). The authors relate the results to the processing condition whereby higher Tg of the homo polymer, PVP K30, requires a much higher extrusion temperature which could potentially resulted in degradation of the added surfactant (Ghebremeskel et al., 2007). As a result, the superiority of the co-polymer PVPVA 6:4 as a HME SD carrier as compared to the homo polymer PVP remains uncertain. This uncertainty will be further studied by incorporating PVPVA 6:4 as one of the investigated carrier system in this study. Table 2.9 lists the main properties of PVPVA 6:4 used in this study.

Table 2.9: Physicochemical properties polyvinylpyrrolidone vinyl acetate (PVPVA 6:4)

Polyvinylpyrrolidone vinyl acetate	Properties	References
Appearance	White to creamy free flowing powder	(Ashland, 2012)
Molecular weight	≈ 47000 g / mol	(Ashland, 2012)
K value	26-29 (1% in water)	(Bühler, 2005)
Glass transition temperature	109 °C	(Ashland, 2012)
Bulk density	0.3 g / cm ³	(Ashland, 2012)
Solubility	<ul style="list-style-type: none"> ➤ Soluble up to 50% in water, ethanol, isopropanol, methanol up to n-butanol. Soluble up to 10% in methylene chloride, glycerol and propylene glycol ➤ Less soluble in ether, cyclic, aliphatic and alicyclic hydrocarbons 	(Bühler, 2005)

2.2.3. Raw Material Sourcing

Table 2.10 lists the APIs, polymer carriers and other materials used in this study and the sources of each product.

Table 2.10: Sources of materials employed in this study

Categories	Substances	Sources
Model drug	PCM	Rhodia Organique, BN: 0312536
	CAF	Acros Organics (New Jersey, USA)
	NAP	AFINE Chemical LTD, BN: 106032456
	KTP	AFINE Chemical LTD, BN: 1102017
	INDO	Signa Aldrich, BN: 115k0689, Italy
	OZP	BN: 20080901, China
Carrier	PVP K29-32	ISP (Switzerland) A.G., Lot: 05000243915
	PVP K17	ISP (Switzerland) A.G., Lot: 05000250512
	PVP K12	ISP Technologies, Inc Lot: 05000242592
	PVP S-630 (PVPVA 6:4)	ISP Technologies, Inc Lot: 05000241890
	Tween 80	Sigma Aldrich, USA
DSC calibrants	n-Octadecane	Fluka, Sigma Aldrich, USA
	Tin	Aldrich Chemical Company, Inc, Lot: HZ02912HZ, USA
	Sapphire disc	TA Instrument
DSC & TGA calibrants	Indium	Aldrich Chemical Company, Inc, BN:05112MU, USA
DVS calibrant	Sodium Bromide	Sigma Aldrich, Lot: SZBB1170V, Germany
Salts used for stability test	Sodium Chloride	Fischer Scientific, UK
	Magnesium nitrate hexahydrate	Fluka, Lot: 1377926, Germany
	Calcium chloride	BDH Laboratory supplies, Lot: A265200 124, England
	Potassium Acetate	Alfar Aesar, Lot: 10152143, UK
	Phosphorus pentoxide	Alfar Aesar, Lot: 10160482, Great Britain
Dissolution test	Hydrochloride Acid	Sigma Aldrich, Lot: SZBB2230V, Germany
	Sodium dihydrogen orthophosphate monohydrate	Fischer Scientific, BN: 0936146, UK
	Sodium phosphate monobasic monohydrate	Sigma Aldrich, Lot: BCBC2211, Japan
	Micro-filter cellulose membrane, 0.45 µm	Sartorius Stedim biotech GmbH, Germany
	Micro-filter polyvinylidene fluoride (PVDF) membrane, 0.45 µm	MILIPORE, Lot: RISA50559K, Ireland
	Distilled water	

2.2.4. Summary of the properties of raw materials

Table 2.11 displays melting and glass transition temperatures of model APIs and glass transition temperatures of the amorphous PVP polymers.

Table 2.11: Melting and glass transition temperatures of model APIs and carriers employed in this study

Components	T _g (°C)	T _m (°C)	References
Paracetamol	≈25	Form I = 169-172	(Qi et al., 2008a, Baird et al., 2010, Di Martino et al., 1997, Di Martino et al., 1996)
Caffeine	≈-13	234-239	(Kishi and Matsuoka, 2010, Descamps et al., 2005a)
Ketoprofen	-5.61	94.6-94.9	(Malaj et al., 2010, Baird et al., 2010)
Naproxen	-6 to -3	155 – 156	(Gashi et al., 2009, Malaj et al., 2010, Mura et al., 2003)
Indomethacin	≈ 43.1	γ form = 161 °C	(Baird et al., 2010, Crowley and Zografis, 2002, Sivert et al., 2009)
Olanzapine	68 °C	194.47	(Freitas et al., 2012, Krishnamoorthy et al., 2012)
PVP K12	120		(ISP Pharmaceuticals, 2007)
PVP K17	126		
PVP K29-32	164		
PVPVA 6:4	109		

2.3. Preparation of solid dispersion : Hot Melt extrusion

Hot melt extrusion is the main manufacturing method of the SD systems used in this study, where the HAAKE Minilab intermeshing twin screw extruder was used to prepare all the PVP based-SD systems. Figure 2.9 presents the extruder used in this study, i.e. HAAKE MiniLab II Micro Compounder.



Figure 2.9: Hot Melt Extruder of Thermo Scientific HAAKE MiniLab II Micro Compounder

The basic principle and the processing zones of this manufacturing method have been described in Chapter 1.4.1. In this section, attention will be paid to the processing parameters of the HME methodology. There are several parameters that need to be considered in order to obtain an acceptable SD extrudate. These include extrusion temperature, torque, screw speed and residence time, which will be further discussed in each of the sub-section below.

2.3.1. Extrusion temperature

The extruder is preheated prior to extrusion process (McGinity et al., 2006). The extrusion temperature should be monitored before each extrusion process in order to ensure the consistent batch to batch production of SD (Stuart J.Kapp, 2007).

The processing temperature can influence the physical and mechanical properties of the obtained extrudates. Crowley et al. (2004 b) suggested that higher processing temperature promotes the formation of guaifenesin-ethyl cellulose SD with less porous matrix which leads to the slower release of guaifenesin. In other studies, attempts were made to demonstrate the influence of temperature control on HME extrudability. The relationship was given by the Equation (2.1),

$$\eta = K' e^{-\frac{Ea}{RT}} \quad (2.1)$$

where η is viscosity, K' is a constant, Ea is the activation energy of melt flow, R is universal gas constant and T is temperature (DiNunzio et al., 2009). Based in Equation (2.1), viscosity of the softened polymer is dependent on the employed temperature. As the extrusion temperature increases, the viscosity of the molten material will decrease which results in better flowability of the molten material (Schilling et al., 2008).

The commonly employed extrusion temperatures are recently reviewed and categorized into two regimes (Shah et al., 2012). Firstly is miscibility regime where $T_{\text{process}} > T_m$ of the API. In the miscibility regime, miscibility of the API and polymer is an important factor in dictating the production and stabilization of amorphous solid dispersion. Secondly is solubilisation regime where the $T_{\text{process}} < T_m$. In this regime, the production of amorphous solid dispersion is mainly depending on the solubilisation of the API into the melted carrier at a certain extrusion temperature (Shah et al., 2012). This regime could be understood by using the well-known Noyes Whitney equation (2.2) (Noyes and Whitney, 1897, Liu et al., 2010).

$$\frac{dM}{dt} = A \times \frac{D}{h} (C_s - C_b) \quad (2.2)$$

where M is the mass, t is the time, A is the total surface area of the drug exposed to the dissolution medium, D is the diffusion coefficient (m^2/s), h is thickness of the diffusion layer and C_s and C_b is the solubility and concentration of the solute, respectively, in the bulk solution which is the softened molten polymer in the hot melt extrusion process. Each of the parameters in Equation (2.2) could be manipulated in order to achieve a better solubilisation of the API in its carrier during extrusion process. Longer residence time of the molten mixture could lead to a better solubilisation of the

API into its carrier during the extrusion process. The increase of API solubility in this regime could also be achieved by increase the diffusivity of the API while extrusion. For instance, additions of plasticizers or shear force by incorporating of kneading paddle will lead to reduction of molten viscosity; thereby enhance the diffusivity and dissolution of the API into its carriers.

2.3.2. Screw Speed

Control of screw speed can impact on the material viscosity by mechanical shearing and affect the degree of mixing of components in the HME barrel (Stuart J.Kapp, 2007, Lyons et al., 2008). Besides, the screw speed adjustment can also have an impact on stability of the polymer. A study by Crowley et al. (2002) indicated that higher screw speed during HME processing may decrease polymer degradation by lowering its residence time in the hot barrel. On the other hand, a high screw speed of HME processing may cause mechanical degradation of polymer such as melt fracture (Crowley et al., 2002b).

Other researchers have also reported that good control of screw speed could increase material transit and reduce the residence time of material in HME barrel which bring a benefit for thermo sensitive components (DiNunzio et al., 2009). In that study, process modulation such as increasing the extrusion temperature and screw speed was carried out to access its impact on the residence time of the molten extrusion. To do that, a tracer dye was added to the formulation to allow visual determination of material transit. Figure 2.10 illustrates the relationship of screw speed, extrusion temperature and residence time of the molten extrusion of hydrocortison in Kinetisol[®] studied by DiNunzio et al. (2009).

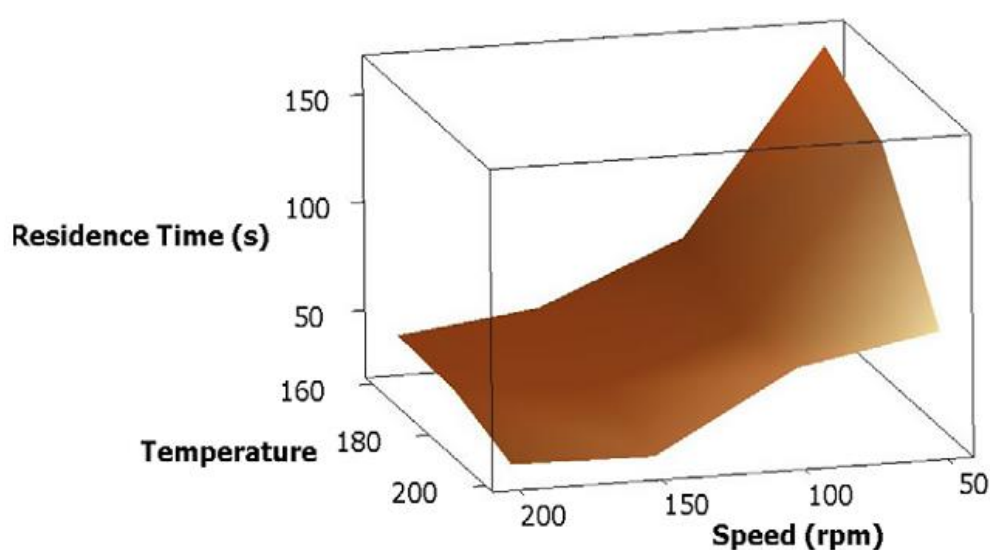


Figure 2.10: The changes of molten residence time as a result from process modulations during HME of binary hydrocortison and Kinetisol[®], i.e. screw speed and extrusion temperature (adopted from reference DiNunzio et al. 2009)

According to Figure 2.10, increases in temperature and screw speed will cause reductions of residence time. At lower screw speeds, a more pronounced effect of temperature on screw speed was observed due to the higher viscosity of the material. However at a higher screw speeds, the residence time of the molten system was less affected due to the low material viscosity (DiNunzio et al., 2009). Thus, DiNunzio et al. (2009) suggested that the residence time of a molten material in a HME barrel could be determined by manipulating the screw speed and extrusion temperature.

2.3.3. Torque

Motor load also known as torque is generally described as a measure of resistance registered by materials to a processing system. These resistances include the viscosity, elasticity, shear sensitivity or temperature sensitivity as indicated by the response of a material to its thermal profile during processing (Martin, 2007).

In the case of HME, torque is a measure of resistance exerted by melt viscosity in the barrel which represents the rate of movement of polymer chains relative to each other, i.e. chain flexibility (Wu and McGinity, 2003). It could also be used as an indicator for batch differentiation or influence of additive such as plasticizer and lubricant on drug-polymer blend (Verreck et al., 2005, Verreck et al., 2006b). An unsteady torque may indicate inconsistent feeding or arching at the feed throat or inadequate speed control (Stuart J.Kapp, 2007). Therefore monitoring the torque is critical for identifying processability as well as quality control of the system during processing. The relationship between torque and other processing conditions such as extrusion temperature and screw speed was also studied by DiNunzio et al. (2009). Figure 2.11 shows the changes of torque as a result from process modulations (screw speed and extrusion temperature) during HME of binary hydrocortisone and Kinetisol[®].

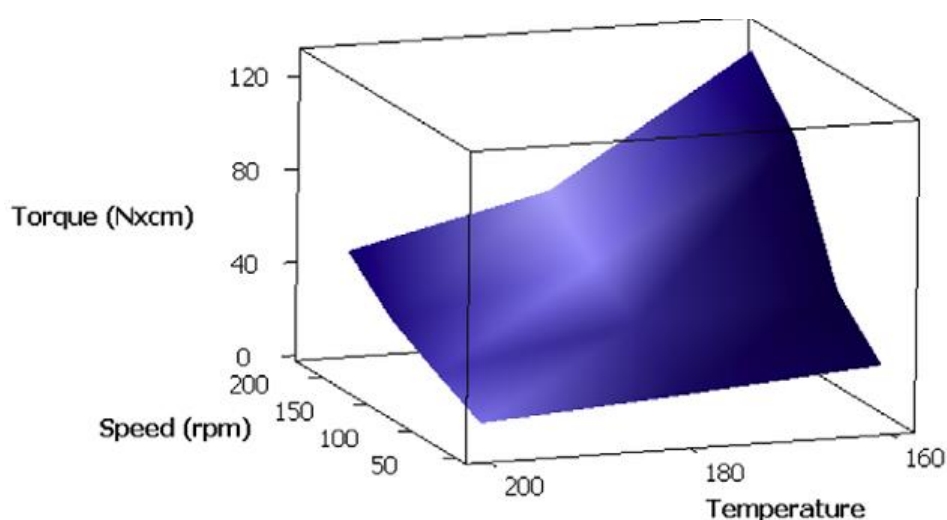


Figure 2.11: The changes of torque as a result from process modulations during HME of binary hydrocortisone and Kinetisol[®], i.e. screw speed and extrusion temperature (adopted from reference DiNunzio, et al. 2009)

According to Figure 2.11, as the temperature increases, material flow was improved due to a reduced viscosity of the melt. However, increases in screw speed result in the increase of torque values. Since the value of torque is proportional to viscosity, the increment of this parameter can be correlated with the non-Newtonian behaviour of the molten material (DiNunzio et al., 2009). Thus, the flow characteristic of the material within the extruder is a function of extrusion temperature and rotational speed.

For the ease of processing, the torque value should not be too high. Thus, in the design of hot melt extrusion equipment, a monitoring device is set up with an alarm or interlock to create alarming alert and automatic shutdown of extruder when the maximum torque is achieved (Verreck et al., 2006b, Dreiblatt, 2007a, Schilling et al., 2010).

Parameter used in this study

In this study, the extrusion temperatures used were adjusted based on the T_m and T_g of the APIs and polymers. Due to the concern of PVP degradation, the overall extrusion temperature of not more than 180 °C was used. The screw speed of 100 rpm was kept constant for all the prepared formulations.

During the extrusion process, torque was recorded as a dependent variable of the resistance of flow and viscosity of the molten material. The obtained extrudates were transported out from the die through a conveyer belt (as shown in Figure 2.12), cooled in ambient condition and then collected into sample tubes.

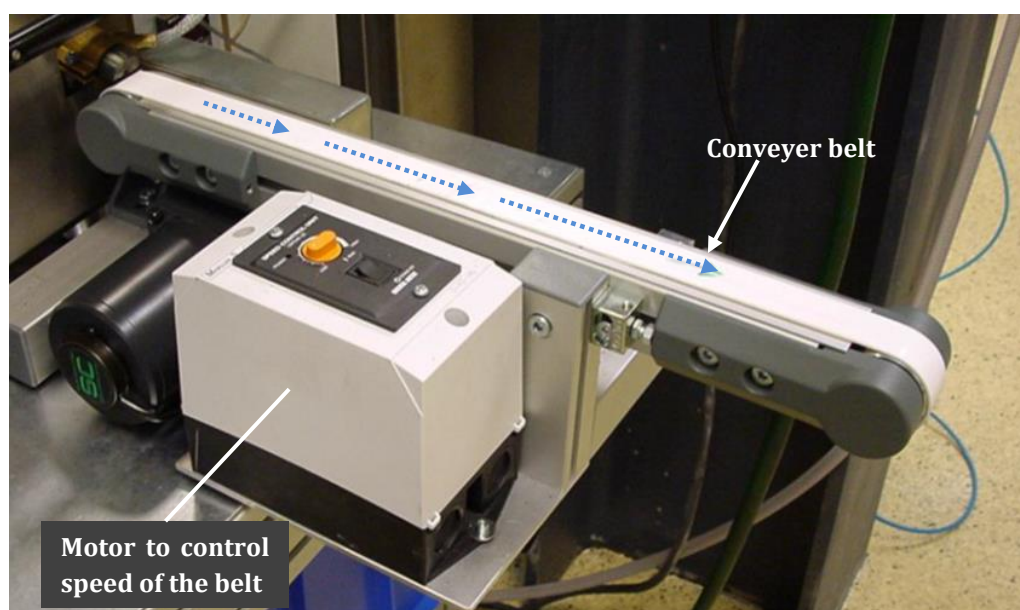


Figure 2.12: Conveyer belt used to collect the extruded material from the HME die

The HAAKE Minilab twin screw extruder enables the circulation of molten materials in the hot barrel before extrusion of the molten mass on activation of the extrusion valve. Therefore, the residence time of the molten mass could be controlled. Table 2.12 lists the parameters used for the production of HME systems.

Table 2.12: Parameter used in the production of HME systems

Formulations (HME % w/w API-carrier)	T _m (°C)	T _g (°C)	Extrusion temperature (°C)	Screw speed (rpm)	Residence time (minutes)
HME 20-70% PCM PVP K29-32	169-172	164	120	100	5
HME 20-50% PCM PVPVA 6:4	169-172	109	120	100	5
HME 10-20% CAF PVP K29-32	234-239	164	155	100	5
HME 10-20% CAF PVPVA 6:4	234-239	109	180	100	5
HME 30-50% PCM PVP K12	169-172	120	160	100	5
HME 30-50% PCM PVP K17	169-172	126	160	100	5
HME 30-50% PCM PVP K29-32	169-172	164	160	100	5
HME 30-50% PCM-PVP PVPVA 6:4	169-172	109	160	100	5
HME 30% KTP PVPVA 6:4	94.6-94.9	109	120	100	10
HME 30% INDO PVPVA 6:4	161	109	160	100	10
HME 30% OZP PVPVA 6:4	194.47	109	180	100	10
HME 10-40% NAP PVPVA 6:4	155 – 156	109	150	100	10
HME 30% NAP PVPVA 6:4+ 2% Tween 80	155 – 156	109	150	100	10
HME 30% NAP PVPVA 6:4 + 10% Tween 80	155 – 156	109	150	100	10
HME 30% NAP PVP K12	155 – 156	120	150	100	10
HME 30% NAP PVP K17	155 – 156	126	150	100	10
HME 30% NAP PVP K29-32	155 – 156	164	150	100	10

* T_m values of model drug were summarised from literature. Please refer to the references of model drug in section 2.2.1 (Table 2.1-2.6). Values of T_g were obtained from the suppliers (ISP Pharmaceuticals, 2007).

2.4. Characterization techniques

2.4.1. Differential scanning calorimetry

Differential scanning calorimetry (DSC) is a technique used for measuring the energy needed in establishing a zero temperature difference between the sample and its reference material. It has been used widely in analysing thermal properties of pharmaceutical materials. Both qualitative and quantitative information could be extracted such as physical and chemical changes of the tested components which involving endothermic, exothermic processes and heat capacity changes of the components upon temperature change (Craig and Reading, 2007).

There are two types of DSC instruments i.e. power compensation DSC and heat flux DSC. In power compensation DSC, the temperature of the sample and reference are made identical by adjusting the power input to two separate furnaces. The change of the power input is a measure of changes in heat capacity or enthalpy of the sample in relative to the reference. On the other hand, heat flux DSC uses only one furnace. In the furnace, sample and the reference are placed on separate crucibles linked by a low resistance heat flow path. The temperature between the sample and the reference are made identical by supplying heat flux (Bhadেশia, 2002). By using the heat flux DSC, any thermal event of the sample that causes the use of heat or release of heat will be recorded as a function of heat flux supply in maintaining an identical temperature between the sample and reference. The differential heat flux for these processes are monitored by thermocouples and recorded as a function of enthalpy and heat capacity changes.

In a conventional DSC, the temperature of the furnace is raised and lowered in a linear fashion. However, there will be difficulties in data interpretation when multiple thermal events of a multi-components system occur at a same temperature in the scanning by using the linear temperature programmer of DSC. To solve the complex interpretation, modulated DSC (MTDSC) was introduced which will be further introduced in the next paragraphs.

In MTDSC, a sinusoidal modulation of temperature program is overlaid on a linear temperature ramp (Gill et al., 1993). With the modulation, the heating rate is no longer constant but varies in a periodic fashion (modulated) of its minimum and maximum values. However, the average heating rate (which is also termed as underlying rate) is the same as conventional DSC. The underlying heating rate, period and amplitude of the superimposed temperature wave determine the range of modulation. The heat flow effect of these parameters is represented by Equation (2.3) (Gill et al., 1993):

$$\frac{dQ}{dt} = -\frac{dT}{dt} [Cp + f'(t, T)] + f(t, T) \quad (2.3)$$

where dQ/dt = heat flow out of the sample, dT/dt = heating rate, C_p = heat capacity of sample, t = time, T = temperature, $f^*(t,T)$ = thermodynamic heat flow component and $f(t,T)$ = kinetically-limited heat flow. From the equation, heat flow components of MTDSC are divided into two. The first term of the right hand side is the function of heat capacity and rate of temperature change which is also known as reversing signal. The heating rate dependent thermal event will be revealed in this part of the signal such as glass transition event. The second term is a function of absolute temperature and time. For absolute temperature dependent transition, once initiated cannot be reversed by cyclic modulation of temperature change and is also known as non-reversing signal. These transitions include enthalpic relaxation, crystallization, evaporation, decomposition and cure (Gill et al., 1993).

In the current study, the thermal properties of the raw materials and formulations were mainly studied by using modulated DSC (Q2000, TA Instrument, Newcastle USA). Samples were weighed accurately (1 to 3 mg) into pinhole aluminium pans (Perkin Elmer) to allow the removal of excessive moisture in the sample in order to minimize influence of water content on the sample's properties. Temperature and cell constant calibration of DSC were performed using indium, n-octadecane and tin. Heat capacity in modulated mode was calibrated with an aluminium oxide sapphire disc provided by TA instruments. The heating rate was 2 °C per minute, 60 sec for the modulation period and ± 0.318 °C for the amplitude or otherwise specified. T_g of the samples were determined from half height of the glass transition event (please refer to Figure 1.2 for half-height of T_g) using the TA propriety software, i.e. Universal Analysis. High-speed standard mode DSC (Q2000, TA Instrument, Newcastle USA) was also used; the details of this method will be covered in Chapter 4.

2.4.2. Thermogravimetric Analysis

Thermogravimetric analysis (TGA) measures the changes of sample weight caused by the chemical or physical processes as a function of temperature or isothermally as a function of time (Craig and Reading, 2007). In the pharmaceutical field, it is often used to detect dehydration, water content and chemical decomposition of solid drugs and pharmaceutical excipients. In the current study, TGA were mainly used for the detection of thermal decomposition temperature as well as water content of raw material and solid dispersion samples.

All TGA experiments were carried out using TGA Q5000 (TA Instruments, Newcastle, USA) to detect the mass changes due to either water loss or decomposition of samples. To effectively identify moisture content, samples were heated from room temperature up to 100 °C at heating rate

of 10 °C per minute and held isothermally for at least 15 minutes before continuing the heating ramp up to 300 °C.

2.4.3. Attenuated total reflectance-Fourier transfer Infrared

Infrared (IR) spectroscopy is a reliable and well-recognized technique for characterizing and analysing a wide range of solids, liquids and gases. When a sample is exposed to an infrared beam, the electric field of the radiation will interact with the electric field generated by the varying dipole of molecules in the sample. These vibrations of molecules (symmetric and a symmetric stretching, bending, rocking, twisting and wagging mode) interact with an electromagnetic wave that matches their frequency of oscillation. Consequently, different functional groups of a molecule absorb the different characteristic frequencies of IR radiation (Sherman Hsu C.P., 1997). The IR radiation, after passing through the sample, is detected and transformed by the spectrometer into a spectrum which reflects the molecular structure. IR information is generally presented in transmittance or absorbance intensities at y-axis versus wave number as the x-axis.

Due to the complication of sample preparation (especially solid sample) in the conventional IR instrument, an attenuated total reflectance (ATR) accessory was utilized. The ATR operates by measuring the changes in a totally internally reflected the IR radiation when the beam is exposed to the sample. The reflectance radiation protrudes only few microns (effective path length) beyond the surface of the crystal (approximately 6 μm) (Larrabee and Choi, 1993). Thus, it is important to have a good contact between the sample and the surface of ATR crystal. This method has reported to be useful due to its non-invasive sample preparation, the small amount of sample required, fast sample preparation and measurement as well as possibility of interfacing with other instruments (Oberg and Fink, 1998, Vrettos and Meuse, 2009).

In this study, attenuated total reflectance-Fourier transfer infrared (ATR-FTIR) was mainly employed to analyse the difference in the peak positions of certain chemical functional groups between the raw API, PM sample, the freshly prepared HME samples and aged HME samples. Infrared spectra of these samples were recorded in the wavenumber range of 4000 to 500 cm^{-1} using IFS-60/S Fourier transform infrared (Bruker Optics, Coventry, UK) with an ATR accessory fitted to a heating system (SPECAC, Orpington, UK). Samples were scanned with a total of 64 scans at resolution 2 cm^{-1} . Spectra were analysed using OPUS software (version 6.0, Bruker Optics, Coventry, UK).

2.4.4. Hot stage microscopy

Hot stage microscopy (HSM) is an optical microscopic method fitted with hot stage accessory. It is often used as a complementary tool to provide corroborating data on melting points, recrystallization, volatilizations, solid-solid transformation, decomposition and etc (Craig and Reading, 2007). During the thermal events, the sample is observed as a function of temperature and time and the appearance recorded by a high resolution color video camera via collection of successive frames.

In this study, polarized light was used to discriminate the crystalline material via birefringence from the amorphous counterpart which does not reveal birefringence. HSM were performed with heating rate of 10 °C per minutes from room temperature up to the thermal event of interest or otherwise specified. The investigated material was placed in the hot stage accessory and placed on the microscope stage. Without the hot stage accessory, it could also be used as an optical microscope, in which only the photography or video microscopy was utilized for the collection of videos or images.

2.4.5. X-ray Powder Diffraction

X-ray is a short wavelength of electromagnetic radiation. It is mainly used for determining the atomic or molecular structure of a crystalline material and quantification of amorphous content in partially crystalline mixture (Du et al., 2011).

A solid matter can be described as crystalline when the molecules are arranged in regular manner by repetition in three dimensions. When an X-ray is exposed to an atom, electron surrounded the atom will be oscillated in the same frequency as the incoming beam. For a crystalline matter, due to regular pattern of the atoms, there will be constructive interference specific to the way of atom arrangement within the crystalline structure. The well-defined X-ray beam will leave the sample at various directions and intensities over a range of incident angle brought about by the periodic arrangement of the atoms / planes. The positions of the diffracted peaks are expressed as Bragg's angle, θ and interplanar spacing d_{hkl} between the diffraction planes. These parameters could be defined by Bragg's law according to Equation (2.4),

$$n\lambda = 2d \sin \theta \quad (2.4)$$

where λ is the wavelength of the diffracted X-ray, d is the interplanar spacing of the diffracting planes and θ is the incidence angle of the X-ray beam (Bandyopadhyay et al., 2005). Conversely,

the atoms of amorphous are randomly distributed or disorder. There is no constructive interference and no resultant energy leaving the sample. Hence, no diffracted peaks would be expected.

There are two types of X-ray instruments, one being single crystal diffractometer and the other is powder diffractometer. Single crystal diffractometer is usually used to elucidate the molecular structure of a compound; whereas the powder application (XRPD) is used for “finger print identification” of a solid matter. Since there is no long range three-dimensional molecular order associated with amorphous system, X-ray Powder diffraction was applied in this study to distinguish crystalline solid from amorphous solid (Scintag Inc, 1999).

X-ray Powder Diffraction analysis of raw materials, PMs and ground HME extrudates were performed with a XRPD, Thermo ARL Xtra model (Switzerland) equipped with a copper X-ray Tube (1.540562 Å). Samples were pressed into a sample holder to generate a flat and smooth plane surface. The samples were then exposed to an X-ray beam with voltage of 45 kV and a current 40 mA. All XRPD experiments were performed at step scan of 0.01° and 1 second for every step. The scanning range is based on the characteristics peaks of the APIs employed in different studies which will be further detailed in each chapter.

2.4.6. Scanning electron microscopy

Scanning electron microscopy (SEM) is a microscopic technique utilizing electron beam in collecting the micrograph. The electron beam was generated via heating a ‘hairpin’ tungsten filament until the electrons are emitted in the electronic optic column. Then the electrons are accelerated at 5-20 kilo voltage at typical working distance of 10 mm. At the same time, the electrons was also demagnetized and focused into a finely focus beam which bombards the sample. While the traverses of the primary electrons beam, secondary electron emitted from the sample surfaces is collected by the electronic console and then figured into the SEM image of the samples (Welton, 1984).

The SEM instrument employed in this study was JSM 5900LV Field Emission Scanning Electron Microscope (Jeol Ltd, Japan) fitted with a Tungsten filament. It was used to investigate surface morphology of the freshly prepared sample, aged sample and the changes of sample appearance after dissolution processes. The fresh of aged extruded were cut into 3 - 4 mm. The cut sample was then attached to a SEM specimen stub (carbon). This step was carried out carefully with disposable gloves and tweezers in order not to introduce artefacts by scrapping the surfaces to be examined. Other samples such as raw API powder and PM of API-polymer were attached directly to the specimen stubs by double-sided tap. All the samples were coated with gold (thickness of 15nm) by

a Polaran SC7640 sputter gold coater (Quorum Technologies, city, country) prior imaging. After coating, the samples specimens were imaged in the highly vacuumed sample chamber equipped with electron optic column and electronics console.

2.4.7. Laser diffraction for particle size analysis

Laser diffraction is a widely used technique in measuring particle size of different physical forms of material such as powder, suspension and emulsion. It is a fast and precise technique for the measurement of a wide range of particle size.

When a sample passes through a broadened beam of laser light, particles scatter the light at an angle onto a Fourier lens. The diffracted laser light data of the analysed particles is a representation of particle size distribution. In this case, the intensity of the scattered light is inversely proportional to the particle size, i.e. large particles scatter the incident light at smaller angles with higher intensities while small particles scatter the incident light at wider angles with lower intensities. Figure 2.13 reveals the example of scattering off a spherical particle.

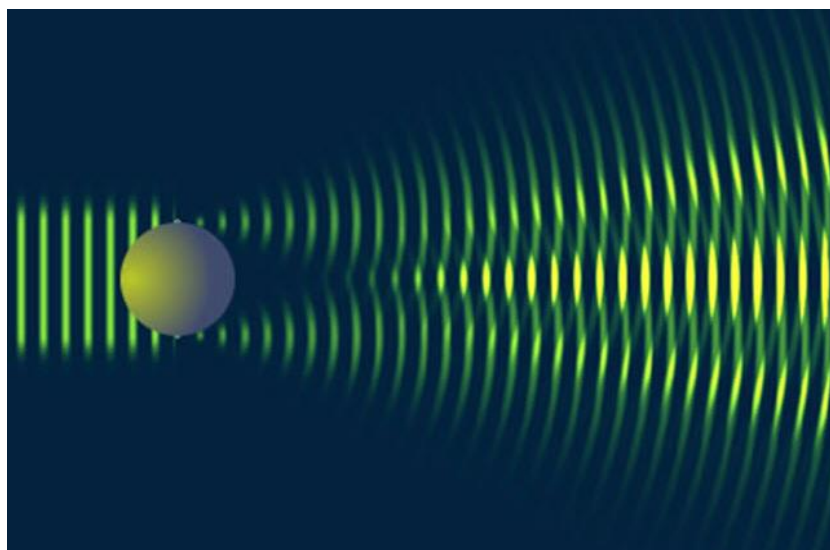


Figure 2.13: example of scattering off a spherical particle (HORIBA Scientific, 2013)

Laser diffraction measurement provides only particle size in an equivalent to volume diameter which assumes all particles to be spherical. Thus, this measurement did not reveal the particle shape of the scanned sample (Tinke et al., 2005). Moreover, this technique is generally used to detect particle larger than 1 μm due to the maximum angular intensity pattern of about 45 degrees (Tinke et al., 2008).

In this project, laser diffraction is used to monitor the particle size changes of the dissolving solid powder during dissolution. The collected sample solutions from dissolution bath was transferred into the quartz cuvette and measured by using Sympatec HELOS/BF (HI146, TYPE: cuv-50 mL / US, Germany) particle size analyser. Each sample was scanned 3 times using a lens of size detection range of 0.25 / 0.45 to 87.5 μm .

2.4.8. Contact angle measurement

Contact angle of a substance is a critical property for the evaluation of adhesion and wettability of the substance. In principle, the higher the contact angle, the lower the adhesion and wetting properties of the solid surface. The theoretical description of the contact angle stems from the relative balance between three different components of interfacial energies, i.e. γ_{lv} , γ_{sl} and γ_{sv} as shown in Figure 2.14 (Tavana and Neumann, 2007).

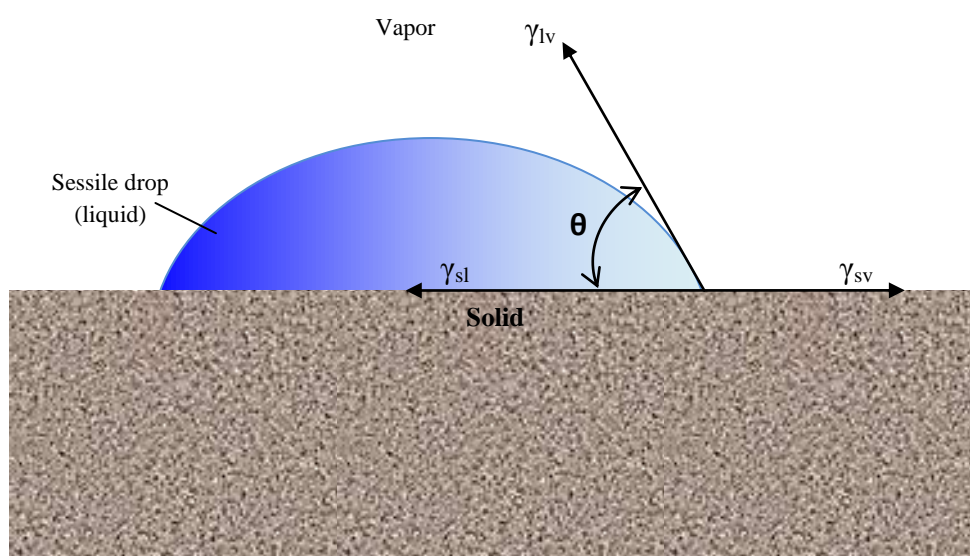


Figure 2.14: Schematic of a sessile drop, contact angle (θ), and the three components of interfacial tensions, i.e. γ_{lv} : liquid-vapor, γ_{sv} : solid-vapor and γ_{sl} : solid-liquid.

γ_{sv} is the solid–vapor interfacial energy, γ_{sl} is the solid–liquid interfacial energy, and γ_{lv} is the liquid–vapor interfacial energy (γ_{lv} is also known as the surface tension). The contact angle, θ is described by the three interfacial components through Young's Equation (2.5) (Young, 1804).

$$0 = \gamma_{sv} - \gamma_{sl} - \gamma_{lv} \cos \theta \quad (2.5)$$

Several methods have been introduced to assess the contact angle of a powder system such as Washburn's method and Wilhelmy plate technique. In Washburn's method, the measurement of the powder wetting is not straight forward as it could be potentially influence by the powder density, size and porosity of the powder bed (Dahlberg et al., 2008). The Wilhelmy plate technique is operated by gluing the powder onto the Wilhelmy plate and measuring the contact angle. However, in that method, the sample preparation can pose a major variable and the effect of the glue is not clear (Buckton et al., 1991, Dahlberg et al., 2008).

Hence, in this study, an indirect contact angle measurements in studying the wetting properties of the PM and HME systems were assessed macroscopically via drop shape analysis performed on a flat surface compressed from the powder materials (Swanepoel et al., 2000, Dahlberg et al., 2008). This method has been reported to be the most widely used method in assessing wetting properties of powder solid (Buckton et al., 1991). Besides, it was also described to be suitable for a reasonable wetting assessment of powdered system (Chibowski and Perea-Carpio, 2002, Chokshi et al., 2007, Dahlberg, 2010, Dahlberg et al., 2008)

In this study, the drop of medium (liquid phase) was saturated with the corresponding API with respect to the analysed surface of solid phase so that the liquid phase could not further dissolve the API on the surface of the solid phase. This is performed to avoid any possible alteration of the wettability study due the API dissolution into the liquid phase of the drop.

Surface tension of the liquid phase was determined via pendent drop measurement. Both the contact angles and surface tension measurements were determined with Theta Optical Tensiometer (zoom lens 0.7 magnifications) (Biolin Scientific, Finland). A liquid dispenser holder with manual control was used to create a drop. Then, OneAttension software was used to analyse the surface tension Young-Laplace surface properties mode. The changes of the surface tension were recorded up to 120 seconds at 1 frame per second.

In the contact angles measurement, a drop of the liquid phase which was pre-saturated with corresponding APIs was deposited on the flat surface of the compressed tablet. Changes of the contact angles at the first 120 seconds were recorded as a video at 6 frames per second for first 10 seconds and 1 frame per second subsequently. All measurements were performed at 25 ± 0.1 °C and 45% RH. All measurements were performed at 25 ± 0.1 °C and 45% RH.

The result of contact angle between a solid and liquid substances can be translated into surface free energy (SFE) information of the solid liquid interfaces by performing mathematical calculation such as using Young's equation (Żenkiewicz, 2007). SFE of a pharmaceutical API may be altered when an excipient is absorbed onto its surface. In this study, interfacial energies between the SD and dissolution medium were determined by using Fowkes method due to its convenient when

applied to polymeric system (Żenkiewicz, 2007). According to Fowkes, SFE of a solid or liquid is a sum of the free energy of the independent components within the solid or liquid associated with their specific interactions i.e. dispersion component and remaining non-dispersive component. At the interface between the two substances, Fowkes assumed that only the dispersive interaction appears. Thus, the assumption of applying this method is that this method is based on the independence and additivity of the dispersion and polar interactions, respectively (Żenkiewicz, 2007). Details calculation of interfacial energies using the Fowkes method was conducted in Chapter 6.2.6, Equation (6.1) to (6.4).

2.4.9. Atomic Force Microscopy

Atomic Force Microscopy (AFM) is a near-field technique which was used to analyse surface of solid or liquid up to atomic scale. The concept behind this technique is the generation of images of surfaces by measuring the physical interaction between a sharp tip / probe and the surface of a sample. The origin of the physical interactions of the tip / probe to the examined surface could be ionic repulsion, Van der Waals forces, capillary, electrostatic or magnetic force, as well as elastic / plastic deformation. These interactions is monitored by the tip / probe attached to a soft cantilever which acts as a spring, and measuring the bending (or deflection) of the cantilever of the tip / probe. AFM could be operated in various mode bases on the requirement of the experiment. These comprise contact mode and non-contact mode, i.e. tapping mode.

In this study, AFM was used to study the surface roughness of compacted tablets whereby the tablets were prepared using an IR press at 5 tons for 1 minute. The investigation of these surfaces was to ensure the comparable surfaces between the prepared tablets which will be utilized for contact angle measurement. AFM images were recorded by using a Veeco Caliber scanning probe microscope head (Veeco, CA) in contact mode. The scan areas for all the AFM images were 50 μm x 50 μm with a resolution of 512 pixels and scan rate of 0.5 Hz.

2.5. Dissolution studies

Dissolution studies are important for formulation development processes. Although there are limitations associated with *in vitro* dissolution process, when a dissolution test was performed correctly, it can provide valuable information and *in vivo* correlation regarding the bio-performance of a dosage form (Swanepoel et al., 2000). Moreover, it can also be used as a quality control tool in monitoring batch - to - batch consistency and manufacturing deviations (Azarmi et al., 2007).

2.5.1. The theory of dissolution

Dissolution of a solid matter is a process when the solid enter into a medium and dissolve into the medium. The dissolution of this solid matter is according to the relative affinity between the affinity of ‘solid molecule - solid molecule’ in the solid substance and the affinity of ‘solid molecule - solvent molecules’ in which, the high affinity between the solid molecule and solvent molecules of a dissolution experiment will promote the dissolution process (Aulton, 2007).

From a broad view, two steps are involved in dissolution of a solid surface. Firstly, drug molecules detach from the solid surface. Secondly, the detached molecule will diffuse through a diffusion layer adjacent to the solid surface into the bulk of the dissolution medium (Sugano et al., 2007). In most cases, step 1 is much faster and step 2 is the dissolution rate limiting step. The rate of drug diffusion can be described by Fick’s first law which stated that the rate of change in the concentration of a dissolved material with time is directly proportional to the concentration between the two sides of diffusion layers as shown in Equation (2.6),

$$\frac{dC}{dt} = k\Delta C \quad (2.6)$$

where C is the concentration of the solute in solution at any time point of t, k is the rate constant and ΔC is the difference between the concentration of the solution at the solid surface (C) and the bulk of solution (C_b). When the dissolution process of the solute at surface of the dissolving front approaches equilibrium, the solution in contact with the solid will be saturated and achieving a concentration where $C=C_s$ (solubility of the solute). At this time, the concentration in the bulk, C_b will be the determining factor for the movement of solute. If $C_b \ll C_s$, dissolution will continue to occur while molecules move from the solid surface to the bulk.

Dissolution mechanism of solid dispersion

Many have shown the dissolution enhancement of poorly soluble drug by the production of SD system. However, as mentioned in Chapter 1.6.1, a few studies have the reported unpredictable dissolution performance of the obtained SDs in water soluble polymer. This might be due to the poor understanding of the mechanism underlying the dissolution process of the API in a SD system. Craig (2002) has reviewed and suggested possible mechanism for dissolution process from solid dispersion in water soluble polymers. Figure 2.15 illustrates the suggested dissolution mechanism of SD in water soluble polymer by Craig (2002). The proposed mechanism is largely determined by the solubility of the solid in the carrier system.

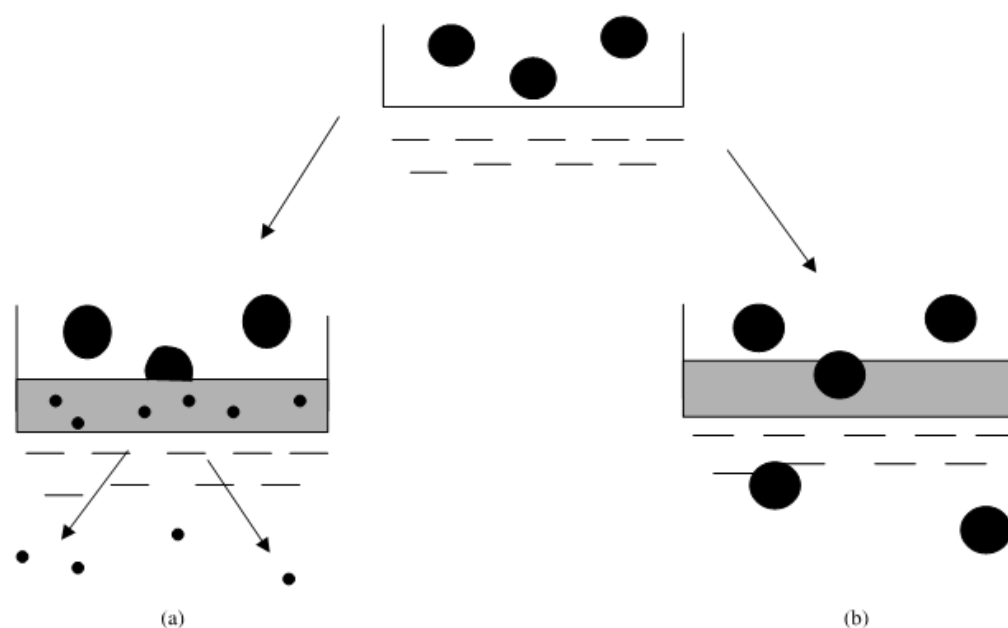


Figure 2.15: : Possible mechanism as proposed by Craig 2002 (a) Carrier-controlled dissolution, whereby the drug dissolves into the concentrated carrier layer prior to release and (b) drug-controlled dissolution whereby the drug is released effectively intact into the dissolution medium. Large spheres represent un-dissolved drug particles, small spheres partially dissolved drug particles, and shaded regions correspond to hydrated material (Figure adopted from Craig 2002).

Pathway (a) involves significant dissolution of the solute in the polymer-rich layer upon wetting of the polymer carrier system. Thus, there is insufficient time for the particles to be released intact into the medium. Consequently, diffusion of the solute is highly dependent to the release of the polymer into the bulk of the medium. Dissolution mechanism of this system is therefore termed as ‘carrier controlled’ release (Craig, 2002). On the other hand, in pathway (b), there is limited dissolution effect of the drug in the diffusion layer of the carrier. Consequently the drug will be released in the medium as solid particle which was termed as ‘drug controlled’ mechanism. With that, properties of the drug (such as size, physical form and etc) will be significant in final dissolution performance of the SD formulations. However, in the latter pathway, dissolution improvement could still be realized due to the improved wetting, de-aggregation and reduction of drug particle size that gives rise to higher effective surface area for the dissolution process.

2.5.2. Factors Affecting the Dissolution Rate

The factors affecting the *in vitro* dissolution rate of a formulation are indicated in the Noyes-Whitney Equation (2.2). These factors include surface area of un-dissolved solid, solid solubility of the sample in the dissolution medium (C_s), concentration of solute in the bulk solution at time t (C_b), thickness of the diffusion layer (h) and diffusion coefficient of the solute in the dissolution medium (D).

2.5.2.1. Surface area of un-dissolved solid

According to Equation 2.2, dissolution rate of a solid is directly proportional to the surface area of the solid. Particle size reduction to about 3 – 5 μm is suggested as a useful strategy in enhancing the dissolution rate of poorly soluble drug with a conventional example of griseofulvin (Hörter and Dressman, 2001).

Solid dispersion is claimed to provide large surface area for dissolution process due to the dispersion of drug at molecular level (Kapsi and Ayres, 2001, Dong et al., 2008b, Biswal et al., 2009). However, the available surface area will be reduced when agglomeration of the solid dispersion powder occurs which will affect the formulations performance significantly. Thus, the available surface area for dissolution process is highly influenced by dispersibility of the powdered solid in the dissolution medium.

2.5.2.2. Solubility of solid in the dissolution medium (C_s)

Solubility of an API is depending on the presence of excipients or additive that can induce complex formation or solubilisation as well as ionization of the API. Other factors such as temperature, the nature of dissolution medium and the solid form in terms of whether it is amorphous or crystalline are also important in affecting the dissolution rate of a system by the solubility effect.

2.5.2.3. Concentration of solute in the bulk solution at time t (C_b)

Assuming that other factors of dissolution are fixed, the concentration of solute in the bulk solution is highly affected by the volume of the dissolution medium. When the medium is small, C_b will be building up to an extent where C_b is approaching C_s , hence no dissolution occurred ($C_s=C_b$). For an effective dissolution study, C_b is usually negligible with respect to C_s by using large volume of dissolution medium which is termed as sink condition. According to USP (US pharmacopeia), sink condition is when the volume of medium used is 3 times more that the volume of medium used to achieved saturation of the solute.

2.5.2.4. Thickness of diffusion layer (h)

Thickness of diffusion layer will determine the rate of movement of the solute molecule across the carrier into the bulk medium. This parameter can be affected by agitation of the medium which is mainly determined by the speed of stirring rate, size and position of the stirrer and viscosity of medium used during in vitro dissolution process.

2.5.2.5. Diffusion coefficient of solute in the dissolution medium (D)

According to Stoke equation, the diffusion coefficient (D) of a solute is depending on the variables presented in Equation (2.7),

$$D = \frac{kT}{6\pi\eta r} \quad (2.7)$$

where k is the Boltzmann constant, T is temperature, η is the viscosity of the dissolution medium and r is the radius of the diffusing molecules. As diffusion rate of an API increase in the carrier, the dissolution rate of the API in the system will be also increased. However, in a SD system, this effect might be irrelevant when the solute is highly soluble in its polymer carrier.

According to Equation (2.7), when a solute is significantly dissolved in its polymer carrier, its diffusion in the polymer is too slow as the r is small at a molecular level, thus the overall release would be irrelevant to the diffusion rate of the API in the carrier system but highly dependent on the release rate of the polymer carrier which is shown as a carrier controlled system as mentioned in the dissolution mechanism proposed by Craig (2002) in Figure 2.15.

2.5.3. Preparation of Dissolution Media

In this study, dissolution medium of 0.1M HCl were prepared by transferring 900 ml of 37% w/w HCl into 10 Litre of container prefilled with 5 L of distilled water. A further amount of distilled water was added up to 10 Litre and the mixture were stirred to achieve homogenous solution. The final pH was checked using a calibrated pH meter, pH was adjusted when necessary.

2.5.4. Dissolution method

Dissolution experiments were carried out using BP Apparatus II (D8000, Copley Scientific Ltd., Nottingham, UK) paddle method. Each vessel was filled with 900 ml dissolution medium. The temperature was set at 37 ± 0.5 °C at 50 rotations per minute. At predetermined time interval, 10 ml sample was withdrawn from each vessel using a 10 ml syringe. The samples were filtered through a 0.45 μ m membrane filter. The collected solution samples were measured at the wavelength of maximum absorbance (λ_{\max}) of each API. All dissolution experiments were carried out in triplicate. The obtained results were presented in percentage of cumulative API release versus time profiles.

2.5.5. Ultraviolet-Visible Spectrophotometer (UV-VIS)

Molecules can absorb energy in the form of ultraviolet or visible light to excite the electron within to higher molecular orbital. This enables the measurement of an analyte of interest by using UV/VIS. Ultraviolet absorbance of a substance could be described by Beer-Lambert law, Equation (2.8),

$$A = \varepsilon . c . l \quad (2.8)$$

whereby A is the light absorbance of molecules at a concentration, c , l is the path length of UV and ε is the molar absorptivity which is also known as the extinction coefficient. To simplify, a path length of 1 cm is usually used to calculate the absorbance and molar absorptivity. The Beer-Lambert law applies when absorbance of sample increases linearly with the concentration of the analyte.

To quantify the API content in a medium sample, a Perkin-Elmer Lambda XLS spectrophotometer (USA) was used. Each sample was scanned at the wavelength of maximum absorbance, λ_{\max} specified for each API which was identified to be devoid of any interference from the added excipients.

Calibration curves were constructed by using Beer Lambert plots for each drug in the corresponding medium or buffer. API was weighed accurately in a weighing boat then transferred into a dry volumetric flask. Then the solution was made up to the desired volume with known concentration of API. The API was dissolved by stirring for at least 48 hours. Once the API solution (stock solution) had been prepared, 1, 2, 3, 4, 5 ml aliquot of the stock solution were transferred into separate 10 ml volumetric flasks for dilution. A further amount of medium was added to each volumetric flask to obtain a series of 10 ml solutions. The series of solutions were analyzed with a Perkin-Elmer Lambda XLS UV/VIS spectrophotometer (USA). The average absorbance readings were plotted against the respective API concentrations to get a calibration line. Each point in the calibration line was an average value of three measurements.

Figure 2.16 to 2.19 display the calibration curve of the all poorly soluble APIs (NAP, KTP, INDO and OZP) in their respective dissolution media.

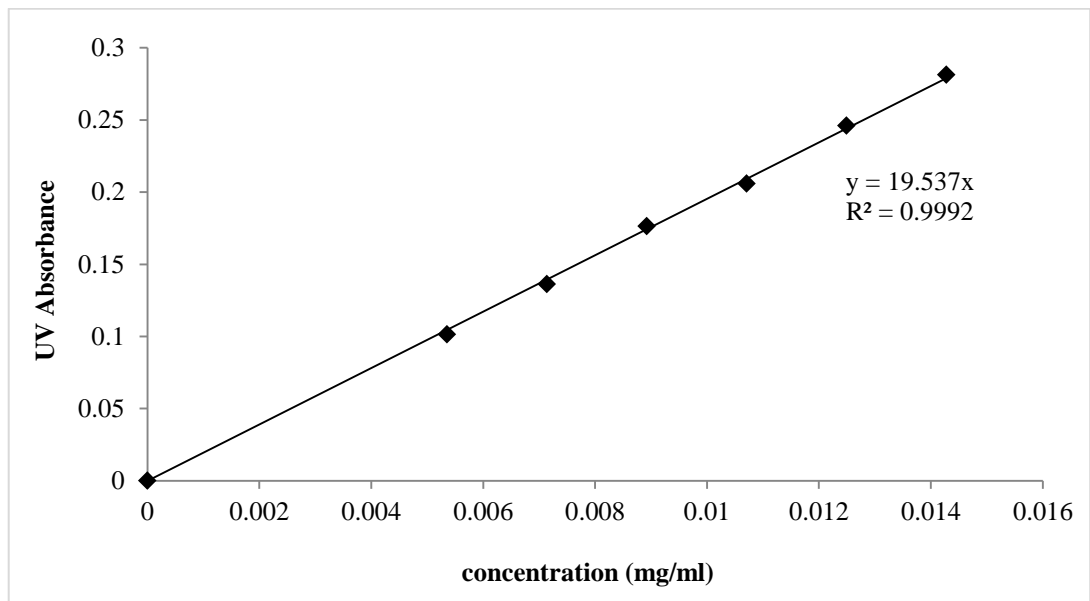


Figure 2.16: Calibration curve of NAP in 0.1M HCl pH 1.2 at 272 nm

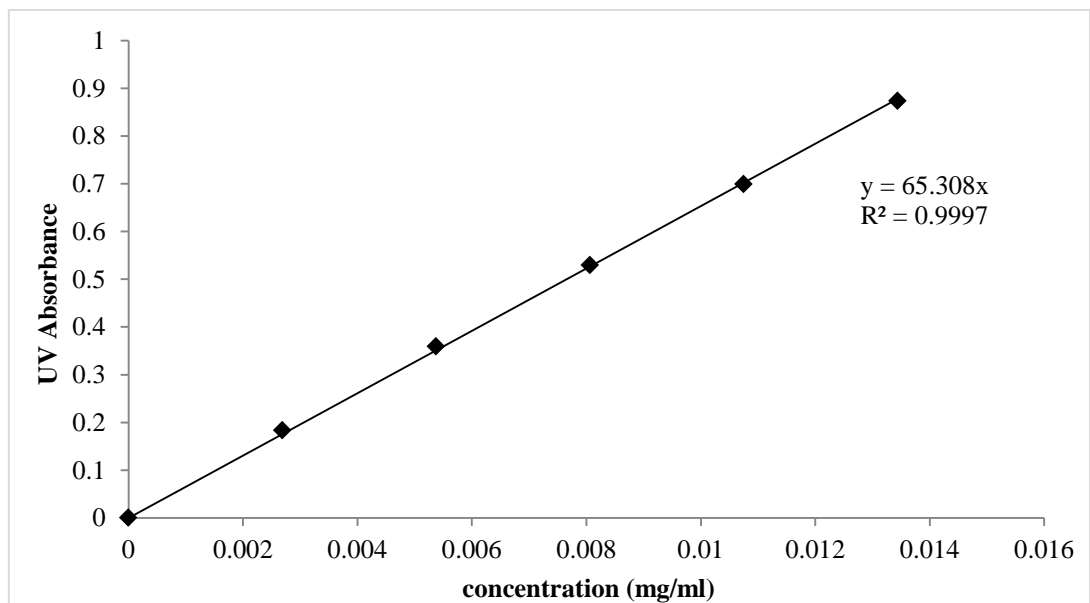


Figure 2.17: Calibration curve of KTP in 0.1M HCl pH 1.2 at 259 nm

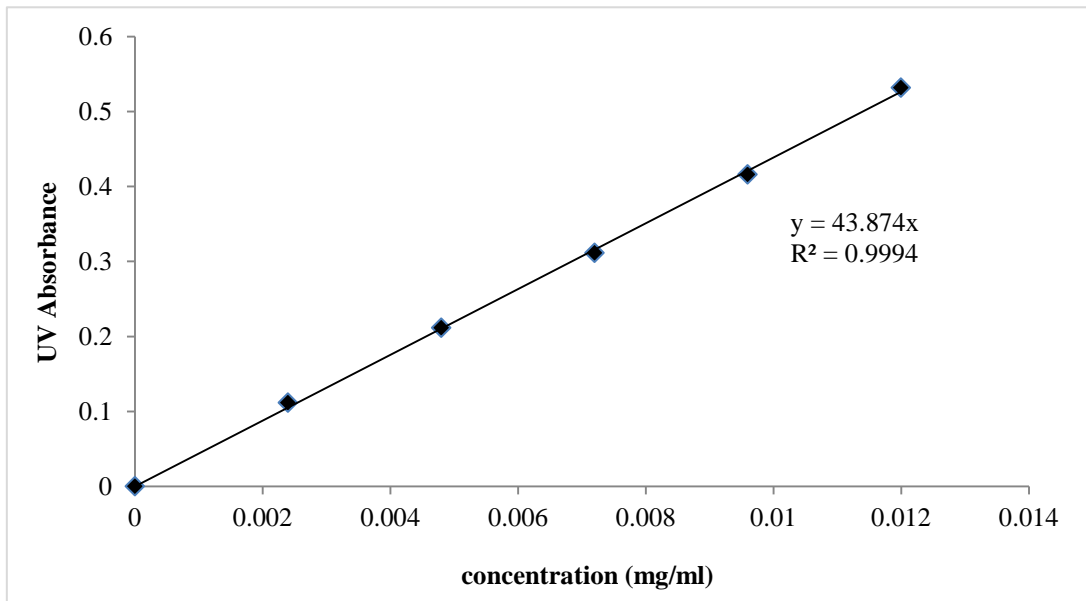


Figure 2.18: Calibration curve of INDO in distilled water at 265 nm

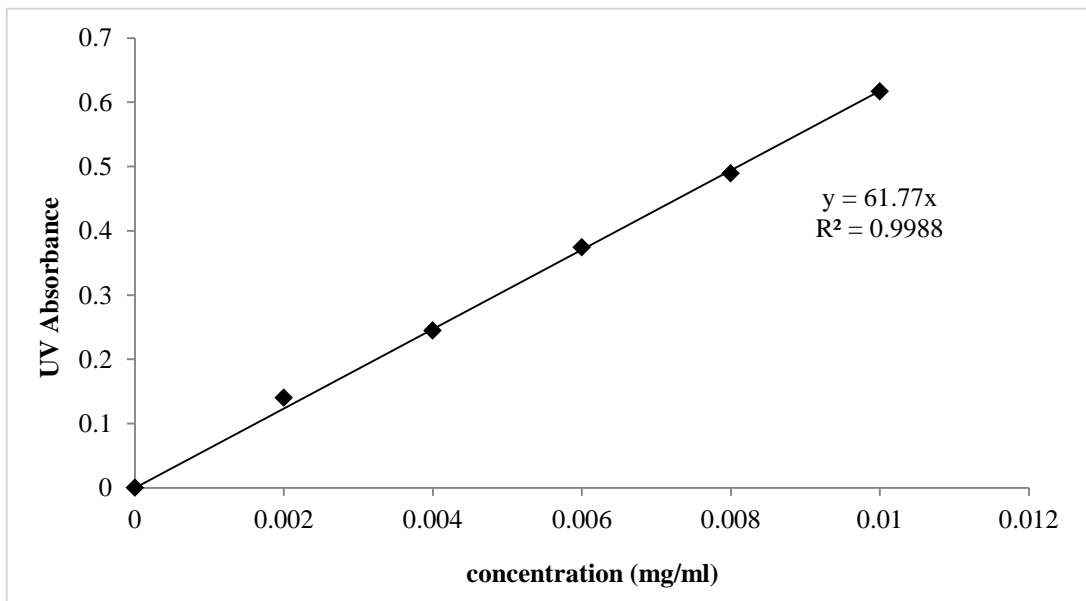


Figure 2.19: Calibration curve of OZP in distilled water at 254 nm

Chapter 3. Theoretical miscibility estimation and basic characterization of hot melt extruded solid dispersions

3.1. Introduction

Hot melt extrusion (HME) has attracted considerable attention in the preparation of solid dispersion (SD) formulations due to its cost sparing and readily scalable production as described in Chapter 1.4 (Hancock et al., 2002). In order to successfully extrude an HME polymer-based amorphous SD, the extrusion temperature is often set at 10 to 20 °C higher than the T_g (glass transition temperature) or T_m (melting temperature) of the polymer to ensure good flowability of the mixture during the extrusion process (Chokshi et al., 2005). However, based on the proposal of employing a high T_g polymer for the physical stabilisation of amorphous solid dispersion (Zhao, 2010, Sathigari et al., 2012, Shah et al., 2012, Hancock and Zografí, 1997), T_g of many pharmaceutical polymers are too high for the extrusion process. Indeed, the use of high processing temperatures is usually not favourable due to the heat induced degradation of many polymeric and drug systems; hence, a more moderate working temperature is required. Nevertheless, simply abandoning potentially useful polymers such as polyvinylpyrrolidone (PVP) without adequate understanding of the processing options and material characteristics could lead to the inefficient use of resources due to premature rejection of polymer candidates.

PVPs are hydrophilic polymers and are the main carriers (i.e. PVP K29-32 and PVP vinyl acetate 6:4) for this study. The advantages of these polymers in solid dispersions have been widely published as described in Chapter 2. However, the use of PVP is lacking in the field of HME SD due to threat of degradation in the hot processing. Therefore, the purpose of this chapter is to investigate the possibility of using PVP polymer in the context of HME. In light of this, the high T_g of PVP polymers may be softened at suitably low temperatures when mixed with a miscible active pharmaceutical ingredient (API), as the low molecular volume of the API compound can plasticize the polymeric matrix (Forster et al., 2001c). This plasticizing effect often confers versatility in terms of widening the extrusion temperature window of HME production.

In the extrusion of HME PVP-based SD, structurally interacting API, i.e. paracetamol and limited-interacting API with PVP, i.e. caffeine (Sekikawa et al., 1978) were employed. Besides, miscibility behaviour of these model APIs and the PVP polymers were determined by measuring the interaction parameters obtained via the Hansen solubility parameter and melting point depression approaches (Marsac et al., 2009). In particular, the intention is to explore whether the production of fully amorphous HME PVP-based SD may be predicted using these theoretical approaches.

3.2. Materials and methods

In this study ‘PVP polymers’ or ‘PVP carriers’ represents both the homopolymer PVP and its derivative copolymer PVPVA 6:4 or otherwise specified.

3.2.1. Preparation of physical mixtures

Physical mixture (PM) of APIs (i.e., Paracetamol (PCM) and caffeine (CAF)) and PVP carriers were weighed according to the desired drug-polymer ratio and the mixtures were gently mixed in a mortar and pestle for approximately 2 minutes.

3.2.2. Estimation of drug-polymer miscibility

Prior to the preparation of solid dispersions, the miscibility of the drug-polymer systems was investigated. The Flory-Huggins theory has been used for calculating free energy mixing and estimating miscibility of drug-polymer components. Although limitations of this approach have been described (Zhao et al., 2011, Marsac et al., 2006, Tian et al., 2012), this method is still useful as a starting point for the understanding of drug-polymer thermodynamics.

In considering the mixing of a large molecular weight polymer and a low molecular weight API, the Flory Huggins theory defines a hypothetical “lattice” in space. It assumes that the probability of the solvent (in this case the API) making contact with the segment of polymer (in this case monomer) is equal to the volume fraction of the polymer segments, i.e. its monomer (Gong et al., 1989). Following the Flory-Huggins theory of polymer solution, with the description of interaction parameter, χ to account for the enthalpy of mixing, the equation for free energy mixing of an API-polymer system, ΔG_m is given by Equation (3.1)

$$\frac{\Delta G_M}{RT} = n_{drug} \ln \phi_{drug} + n_{polymer} \ln \phi_{polymer} + n_{drug} \phi_{polymer} \chi_{drug-polymer} \quad (3.1)$$

where n_{drug} is number of mole of the drug, $n_{polymer}$ is number of moles of polymer, ϕ_{drug} is volume fraction of the drug, $\phi_{polymer}$ is the volume fraction of the polymer, $\chi_{drug-polymer}$ is the interaction parameter between the drug and polymer, R is gas constant, and T is absolute temperature. By the knowledge of the interaction parameter, χ , one can estimate the mixing behaviour of an API to polymer system using the Flory-Huggins theory via estimation of the free

energy of mixing which in turn indicates the driving energetics of the process. However the approach requires the interaction parameter χ to be known.

Earlier reports indicated that the solubility parameter and melting point depression approaches maybe used to estimate the interaction parameter of a blend and hence, possibly, the degree of miscibility and solid solubility (Marsac et al., 2009, Marsac et al., 2006, Zhao et al., 2011, Tian et al., 2012). Both of these approaches were tested in the current study in relation to the characteristics of both the raw materials and the prepared products.

3.2.2.1. Solubility parameter approach

The solubility parameter approach is a widely used method in estimating the miscibility and compatibility of a mixture system. The origin concept of this approach is described by Hildebrand (1961) who stated that solubility of a given solute in a solvent is determined by the cohesive energy density, i.e. cohesive energy per unit volume of the substance (Van Krevelen and Te Nijenhuis, 2009). This concept is developed to specify a parameter (the solubility parameter) that is defined to be the square root of the cohesive density energy. According to Van Krevelen and Te Nijenhuis (2009) the solubility of a given solute is largely determined by the chemical structure. As a general rule, similar chemical structure between the solute and solvent favours solubility, i.e. solubility is favoured when structures of solute and solvent possess similar solubility parameters (Van Krevelen and Te Nijenhuis, 2009).

In a low molecular weight liquid, the cohesive energy is closely related to the molar heat of evaporation ΔH_{vap} , as presented in Equation (3.2)

$$E_{coh} = \Delta H_{vap} - p\Delta V \approx \Delta H_{vap} - RT \quad (3.2)$$

where E_{coh} is cohesive energy, p is pressure, ΔV is volume changes, R is universal gas constant and T is temperature. Since it is not possible to obtain the vaporization energy of a polymer directly, an indirect method was developed to estimate the solubility parameter of polymer system i.e. via group contribution methods.

In the literature, two chemical group contribution methods are reported for the indirect prediction of solubility parameter of the API and polymer system, i.e. the Hoftyzer/ Van Krevalen method and the Hoy method (Van Krevelen and Te Nijenhuis, 2009). Based on these methods, the cohesive energy of a molecule is dependent on different forces in the chemical structure of the molecule which include dispersive force (F_{di}), hydrogen bond force (E_{hi}), as well as polar force (F_{pi}). The

values of these forces are given as a reference table in Van Krevelen and Te Nijenhuis (2009). With the known of these forces, the solubility parameter of a molecule can be estimated.

3.2.2.2. Melting point depression approach

Apart from the solubility parameter approach, the melting point depression approach is another method that can be used to estimate the miscibility in a mixture of different components. The miscibility of the components is presented by the negative value of a defined parameter, namely interaction parameter, as a function of melting point depression phenomenon.

Additionally, this approach is also introduced for the prediction of solid solubility of a drug in a polymer system which is strongly attributed to the drug-polymer interaction. When a drug interacts with a polymer system, the chemical potential of the mixture will be reduced and thus the melting point of the drug would be reduced (Tian et al., 2012). Consequently, by accessing the degree of melting point depression as a function of polymer composition, the energy density of the interaction between the two systems could be anticipated (Marsac et al., 2009, Zhao et al., 2011). This density of interaction is frequently represented by the interaction parameter, χ_{12} , where subscript 1 denotes the first component and subscript 2 denotes the second component.

To predict the interaction parameter by using the melting point depression method, PM API-carriers were prepared in drug rich proportions (from 70 - 90% w/w drug loading) and scanned by modulated DSC with ± 0.212 °C every 40 s at 2 °C per minute to 200 °C using pin hole pan. MTDSC was used to separate the Tg or relaxation endotherm of the polymer particularly, PVP K 29-32 from the melting endotherm of PCM. This is to avoid misinterpretation of the Tg related endotherm (particularly PVP K29-32) as a depressed melting point of PCM.

3.2.3. Preparation of hot melt extruded solid dispersions

HME sample of PCM PVP K29-32 ranging from 20%-70% of PCM loading was prepared. While 20%-50% of PCM loading were prepared in HME PCM PVPVA 6:4. For both HME systems of CAF PVP K29-32 and CAF PVPVA 6:4, only 10% and 20% loading of CAF systems were prepared. The discrepancy of the API loading is dependent on the experimental observation whereby the loading limit of preparation was extruded up to a point where the appearance of the extrudate was opaque. Please refer to Table 2.12 for the processing parameters used in the production of HME systems.

3.2.4. Hot stage microscopy

The melting or T_g temperature of pure PCM, CAF, PVP polymers and fusion temperatures of the PM of drug and polymer were observed by hot stage microscopy (HSM). Samples were heated from room temperature up to 200 °C at a heating ramp of 10 °C per minute. Events that occurred in the samples while heating were recorded using a JVC colour video camera with studio capture software.

3.2.5. Thermogravimetric analysis

Thermogravimetric analysis (TGA) was used to measure the water content and detect the decomposition temperature of the raw materials and the prepared HME PVP-based formulations. Raw powders or intact extrudates (3-4 mm) were heated from room temperature and isothermed at 100 °C for 15 minutes before further heating to 350 °C at a heating rate of 10 °C per minute. Weight loss after 15 minutes of isotherm at 100 °C was taken as water content of the samples. Dramatic weight loss at higher temperatures was regarded as being indicative of the decomposition temperature.

3.2.6. Modulated temperature differential scanning calorimetry

All samples, including the drugs, polymers, physical mixtures and HME PVP-based extrudates were analysed using a DSC with modulated mode (MTDSC). Pin-hole lids were used to allow removal of water, particularly given the hygroscopic nature of the PVP polymers (Callahan et al., 1982). Samples were heated from 0 °C in modulated mode (± 0.212 °C every 40 s) at 2 °C per minute to 200 °C. All experiments were run in triplicate.

3.2.7. Attenuated total reflectance -Fourier transform infrared spectroscopy

Attenuated total reflectance -Fourier transform infrared spectroscopy (ATR-FTIR) measurements were carried on freshly ground extrudates. The spectra were recorded over a wavenumber range of 500 cm⁻¹ to 4000 cm⁻¹ with a resolution of 2 cm⁻¹ and 64 scans. To detect changes as a function of heating, the ATR crystal was heated to the desired temperature (ranging from room temperature to 200 °C) before scanning. Extrudates were scanned in powder form by gently grinding in a mortar and pestle.

3.2.8. Powder X-ray diffraction

Powder X-ray diffraction (XRPD) experiments were performed on freshly prepared HME PVP-based extrudates. The extrudates were crushed into powder form and compacted into the sample holder of the XRPD. Measurements were performed from 10° to 30° (2θ) coupled with scanning speed of 0.01° / step and 1 second for every scan step to cover the characteristic peaks of the crystalline PCM and CAF.

To detect crystallinity of the HME PVP based extrudates using XRPD method, a calibration curve was constructed based on the relationship between the area under the characteristic peaks and the crystallinity of PM was performed. This method of quantifying PCM using XRPD was reported before by de Villiers et al., 1998 (de Villiers et al., 1998). PMs of 10% to 80% w/w were prepared by simple mixing in a mortar and pestle. The PMs were then compacted into the X-ray sample holder and scanned from 10° to 30° (2θ) to cover the characteristic peaks of the crystalline PCM and CAF. Calibration curves were constructed according to the intensity of the two sharp peaks at 23.4 and 24.5° 2θ Bragg diffraction peaks versus the known crystal content.

3.2.9. Scanning electron microscopy

The surface morphology of the fresh extrudates was investigated using scanning electron microscopy (SEM). The extrudates were cut through by cross section using a microtome. Both the cut extrudates and whole spaghetti-like extrudates were placed on a sample stub and sputtered with a thin layer of gold prior to imaging.

3.3. Results

3.3.1. Estimation of drug-polymer miscibility

3.3.1.1. Solubility parameter approach

In this study, the solubility parameters of the drug and polymer were both estimated. Theoretical background of this approach has been described in section 3.2.2.1. Table 3.1 and Equation 3.3 provide the example of solubility parameter calculation of PCM. Table 3.1 lists the values of the chemical group forces of PCM based on the cohesive energy values given in Van Krevelen and Te Nijenhuis (2009). By knowing the forces of each chemical group, the summation of all the forces was carried out in each column of Table 3.1.

Table 3.1: Solubility parameter calculations for PCM using the Hoftyzer and Van Krevelen methods. Column 1 represents the chemical group contribution of PCM. Columns 2 to 4 represent the respective forces attributed by each of the chemical group. The last column represents the molar volume of the contributed groups (Van Krevelen and Te Nijenhuis, 2009).

Structural Group	F_{di} (MJ/m ³) ^{1/2} mol ⁻¹	F_{pi}^2 (MJ/m ³) mol ⁻²	E_{hi} J/mol	V cm ³ / mol
1-CH3	420	0	0	33.5
1-OH	210	250000	20000	10
1-CO-	290	592900	2000	10.8
1-NH-	160	44100	3100	4.5
1 Ring	1430	12100	0	71.4
Σ	2510	899100	25100	117.2

Then, the solubility parameter was calculated from Equation (3.3).

$$\delta_{drug} = \sqrt{\left(\frac{\sum F_{di}}{V}\right)^2 + \left(\frac{\sqrt{\sum F_{pi}^2}}{V}\right)^2 + \left(\frac{\sum E_{hi}}{V}\right)^2} = 27.17 \quad (3.3)$$

where V is the molar volume F_{di} is dispersive force, F_{pi} is polar force and E_{hi} is hydrogen bond. By using Equation (3.3), the solubility parameter of PCM could be obtained by combination of the square root of the cohesive energy density of the different contributions forces. The solubility parameter of PCM molecule was calculated to be 27.17.

On the other hand, Hoy has incorporated the molar attraction constant in the calculation of solubility parameter (Van Krevelen and Te Nijenhuis, 2009). For comparison, Table 3.2 presents the example of solubility parameter estimation of PCM via the Hoy method. In a similar manner to the Hoftyzer/ Van Krevalen method, the Hoy method entails the calculation of density of the cohesive energy which involves the molar attraction function (F_c), its polar component (F_p), molar volume (V) of the solvent molecule or structural unit of the polymer and the Lydersen correction for non-ideality (Δ_{Ti}). These values could be obtained from a reference table published in Van Krevelen and Te Nijenhuis (2009). Table 3.2 lists the values the involved forces obtained from Van Krevelen and Te Nijenhuis (2009). Values of each column in Table 3.2 was summed up and used for further calculation of the solubility parameters by using Equation (3.4) or (3.5).

Table 3.2: Solubility parameter calculations for PCM using the Hoy methods. Column 1 represents the chemical group contribution of PCM. Columns 2 and 3 represent the molar attraction function and polar component, respectively attributed by each of the chemical group. Column 4 represents the molar volume of the contributed groups and the last column is the Lydersen correction for non-ideality of each chemical group (Van Krevelen and Te Nijenhuis, 2009).

Structural Group	F_t (MJ/m ³) ^{1/2} mol ⁻¹	V cm ³ / mol	Δ_{Ti}
1-CH3	303.5	21.55	0.023
4- CH aromatic	964	53.68	0.044
2 -C aromatic	402	14.84	0.22
1-CONH	1131	28.3	0.054
1-OH-(phenol)	350	12.45	0.031
1Aromatic substitution-para	83	0	0
Σ	3233.5	130.82	0.174

$$\delta_t = \frac{F_t + B}{V} = 26.83 \quad (3.4)$$

$$\delta_t = \frac{F_t + (B/n)}{V} \quad (3.5)$$

From Equation 3.4, δ_t is the solubility parameter, F_t is molar attraction function, F_p is polar component and the B is a base value which has been proved to be essential to be incorporated (Traube 1895). B is equal to 277 for low molecular weight liquids. For calculations for the amorphous polymer Equation (3.5) should be used where 'n' is an auxiliary number which could be obtained by Equation (3.6) with the knowledge of the value of Lydersen correction for non-ideality, $\Delta_T^{(p)}$, which is obtained by summation of value of Δ_{Ti} as shown in Table 3.2.

$$n = 0.5/\Delta_T^{(p)} \quad (3.6)$$

The average magnitudes of solubility parameters obtained from the Hoftzyer/Van Krevelen method and Hoy method has been previously suggested to be the best prediction due to the good agreement between the theoretical calculation and experimental data obtained from heat of vaporization of low molecular weight molecules (Van Krevelen and Te Nijenhuis, 2009). Therefore, in this study, solubility parameters of the materials were the average values obtained from both Hoftzyer/Van Krevelen (Table 3.1 and Equation (3.3)) and Hoy (Table 3.2 and Equation (3.4) or (3.5)) methods Table 3.3 displays the calculated solubility parameter for each method and their average and the difference between the solubility parameters of drug and polymer carriers.

Table 3.3: Solubility parameters of APIs and PVP polymers

Compound	Solubility parameter, δ			$\Delta\delta$ ($\delta_d - \delta_p$)	
	Hofsteyer/ Krevelen (MPa) ^{1/2}	Van Hoy (MPa) ^{1/2}	Average	PVP K2932	PVPVA 6:4
Paracetamol	27.17	26.83	27.00	3.68	4.17
Caffeine	35.19	27.48	31.34	8.16	9.01
PVP K29-32	26.29	20.05	23.17		
PVPVA 6:4	24.38	20.54	22.32		

The difference of the solubility parameters between the drug and polymer is an indication for drug-polymer miscibility. When the difference is more than 10 MPa^{1/2}, there is potential for immiscibility between the mixture components. Conversely, when the difference is less than 7 MPa^{1/2}, the mixture is expected to show good miscibility (Forster et al., 2001c).

The last two columns of Table 3.3 (highlighted in grey) represent the differences of solubility parameters between the drug and polymer carriers. Binary systems of PCM-PVP K29-32 and PCM-PVPVA 6:4 were expected to show good miscibility as indicated by the low differences between the PCM and its carrier systems (PVP K29-32 and PVPVA; < 7 MPa^{1/2}). On the other hand, difference of the solubility parameters between the drug and polymer in binary systems of CAF-PVP K29-32 and CAF-PVPVA 6:4 are $\Delta\delta > 8$ MPa^{1/2} suggesting limited miscibility of the drug and carriers. These results further discussed based on the nature of the prepared extrudate formulations in the subsequent sections.

3.3.1.2. Melting point depression approach

Drug-polymer miscibility was also estimated using melting point depression approach as described in section 3.2.2.2. Figure 3.1 shows an example of MTDSC thermograms of the depressed melting point of PCM in the PM of binary PCM-PVP K29-32 ranging from 70% to 95% of drug loading.

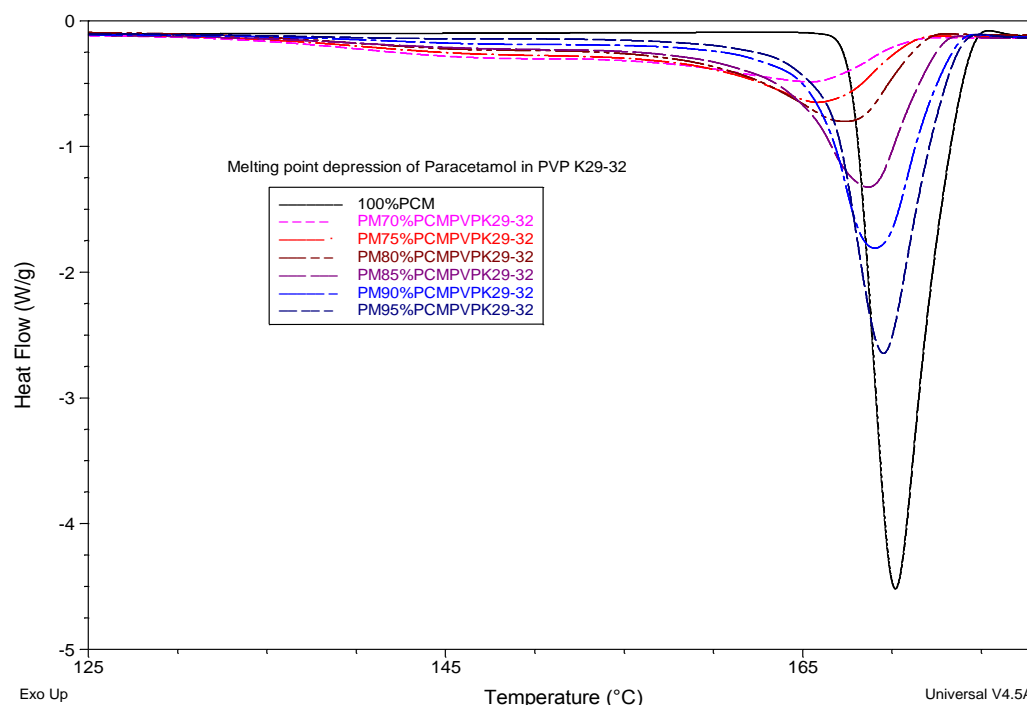


Figure 3.1: DSC thermograms of PM of PCM-PVP K29-32 (from 70% w/w to 90% w/w drug loading) measured at 2 °C/min. Onset melting point of the DSC thermograms was taken as the melting temperature of the systems.

Apparent melting point depression was detected for PCM in the presence of PVP K29-32 in which the onset of T_m of PCM was recorded as 150 °C at 70% w/w PCM loading.

Figure 3.2 compares the changes in melting temperatures of PCM and CAF in the presence of PVP K29-32. In presence of PVP K29-32 systems, PCM displays a higher melting point depression than CAF as indicated by the steeper slope of the curves of PM PCM-PVP K29-32 in Figure 3.2. Besides, the onset melting point of PCM and CAF also decreased with the higher proportion of polymer.

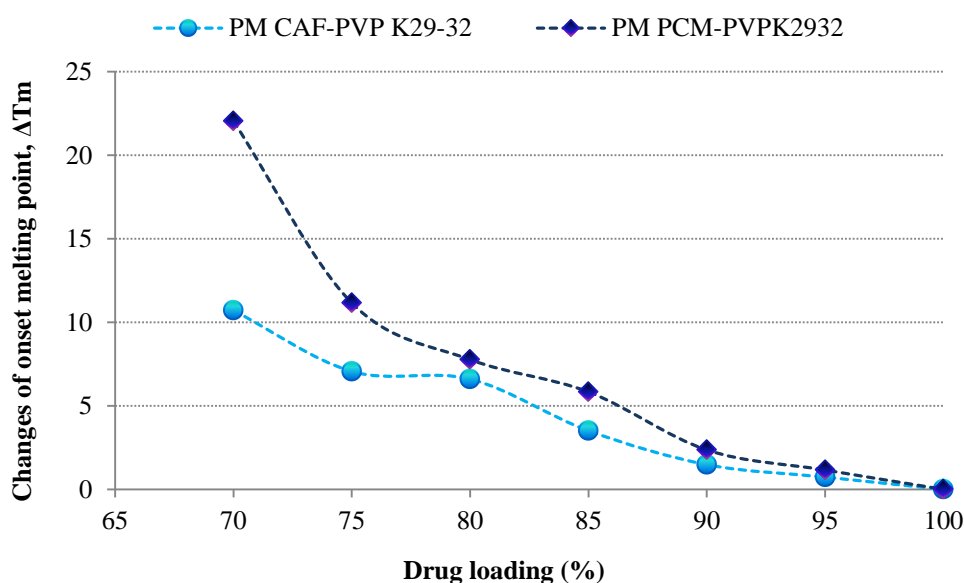


Figure 3.2: Change in onset of T_m of PM PCM and CAF in PVP K29-32 as a function of percentage API loading

As mentioned in the beginning of this section (Chapter 3.2.2.2), melting point depression of the drug system is attributed to the change in overall chemical potential of the mixture as a result of interaction between the drug and the polymer (Zhao et al., 2011, Tian et al., 2012). These interactions include Van der Waal interaction, hydrogen bond interaction, charge transfer complexation as well as ionic interaction.

Structurally, hydrogen bond formation was anticipated between PCM and PVP K29-32 due to the presence of proton donor in PCM and proton acceptor in pyrrolidone of PVP K29-32. However, this is not anticipated in the binary CAF and PVP K29-32 because of the lack of proton donor in the chemical structure of the CAF molecule. Therefore, the difference in ability of hydrogen bond formation in PCM-PVP K29-32 system and CAF-PVP K29-32 may explain the different degree of depressed melting point of PCM and CAF in the presence of PVP K29-32. In the context of HME, the depressed melting temperature of the melted API will promote flowability of the mixture in the HME barrel as the solid of the drug melts into its liquid state. This might allow the good mixing process between the drug and polymer.

Interaction parameters

To predict the drug-polymer interaction parameter by using the melting point depression approach, the data of the depressed melting point detected from MTDSC scan was used in Equation (3.7) (Paudel and Mooter, 2012, Marsac et al., 2006, Zhao et al., 2011).

$$\left(\frac{1}{T_{Mmix}} - \frac{1}{T_{Mpure}} \right) = \frac{-R}{\Delta H_{fus}} \left[\ln \phi_{drug} + \left(1 - \frac{1}{m} \right) \phi_{polymer} + \chi_{12} \phi_{polymer}^2 \right] \quad (3.7)$$

where T_{Mpure} is the melting temperature of the pure API, T_{Mmix} is the depressed melting temperature of the mixture, R is universal gas constant, ΔH_{fus} is heat of fusion of the pure API, m is the volume ratio of polymer to its volume lattice (which is taken as the volume of drug), χ_{12} is interaction parameter, ϕ_{drug} and $\phi_{polymer}$ is the volume fraction of the drug and polymer respectively which were obtained from Equation (3.8).

$$\phi_{drug} = \frac{V_{drug}}{V_{drug} + V_{polymer}} \quad (3.8)$$

where V is volume of the component which is denoted by its subscription. Volume of a component is calculated from the value of weight divided by value of density, i.e. $V = m/\rho$.

By rearranging Equation (3.7) into Equation (3.9), the interaction parameter, χ_{12} between the drug-polymer could be obtained by plotting the function of depressed melting temperature (left side of Equation (3.9)) of PCM against the volume fraction of the polymer (right side of Equation 3.9), i.e.

$$\left[(T_{Mmix}^{-1}) - (T_{Mpure}^{-1}) \times \frac{\Delta H_{fus}}{-R} \right] - \left[1 - \left(\frac{1}{m} \right) \times \phi_{polymer} \right] - [\ln \phi_{drug}] = \chi_{12} \times \phi_{polymer}^2 \quad (3.9)$$

Figure 3.3 displays the example plots of the function of depressed melting temperature against volume fraction of PVPs polymer with good correlations. The slopes of the lines in Figure 3.3 were taken as interaction parameter, χ_{12} .

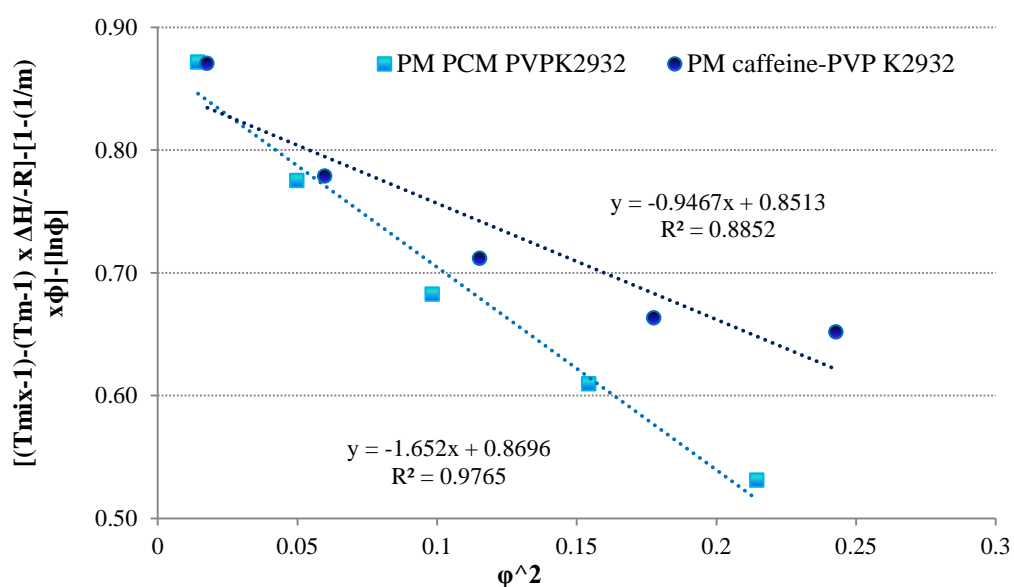


Figure 3.3: Plot used to determine the interaction parameter of PCM-PVP K29-32 and CAF-PVP K 29-32

According to the relationship between the free energy mixing and interaction parameter as presented in Equation (3.1), a favourable mixing can be realized only if the drug-polymer interaction parameter is negative. Besides, the smaller the magnitude of interaction parameter would give rise to a more negative free energy mixing, ΔG_m which indicating a bigger change in chemical potential between the mix and unmixed state. Thus a more negative interaction parameter indicates a higher potential of drug-polymer interaction.

Table 3.4 summarise the interaction parameters of the investigated API-polymer systems. From Table 3.4, interaction parameters for both PCM and CAF with both PVP K29-32 and PVPVA 6:4 system are negative.

Table 3.4: Flory-Huggins interaction parameters based on melting point depression

Formulation	Interaction parameters, χ_{12}	Correlation, R^2
PM PCM / PVP K29-32	-1.652	0.9765
PM PCM / PVPVA 6:4	-0.7752	0.8974
PM CAF / PVP K29-32	-0.9467	0.8852
PM CAF / PVPVA 6:4	-0.4992	0.7908

Interaction parameters of PCM – PVP carriers are slightly more negative than CAF – PVPs. This suggests better interactions between PCM and both PVPs carriers (PVP K29-32 and PVPVA 6:4) as compared to the interaction between CAF and PVPs carriers (PVP K29-32 and PVPVA 6:4). Furthermore, the interaction parameter of PCM-PVP K29-32 is more negative than PCM-PVPVA 6:4 at a temperature close to the melting of the APIs which implies a better interaction between PCM and PVP K29-32 than between PCM and PVPVA 6:4.

To extend the discussion, the free energy of mixing (ΔG_m) of the systems were also calculated based on the interaction parameters from Table 3.4 by using Equation (3.1) in section 3.2.2.. Figure 3.4 displays the obtained Gibbs free energy values plotted against the volume fraction of PVP carriers.

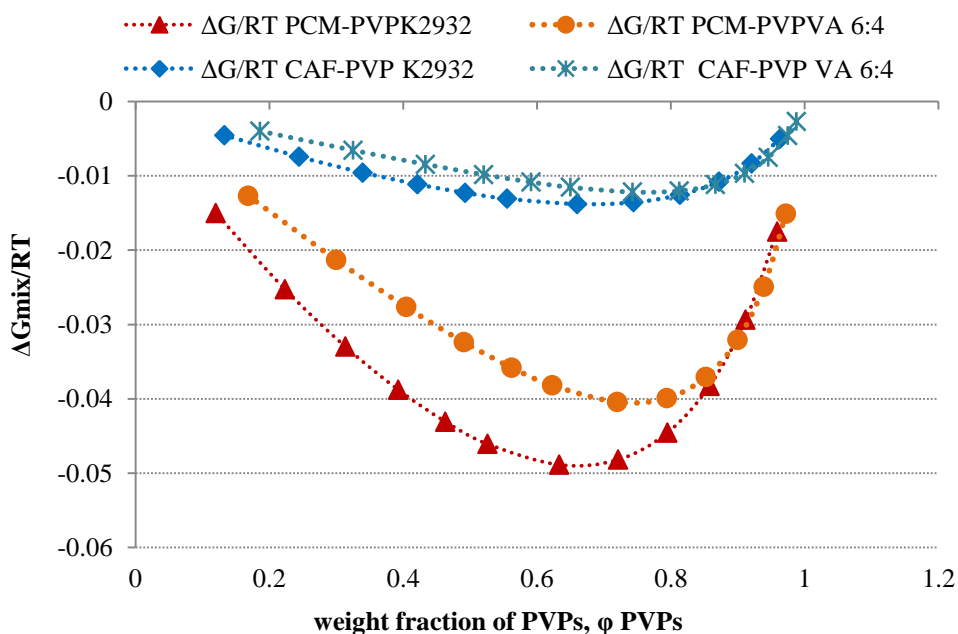


Figure 3.4: The changes in free energy of mixing as a function of volume fraction of polymer as predicted using interaction parameter of Flory-Huggins lattice theory

The Gibbs free energies for the PCM-PVPs (PVP K29-32 and PVPVA 6:4) were negative which indicated miscibility of the PCM and PVP-carriers. This is in good agreement to the conclusion drawn from the close values of solubility parameters (Table 3.3).

However, the Gibbs free energy curves of CAF and PVPs carriers (PVP K29-32 and PVPVA 6:4) were also found to be negative which suggested some extent of miscibility between the CAF and PVP carriers. This is in agreement with the prediction from solubility parameters whereby the high difference ($> 8 \text{ MPa}^{1/2}$) between solubility parameters of the CAF and PVPs infers potential immiscibility (Chapter 3.3.1.1, Table 3.3).

According to Gibb free energy curves in Figure 3.4, the minimum negative value of the concave of PCM-PVPVA 6:4 system lies at a higher value of polymer fraction (i.e. at 0.7 mole fraction of PVPVA 6:4) as compared to PCM-PVP K29-32 which has a minimum at 0.6 mole fraction of PVP K29-32. This indicates that a higher PVPVA 6:4 fraction is needed to achieve a maximum miscibility between PVPVA 6:4 and PCM in comparison to the homopolymer PVP K29-32. A similar trend was also noted in the binary system of CAF and PVPs carriers. These predictions will be correlated to the nature of the prepared SD extrudates in a later section (Chapter 3.3.3.4).

Based on the miscibility prediction using both the Hansen solubility approach and melting point depression approach, the structurally interacting API, i.e PCM was shown to be highly miscible with PVP K29-32 and PVPVA 6:4. On the other hand, the limited-interacting API, i.e. CAF was revealed with limited miscibility with PVP K 29-32 and PVPVA 6:4.

Solid solubility prediction

With the knowledge of interaction parameter, solid solubility of the product could be determined. Here, the interaction parameters that were predicted from melting point depression approach were used for the calculation of solid solubility by using Equation (3.10).

$$\ln(\gamma_{drug} \cdot x_{drug}) = -\frac{\Delta H_{fus}}{RT} \left[1 - \frac{T}{T_m} \right] - \frac{1}{RT} \int_{T_m}^T \Delta C_P^{config} dT + \frac{1}{R} \int_{T_m}^T \frac{C_P^{config}}{T} dT \quad (3.10)$$

where γ_{drug} is activity coefficient and x_{drug} is the mole fraction. ΔH_{fus} is heat of fusion for API, C_p is the change of heat capacity, T_m is the melting point of API, R is universal gas constant and T is the temperature where is the solid solubility was predicted. In the context of HME (i.e. in this study), the expected 'extrusion temperatures of preparing the formulations' was used as the values of T in predicting the solid solubility. According to the Flory-Huggins lattice theory, the activity coefficient of a drug substance can be obtained from Equation (3.11) (Marsac et al., 2009).

$$\ln \gamma_{drug} = \ln \frac{\phi_{drug}}{x_{drug}} + \left(1 - \frac{1}{m}\right) \phi_{polymer} + \chi_{12} \phi_{polymer}^2 \quad (3.11)$$

where m is the ratio of the volume of the polymer to that of the lattice site which is defined as volume of the drug (Marsac et al., 2009). Other terms in Equation 3.11 have been previously defined. It is clear from Equation (3.11) that the activity coefficient of the drug is highly dependent to the interaction parameter and the discrepancy in molecular size between the drug and polymer. If there is only minimal difference in molecular size between the drug and monomers of polymer, ideal mixing entropy can be assumed. By assuming ideal mixing, the first two terms on right hand side are equal to zero. Thus the solid solubility in mole fraction of the drugs in PVPs polymer can be calculated by substituting value of activity coefficient from Equation (3.11) into (3.10). The predicted solid solubility values, x_{drug} in molar ratio could be obtained. These calculated molar ratios x_{drug} were converted into its weight ratios (% w/w) as listed in Table 3.5.

Table 3.5: Theoretical solid solubility of APIs in PVP carriers at their corresponding extrusion temperatures predicted by using melting point depression approach

Solid Solubility of APIs in polymer (% w/w)			
PCM-PVP K29-32	PCM-PVPVA 6:4	CAF- PVP K29-32	CAF-PVPVA 6:4
32 - 55	27- 40	23- 31	31- 42

* Solid solubility prediction via the melting depression approach involves the estimation from drug rich proportions of the drug and polymer systems i.e. 75% to 95% of API. A different concentration of drug will result in a different predicted value of the solid solubility (based on Equation 3.11), thus, a range of apparent solid solubility results will be if a different range of mixtures system is used.

From Table 3.5, the solid solubility of PCM is relatively higher in PVP K29-32 than in PVPVA 6:4. On the other hand, solid solubility of CAF is higher in PVPVA 6:4 than in PVP K 29-32. This might be due to the different magnitude of T used in the calculation as a higher T value was used in the solid solubility calculation of CAF-PVPVA 6:4 system. This is because of the higher expected processing temperature that will be used in producing CAF-PVPVA 6:4 extrudates system (please refer to Table 2.12 for processing temperature).

3.3.2. Preparation of HME PVP-based SDs

3.3.2.1. HME parameter investigation: Extrusion temperature

Before the extrusion of an HME formulation, it is important to understand the thermal properties of the raw materials in order to avoid the inappropriate use of processing parameters (such as high extrusion temperature and long residence time of extrusion). To do this, TGA was used to measure the degradation temperature and water content (%) of the raw materials. On the other hand, DSC was used to measure the T_m or T_g of the drug and polymer, respectively. Table 3.6 lists the thermal properties of the raw materials from both DSC and TGA analysis.

Table 3.6: Thermal properties of raw materials from DSC and TGA analysis

Compounds	Melting (T_m)/ T_g temperature ($^{\circ}\text{C}$)	Degradation temperature ($^{\circ}\text{C}$)	Water content (%)
PCM	$T_m=169-172$	199.1 ± 9.1	0.12 ± 0.14
CAF	$T_m=231-234$	172.4 ± 6.7	0.15 ± 0.06
PVP K29-32	$T_g=164$	177.6 ± 1.7	5.53 ± 0.94
PVPVA 6:4	$T_g=106$	282.1 ± 2.3	3.97 ± 0.91

It is interesting to note that an apparent weight loss was seen for raw CAF powder well below the reported melting temperature (Table 3.6). This is ascribed to the sublimation of CAF molecule at a temperature around $\approx 175^{\circ}\text{C}$ (Moura Ramos et al., 2006).

The water contents for both the crystalline PCM and CAF are almost negligible. In contrast, the water content of homopolymer was noted to be relatively high as compared to PVPVA 6:4. This is due to the hygroscopic nature of the PVP (Callahan et al., 1982). The relationship between the water content of the raw material and the extrudates will be further commented on in a later section (Chapter 3.3.3.1).

To determine an appropriate extrusion temperature, HSM was used to identify the fusion temperature of the drug and polymer. The purpose of identifying the fusion temperature, a temperature which leads to the liquid state formation of the mixture, is to anticipate an appropriate extrusion temperature that will ease the flowability of the mixture in the HME barrel while processing. It should be emphasized that the fusion temperature here refers to a temperature that causes the transformation of the solid state of the mixture to a liquid or fluidized state. Thus, it may not necessary be equivalent to the T_m or T_g of the drug and polymer, respectively. Figure 3.5 (I) to (IV) show images of the 50% API-polymer physical mixture which were captured during heating.

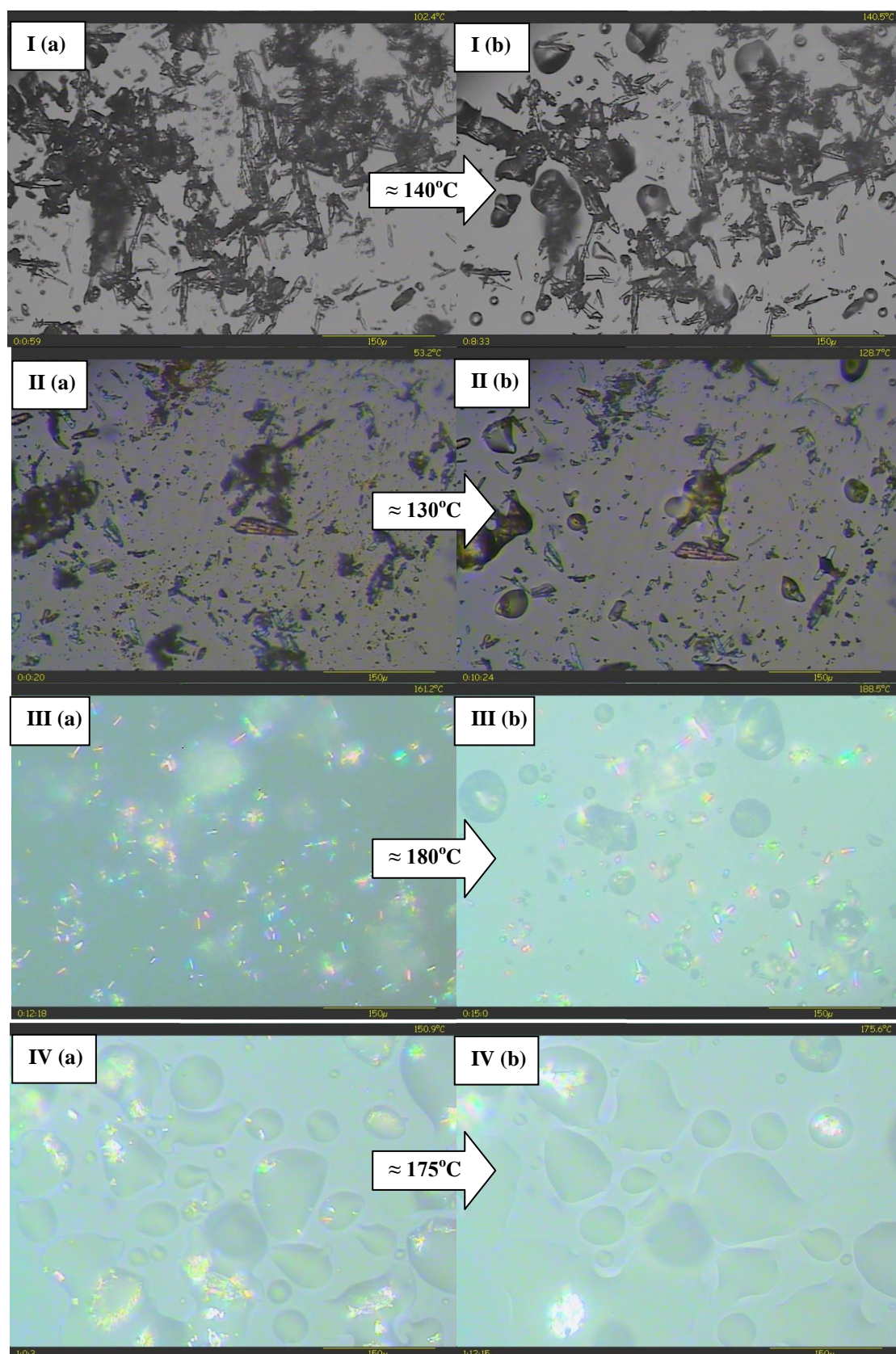


Figure 3.5: HSM screens of PM of 50% API-polymers. I) Fusion of PCM- PVP K29-32 at $T \approx 140^{\circ}\text{C}$, II) Fusion of PCM- PVPVA 6:4 at $T \approx 130^{\circ}\text{C}$, III) Fusion of CAF- PVP K29-32 at $T \approx 180^{\circ}\text{C}$, and IV) Fusion of CAF- PVPVA 6:4 at $T \approx 175^{\circ}\text{C}$. Figures on the left which is denoted as (a) are screens captured before the apparent fusion was noted and figures on the right which is denoted as (b) are screens captured when the fusion event was clearly seen.

The fusion temperature between the PCM and PVP K29-32 (Figure 3.5 I (a) and (b)) occurs at a temperature well below (i.e. circa 140 °C) the T_m and T_g of the PCM and PVP K29-32, respectively. The depressed temperature is in good agreement to the melting point depression data obtained previously in the DSC scan (Figure 3.2). It may therefore be expected that the extrusion of PCM in PVP K29-32 could be performed at lower temperatures than their individual thermal properties would indicate.

On the other hand, the fusion temperature between the PCM and PVPVA 6:4 occurred at temperature around 130 °C in the presence of PVPVA 6:4 (Figure 3.5 II (a) and (b)). This is due to the low T_g of PVPVA 6:4 leading to its softening below the melting of PCM and, subsequently, the dissolution of PCM into the softened PVPVA 6:4. Thus, it was also expected that this mixture could also be extruded at temperatures lower than the melting point of PCM.

HSM screens of the PM CAF-PVP carriers also show lower fusion temperatures i.e. ≈ 180 °C and ≈ 175 °C for PM CAF PVP K29-32 and PM CAF PVPVA 6:4, respectively. Both temperatures were below the T_m of the drug (Figure 3.5 (III) and (IV)). However, due to the low degradation temperature of PVP K29-32 (i.e. 180 °C from TGA data) it was thus expected that extrusion of the CAF PVP K29-32 needed to be performed at a lower temperature than 180 °C, whereas mixture of CAF PVPVA 6:4 could be extruded at 180 °C as the polymer degradation temperature is > 200 °C.

The extrusion of PCM PVPs and CAF PVPs

Previous studies have indicated that the extrusion processes may be performed at temperatures below the melting point of PCM due to the melting point depression of the PCM in the presence of PVP polymers. Thus, HME PCM-PVPs extrudates was prepared using an extrusion temperature of 120 °C. Clear extrudates were obtained up to 40% and 50% of PCM PVPVA 6:4 and PCM PVP K29-32 system, respectively. On the other hand, only 10% and 20% caffeine loading produced clear extrudates for PVPVA 6:4 and PVP K29-32, respectively. However, it should be emphasized that the extrusion of 10% HME PVP based extrudates was difficult as a low yield and high value of processing torque was noted. This is ascribed to the insufficient plasticization of the small fraction of API to the high fraction of PVP polymers which causes high viscosity of the resultant molten system.

Figure 3.6 illustrates the example of HME 20 to 70% PCM and PVP K29-32 extrudates that had been prepared at 120 °C. It was suspected that the extrudates with an opaque appearance provided evidence of incomplete drug solubilisation, while the transparent extrudates showed complete solubilisation of the drug. However, further investigation was needed to confirm the amorphicity of the clear extrudates.

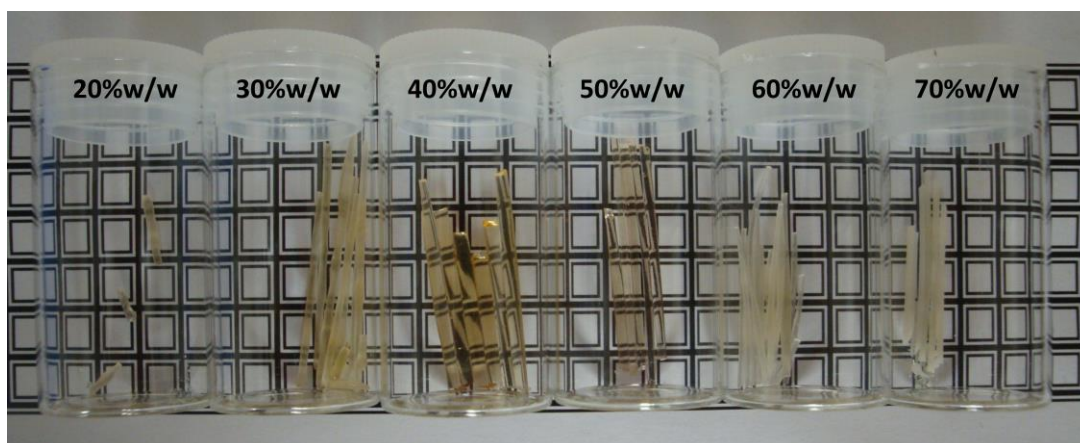


Figure 3.6: Appearance of extrudates of HME 20 - 70% PCM-PVP K29-32 prepared at 120 °C

3.3.2.2. HME parameter investigation: Torque

During the processing of the HME products, the viscosity of the molten material in the HME barrel was recorded as torque. This is a processing dependent variable, the value of which is a result of the parameters used in the processing such as temperature, residence time and screw speed. In this section, the effect of torque change during the extrusion process was studied. The effect of API loading, API types (interacting versus non-interacting) and polymer types (homopolymer and copolymer) on the torque are discussed.

The influence of API loading on torque

Figure 3.7 plots the changes of torque value while preparing the HME PCM PVPs as a function of PCM loading after 5 minutes of molten circulation.

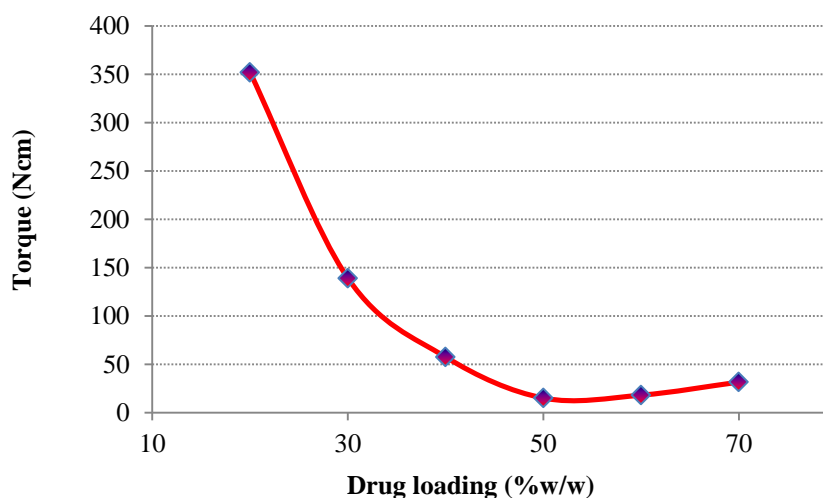


Figure 3.7: Torque value recorded during the processing of HME 20-70% w/w at 120 °C after approximately 5 minutes of molten circulation

As the API loading increased, the observed torque values were reduced. This is due to the plasticization of the polymer by the API in which the extent of plasticization increases with API loading. At 60% w/w of PCM, there was no further reduction in torque of the process which matches the appearance of the opaque extrudates as shown in Figure 3.6. Thus it is suggested that at the processing temperature of 120 °C, the viscosity of the molten system was at a minimum at a loading of PCM lower than 60%, i.e. 50%, which imply a maximum plasticizing effect of PCM on the PVP carriers. In other words, the higher drug loading led to increased plasticization of the system and hence a lower torque value. At the same loading system (50% PCM), the yields and output rates of the extrudates were also recorded to be the highest due to the good flowability of the molten mixture at a maximum plasticizing level.

It is worth mentioning that, during the extrusion process, the torque values were noted to increase gradually with time. This increment is particularly obvious for low drug loading systems. The mechanism of this change will be further discussed in the next sections.

The influence of the interacting and non-interacting API on torque

As mentioned previously, the torque values were noted to increase over the time of the processing, particularly at low drug loading. To effectively compare the influence of API types on the torque profile of HME PVP-based SD, both CAF and PCM were extruded with PVP K29-32 at a same processing temperature 160 °C. Figure 3.8 compares the torque profiles of PCM-PVP K29-32 and CAF PVP K29-32 across 5 minutes processing time.

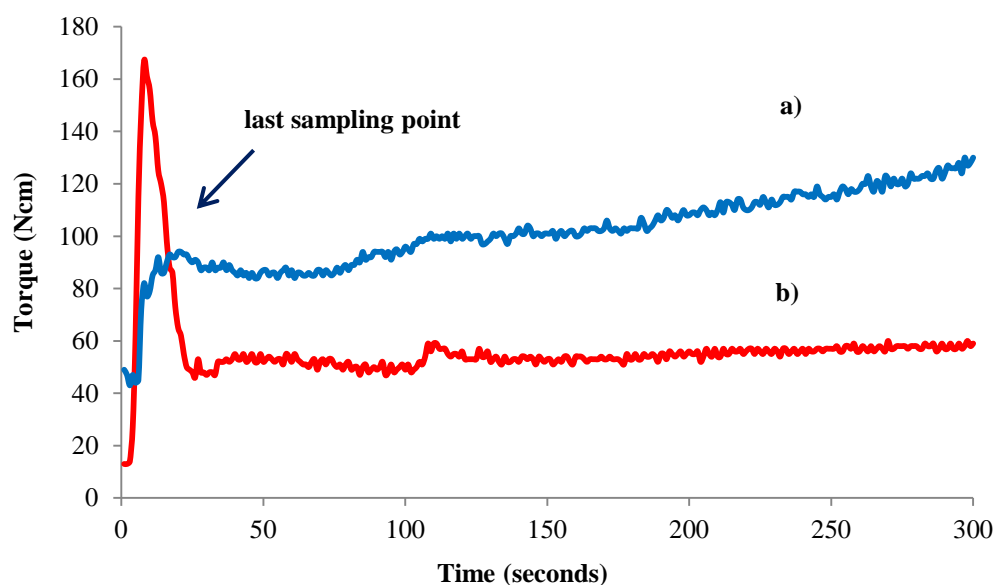


Figure 3.8: The comparison of torque profiles of a) HME 20% PCM-PVP K29-32 and b) HME 20% CAF-PVP K29-32. The peak at beginning of the profiles indicated the manual pressure applied to the raw material upon loading. The profile of torque was thus considered after this peak.

The peak noted at the beginning of the torque profile was attributed to the pressure applied while manual feeding of the mixture. It indicates the last sampling point of the mixture into the barrel. Thus, the torque profile of the molten mixture starts after the torque surge of the last sampling point. According to Figure 3.8, the torque value of HME 20% PCM in PVP K29-32 was higher (120 Ncm) than HME 20% CAF PVP K29-32 system (60 Ncm) after 5 minutes of extrusion, at the same extrusion temperature.

It is worth reminding that, extrusion process of PCM and PVP was performed at a temperature lower than T_g of the PVP, i.e. $T_{\text{process}} < T_g$. This extrusion process is feasible due to the plasticization effect of the tested drugs to PVP. However, this plasticization effect could be opposed by the drug-polymer interaction (Immergut and Mark, 1965). According to Figure 3.8, the torque profile of HME PCM -PVP K29-32 system increased gradually over time which suggests an increase in viscosity of the molten over time (Alsarra et al., 2011). This is an indication of opposing plasticization effect as a result of hydrogen bond interaction between the PCM with PVP during circulation of the molten in the barrel. Such behaviour was reported earlier for PVP hydrogels with PEG and thermal processing of Zein or Kafirin protein (Di Maio et al., 2010, Alsarra et al., 2011). In Alsarra et al. (2011), the increase in viscosity of the mixture at a constant shear was reported to be a result of inter-particulate interaction build-up in the mixture during shearing (Alsarra et al., 2011).

Unlike the torque profile of HME 20% PCM in PVP K29-32, the torque values of HME 20% CAF-PVP K29-32 remain almost constant for 5 minutes during the molten circulation period. This is due to the small molecular size of CAF in comparison to PVP which causes plasticization of PVP polymer chain. The constant torque profile was expected as the non-interacting CAF with respect to PVP polymer will not lead to the phenomena of opposing plasticization which was seen with PCM. Hence, it is suspected that hydrogen bond interaction between the API and PVPs could affect the flow properties of the mixture. The difference in flow properties of a molten mixture during production may cause a different mixing efficiency between the drug and polymer which could eventually alter the overall performance of solid dispersion.

The comparison of torque profile between PVP K29-32 and PVPVA carrier HME PCM system

The influence of different types of PVPs on the torque profile was also investigated. Figure 3.9 displays the torque profiles for HME 40% PCM system using both the PVP K29-32 and PVPVA 6:4 carrier system.

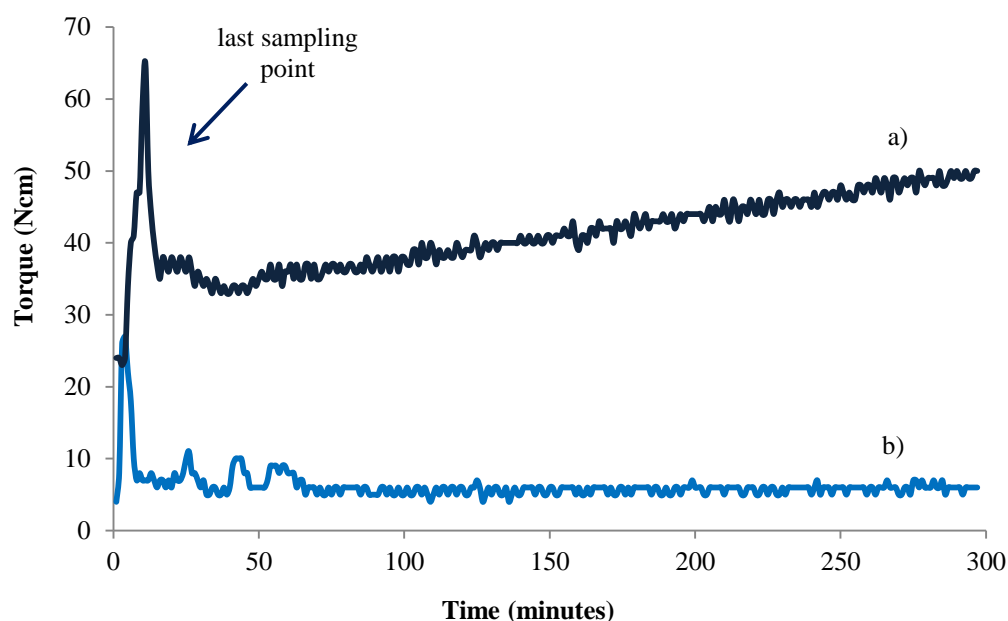


Figure 3.9: Torque of the HME twin-screw during hot melt extrusion at 120 °C as a function of processing time, a) HME 40% PCM PVP K29-32, b) HME 40% PCM PVPVA 6:4. The peak at beginning of the profiles indicated the manual pressure applied to the raw material upon loading. The profile of torque was considered after this peak.

As presented in Figure 3.9, HME PCM PVP K29-32 revealed an apparent increase in torque values across time which indicating the occurrence of opposing plasticization phenomena at the extrusion temperature, i.e. 120 °C lower than its T_g . Whereas, HME APIs in PVPVA 6:4 systems revealed relatively smaller torque values with minimal torque profile increment at HME 40% PCM-PVPVA 6:4 at the extrusion temperature of 120 °C. The different torque profiles seen for both the PVPs carrier system might be related to the T_g of the carrier in relation to the extrusion temperature, i.e. 120 °C. A more apparent opposing plasticization phenomenon would be seen in the processing of PVP K29-32 whereby, $T_{process}$ is less than T_g . In comparison, the effect of opposing plasticization was not seen in PVPVA 6:4 system as the $T_{process}$ is higher than its T_g .

To summarise, the torque value of a HME process is a dependent variable. It reflects the viscosity changes of the melt within the barrel (Chokshi et al., 2005). In this study, the decrease in torque value with higher PCM loading supports the suggestion of a plasticization effect exerted by PCM. An increase in torque values over the processing time was only noted in the interactive API (PCM) but not observed in the not-interactive API (CAF). On comparing PVP K29-32 and PVPVA 6:4, HME PVPVA 6:4 molten system was showed to have lower torque values with lower increase of torque values over the processing time. Following these observations, it should be kept in mind that the extent and direction of change in torque for different formulations may vary and hence may exert a variable effect on the final performance of the HME PVP-based SD.

3.3.3. Characterization of HME solid dispersions

After exploring the processing parameters in the preparation of HME PVP-based SD, the characterization of the extrudates was performed. In order to allow comparison between the interactive API, PCM to the non-interactive API, CAF, the extrusion temperatures used were each approximately 50 °C below the corresponding melting point of each API unless the degradation of the polymer necessitated use of a lower temperature. On that basis, mixtures of PCM-PVP K29-32 and PCM-PVPVA 6:4 were extruded at 120 °C. On the other hand, CAF-PVPVA 6:4 was prepared at 180 °C; however, extrudates of CAF-PVP K29-32 was prepared at temperature 155 °C due to possible degradation of PVP K29-32 at 180 °C.

3.3.3.1. Water content of physical mixtures and hot melt extrudates

Sorbed water could compromise the stabilizing effect of PVPs by plasticising the polymer, resulting in an increase in molecular mobility of the system (Tamaki et al., 2004). Hence, water content determination of the PVP based extrudates is a crucial step for better understanding of the effect of the HME process on stability of HME PVP-based SD (Callahan et al., 1982). To do this, water content of the prepared extrudates were investigated using TGA. Figure 3.10 shows an example of water content determination of HME 40% PCM-PVP K29-32 system by performing isothermal analysis on the samples at 100 °C for 30 minutes. This was conducted to erase the possible masking of water-related weight changes upon approaching the decomposition temperature (Peniche et al., 1993).

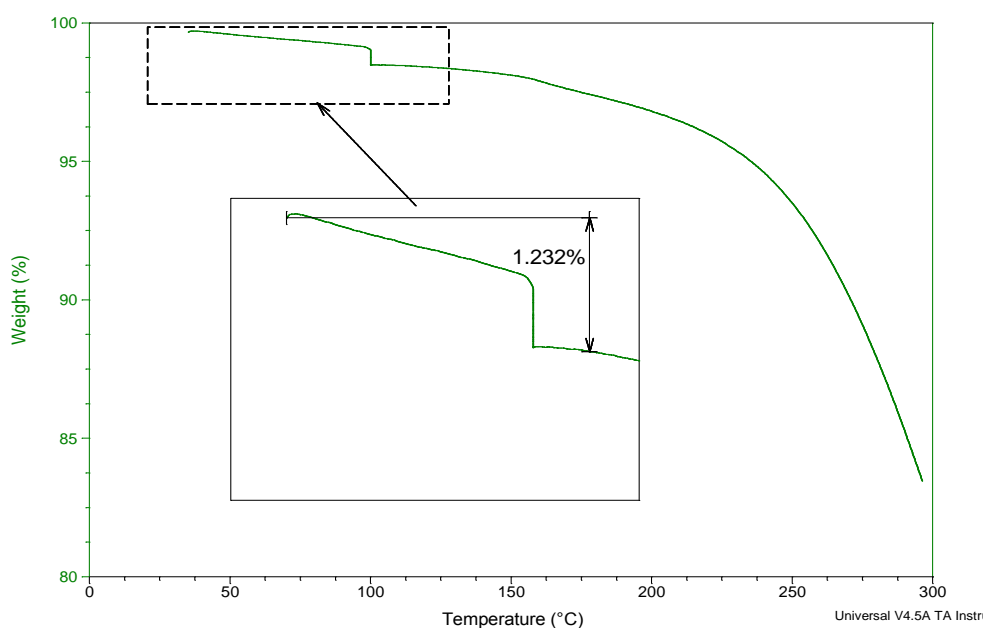


Figure 3.10: Water content determination of HME 40% PCM-PVP K29-32 system by performing isothermal analysis on the samples at 100 °C for 30 minutes. The marked value (1.232%) is the water content of this SD

All the freshly prepared HME PVP-based SDs were found to have lower water content as compared to their corresponding PM. Table 3.7 displays the values of water content for all the prepared extrudates.

Table 3.7: Water content (% w/w) of freshly prepared extrudates as a function of composition

Drug loading % w/w	Water content (%w/w)			
	HME PCM- PVP	HME PCM-	HME CAF-PVP	HME CAF-PVPVA
	K29-32	PVPVA 6:4	K29-32	6:4
10	-	-	2.59 ± 0.52	2.25 ± 0.38
20	1.73 ± 0.26	2.16 ± 0.39	2.44 ± 0.08	2.07 ± 0.38
30	1.45 ± 0.14	1.56 ± 0.13	-	-
40	1.27 ± 0.17	1.57 ± 0.16	-	-
50	1.24 ± 0.11	1.24 ± 0.15	-	-
60	1.20 ± 0.26	-	-	-
70	1.45 ± 0.18	-	-	-

The low moisture content of HME PVP-based SD was ascribed to the water evaporation of the mixture while hot melt processing condition. Interestingly, the HME CAF formulations possessed slightly higher moisture content despite the used of higher extrusion temperatures in preparing this formulations (please refer Table 2.12 for processing conditions).

3.3.3.2. MTDSC of HME PVP-based SD

3.3.3.2.1. MTDSC of HME PCM in PVP K29-32 and PVPVA 6:4

The thermal behaviours of the HME PVP-based SD were studied using MTDSC. Figures 3.11 and 3.12 display the thermograms of the HME PCM in PVP K29-32 and PVPVA 6:4 systems, respectively. From Figure 3.11 and Figure 3.12, it can be seen that a single T_g was obtained for the tested HME PVP-based extrudates; this allowed elucidation of the miscibility of PCM in both the PVP K29-32 and PVPVA 6:4 carrier systems. More specifically, the T_g(s) of the extrudates were numerically in between the T_g(s) of the API and carriers. These values indicated a strong plasticizing effect of PCM within PVP K29-32 and PVPVA 6:4. The T_g values reduced consistently with increased PCM loading, as is consistent with the plasticizing behaviour of PCM to its PVPs carrier.

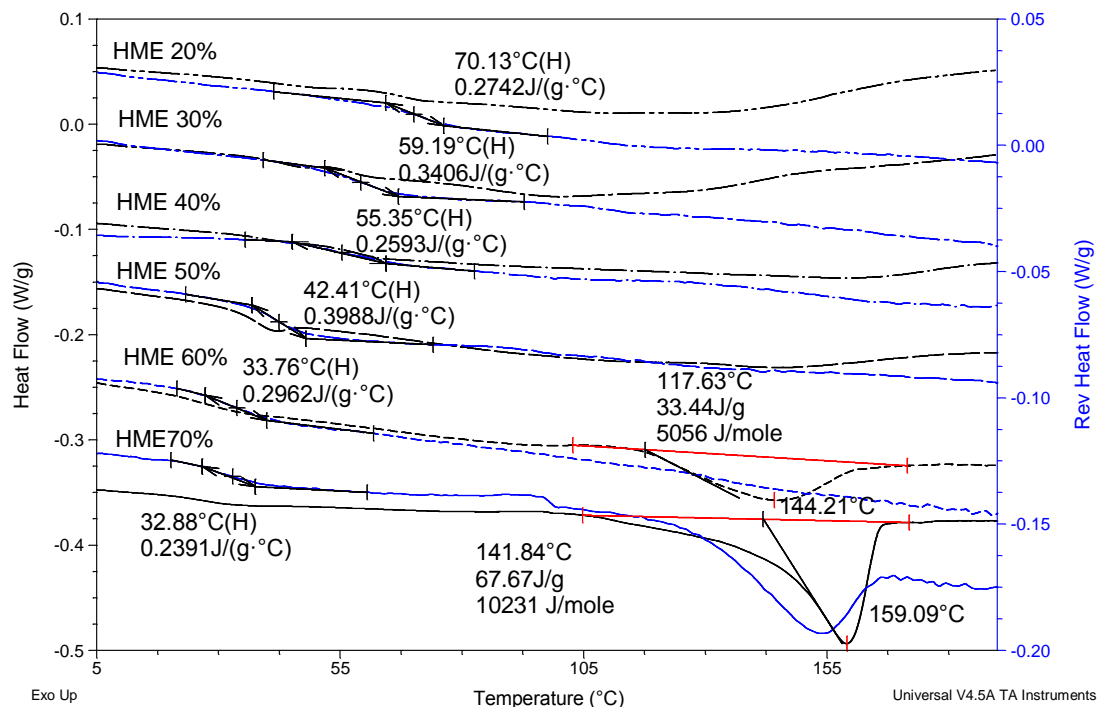


Figure 3.11: MTDSC thermograms of HME 20% - 70% PCM-PVP K29-32 using aluminum pin-hole pans

From Figure 3.11, no melting endotherm was noted in the thermograms (first heating cycle) of formulations ranging from 20% to 50% w/w PCM loading, suggesting the production of a wholly amorphous dispersion. However, melting peaks were noticeable for 60% and 70% w/w PCM loaded systems which indicated the existence of crystalline traces within these formulations. Dividing the melting enthalpy of the extrudates by the melting enthalpy of the pure crystalline PCM, there were approximately 14.43% and 29.17% crystalline drug detected in HME 60% PCM-PVP K29-32 and HME 70% PCM-PVP K29-32 respectively.

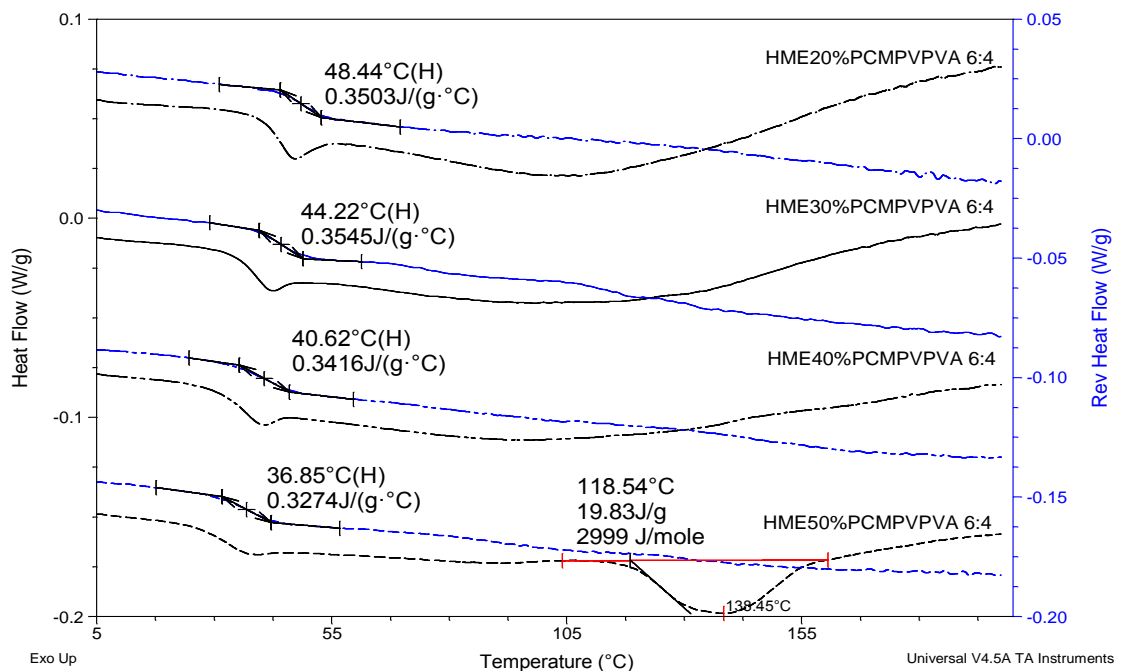


Figure 3.12: MTDSC thermograms of HME 20% - 70% w/w PCM-PVP VA 6:4

According to Figure 3.12, MTDSC thermograms of PVPVA 6:4 carrier systems show an apparent endotherm melting peak in the sample of HME 50% PCM-PVPVA 6:4. This implies the inability of the excess PCM to be dissolved in carrier matrix at the operating temperature. According to the melting endotherm, the amount of crystalline materials detected in the sample of HME 50% PCM PVPVA 6:4 was 8.91% of PCM, calculated from the ratio of the sample heat of fusion to that of the pure crystalline PCM.

Comparison between the theoretical Tg and experimental Tg

The nature of drug-polymer mixing can be studied by comparing the measured Tg(s) of the extrudates to the theoretical Tg(s) as estimated from the Gordon-Taylor (G-T) equation (Gordon and Taylor, 1952). Strongly interacting components tend to give a mixture with Tg value higher than that would be expected theoretically. Assuming ideal mixing, Tg values of a mixture could be estimated based on volume additivity theory as described in Equation (3.10) (Gordon and Taylor, 1952).

$$Tg = \frac{w_1 Tg_1 + K w_2 Tg_2}{w_1 + K w_2} \quad (3.10)$$

where w_1 and w_2 are the weight fractions of drug and polymer, and Tg_1 and Tg_2 are glass transition temperatures of drug and polymer, respectively. Based on the thermodynamically consideration, Couchman and Karasz has derived an equation similar to G-T Equation (3.10) but the K-value was obtained by Equation (3.11) (Couchman and Karasz, 1978),

$$K = \frac{\Delta Cp_2}{\Delta Cp_1} \quad (3.11)$$

where ΔCp is the change in heat capacity between the liquid-like and glassy state. Many have found that this equation is useful for prediction of Tg of a mixture (Shamblin et al., 1998, Hancock and Zografis, 1994). Thus in this study, Tg of the mixture were estimated from Equation (3.10) with K-value obtained from Equation (3.11).

It is noted from the previous TGA that there were appreciable water content detected from the HME PVP-based extrudates (circa 1.2 - 2%). Thus the resultant HME extrudates is effectively a ternary system of the mixture of API-carrier-water. To predict the theoretical Tg for the ternary systems (PCM-polymer-water), Equation (3.12) and (3.13) was used (Truong et al., 2002).

$$Tg = \frac{w_1 Tg_1 + K_{12} w_2 Tg_2 + K_{13} w_3 Tg_3}{w_1 + K_{12} w_2 + K_{13} w_3} \quad (3.12)$$

where the w_1, w_2 and w_3 are the weights of PCM, polymer, and water respectively, the $Tg_1, Tg_2,$ and Tg_3 are the glass transition temperatures of API, polymer, and water respectively, and the $\Delta Cp_1, \Delta Cp_2,$ and ΔCp_3 are the changes in heat capacity of of API, polymer, and water respectively, between the liquid-like and glassy state of the components. The constant value of K_{12} and K_{13} can be estimated by Equation (3.13).

$$K_{12} = \frac{\Delta Cp_2}{\Delta Cp_1} \quad \text{and} \quad K_{13} = \frac{\Delta Cp_3}{\Delta Cp_1} \quad (3.13)$$

Along with the calculation, the numbers used for the calculation of theoretical Tg values were presented in Table 3.8.

Table 3.8: Values used to calculate the theoretical Tg of the mixture of Ternary PCM-Polymer-Water system

Component	Tg (K)	Heat Capacity (J/g. K)	Reference
PCM	298.29 ± 0.0954	0.713 ± 0.022	-
PVP K29-32	437.33 ± 0.249	0.291 ± 0.012	-
PVPVA 6:4	375.5 ± 0.821	0.293 ± 0.036	-
Water	136 ± 1	0.089 ± 0.005	(Hallbrucker et al., 1989)

Figure 3.13 demonstrated the theoretical and experimental Tg values for the binary and ternary systems of PCM PVPs (for both PVP K29-32 and PVPVA 6:4) and PCM-PVP-water, respectively.

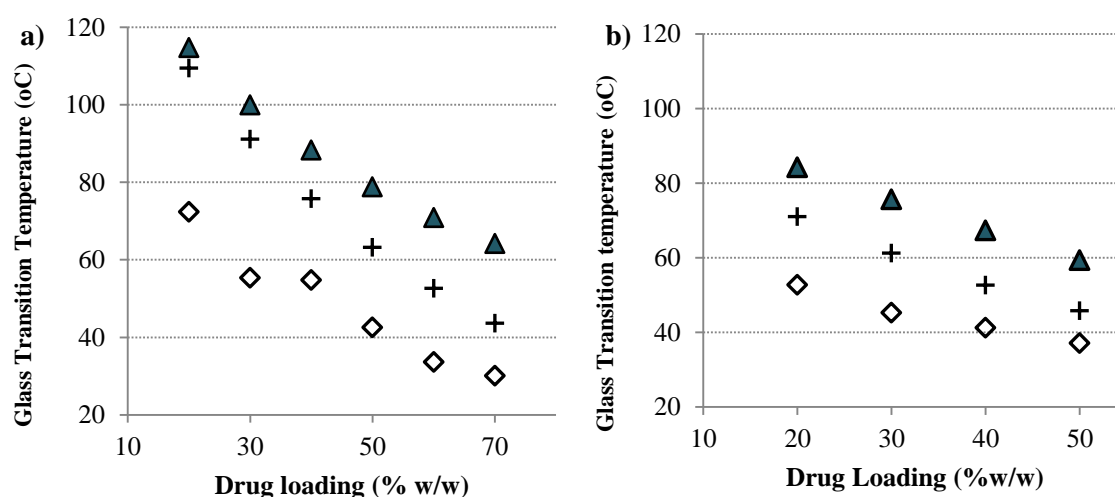


Figure 3.13: Comparison of experimental Tg(s) to calculated Tg(s) based on Gordon Taylor equation a) HME PCM PVP K29-32, b) HME PCM PVPVA 6:4: binary PCM-PVPs polymer theoretical value based (Δ), ternary PCM-PVPs polymer-water theoretical value (+) and experimental glass transition values (\diamond)

It is known that the existence of drug-polymer interactions may cause the observation of experimental T_g values higher than the theoretical ones. However, in this study, a reverse trend was seen, whereby the T_g (s) of the products were unexpectedly lower than the values predicted via G-T equation (Figure 3.13). Van de Mooter et al. (2001) suggested that the incorporation of water content in GT-prediction could accurately estimate the T_g of the mixtures which contain moisture traces (Van den Mooter et al., 2001). After the consideration of moisture content in calculations of the theoretical T_g in the ternary system as shown by the + in Figure 3.13, the predicted T_g values remain higher than the experimental T_g (s) of the HME PVP-based SD extrudates.

The large negative deviations of the experimental T_g (s) of HME PVP-based SD from the predicted T_g (s) suggests non-ideal mixing between the two components. Similar findings have also been encountered in previous publications where negative deviation of the detected T_g (s) were noted (Shakhtshneider et al., 2007a, Shakhtshneider et al., 2007b, Di Martino et al., 2004, Hancock and Zografi, 1997, Malaj et al., 2010, Gashi et al., 2009). The authors explained this effect in terms of the small molar volume of drug molecules that led to their diffusion inside the polymer which causes a higher free volume of the system than the theoretically anticipated state. Furthermore, according to Nair et al. (2001) the negative deviation from the theoretical predicted values could also be accounted for the lower intermolecular strength of the blend as compared to the intermolecular strength of the single components, i.e. adhesive energy is lower than cohesive energy of the system (Nair et al., 2001).

With the presence of the proton acceptor in PVP structure and the proton donor in PCM molecule, hydrogen bond between these two compounds is reported before (Sekikawa et al., 1978, Garekani et al., 2003). On one hand, PVP is a hygroscopic homopolymer which interacts preferentially with water through its carbonyl group and did not interact among the main chain (Gangopadhyay, 2008, Callahan et al., 1982). Therefore the cohesive interaction of PVP alone is expected to be low. On the other hand, when the crystalline PCM is turn into amorphous form, it loses its intermolecular hydrogen bond which also infers its low cohesive energy. Thus, in this study, the lower intermolecular strength of the blend as compared to the intermolecular strength of the single components could not be the main reason for the observed negative deviation. Further investigations were performed to understand the unexpected T_g values deviation.

Conventionally, T_g is easily lowered by the presence of small molecules such as water. Here, the effect of water molecules was further explored to test if water causes the large negative deviation of T_g (s) as seen in Figure 3.13. To do this, T_g (s) of the ground extrudates (prepared by gently milling in a mortar and pestle) and intact extrudates were compared by scanning both samples in pinhole pan using MTDSC. Figure 3.14 shows the MTDSC thermograms of HME 20% PCM PVP K29-32 for both the ground and intact extrudates with total heat flow and reversing heat flow signals.

It is obvious from Figure 3.14 that the MTDSC thermogram of the ground extrudates indicates an obvious endotherm in the region of 60-80 °C which is ascribed to the efficient moisture removal upon heating the sample in pin-hole pan. On the other hand, MTDSC thermograms of the intact extrudates show no apparent endotherm signal in the same region of 60-80 °C which implies inefficient water loss from the intact extrudates.

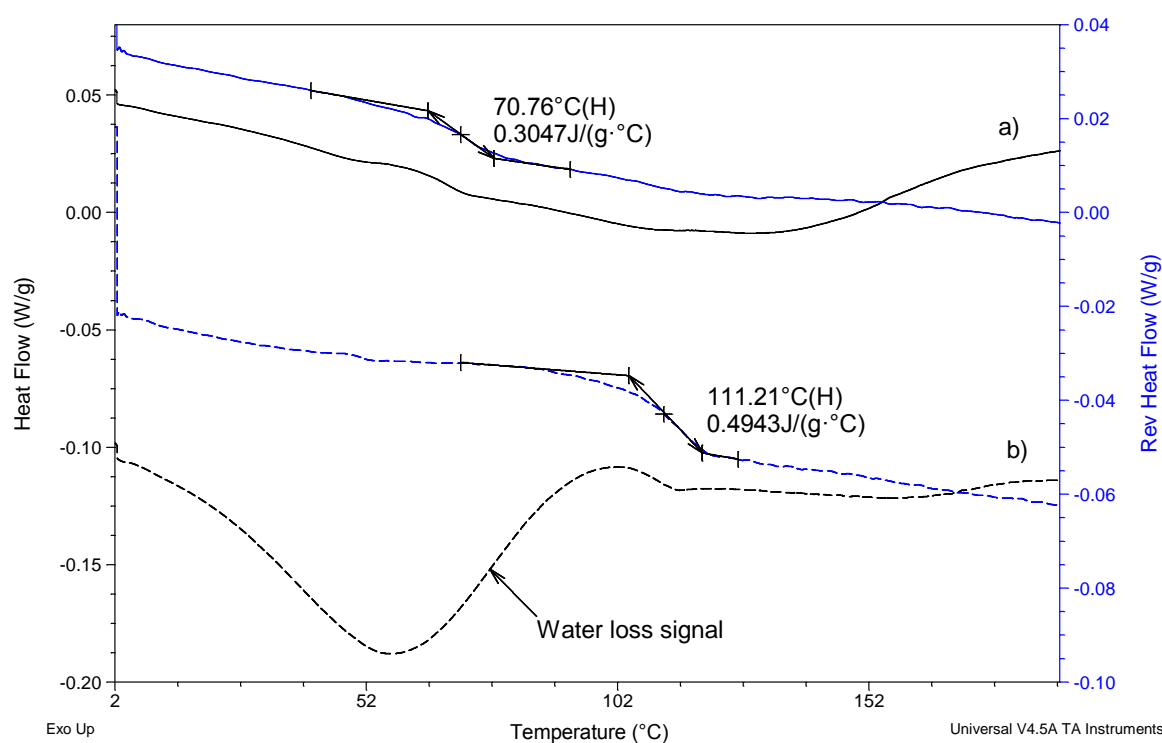


Figure 3.14: MTDSC thermograms of HME 20% PCM PVP K29-32 a) intact extrudates of circa 4 mm, b) ground extrudates from the same sample by using aluminium pin-hole pan

Furthermore, the T_g value in the ground extrudates is higher than the same sample of intact extrudate, despite the possibility of absorbing moisture during the grinding process. This is due to the more efficient removal of moisture from the ground extrudate than the intact one. Accessing T_g values of the ground extrudates, the newly detected T_g values coincide well with the predicted values from the G-T equation of binary system. Following this observation, it is suggested that there were excess moisture trapped in the matrix of extrudates which increased molecular mobility of the solid dispersion systems while DSC experiments. This results in the large negative deviation of the experimental T_g from the theoretical one as seen in Figure 3.13.

3.3.3.2.2. MTDSC of HME CAF PVP K29-32 and PVPVA 6:4

After analysing the DSC data of HME PCM system, this section will outline the DSC characteristics of the non-interactive API, CAF, in HME PVP systems. CAF is an easily crystallisable drug (Sekikawa et al., 1978). There is no reported T_g for CAF but there have been some reports of an anomalous event at $-13\text{ }^\circ\text{C}$ to $-10\text{ }^\circ\text{C}$ which might be associated with its T_g (Descamps et al., 2005b, Moura Ramos et al., 2006). In this study, recrystallization of molten CAF was immediate upon quench cooling in the DSC (data not shown) and all attempts to produce the glassy CAF by preventing its recrystallization were unsuccessful, as shown by the absence of T_g in the DSC thermogram. This is mainly due to the intensive molecular motion of CAF molecules which favors its free energy loss and recrystallization process (Descamps et al., 2005b). On this basis, G-T calculations were not performed due to the perceived unreliability and experimentally undetectable of the glass transition temperature value for the CAF alone.

HME CAF-PVP K29-32

Figure 3.15 shows the MTDSC thermograms of HME 10% CAF-PVP K29-32 extruded at $155\text{ }^\circ\text{C}$.

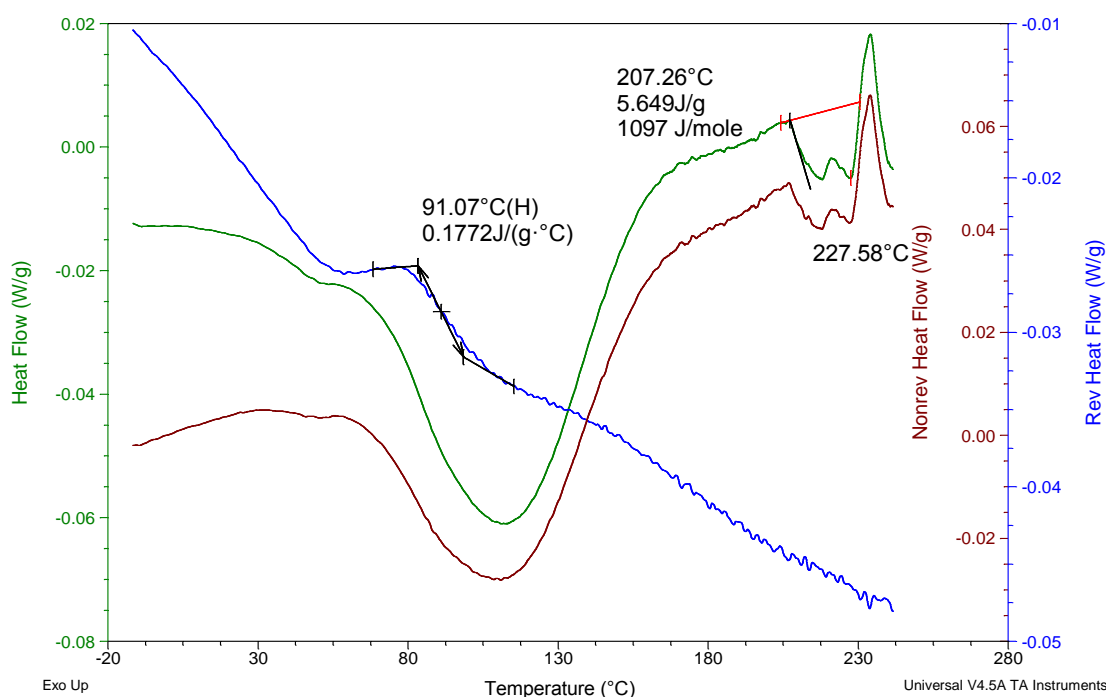


Figure 3.15: MTDSC thermograms of HME 10% CAF-PVP K29-32 by using pin-holed pan

According to Figure 3.15, HME 10% CAF-PVP K29-32 exhibited partially glassy behaviour as indicated by a single T_g detected at $95.6 \pm 4.1\text{ }^\circ\text{C}$ and a small melting peak at circa $207\text{ }^\circ\text{C}$.

Figure 3.16 shows the MTDSC thermograms of HME 20% CAF-PVP K29-32 extruded at 155 °C. Similar observation was seen in HME 20% CAF-PVP K29-32 extrudate as it shows a single T_g at 75.4 ± 3.9 °C, and a melting endotherm at 212 °C in its DSC thermogram. However, an anomalous peak at around 115 °C was also noted in the total heat flow and non-reversing heat flow of Figure 3.16. The cause of the anomalous exothermic peak at 115 °C was unknown. It is suspected that the anomalous peak may be related the recrystallization of the amorphous CAF which will be further confirmed by HSM investigation in the later part of this section.

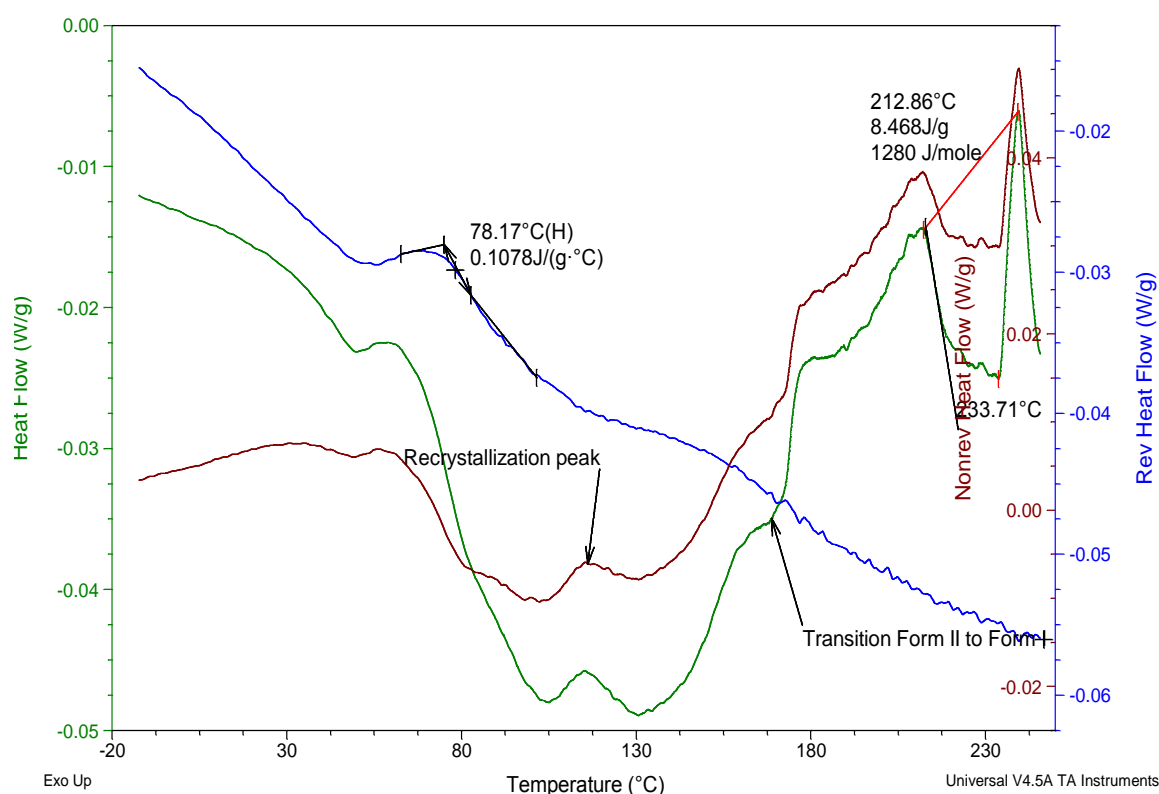


Figure 3.16: MTDSC thermogram of HME 20% CAF - PVP K29-32 by using pin-holed pan

The detected melting endotherm in both HME 10% and 20% CAF-PVP K29-32 formulations suggested the existence of surplus crystalline material within the extrudates.

HME CAF-PVPVA

Figure 3.17 displays the MTDSC thermogram for HME 10% CAF – PVPVA 6:4. According to Figure 3.17, the thermogram showed a T_g at around 60.9 ± 1.0 °C and an anomalous exothermic transition temperature at about 115 °C similar to that detected in HME 20% CAF-PVP K29-32 in Figure 3.16. No melting endotherm was noted from the profile which suggested the absence of crystalline material in the sample or dissolution of the crystalline material into the polymer carrier upon heating.

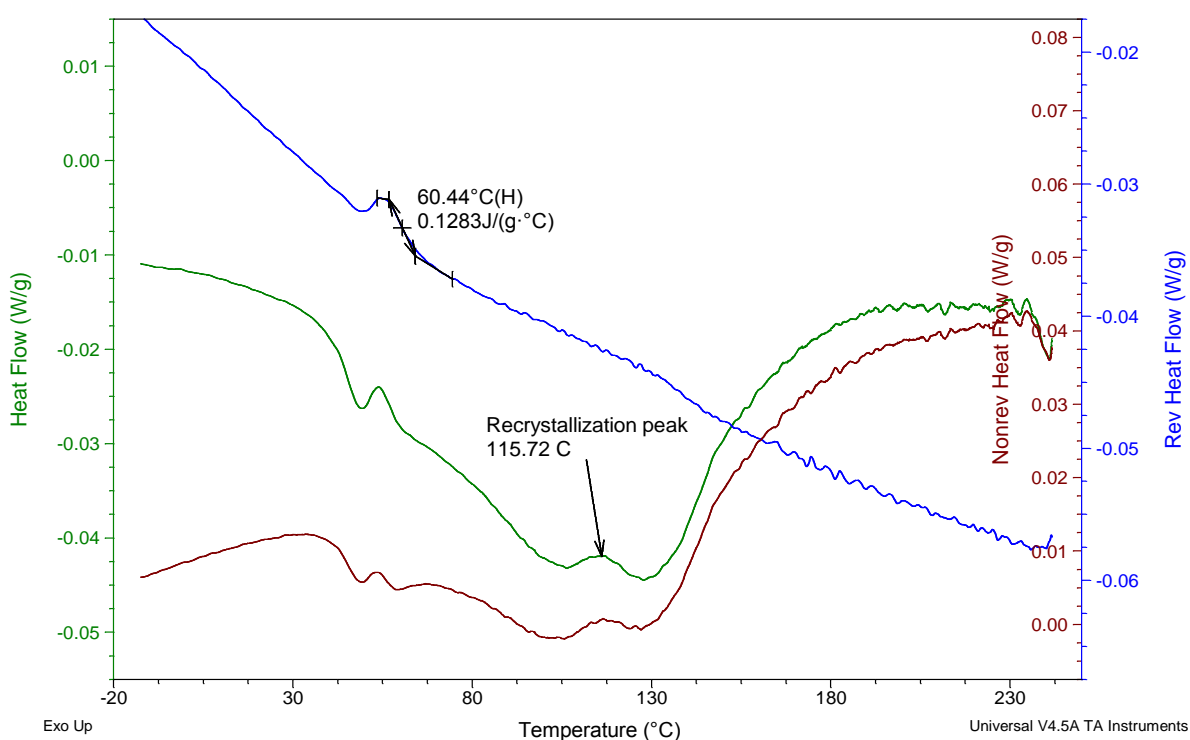


Figure 3.17: MTDSC thermogram of HME 10% w/w CAF in PVPVA 6:4 by using pin-holed pan

The MTDSC thermograms of the 10% CAF in PVPVA 6:4 (Figure 3.17) is complex, with transitions seen at circa 50 °C, 115 °C and 140 °C. Given the non-linear nature of the baseline, interpretation becomes even more challenging as the exothermic, endothermic and reversing or non-reversing nature of the transitions becomes unclear. Nevertheless, it is possible to gain insights into these events via a combination of supportive HSM experiments and consideration of previous work on CAF polymorphs performed by Descamps et al. (2005). Figure 3.18 displays the captured screens of HME 10% CAF-PVPVA 6:4 upon heating from room temperature up to 250 °C by using HSM.

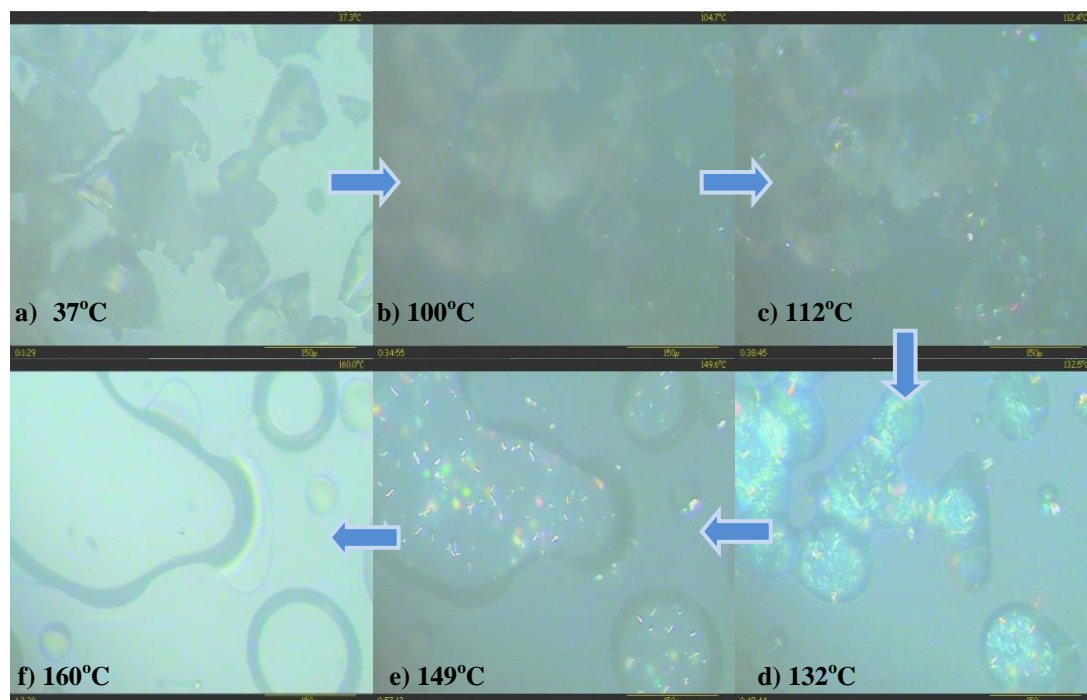


Figure 3.18: HSM investigation of HME 10% CAF-PVPVA 6:4 at a heating rate of 10 °C per minute. The marked temperatures at left bottom corner of each screen indicates the temperature of sample

HSM screens in Figure 3.18 (c) show the appearance of crystalline material at circa 112 °C, which was in coherent to the anomalous exothermic peaks observed in both HME 20% CAF-PVP K29-32 (Figure 3.16) and HME 10% CAF-PVPVA 6:4 (Figure 3.17). Thus it is suggested that the anomalous exothermic peaks observed in these thermograms were related to the recrystallization of some of the amorphous CAF from the dispersion.

Besides, these observed crystals were disappearing at circa 140 °C (in Figure 3.18 (e)) which is well below the melting point of the drug but coincident with the transition between Form II and Form I caffeine. Descamps et al. (2005) have suggested that the transformation between Form II and Form I on heating is accompanied by a significant change in dielectric mobility, in turn reflecting a sizeable increase in molecular mobility as the drug goes through this enantiotropic transition on heating. The disappearance of the crystals may well be associated with this increased mobility leading to a greater tendency to dissolve in the PVPVA 6:4 on formation of the more mobile Form I at circa 140 °C.

Figure 3.19 shows the MTDSC thermogram of HME 20% CAF-PVPVA 6:4. From the Figure, a T_g was noted at 48.0 °C which indicated certain extent of amorphicity of the HME 20% CAF-PVPVA 6:4 extrudate.

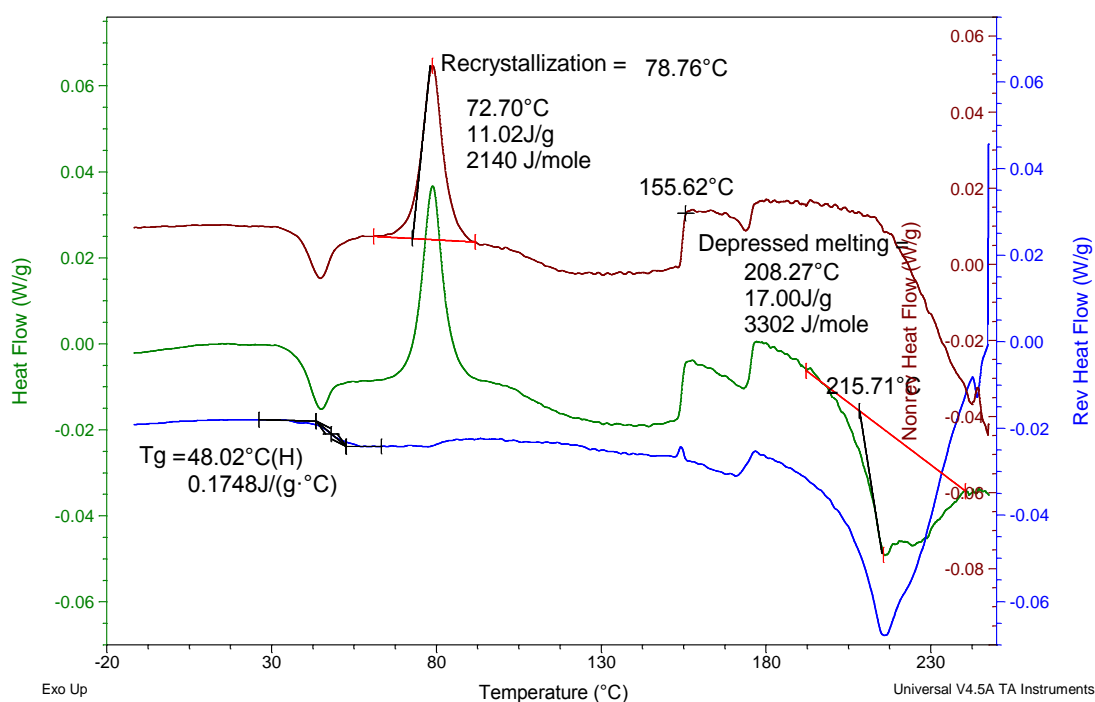


Figure 3.19: MTDSC thermogram of HME 20% CAF PVPVA 6:4 by using pin-holed pan

Unlike the HME sample with 10% loading of CAF, the recrystallization phenomenon was clearly shown in MTDSC curve of HME 20% CAF-PVPVA 6:4. The obvious recrystallization occurred at 78.8 °C which revealed at a slightly lower temperature than the recrystallization temperature in HME 10% CAF-PVPVA 6:4. This is due to the lower proportion of polymer in retarding the recrystallization event in the HME 20% CAF-PVPVA 6:4 system. Finally, an apparent melting endotherm of CAF was seen at temperature 208 °C which was suggested the partially crystalline nature of this system (HME 20% CAF-PVPVA 6:4). An end point endotherm of 155 °C was observed which might be ascribed to the prolonged process of polymorphic transformation of Form II to Form I CAF in the presence of PVPVA 6:4 started from 140 °C which was anticipated by the HSM data in Figure 3.18 (Moura Ramos et al., 2006, Pinto and Diogo, 2006).

In summary, therefore, it is suggested that the system in PVPVA 6:4 is initially amorphous and undergoes a glass transition at circa 50 °C; on further heating the Form II crystallizes out at around 72 °C (for HME 20% CAF-PVPVA 6:4) or 115 °C (for HME 20% CAF-PVP K29-32 and HME 10 CAF-PVPVA 6:4) and converts to Form I at circa 140 to 150 °C which subsequently melts at circa 200 °C. This is in contrast to dispersions in PVP K29-32, (Figure 3.15 and 3.16) whereby the system appears to be largely but not entirely amorphous, with a T_g coincident with the water loss peak, and a small melting peak detected at the melting point of Form I.

3.3.3.3. ATR-FTIR studies of HME preparation

It is worth emphasizing at this point that PCM was chosen as an interactive API due to the availability of proton donor in its chemical structure. Whereas, CAF is chosen as a non-interactive API as there is no proton donor available in its chemical structure for the interaction with proton acceptor of PVP monomer. This could be further confirmed from ATR-FTIR study of the prepared samples.

3.3.3.3.1. ATR-FTIR studies of HME PCM - PVP K29-32

Figure 3.20 shows the ATR-FTIR spectra of pure PCM, PVP, PM and HME of 20-70% PCM PVP K29-32.

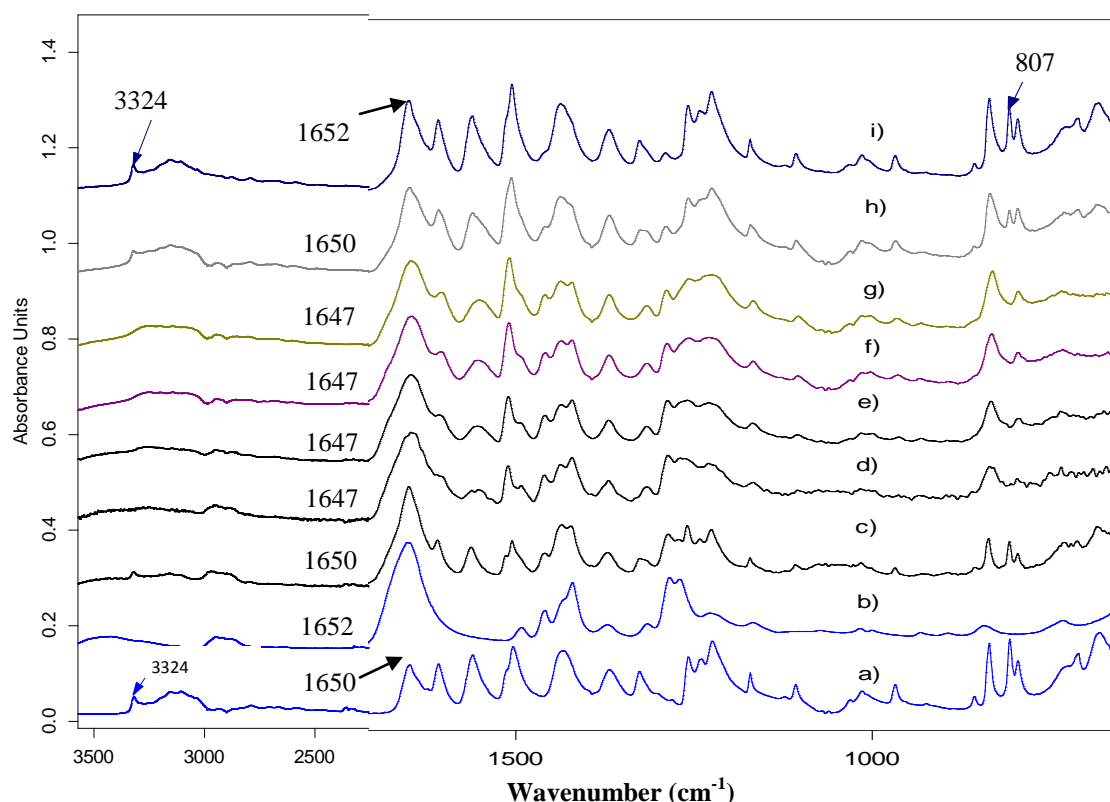


Figure 3.20: ATR-FTIR spectra of PM and HME PCM-PVP K29-32 a) Form I PCM, b) raw PVP K29-32, c) PM 50% PCM and PVP K29-32, d) HME 20% PCM-PVP K29-32, e) HME 30% PCM-PVP K29-32, f) HME 40% PCM-PVP K29-32, g) HME 50% PCM-PVP K29-32, h) HME 60% PCM-PVP K 29-32, i) HME 70% PCM-PVP K29-32

Carbonyl (C=O) group of PVP monomer reveals stretching at 1652 cm^{-1} . After the HME processing of PVP K29-32 with PCM, this band was slightly shifted to the lower frequency i.e. 1647 cm^{-1} . This indicated a certain extent of interaction that occurred at the carbonyl group of PVP monomer.

The ATR-FTIR spectrum of crystalline PCM indicates a characteristic band at 3324 cm^{-1} which is attributed to the NH stretching of PCM. This band was broadened in HME product which suggested the weakening or disappearing of the original –NH stretching vibration. Furthermore, the –OH stretching band of crystalline PCM at region 3100 cm^{-1} was also broadened in the HME PCM PVP K29-32 products as compared to its pure crystalline ATR-FTIR spectrum which shows a moderate stretching band. Both changes of the characteristic peaks in the regions of 3100 cm^{-1} and 3324 cm^{-1} indicated different vibration mode of –NH and –OH in the HME PVP-based SD. This might be due to the breaking of intermolecular hydrogen bonds of the crystalline PCM that dissolves into the polymer carrier while HME processing.

At the fingerprint region of circa $900\text{-}700\text{ cm}^{-1}$, triplet peaks were seen for pure PCM and PM 50% PCM-PVP K29-32. However, in HME products, only a doublet was seen. According to Qi et al. (2008), the triplet peaks in this region was attributed to the crystalline material of PCM, whereas a doublet peaks infer amorphousness of the PCM. Therefore, based on the ATR FTIR spectra in Figure 3.20, HME 10% to 50% PCM PVP K29-32 extrudates were amorphous in nature as shown by the double band in print region of $900\text{-}700\text{ cm}^{-1}$. At higher PCM loading of HME PVP-based (60% and 70%) SD, the ATR-FTIR spectra show the reappearance of the diagnostic peaks of crystalline PCM (3100 , 3324 and 807 cm^{-1}) which implies the minor crystal trace in these samples. This result is in agreement to the MTDSC thermograms as presented in Figure 3.11.

Combining the observations of down-shifted carbonyl stretching band in PVP monomer and the broadening in –NH/–OH stretching band of PCM molecules, it was thus suggested that hydrogen bond interactions were formed between the C=O group of PVP monomer and NH or OH groups of PCM (Nair et al., 2001, Wang et al., 2002). Attributions of each band from the spectra of HME products are further detailed in Table 3.9.

Table 3.9: Infrared bands of hot melt extrudate of PCM PVP in comparison to the corresponding PM

Wavenumber (cm ⁻¹)	Attribution in pure PCM (Wang et al., 2002)	Changes observed in HME extrudates
3324	NH stretching vibration	Broadening of the band indicated stretching of -NH via intermolecular hydrogen bond within the crystal disappears, i.e. irregularity induced by incorporation of PVP or dissolved PCM molecules.
3126	H-OH/OH stretching vibration plus combination band	The glassy state of HME products causes slight shift in this band to higher wave-number which representing the solidified state of solid solution
3174	H-OH/OH	This band is still observed due to intra and intermolecular hydrogen bond with polymer molecules
1650	C=O stretching vibration	The glassy state of HME products causes slight shift in this band to lower frequency representing the hydrogen bond interaction
1560	NH in plane bending	It reduced intensity, shifted to lower frequency due to intermolecular hydrogen breaking in PCM crystal thus indicated amorphous formation
1609, 1504, 1433	Aromatic mode	1512-shift to higher wavenumber due to solid solution form
1374	CH bend	Higher peak relatively to aromatic mode
1328	OH bending vibration	Shifted to lower wavenumber indicated stronger hydrogen bond interaction
1226-1259	C-O/C-N stretching vibration	broaden and higher frequency due to dispersive within polymer and amorphous have weaker bonds than crystal

3.3.3.3.2. ATR-FTIR studies of HME PCM in PVPVA 6:4

Figure 3.21 shows the ATR-FTIR spectra of pure PCM, PVPVA 6:4 and HME PCM-PVPVA 6:4 systems. According to Figure 3.21 (b), ATR-FTIR spectra of PVPVA 6:4 indicates two peaks at C=O stretching region, i.e. 1734 cm^{-1} and 1667 cm^{-1} which correspond to the C=O stretching of vinyl acetate and pyrrolidone, respectively.

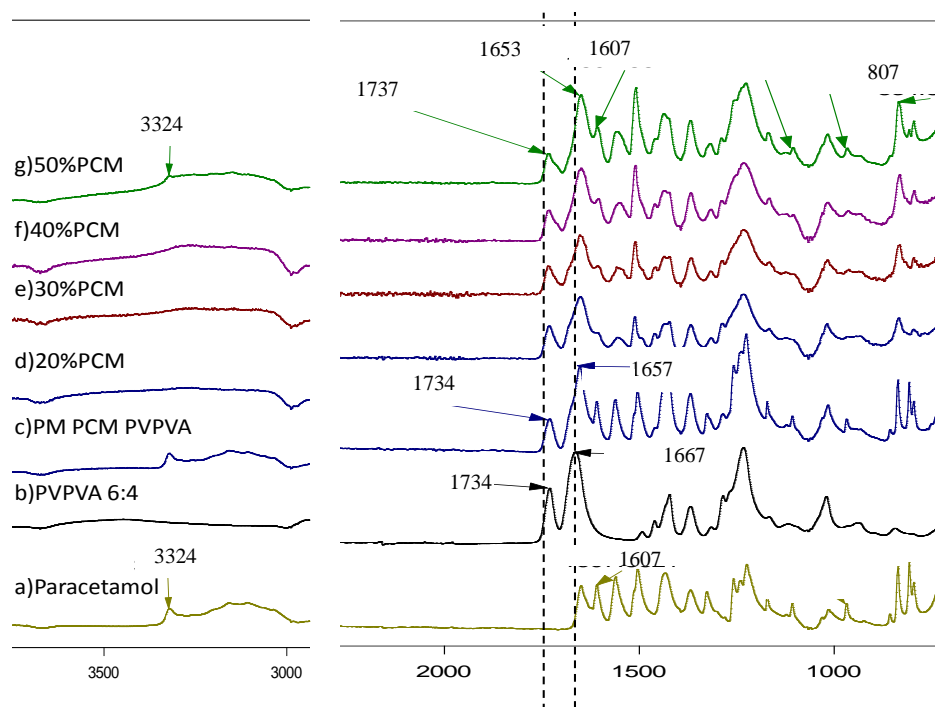


Figure 3.21: ATR-FTIR spectra of PCM, PVPVA 6:4 and HME PCM-PVPVA 6:4 systems

Interestingly, it is found that the C=O stretching (1734 cm^{-1}) of the VA moiety in both PM and HME preparations of binary PCM-PVPVA 6:4 did not shift in comparison to the spectra of PVPVA 6:4 alone. This is in contrast to the C=O stretching of pyrrolidone where down-shifting of its peak position (from 1667 cm^{-1} to 1656 cm^{-1}) was noted in HME PCM-PVPVA 6:4 in comparison to the PM and raw PVPVA 6:4. Therefore it was believed that the main interactions between PCM and PVPVA 6:4 occurs preferentially at the C=O group of the pyrrole group rather than the C=O in vinyl-acetate group. On that basis, the intensity of PCM-polymer interaction was higher in PVP K29-32 carrier system than in HME PVPVA 6:4 system.

3.3.3.3.3. ATR-FTIR studies of HME CAF-PVP K29-32 and PVPVA 6:4

Figure 3.22 compares the ATR-FTIR spectra of CAF, PVP K29-32 and HME CAF in PVP K29-32. ATR-FTIR spectra of HME 10-20% CAF in PVP K29-32 did not show any significant peak position shift in the carbonyl stretching region of the PVP as compared to its corresponding PM

(Figure 3.22). This was attributed to the absence of physical interactions between the CAF and PVP (PVP K29-32 and PVPVA 6:4) molecules.

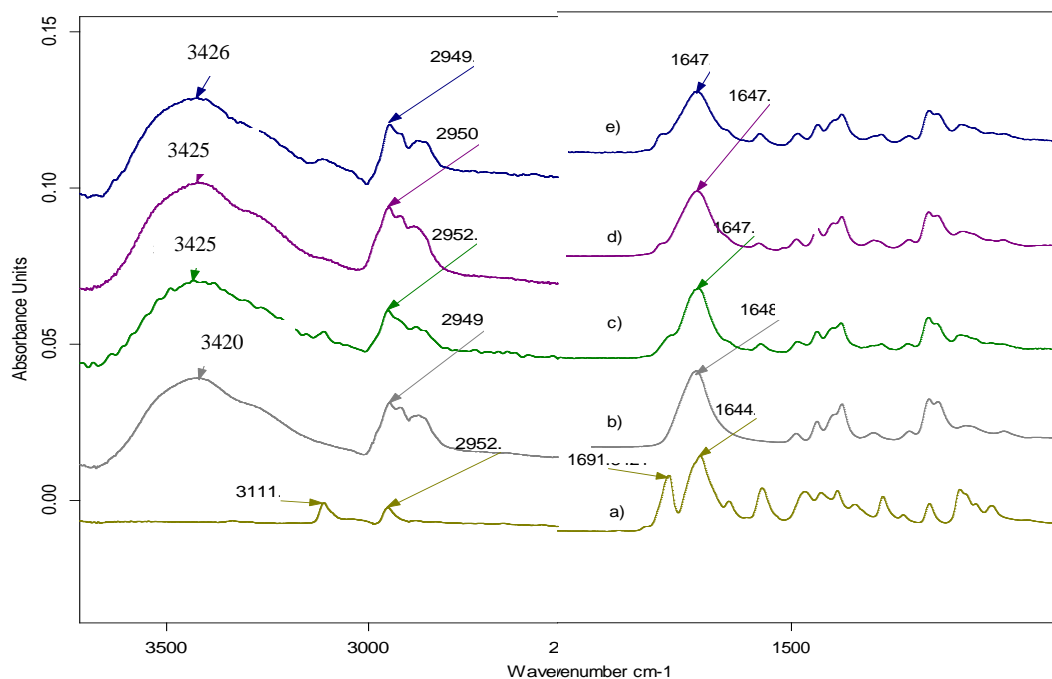


Figure 3.22: FTIR spectra for a) CAF, b) PVP K29-32, c) PM 10% CAF-PVP K 29-32, d) HME 10% CAF-PVP K29-32, e) HME 20% CAF-PVP K29-32

Figure 3.23 shows the ATR-FTIR spectra of CAF, PVPVA 6:4 and HME CAF-PVPVA 6:4. Similarly, no significant peak shift is noted in the PM and HME of CAF-PVPVA 6:4 which reconfirms the lack of drug-polymer interaction in these systems.

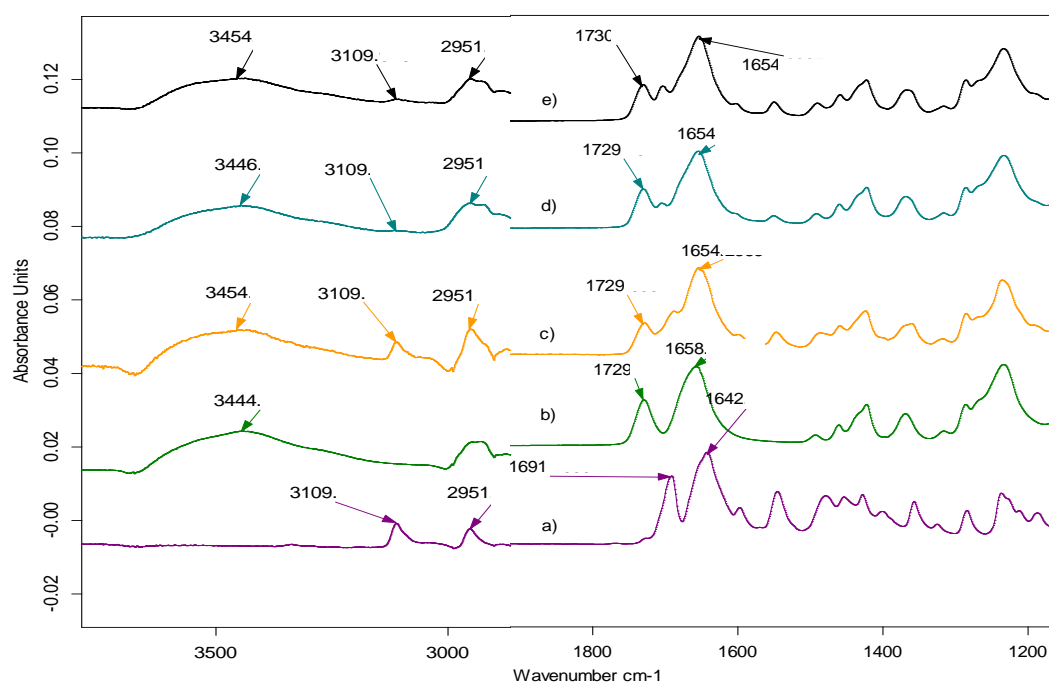


Figure 3.23: ATR-FTIR spectra for a) CAF, b) PVP VA 6:4, c) PM 10% CAF-PVPVA 6:4, d) HME 10% CAF-PVPVA 6:4 e) HME 20% CAF-PVPVA 6:4

3.3.3.4. X-ray Powder Diffraction of HME solid dispersions

The ability of PVP polymers to maintain molecules in a non-crystalline form has been studied by several groups (Tamaki et al., 2004, Nair et al., 2001, Thybo et al., 2008b, de Villiers et al., 1998). In this context, X-ray Powder Diffraction (XRPD) measurement was frequently performed to confirm the presence or absence of crystallinity in the SD formulation. Thus, to reconfirm the nature of the prepared HME PVP-based extrudates, their XRPD behaviour was measured. The percentage of crystalline material within the extrudates was calculated based on a calibration curve that could be found in Appendix I (Figure (i)).

3.3.3.4.1. XRPD of HME PCM in PVP K 29-32

Figure 3.24 shows the XRPD diffractograms of HME PCM PVP K29-32 systems. The diffractograms showed halo patterns up to 50% drug loadings. At higher PCM loading i.e. 60%-70%, clear diffraction peaks were noted as anticipated from the opaque appearance of the extrudate at these loadings.

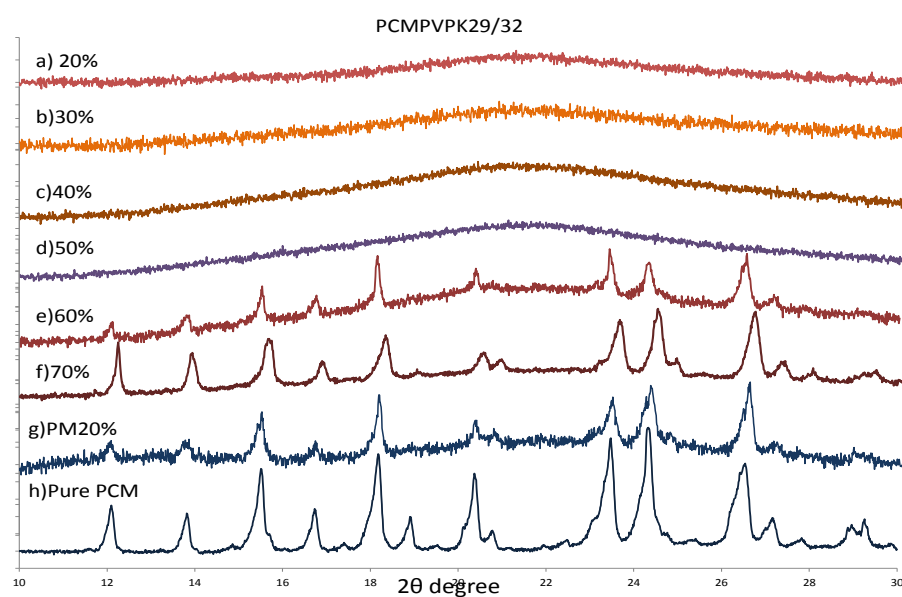


Figure 3.24: X-ray Diffraction patterns of PCM and PVP K29-32, a) HME 20% PCM, b) HME 30% PCM, c) HME 40% PCM, d) HME 50% PCM, e) HME 60% PCM, f) HME 70% PCM, g) PM 20% PCM and h) Pure PCM

The diffracted peaks in the X-ray diffractograms of HME 60% and 70% PCM PVP K29-32 (Figure 3.24) corresponded to the initially used polymorphs form, i.e. Form I crystals (Al-Zoubi et al., 2002). The detection of crystalline material for HME 60% PCM-PVP K29-32 and above was due to the use of a relatively low extrusion temperature, i.e. 120 °C, which rendered only a certain solid

solubility limit at about 50% of drug loading in PVP K29-32. However, the reduction of crystal content were still seen in extrudates of 60% and 70% drug loading compared to the PM. The percentage of crystalline PCM is compared to the calculated crystallinity from previous section on MTDSC (Figure 3.11). Table 3.10 summarise the percentage of crystalline PCM detected by using both XRPD and MTDSC methods. It was noted that the calculated percentages of crystalline PCM were in good agreement to that prediction from MTDSC data.

Table 3.10: Percentage crystalline PCM in HME PCM- PVP K29-32

Samples	XRPD Crystallinity (%)	MTDSC Crystallinity (%)
HME 60% PCM-PVP K29-32	13.72	14.43
HME 70% PCM-PVP K29-32	29.25	29.17

3.3.3.4.2. XRPD of HME PCM in PVPVA 6:4

Figure 3.25 shows the XRPD data of HME PCM in PVPVA 6:4 systems. Unlike PVP K29-32 carriers system of PCM, HME 50% w/w PCM-PVPVA 6:4 gave rise to X-ray diffraction peaks. This in turn implies that the solubility limit of PCM in PVPVA 6:4 is lower than that in PVP K29-32. Table 3.11 outlines the percentage of crystalline material in HME 50% PCM in PVPVA 6:4.

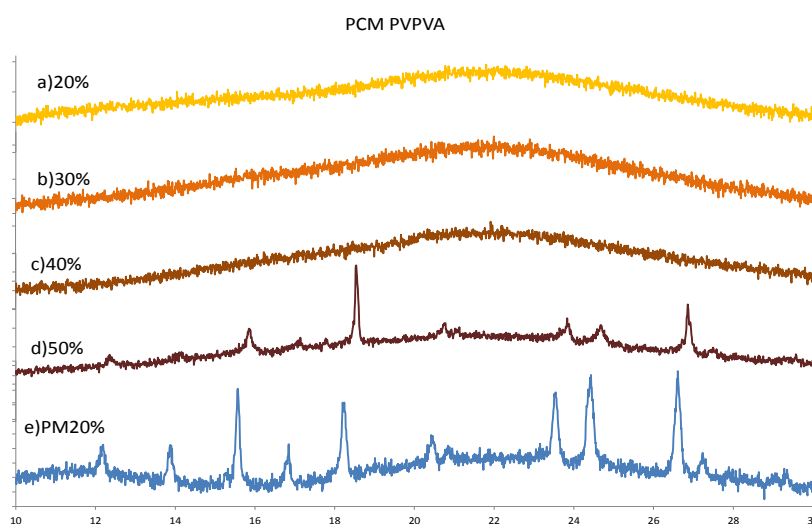


Figure 3.25: X-ray diffraction patterns of PCM with PVPVA 6:4, a) HME 20% PCM, b) HME 30% PCM, c) HME 40% PCM, d) HME 50% PCM, e) PM of 20% PCM-PVPVA 6:4

Table 3.11: Percentage of crystal based on Bragg reflection peak from XRPD

Samples	XRPD Crystallinity (%)	MTDSC Crystallinity (%)
HME 50% PCM-PVPVA 6:4	10.52	8.91

The excess crystalline material seen in HME 60% PCM PVP K29-32 and HME 50% PCM in PVPVA 6:4 led to the conclusion that the solid solubility of PCM in the presence of PVP K29-32 and PVPVA 6:4 at 120 °C were circa 50% and 40% of drug loading, respectively. Interestingly, this observation corresponded to the theoretical estimation in Chapter 3.3.1.2, Table.3.5.

3.3.3.4.3. XRPD of HME CAF in PVP K29-32 and PVPVA 6:4

X-ray Powder diffraction was also used to analyse extrudates of HME CAF in PVP systems. Since the diffracted peaks in the X-ray diffractograms of HME PVP-based CAF systems indicated a different polymorphic form of CAF which was different from the PM of raw CAF, percentage of CAF crystallinity in the HME extrudates was not performed. Thus the discussion below describes only the XRPD characteristic of the HME CAF-PVP based samples without quantification of the crystalline CAF.

HME CAF-PVP K29-32

Figure 3.26 displays the XRPD spectra of CAF, PM and HME of CAF PVP K29-32 systems. A halo pattern was only detected in HME 10% CAF-PVP K29-32.

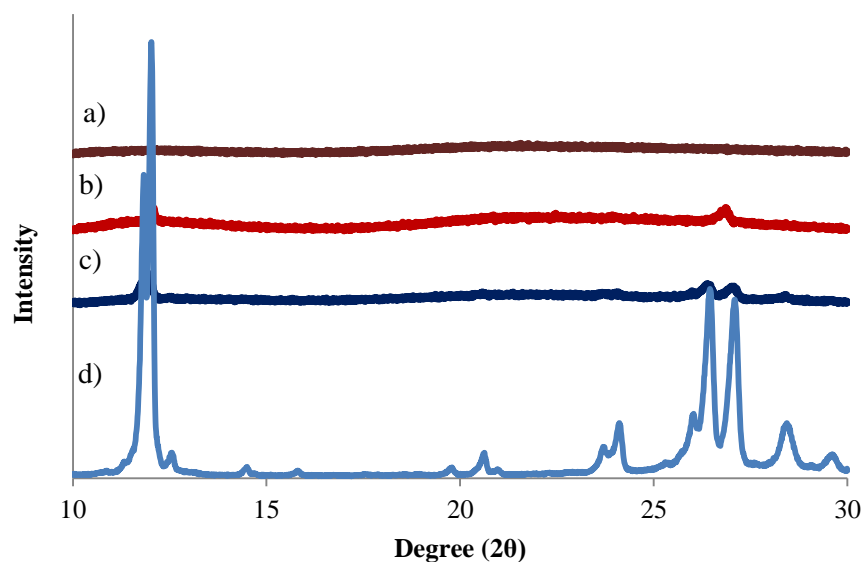


Figure 3.26: X-ray diffraction patterns of CAF and PVP K29-32, a) HME 10% CAF, b) HME 20% CAF, c) PM of 10% CAF d) commercial CAF as received

In XRPD diffractograms of HME 20% CAF-PVP K29-32, a single characteristic peak at $2\theta = 26.86^\circ$ was noted which is attributed to Form I CAF (Figure 3.26 (b)). The detection of Form I in the hot processed HME PVP-based extrudates was not unexpected as Form I CAF was reported to

be stable at high temperatures (Descamps et al., 2005b, Moura Ramos et al., 2006, Kishi and Matsuoka, 2010). Besides, X-ray diffractogram of HME 20% CAF PVP K29-32 shows a reduction in degree of crystallinity of CAF as compared to its PM. Therefore, it is suggested that CAF dissolves into PVP K29-32 to a minor extent upon heat processing.

Recalling the DSC thermogram of HME 20% CAF PVP K29-32, an anomalous peak and a melting peak were noted at 115 °C and 212 °C, respectively. The melting peak corresponds to the detection of crystalline trace which is in accordance to the diffracted peak seen in the XRPD diffractogram (Figure 3.26).

HME CAF-PVPVA 6:4

Figure 3.27 presents XRPD diffractograms of HME CAF-PVPVA 6:4 systems. From Figure 3.27, HME CAF-PVPVA 6:4 reveals a halo pattern for HME 10-20% CAF-PVPVA 6:4 systems. This result did not agree with the data obtained from MTDSC and HSM (refer to Chapter 3.3.3.2.2, Figure 3.17 to 3.18) which indicated the presence of crystalline material in both 10% and 20% of HME CAF PVPVA 6:4 system. This might be due to the limited sensitivity of XRPD in detecting low percentage of crystalline material (Saleki-Gerhardt et al., 1994).

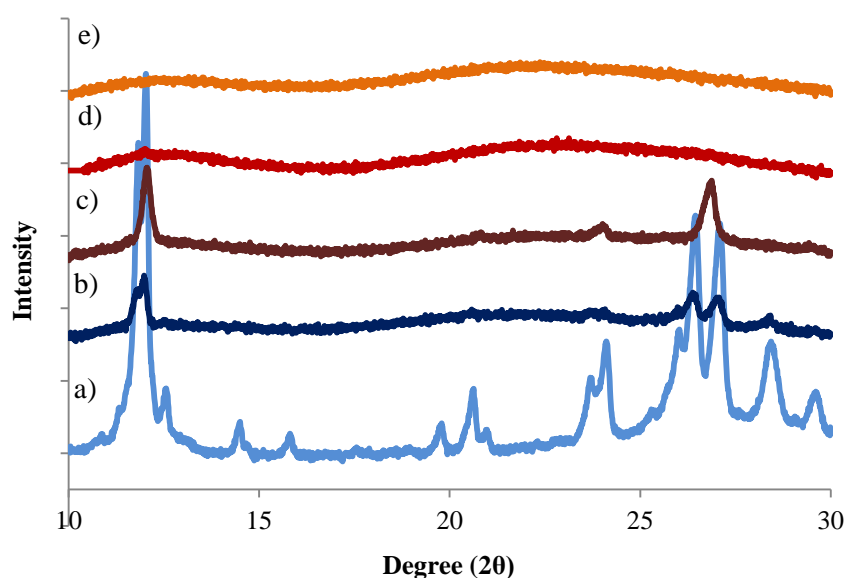


Figure 3.27: X-ray diffraction patterns of CAF and PVPVA 6:4, a) CAF, b) PM of 10% c) HME 30%, d) HME 20%, e) HME 10%

Unlike HME CAF-PVP K29-32, a higher amorphous content was noted in HME CAF 20% PVPVA 6:4 as shown by its halo patterns in XRPD diffractograms. This might be ascribed to the higher extrusion temperature employed in HME PVPVA 6:4 system (i.e. 180 °C) as compared to

PVP K29-32 (i.e. 155 °C). Similar to the HME 20% CAF-PVP K29-32, XRPD diffractograms of HME 30% CAF-PVPVA 6:4 system indicated single peaks at $2\theta = 26.86^\circ$ which was attributed to the Form I CAF (Lehto and Laine, 1998). This is due to the transformation of CAF Form II (raw) to Form I while hot processing at 180 °C. Therefore, at 30% CAF loading of HME CAF-PVPVA 6:4, system, there was certain amount of un-dissolved crystalline CAF in the formulations.

3.3.3.5. Scanning Electron Microscopy

3.3.3.5.1. SEM of HME PCM in PVPK29-32 and PVPVA 6:4

SEM was used to image the surface and cross sectional morphology of extrudates. Figure 3.28 shows the SEM micrographs of PM 40% PCM-PVP K29-32, the surface of the freshly prepared HME 40% PCM-PVP K29-32 extrudates and the corresponding cross section and also the surface of HME 60% PCM-PVP K29-32.

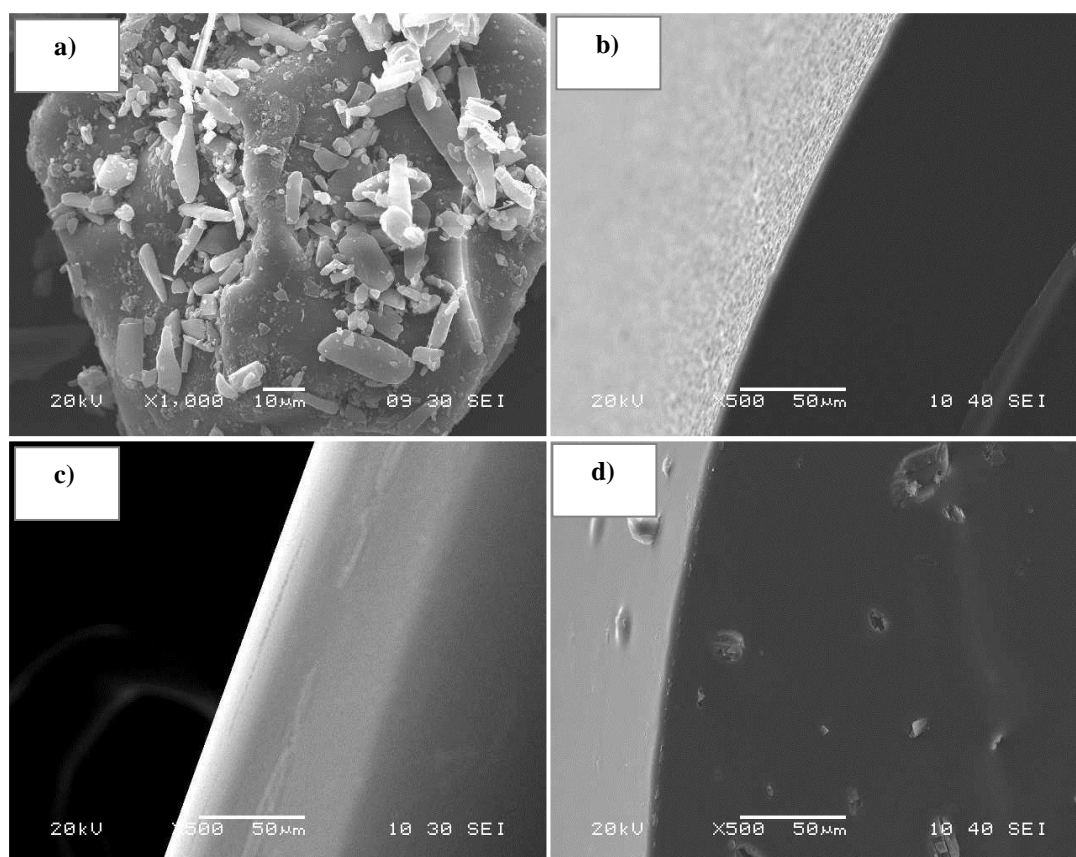


Figure 3.28: SEM image of a) PM of PCM-PVP K29-32, b) fresh extrudate of HME 40% PCM-PVP K29-32 surface, c) fresh extrudate of HME 40% PCM-PVPVA 6:4, d) Cross section of extrudates of HME 60% PCM-PVP K29-32

SEM image of PM PCM and PVP K29-32 (Figure 3.28 (a)) reveals needle-shape crystals of PCM embedded on the raw spherical PVP K29-32 particles which were prepared commercially via spray

drying. As displayed in Figure 3.28 (b), extrudates of PVP K29-32 with drug loading of 40% indicated shark skinning features on its surface. This was due to the high friction and low flowability of the molten material during the extrusion process at temperature lower than T_g of the polymer. However, for HME 40% PCM-PVPVA 6:4 system, smooth surfaces were noted (Figure 3.28 (c)). At high loading of PCM, i.e. HME 60% PCM-PVP K29-32 systems, small crystals were embedded at both the surface and cross section of the HME 60% PCM-PVP K29-32 extrudate (Figure 3.28 (d)). This is in good agreement to the proposed solubility threshold of PCM in PVP K29-32 prepared at 120 °C whereby 55% of PCM is the solubility limit of PCM in PVP K29-32 (please refer to Table 3.5 for solubility threshold). To summarise, all the observed features of extrudate in SEM were in agreement with the concluded amorphicity / crystallinity of HME PCM-PVP K29-32 and HME PCM-PVPVA 6:4 systems deduced from XRPD data in Chapters 3.3.3.4.1 and 3.3.3.4.2.

3.3.3.5.2. SEM of HME CAF in PVP K29-32 and PVPVA 6:4

Figure 3.29 displays the SEM micrographs of raw CAF (Form II), Form I CAF and HME PVP-based dispersions of CAF.

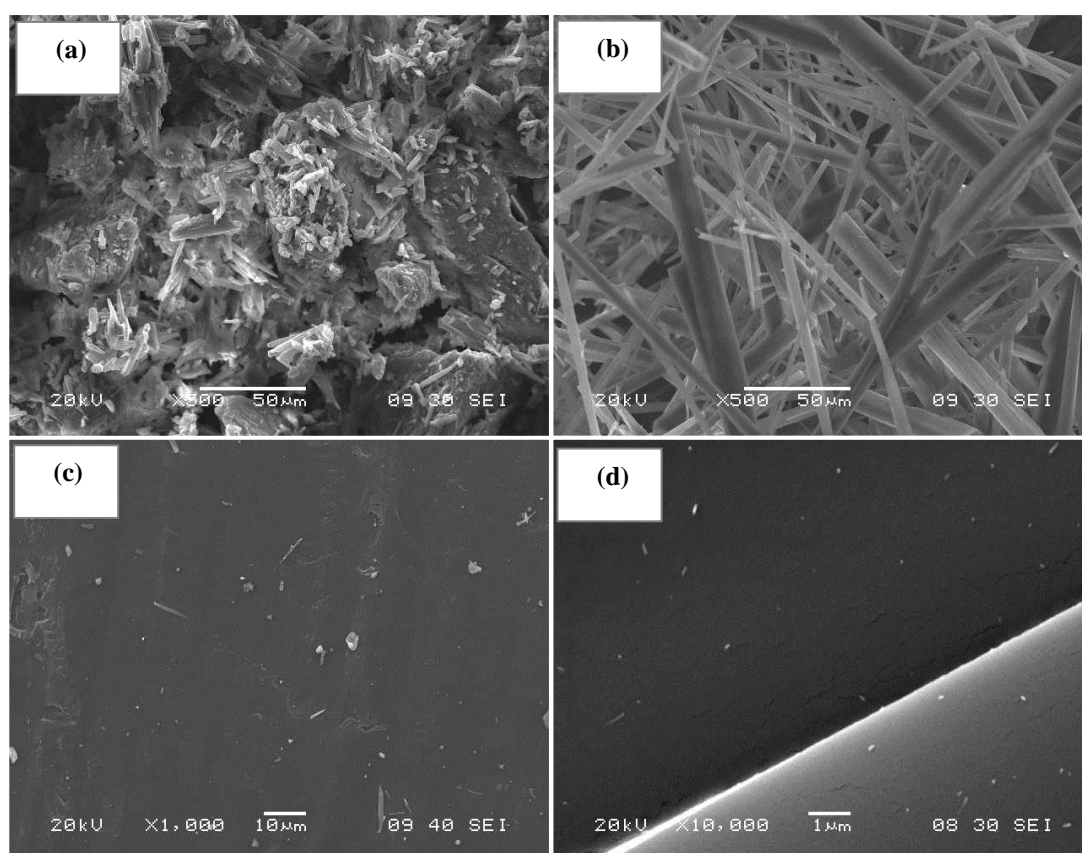


Figure 3.29: a) raw CAF (Form II), b) heated CAF (Form I was prepared by heating the Form II in a covered petri-dish condition. The sublimated product were Form I as confirmed by XRPD), c) HME 10% CAF-PVPVA 6:4 and d) c) HME 10% CAF-PVP K29-32

As expected from the lower miscibility of CAF with both the PVP carrier systems (predicted from solubility parameter and Gibb free energy of mixing), Figure 3.29 (c) and (d) reveal tiny crystal traces of needle-shape in both HME 10% CAF in PVP K29-32 and HME 10% CAF in PVPVA 6:4 which corresponds to the Form I CAF as shown in Figure 3.29 (b). This might be attributed to the recrystallization upon extrusion or incomplete solubilising of these materials during the HME manufacturing process. These observations agree with the results from the DSC thermograms but the contradict XRPD data which did not indicate the presence of crystalline material. This might due to different sensitivity of the analysis methods in which XRPD was reported to have the detection limit down to only 10% of crystalline material in a mixture (Saleki-Gerhardt et al., 1994).

To summarise this section, SEM images showed the partially crystalline nature in all the HME CAF PVP-based systems. Hence, SEM images of all the HME PVP-based systems have supported the results of extrudate characterization studies described in the previous sections.

3.4. Discussion

3.4.1. Theoretical estimation of miscibility

It is reported that when difference in solubility parameters of drug-polymers is $< 7.0 \text{ MPa}^{1/2}$, significant miscibility between the two components is expected (Forster et al., 2001c, Maniruzzaman et al., 2013). In this study, good miscibility was predicted in the binary system of the interacting API, i.e. PCM and PVPs polymers as shown by the small difference in their solubility parameters. In contrast, solubility parameters of the non-interacting API, i.e. CAF with PVPs polymers show differences of $> 8 \text{ MPa}^{1/2}$ which imply limited miscibility. As a result it is expected that the CAF and PVP carriers may not easily form fully amorphous solid dispersions in the HME processing. Similarly, interaction parameter prediction from melting point depression studies also implied the trend described above. Larger negative values, indicating high miscibility, of the interaction parameter were obtained for PVP K29-32 and PVPVA 6:4 with PCM (the structurally interacting API) as compared to CAF (the structurally non-interacting API). This result is in agreement to a recently published paper whereby the authors reported the importance of drug-polymer interaction in promoting miscibility of the components (Maniruzzaman et al., 2013).

On comparing the homopolymer (PVP K29-32) and co-polymer (PVPVA 6:4), more negative values of interaction parameter were seen in the former with both the APIs. This is because of the higher interactive units available in PVP K29-32 for drug-polymer interaction than the co-polymer, PVPVA 6:4. This difference might potentially affect the ability to produce fully amorphous solid dispersions as well as influencing the stability of the systems. Production of amorphous solid

dispersions will be detailed out at later section and the influence of carrier system on the stability issues of the prepared extrudates will be presented as separate chapter (Chapter 4).

3.4.2. Production of amorphous solid dispersion

The non-interacting CAF which was shown to have limited miscibility was not successfully extruded as a fully amorphous solid dispersion. On the other hand, the interacting PCM, which was predicted to have good miscibility with PVP was shown to be extruded as fully amorphous solid dispersion up to 40% and 50% of PCM loading in PVPVA 6:4 and PVP K29-32, respectively. This result is in agreement to some recently published reports whereby the use of Hansen solubility parameter has been shown to be useful in predicting miscibility of API and polymer for the production of solid dispersion (Djuris et al., 2013b, Forster et al., 2001c, Maniruzzaman et al., 2013, Sarode et al., 2013). The drug polymer miscibility is attributed by balancing the energy of mixing released from the intermolecular interaction between the API and polymer with the energy release from the intramolecular interaction in the components (Maniruzzaman et al., 2013). As a result, an interacting API is preferred in the production of fully amorphous solid dispersion at temperature lower than its melting temperature. In this context, the prediction of miscibility could be estimated from the Hansen solubility parameter as well as melting point depression approach.

In addition, the limits of PCM loading in PVPs polymer (up to 40% and 50% of PCM loading in PVPVA 6:4 and PVP K29-32) were found to have good correlation to the solid solubility calculated using Equation (3.10) and (3.11) as tabulated in Table 3.5. It is worth mentioning that the T envisaged in this calculation was the extrusion temperature employed during the extrusion process (i.e. $T_{\text{process}} < T_m$). Thus, the calculated solid solubility in this case may only represent the loading of drug that could be incorporated in the formulation in order to achieve a fully amorphous solid dispersion at $T_{\text{process}} < T_m$. On the other hand, solid solubility prediction of CAF in PVPs by using the melting point depression approach did not agree to the results obtained experimentally in that some miscibility was predicted but at concentrations of 10% w/w and above, crystalline material was detected in both polymer systems. This was probably due to the sublimation characteristics of CAF molecules near to its melting temperature (as shown in TGA result, Table 3.7), hence, complicating the use of the melting point depression approach for this material.

On comparing the homopolymer (PVP K29-32) and co-polymer (PVPVA 6:4) as a carrier in SD system, the former was found to have higher accommodation of PCM (higher PCM loading) in producing fully amorphous dispersions. This is attributed to the higher extent of hydrogen bond interaction between PCM and carrier in HME PCM PVP K29-32 system than in HME PCM PVPVA 6:4 system which was confirmed by their ATR-FTIR spectra. According to the infrared

spectra, hydrogen bond interaction between PCM and carrier occurred preferentially at the C=O group of PVP monomer (for both PVP K29-32 and PVPVA 6:4) compared to the C=O of the vinyl acetate. These results are comparable to a previous work on colyophilized indomethacin with PVP and PVPVA 6:4 (Shamblin et al., 1998) where the drug polymer interaction occurs preferentially in the C=O group in the pyrrole ring as compared to the C=O found in vinyl acetate.

The preferential hydrogen bond interaction on C=O of pyrrolidone group compared to the C=O of the vinyl-acetate group is reported to be due to the stronger basic nature and the higher partial atomic charges on the oxygen functional group of the C=O in pyrrolidone which acts as a stronger proton acceptor as compared to the C=O of vinyl acetate (Trasi and Taylor, 2012, Shamblin et al., 1998, Matsumoto and Zografi, 1999). Thus the C=O of vinyl-acetate in PVPVA 6:4 system was found to not play a significant role in the drug-polymer interaction which may be associated with the lower solubilizing effect of this polymer on the crystalline drug during the hot melt extrusion process.

3.4.3. Extrudate properties

Water contents of the HME extrudates were consistently lower than their corresponding PMs. This was due to the nature of the process whereby heating of the mixture allowed the removal of moisture. Even so, HME is a closed barrel process whereby less than 100% of the moisture could be released during the feeding process and upon extrusion, thus a certain amount of moisture could be trapped within the extrudate. This is clearly evidenced by the grinding experiment in Figure 3.14 that led to the observation of reduced glass transition temperature from the theoretical prediction via Gordon-Taylor (G-T) equation (Figure 3.13). Similar observations were noted by Patterson et al (2008) in comparison between the T_g of SD obtained from melt extrusion and spray drying processes. In that study, the melt extrusion product possessed lower T_g values than the spray dried equivalents, despite the use of higher processing temperatures in HME process (Patterson et al., 2008).

3.5. Conclusion

The agreement between the experimental data and miscibility behaviour predicted from a theoretical group contribution approach was found to be very good. Since the reference table of the chemical group contributions forces is widely available and it provides a good estimation in most cases, it is suggested that this approach could be suitable for predicting the suitability of a material to be processed by HME. The Flory Huggins interaction parameter predicted from melting point

depression approach was also in agreement to the data obtained from experimental studies. This implying that both theoretical predictions of miscibility (Hansen solubility parameters and melting point depression) may be used to anticipate the successful formulation of a molecularly dispersed hot melt extruded system.

Similarly, the solid solubility prediction for HME PCM PVPs system shows good agreement to the limit of PCM loading in producing a fully amorphous solid dispersion obtained from characterization of the extrudates experimentally. This suggested the good predictability of the melting depression method in estimating the loading limit of API in the production of fully amorphous HME PVP-based SD at $T_{\text{process}} < T_m$. This is provided there is not complication in data interpretation of the depressed melting point of API in the DSC thermogram.

In the context of processing, small molecular size of API was found to plasticize the big molecular size of PVP polymer which leads to its flowability at temperature lower than its T_g which resolve the worries of PVP degradation at temperature higher than its T_g . In this respect, the interacting API could further aid the production into fully amorphous solid dispersion due to the melting point depression of API in the presence of PVP polymer alongside with its good miscibility with the PVP polymer. However, one should bear in mind on the processing condition of interacting PCM with PVP whereby an increase in viscosity of the molten system were noted with the $T_{\text{process}} < T_g$ of polymer. The rigidity build-up of the molten during the extrusion process might limit subsequent diffusivity of the API within the polymer system. At a macroscopic level, this parameter was seemed to be irrelevant in the properties of freshly prepared extrudates. However, the effect of this parameter in other performances of solid dispersion such as physical stability shall not be overlooked. This will be further correlated to the physical stability of the extrudates in next chapter (Chapter 4).

Chapter 4. An investigation into the recrystallization of paracetamol in HME PCM PVP-based solid dispersions

4.1. Introduction

HME is a well-known process for the production of amorphous SDs with relatively good physical stability profiles as reviewed in Chapter 2.2.2.1, (Dong et al., 2008b, Verreck et al., 2004, De Brabander et al., 2003, Fukuda et al., 2006a). In this process, the use of PVP, despite its good physical stabilization capacity (Balani et al., 2010, Berggren and Alderborn, 2004, Yoshioka et al., 1995), is discouraged due to the possible degradation of PVP at high temperature (Chokshi et al., 2005). Previous chapter (Chapter 3) has suggesting the feasibility of employing PVP polymers in HME processes based on the phenomenon of melting point (T_m) depression of API in the presence of polymer, thereby providing a means by which the issue of PVP degradation may be overcome. As there are only limited studies of PVP in the context of HME processes, understanding of the physical instability of the PVP-based HME formulations is somewhat lacking. Thus in this chapter, the physical stability of the HME PVP-based SD was investigated by studying its recrystallization behaviour.

The previous chapter (Chapter 3) has shown the different molten flowability of API in the homopolymer of PVP K29-32 and copolymer PVPVA 6:4 during the extrusion process. This difference might affect the characteristics of the system at a molecular level, potentially causing the physical stability variation of the HME product. Therefore, a physical stability study of the HME PVP-based product was carried out with a focus on the possible effect of molten flowability of the samples during the HME process. In this case, in addition to both PVP K29-32 and PVPVA 6:4, polymers with lower molecular weights (i.e. PVP K17 and PVP K12), which represents low molten flowability SD systems during processing, were investigated in this study.

In this chapter, the physical stability of the HME PVP-based SD was reflected by recrystallization profile of the PCM in the PVP matrix of HME product. To access the crystallinity of PCM, a method for quantifying the crystalline content of paracetamol (PCM) was developed by using Attenuated Total Reflectance - Fourier Transform Infrared (ATR-FTIR). This was achieved by investigating the relationship between a characteristic crystalline peak in the ATR-FTIR spectrum of the PCM and its thermal behaviour using Differential Scanning Calorimetry (DSC), which forms the first part of the chapter. Then, the developed ATR-FTIR method was used at the later sections of this chapter to probe the crystallinity the aged HME PCM PVPs-based samples under heat and humidity conditions which will be presented.

4.2. Material and methods

4.2.1. Establishment of quantification methods for crystalline PCM

4.2.1.1. Preparation of amorphous and Form II of PCM

Form I polymorph of PCM was used as received. Form II PCM was prepared by slow cooling of the melted PCM (Qi et al., 2008a). To do this, the raw PCM was melted on a hot plate at 180 °C for 1 minute, and then the molten PCM was slow-cooled on the same hot plate in power off conditions (switched off). The prepared forms of PCM were re-confirmed by using XRPD with detailed scanning parameters being presented in section 4.2.2.1. On the other hand, amorphous PCM was prepared by freshly quench-cooling (QC) PCM. This was carried out by heating the raw PCM above the melting temperature, i.e. at 180 °C for 1 minute by using a hot plate (noting that TGA had previously indicated that this would not result in degradation), and then quench cooling the melted sample in liquid nitrogen for 10 seconds. However, it is worth emphasizing that, QC PCM will lose its fully amorphous nature when it is left under room conditions for more than 1 minute. This is ascribed to the low T_g of the amorphous PCM i.e., circa 23 °C that prone to undergo recrystallization at room temperature (Qi et al., 2008a, Di Martino et al., 1997, Di Martino et al., 1996, Di Martino et al., 2000).

4.2.1.2. The detection of crystalline PCM by using ATR-FTIR and high speed DSC

Detection of crystalline PCM using ATR-FTIR

The prepared forms of PCM (Chapter 4.2.1.1) were distinguished by using ATR-FTIR. According to the literature, ATR-FITR spectra could be used to distinguish the different forms of crystalline PCM. In particular, it is suggested that band of 807 cm⁻¹ in the spectra of PCM can be used as specific identification for Form I PCM as this band is absent in Form II PCM (Ivanova, 2005, Al-Zoubi et al., 2002, Qi et al., 2008b). In order to observe the recrystallization behaviour of QC PCM as reflected by the growth of 807 cm⁻¹ over time, multiple infrared measurements of the QC PCM were performed at the rate of 1 measurement per minute over 2 hours. In each measurement, the infrared spectra were collected between 500 - 4000cm⁻¹ with a resolution of 2 cm⁻¹ and 32 scans.

Quantification of crystalline PCM using DSC

DSC was used to determine the percentage of crystalline material in the QC PCM over time. The freshly prepared QC PCM was immediately analysed using conventional DSC run at high speeds heating, i.e. from -50 to 300 °C at a calibrated rate of 100 °C per minute. This speed was chosen so

as to minimise polymorphic conversion during the run itself. In this measurement, pinhole aluminium pan was used based on preliminary work, which indicated the recrystallization of the QC PCM into only Form I of PCM. Then, the recrystallization of the QC PCM was tracked as a function of time by DSC measurement. Crystalline content of the recrystallized QC PCM obtained from DSC data was correlated to the profile of relative peaks intensity (band 807 cm^{-1} to 797 cm^{-1}) changes obtained from ATR-FTIR method. Details of the correlation will be presented in section 4.3.1.

4.2.2. Preparation of amorphous HME solid dispersions

In the preparation of HME PVP-based SD, four different types of carrier were employed. These include three different molecular weights of homopolymers, i.e. PVP K12, PVP K17, PVP K29-32 and a co-polymer, PVPVA 6:4. HME 30-50% (w/w) PCM loading in PVP carriers were prepared. Please refer to Table 2.12 for the processing parameters used in the manufacturing of HME 30-50% PCM-PVP K29-32, 30-50% PCM-PVP K17, 30-50% PCM-PVP K29-32, 30-50% PCM-PVPVA 6:4 systems.

4.2.2.1. Basic characterisation of HME solid dispersions

The amorphicity of the SD extrudates (HME 30-50% PCM in PVP(s) and PVPVA 6:4) was confirmed by using complementary results obtained from ATR-FTIR and XRPD. The scanning parameters as presented in Chapter 3, section 3.2.6 and 3.2.7 were used for ATR-FTIR and XRPD, respectively.

4.2.2.2. Fragility calculation of the HME solid dispersions

DSC was used to measure the T_g of the prepared extrudates. In order to calculate the fragility index of the HME sample, which was correlated to their physical stability, DSC measurements of the freshly prepared extrudates were performed in standard mode at different heating rates (5, 10, 20, 50 °C per minute). The changes of T_g obtained at different heating rates were used to estimate the fragility index of the extrudates.

4.2.3. Recrystallization studies of HME PCM-polymers system

The influence of storage humidity

In recrystallization studies, the SD extrudates were cut into pieces of extrudates circa 3-4 mm long prior to storage. The influence of the degree of relative humidity on recrystallization behaviour of HME 40% PCM-PVPVA 6:4 system were studied by desiccating the cut extrudates in different humidity conditions ranging from 0% RH (phosphorus pentoxide), 22% RH (potassium acetate), 33% RH (magnesium chloride), 53% RH (magnesium nitrate) to high humidities of 75% RH (sodium chloride) at the room temperature. The humidity condition of the desiccator was confirmed by using a hygrometer before the storage of extrudates.

The influence of different PVPs carriers and PCM loading

Subsequently, an accelerated storage condition, i.e. 75% RH was used to study other factors in affecting recrystallization behaviour of the HME PCM-PVP based system. These factors include the effect of different carriers system and the effect of drug loadings.

In studying the effect of different carriers (three homopolymers of different molecular weights, i.e. PVP K12, PVP K17, PVP K29-32 and a co-polymer), HME 40% PCM different carriers systems were aged in the 75% RH for up to 3 months. On the other hand, the effect of drug loading was studied by storing the HME 30% PCM-carriers system and HME 50% PCM-carriers system at the accelerated humidity condition, i.e. 75% RH at 25 °C. Their recrystallization patterns were compared to the recrystallization pattern of formulations with 40% PCM loading under the same storage condition.

The influence of storage temperature

The effect of temperature on recrystallization behaviour of the HME 40% PCM-carrier was also studied by storing the extrudates under 0% RH / 40 °C oven. The annealed extrudates were sampled at predetermined time points and tested by using DSC, ATR-FTIR, and SEM for the detection of crystalline material.

4.2.3.1. DSC studies

For the recrystallization study, the aged SD of HME 30-50% PCM-carriers were analysed using a DSC with modulated mode (MTDSC). Pin-hole lids were used to allow removal of water, particularly given the hygroscopic nature of the PVP polymers (Callahan et al., 1982). Samples were heated at 2 °C per minute from -20 °C with modulation of ± 0.212 °C every 40s to 200 °C. All experiments were run in triplicate.

4.2.3.2. TGA studies

Thermogravimetric analysis was performed to quantify the water content of the aged HME 30-50% PCM-carriers after humidity storage. The same parameters as stated in Chapter 3, section 3.2.5 were used.

4.2.3.3. ATR-FTIR

ATR-FTIR measurement of the aged HME 30-50% PCM-PVPs were performed daily for the first 14 days of sample storage in humidity conditions using the same parameter. After that, the ATR-FTIR measurements of the aged extrudates were performed monthly up to 3 months. The same scanning parameters as stated in section 4.2.1.2 were used.

4.2.3.4. XRPD

XRPD experiments were also performed on the aged HME 30-50% PCM-carriers. Upon XRPD measurement, the aged extrudate was ground gently in a mortar and pestle before compaction into the sample holder of XRPD machine. Measurements were performed using the same parameters as described in Chapter 3, section 3.2.8.

4.2.3.5. SEM

Surface morphology of the aged extrudate was investigated using Scanning Electron Microscopy (SEM). Please refer to Chapter 3, section 3.2.9 for experimental details.

4.3. Results

4.3.1. Development of ATR-FTIR method as a quantification method for crystalline PCM

In order to study the recrystallization behaviours of the HME PVP-based SD, a quantification method of the recrystallized API was developed. DSC is an excellent technique in recrystallization study of a pure API. However, this technique might post a problem in recrystallization study of a drug-polymer blend system due to the possible drug dissolution into the polymer during heating scan of DSC that might lead to complex data interpretation. Hence, the quantification of the recrystallized material in the aged HME systems was assessed by using ATR-FTIR. Nevertheless, DSC was employed in the later sections to study the T_g (s) of the aged samples in order to detect possible phase separation after storage.

Prior to the recrystallization study, a quantification method of PCM by using ATR-FTIR is developed based on the recrystallization kinetic of PCM in its pure amorphous state. This will be further detailed in the subsequent sections.

4.3.1.1. Identification of different polymorphs of PCM in ATR-FTIR

Prior to the quantification of crystalline PCM, different forms of PCM were distinguished by using the ATR-FTIR. Figure 4.1 displays the ATR-FTIR spectra of amorphous, Form I and Form II of PCM that were produced as outlined in section 4.2.1.1.

According to Figure 4.1, Form I PCM was characterized by a unique absorption band at 807 cm⁻¹ which is attributed to the out of plane bending mode of methyl group in PCM molecule (Al-Zoubi et al., 2002, Ivanova, 2005). This band (807 cm⁻¹) is absent in both the Form II and amorphous PCM. Thus it is suggested that this peak (807 cm⁻¹) could be useful for the identification of Form I PCM.

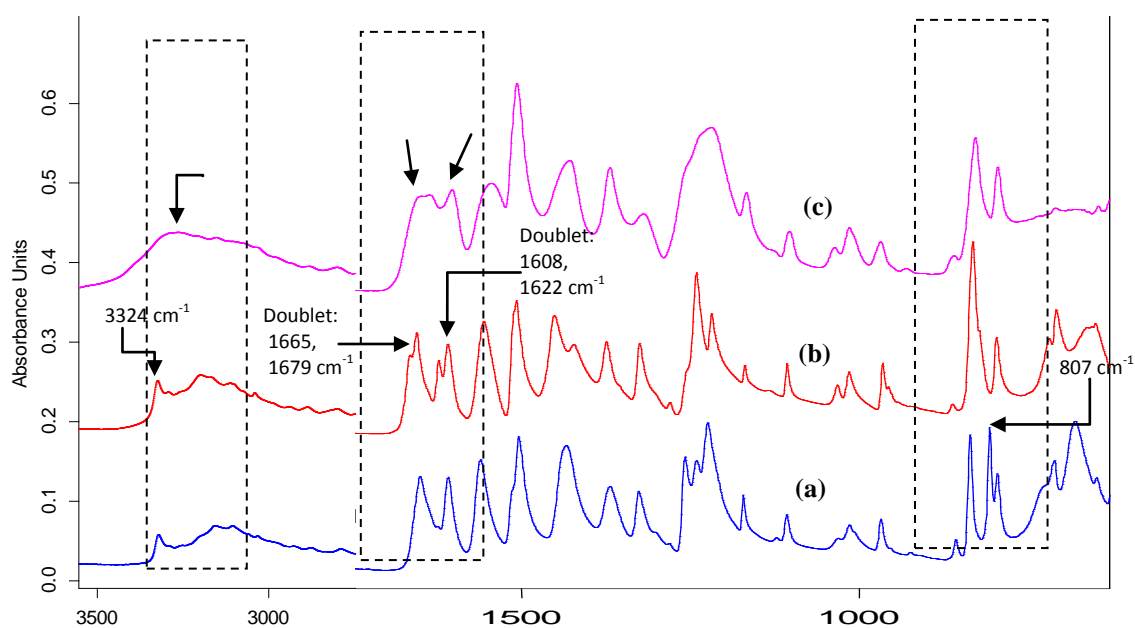


Figure 4.1: ATR-FTIR spectra of different solid-state forms of PCM. (a) Form I was scanned as received (raw), (b) Form II was prepared by slow cooling as described in the method section, (c) ATR-FTIR spectra of amorphous PCM which was obtained by immediately scanning after the quenched-cooling of the molten PCM.

On the other hand, Form II PCM reveals a different ATR-FTIR spectrum from the amorphous form and Form I PCM. According to Figure 4.1, Form II gave rise to double bands in the region of 1665 cm^{-1} and 1608 cm^{-1} which was shown as single broad band in the spectra of amorphous and Form I PCM. Furthermore, ATR-FTIR spectrum of Form II could also be distinguished from the amorphous PCM by the peak at 3324 cm^{-1} which is absent in spectrum of amorphous PCM. This peak (3324 cm^{-1}) is responsible for the NH stretching of the intermolecular H-bond within the crystal (Wang et al., 2002), which is not present in the non-crystalline structure of amorphous PCM (Al-Zoubi et al., 2002, Ivanova, 2005).

4.3.1.2. Tracking of the relative intensity of 807 cm^{-1} in QC PCM by using ATR-FTIR

From the identification of different forms of PCM in ATR-FTIR, it was noted that 807 cm^{-1} could be used to exclusively represent Form I PCM. By detecting the intensity of this peak in the ATR-FTIR spectra, the amount of Form I PCM presence in a sample could be estimated. With that, the freshly prepared QC PCM was scanned by ATR-FTIR as a function of time. Figure 4.2 shows the multiple ATR-FTIR spectra of the freshly prepared QC PCM over 2 hours.

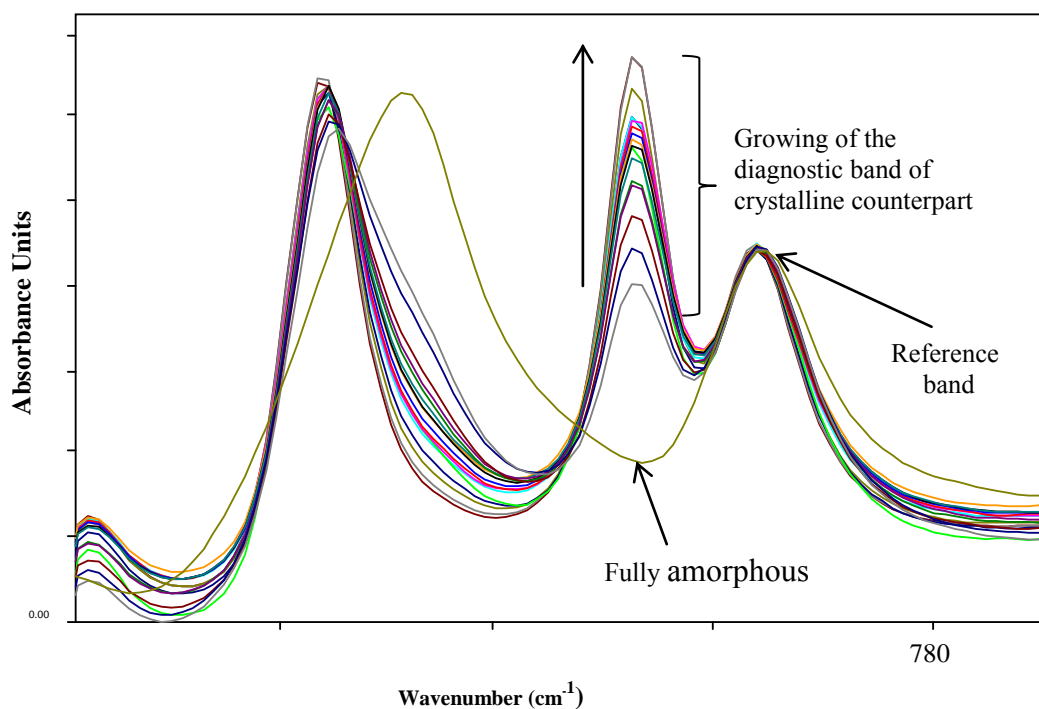


Figure 4.2: Multiple ATR-FTIR spectra of quench-cooled PCM that were taken every 2 minutes. Growing of the diagnostic 807 cm^{-1} band was started from the grey line (lowest absorbance), in which its IR absorbance was found to increase with time.

Immediate scanning of the QC PCM revealed no characteristic band of 807 cm^{-1} , (as indicated by the arrow corresponding to ‘fully amorphous’ material), which indicated the amorphous nature of the PCM immediately after the QC process. However, this band started to appear in the second spectrum, which was scanned after 1 minute of the quench-cooling procedure. In addition, the band of 807 cm^{-1} was found to increase with time, which indicating the progress of recrystallization into Form I PCM. The relative intensity of this band was expressed as a ratio to a band with constant intensity, i.e. 797 cm^{-1} as shown in Equation (4.1).

$$\text{Relative Intensity} = \frac{\text{Intensity of } 807\text{ cm}^{-1}}{\text{Intensity of } 797\text{ cm}^{-1}} \quad (4.1)$$

According to Equation (4.1), the percentage of crystallinity could be estimated if the relationship of the relative intensity and its real crystalline content is known. This was performed by correlating the relative intensity in Equation (4.1) to the percentage of crystallinity calculated from the high speed DSC which will be presented in the subsequent sections.

4.3.1.3. Quantification of the recrystallized PCM using DSC

DSC was used to determine the amount of crystal PCM in the QC PCM. This estimation was based on the melting endotherm of PCM by scanning the QC PCM. DSC measurements of the QC PCM were performed at the corresponding time points of ATR-FTIR spectra of the QC PCM that were presented in Figure 4.2. Figure 4.3 displays DSC profiles of the QC PCM at 3 different time points.

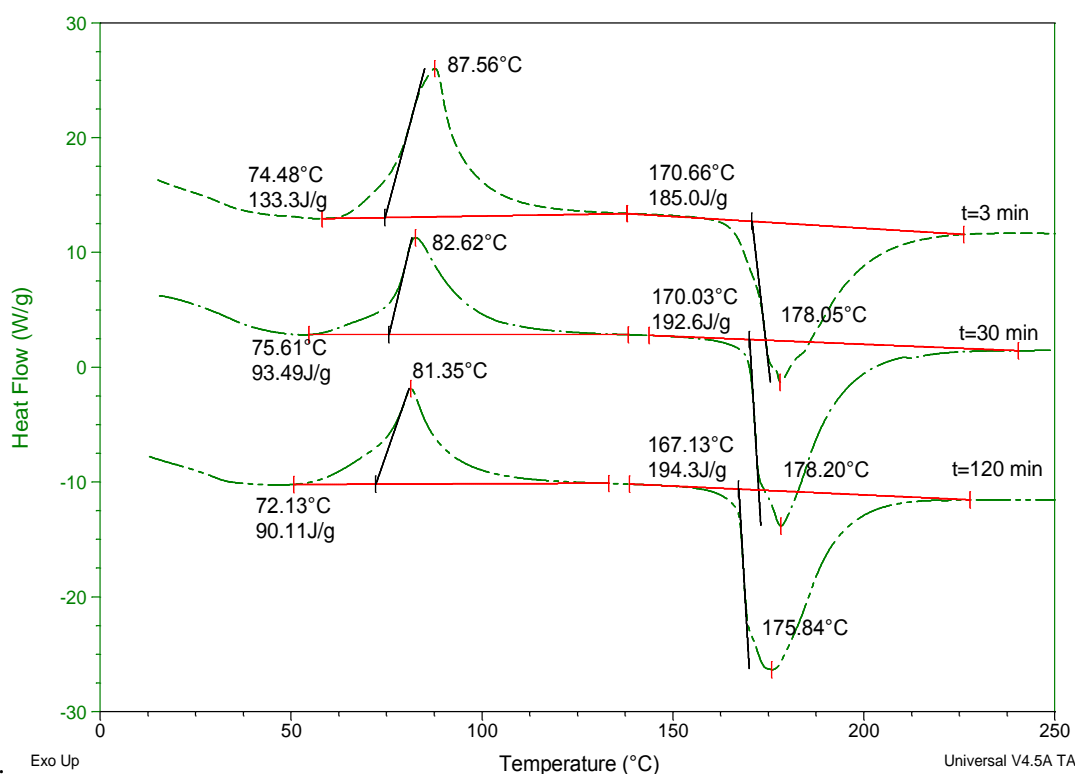


Figure 4.3: Examples of DSC profile of QC PCM run at 100 °C / minute with pin-holed pans at the specified time points

According to Figure 4.3, recrystallization peak of the QC PCM was seen at an onset temperature of circa 73 °C. Subsequently, a melting of the crystalline material in the sample was measured at an onset temperature of around 169 °C which agrees well with the onset melting temperature of Form I PCM in the literature (Qi et al., 2008a, Di Martino et al., 1997, Di Martino et al., 1996, Di Martino et al., 2000). Based on the DSC thermogram of QC PCM in Figure 4.3, crystal content of the scanned samples could be approximated by comparing the recrystallization enthalpy and melting enthalpy of the QC sample to the melting enthalpy of the pure crystalline material as shown in Equation 4.2 (Mooter et al., 2001).

$$\% \text{ Crystal} = \frac{\text{melting enthalpy} - \text{recrystallization enthalpy}}{\text{melting enthalpy of pure crystal}} \times 100\% \quad (4.2)$$

However, as the two thermal events (recrystallization and melting) take place at different temperatures, correction on the values of temperature dependence enthalpies is thus necessary. The mean of achieving this was reported before (Grisedale et al., 2011, Lefort et al., 2004). In this correction, it does not assume complete recrystallization on heating. Therefore the correction was done by defining the ratio, α , which is the fraction of amorphous material that may not have recrystallized on heating. The α ratio could be obtained from Equation (4.3)

$$1 - \alpha = \frac{\Delta H_m(T_m)}{\Delta H_m^*(T_m)} \quad (4.3)$$

where $\Delta H_m(T_m)$ is the melting enthalpy of the partially amorphous material and $\Delta H_m^*(T_m)$ is the melting enthalpy of the fully crystalline material. Then the initial amorphous content, τ could be estimated by Equation (4.4) taking into consideration the corrected melting enthalpy which theoretically occurs at the recrystallization temperature.

$$\tau = \frac{\Delta H_c(T_c)}{\Delta H_m^*(T_c)} \times \frac{1}{(1 - \alpha)} \quad (4.4)$$

According to Equation (4.4), $\Delta H_c(T_c)$ is the experimental enthalpy of recrystallization occurring at recrystallized temperature and $\Delta H_m^*(T_c)$ is the corrected melting enthalpy which theoretically takes place at the temperature of recrystallization. This corrected enthalpy could be estimated by using Equation (4.5),

$$\Delta H_m^*(T_c) = \Delta H_m^*(T_m) - (T_m - T_c) \Delta C_p \quad (4.5)$$

where T_c and T_m are recrystallization and melting temperatures, respectively. ΔC_p is the difference in heat capacity of the liquid and solid phase which is assumed to be a constant (Grisedale et al., 2011, Lefort et al., 2004). Thus, by knowing the initial amorphous content, one could also easily calculated the initial crystalline content of the sample by the subtraction the obtained amorphous content (obtained using Equation (4.4)) from unity. Crystallinity of the QC PCM at the corresponding time points of ATR-FTIR spectra in Figure 4.2 was calculated by using correction presented in Equation (4.3) to (4.5).

Correlation between ATR-FTIR and DSC data

Figure 4.4 (a) and (b) exhibits the relative intensity changes of $807 \text{ cm}^{-1}/797 \text{ cm}^{-1}$ detected from ATR-FTIR of QC PCM, and the percentage of crystalline PCM detected from DSC, respectively. The growth of crystallinity as estimated by DSC methods indicated exponential growth which is in

coherent to the exponential growth of the characteristic peak, 807cm^{-1} (Figure 4.4 (b)) as demonstrated by the multiple ATR-FTIR spectra of QC PCM in Figure 4.2.

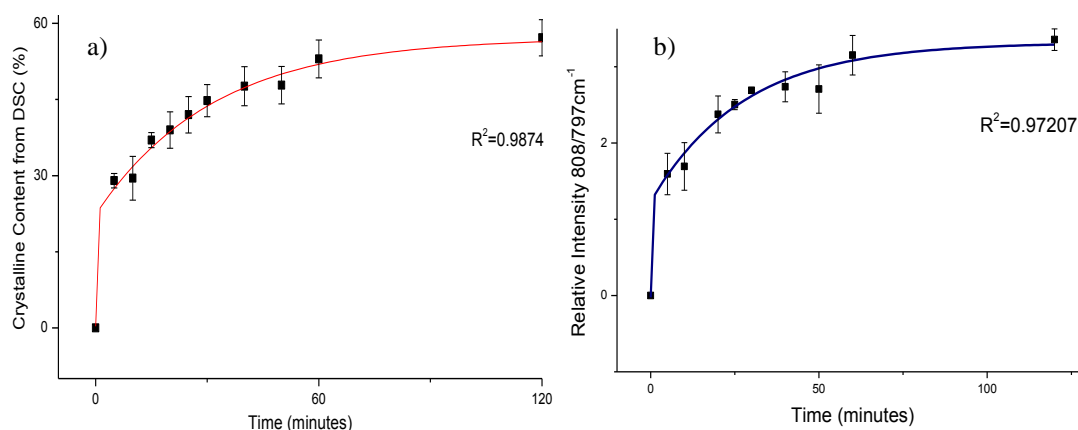


Figure 4.4: a) Exponential recrystallization profile of PCM as a function of time predicted by DSC b) Exponential profile of relative peak intensity $807\text{ cm}^{-1} / 797\text{ cm}^{-1}$ as a function of time predicted by ATR-FTIR.

As both the ATR-FITR data and DSC data display an exponential growth as shown in Figure 4.4, simple regression of these data sets was performed. Figure 4.5 showed the simple regression of the data sets from ATR-FTIR and DSC at their corresponding time points.

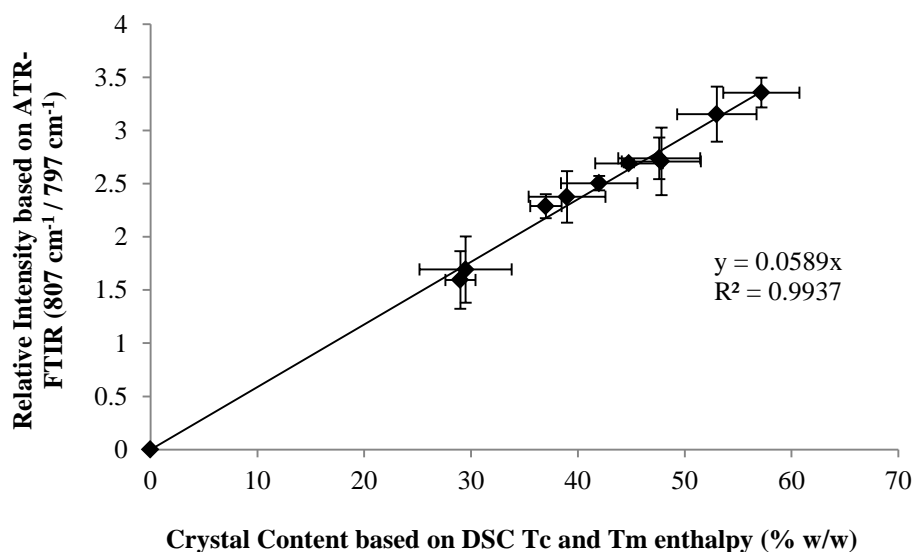


Figure 4.5: Correlation curves between the relative peak intensity of $807\text{ cm}^{-1} / 797\text{ cm}^{-1}$ as obtained of ATR-FTIR spectra of QC PCM and the crystal percentage of QC PCM as approximated from DSC thermograms.

The value of $R^2 = 0.9937$ in Figure 4.5 indicates good correlation between the percentage of crystal calculated from DSC and the relative intensity obtained from ATR-FTIR. Based on this relationship, crystal content of PCM in a sample could be described by using Equation 4.6,

$$\text{Crystal content (\%)} = \frac{\text{Relative intensity of } \frac{807\text{ cm}^{-1}}{797\text{ cm}^{-1}}}{0.0589} \quad (4.6)$$

Equation 4.6 enables the determination of the content of Form I PCM from an ATR-FTIR spectrum of a sample with a known relative intensity of 807cm^{-1} to 797cm^{-1} . The applicability of this quantification method in the crystallinity detection of HME partially crystalline SD was also verified by using XRPD and DSC heat capacity / melting endotherm methods which was presented as a separated work in Appendix (II). In the subsequent sections, the developed quantification method of crystalline PCM will be employed for crystallinity detection of the PCM in HME PVP-based SD.

4.3.2. Fully amorphous HME solid dispersions

Before the detailed recrystallization studies of HME PCM-PVPs extrudates, physical state of the freshly prepared extrudates was examined. All the freshly prepared hot melt extruded PCM-PVPs products, with a drug loading ranging from 30 to 50% w/w, revealed amorphous characteristics as confirmed via the halo pattern seen for XRPD spectra (data not shown). This is further supported by the absence of the characteristic peak of crystalline PCM, i.e. 807 cm^{-1} and 3324 cm^{-1} in the ATR-FTIR spectra of the freshly prepared HME systems.

Prior to recrystallization study, the commonly used stability predictive parameters such as glass transition temperature and fragility index, m were determined. In this context, T_g of the HME 30 to 50% w/w PCM-PVPs system were analysed by using DSC measurement.

The concept of fragility was previously discussed in Chapter 1.2.1.2. This parameter is an indicator of the molecular transport via thermally activated hopping barriers (Ojovan and Lee, 2005). A fragile glass will undergo rapid thermal excitation with high configurationally change of the molecule in order to approach its structural equilibrium which promotes recrystallization process (Ojovan and Lee, 2005). On the other hand, molecular mobility of a relatively strong glass is less influenced by a temperature variation. Hence, this system is less susceptible to solid state changes which resulting in a better physical stability profile. In relation to physical stability, this parameter was used to predict physical stability of a system by estimating its susceptibility to solid state change upon annealing process.

To estimate fragility of the HME PCM-PVPs system, samples were scanned in DSC at different heating and cooling rates. Then, natural logarithm heating rate was plotted against the T_g values with the corresponding measurements. Figure 4.6 shows an example of natural logarithm of the heating rate versus the inverse of the glass transition temperatures of HME 40% PCM-PVPVA 6:4 at the corresponding scanning rate.

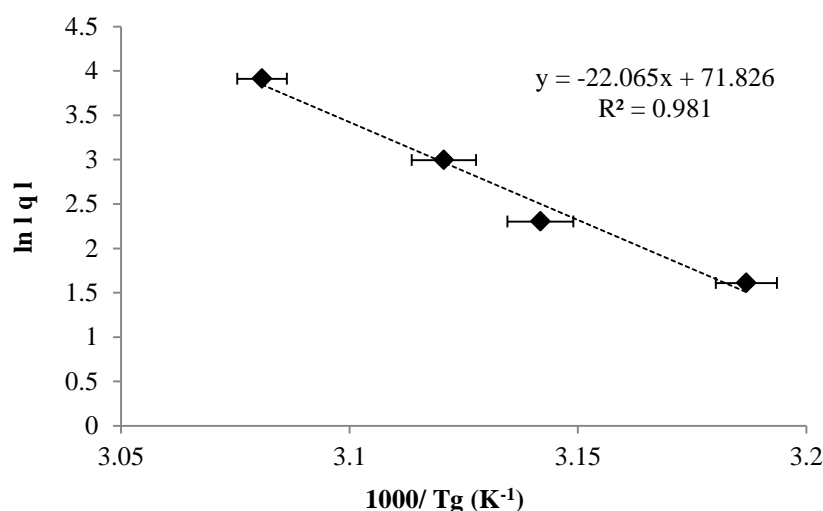


Figure 4.6: An example of heating rate dependence of the glass transition temperature of extrudates (HME 40% PCM-PVPVA 6:4). Error bars indicate the standard deviation, $n = 3$

Activation energy, E_a was calculated from the slope of Figure 4.6 (which represents $-E_a/R$) using Equation (1.4). The value of E_a was then used in the calculation of fragility using Equation (1.3) as presented in Chapter 1.2.1.2. Table 4.1 displays the glass transition temperature of the sample at heating rate of 2 °C / minute, activation energy obtained (calculated from Equation (1.4)), fragility index of the HME PCM-PVPs systems (calculated from Equation (1.3)), and R^2 which indicated the correlation between the scanning rate and changes of $1000/T_g$ as presented in Figure 4.6.

Table 4.1: Glass transition temperature/ activation energy/ fragility for different HME PCM-PVP systems

Drug loading (%w/w)	Glass transition temperature, T_g (°C)	Activation Energy, E_a (kJ / mol)	Fragility, m	R^2
PVP K29-32				
30	84.97 ± 2.74	205.62	30.77	0.8688
40	68.40 ± 2.10	193.06	29.54	0.8729
50	51.34 ± 0.07	172.90	28.29	0.8490
PVPVA 6:4				
30	61.34 ± 0.13	167.97	26.81	0.9825
40	52.20 ± 0.20	183.45	30.55	0.9810
50	44.10 ± 0.23	180.16	30.49	0.983
PVP K12				
30	58.68 ± 0.20	210.80	32.31	0.9238
40	54.66 ± 1.67	235.50	37.95	0.971
50	48.32 ± 0.34	193.70	32.08	0.9332
PVP K17				
30	54.40 ± 0.61	208.53	32.08	0.9298
40	48.78 ± 0.42	181.20	29.92	0.9397
50	42.54 ± 0.12	173.98	29.30	0.9811

As shown in Table 4.1, fragility indexes of the HME PCM-PVPs systems that being less than 40, i.e. $m < 40$ (Table 4.1) were categorized as strong glasses. These values are considerably lower than the at corresponding fragility of the pure amorphous PCM, i.e. 86.7 (Yu, 2001, Qi et al., 2008a), which was categorised as a fragile glass ($m > 75$) (Yu, 2001, Qi et al., 2008a). This indicates the less susceptibility of the solid state changes of the prepared HME systems upon annealing.

Table 4.2 summarise the trend of stabilization based on the magnitude of fragility (where a product with a higher m value was deemed to have lower stability and vice versa) and T_g estimation.

Table 4.2: The predicted trend of product stability based in fragility and T_g prediction

HME PCM carriers (drug loading, % w/w)	Trend of stabilization (most stable from the left to less stable on the right)	
	Based on Fragility	Based on T_g
30%	PVPVA > PVP K29-32 > PVP K17 > PVP K12	PVP K29-32 > PVPVA > PVP K12 > PVP K17
40%	PVP K29-32 > PVP K17 > PVPVA > PVP K12	PVP K29-32 > PVP K12 > PVPVA > PVP K17
50%	PVP K29-32 > PVP K17 > PVPVA > PVP K12	PVP K29-32 > PVP K12 > PVPVA > PVP K17

T_g is generally thought to be a ‘thermodynamic necessity’ to prevent ‘entropy crisis’ of an amorphous material toward recrystallization (Hancock et al., 1995). Researchers suggest that the storage conditions of an amorphous material should be 50 °C below the T_g in order to prevent devitrification of the amorphous material (Hancock et al., 1995). Therefore, the highest T_g of HME PCM-PVP K29-32 is expected to be the most stable followed by HME PCM-PVP K12 or HME PCM-PVPVA 6:4 and finally HME PCM PVP K17.

Unlike the T_g values of the products, there is not a general trend of stabilization prediction among the different drug loading systems based on fragility prediction as the predicted fragility index were all very similar (Table 4.1). However, among the carriers examined, PVP K12 carrier systems consistently revealed the highest fragility value in all the different drug loading systems and hence this polymer may be predicted to produce the most unstable HME systems (Table 4.2). The rank order of physical stability of HME PCM-different PVPs based on the T_g and predicted fragility index will be correlated to the stability profile of the products under recrystallization studies in the next section.

4.3.3. Recrystallization profile of aged HME PCM-PVPs on storage at elevated humidities

Recrystallization of HME PCM PVP-based systems in humidity induced conditions was investigated in two aspects. In the first instance, the influence of different humidity storage conditions on recrystallization behaviour of HME 40% PCM-PVPVA 6:4 system was investigated. This is carried out by storing the HME 40% PCM-PVPVA 6:4 systems in different relative humidity conditions, i.e. 22% RH, 33% RH, 53% RH and 75% RH, at room temperature. Subsequently, the effects of PCM loading, i.e. 30 - 50% w/w on the recrystallization behaviours of the aged HME different carriers systems (PVP K12, PVP K17, PVP K29-32 and PVPVA 6:4) were also studied exclusively at 75% RH.

The recrystallization studies of PCM under various humidity conditions were investigated up to 3 months. Different analytical methods were used to study the solid state changes. ATR-FTIR was used to probe the incremental change in crystalline content over time. As stated in section 4.2.3.3, samples were scanned daily for the first 14 days, then weekly up to one month, and subsequently monthly up to 3 months. DSC was used to detect the T_g changes of the samples after 3 months humidity storage. SEM was utilized for surface morphology inspection which was particularly useful for early stage of stability study as the content of crystalline material remained below the detection limit for other analytical methods. Thus SEM micrographs of early stability study (few hours, 1 week or 1 month) are preferentially presented.

4.3.3.1. Recrystallization of HME 40% PCM PVPVA 6:4 at different humidity conditions

Moisture-induced immiscibility upon storage has been widely reported for PVP-based SD due to its hygroscopic nature (Rumondor et al., 2009). Thus, it is important to study the influence of moisture content on the miscibility of the HME PVP-based SD upon storage. Figure 4.7 depicts the representative DSC thermograms of HME 40% PCM-PVPVA 6:4 system after 3 months storage at various humidities (22% RH – 75% RH).

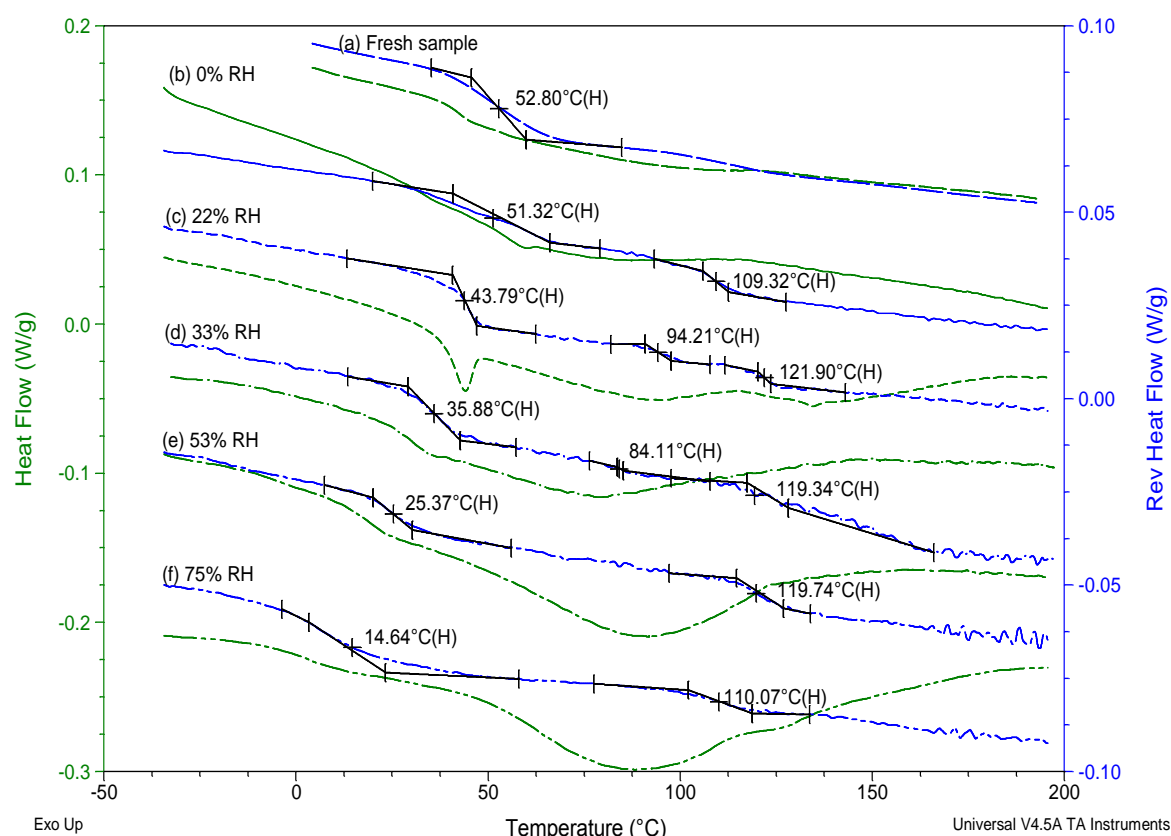


Figure 4.7: DSC curves for HME 40% PCM-PVPVA 6:4 system after 3 months storage under different humidity conditions a) 0% RH, b) 22% RH, c) 33% RH, d) 53% RH and e) 75% RH

Freshly prepared sample indicated a single T_g at 52.80 °C. After 3 months storage in the dry condition, i.e. 0% RH, two T_g (s) were detected which is an indication of classical phase separation. This phenomenon was also seen in all of the aged samples under higher humidity conditions.

First T_g in the thermograms of the aged HME 40% PCM-PVPVA 6:4 system reveals a consistent reduction with the increase in storage humidity (Figure 4.7). This might be ascribed to the plasticization of the absorbed moisture content in the sample which was more considerable in the higher relative humidity conditions. This is further indicated by the noticeable water loss endotherm in the total heat flow signal at 60 to 100 °C, and this endotherm increased with higher humidity storage conditions. The absorbed water molecules have resulted in an increase in the free volume of the system which subsequently increases the molecular mobility of the system. With the increase free volume of the system, the small molecule of drug will diffuse within the polymeric network and separate from the polymer into an amorphous API rich phase which gave rise to the first separated T_g as observed from the DSC profile (Vasanthavada et al., 2004). Figure 4.8 presents the overall picture of the T_g values and water content of the aged HME 40% PCM-PVPVA 6:4 after 1 month storage.

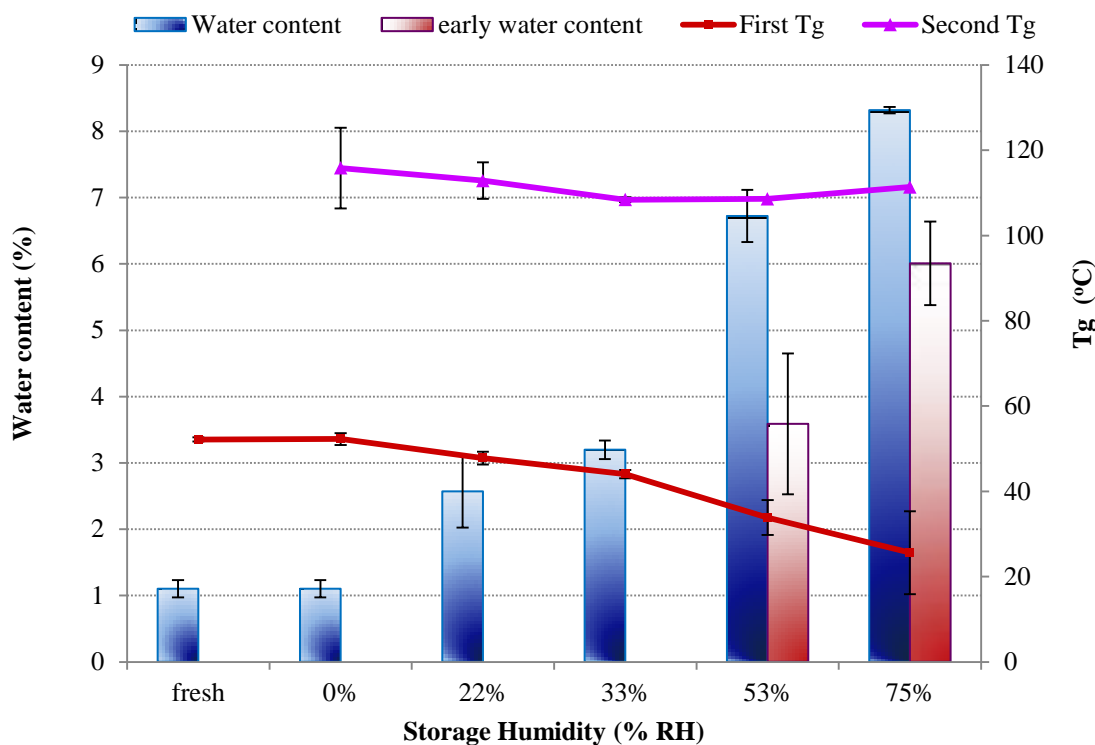


Figure 4.8: Moisture contents and Tg values of aged HME 40% PCM PVPVA 6:4 after 1 month storage in different humidity conditions. Bar chart in red indicated the early water content of the aged HME 40% PCM PVPVA 6:4 after 9 days and 3 days storage in 53% and 75% RH, respectively

The second Tg detection in the DSC thermograms of the aged HME PCM-PVPVA 6:4 sample might be attributed to two possibilities. Firstly, it may be indicating moisture induced separation of PVPVA 6:4 polymer in the aged HME 40% PCM-PVPVA 6:4 (Figure 4.7). Based on Figure 4.8, the second Tg values of the aged HME PCM-PVPVA 6:4 in different humidity conditions were almost constant and closed to the Tg value of pure PVPVA 6:4, despite its extensive plasticization that expected from the presence high water content (blue bar chart). This might be ascribed to the moisture evaporation through the pinhole cover as could be evidenced noticeable endotherm in the DSC thermogram during the DSC scan (Figure 4.7), which leads to the detection of the Tg value close to its original Tg instead of the plasticized one. Secondly, the detected second Tg may be an indication of polymorphic transformation of the possibly recrystallized Form III PCM which was reported to reveal a transition temperature at circa 120 °C into Form II PCM (Di Martino et al., 1997).

As the detected second Tg (s) in these highly plasticized samples were circa 110 °C which were slightly higher than the pure Tg of PVPVA 6:4, i.e. 106 °C, the second possibility is more likely. However, further study is required to confirm the presence of form III PCM in the aged HME PCM-PVPs system which will be included as future work.

Recrystallization of the aged HME 40% PCM-PVPVA 6:4 system was further studied by using ATR-FTIR. The fast analysis of this method enables the tracking of the crystallinity on a daily basis with minimal sample preparation procedure. No characteristic peak of 807 cm^{-1} was detected in the ATR-FTIR spectra of HME 40% PCM-PVPVA 6:4 stored in 22% RH. However, in 53% RH and 33% RH, this peak was seen after 14 days and 1 month storage, respectively. In 75% RH conditions, this characteristic peak was seen 48 hours after storage which indicated the highest recrystallization rate of HME 40% PCM-PVPVA 6:4 in high humidity condition. The presence of peak at 807 cm^{-1} in ATR-FTIR spectra of aged HME systems suggested the presence of Form I crystal in the aged HME 40% PCM PVPs-based system. Instead of doublet peaks, a single peak was shown in the region of 1608 cm^{-1} and 1655 cm^{-1} which indicated the absence of Form II crystals as previously discussed in section 4.3.1.1 and Figure 4.1. The recrystallized polymorph was further confirmed by scanning the aged sample in XRPD (data not shown).

Crystallinity of the aged sample was approximated from the quantification method that was developed in the earlier section (section 4.3.1) to obtain a recrystallization profile of the aged samples. Figure 4.9 shows the recrystallization profiles of the HME 40% PCM-PVPVA 6:4 system at different humidity conditions.

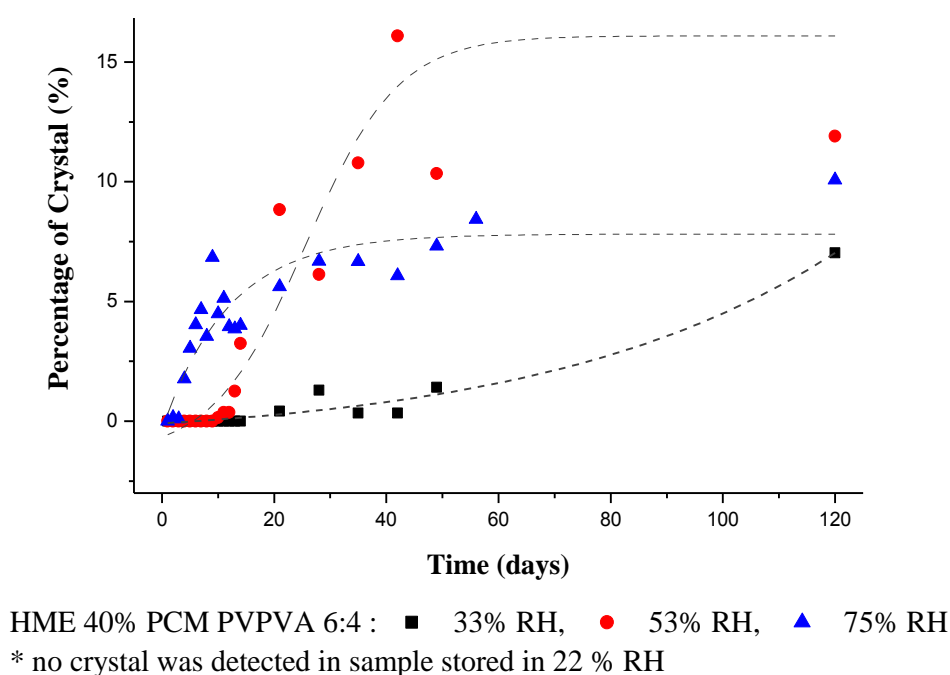


Figure 4.9: Recrystallization profiles of HME 40% PCM-PVPVA 6:4 under different humidities condition at room temperature detected by scanning the aged samples overtime using the developed ATR-FTIR quantification method. Dotted lines shown in the Figure is just a guide in following the data points

The results show a trend of faster recrystallization at higher humidity conditions. Calling back to the early water content detected in the aged HME 40% PCM-PVPVA 6:4 system in Figure 4.8, a lower water content of the aged sample stored in 22% RH has led to the undetectable of crystalline material in this system which infers its limited recrystallization in this storage condition. However, in 33% RH, the aged sample showed a higher water content i.e., circa $3.20 \pm 1.05\%$ with a small percentage of crystalline materials detected after 1 month storage at this condition. Furthermore, aged samples stored in 53% RH reveal an absence of detectable crystal until day 9 whereas an exponential growth of crystal was measured and its water content was found to be circa $3.58 \pm 1.06\%$ (Figure 4.8). As anticipated, crystalline materials were detected in the aged sample with a water content of $6.08 \pm 0.63\%$ after 3 days storage in 75% RH. Therefore, the amount of water content required for the initiation of recrystallization event is predicted to be between 3.5 - 6%.

The result of ATR-FTIR is in contrast to DSC thermograms whereby no melting endotherm was detected (Figure 4.7). This suggested the potential dissolution of the existing crystalline material upon the DSC heating scan which was further confirmed by scanning the aged sample using variation temperature of ATR-FTIR (Appendix III). Besides, the principle in detecting the crystalline materials of both the analytical instrument should be taken into consideration. Firstly, DSC is a techniques that scanning the whole of the extrudate which including the bulk and the surface. On the other hand, ATR-FTIR is a surface detection techniques, where its measurement is limited to only approximately 6 μm beyond the surface of the ATR accessory (Larrabee and Choi, 1993). Thus, the recrystallization profile obtained by using the ATR-FTIR techniques might only be used to represent the percentage of crystal that was detected near the surface of the extrudates. This will be further confirmed in a later section in HME 50% PCM-PVPs-based system.

4.3.3.2. Recrystallization of HME 40% PCM with different PVPs carriers

After the recrystallization study of HME 40% PCM-PVPVA 6:4 system in different humidity storage conditions, the effect of different carriers on recrystallization behaviour of the HME products was also studied. In this case, recrystallizations of the samples were studied only in 75% RH. Figure 4.10 and Figure 4.11 display the DSC thermograms of freshly prepared HME 40% PCM- carriers and aged HME 40% PCM- carriers, respectively after 3 months storage in 75% RH.

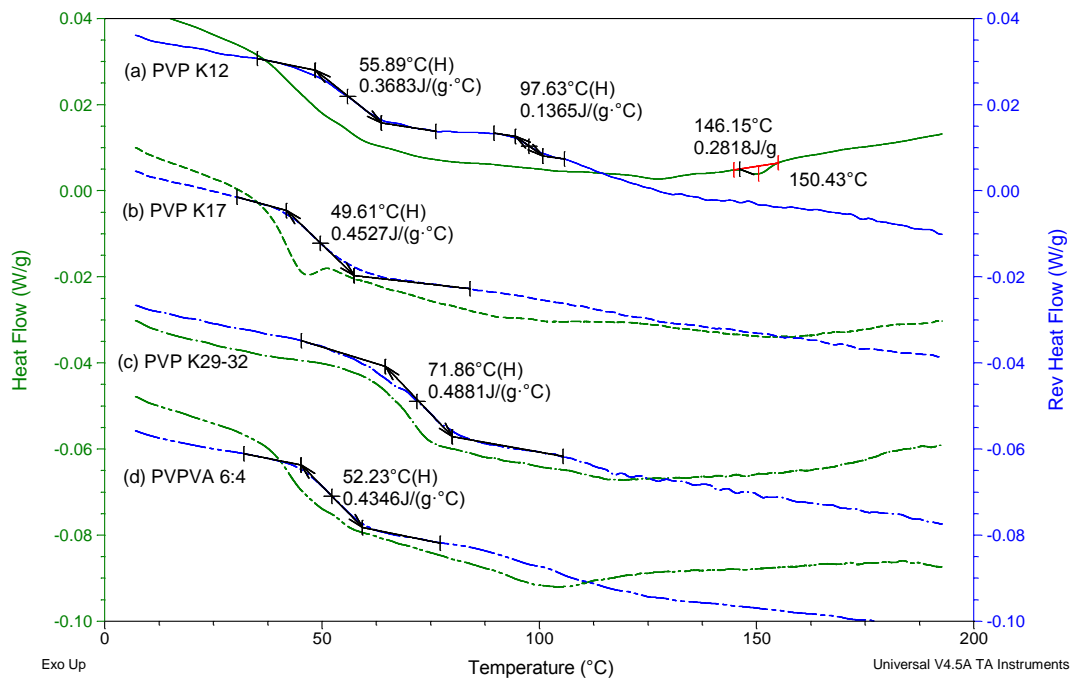


Figure 4.10: DSC thermograms of the freshly prepared HME 40% PCM -carriers, (a) PVP K12, (b) PVP K17, (c) PVP K29-32 and (d) PVPVA 6:4

As demonstrated in Figure 4.10, the HME 40% PCM-PVPs systems revealed a single Tg except HME 40% PCM-PVP K12 whereby two apparent Tg(s) were seen. There is a minor endotherm in the same thermogram at a temperature slightly lower than the normal melting temperature of PCM. This could be possibly ascribed to the depressed melting point of the PCM in the presence of PVP K12.

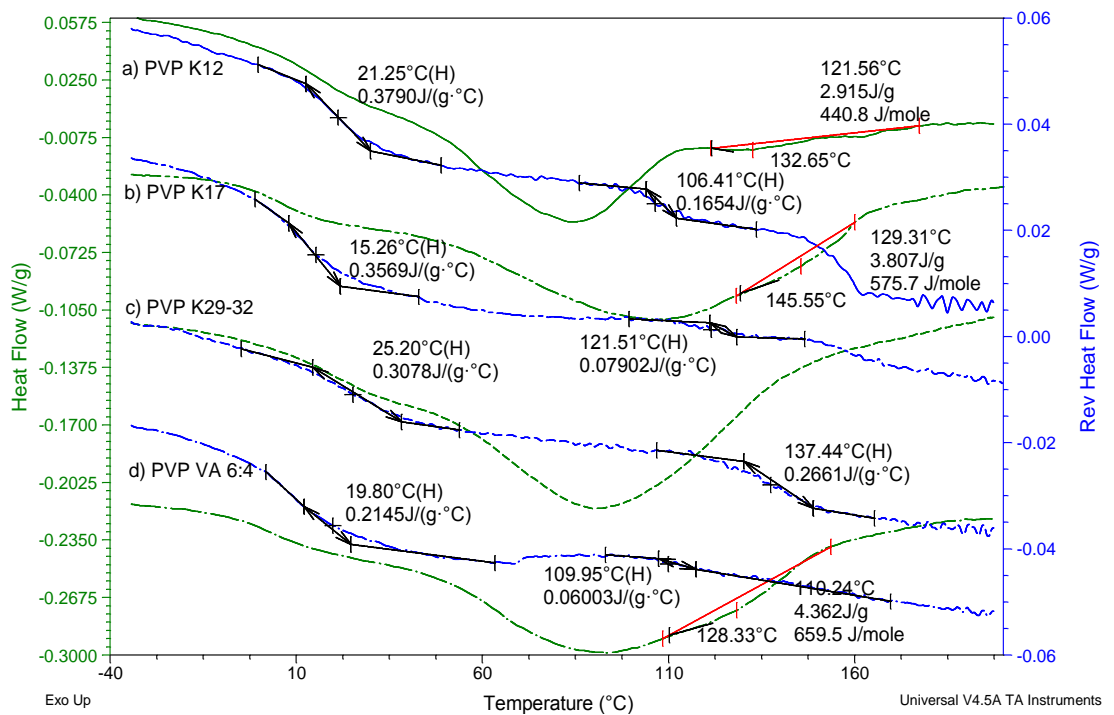


Figure 4.11: DSC curve for HME 40% PCM-carriers at 75%RH after 3 months storage

In the DSC thermograms of aged samples as shown in Figure 4.11, two T_g (s) were noted for all the different carriers based system of 40% HME which indicated a phase separation after humidity storage. The two separated T_g (s) coincided to the T_g of amorphous PCM, i.e. 25 °C and T_g of the pure polymer phase with the exception for PVP K29-32 system. In PVP K29-32 carrier system, the second T_g remained much lower than the T_g of the pure polymer phase. This indicated that a fraction of drug molecules remains miscible with PVP K29-32 (Vasanthavada et al., 2004). As described previously (section 4.3.3.1), the detection of the high value of second T_g might be related to the water evaporation during DSC heating scan as a result of the used of pin-holed pans or the possibility of the presence of Form III PCM in the aged samples.

From Figure 4.11, minor endotherm was seen in HME 40% PCM-PVP K12 at circa 121°C which was accompanied by an obvious transition in the reversing heat flow signal. Similar minor endotherm was also seen in both HME 40% PCM-PVP K17 and PVPVA 6:4 system, where both show the endotherm at an onset of 129 °C and 110 °C respectively. To summarise, phase separation were seen in all the HME 40% PCM-PVP systems.

Recrystallization profiles of the HME 40% PCM in different carriers were produced by using the quantification method that has been developed in the section 4.3.1. Figure 4.12 displays the recrystallization of 40% HME of PCM in different carrier systems at 75% RH over 120 days based on ATR-FTIR data using Equation (4.1).

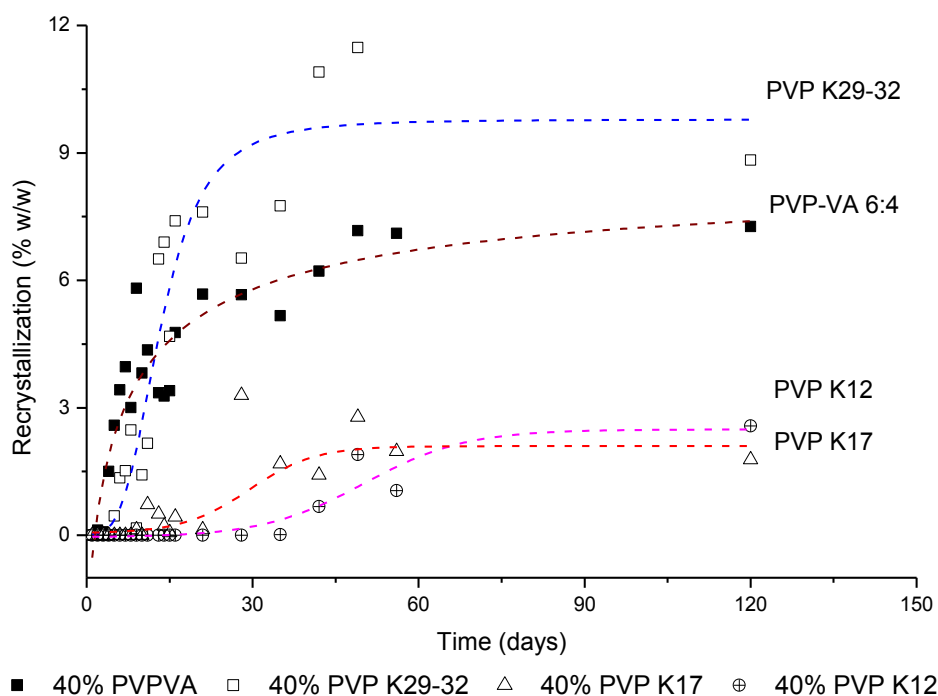


Figure 4.12: Recrystallization of 40% loading of PCM in different carriers at 75% RH calculated based on characteristic peak of 807 cm⁻¹ /797 cm⁻¹ in ATR-FTIR spectra of the aged sample using Equation 4.6. Dotted lines shown in the Figure is just a guide in following the data points

As could be seen in Figure 4.12, HME 40% PCM-PVPVA 6:4 system appeared to show the earliest crystal detection (highest early recrystallization rate) using the ATR-FTIR method. This is followed by HME 40% PCM-PVP K29-32 where the crystalline content was detected in ATR-FTIR after 5 days of storage in 75% RH. However, the percentage of crystals in HME PCM-PVP K29-32 system was higher than HME PCM-PVPVA system after one week of storage in 75% RH, as shown by overshooting of the crystal growth profile of HME 40% PCM-PVP K29-32 over HME 40% PCM-PVPVA 6:4 (Figure 4.12). Under the same storage conditions, the crystal content in HME 40% PCM-PVP K17 and PVP K12 was detected only after 12 days and 21 days, respectively. Lag phases were seen in the profiles of these samples (HME 40% PCM in PVP K17 and PVP K12) which might be attributed to the nucleation phase of the aged extrudates. The lower crystal content detected in the low MW carrier of HME PCM PVPs system was unexpected. This is because a low MW carrier should impose a lower physical hindrance toward the recrystallization process of the drug molecule as compared to the high MW carrier system which might possibly lead to its higher recrystallization rate (Prodduturi et al., 2005). This unexpected result will be further communicated in a latter section (section 4.4.4) in relation to the processing conditions of HME.

In order to confirm the recrystallization trend obtained from the Figure 4.12, surface morphologies of the aged HME SD extrudates were also investigated under SEM. Figure 4.13 shows the SEM micrographs of HME 40% PCM PVPs after 1 month storage in 75% RH (next page).

It was found that the aged HME 40% PCM-PVP K12 and 17 did not show any apparent drug crystalline structure on their surfaces (Figure 4.13 (a) i and (b) i). However their magnification images reveal some interesting features (Figure 4.13 (a) ii and (b) ii). In addition, HME 40% PCM-PVP K29-32 demonstrated tiny pores visible on its surface after humidity storage. Magnification of this image reveals some particles on its surface. Unlike the other HME PVP carrier systems, surface of the aged HME 40% PCM-PVPVA 6:4 (Figure 4.13 (d) i) was rough. The magnification of this image in Figure 4.13 (d) ii indicated small indentations on its surface. Overall, the observed features on the surface of the extrudate were not conclusively to be regarded as distinctive crystalline structure. However, the trend of the significance of this surface features was coincided to the trend of early recrystallization rate of the aged HME 40% PCM-PVPs system as deduced from Figure 4.12.

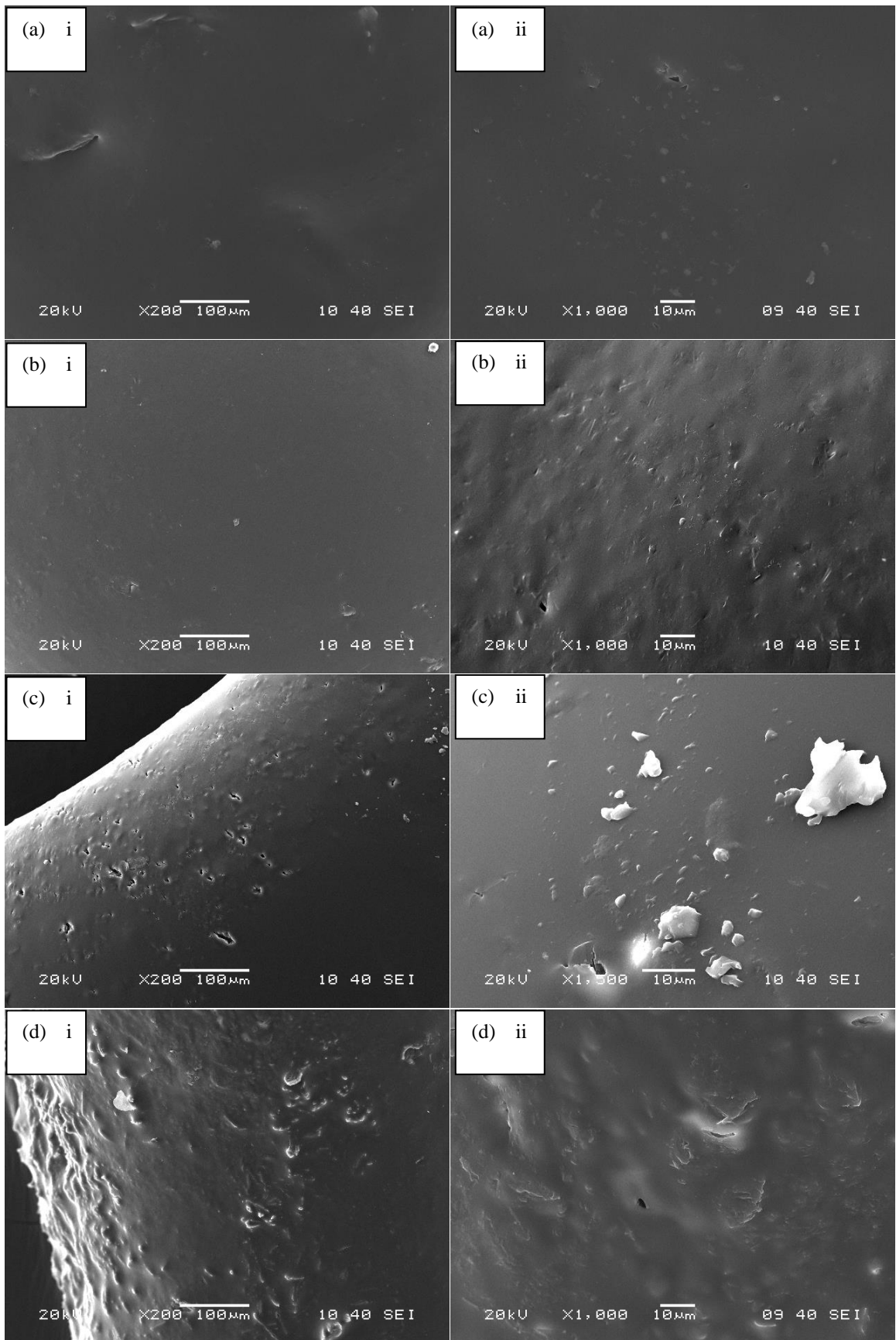


Figure 4.13: Surface morphology of HME 40% PCM-PVPs after 1 month storage in 75% RH a) PVP K12, b) PVP K17, c) PVP K29-32 and d) PVPVA 6:4. Right (ii) images are the corresponding magnification of the left (i) images.

To summarise, recrystallization rate and extent of HME 40% PCM-PVP systems were highly dependent on the storage humidity. In particular, the recrystallization process was faster under the higher humidity storage conditions. Apart from that, in 75% RH storage condition, PVPVA 6:4 carrier displayed the earliest onset crystallisation followed by PVP K29-32, PVP K17 and PVP K12. This recrystallization trend based on the carrier system is not in agreement to the trend predicted by the values of fragility index and T_g as tabulated in Table 4.1. Therefore, more studies were carried out afterwards to further investigate this as will be discussed in the following sections.

4.3.3.3. Effect of PCM loading on the recrystallization behaviour of HME different PVPs carrier system

The previous section has shown the disadvantageous physical stability of HME sample utilizing PVPVA 6:4 as the carrier system. This was unexpected as PVPVA 6:4 was less hygroscopic as compared to the homopolymer carriers. In order to further understand this unexpected result, the effects of drug loading on the relative recrystallization behaviours of different carriers of interest were investigated. This was performed by studying the recrystallization profiles of both the high loading of PCM, i.e. 50% and the low loading of PCM i.e., 30% in the HME different carriers system. In the subsequent sections, recrystallization profiles of both the aged systems of HME 50% PCM-PVPs and HME 30% PCM-PVPs will be presented and complemented by the results deduced from SEM micrographs.

4.3.3.3.1. Recrystallization profile of aged HME 50% PCM-carriers at 75% RH

The crystal growth profile of HME 50% PCM-PVP-based SD after 75% RH storage was probed by using ATR-FTIR scanning. The diagnostic band at 807 cm^{-1} was detected in the spectra of HME 50% PCM-PVPs system after 12 hours of storage at 75% RH which indicated the presence of crystalline content. The relative intensity of this band was used to calculate the percentage of crystallinity using Equation (4.6). Figure 4.14 presents the crystallization profile of the HME 50% PCM PVPs-based SD up to 3 months using the ATR-FTIR method.

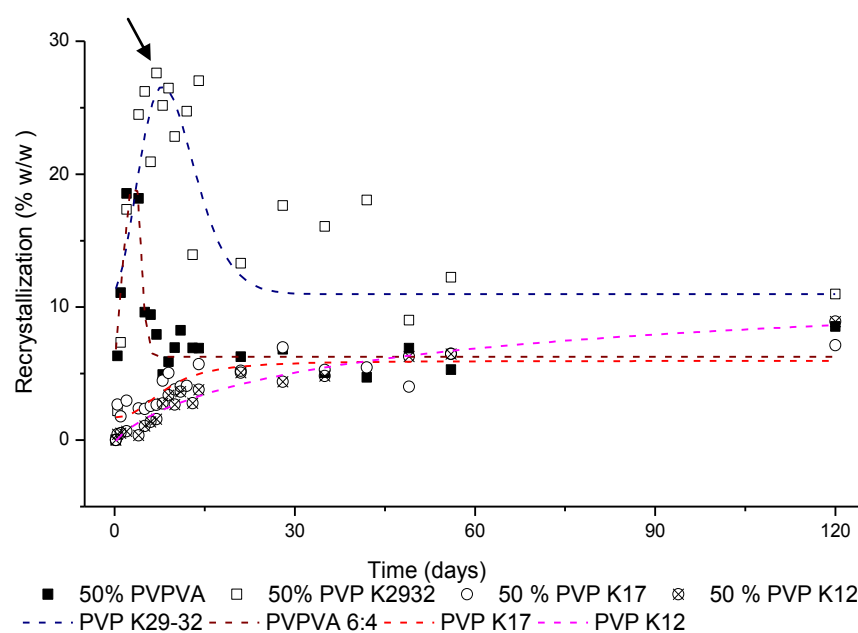


Figure 4.14: Recrystallization of HME 50% PCM in different polymer systems at 75% RH measured by using ATR-FTIR. Dotted lines shown in the Figure is just a guide in following the data points

According to the Figure 4.14, a single maximum profile (as indicated by the arrow in Figure 4.14) was observed for the recrystallization of HME 50% PCM-PVP K29-32 and PVPVA 6:4 systems after the exposure to 75% RH. A surge of crystal growth in the early stage of storage in 75% RH was noted in the recrystallization profile of the aged samples (HME 50% PVP K29-32 and PVPVA) detected by using ATR-FTIR. Eventually, the crystallinity of aged samples (HME 50% PVPVA 6:4 and PVP K29-32) achieved a constant value up to 3 months storage (Figure 4.14). However, this behaviour was not observed in the aged 50% PCM extrudate of PVP K12 and PVP K17 carriers.

The single maximum recrystallization profile of HME 50% PCM in PVP K29-32 and PVPVA 6:4 may have occurred due to two possibilities. Firstly, this might be ascribed to the nature of the crystal PCM, which is a water soluble drug. During the sample storage, there is a continuation of water absorption of the extrudates due to the hygroscopic nature of PVP, which initiated the recrystallization of the crystal on the surface of the extrudates. However, when the water content reached a certain value above the rubbery state of the sample, chain re-orientation of the polymer occurs. This may cause the dissolution of the recrystallized PCM (generated from an early recrystallization process) into the co-solvent of PVP and the absorbed water which gave rise to a reduction in crystal content after certain period of humidity storage (Figure 4.14).

Secondly, it might be caused by the better drug-polymer interaction following high humidity storage that eventually dissolves the present crystal. Recent study has indicated that the pyrrolidone subgroup of PVP possesses different conformations in the dry and humidified state as indicated by the molecular docking and intermolecular energies studies (Malaj et al., 2010). In that study,

crystallinity of the poorly soluble drugs was observed to reduce with time at high humidity storage. The authors presented that pyrrolidone subgroups are folded along the main chain in the dry PVP, whereas the pyrrolidone subgroups appears to be perpendicular to the main chain in a hydrated PVP, thus leading to the higher accessibility for interaction. Therefore, it is suggested that the combination of both of the ‘water soluble nature of PCM’ and ‘higher drug-polymer interaction’ following humidity storage have contributed to the single maximum profile of recrystallization observed in Figure 4.14. Further study is required to understand the effect of high humidity storage on crystal re-dissolution phenomena which is beyond the scope of this study.

In addition, it is unexpected that the samples with high MW carrier recrystallized (HME 50% PCM-PVP K29-32) faster than the same composition of sample extruded with a low MW (HME 50% PCM in PVP K12 and PVP K17). This might be ascribed to the different tendencies of recrystallization process between the surface and bulk of the extrudates in different MW PVP systems, as ATR-FTIR is a surface technique that scanned up to approximately 6 μm beyond the surface of the ATR accessory (Larrabee and Choi, 1993). This phenomena will be further presented in the next section by comparing the crystallinity of PCM on the surface and ground extrudates.

Crystallinity comparison between surface and whole extrudates by using ATR-FTIR

It is expected that the ground extrudate would give rise to a value of total crystallinity of the sample as the grinding process has mixed the crystals on the surface and the bulk to produce a homogeneous powdered system. The crystallinity of the ground extrudates were probed by using ATR-FTIR and compared to the crystallinity of the system measured on the surface of the extrudates. Figure 4.15 indicates the percentage of crystallinity obtained from both ground and surface of the extrudates (next page).

As demonstrated in Figure 4.15, the overall crystal content of the extrudates (spectra obtained from ground extrudates) and the crystal contents on its surface (spectra obtain from intact extrudate) were different. Crystal content on the surfaces of the higher MW HME carrier systems, i.e. PVP K29-32 and PVPVA 6:4, was higher than that of their ground form (ground extrudates). However, crystal content on the surface of the extrudates with low MW carrier system, i.e. PVP K12 and PVP K17 were slightly higher than the crystal content in their ground state. Overall, crystal contents of all the ground extrudates of homopolymer carriers are comparable. However, PVPVA 6:4 shows a consistently highest crystalline content in both the surface and the bulk extrudates. This coincides to the relative instability of HME system with PVPVA 6:4 as a carrier as deduced from the previous section in recrystallization of HME 40% PCM-PVPVA 6:4.

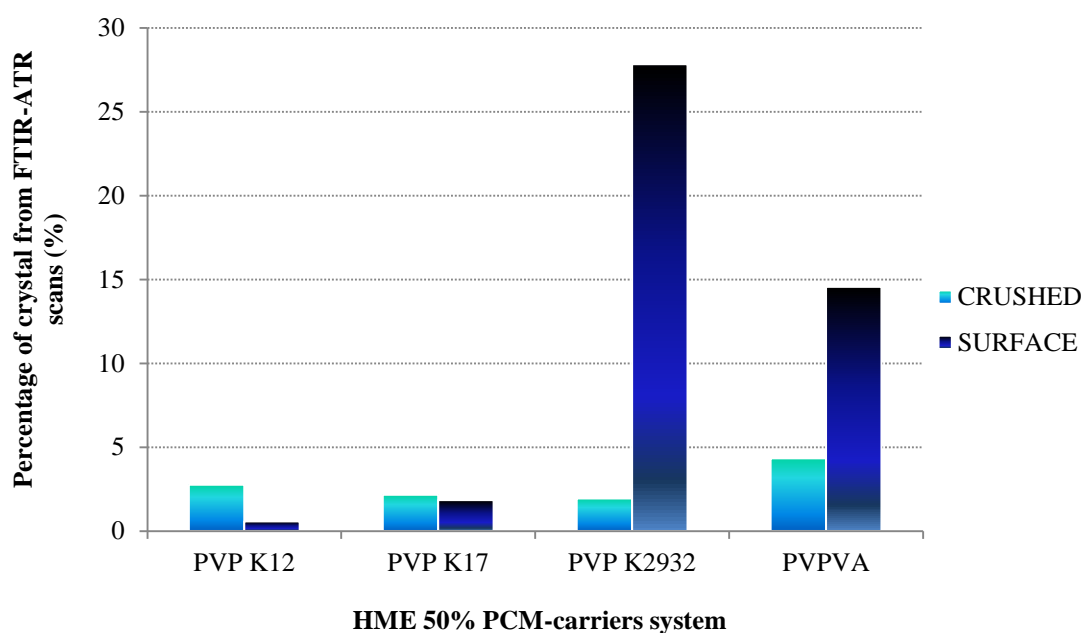


Figure 4.15: The comparison of crystallinity on surface and bulk extrudates after 4 days in 75 % RH measured by using ATR-FTIR

The reason behind the different recrystallization of the surface and the bulk extrudates of the high MW carrier HME system may be related to the high MW carrier matrix that exerts a restraining pressure in preventing the internal crystal growth (Bruce et al., 2007). Besides, it could also be explained by the different relaxation processes occurring on the surface and bulk of a solid dispersion system as suggested by Ke et al., 2012 who differentiated the surface and bulk relaxation of the SD system with inverse gas chromatography (ICG) and DSC methods (Ke et al., 2012). However, the discrepancies of difference in crystalline content between the surface and bulk of the four different PVPs carrier system were unexpected. This is because all the aged HME 50% PCM-PVPs systems show similar values for the first T_g and the second T_g which implies that phase separation have occurred in all the aged systems. The phase separation indicated the presence of partially rubbery state and partially glassy state in the aged samples at the temperature of room condition, i.e. 25 °C. However, the relative portion of the rubbery and glassy state of the different carrier of aged HME system may be responsible for the discrepancies of differences in crystalline content seen between surface and bulk of the extrudates which will be served as a ramification for future study.

The surface of the aged HME 50% PCM-PVPs systems after exposed to the 75% RH was also investigated by SEM. The investigation was performed at 2 time points (after 4 hours and 1 week of storage) in order to understand the different recrystallization rates at early and later stages of humidity exposure. Figure 4.16 displays the SEM images of the aged samples after 4 hours in 75% RH.

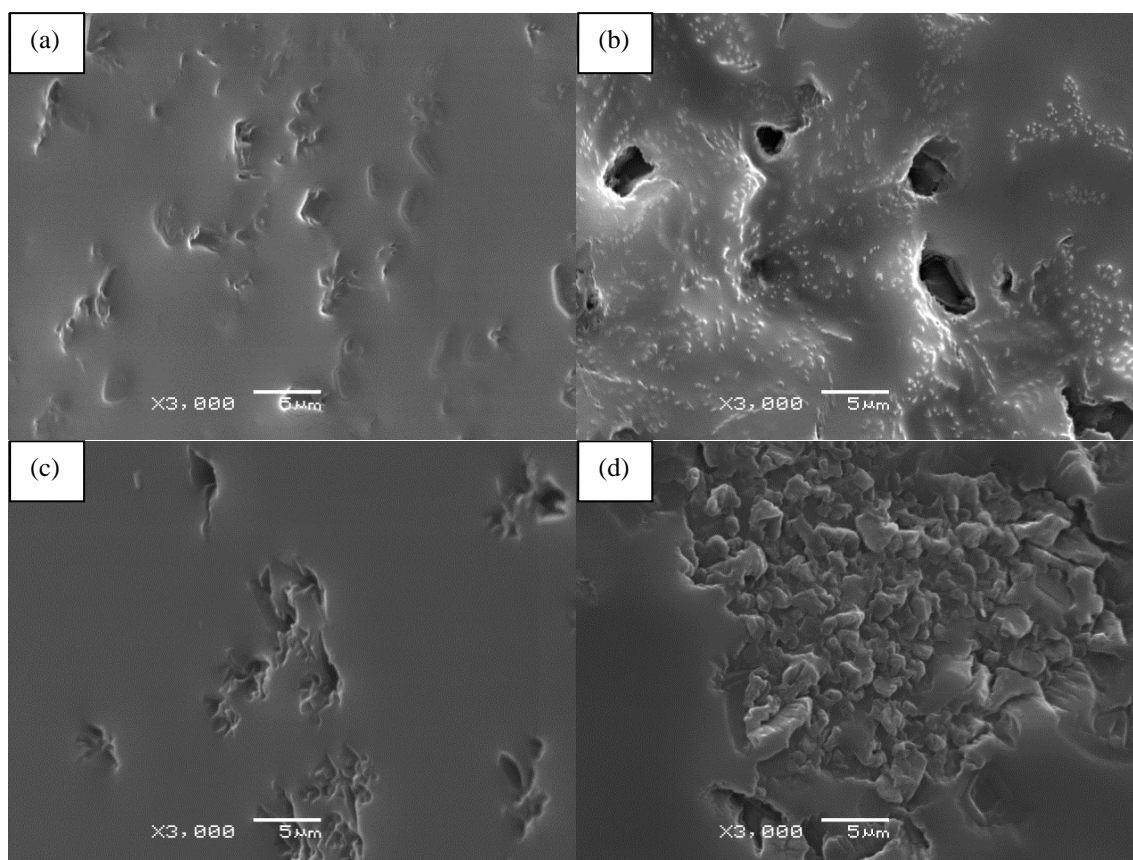


Figure 4.16: Surface images after 4 hours in 75% RH HME 50% PCM-PVPs a) PVP K12, b) PVP K17, c) PVP K29-32, and d) PVPVA 6:4

After 4 hours storage of RH HME 50% PCM-PVPs in 75% RH (Figure 4.16), small angular structures were seen on the surfaces of the PCM PVP K12 system (Figure 4.16 (a)). Obvious indentation were noted on the surface of HME 50% PCM-PVP K17 system as seen in Figure 4.16 (b). Similarly to HME PVP K29-32 carrier system, tiny pores were seen. However, no obvious crystal shapes were noted in all the homo-polymer carrier system (PVP K12, PVP K17 and PVP K29-32). Based on the SEM micrographs (Figure 4.16), PVPVA 6:4 carrier system exhibited the highest surface changes intensity, (Figure 4.16 (d)) which might indicate the beginning of recrystallization process in this samples.

Figure 4.17 shows the surface of the extrudates after 1 week storage under 75% RH. After 1 week storage in 75% RH, SEM micrographs of HME 50% PCM-PVPs revealed regular repeating unit on surface of PVP K12 carrier system (Figure 4.17 (a)). Surface of the aged HME 50% PCM-PVP K17 shows some indentations and elongated shaped features. On the other hand, an obvious crystalline structure was seen in HME 50% PCM high MW carrier Figure 4.17 (c). Also, well-ordered block-like structures (circa 5 μ m) were noted on the surface of the HME 50% PCM-PVPVA 6:4 carrier Figure 4.17 (d). This result is in agreement to the recrystallization trend of the different HME carriers system obtained by using ATR-FTIR method where the rank order of recrystallization is PVPVA 6:4 > PVP K29-32 > PVP K17 > PVP K12.

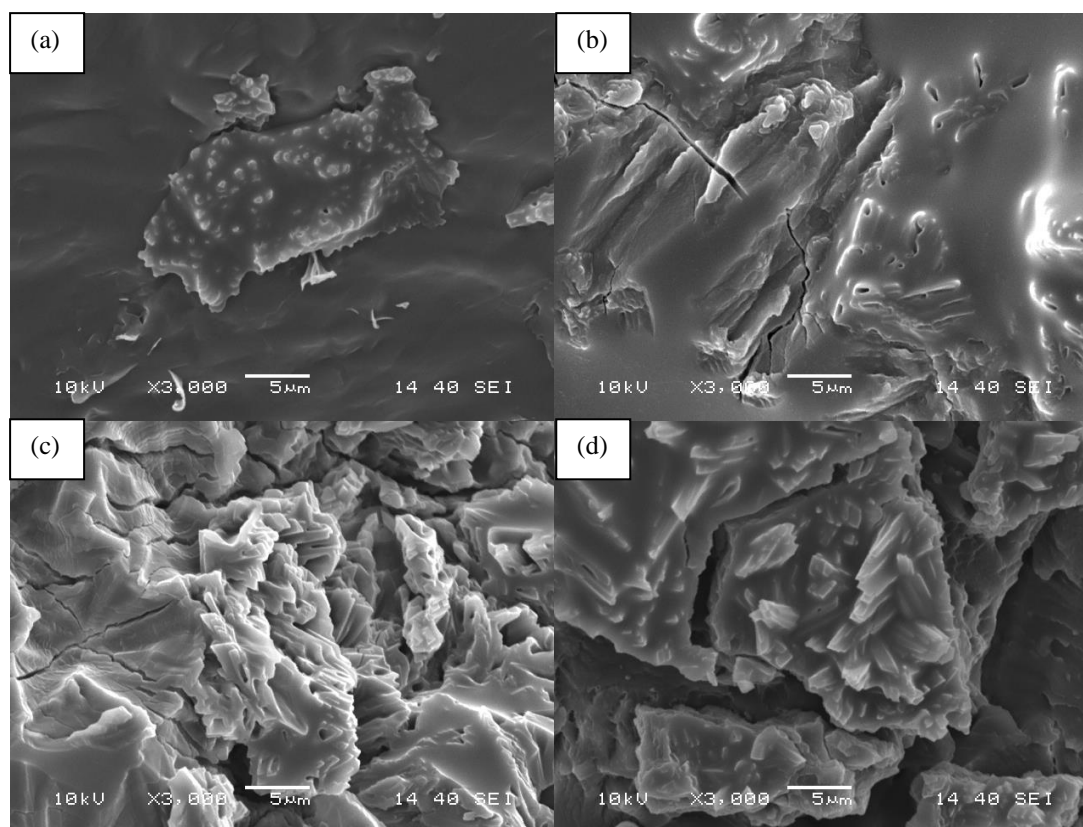


Figure 4.17: SEM images of HME of 50% PCM PVPs (a) PVP K12, (b) PVP K17, (c) PVP K29-32 and (d) PVPVA 6:4 after 1 week in 75% RH

To summarise the stability study of HME 50% PCM-PVPs carriers, HME PVPVA 6:4 carrier system showed the poorest stabilising effect on recrystallization of PCM. In addition, the recrystallization of PCM was preferentially occurred on the surface of the extrudate when a high MW carrier was used. Overall, PVPVA 6:4 carrier remains inferior in physical stabilization of PCM where the stability trend of HME 50% PCM-PVP is in the order of $\text{PVP K29-32} \geq \text{PVP K17} \geq \text{PVP K12} > \text{PVPVA 6:4}$

4.3.3.3.2. HME 30% PCM-carriers on storage at 75% RH

With the recrystallization trend of HME PCM in different PVPs system at high PCM loading, the recrystallization trend of the HME PCM in different PVPs at low PCM loading system were investigated. This is to provide a further insight into the recrystallization behaviour of the drug in the different carriers of HME system. Figure 4.18 indicated the recrystallization profiles of the aged formulations of HME 30% in different PVPs systems. Recrystallization of the HME 30% PCM-PVPs were observed only after 10 days storage in 75% RH as measured by using ATR-FTIR method.

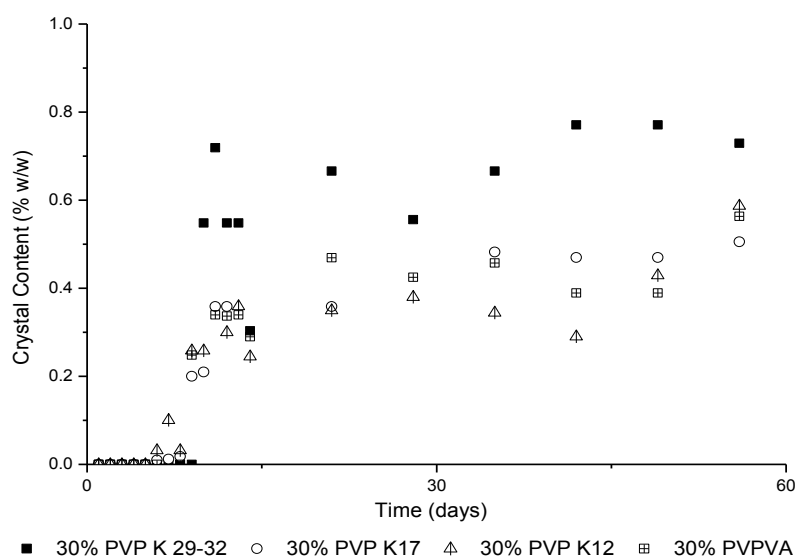


Figure 4.18: Recrystallization profile of HME 30% PCM PVPs system at 75%RH over 120 days produced by using the data from ATR-FTIR

Unlike the recrystallization trend seen in higher drug loading system, HME 30% PCM-PVPVA 6:4 system showed a similar crystalline content to the HME 30% PCM-low MW carrier systems i.e. PVP K12 and PVP K17 as shown in Figure 4.18. This implies similar stability among HME 30% PVPVA 6:4, PVP K12 and PVP K17 systems under 75% RH. The aged extrudates of HME 30% PCM-PVP K29-32 exhibited the highest crystallinity on its surface as indicated by the characteristic peak of 807 cm^{-1} in its ATR FTIR spectrum. However, it is noteworthy from Figure 4.18 that the percentages of crystallinity detected for the HME 30%-different PVPs were all below 1% w/w.

To confirm the recrystallization trend of the different PVP polymers in the HME PCM systems, surface morphologies of the aged HME 30% PCM different PVPs system were investigated. Figure 4.19 show the SEM images of the HME 30% PCM different PVPs carrier after two weeks storage in 75% RH. According to the SEM images, surfaces of the HME 30% PCM with homo-polymers revealed tiny repetitive features especially in PVP K17 carrier system. This feature was not noted in HME 30% PCM-PVPVA 6:4 after storage (Figure 4.19 (d)). However, the topography of the HME 30% PCM-PVPVA 6:4 surface was distorted and rough which was suspected to be attributed to the ingress of moisture under humidity storage. Hence, the aged HME 30% PCM-PVPVA 6:4 was suggested to have a similar recrystallization behaviour in comparison to the homopolymer carrier system. This trend of recrystallization base on the carrier types is not in coherent to the trend shown in the previous studies of HME 40% and 50% PCM-PVPs system.

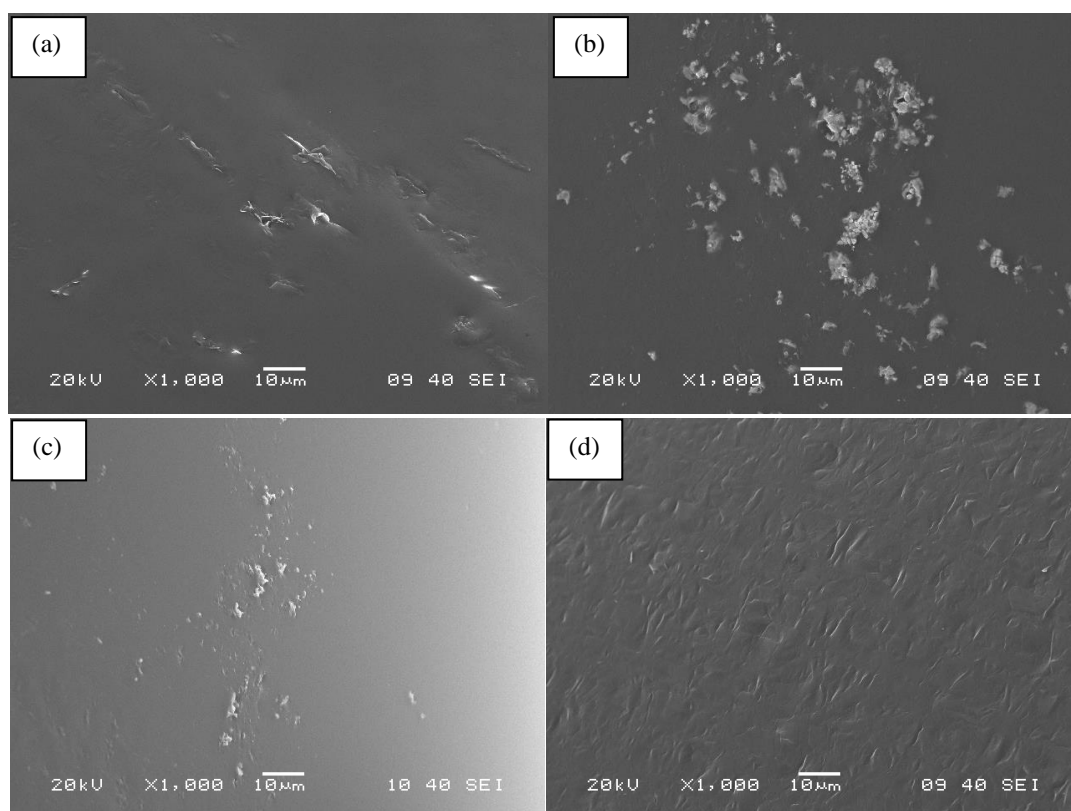


Figure 4.19: SEM images of HME of 30% PCM different PVPs carriers (a) PVP K12, (b) PVP K17, (c) PVP K29-32 and (d) PVPVA 6:4 after 2 weeks in 75% RH

To summarise the recrystallization study of 30 to 50% PCM-PVP carriers under 75% RH storage condition, a bar chart in Figure 4.20 is presented. It is based on the recrystallization rate of each formulation at early recrystallization process (first 5 days).

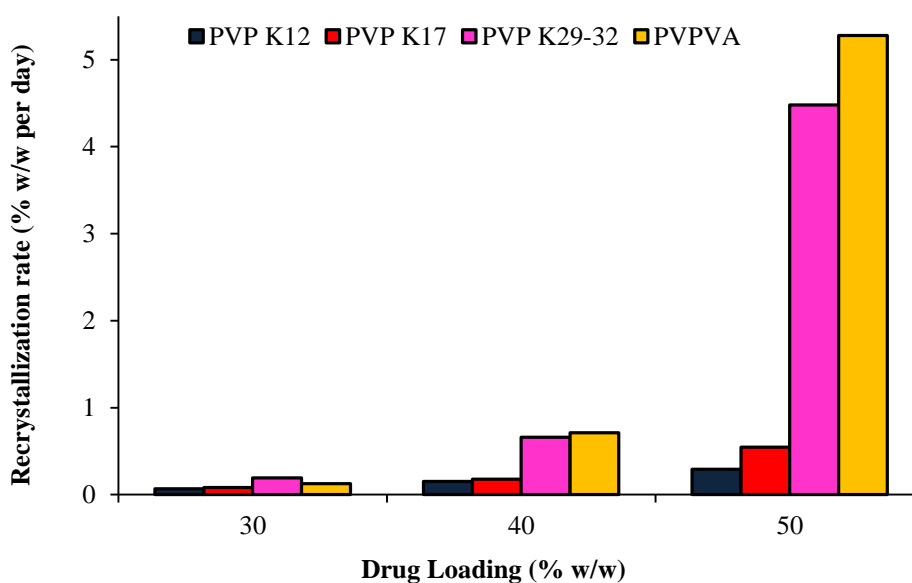


Figure 4.20: The summary of recrystallization rate of HME 30 to 50% PCM-carriers system. The rate of the recrystallization was obtained from the slope of initial (first 5 days) crystallization profile of each formulations detected from ATR-FTIR method

According to Figure 4.20, PVPVA 6:4 carrier was found to be inferior in stabilising HME PCM-PVPs system under high humidity conditions (75% RH) particularly in extrudates with 40% and 50% of PCM loading. However, at low loading of PCM, the trend of stabilising the PCM was not following the same trend as that observed in higher PCM loading. In the low PCM loading system (30% drug loading), PVPVA 6:4 carrier showed a lower surface recrystallization rate than PVP K29-32 system and revealed almost similar degree of recrystallization to the low MW PVP carrier system (PVP K12 and PVP K17). The reason behind these observations will be discussed in Chapter 4.4.3.

4.3.4. Influence of storage temperature on the stability of HME PVP-based SD

Temperature is another important factor for the determination of stability of a thermodynamically unstable solid dispersion. Thus, it is essential to understand the influences of temperature on the recrystallization behaviour HME PVP-based system. In this case only HME 40% PCM different PVPs were investigated. Samples were stored at room temperature and at 40 °C / 0% RH for the 3 months temperature storage study.

4.3.4.1. Annealed sample of HME 40% PCM with different polymers

The annealed HME 40% PCM PVPs system did not indicate the appearance of 807 cm^{-1} in the ATR-FTIR spectra which indicated the absence of Form I PCM (data not shown). This is further supported by the halo pattern of their XRPD diffractograms after 3 months storage in 0% RH, 40 °C (data not shown). Tg changes of the system were analysed by DSC measurement. Figure 4.21 shows the representative DSC thermograms of the aged sample HME 40% PCM-PVP carriers after 3 months storage in 40°C / 0%RH.

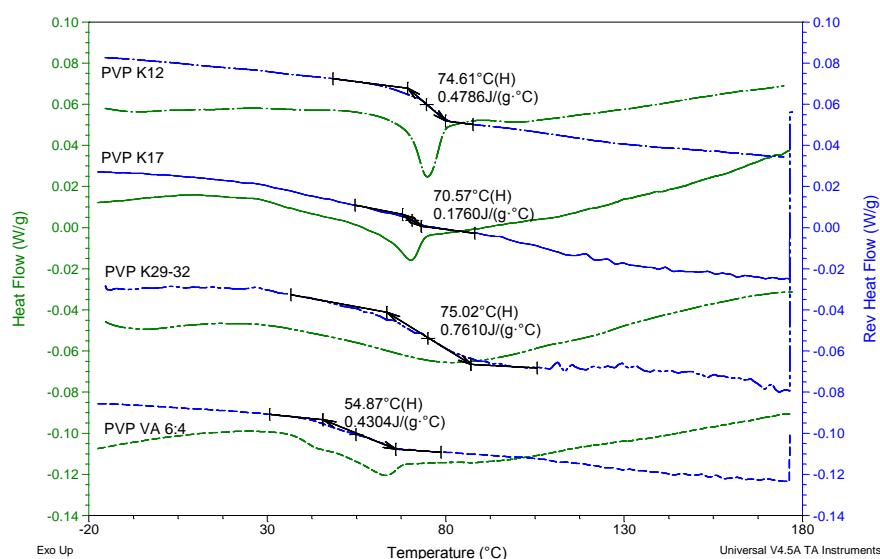


Figure 4.21: DSC thermograms of HME 40% PCM PVPs after 3 months storage at 0RH 40°C

As expected, no apparent melting endotherm of API was detected in the DSC thermograms of the annealed HME 40% PCM-PVPs samples. However, T_g of the annealed samples were clearly increased as compared to the freshly prepared samples (refer to Figure 4.10 for DSC thermograms of fresh samples) due to the evaporation of moisture under the dry (0% RH) and warmer conditions. Based on Figure 4.21, relaxation event were also noted superimposed upon the glass transition of the tested HME 40% PCM-carriers samples. The magnitude of this endotherm is then an indication of the non-equilibrium fraction of the samples which dictate the thermodynamically driving force for recrystallization process (Figure 4.21).

As crystalline material could not be detected using the previously presented technique, SEM was used in this case to study crystallinity on the surface of the annealed extrudates qualitatively. Figure 4.22 presents the SEM images of the annealed HME 40% PCM-PVPs at 40 °C. Some minor features were seen on the surface of extrudates. These were more profoundly observed on surface of HME 40% PCM-PVPVA 6:4 system (Figure 4.22 (d)) where the observed feature was crystal-like as compared to other carriers. Thus, it is suggested that, HME 40% PCM-PVPs system is relatively stable in temperature-induced condition, i.e. 40 °C in this study rather than in humidity induced conditions.

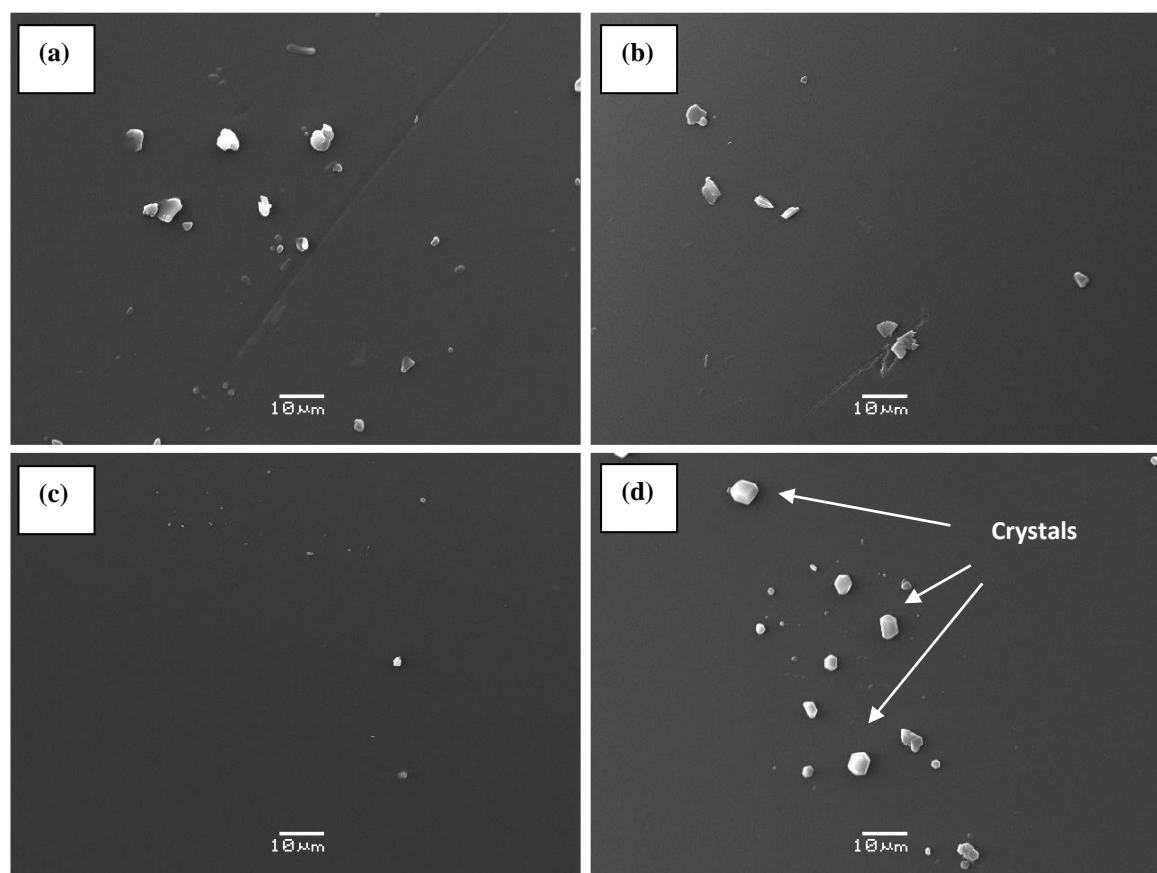


Figure 4.22: SEM images of HME of 40% PCM in polymer for different carriers (a) PVP K12, (b) PVP K17, (c) PVP K29-32 and (d) PVPVA 6:4 after 3 months in 40°C

4.4. Discussion

4.4.1. Establishment of quantification methods for crystalline PCM

One of the key aspects of this chapter was the development of reliable quantification methods to detect crystalline materials. In this respect, the diagnostic band of 807cm^{-1} detected in ATR-FTIR was calibrated using crystallinity changes of QC PCM calculated from DSC scan. In this development, data obtained from DSC was served as a calibrant whereby it could convincingly and accurately measure a single compound such as QC PCM samples.

Complications arise if DSC was used for the detection of minute crystal in a mixture of different components (Biswal et al., 2009). This is because drug might potentially dissolve into the mixed polymer upon heating especially the scanning with a low heating rate (Craig and Reading, 2007, Yang et al., 2010b). Moreover, huge moisture sorption of the aged HME PVP-based systems would further complicate the data analysis of DSC thermograms. The endothermic water loss signal may mask some of the thermal events such as recrystallization or glass transition which will be recorded in the same temperature region of water loss. Even though the masking effect of water could be effectively separated in modulated mode of DSC (heating or cooling rate of $< 2^\circ\text{C}$), however the use of the low heating rate would promote the drug dissolving problem. Therefore, in this study, DSC was not employed as a method for crystallinity detection in the blend system of HME PCM-PVPs but instead it was used to detect the Tg changes of the aged sample after storage.

4.4.2. The influence of humidity on HME PCM in PVP-based polymers

During the humidity storage HME system absorbs a considerable amount of water due to the hygroscopic nature of its PVP carriers (Callahan et al., 1982). This lead to the observation of phase separation of the aged system following humidity storage system as inferred from the 2 detected Tg (s) shown in Figure 4.7 (Vasanthavada et al., 2004, Vasanthavada et al., 2005, Rumondor et al., 2009). Water is well-known plasticizer due to its low molecular size that increases the free volume of the system and alters the chain conformation of the macromolecule polymer (Airaksinen et al., 2005, Szakonyi and Zelkó, 2012). This phenomenon is particularly augmented by the hydrogen bond interaction between the polymer-water, as the water molecule could replace the bonded polar group of the polymer (i.e pyrrolidone group in PVP polymer of this study) and weaken the attracting forces between the polymeric chains, consequently increase the free volume of the whole polymeric system (Szakonyi and Zelkó, 2012).

This increment in free volume of an amorphous system leads to the greater molecular mobility of the API molecule embedded in the polymer. This molecular mobility of the API can be further promoted by the replacement of water molecules on the polar group of PVP which was previously bonded with API. Thus, with the higher molecular mobility of API, recrystallization of API could easily ripen (Heljo et al., 2012). This is clearly shown in the recrystallization rate and extent of the aged HME 40% PCM-PVPVA 6:4 that were found to be directly correlated to the absorbed moisture after humidity storage. Therefore, recrystallization of the HME 40% PCM-PVPVA 6:4 system was found to be highly humidity dependent.

Based on the crystallization profile in Figure 4.9, a lag time occurred before crystallization. This lag time was longer in lower humidity storage conditions. According to the ATR-FTIR results of the HME 40% PCM-PVPs system, samples stored in 22% RH did not reveal apparent diagnostic band of 807 cm^{-1} which implied the absence of crystalline material on the surface of these samples. Nevertheless, these samples underwent moisture absorption (moisture content of fresh samples < 2%) with water content of circa $2.57 \pm 1.04\%$ (refer to Figure 4.8). At 33% RH storage condition, the aged HME 40% PCM-PVPVA 6:4 system absorbed circa $3.20 \pm 1.05\%$ of water content after 1 month storage. This amount of water coincides to the onset of crystalline material detection by using ATR-FTIR. This could be further confirmed by the early water content of the aged samples stored in 53% RH. In 53% RH, the crystalline PCM was detected after 9 days of storage whereby its water content was in coherent to the amount of water detected for the initiation of recrystallization, i.e. $3.58 \pm 1.06\%$. Thus, it is not unexpected to note the immediate recrystallization of the aged HME 40% PCM-PVPVA 6:4 in 75% RH as the sample absorbed a considerable amount of water in a short period of storage time, i.e. $6.08 \pm 0.63\%$ just after 3 days of storage in 75% RH. Thus, it is suggested that there is a minimum amount of moisture that dictates the minimum mobility of drug molecules in ripening the event of recrystallization. On the basis of the moisture content detected from TGA and the trend of immediate recrystallization profiles (recrystallization profiles in Figure 4.9), the minimum moisture level for the initiation of recrystallization of aged HME 40% PCM-PVPVA 6:4 is estimated to be between 3.5 to 6%.

4.4.3. Hydrogen bonding between drug and polymer: a key for physical stability?

Base on the recrystallization studies of HME PCM-in different PVPs carrier, PVPVA 6:4, a relatively hydrophobic polymer with its lowest moisture absorption following humidity storage, revealed consistently the highest recrystallization tendency in HME 40% and 50% PCM PVPs systems. As the recrystallization tendency was correlated to the ability of the water molecule in replacing the API on the polar group of the pyrrolidone monomer, it is hypothesized that hydrogen bonds interaction between the drug-polymer might critically determine the recrystallization

behaviour of HME PCM PVP-based system. This effect was previously identified to be important in stabilization of solid dispersions (Matsumoto and Zografi, 1999, Trasi and Taylor, 2012). In further understand this, the relationship between the hydrogen bond tendencies to the recrystallization process was considered.

PCM molecules possess two proton donors whereas PVP monomer possesses one proton acceptor in the carbonyl group of pyrrolidone. The quantities of carbonyl groups from each monomer were correlated in molar ratio of possibility of hydrogen bond formation resulting in 1:2, PCM: PVP monomer ratio. Since the possibility of hydrogen bonds formation is in 1:2 PCM : PVP monomer ratio, thus any value of the ratio that is above 1:2 (i.e. > 0.5) is deemed to have the PCM oversaturated in view of drug-polymer hydrogen bond interaction. Table 4.3 presents the ratio of PCM: polymer based on hydrogen bond capacity of the proton acceptor of pyrrolidone or vinyl-acetate. The highlighted rows in Table 4.3 indicate the limit of PCM loading where the molar ratios of the PCM : PVP monomer are just below 0.5.

Table 4.3: Ratio of PCM to polymer in different composition (hydrogen bonding limit of PCM-PVP polymers are highlighted in pink)

Drug loading (% w/w)	Ratio of PCM: monomer of Polymers		
	PVP Homo-polymers	PVPVA 6:4 Pyrrolidone	PVPVA 6:4 pyrrolidone + acetate
20	0.19	0.28	0.17
30	0.33	0.47	0.28
40	0.49	0.73	0.44
50	0.76	1.10	0.66
60	1.13	1.65	0.99

According to Table 4.3, the drug-homopolymer (PVP) hydrogen bonding interaction limit is lies in composition of 40% w/w PCM loading (Table 4.3, column 2). Base on this, HME of 50% PCM-PVPs is existed in the oversaturated (in term of hydrogen bond interaction) state which coincides to its immediate recrystallization upon humidity storage as the non-bonded amorphous PCM is readily to recrystallize (recrystallized within 12 hours of 75% RH storage). On the other hand, a lag time was observed for formulations with 40% drug composition possibly due to its optimum drug-polymer hydrogen bond interaction.

From the relative recrystallization behaviours of different PVP carrier, HME 40% PCM PVPVA 6:4 system revealed an immediate recrystallization profile despite its optimum hydrogen bond interaction between the PCM and PVPVA 6:4 as anticipated from involving both the carbonyl groups from pyrrolidone and vinyl acetate. However, according to the ATR-FTIR spectra of HME PCM-PVPVA 6:4 copolymer system (Chapter 3), red-downshift was only seen in carbonyl

stretching region of pyrrolidone but not in the carbonyl region of vinyl acetate. Thus, it is suggested that hydrogen bonding of the PCM and PVPVA 6:4 is preferential formed through the pyrrolidone rather than vinyl acetate groups. This might be due to the reported lower partial atomic charges on the oxygen functional group of the vinyl acetate (i.e. poorer proton acceptor) as compared to pyrrolidone (Trasi and Taylor, 2012). Therefore, the intensity of hydrogen bond interaction between PCM-PVPVA 6:4 is relatively lower as compared to the PCM-PVP homopolymer. This leads to a higher proportion of free amorphous PCM molecule in PVPVA 6:4 carrier system which in turn promotes its higher recrystallizations tendency as compared to the HME PCM homopolymer, PVP system.

The important of drug-polymer interaction in recrystallization behaviour of PCM was further confirmed by studying HME 30% PCM- carriers systems. At the end of 3 months stability studies, all the different HME 30% polymer systems (PVP K29-32, PVP K17, PVP K12 and PVPVA 6:4) displayed <1% crystal content with a similar lag time (i.e. 10 days) and recrystallization profile. Based on Table 4.3, composition of 30% PCM-PVPs systems would theoretically have all the PCM drug molecules hydrogen bonded to the polymer carrier, thereby, no drug molecules existed in surplus for the driving of crystallization.

The comparison of recrystallization behaviours in HME PCM-PVPs of different carriers and PCM composition systems suggested that hydrogen bond interaction between the drug and polymeric is a decisive factor in the recrystallization process of the HME PVP-based SD upon humidity storage.

4.4.4. The effect of molecular weight of PVP on physical stability of HME formulations

Among the homopolymer carrier systems, HME PCM-PVP K29-32 consistently revealed a highest crystalline content on its surface after humidity storage. This is unexpected as the high MW PVP K29-32 might exert a higher physical hindrance for the recrystallization of PCM as compared to the carrier with low MW. Besides, PVP homopolymers in their same composition of PCM-polymer shall possess the same number of available interaction unit (carbonyl group from pyrrolidone) with the PCM which give rise to their similar recrystallization behaviour, however, it is not as such. The result in Figure 4.18 demonstrated that PCM dispersion in PVP K29-32 was relatively unstable as compared to the PCM dispersion in low MW systems, i.e. PVP K12 and PVP K17 which show similar recrystallization profiles of the both.

Generally, it is reported that the extrusion temperature should be 10-20 °C higher than the polymer in order to achieve good flowability in the hot melt barrel during preparation (Chokshi et al., 2005). However, this principle was not employed in this study due to the potential degradation of PVP polymer at high temperature. In this study, solubilisation regime of processing temperature was

employed whereby T_{process} (at 160 °C) is lower than T_m and T_g of PCM and PVP K29-32, respectively (please refer to Chapter 2.3.1 for the review of the processing temperature regimes summarised in literature). Based on this regime, viscosity of the molten dictate diffusivity of the API and hence the extent of API solubilisation. High torque values (i.e. 20-30 Ncm for PVP K29-32 carrier and 0 - 2 Ncm for PVP K12 and K17 carrier) in the extruder barrel, indicated high viscosity of the extruded material in the barrel, which could led to suboptimal drug polymer interaction and limited solubilisation of the PCM in PVP K29-32 (Lakshman et al., 2008). Thus, it is proposed that the suboptimal drug polymer interaction and limited solubilisation of the PCM in PVP K29-32 during the HME process has led to the higher recrystallization of HME PCM PVP K29-32 system tendency as compared to low MW carriers, i.e. PVP K12 and PVP K17.

However, the effect chain conformation change of polymer following high humidity storage that lead to a better accessibility of the carbonyl group of the pyrrolidone for drug-polymer interaction should not be overlooked, as it might be a possible reason of the undetectable crystalline material in the low MW HME PCM PVPs system. This phenomenon might be closely related to the solid state conversion, i.e. from glassy state to the rubbery state. Thus, the relationship on the relative portion of the glassy and rubbery state of the aged HME PCM-PVP system in recrystallization behaviour of the system shall serve as a study for the future work.

4.4.5. The influence of temperature on physical stability of HME PCM-PVPs

Amorphous solid dispersion may undergo mixing and de-mixing under the influence of temperature. In this study, endothermic relaxations accompanied by the glass transition temperature were seen (Figure 4.21) in DSC thermograms of HME PCM-PVPs sample after 3 months storage at 40 °C / 0% RH .

Preparation of HME products involves the extrusion of sample from a high temperature (i.e 160 °C in this study) to room temperature which led to the production of a supercooled liquid after extrusion. Therefore, the HME samples possess an excess amount of configurationally enthalpy through frozen-in of the degree of orientation freedom from the molten state (Suga, 2000). Hence, the relaxation endotherm shown in DSC thermogram implies a change of the annealed samples from a non-equilibrated state to an equilibrated state upon heating up to above the glass transition temperature.

Despite the detection of samples relaxation, there was no significant recrystallization observed over the timescale of experiment using the analytical approaches of DSC, ATR-FTIR and XRPD except SEM, where crystalline materials were noted on the surface of the annealed HME 40% PCM-PVPs system. Besides, surface of annealed HME 40% PCM-PVPVA 6:4 system consistently shows a

higher amount of crystalline materials as compared to the other carrier of HME PCM-PVPs system (SEM images in Figure 4.22). This trend is in agreement to the stability profiles of the HME different carriers system whereby the stabilizing effect of PVPVA 6:4 was inferior as compared to the homopolymer PVP at HME 40 % PCM-PVPs system.

Based on the trend of fragility index in Table 4.1, HME PVPVA 6:4 carrier system shows a lower value than the HME PVP K12 system in which the former system was theoretically predicted to be relatively more stable than the PVP K12 system. However, this is not as such as the annealed HME PVPVA 6:4 carrier system shows highest crystalline proportion on its surface as compared to the PVP K12 system. This indicated that the annealed HME 40% PCM-PVPVA 6:4 had undergone the highest recrystallization rate as compared to the other system annealed in the same condition, 0% RH and 40 °C. Therefore, it is suggested that there is poor correlation between the fragility index of a material and physical stabilization of the product which is in agreement to some recently published literature (Graeser et al., 2009, Kawakami et al., 2012, Graeser et al., 2009a, Ke et al., 2012).

4.5. Conclusion

A quantification method of Form I PCM was developed using ATR-FTIR measurement. This method was found to be suitable in detecting low crystalline content of the sample. Besides, it should be reminded that ATR-FTIR is a surface technique whereby the only approximately 6 µm of the surface contacted to the ATR accessory was detected. Nonetheless, it is a valuable technique which has been found to be particularly useful to complement the result of DSC that may be affected by the kinetic dissolution of the crystal during DSC heating scan.

Recrystallization tendency of HME PVP based products was found to be highly humidity dependent as higher recrystallization rate was detected in storage condition of higher humidity. Preceding the dramatic crystallization growth in recrystallization profiles of the aged HME PCM PVPs system, a lag phase of the profiles was noted. This lag phase was found to be highly correlated to its water content which might be responsible for the nucleation phase of the aged HME PVP-based sample. Besides, recrystallization profiles of HME PVP-based systems indicated that the early crystallization process was predominantly controlled by hydrogen bond interaction between drug and polymer systems at an early stage of the humidity storage.

Furthermore, drug-polymer composition of a HME PVP-based SD is preferably accord to the optimum or under-saturated of hydrogen bond interaction between drug-polymer in order to reduce the driving force of recrystallization. This could be clearly seen in the immediate recrystallization of the hydrogen bond supersaturated state in the high drug loading of HME PCM-PVP (i.e. 50%

PCM for homopolymer carrier and > 40% PCM for PVPVA 6:4 carrier systems). On the other hand, the under-saturated (hydrogen bond between drug and polymer) of HME 30% PCM-PVPs systems show no immediate recrystallization (recrystallized only after 10 days) of PCM occurred even in the high humidity condition (75% RH). Above all, it should be re-emphasized that, the degree of drug-polymer hydrogen bond interaction of HME product stems from the HME preparation process, where a lower viscosity (low torque value) and optimum flowability of the molten mixture is preferred in order to obtain an optimum hydrogen interaction between the drug and polymer.

Apart from that, this chapter has shown that HME PVP based products exhibited a better physical stability in 'temperature induced' condition as compared to the 'humidity induced' condition. Moreover, the trend of T_g and fragility index did not correlate well to the recrystallization rate of the aged HEM PCM-PVPs carrier system. Therefore, the factor of T_g and fragility index was concluded to have minimal roles in the physical stabilization of HEM PCM-PVPs carrier system.

Chapter 5. An investigation into factors governing the drug release mechanism of PVP-based hot melt extrusion formulations Part I: Dissolution performances of HME of poorly soluble drugs with PVPVA 6:4

5.1. Introduction

Solid dispersions (SD) are often associated with the dissolution and bioavailability enhancement of poorly soluble drugs (Chawla and Bansal, 2008, Craig, 2002, Hülsmann et al., 2000, Kalivoda et al., 2012b). This is mainly attributed by several factors that have been discussed in Chapter 1.6 which include, the conversion of crystalline into amorphous dispersion in SD, carrier solubilisation effect, hydrophilicity and wettability enhancement by the carrier, formation of complexes and high surface area of the dissolving API in the SD system due to their molecularly dispersed nature (Kapsi and Ayres, 2001, Dong et al., 2008b, Biswal et al., 2009).

Many studies reported the significant increases in dissolution rate of poorly soluble compounds when they are formulated into a SD (Corrigan, 1985, Craig, 2002, Fernandez et al., 1989, Biswal et al., 2009, Chawla and Bansal, 2008). However, a number of papers have revealed undesired dissolution behaviour of SD whereby a slower release of drug was noted when the drug was processed into a SD as compared to their corresponding physical mixture (PM) (Verheyen et al., 2002, Tajarobi et al., 2011a, Moneghini et al., 1998, van Drooge et al., 2004, Saers and Craig, 1992). Further details of this contradiction were reviewed in Chapter 1.6 and 1.6.1. Based on this literature, there are no general principles regarding the benefit of production of SD that can be guaranteed to the user, hence there remains uncertainty regarding the relationship between structure of API-polymer and dissolution performance for these systems.

Therefore, a detailed understanding on the dissolution mechanism of the SD system is required to guide the formulation scientist in developing a successful SD system. In this chapter, the aspect of formulation performances of HME PVP-based SD was focused on. Here, dissolution performances of SD of four different poorly soluble active pharmaceutical ingredients (APIs) were investigated. PVPVA 6:4, a hydrophilic polymer, was employed as a carrier with a view to enhance the dissolution performance of the poorly soluble APIs. Possible factors in affecting the desired dissolution performance that arise from the use of different APIs in the prepared HME PVP-based SD system were investigated.

5.2. Material and methods

The APIs employed in this study include ketoprofen (KTP), naproxen (NAP), indomethacin (INDO) and olanzapine (OZP). Chemical structures and physicochemical properties of these four APIs and PVPVA 6:4 could be found in Chapter 2.21. To compare the effect of the four different APIs in dissolution performance of HME PVP-based SD, the carrier of the systems was made constant, i.e. PVPVA 6:4.

5.2.1. Estimation of the amorphous solubility advantage

The dissolution advantage of an immediate release SD system is often linked to its amorphous nature due to the lack of strong bond in the structure of API in this state. In amorphous state, the API exists in its readily dissolvable state which is deemed to be an advantage of its form. This amorphous advantage could be reflected by the free energy difference between the amorphous and its crystalline form (Hancock and Parks, 2000) as described by Hoffman Equation (5.1) (Hoffman, 1958),

$$\Delta G = \frac{\Delta H_f \cdot \Delta T \cdot T}{T_m^2} \quad (5.1)$$

where ΔH_f is the enthalpy of melting which could be obtained from DSC experiment, T_m is the melting temperature of the crystalline form, and ΔT is $T_m - T$ (Alonzo et al., 2010, Hancock and Parks, 2000). Besides, the free energy differences is also a function of solubility advantage offered from the amorphous form (Alonzo et al., 2010). This ratio of solubility advantages could be approximated from Equation (5.2),

$$\frac{\sigma^{amorph}}{\sigma^{crystal}} = e^{\frac{\Delta G}{RT}} \quad (5.2)$$

where $\sigma^{amorph} / \sigma^{crystal}$ represent the ratio of the solubility of amorphous API to the solubility of its crystalline counterpart, ΔG is the different of free energy between the amorphous and crystalline forms, R is universal gas constants and T is the respective solubility temperature at Kelvin (Alonzo et al., 2010).

5.2.2. Solubility testing

Solubility tests of the pure APIs were performed in their corresponding discriminatory media as outlined in Table 5.1. Apparent solubility of the APIs in the presence of low (0.0001% w/v), intermediate (1% w/v) and high concentration (10% w/v) of PVPVA 6:4 in the corresponding discriminatory medium were also performed.

Table 5.1: Medium and UV wavelength used for the solubility measurement of pure API and PM API-PVPVA

Drugs / carrier	Medium	UV wavelength (λ_{\max})
Ketoprofen	0.1M HCl	259 nm
Naproxen	0.1M HCl	272 nm
Indomethacin	Distilled water	265 nm
Olanzapine	Distilled water	254 nm
PVPVA 6:4	0.1M HCl/ distilled water	No absorbance after 240nm

In general, the solubility of APIs were carried out by dissolving excess powder of APIs in 200 ml of the medium (with or without the presence of PVPVA 6:4) to form a mixture which were stirred for at least 48 hours at 37 °C. Then, these mixtures were filtered using a 0.45 μm polyvinylidene fluoride (PDVF) filtration unit and examined spectrophotometrically at the corresponding UV wavelength, λ_{\max} of the APIs (Table 5.1).

5.2.3. Preparation of PM

PMs were prepared by mixing the API and PVPVA 6:4 using a ball milling equipment without the insertion of ball. Both the powders of APIs and PVPVA 6:4 were sieved into a control particle size range of 63 - 106 μm . Then, 30% (w/w) of API loading and 70% (w/w) of PVPVA 6:4 were weighed accordingly and transferred into the ball-milling chamber without the insertion of ball. Subsequently, the milling chamber was fixed to the milling equipment and oscillated horizontally at 30 Hz for 10 minutes. The used of this technique allows the preparation of a homogenous and reproducible PMs between the API and PVPVA 6:4 that has been verified from preliminary data.

5.2.4. Hot melt extruded products

HME of the binary APIs-PVPVA 6:4 were prepared using a hot melt extruder. Details of the extruder used in this study could be found in Chapter 2.3. Please refer to Table 2.12 for the processing parameters used in the manufacturing of HME 30% KTP PVPVA 6:4, HME 30% NAP PVPVA 6:4, HME 30% INDO PVPVA 6:4 and HME 30% OZP PVPVA 6:4 systems.

5.2.5. Characterization of the amorphous solid dispersions

5.2.5.1. Differential scanning calorimetry

API and the freshly prepared HME API-PVPVA 6:4 systems were scanned in DSC by using modulated mode at ± 0.318 °C every 60 seconds, 2 °C / min. In these measurements, pierced aluminium pans were used in order to allow the removal of moisture during the heating processes.

5.2.5.2. Attenuated total reflectance-fourier transform infrared

The same parameters of ATR-FTIR as described in Chapter 3, section 3.2.7 were used to scan the prepared HME APIs-PVPVA 6:4 systems.

5.2.5.3. X-ray diffraction

X-ray powder diffraction (XRPD) experiments were performed on the freshly prepared HME API-PVPVA SDs. These extrudates were gently crushed into powder form (in a mortar and pestle) and compacted into the sample holder of the XRPD prior scanning. Measurements were performed from 3° to 40° (2 θ) coupled with scanning speed of 0.01° / step and 1 second for every scan step to cover the characteristic peaks of each APIs.

5.2.6. Dissolution studies of PM and HME of APIs – PVPVA 6:4

Dissolution studies of the HME APIs-PVPVA 6:4 formulations were performed in the corresponding discriminatory dissolution media as outlined in Table 5.1. Dissolution experiments were carried out using the USP paddle method at 37 °C, 50 rpm. At pre-determined time intervals, 10 ml of solution was withdrawn and filtered with a 0.45 μ m PVDF membrane syringe filter. The filtrate was then analyzed spectrometrically to evaluate the concentration of API in the medium. For comparison, dissolution behaviors of the API and PM systems were also studied. All the dissolution studies were performed under sink condition with the exception of the pure INDO due to its extremely poorly solubility properties in the dissolution medium.

To compare the dissolution performances between the PM and HME systems, similarity factor (f_2) was used. This is a model independent approach that measures the similarity in percentage between

the 2 profiles of dissolution (FDA, 1997). Similarity factor (f_2) is a logarithmic reciprocal square root transformation of the square error, which could be expressed by Equation (5.3).

$$f_2 = 50 \times \log \left\{ \left[1 + \left(\frac{1}{n} \right) \times \sum_{t=1}^n (R_t - T_t)^2 \right]^{-0.5} \times 100 \right\} \quad (5.3)$$

where n is the number of time points, R_t is the percentage of drug release of a reference batch at the time t and T_t is the percentage of drug release of the comparison batch at time t . When f_2 is greater than 50 (i.e. 50-100), this indicates the sameness or equivalence of the both compared profiles. Conversely, when f_2 is less than 50 then it is taken as which both the profiles are different. Generally, it is used for comparison of a product before and after minor changes in a formulation for industrial approval. In this study, dissolution profiles were compared up to a point after 80% drug release of the formulation. Similarity factor was utilised as a tool to provide a gross idea on the rank order of the dissolution performance differences of different API systems between the prepared amorphous SD and their PM systems.

5.2.6.1. Light microscopy observation

The change in particle appearance of the HME SD system upon contact with the dissolution medium was observed using a light microscope. The freshly ground HME API-PVPVA 6:4 particles were loaded on a slide under the microscope with a pre-focused position of the lens. Then, 2 drops of selected dissolution mediums were dropped on the particles and immediately covered with a cover slide. The appearances of the particles shown under the microscope were captured up to 60 minutes.

5.2.6.2. Particle size analysis

Particles size changes of the HME SD system during the dissolution experiment were measured using a particle size analyser. This experiment is aimed to detect the possible agglomeration of the dissolving particles while dissolution process. To do this, 20 ml of dissolution medium was collected from the dissolution bath after 2, 15, 30 minutes of dissolution experiment and immediately (within 1 minute) analysed by using particle sizer.

5.2.6.3. Scanning electron microscope

Surface morphologies of the particles collected from the dissolution vessel during the dissolution experiment were investigated using scanning electron microscopy (SEM). These collected particles were placed on a sample stub and dried for not more than 1 hour at room temperature before sputtered with a thin layer of gold prior to SEM imaging.

5.2.6.4. Contact angle measurement

As mentioned in Chapter 2.4.8, an indirect contact angle measurements were used in studying the wetting properties of the PM and HME systems. Contact angle measurements between the surface of compacted tablets (which includes tablets of raw API, PM API-polymer and ground HME API-polymer) and their corresponding dissolution media were performed with surface drop shape analysis. This method has been reported for reasonable wetting assessment of powdered system (Swanepoel et al., 2000, Dahlberg et al., 2008, Buckton et al., 1991).

Powder compaction parameters

PMs with a controlled particle size (63-106 μm) were produced using the same method outlined in Chapter 5.2.3. On the other hand, HME API-PVPVA SDs, which were prepared in Chapter 5.2.4, were gently milled in a mortar and pestle and then sieved into the 63-106 μm particle size range. 300 mg of the powdered samples (both PM or HME) were weighed and compressed into tablet by using an GRASEBY SPECAC hydraulic press. The powders were pressed with a pressure of 5 tons for 60 seconds. The resultant flat surface was examined for their surface roughness using atomic force microscopy (AFM). 'z' variations of the piezoelectric scanner of AFM were used to provide the surface roughness information which could be found in Appendix IV.

Surface tension and contact angles analysis

The equipment used for the surface tension and contact angle measurement has been described in Chapter 2.4.8. To determine surface tension of the dissolution media and 1% w/v PVPVA 6:4 solutions, pendent drop measurements were performed. A liquid dispenser holder with manual control was used to create a drop. Then, OneAttension software was used to analyze the surface tension by Young-Laplace surface properties mode. The changes of the surface tension were recorded up to 120 seconds at 1 frame per second.

In the contact angles measurement, a drop of the liquid phase which was pre-saturated with corresponding APIs was deposited on the flat surface of the compressed tablet by using a dispenser holder (pure APIs, PMs of APIs and PVPVA and HME APIs-PVPVA). The changes of the contact angles at the first 120 seconds were recorded as a video at 6 frames per second for first 10 seconds and 1 frame per second subsequently. All measurements were performed at 25 ± 0.1 °C and 45% RH. Table 5.2 summarises the combination of solid phases to their corresponding liquid phase in the contact angle experiments.

Table 5.2: Experiments of contact angles between the solid phase and the liquid phase

Surfaces (tablets)	Medium			
	Distilled water (DW)	1% w/v PVPVA in DW	0.1M HCL	1% w/v PVPVA in 0.1M HCl
PVPVA 6:4	√		√	
NAP	√		√	√
KTP	√		√	√
INDO	√	√		
OZP	√	√		
PM 30% NAP PVPVA 6:4	√		√	
PM 30% KTP PVPVA 6:4	√		√	
PM 30% INDO PVPVA 6:4	√			
PM 30% OZP PVPVA 6:4	√			
HME 30% NAP PVPVA 6:4	√		√	
HME 30% KTP PVPVA 6:4	√		√	
HME 30% INDO PVPVA 6:4	√			
HME 30% OZP PVPVA 6:4	√			

These combinations are based on the types of media used in the solubility and dissolution test of the API and its HME PVPVA formulations. Besides, 1% of PVPVA used in the respective medium was to understand the influence of high polymer concentration in the wettability of the hydrophobic API, as a dissolving system was reported to have a high polymer concentration at its dissolving front (Tajarobi et al., 2011b, Baumgartner et al., 2005, Siepmann and Peppas, 2001).

5.3. Results

5.3.1. Estimation of amorphous solubility advantages ratio of APIs

The advantages of an amorphous pharmaceutical have been discussed in Chapter 1.2. These amorphous advantages are mainly ascribed to the difference in free energy of the amorphous form and its crystalline counterpart (Hancock and Parks, 2000). Thus, in this study, the free energy difference between the amorphous and crystalline form of the studied APIs were calculated according to the Hoffman Equation (5.1) based on the DSC data of the pure APIs. At the same time, the 'solubility ratio' between the amorphous form to the crystalline form could be also estimated according to Equation (5.2). Table 5.3 displays the melting temperatures and enthalpies of the different APIs, free energy difference between the amorphous form and crystalline form of different APIs, experimental solubility of the APIs and calculated solubility ratio of crystalline drugs to their corresponding amorphous forms using Equation (5.2).

Table 5.3: Experimental solubility of APIs, free energy difference between the crystalline APIs and their amorphous form, solubility ratio and theoretical amorphous of amorphous form to their crystalline counterpart in the selected media

Drug-PVPVA	Melting Temperature (K)	Melting enthalpy ΔH (KJ/mole)	Free energy difference, ΔG , (KJ/mole)	Experimental Solubility (mg/ml)	Solubility ratio	Theoretical amorphous solubility (mg/ml)	Medium
KTP	366.76	29.37	3.83	0.170	4.24	0.7531	0.1M HCl
NAP	428.53	30.94	6.18	0.032	11.01	0.3522	0.1M HCl
INDO	434.15	37.56	7.66	0.0094	19.53	0.1941	Distilled water
OZP	467.62	38.42	8.58	0.069	27.88	1.9237	Distilled water

Based on Table 5.3, OZP was shown to have highest free energy difference between its amorphous and crystalline state (column 4). This is followed by INDO > NAP and > KTP. This trend is in parallel to the predicted solubility ratio (amorphous API to crystalline API) of the APIs as shown in column 6 of Table 5.3.

According to the well-known Noyes-Whitney Equation (2.2), dissolution rate of a substance can be correlated to the concentrations difference between the solid surface (C_s) and the bulk of solution (C_b) in which the solution at the dissolving front would be equivalent to the solubility of the API upon achieving a constant release rate at the dissolving front (Aulton, 2007). Thus, the higher solubility advantage of an amorphous API could drive its dissolution process assuming other parameters in the Equation (2.2) are constant. Consequently, the release enhancement of

amorphous OZP as compared to its crystalline form would be expected to be highest followed by INDO > NAP > KTP.

5.3.2. Equilibrium phase solubility studies of APIs in the presence of PVPVA 6:4

A few papers have suggested the solubilising effects of hydrophilic polymer in contributing to the dissolution enhancement of poorly soluble API (Nokhodchi et al., 2005, Sjobkist et al., 1992, Craig, 2002). This may be attributed to the enhanced solubility of API in the polymer rich diffusion layer which could subsequently drive the dissolution of the poorly soluble API (Doherty and York, 1987). According to Craig (2002), the carrier controlled release mechanism of a SD system is mainly attributed to the high solubility of the API into the hydrophilic polymer carrier which may allow the dissolution of the API to occur before the reaching of dissolution front to the API particles. On the other hand, when the solubility of API in its hydrophilic polymer carrier is low, the particle may be released intact into the bulk of the medium. Therefore, in order to understand the effect of solubilising capacity of the PVPVA 6:4 in its influence on dissolution process of the HME SDs, the solubility of the APIs in the PVPVA 6:4 solutions were studied.

Besides, API solubility is reported to increase disproportionately in higher polymer concentration solutions (Craig 2002). Thus, the significance of the PVPVA 6:4 concentration in the solubilisation of APIs was also examined by performing the apparent solubilities studies of the tested APIs in three different concentrations of PVPVA 6:4 solutions in distilled water, i.e. high concentration (10% w/v), intermediate concentration (1% w/v) and low concentration (0.0001% w/v) of PVPVA 6:4. Figure 5.1 displays the multiple of solubility enhancement of the APIs at the tested concentrations of PVPVA 6:4 solutions using solubility of API in the media without PVPVA 6:4 as a reference.

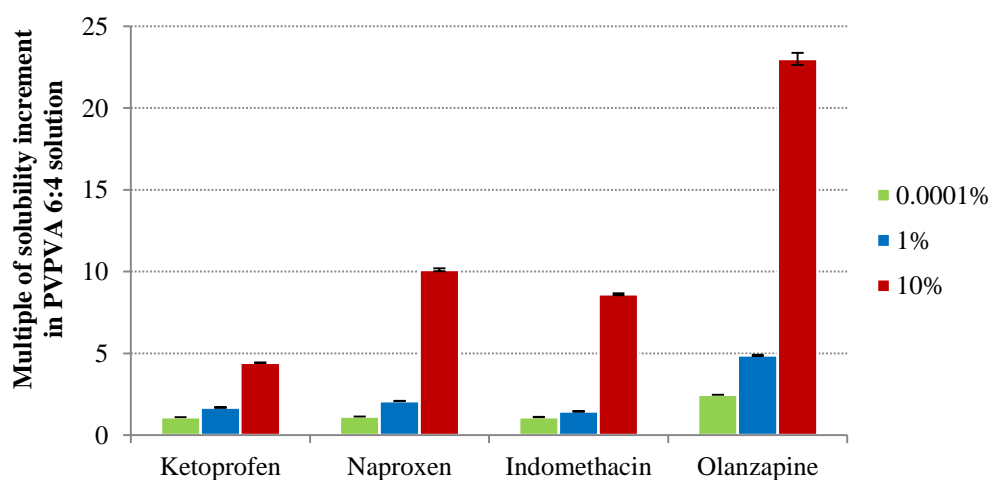


Figure 5.1: Apparent solubility of APIs in the presence of PVPVA 6:4 after 48 hours at 37 °C

According to Figure 5.1, OZP was showed to have the highest apparent solubility enhancement for all the tested concentrations of PVPVA 6:4. However, there is no apparent difference in the apparent solubility enhancement of the acidic APIs (KTP, NAP and INDO) at low PVPVA 6:4 concentration (0.0001% w/v). In contrast, noticeable differences in solubilities enhancements of the acidic APIs were seen at the high concentration of PVPVA 6:4 (10% w/v PVPVA 6:4), in which the solubility enhancement was in a trend of NAP > INDO > KTP. This implies the importance of high concentration of PVPVA 6:4 in any possible solubilizing effects of these APIs.

5.3.3. Basic characterization of HME products: XRPD and DSC

Before investigating the dissolution performances of HME API-PVPVA 6:4 extrudates, basic characterisation of the extrudates was performed. Figure 5.2 displays the XRPD curves of the freshly prepared HME API-PVPVA 6:4.

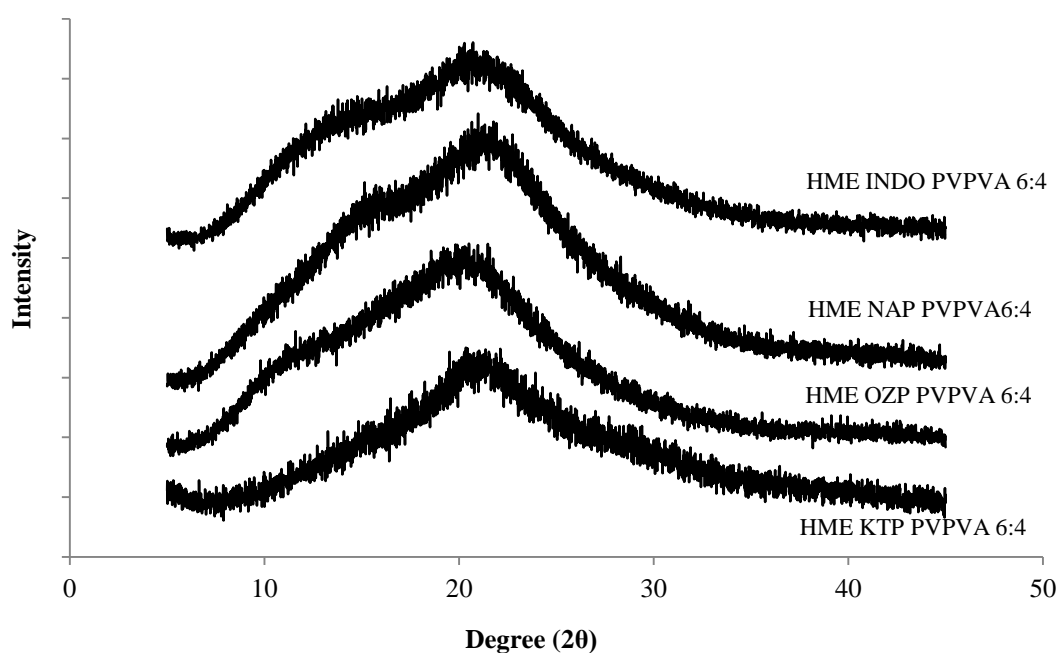


Figure 5.2: XRPD profiles of HME 30% APIs-PVPVA 6:4

All the extrudates were predominantly amorphous in nature as indicated by the halo pattern of X-ray diffractograms in Figure 5.2. This result can be further complemented by MTDSC scanning of the prepared HME API-PVPVA 6:4 systems. Figure 5.3 shows MTDSC thermograms of the freshly prepared HME 30% APIs-PVPVA 6:4 systems

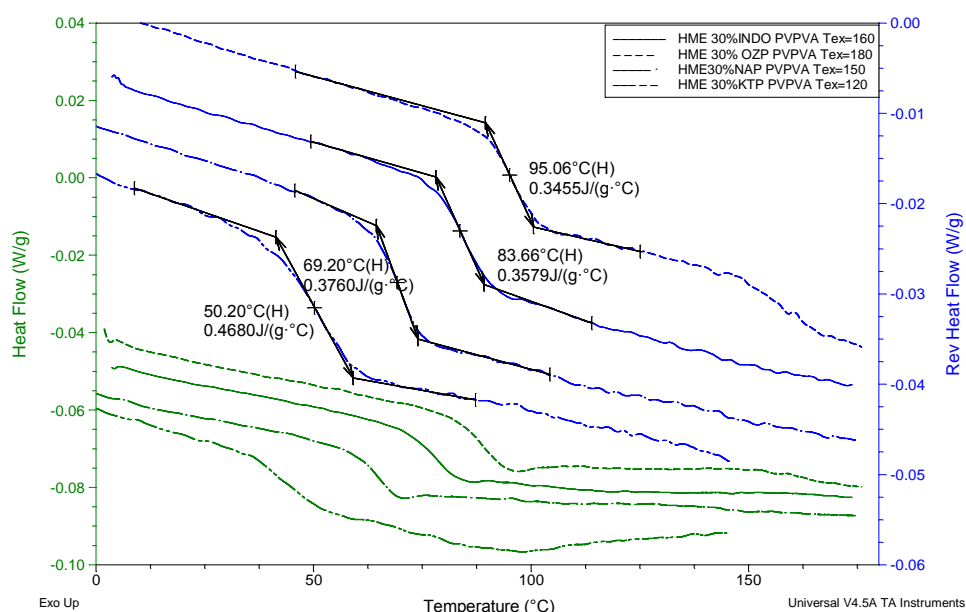


Figure 5.3: MTDSC thermograms of HME 30% APIs-PVPVA 6:4. Blue lines present the reversing heat flow signal, whereas the green lines present the total heat flow of the corresponding samples

According to the thermograms in Figure 5.3, a single T_g was observed in the reversing signal (blue lines) of the freshly prepared HME SD, which is a classical indication for homogeneity of the SD system. The detected T_g of the HME system as shown in Figure 5.3 were all lower than the T_g of the PVPVA alone (data not shown) due to the plasticization effect of the APIs. Besides, there were no apparent melting endothermic peaks detected in the total heat flow signal (green lines) of each of the HME systems, which supports the conclusion obtained from XRPD data as the HME systems were amorphous in nature.

5.3.4. Interaction between APIs and PVPVA 6:4

Drug polymer interaction has been reported to be important in the dissolution performance of SD due to the formation of soluble complexes and reduction of agglomeration of the hydrophobic particles (Karavas et al., 2006, Ilevbare et al., 2012a). Therefore, in this study, interaction between the APIs-PVPVA 6:4 was also investigated to check its effect on dissolution rates enhancement of HME SD system.

ATR-FTIR spectra of PMs API and PVPVA 6:4 revealed a summation of the individual ATR-FTIR spectra of the respective components with no apparent wavenumber shift of the peak (data not shown). This suggests only a limited interaction between API and PVPVA 6:4 in their PM systems.

On the other hand, ATR-FTIR spectra of the investigated HME systems shows significant peak shift in as compared to the ATR-FTIR spectra of the pure API and PVPVA 6:4. Figure 5.4 shows the theoretical PVPVA 6:4 spectra from the all the HME APIs-PVPVA 6:4 system which were obtained via subtraction of the HME APIs-PVPVA 6:4 systems by their corresponding API spectra, i.e. HME API- PVPVA 6:4 spectra-API spectra.

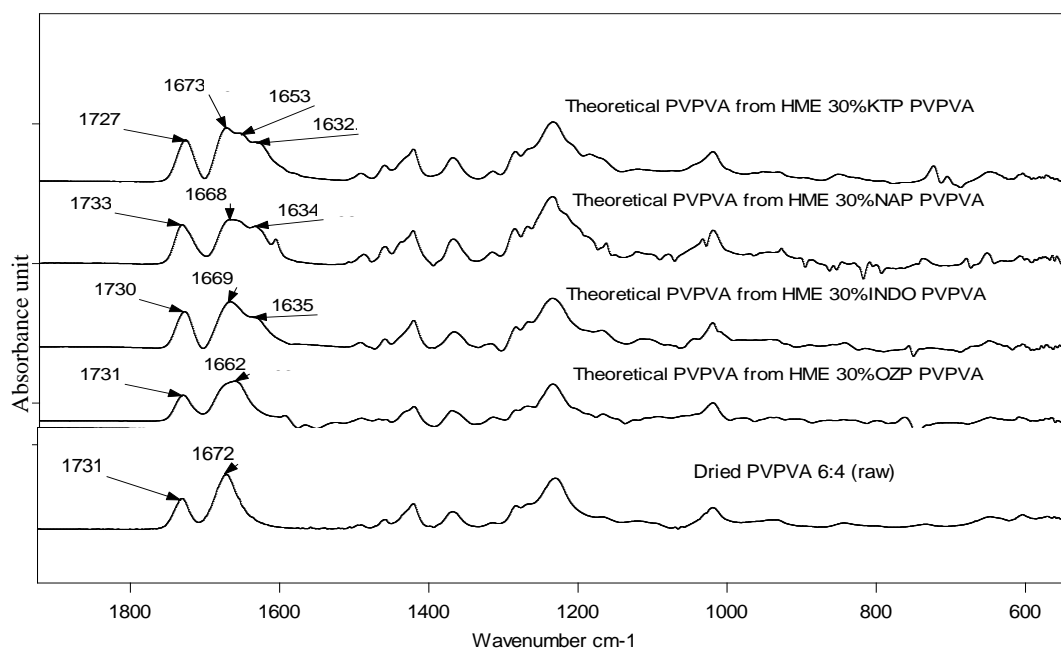


Figure 5.4: Theoretical FTIR-ATR spectra of PVPVA 6:4 from different HME-drugs-PVPVA 6:4 systems

According to Figure 5.4, dried PVPVA 6:4 possesses an amide carbonyl stretching from its pyrrolidone group at 1672 cm^{-1} . This peak was shifted down in the theoretical spectra of PVPVA 6:4 obtained from the HME systems (Figure 5.4) which indicating the existence of interactions on the C=O group of the pyrrolidone in PVPVA 6:4. Besides, new peaks were observed in the theoretical PVPVA 6:4 spectra obtained from all the tested HME systems. The appearance of these new peaks are possibly due to the new stretching mode of the C=O following the hydrogen interaction of API with the PVPVA 6:4 (Paudel and Van den Mooter, 2011). This interaction between the APIs and PVPVA 6:4 was also confirmed by the observation of downshifting in the wavenumber of OH / NH stretching of the APIs (data not shown).

The extent of C=O downshifting reflects the trend of hydrogen interaction between the APIs and polymer as weakening of the vibration energy of carbonyl stretching causes the down-(red) shift to lower wavenumber (Van Eerdenbrugh and Taylor, 2012, Marsac et al., 2009). From Figure 5.5, the highest extent of down-(red) shift of the C=O peak is seen in OZP followed by $> \text{NAP} > \text{INDO} > \text{KTP}$. This trend was observed to be following the similar trend of enhanced solubility of APIs in the PVPVA 6:4 solution (Chapter 5.3.2, Figure 5.1).

5.3.5. Comparison of dissolution profiles of PM and HME products

After the basic characterisation of the prepared HME APIs-PVPVA 6:4 system, their dissolution performances were investigated. To assess the advantages in dissolution performance of SD system, dissolution performances of their corresponding pure APIs and PMs were also performed. Figure 5.5 displays the dissolution profiles of the four different APIs in their pure powder form, PMs and HME APIs-PVPVA systems.

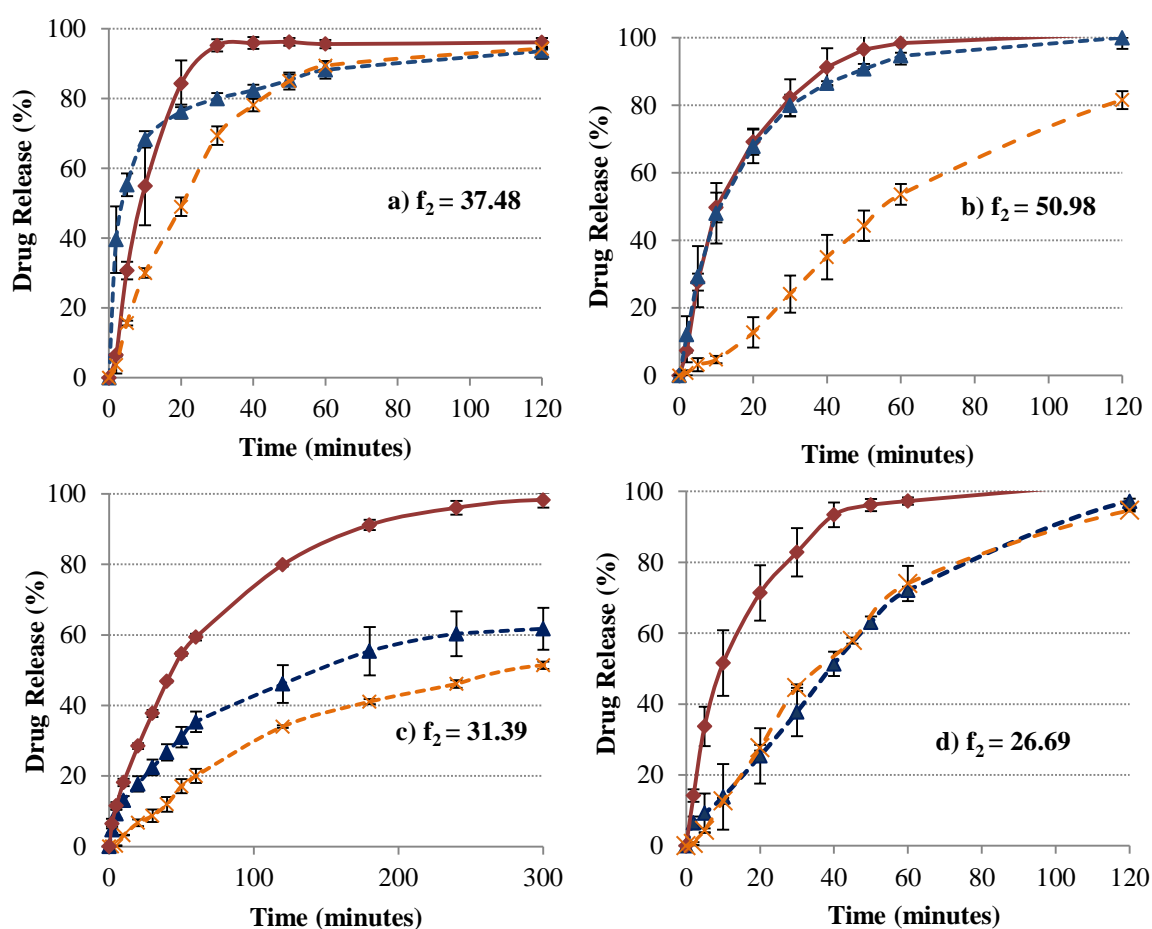


Figure 5.5: Dissolution profiles of pure API (orange dotted line), HME 30% API-PVPVA (in red) and their corresponding PM (blue dotted line) in their respective dissolution media: a) KTP, b) NAP, c) INDO and d) OZP. The similarity factors, f_2 indicated the comparison of dissolution profile between PM and HME formulations.

According to Figure 5.5, dissolution rates of the APIs were noted increased in the PM of the acidic drugs (KTP, NAP and INDO) but not in the PM OZP PVPVA 6:4 system. This might be ascribed to the wetting effect of the PVPVA 6:4 which will be further investigated in a later section (Chapter 5.3.6.1).

Comparison between the HME and PM

Based on Figure 5.5, it is interesting to note that the dissolution rate of HME amorphous API-PVPVA 6:4 systems (red lines) did not consistently show a higher release rate than their corresponding PM crystalline API-PVPVA 6:4 systems (blue-lines). These could be quantitatively analysed by using magnitude of similarity factor f_2 that has been described in Chapter 5.2.6 which indicates similar dissolution profiles between the comparing systems when its value of f_2 is more than 50 and a difference profile when f_2 is less than 50.

Among the tested APIs, the lowest similarity factor f_2 between the HME and PM was noted in OZP system which indicating its highest dissolution performance difference between its HME and PM systems (Figure 5.5 (d)). It was then followed by HME 30% INDO-PVPVA 6:4 which also shows a difference in the dissolution performance between the HME and its PM systems (Figure 5.5 (c)), but the difference was slightly lower as compared to OZP system. In NAP system (Figure 5.5 (b)), there was almost no difference in the dissolution profiles between its HME and PM as indicated by the similarity factor $f_2 > 50$. Whereas for KTP system (Figure 5.5 (a)), although f_2 is less than 50 which indicates a difference between PM and HME KTP PVPVA 6:4. However, this difference is based on the higher dissolution rate of PM KTP PVPVA 6:4 than its HME systems which is in oppose to the differences seen in OZP and INDO system whereby their HME systems release faster than PM system. These observation give rise to a rank order of the increased release rate of API in HME in comparison to their PM, i.e. OZP > INDO > NAP > KTP which was found to be following the exact trend seen in solubility advantages ratio of APIs calculated from the difference in free energy of the amorphous form and crystalline form of the APIs (Table 5.3).

Table 5.4 display the summary of dissolution rate comparison among the APIs, PMs and HME systems for the tested APIs in this study.

Table 5.4: Summary of the dissolution performances among pure APIs, PMs and HME PVPVA systems

HME	Dissolution rate	PM	Dissolution rate	API
KTP-PVPVA 6:4	<	KTP-PVPVA 6:4	>	KTP
NAP-PVPVA 6:4	= / <	NAP-PVPVA 6:4	>	NAP
INDO-PVPVA 6:4	>	INDO-PVPVA 6:4	>	INDO
OZP-PVPVA 6:4	>	OZP-PVPVA 6:4	=	OZP

Following the summary in Table 5.4, two main phenomena were observed in the dissolution experiments. On one hand, API release rate was significantly improved by physical addition of PVPVA 6:4 as shown in the dissolution performances of the PM API-PVPVA 6:4 system with the exception for OZP system. On the other hand, HME APIs-PVPVA 6:4 formulations show only limited dissolution rate enhancement in comparison to their corresponding PM system with the

exception of OZP system. These inconsistent observations of SD leave the formulation scientist in an uncertain position as one may argue that some of the PM systems seem to sufficiently enhance the API release rate without necessitating the generation of an SD at all. This entails more fundamental investigation into the factors affecting the dissolution behaviours of the PM and HME systems.

5.3.6. Investigation of factor governing dissolution performance of HME API-PVPVA 6:4 system

Following the inconsistent dissolution profiles of the PM and HME systems, possible factors that could influence the dissolution performance of HME 30% APIs-PVPVA 6:4 systems were investigated. These factors include wetting properties, agglomeration tendency and recrystallization behaviour of the HME API-PVPVA 6:4 systems during their dissolution processes.

5.3.6.1. Wetting properties of the solid system

Wetting effects of a hydrophilic polymer are generally deemed to be relevant to the dissolution process of an immediate release SD formulation due to the associated increase in effective surface area for well wetted systems (Chokshi et al., 2007, Dahlberg et al., 2008). Dahlberg et al. (2010) have demonstrated that the combination of API and hydrophilic polymer into a SD system may affect the wetting of the surface system in an unexpected and nontrivial manner. This situation could be further complicated by the manufacturing method of the formulation system which may cause a change of the functional group of the system that are present on the surface of the system (Dahlberg et al., 2008). Thus, it is essential to understand the change in wetting properties of both PM and HME of binary API-PVPVA 6:4 in comparison to their API which will be presented in the next sections.

Firstly, contact angle studies of APIs/ medium, APIs/ PVPVA solution and their PMs/medium were investigated to understand the wetting effect of PVPVA 6:4 in these systems which are being presented in section 5.3.6.1.1. The relative wettability between the PM and HME systems were subsequently compared in section 5.3.6.1.2. It is worth mentioning that the liquid phase of the contact angle measurement was based on the medium used in dissolution experiments (please refer to Table 5.1 for the medium type). The use of these dissolution media as a liquid phase in the contact angle measurements was undertaken in order to understand the wettability effect of these systems, with a view to explaining the unpredictable dissolution performance as seen in the dissolution experiments in section 5.3.5.

Contact angle profile of pure APIs-dissolution medium

Figure 5.6 shows the contact angle of the compacted crystalline APIs in response to the corresponding saturated medium.

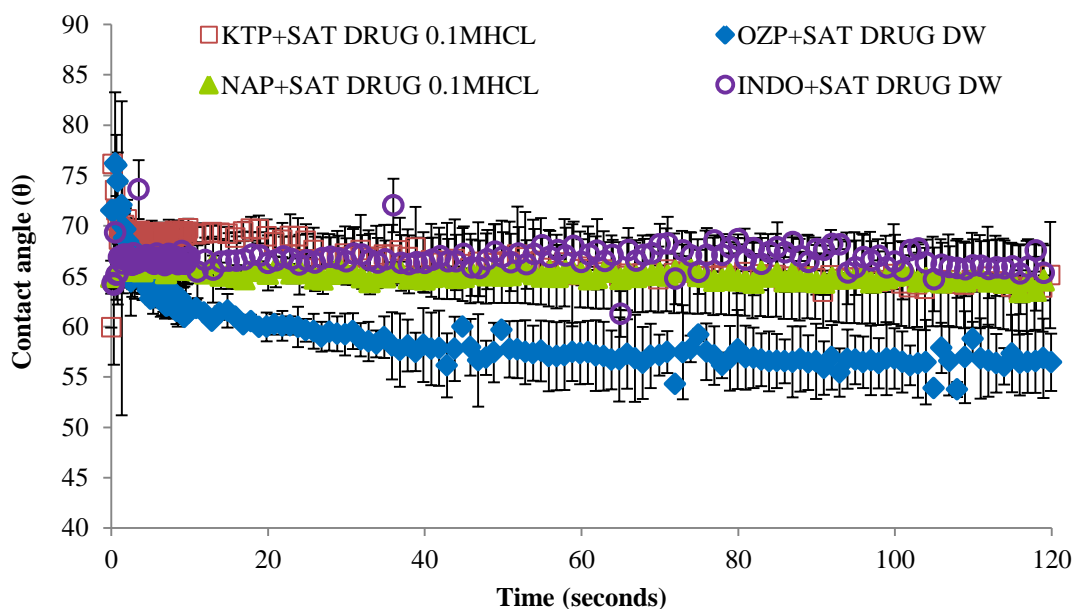


Figure 5.6: Contact angles between the pure APIs and their dissolution media. 0.1 M HCl was used as the liquid phase in contact angle measurement of KTP and NAP, whereas distilled water was used as a liquid phase in the measurement for the surfaces of INDO and OZP.

From Figure 5.6, KTP, NAP and INDO were showed to possess superimposable contact angle profiles which were higher than the contact angle profile of OZP. This implies that wettability of crystalline OZP is relatively better than the other tested APIs.

5.3.6.1.1. Wetting properties of PM APIs-PVPVA 6:4 in comparison to their APIs

Dissolution enhancement of poorly soluble API in PM is always associated to the increased in wetting of the API with the presence of the hydrophilic polymer. Thus, to understand the change in wetting properties of the system in the presence of the hydrophilic polymer, the contact angles of the PM systems were performed.

Before detailing the contact angle data, it should be pointed out that the use of compacted surface in determining the wetting of the system via contact angle might not be directly related to the exact wettability of the powder form during their dissolution experiments. However, the relative values of the contact angles among the different tested systems could still be useful for the approximation of relative wettability of the different APIs in their PM systems. Figure 5.7 displays the contact angle profiles of the PM systems in contact to their corresponding dissolution mediums.

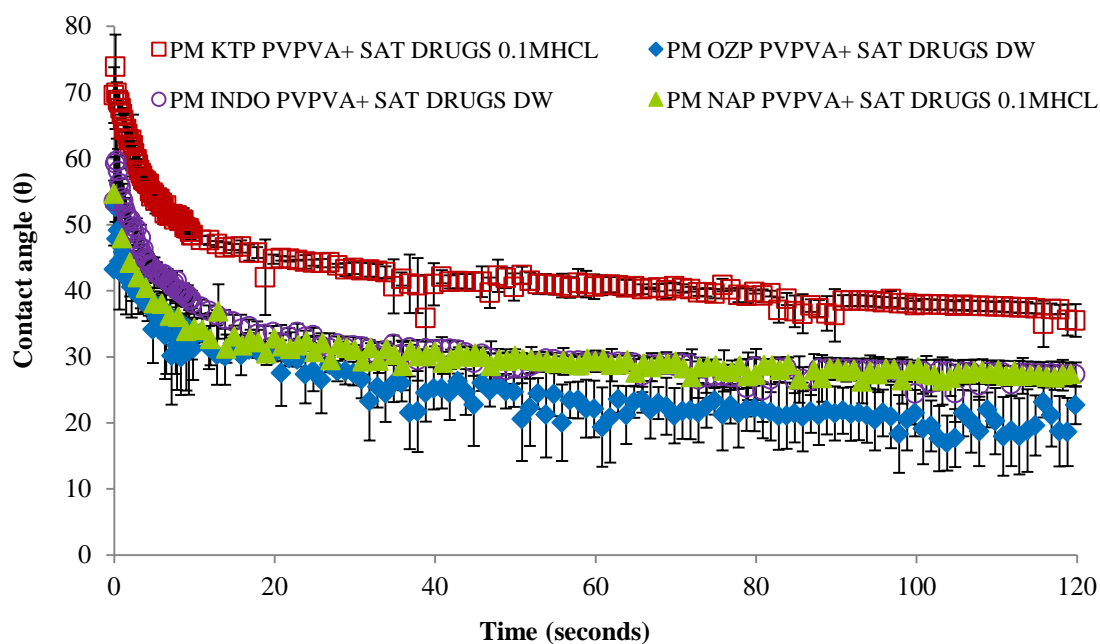


Figure 5.7: Contact angles of the compacts PM APIs-PVPVA 6:4 to its corresponding dissolution medium. 0.1 M HCl was used as the liquid phase in contact angle measurement of KTP and NAP, whereas distilled water was used as a liquid phase in the measurement for the surfaces of INDO and OZP

Unlike the contact angle profile of pure API, contact angles profile of the PM shows time dependent receding angle in the first 10 seconds which suggests some changes in the interface of the measurement (Figure 5.7). As a high proportion of PVPVA 6:4 was covering the surface at this composition (70%) it is plausible that the time dependent receding contact angle profiles is a reflection of change in configuration of the surface polymer upon contact with the liquid phase. This change can take place through short-range motion such as diffusion of the hydrophilic moieties of the polymer into the liquid phase, swelling and reorientation of polymer chain that might potentially reduce the surface tension and reorganisation of the liquid molecules at the solid-liquid interface (Lam et al., 2002, Tavana and Neumann, 2007). All the PM systems revealed almost similar contact angle profiles except PM of KTP-PVPVA 6:4 which reveal a higher contact angle.

By comparing the contact angle profile of the PM API PVPVA (Figure 5.7) and its pure API alone (Figure 5.6), the reduction of contact angle could be assessed. It is a reflection of increased wettability of the PM system as compared to its pure APIs. The contact angle reductions of all PM systems were circa 30° in comparison to their corresponding APIs except PM KTP PVPVA 6:4 system which show a reduction of circa 22°. These similar reductions in contact angle of PM systems did not show any trend in affecting their degree of dissolution rate enhancement. Hence, it could be suggested that the increased wettability of the PM system at the pre-dissolved state of PVPVA 6:4 is not a major factor in determining the extent of dissolution enhancement of PM in comparison to their pure APIs.

Dissolution rate enhancement of PM was also reported to occur via wetting the hydrophobic drug particles by the surrounded polymer layer which provides a lower energy pathway for its dissolution (Yadav and Yadav, 2009). In this case, it is hypothesized that the carrier shall be in its dissolved state to exert the wetting effect. To test this, wetting effect of PVPVA 6:4 in its post-dissolved state were carried out by measuring the contact angle of API with the 1% PVPVA 6:4 solutions as liquid phase. The obtained data (data not shown) were compared to the contact angles profiles of APIs/media without PVPVA 6:4 (Figure 5.6). This was done by subtracting the contact angle profiles of 'API /1% w/v PVPVA 6:4 medium' from the contact angle profiles of 'API/medium without PVPVA 6:4'. Figure 5.8 displays the results of the subtracted contact angles profiles for all the 4 tested APIs.

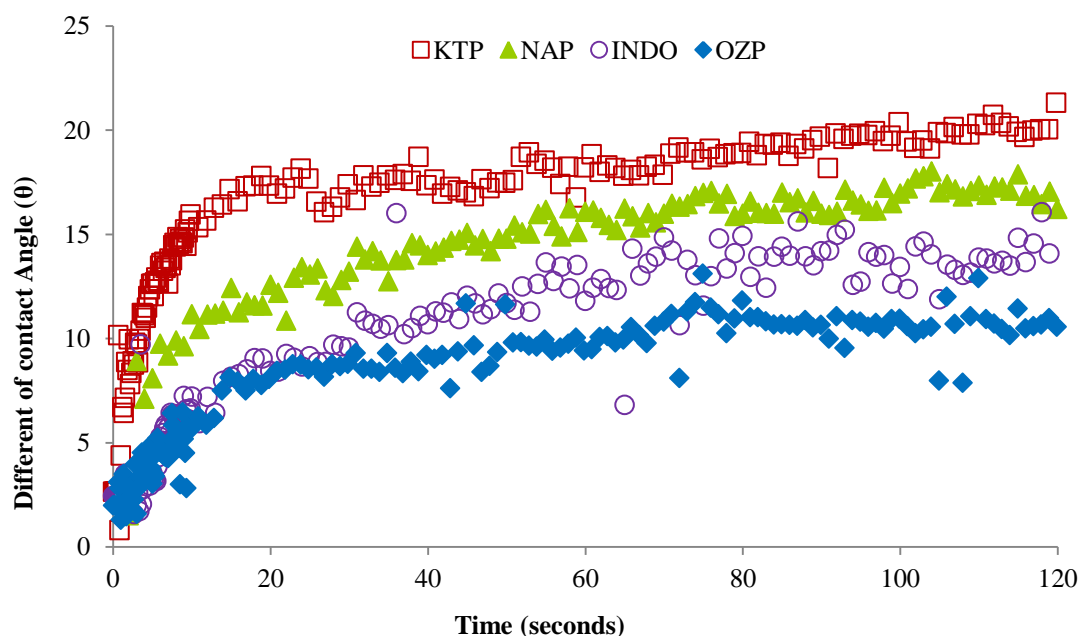


Figure 5.8: The differences of contact angles profiles between 'APIs-dissolution medium' and 'APIs -1% w/v PVPVA in dissolution medium'

It is noted from Figure 5.8 that the extent of the contact angle differences between API/1%PVPVA in media and API/media exhibit a rank order of wettability enhancement, i.e. $KTP > NAP > INDO > OZP$ which is similar to the rank order in the extent of dissolution rate enhancement of PM API-PVPVA 6:4 as compared to their APIs alone (Figure 5.5). Therefore it is suggested that the increase wettability of API at post-dissolved state of the PVPVA 6:4 might be the decisive role in determining the extent of dissolution rate enhancement of the APIs in their PM systems.

5.3.6.1.2. Wetting properties of the HME and PM system

After acknowledging the importance of wetting properties in the dissolution of the PM system, the relative wettability between the PM and HME system was also investigated. With the same compositional surface of HME and PM system, the contact angle profiles of both these systems are deemed to be comparable. Figure 5.9 displays the comparison of contact angles between the HME and PM systems.

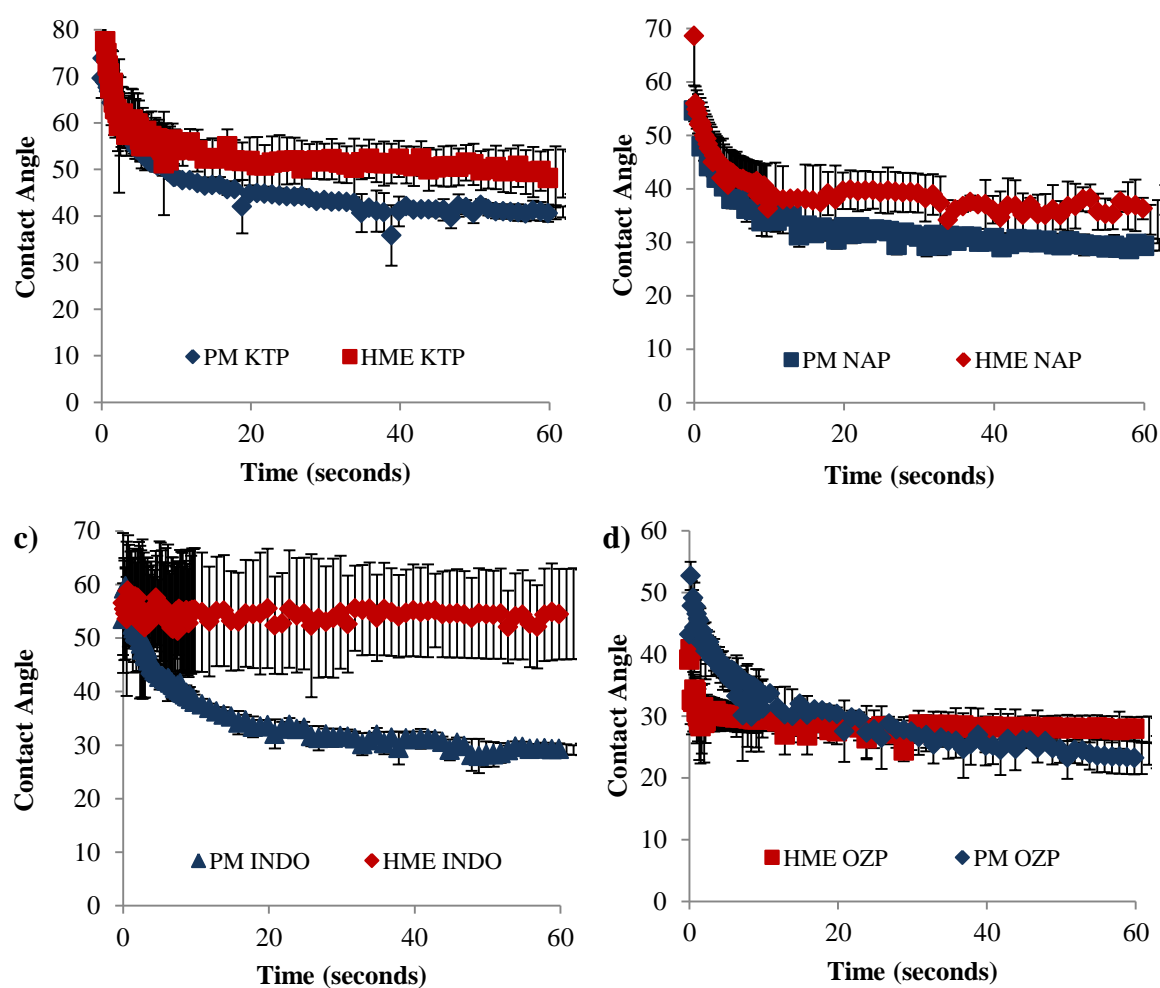


Figure 5.9: Comparison of contact angle profiles between PM and HME API-PVPVA 6:4 solid dispersions using corresponding dissolution medium a) KTP, b) NAP, c) INDO, and d) OZP

According to Figure 5.9, it is interestingly to note that HME systems displayed higher contact angle values as compared to their corresponding PM except HME OZP-PVPVA 6:4 system (Figure 5.9 (d)). This implies the poorer wettability of the HME API PVPVA 6:4 systems as compared to their PM system except HME OZP-PVPVA 6:4 system which suggests a negative influence on wettability of the binary API-PVPVA 6:4 system after the production into HME API-PVPVA 6:4 systems. Similar observations were noted before in literatures whereby the PVP-based SD

possessed a higher contact angle than its corresponding PVP-based PM (Chokshi et al., 2007, Dahlberg, 2010, Dahlberg et al., 2008). Among these systems, the highest negative impact was seen in HME INDO PVPVA/media as compared to its PM. However, in OZP system, it could be deduced that the wettability between the PM and HME systems was similar as indicated by their superimposable contact angle profiles in Figure 5.9 (d).

The reduced wettability of the HME system may be related to two possibilities. Firstly, it might be ascribed to the dissolution of the hydrophobic API into the polymeric system to form a one phase HME system while hot melt extrusion process. This may reduce the overall hydrophilicity of the PVP carrier. Secondly, the reduced wettability of HME system might also be associated with the orientation of its hydrophilic polymer chain as compared to the PM system. In PM, the hydrophilic PVPVA 6:4 polymer could orientate freely and swell upon contact with the medium. This may cause a reduction in surface tension of the liquid phase which spread well on the solid surface (Lam et al., 2002). However, this is limited for the HME system, as the coordination of the hydrophilic polymer was restricted as a result of API-polymer interaction as evidenced in Figure 5.4. This result is in agreement with Dahlberg et al. (2010) who have demonstrated that the high possible hydrogen bonding site of hesperetin with the PVP carrier in SD has caused a higher contact angle of the SD system as compared to its PM system.

To summarise, wettability of the system was evaluated by using contact angle measurements. Based on the results, the wetting of API was greatly enhanced with the presence of PVPVA 6:4 in a post-dissolved state in a rank order similar to the dissolution rate enhancement of the PM system (Figure 5.5). This indicated the significance of post-dissolved PVPVA 6:4 in dissolution rate enhancement of the PM system. Besides, the results also show lower wettability of HME system as compared to their corresponding PM systems. This might cause a change in the agglomeration tendency of the HME system as a result of surface hydrophobicity which could potentially alter the desired dissolution rate enhancement of SD system. This effect will be further investigated in the next section.

5.3.6.2. Agglomeration of the dissolving solid

During the dissolution experiments of the HME API- PVPVA 6:4 systems, opaque-white particles were visibly formed and floated within the dissolution media. Figure 5.10 illustrates the example of opaque particles observed during the dissolution experiment of HME 30% NAP-PVPVA 6:4.



Figure 5.10: Observation during dissolution process of HME 30% NAP-PVPVA 6:4

According to the well-known Whitney Noyes Equation (2.2), the surface area of the dissolving particles could potentially affect the dissolution rate of a dissolving system (Noyes and Whitney, 1897). Therefore, the precipitated particles observed in this study (Figure 5.10) may cause a reduction in the effective surface area for dissolution which may be the potential reason for the low dissolution rate of HME API-PVPVA 6:4 systems as seen in Figure 5.5. Similar events were also observed in previous works where the dissolution rate was reduced as a result of large particle formation (de Waard et al., 2008, Karavas et al., 2007). According to this literature, the reduced dissolution rate is due to the uncontrolled formation of large crystal particle following the saturation of drug concentration in the direct vicinity of the dissolving front. Hence, the overall dissolution rate is the net result of the solubilisation of the solid dispersion in its original form and the low specific area of the agglomerated particles.

Particle size analysis

In order to access the influence of the surface area changes in dissolution process of the HME APIs-PVPVA 6:4 systems, a light scattering particle size analyser was employed to track the particles size changes of the dissolving HME systems during their early dissolution process. Figure 5.11 presents an example of the results obtained from particle size analyses of HME 30% KTP-PVPVA 6:4 after 2 minutes of dissolution.

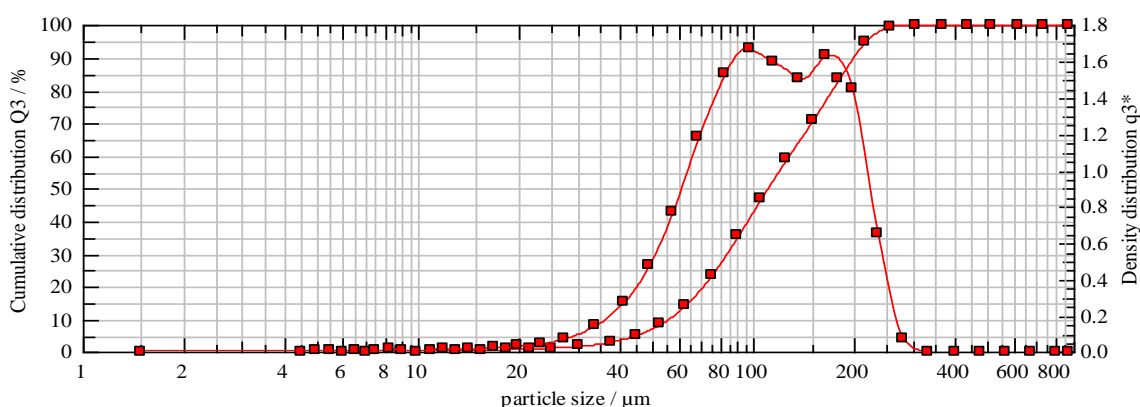


Figure 5.11: Examples of particle size analysis of HME 30% KTP-PVPVA in dissolution medium after 2 minutes of the dissolution experiment

Based on Figure 5.11, particles with sizes up to 300 μm were noted, which was larger than the initial controlled size (63-106 μm). Besides, the all tested formulations showed almost bimodal particle size profiles except the HME NAP-PVPVA 6:4 system (data not shown). Figure 5.12 summarises the 90 % of the cumulative undersize distribution of particles during the first 30 minutes for the four studied HME API-PVPVA 6:4 systems. An increased in particle sizes upon dissolution process was noted that in all the HME API-PVPVA 6:4 systems which indicated the occurrence of agglomeration or precipitation.

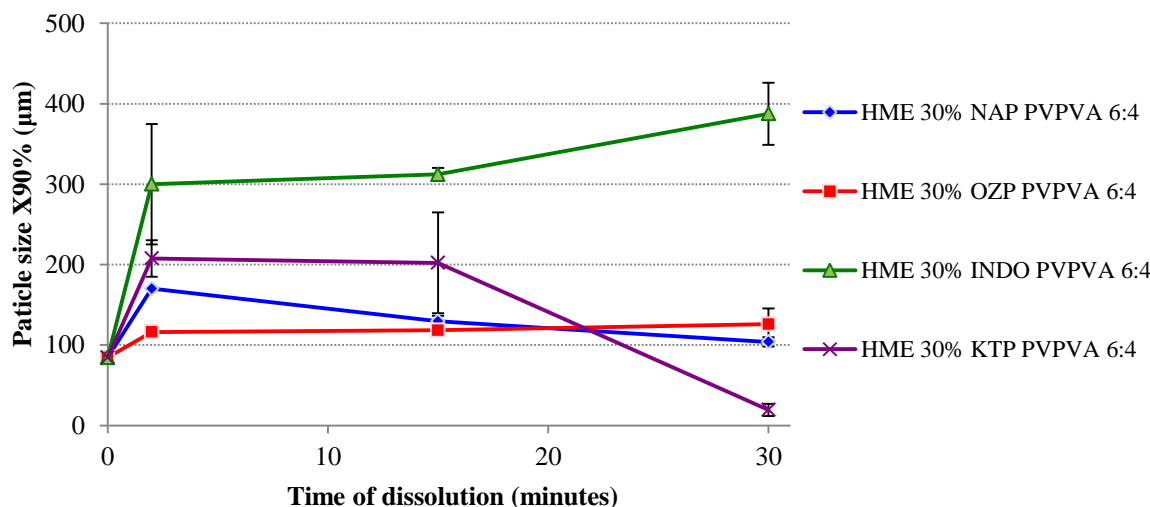


Figure 5.12: Particle size analysis: 90% of the cumulative undersize distribution of HME 30% APIs-PVPVA 6:4 in dissolution medium

From Figure 5.12, larger particle size was noted after 2 minutes of dissolution. The trend of particle size of the HME API- PVPVA systems was INDO > KTP > NAP > OZP. This trend is noted to be in the same rank order with contact angle of HME APIs PVPVA 6:4 systems as presented in Figure 5.9. Thus, the appearance of the big particles was attributed to the agglomeration of the dissolving particles due to the hydrophobic nature of their surfaces.

5.3.6.3. Recrystallization of APIs during dissolution

In order to gain an understanding regarding the physical state of the HME API-PVPVA 6:4 systems during the dissolution experiment, their behaviours on exposure to the dissolution medium were investigated by using polarized light microscope as described in Chapter 5.2.6.1. It is expected that birefringence of the crystalline materials will be revealed under the polarized light microscope observation if recrystallization of APIs occurs upon medium addition. Figure 5.13 displays the images recorded over the time scale of the experiment.

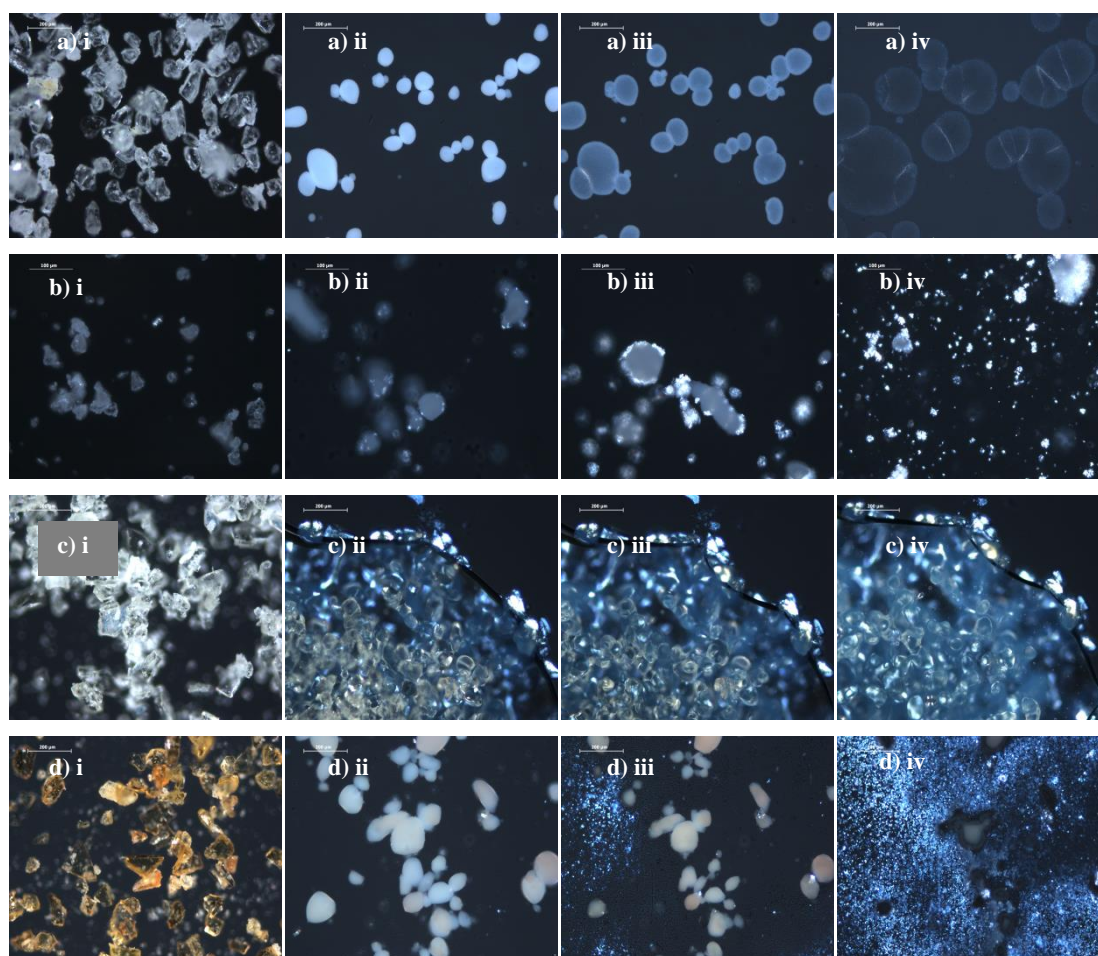


Figure 5.13: Images captured upon addition of dissolution media to HME 30% APIs-PVPVA 6:4. From top to bottom of the images a) KTP, b) NAP, c) INDO, d) OZP and from left to right: (i) t=0, (ii) t=1, (iii) t=30, (iv) t=60 minutes

Based on Figure 5.13 (a) i, HME KTP-PVPVA 6:4 SD particles did not show any birefringence of crystalline material after 1 minute of the medium fluid addition. Instead, an opaque appearance of the particles was observed. These opaque particles were noted to swell with time before complete dissolution of the particle took place (Figure 5.13 (a) ii to (a) iv). On the other hand, HME NAP-PVPVA 6:4 SD revealed birefringence on the ground particles which became more intense with

time (Figure 5.13 (b) i to (b) iv) from left to right). This indicates the recrystallization of NAP on the surface of the ground extrudates after exposure to 0.1M HCl. For HME INDO-PVPVA 6:4 SD, no obvious changes such as birefringence of the wetted particles could be detected under microscopic investigation. Also, the particles of this system did not show an opaque appearance after the medium contact (Figure 5.13 (c) ii to (c) iv). However, the outer layer of the HME INDO-PVPVA 6:4 SD particles was slightly depleted and the size of these particles remained largely constant up to one hour despite their contact with the dissolution medium.

HME OZP-PVPVA 6:4 SD (Figure 5.13 (d) ii to (a) iv) revealed an opaque appearance similar to that of KTP upon contact with the dissolution medium. Unlike KTP, the opaque particles of HME OZP-PVPVA experienced apparent size reduction with time instead of particle swelling as noted in the HME KTP PVPVA 6:4 system (Figure 5.13 (a) ii to (a) iv). Besides, birefringence was also noted in the HME OZP-PVPVA 6:4 system similar to HME NAP PVPVA 6:4 system. However it took a relatively longer time in revealing the birefringence of crystalline material (i.e. after 30 minutes of medium contact as shown in Figure 5.13 (d) iii) as compared to HME NAP PVPVA 6:4 system (i.e. after 1 minutes of medium contact as shown in Figure 5.13 (b) ii). This suggested a slower recrystallization rate of OZP as compared to the HME NAP PVPVA 6:4 system.

The observations deduced from microscopic investigation could be further supported by examining the surface morphologies of particles collected from the dissolution bath after 2 minutes dissolution were observed using scanning electron microscopy. Figure 5.14 shows the surface morphologies of the particles collected after 2 minutes of the dissolution experiment of HME API-PVPVA 6:4.

According to Figure 5.14 (a), surface of HME 30% KTP-PVPVA 6:4 particle was shown to have some star shape cluster with the square-like crystal on its surface which is an indication of particle recrystallization during the dissolution process (Figure 5.14 (a)). Based on this observation, it is reasonable to suggest that the opaque appearance of HME KTP-PVPVA 6:4 in the HSM images (Figure 5.14 (a) ii) is a sign of early recrystallization of the KTP on the extrudate upon contact with dissolution medium. The covering of the recrystallized KTP at the surface dissolving may cause a reduction in dissolution of the surface, in which a continuation of medium ingress into the core of the particle resulted in polymer swelling inside the core of the particles as could be seen in Figure 5.14 (a) iii and iv.

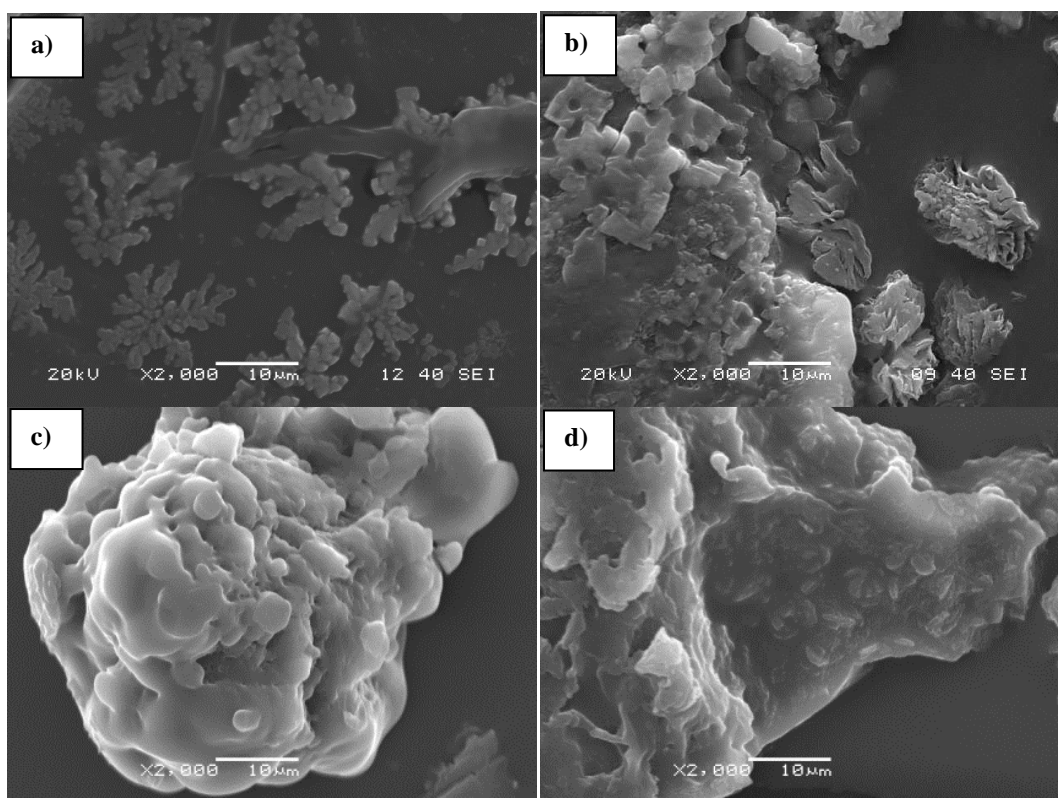


Figure 5.14: SEM images of particle collected from dissolution of HME 30% APIs-PVPVA after 1 minute of dissolution process a) KTP, b) NAP, c) INDO and d) OZP

Similarly, distinctive edges were also seen on the surface of HME 30% NAP-PVPVA 6:4 samples (Figure 5.14 (b)) which implying the appearance of crystalline material on the surface of these collected particles. On the other hand, particles of HME 30% INDO-PVPVA 6:4 in Figure 5.14 (c) indicate smooth surface of this system which suggesting the absence of crystalline material on its surfaces (Figure 5.14 (c)). This was in agreement with the observations of polarized light microscopy whereby the no recrystallization was expected from the HME 30% INDO-PVPVA 6:4 system (Figure 5.13 (c) ii to (c) iv). However, some ‘flaky’ structures precipitated near the surface of particle collected from the dissolution vessel of HME 30% OZP-PVPVA 6:4 system was seen (Figure, 5.14 (d)). This might indicate a potential of early recrystallization of OZP on the surface of the HME OZP-PVPVA 6:4 system as complemented by the opaque appearance of these particles upon medium contact (Figure 5.13 (d) ii to (d) iv).

Results obtained from both the polarized light microscope and SEM deduced that there were some extent of recrystallization occurred in all the investigated HME system upon media contact except the HME INDO-PVPVA 6:4 system. In summary, the recrystallization tendency were noted to be highest in HME NAP-PVPVA 6:4 system follow by HME OZP-PVPVA 6:4 > HME KTP-PVPVA 6:4 > HME INDO-PVPVA 6:4 systems. This trend of recrystallization does not follow the same trend of dissolution rate difference between the HME different API-PVPVA 6:4 and their PM systems.

5.4. Discussion

According to Figure 5.5 and Table 5.4, the production of poorly soluble APIs into an HME formulation did not show a consistent dissolution rate enhancement of the APIs as compared to their corresponding PM, despite the production of fully amorphous HME SDs as shown by the XRPD diffractograms (Figure 5.2). Hence, the production of a fully amorphous HME SD system may not necessarily be advantageous as compared to the product prepared by simple physical mixing procedure. Following this observation, the immediate question that arises is: what properties of the API are responsible for the different dissolution enhancement effects of the HME amorphous SD? This question can be answered by considering the factors determining the release rate enhancement of PM and amorphous system, as well as recognising the potential problems of dissolution process that have been observed during the dissolution process.

5.4.1 Dissolution performance of APIs in comparison their PM API-PVPVA 6:4

Dissolution enhancements of the investigated PM systems as compared to their pure API were seen for PM KTP, NAP and INDO PVPVA 6:4 system with the exception of OZP system which shows a superimposable dissolution profile to its pure API. The observed improvements may be due to the better wettability of the PM system as revealed by their reduced contact angles in comparison to the pure API.

Based on Figure 5.5, the degrees of dissolution rate enhancement of the PM systems were different for different APIs. It was interesting to found that the rank order of the degree of dissolution enhancement were not correlated to the reduced contact angles of the PM system but instead correlated well to the degree of wettability increment of the tested APIs by dissolved PVPVA 6:4 (Figure 5.7). In particular, the limited wettability enhancement of OZP by the dissolved PVPVA 6:4 was in agreement with the limited dissolution rate enhancement in its PM system, hence it is reasonable to suggest that the PM enhancement in dissolution is directly related to the wetting of the drug by the dissolved polymer.

It is worth mentioning that the wettability study of the API/PVPVA solution in Figure 5.8 was performed with high concentration of dissolved PVPVA, i.e 1% w/v PVPVA 6:4. Thus it is proposed that the dissolution enhancement of a PM system is highly dependent on the wettability enhancement of the API by the dissolved PVPVA 6:4 at early dissolution process as the high polymer concentration surrounding the API could only be formed at this early phase. A similar role of the PVP polymer has been reported previously as authors have recognized that a polymer rich layer is important for dissolution process of poorly soluble APIs (Chawla and Bansal, 2008).

Besides, solubilisation of the API by its carrier may also contribute to the observed dissolution enhancement of the PM system based on the well-known Noyes Whitney equation that identifies solubility in driving a dissolution process (Noyes and Whitney, 1897). This can be seen for the dissolution of PM NAP PVPVA 6:4 system which shows its relatively high solubility in 10% w/v PVPVA 6:4 solution. In this case, dissolution rate enhancement of the PM NAP PVPVA 6:4 system was 2 fold as compared to the pure NAP alone. In contrast, the high solubilisation of OZP by PVPVA 6:4 solution did not give rise to dissolution enhancement of its PM OZP PVPVA 6:4 system. This might be attributed to the strong crystal lattice of OZP which could be inferred by its high free energy difference of the crystalline material to its non-crystal state base on its T_m (as shown in Table 5.3) (Ivanov and Tsokeva, 2009). Therefore, apart from the limited wettability enhancement of OZP by PVPVA 6:4, the strong crystal lattice energy of the OZP has also caused the limited dissolution enhancement of PM OZP PVPVA 6:4 (Reutzel-Edens et al., 2003, Gao and Olsen, 2013).

The crystal strength of all the tested APIs as reflected from the free energy differences showed a trend of OZP > INDO > NAP > KTP (Table 5.3 and column 4). This is found to be in the reverse trend as seen in dissolution enhancement of PM as compared to its API, i.e. OZP < INDO < NAP < KTP, which implies that higher strength of a API crystal may cause ineffective dissolution enhancement of its PM prepared by simple mixing procedure. Hence, the role of crystal strength in dissolution enhancement of the PM API-PVPVA 6:4 as compared to its API alone was further confirmed.

5.4.2 Dissolution performance of HME APIs-PVPVA 6:4 in comparison to PM

It is interesting to note that different APIs behaved differently in term of wetting and dissolution performance in their PMs and HME SD systems. In this context, some APIs showed faster dissolution profiles in HME SD in comparison to the corresponding PM e.g. OZP and INDO-PVPVA 6:4 and others, in contrast, showed slower dissolution rates for the HME systems e.g. KTP and NAP-PVPVA 6:4 despite the use of the same carrier system.

Wettability of the HME formulations

Wetting properties of the tested HME KTP, NAP, INDO systems were lower than their corresponding PM which was shown by the higher contact angle of the HME system as compared to the PM system. This might be the reason of the limited dissolution rate enhancement of HME systems as compared to their PM system. During the dissolution process of the PM system, the

hydrophilic polymer could be easily wetted due to the flexibility of the hydrophilic polymer system in its PM state. Then, the polymer can swell and form a layer of polymer rich continuum between the dissolving particle and the liquid bulk (Craig, 2002, Miller-Chou and Koenig, 2003). In this state, the drug could dissolve into the high concentration of the polymer prior to release into the bulk. However, this polymer rich layer is limitedly formed in HME system. This is mainly due to the reduced coordination of polymer chain as a result of drug-polymer interaction in the one phase system of HME (Dahlberg, 2010) as detailed in Chapter 5.3.6.1.2. The exception of OZP system which shows a similar wettability between the HME and its PM system might be due to the high solubility advantage of the amorphous form of OZP (Table 5.3 and column 7) that reflects its possibly low hydrophobicity properties at its amorphous state. Furthermore, the wetting effect of HME SD systems can be further deteriorated in by the intensive recrystallization of the amorphous API on the surface of dissolving particles during the dissolution process which will be further discussed in a later section.

Agglomeration and precipitation

The high tendency of particle agglomeration and precipitation of SD during the dissolution process could potentially reduce the drug release rates of the SD (Kapsi and Ayres, 2001, Karavas et al., 2007). During dissolution experiment of HME formulations, pronounce agglomeration and precipitation was noted as indicated by the sizes of particles dispersed in the dissolution medium being larger than the initial controlled particles size range (63-106 μm). In this context, the extent of agglomeration was reflected by the particle size of the dissolving particle which showing the trend of particle as INDO > KTP > NAP > OZP. This may be ascribed to the high hydrophobicity of the surface system of the HME which could be correlated well to the value of contact angle found in HME system as highest values was seen in INDO followed by > KTP > NAP > OZP. Furthermore, the agglomeration of the dissolving solid during the dissolution process could also potentially lead to crystallization of the API depending on the crystallization tendency of the tested API which will be further discussed in the next paragraphs.

Recrystallization

In this study, microscopic observations confirmed recrystallization of all the tested formulations upon dissolution except HME INDO-PVPVA 6:4. For instance, HME NAP-PVPVA 6:4 showed intense recrystallization after agglomeration of particle upon medium addition as shown from the birefringence of crystalline material in Figure 5.13 (b). This was further supported by high magnification investigations using SEM where crystalline features was seen on the surface of the

particle collected while dissolution experiment (Figure 5.14). The recrystallization of API on the surface can lead to the lining of crystalline material at the dissolving front of particle which could hinder the movement of large molecular polymer from the core of particle to the outer layers of the particle. Consequently, this could hinder the formation of polymer rich layer at vicinity of the dissolving front in exerting its wetting effect which was shown to be important for dissolution enhancement of a poorly soluble API as shown in the contact angle measurement in Figure 5.8. Hence, it is proposed that the limited dissolution rate enhancement of HME KTP, NAP, and INDO PVPVA 6:4 in comparison to their PM systems could also be associated with the secondary phenomena of recrystallization which further reduces the wettability of the API.

The previous chapter (Chapter 4) has shown the importance of drug polymer interaction in preventing physical recrystallization of HME PVP-based. Nevertheless, in this chapter, recrystallization trend of the dissolving systems as deduced from both the HSM and SEM images were not in coherent to the trend of hydrogen bond interaction between the API-PVPVA 6:4 as predicted by ATR-FTIR. This is attributed to the hydrodynamic dissolution process that causes different recrystallization trend of the HME system. During dissolution, the effect of drug polymer interaction in controlling the recrystallization of HME API-PVPVA 6:4 has been diluted as other events might come into play in the recrystallization of API while dissolution, such as ionization or solubilisation of the API in the dissolution medium.

Theoretical solubility advantages of amorphous API and its phase solubility behaviour in PVPVA solution

As mentioned in previous paragraph, the dissolution rate of an API has been long established to be associated to its solubility in which a high solubility of an API could drive the its dissolution rate (Noyes and Whitney, 1897). In amorphous systems, beside the absence strong crystal lattice bonds between the molecules which lead its readily dissolvable state, high apparent solubility of the amorphous API can also drive the dissolution rate. The apparent solubility of an amorphous API could be theoretically estimated by calculating the free energy difference between the crystalline and amorphous state as presented in Table 5.3. The rank order difference in free energy of amorphous and crystalline state of the tested API as shown in Table 5.3 was found to correlate well to the trend of extent in dissolution rate enhancement of the HME systems as compared to its PM, i.e. HME OZP-PVPVA 6:4 > HME INDO-PVPVA 6:4 > HME NAP-PVPVA 6:4 > HME KTP-PVPVA 6:4. This suggested that the dissolution performance of a HME API-PVPVA 6:4 system is API specific where the free energy difference between the amorphous and crystalline form largely dictate the overall dissolution performance of a HME amorphous SD system.

The enhanced dissolution rate of the HME amorphous systems could be further driven by the enhanced phase solubility of the APIs in the concentrated polymer rich layer. For instance, the highest extent of solubility enhancement of OZP in the concentrated PVPVA 6:4 solution (Figure 5.1) has promoted its high dissolution rate of HME OZP-PVPVA 6:4. This is due to the high concentration gradient of the dissolving system that fastens the dissolution rate of the system based on the classical Noyes-Whitney Equation (2.2). However, this solubilising effect can be potentially affected by the intense recrystallization of API which was clearly shown in dissolution process of HME NAP-PVPVA 6:4. In this system, the dissolution enhancement of NAP was not observed despite the apparent solubility enhancement of NAP in the presence of PVPVA 6:4. This is due to the high recrystallization tendency of the HME NAP PVPVA 6:4 system that has counter-balanced the positive effect anticipated from the solubility enhancement of NAP by PVPVA 6:4 solution.

5.5. Conclusion

This chapter have highlighted the issues arise in dissolution performance of HME PVP-based SD system. The limited wetting properties of HME poorly soluble API-PVPVA 6:4 system as compared to their PM may be a potential reason for the limited dissolution rate enhancement of the HME systems. The wettability alteration of the HME system has cause secondary dissolution limiting effect such as hydrophobic agglomeration which further promotes the recrystallization of the drug during dissolution process. Following the solid state changes of the HME API-PVPVA 6:4 system upon dissolution, the subsequent dissolution dynamic is largely dictated by a combination of the total surface area for dissolution and the amorphous advantages of the APIs. The interactions between the different API and PVPVA 6:4 has shown to have minimal effect on the dissolution rate enhancement of the HME PVPVA 6:4 based system.

Besides, the ‘solubility advantage’ of an amorphous API has shown to be an important parameter in determining the dissolution performance of solid dispersion of a poorly soluble API. In this study, it was found that an API candidate with its high ‘solubility advantage’ ratio is worth to be formulated into its solid dispersion form. This is clearly shown by the example of OZP system which reveals its high dissolution rate enhancement in its HME PVPVA system as compared to its PM system. On the other hand, a relatively low ‘solubility advantage’ of an API may not exert a big benefit in formulating into HME PVP-based SD. This is shown by the dissolution experiment of HME KTP and NAP systems where their HME systems revealed a similar dissolution profiles to their corresponding PM systems. The low ‘solubility advantages’ offered from the amorphous state of these APIs (KTP and NAP) could be easily counter-balanced by the secondary dissolution limiting processes of agglomeration and recrystallization which have been identified in this chapter.

Chapter 6. *An investigation into factors governing the drug release mechanism of PVP-based hot melt extrusion formulations Part II: Dissolution performance of hot melt extruded naproxen-carrier systems*

6.1. Introduction

Conventionally, transforming a poorly soluble crystalline API into amorphous form is beneficial to its dissolution performance as no additional bonds are necessary to be broken before complete dissolution of the system. However, previous chapter (Chapter 5) has found an inconsistent dissolution performance of HME amorphous SDs in comparison to their corresponding physical mixture (PM) system. In particular, the dissolution rate of the HME NAP-PVPVA 6:4 has shown a superimposable dissolution profiles to its corresponding PM system. This observation contradicts the general belief of ‘solubility advantages’ of amorphous pharmaceutical in the in-vitro dissolution performance of SD system (Hancock and Parks, 2000). Furthermore, the dissolution profile of the PM revealed a 2-fold increase in drug release rate as compared to the dissolution rate of the NAP alone. Therefore, PM NAP PVPVA 6:4 system seems to have reasonably increased the release rate of the poorly soluble NAP which makes its formulation into an HME system unnecessary.

Thus, the purpose of this chapter is two-fold. On one hand, factors contributing to the dissolution enhancement of PM NAP-PVPs system will be explored. In this context, dissolution behaviour of a series of PVP homopolymers and a copolymer in PM will be studied. On the other hand, the root causes of the limited dissolution rate enhancement of HME API-PVPs system will be further investigated as an extension study from chapter 5, which has suggested an API dependency on dissolution performance of HME PVP-based SD systems. Here, other factors that affecting the dissolution performance of HME NAP PVP-based SD system will be explored. These factors include the effect of NAP loading, different molecular weight (MW) of PVP polymers and the effect of surfactant incorporation in the extrudate system on dissolution performance of HME NAP PVP-based SD.

6.2. Materials and Methods

NAP was chosen as the API for the study on the effect of drug loading and carrier types in dissolution performances of PM and HME formulations. In this context, various grades of PVP were tested, which included PVP K12, PVP K17, PVP K29-32 and their copolymer, PVPVA 6:4. Therefore, the word ‘PVPs’ represents all the tested PVP carriers (PVP K12, PVP K17, PVP K29-32 and PVPVA 6:4) and PVPVA 6:4 copolymer or otherwise specified.

6.2.1. Preparation of PM

PMs were prepared according to the same method as described in Chapter 5, section 5.2.3.

6.2.2. Dissolution studies of pure NAP and its PMs

Dissolution of the NAP systems was performed in 0.1M hydrochloric acid (0.1M HCl) at 37 °C and at 50 rpm. The particle size of NAP and the polymers was maintained in the range of 63-106 µm prior to the dissolution experiments. Then, the samples equivalent to 10 mg of NAP (based on formulation composition) was transferred into the dissolution media for the NAP release measurement. At predetermined intervals, 10 ml of solution was withdrawn and filtered with a 0.45µm polyvinylidene fluoride (PVDF) syringe filter. The filtrate solution was then scanned by UV spectrometer at 272 nm to determine the concentration of the released NAP.

The release behaviour of NAP in the presence of PVPVA is evaluated in this study. The effect of PVPVA 6:4 on the release behaviour of NAP was measured in various conditions as shown in the dissolution experiments given in Table 6.1.

Table 6.1: Dissolution experiments of NAP with the presence of PVPVA 6:4 in various conditions

Sample		Dissolution medium	Explanation of experiment conditions	Code
Component 1	Component 2			
10 mg NAP	-	0.1M HCl	Pure NAP dissolution	-
10 mg NAP	-	0.1M HCl + 23.33 mg PVPVA 6:4	PVPVA 6:4 was pre-dissolved in the 0.1 M HCl prior dissolution of NAP alone	-
10 mg NAP	23.33 mg PVPVA 6:4	0.1M HCl	Addition of 23.33 mg PVPVA after 20 minutes of NAP dissolution started	Exp A
PM30% NAP-PVPVA 6:4		0.1M HCl	Pre-mixing of NAP and PVPVA 6:4 as described in Chapter 6.2.1	PM
10 mg NAP	23.33 mg PVPVA 6:4	0.1M HCl	NAP and PVPVA were transferred into the dissolution vessel at opposite ends.	Exp S

'Exp S' was carried out by transferring both the NAP and PVPVA 6:4 components from opposite ends of the dissolution vessel into the medium at the same time (also coded as 'Exp S' in Table 6.1) as illustrated in Figure 6.1. The dissolution profile of NAP in this experiment was used as a comparison to the dissolution profile of PM system in order to check the significance of the premixing step in dissolution enhancement of PM NAP PVPVA systems.

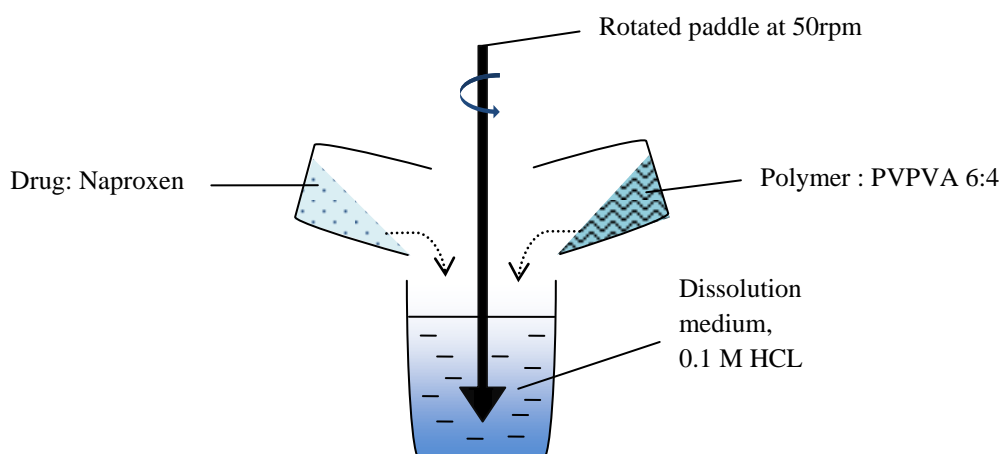


Figure 6.1: Schematic to illustrate the dissolution experiment performed with addition of two components at different ends of the dissolution vessel, 'Exp S'

6.2.2.1. Phase solubility of PVP and NAP

Solubility of NAP in PVP solutions was determined by stirring excess of NAP powder in 10 ml 0.1M HCl at 37 °C for 48 hours. The saturated solution was then filtered with a 0.45 μm PVDF syringe filter and the filtrate was measured for NAP content using a UV spectrophotometer at 272 nm. Each sample was measured in triplicate.

6.2.2.2. Surface tension of PVPs solutions

Surface tension of the dissolution media and 1% w/v PVPVA 6:4 solution was determined by using a pendent drop measurement. A liquid dispenser holder with manual control was used to create the drops. OneAttension software was used to analyze the surface tension by Young-Laplace surface properties mode. The changes in the surface tension were recorded up to 120 seconds at 1 frame per second.

6.2.3. Production of HME NAP PVP-based SDs

HME NAP PVPs SD systems were prepared using co-rotating twin-screw extruders (Thermo HAAKE MiniLab Micro Compounder). NAP and polymers (total amount of 5g) were gently mixed in mortar and pestle for 2 minutes prior to extrusion. In the preparation of HME NAP-PVPVA 6:4-Tween 80 system, Tween 80 (liquid surfactant) was premixing in the PM of NAP and PVPVA 6:4 using a mortar and pestle prior extrusion. Please refer to Table 2.12 for the processing parameters used in the manufacturing of the HME systems. Table 6.2 lists the different compositions of HME SD system prepared in this study and the aims of each experiment.

Table 6.2: HME formulations that were prepared and investigated in this study. All the HME formulations were prepared at 150 °C, 100rpm with a residence time of 10 minutes.

HME formulation	Purpose of investigation
HME 10% NAP PVPVA 6:4	To test the effect of NAP loading on dissolution performance
HME 20% NAP PVPVA 6:4	HME PVPVA-based SD system
HME 30% NAP PVPVA 6:4	
HME 40% NAP PVPVA 6:4	
HME 30% NAP PVP K12	
HME 30% NAP PVP K17	HME PVP-based SD system
HME 30% NAP PVP K29-32	
HME 30% NAP PVPVA 6:4-2% Tween	To test the effect of incorporation of surfactant into extrudates in dissolution performance of the HME PVP-based SD system
HME 30% NAP PVPVA 6:4-10% Tween	

6.2.4. Basic characterisation of HME NAP PVPs SD systems

6.2.4.1. Differential scanning calorimetry

Please refer to Chapter 5, section 5.2.5.1, as the experimental conditions used were the same.

6.2.4.2. Attenuated total reflectance-fourier transform infrared

Please refer to Chapter 5, section 5.2.5.2, as the experimental conditions used were the same.

6.2.4.3. X-ray diffraction

Please refer to Chapter 5, section 5.2.5.3, as the experimental conditions used were the same.

6.2.5. Dissolution studies of HME NAP PVP-based SD

Dissolution behaviours of HME NAP-PVP based SDs were performed by using the same conditions as stated in Chapter 6.2.2.

6.2.5.1. SEM

Please refer to Chapter 5, section 5.2.6.3, as the experimental conditions used were the same.

6.2.5.2. Hot stage microscope

The appearance of the HME particles upon contact with dissolution medium was observed and recorded using a HSM as a function of time, where the freshly ground HME particles were loaded on a slide under a microscope with a pre-focused position of the lens. Two drops of the medium were added to the particles and appearance of the extrudates was immediately recorded with HSM after covering the samples with a cover slide.

6.2.5.3. Particle size of residue

Please refer to Chapter 5, section 5.2.6.2, as the experimental conditions used were the same.

6.2.6. Contact angle measurement

Previous chapter has concluded the potential of reduced wettability of HME as a cause of the low dissolution rate of HME as compared to their PM systems. Therefore in this study, contact angle measurements of both the PM and HME systems of NAP in different PVPs systems were also assessed. These contact angle measurements were performed on the surface of the compressed tablet with drop analysis, which have been described in a previous chapter (Chapter 5.2.6.4). Table 6.3 summarises the contact angle experiments that have been carried out in this chapter.

Table 6.3: Experiments of contact angle measurement between the solid phase and liquid phase.

Surfaces of the solid phase	Liquid phase		
	Distilled water (DW)	0.1M HCL saturated with NAP	Diiodo-methane
NAP	√	√	√
PM 30% NAP PVP K12	√	√	√
PM 30% NAP PVP K17	√	√	√
PM 30% NAP PVP K29-32	√	√	√
PM 30% NAP PVPVA 6:4	√	√	√
HME SD 30% NAP PVP K12	√	√	√
HME SD 30% NAP PVP K17	√	√	√
HME SD 30% NAP PVP K29-32	√	√	√
HME SD 30% NAP PVPVA 6:4	√	√	√

Determination of Interfacial tension

The contact angle measurements of system/distilled water and system / diiodomethane are intended for the calculation of interfacial tension. Interfacial tension between the solid surface and the dissolution media could be calculated by using Fowkes Equation (6.1), (6.2) and (6.3) (Żenkiewicz, 2007).

$$\gamma_s = \gamma_s^d + \gamma_s^p \quad (6.1)$$

$$\gamma_s^d = 0.25\gamma_l(1 + \cos\theta_d)^2 \quad (6.2)$$

$$\gamma_s^p = [0.5\gamma_l(1 + \cos\theta_p) - (\gamma_s^d \gamma_l^p)^{0.5}]^2 / \gamma_l^p \quad (6.3)$$

where γ_s is the measured surface tension of the solid, γ_s^d is attributed to the dispersive component (determined from diiodomethane) of the solid surface tension and γ_s^p is attributed to the polar component of the solid surface tension which could be obtained from the polar medium i.e. water. γ_l is the surface tension of the liquid phase i.e. either the apolar liquid in Equation (6.2) or polar liquid in Equation (6.3). The θ_d or θ_p could be obtained from contact angle measurement. After obtaining the solid surface tension in Equation (6.1), the interfacial energy, γ_{sl} between the solid formulation and dissolution medium or solution of interest could then be calculated by using Young's equation, as described in Equation (6.4).

$$\gamma_{sl} = \gamma_s - \gamma_{l(0.1M\ HCl)} \cos \theta \quad (6.4)$$

where γ_s is the solid surface tension, γ_l is the liquid surface tension which is dissolution medium in this study and θ is the contact angle between the solid surface of the prepared formulation and the dissolution media which have been measured in the previous section. Table 6.4 displays the values used for the calculation of interfacial energy by using Equation (6.1) to (6.4).

Table 6.4: Values used for the calculation of interfacial energy by using Fowkes Equation (6.1) to (6.4)

Liquid phase	Surface tension (mJ/m ²)	References
γ_l of diiodomethane	51.84 ± 0.09	Experimental value
γ_l of water	71.81 ± 0.39	Experimental value
γ_l^d of water	21.8	(Żenkiewicz, 2007)
γ_l^p of water	51	(Żenkiewicz, 2007)
γ_l of 0.1MHCl saturated with NAP	70.34 ± 1.99	Experimental value

6.3. Results

The first part of the results (i.e. Chapter 6.3.1) will explore the reasons for dissolution enhancement of NAP in its PM NAP-PVPVA 6:4 system, whereby the effects of wetting and solubilising of polymer in the dissolution performance of the PM NAP PVPVA 6:4 system were investigated. Secondly, dissolution behaviour of HME NAP-PVP-based SDs (Chapter 6.3.2) with different combinations of NAP loading and PVPs carrier system will be presented in sections 6.3.2.1 and 6.3.2.2, respectively. Then, an attempt was made to incorporate a non-ionic surfactant, i.e. Tween 80 in the HME NAP-PVP based SD and their dissolution behaviours will be presented in Chapter 6.3.2.3. The last part of the results will reveal whether amorphous nature of a SD system is essential for the dissolution enhancement of HME NAP PVP-based SD (Chapter 6.3.3).

6.3.1. Investigation of dissolution behaviour of PM formulations

Several factors have been suggested to cause dissolution enhancement of PM of a poorly soluble API with their API. Crystallinity changes of API upon physical mixing with polymer has been suggested as one of the causes in dissolution rate enhancement of PM API-polymer (Rawlinson et al., 2007). However, this effect was excluded in dissolution enhancement of the PM NAP PVPVA 6:4, in this study, as there is no crystallinity change of NAP in its PM system which was confirmed by the XRPD diffractograms of PM NAP in PVPVA 6:4 (data not shown). Therefore, other possible factors were subsequently explored.

Previous chapter has shown the important wetting effect of PVPVA 6:4 in increasing dissolution rate of NAP in its PM NAP PVPVA 6:4 system. In that case, the extent of dissolution rate increase of the APIs in their PM systems was proved to be related to the degree of increase wettability by the hydrophilic PVPVA 6:4 in its dissolved state. This implies that the premixing of the drug and polymer might be insignificant in enhancing of the dissolution rate of a poorly soluble drug. Therefore, in order to explore the root cause of dissolution rate enhancement of NAP in its PM system, dissolution experiments of NAP in different conditions of the presence of PVPVA 6:4 was performed as described in Table 6.1 (Chapter 6.2.2). Figure 6.2 shows the dissolution profiles of NAP that were performed according to the dissolution experiments listed in Table 6.1.

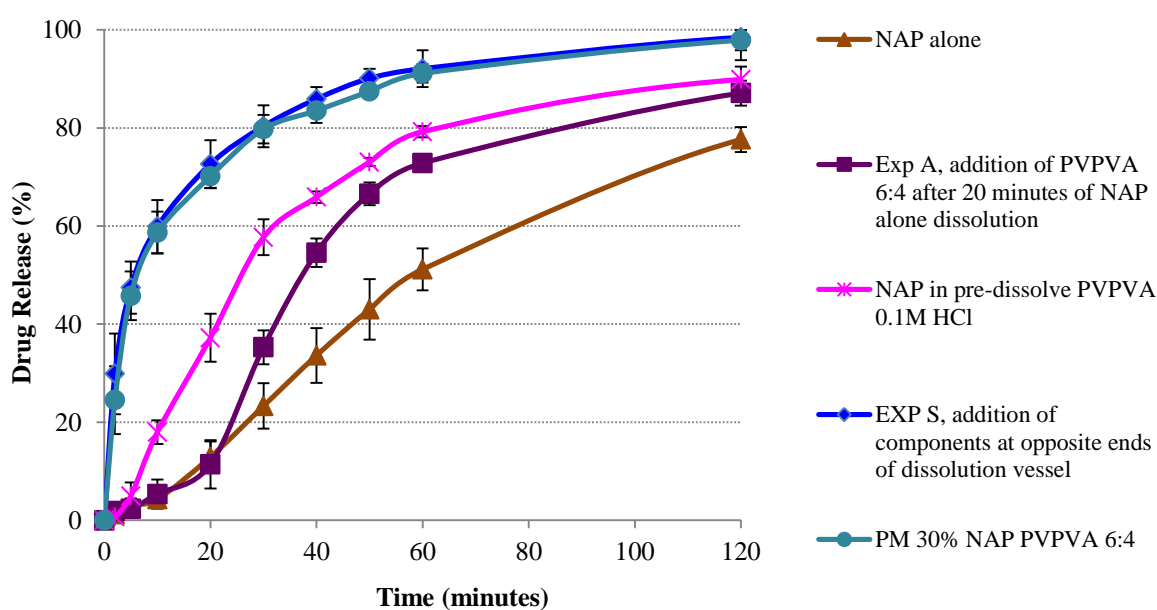


Figure 6.2: Dissolution profiles of NAP in the presence of PVPVA 6:4 at various ways as presented in Table 6.1.

According to Figure 6.2, the release of NAP was slow, as only 50% of NAP was released after 1 hour of dissolution (brown line). On the other hand, release rate of NAP in a pre-dissolved PVPVA 6:4 0.1M HCl medium (pink line) was increased, implying a wetting effect by the dissolved PVPVA 6:4 in the 0.1M HCl medium. This wetting effect could be further indicated by the marked increase in the release rate of NAP in 'Exp A' after the addition of PVPVA 6:4 at 20 minutes of the NAP dissolution experiment (purple line). In this experiment ('Exp A'), the initial dissolution rate of NAP without the presence of PVPVA 6:4 was 0.57 mg/min (in NAP alone in 0.1M HC); it was then increased to 2.39 mg/min upon the addition of polymer (an increase of approximately 4 - fold). This increased release rate of NAP was found comparable to the dissolution rate of NAP in the pre-dissolved PVPVA 6:4 0.1M HCl medium (pink line) which confirmed the essentiality of the presence of PVPVA 6:4 in dissolution rate enhancement of NAP. A further increase in the

initial dissolution rate of NAP was noted in its PM NAP PVPVA 6:4 system (light blue line in Figure 6.2). This might be attributed to the solubilising effect of PVPVA 6:4 on top of its wetting effect in the PM system.

In ‘Exp S’ (navy blue line in Figure 6.2) where both the PVP polymers and NAP were added from different ends of the dissolution medium (Figure 6.2), the release NAP was surprisingly superimposed to the dissolution profile of PM NAP PVPVA (pre-mixing prior to dissolution experiment). This implies that the pre-mixing procedure of the NAP and PVPVA 6:4 does not exert beneficial effect on dissolution enhancement of PM NAP PVPVA 6:4 formulations.

6.3.1.1. Dissolution behaviour of PM NAP in different carriers system: PVP K12, PVP K17, PVP K29-32, PVPVA 6:4

The insignificance of premixing step in dissolution enhancement of a PM NAP-PVPVA 6:4 was not expected. To further understand these phenomena, the dissolution experiments of PM and “Exp S” of NAP-homopolymers with different MW of PVPs were also studied. Figure 6.3 compares the dissolution profiles of NAP among different MW of PVPs, whereby dissolution profiles of both the PM and ‘Exp S’ in each grade of PVPs were compared quantitatively by using similarity factors, f_2 values, a term that was described in Chapter 5.2.6.

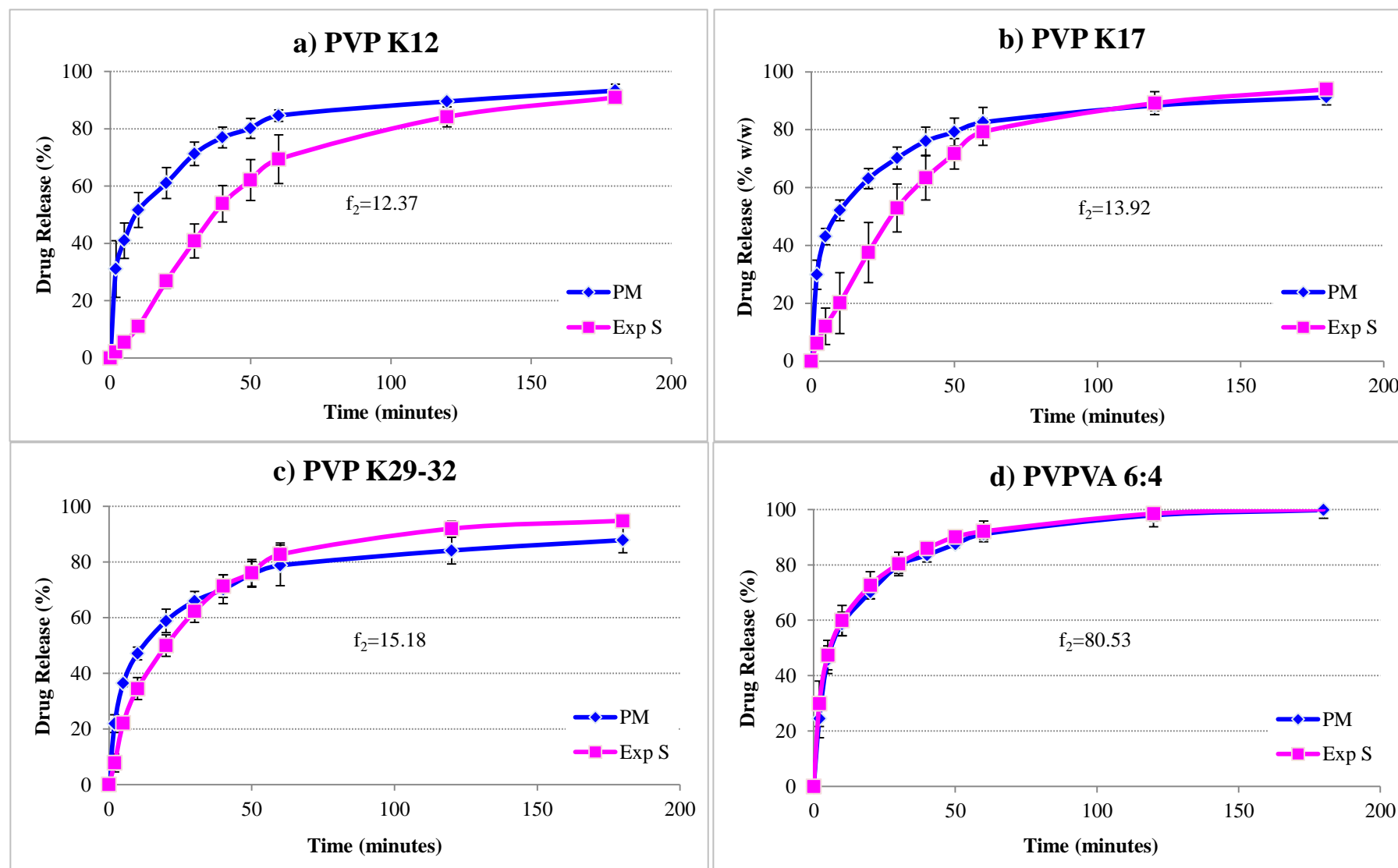


Figure 6.3: Comparison of the dissolution profiles for PM (blue \diamond) and 'Exp S' (pink \square) of binary NAP PVPs systems a) PVP K12, b) PVP K17, c) PVP K29-32 and d) PVPVA 6:4.

Unlike the NAP-PVPVA 6:4 system, significant differences between the release of NAP in PM and ‘Exp S’ were noted in NAP-homopolymer PVP as indicated by the f_2 factor, i.e. $f_2 < 50$ (Figure 6.3 (a) to (c)). The trend of dissolution profiles differences between the HME and PM system based on similarity factors as presented in Figure 6.3 is PVP K29-32 > PVP K17 > PVP K12. This trend implies the effect of pre-mixing is in the rank order of PVP K12 > PVP K17 > PVP K29-32 which in turn implies the importance of the pre-mixing step in the dissolution of NAP in the PM NAP homopolymer systems, particularly in LMW PVP systems. The observed discrepancy in significance of the premixing step among the different PVPs carriers might be ascribed to their different degrees of wetting or solubilising effect onto the poorly soluble NAP, which will be further explored in the next section.

6.3.1.2. Solubility tests of NAP in PVP solutions

The solubility of NAP in PVP solutions were examined in order to establish the possible role of solubility enhancement in promoting dissolution of both PM NAP formulations and ‘Exp S’ as shown in Figure 6.3. Figure 6.4 represents the profiles of phase solubility of NAP in different concentrations of PVP polymers.

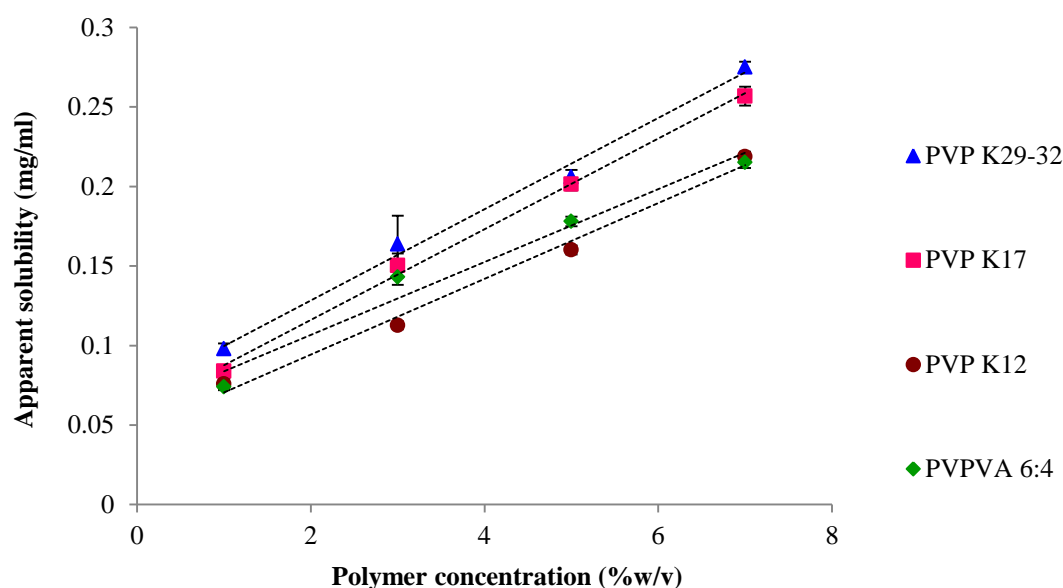


Figure 6.4: Phase solubility relationships between different polymer concentrations and solubility of naproxen after stirring for 48 hours at 37 °C

Based on the solubility results in Figure 6.4, PVP K29-32 was found to exert the highest increase in the apparent solubility of NAP. This trend was observed to increase linearly up to 7% w/v of polymer (with an approximately 10 fold increment in solubility of NAP at 37 °C). The solubilizing effect of the PVP polymer onto the poorly soluble NAP was then followed by PVP K17 > PVPVA

> PVP K12. The solubilizing effect of homopolymer was appeared to be directly related to the molecular weight of the PVP homopolymer used, i.e. PVP K29-32 > PVP K17 > PVP K12. This solubilizing trend was noted to be similar to the trend of ‘significance of the premixing step in dissolution’ that was compared between the PM and ‘Exp S’ (the significance was reflected by the similarity factor, f_2 as shown in Figure 6.3). This suggested that dissolution enhancement of a physical mixture of NAP and homopolymer might be related to the solubilisation of NAP by its homopolymer carrier during the dissolution process.

6.3.1.3. Surface tension properties

Dissolution rate enhancement of both the PM NAP-PVPs and ‘Exp S’ have shown to be related to the solubilising effect of the PVP carrier on the solubilisation of the poorly soluble NAP. However, despite the relatively lower solubilising effect of PVP K12 carrier on the solubilisation of NAP, the PM of NAP in this polymer system showed a similar dissolution profile to those of other tested PVPs, i.e. PVP K17, PVP K29-32 and PVPVA 6:4. This might be due to the wetting effect of this polymer which was further investigated.

The previous chapter (Chapter 5) has shown the significance of surface properties in dissolution behavior of poorly soluble API in its PM formulation. Hence, in this study, the surface tension of the dissolved PVP polymer solutions was also studied to understand the wetting effect of the polymer onto NAP. Table 6.5 lists the surface tension of the dissolution media and solution with the pre-dissolved polymer system.

Table 6.5: Average surface tensions and average volume of drops during the 120 seconds of the experiment time frame. All the solutions were saturated with NAP which was denoted as ‘sat NAP’.

Medium	Average surface tension ± STDEV (mN/m)	Average Volume ± STDEV (µl)
sat NAP 0.1M HCl	70.34 ± 1.98	14.90 ± 0.12
sat NAP Distilled water	70.91 ± 1.40	13.74 ± 0.20
0.1MHCl+1%w/v PVPVA 6:4 with sat NAP	55.66 ± 0.77	12.68 ± 0.11
0.1MHCl+1%w/v PVP K12 with sat NAP	58.37 ± 0.35	12.79 ± 0.11
0.1MHCl+1%w/v PVP K17 with sat NAP	62.91 ± 0.95	14.22 ± 1.99
0.1MHCl+1%w/v PVP K29-32 with sat NAP	61.90 ± 1.15	13.49 ± 0.42

According to Table 6.5, the surface tensions of distilled water and 0.1 M HCl that were pre-saturated with NAP are similar. As anticipated, the surface tensions of the media were reduced slightly with the addition of PVP homopolymers which was reported earlier (Huang and Wang,

1996, Bolten and Türk, 2011). The marginal reduction in surface tension of the PVP homopolymer is probably ascribed to the small tendency of the PVP migration to the interface, particularly at high concentration of PVP (Huang and Wang, 1996, Bolten and Türk, 2011). In this case, PVP K12 was shown to have the lowest surface tension among the tested PVPs homopolymer solution which is in agreement with Huang and Wang (1996) whom have demonstrated the molecular weight dependence of surface tension at high (above 10^{-4} g/ml) polymer concentration (Huang and Wang, 1996). This explained the high dissolution enhancement of NAP in PM NAP PVP K12 as compared to 'Exp S' system despite its relatively low solubilizing capacity as compared to other PVP homopolymer system.

Furthermore, the surface tension of 0.1M HCl was found to be reduced greatly with the addition of 1% w/v PVPVA 6:4 in the 0.1M HCl. This might be attributed to the 40% of the hydrophobic vinyl-acetate monomer in the PVPVA 6:4 that lead to the higher hydrophobic to hydrophilic balance which increases its surface active nature as compared to the PVP homopolymer. This might be the main reason for the superimposable dissolution profile of PM and 'Exp S' that suggested the insignificant pre-mixing step in the release rate of NAP.

Summary of dissolution studies of PM

To summarise, solubilizing and wetting effects of the concentrated PVPs polymer are the main reasons for the increase release rate of NAP in its PM system. Thus it is essential to have the hydrophilic PVP presence at vicinity of the poorly soluble NAP during its dissolution process. In this context, PVPVA 6:4 carrier system showed a more apparent wetting effect which leads to the insignificant of the premixing step in enhancing the dissolution of NAP in PVPVA 6:4 system.

6.3.2. Dissolution performances of amorphous HME PVP-based SDs

After detailed studies of the reason for dissolution rate enhancement of the PM NAP-PVPVA 6:4 system, dissolution performances of the HME NAP-PVPVA 6:4 systems were also studied.

The previous chapter (Chapter 5) has suggested that dissolution performance of the HME system as compared to their PM counterpart is highly API dependence. However, the effect of carrier system in dissolution performance of HME SD shall not be overlooked. Therefore, dissolution performances of HME SD systems were studied from the perspective of the drug loading and carrier system in the subsequent sections of this chapter. This is to complement the limited understanding of the release mechanism of HME SD system.

Basic characterisation of HME NAP SD extrudates

The physical state of the freshly prepared HME NAP PVPs systems were confirmed prior to the detailed study on their dissolution performance. These physical states were characterised by using XRPD, ATR-FTIR and DSC measurements. Figure 6.5 display the DSC thermograms of the freshly prepared HME 10% to 40% NAP-PVPVA 6:4.

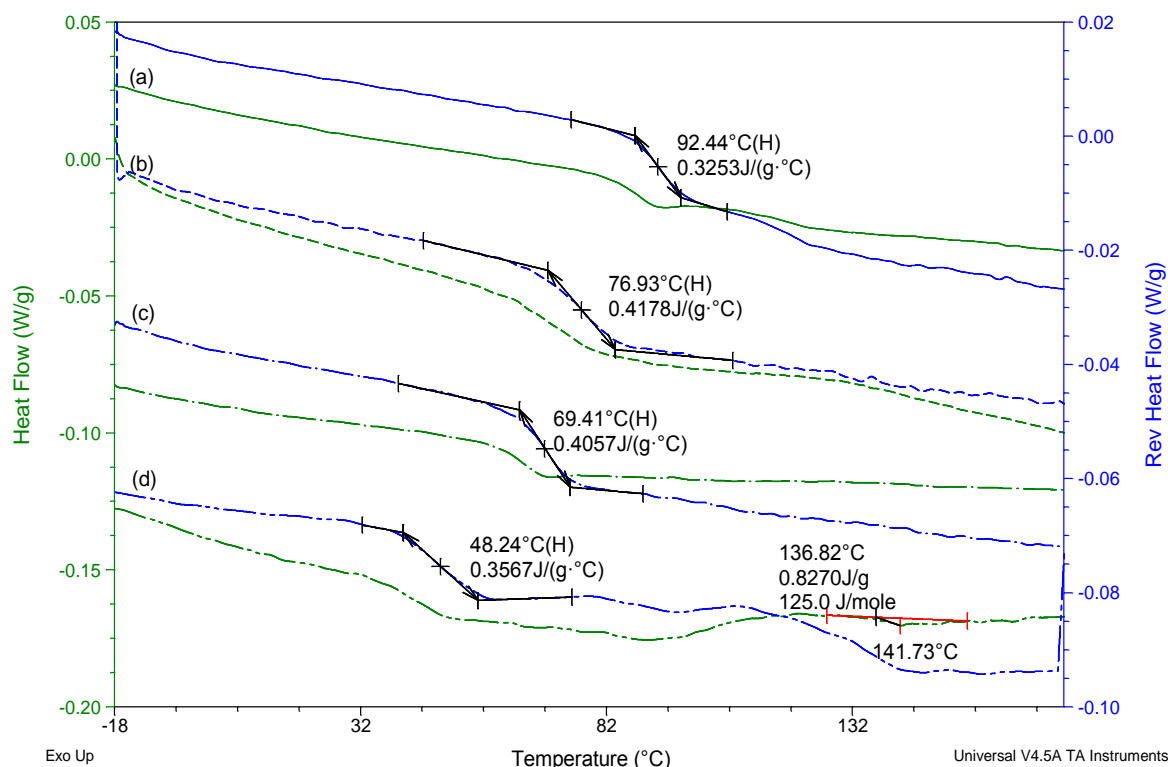


Figure 6.5: MTDSC thermograms of HME NAP PVPVA 6:4 with different NAP loading (a) 10% NAP, (b) 20% NAP, (c) 30% NAP and (d) 40% NAP. Green lines of the thermograms are total heat flow profile whereas blue line represents reversing heat flow of the DSC thermograms.

According to Figure 6.5, a single T_g was obtained for the HME 10 - 30% NAP-PVPVA 6:4 which indicated the production of homogenous HME systems. These T_g values were NAP loading dependent, whereby a higher content of PVPVA 6:4 increased the value of the T_g . Besides, no apparent melting point was detected in the HME NAP-PVPVA 6:4 SD except HME 40% NAP PVPVA 6:4. In HME 40% NAP-PVPVA 6:4 system, a minor melting endotherm at circa 141 °C was detected which was believed to be due to the depressed melting point of crystalline NAP. However, both XRPD and ATR-FTIR results of these formulations suggest the absence of detectable crystalline trace through the halo pattern and the disappearance of characteristic crystalline peak of NAP in both the XRPD and ATR-FTIR spectra, respectively.

To study the effect of different carrier types in dissolution performance of HME system, HME with different MW of PVP carriers (PVP K12, PVP K17, PVP K29-32, PVPVA 6:4) at 30% of NAP SD systems were produced. Basic characteristic of these systems were also studied. Figure 6.6 depicts the thermograms of the HME 30% NAP in different PVP carriers system.

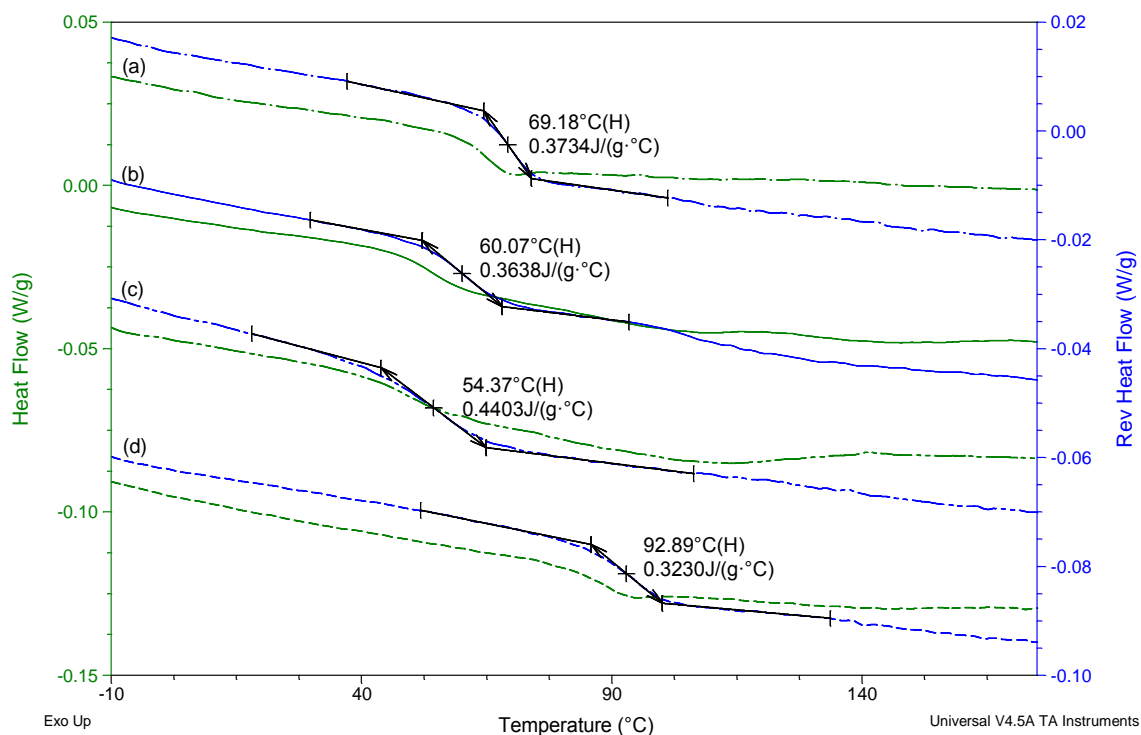


Figure 6.6: MTDSC profiles of HME 30% NAP-PVPs different carriers system, i.e. (a) PVPVA 6:4, (b) PVP K12, (c) PVP K17 and (d) PVP K29-32. Green lines of the thermograms are total heat flow profile whereas blue line represents reversing heat flow of the DSC thermograms.

No apparent melting endotherm was detected in the DSC thermogram of HME 30%-different PVPs carrier, which implied complete amorphizing of NAP-PVPs via HME process. These systems were homogenous as indicated by the single T_g (s) of HME NAP-PVPVA 6:4. The T_g (s) values were closely related to the T_g of the different MW of PVP carriers whereby the highest T_g was recorded for HME NAP-PVP K29-32 > HME NAP-PVP K12 > HME NAP-PVP K17 > HME NAP-PVPVA 6:4. Similarly, XRPD and ATR-FTIR spectra of these systems indicate halo patterns and absence of characteristic crystalline peak of NAP, respectively (data not shown), which suggests the absence of detectable crystalline NAP.

To summarise, all the freshly prepared HME NAP-SD extrudates shows amorphous nature in XRPD (data not shown). However, DSC analysis of these systems also suggested the amorphous nature for all the prepared HME NAP SD system except HME 40% NAP-PVPVA 6:4 system as indicated by the minor melting endotherm in its DSC thermograms.

6.3.2.1. Dissolution studies of different NAP loading on HME NAP PVPVA 6:4 SDs

After basic characterisation of the HME SD system, dissolution behaviours of these systems were studied. It is worth mentioning that the dissolution behaviours of the PM 10% up to 40% of NAP PVPVA 6:4 show superimposable dissolution profiles (data not shown). Therefore, in order to simplify the comparison of dissolution profiles between the different HME systems, Figure 6.7 displays the dissolution profiles of only the PM 10% NAP-PVPVA 6:4 and all the different NAP loading, i.e. 10-40% of HME NAP-PVPVA in comparison with NAP alone.

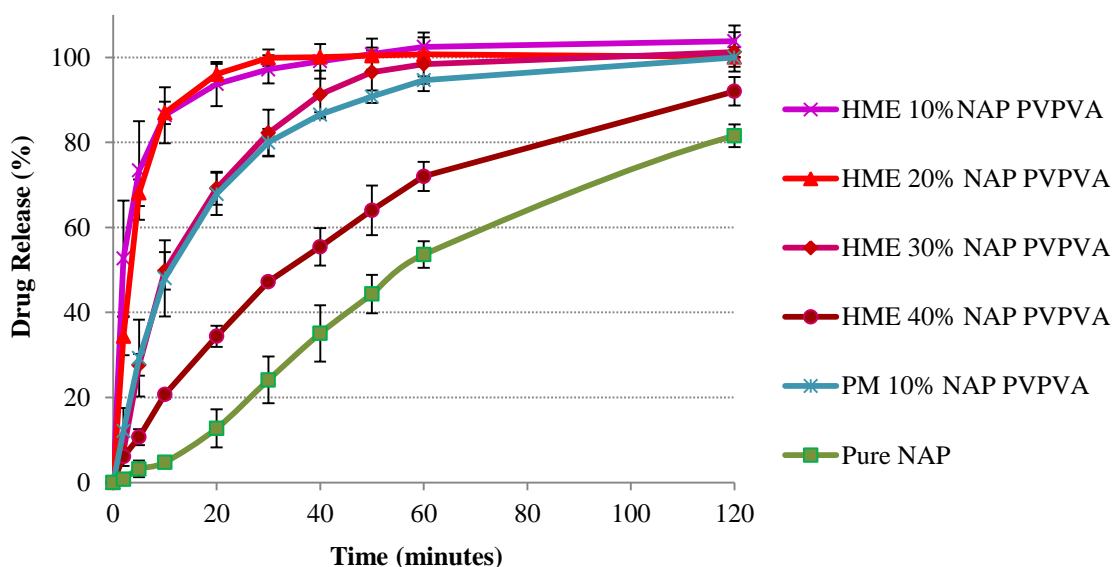


Figure 6.7: Dissolution of HME formulations of NAP-PVPVA 6:4 in 0.1M HCl pH 1.2.

According to Figure 6.7, dissolution of NAP was markedly enhanced in the HME 10% and 20% NAP-PVPVA 6:4 systems in which 100% of NAP was released after 30 minutes of dissolution experiment. Whereas, the dissolution profile of NAP in HME 30% NAP-PVPVA 6:4 was superimposed with the PM NAP-PVPVA 6:4 system. However, dissolution of HME 40% NAP PVPVA 6:4 was slower than the PM NAP-PVPVA 6:4. This was not expected as there is some extend of amorphocity of the NAP in HME 40% NAP-PVPVA 6:4 formulation as compared to the full crystallinity of NAP in the PM system. Thus, the role of amorphicity in dissolution rate enhancement of a SD is questionable, which will be further addressed in a latter section Chapter 6.3.3.

Overall, dissolution of HME NAP-PVPVA 6:4 SD was found to be NAP-loading dependent where the enhancement effects were found to decrease with an increase in loading of the NAP. Figure 6.8 illustrates a comprehensive picture of the initial dissolution rate of PM and HME 10-40% NAP-PVPVA 6:4.

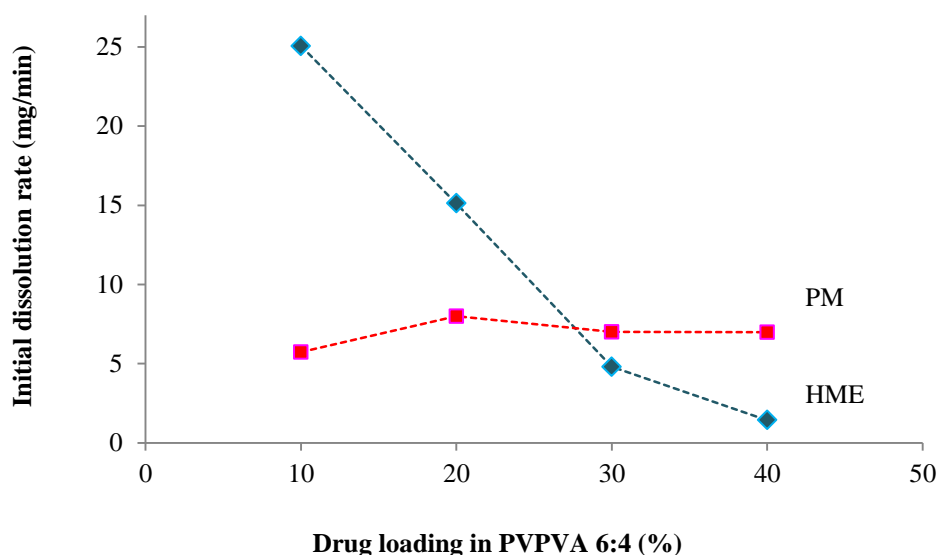


Figure 6.8: The effect of NAP-PVPVA 6:4 compositions in HME and PM products on the initial dissolution rate (at first 5 minutes) of solid dispersion

It is clear from Figure 6.8 that different loadings of NAP had little effect on initial dissolution rate of the PM systems. On the other hand, the initial dissolution rate of NAP in HME systems was noted to decrease with an increase of NAP loading (Figure 6.8). In this case, a critical loading of the NAP that leads to the effectiveness in dissolution performance of HME SD systems in comparison with their PM systems was found to be approximately 30% NAP loading. This critical loading of NAP in its dissolution performance of HME PVPVA 6:4 SD might be ascribed to the turning point of the drug release mechanism of SD, i.e from the carrier-controlled mechanism to drug controlled mechanism (Craig, 2002, Karavas et al., 2007). The different release rates of the NAP at different NAP loading of HME system were further investigated base on the identified limiting step such as agglomeration and recrystallization of the dissolving system that have been shown in Chapter 5.

6.3.2.1.1. Agglomeration

During the dissolution process, large particles were visible by eye in the dissolution medium possibly attributed to the extensive agglomeration of the dissolving system. This may cause a dramatic change in the effective surface area of dissolution which is essential in determining the dissolution rate of a system (Noyes and Whitney, 1897). Thus, particle size changes as a result of particles agglomeration during the dissolution processes of the HME SD were evaluated using a laser diffraction particle size analyser. Figure 6.9 shows the particle size distributions of HME 10% to 40% NAP PVP systems after 2 minutes of dissolution.

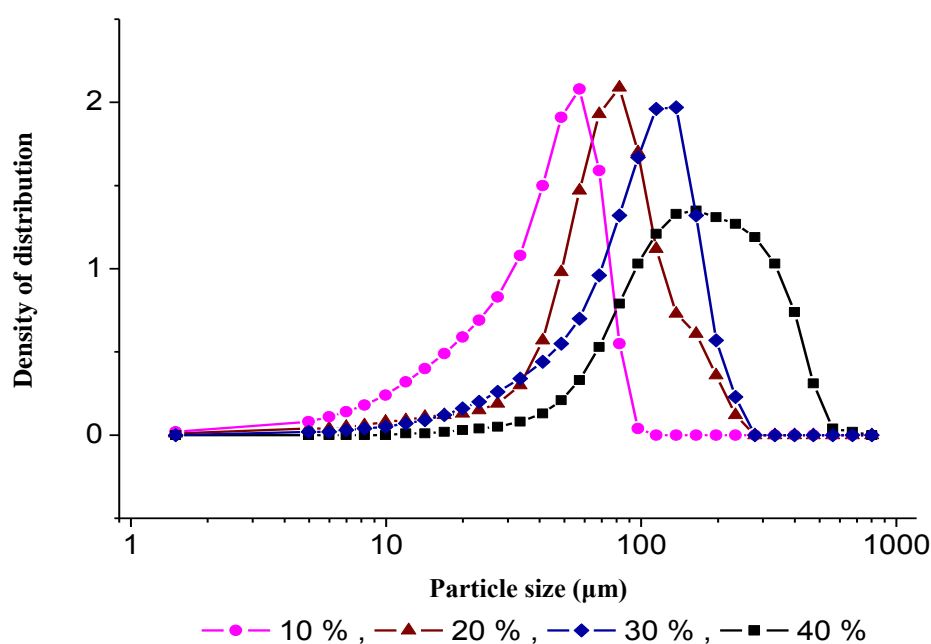


Figure 6.9: Particle size distribution of particles collected from the dissolution vessel at 2 minutes of dissolution of HME 10-40% NAP PVPVA 6:4 systems

It should be remembered that the particle size of all formulations was initially controlled within the range of 63-106 μm . The pronounced particle size reduction of HME 10% NAP-PVPVA 6:4 after 2 minutes of dissolution process indicated the fast dissolution of the particle in this system (Figure 6.9), which was consistent with the dissolution profiles found in Figure 6.7. Besides, particle size of HME 20% NAP-PVPVA 6:4 was remained at around the initial controlled size range with some distribution of particle up to 200 μm . However, larger size particles were detected in HME 30% and 40% NAP-PVPVA 6:4 system which indicated the extensive agglomeration of these HME particles during the dissolution process. This result is in agreement with a previous work on dispersions of felodipine in PVP and PEG SD whereby a higher extent of agglomeration was seen in higher API loading systems (Karavas et al., 2007).

Particle morphology by SEM

The size and morphology of the dissolving particles during dissolution experiment could also be evaluated using SEM. Figure 6.10 presents the SEM micrographs of the collected particles at different time points from the dissolution vessel of HME 40% NAP-PVPVA 6:4 during the dissolution experiments.

According to Figure 6.10 (a), agglomerated particles with their size larger than the initially controlled size range (60-106 μm) were observed. Ordered features were also seen in these particles which imply the formation of crystalline material on their surfaces (Figure 6.10 (b) and (c)). This might be due to the uncontrolled agglomeration and recrystallization of the system upon dissolution process. After 1 hour of dissolution, the edges seen on the particle faded and became relatively round after continuous dissolution of the particles (Figure 6.10 (d)).

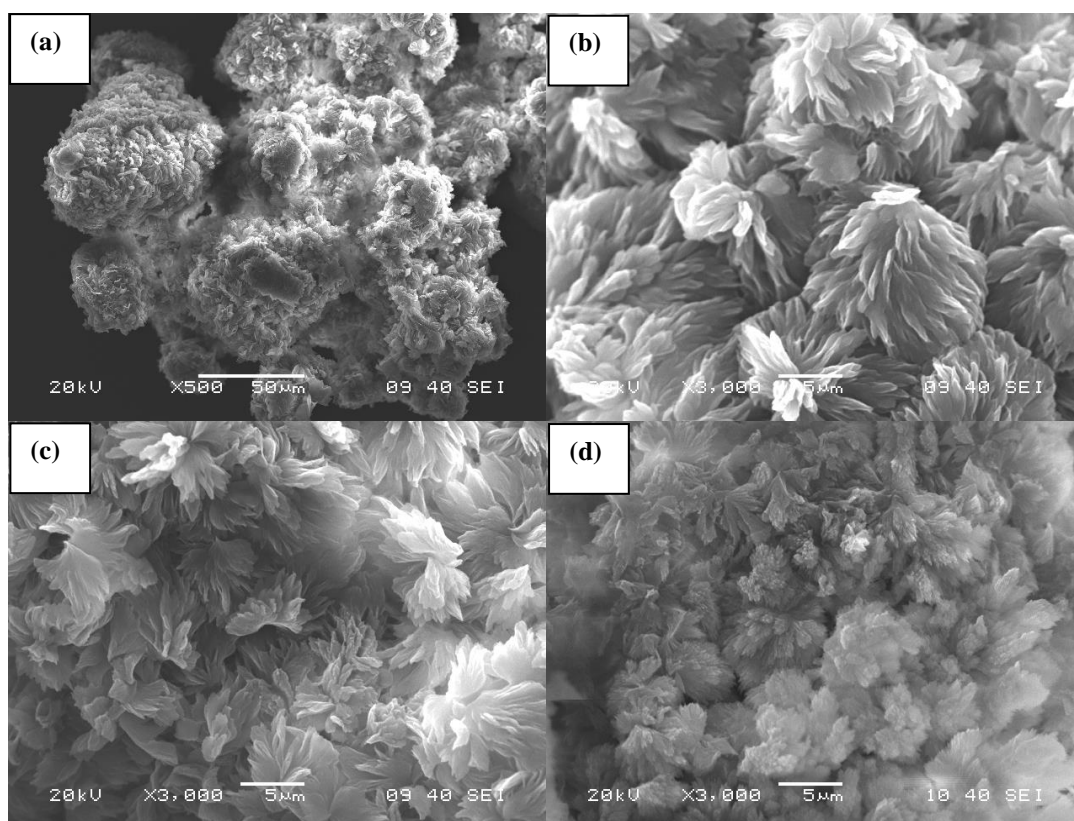


Figure 6.10: SEM images of residues collected from a dissolution experiment of HME 40% NAP-PVPVA 6:4 system at a) 1 minute, b) high magnification for particles at 1 minutes, c) 2 minutes, and d) 1 hour

6.3.2.1.2. Recrystallization

Birefringence of crystalline NAP observed via polarise light microscope

To further confirm the recrystallization of the HME NAP-PVPVA 6:4 powder while dissolution process, the change in particle appearance of HME 10-40% NAP-PVPVA 6:4 samples upon dissolution medium contact were analysed by using HSM as described in Chapter 6.2.5.2. Birefringence of the tested sample observed under HSM is an indication of recrystallization of the system upon contact with the dissolution medium. Figure 6.11 displays the captured screens of HSM for HME 10-40% NAP-PVPVA 6:4 upon medium contact as the function of time.

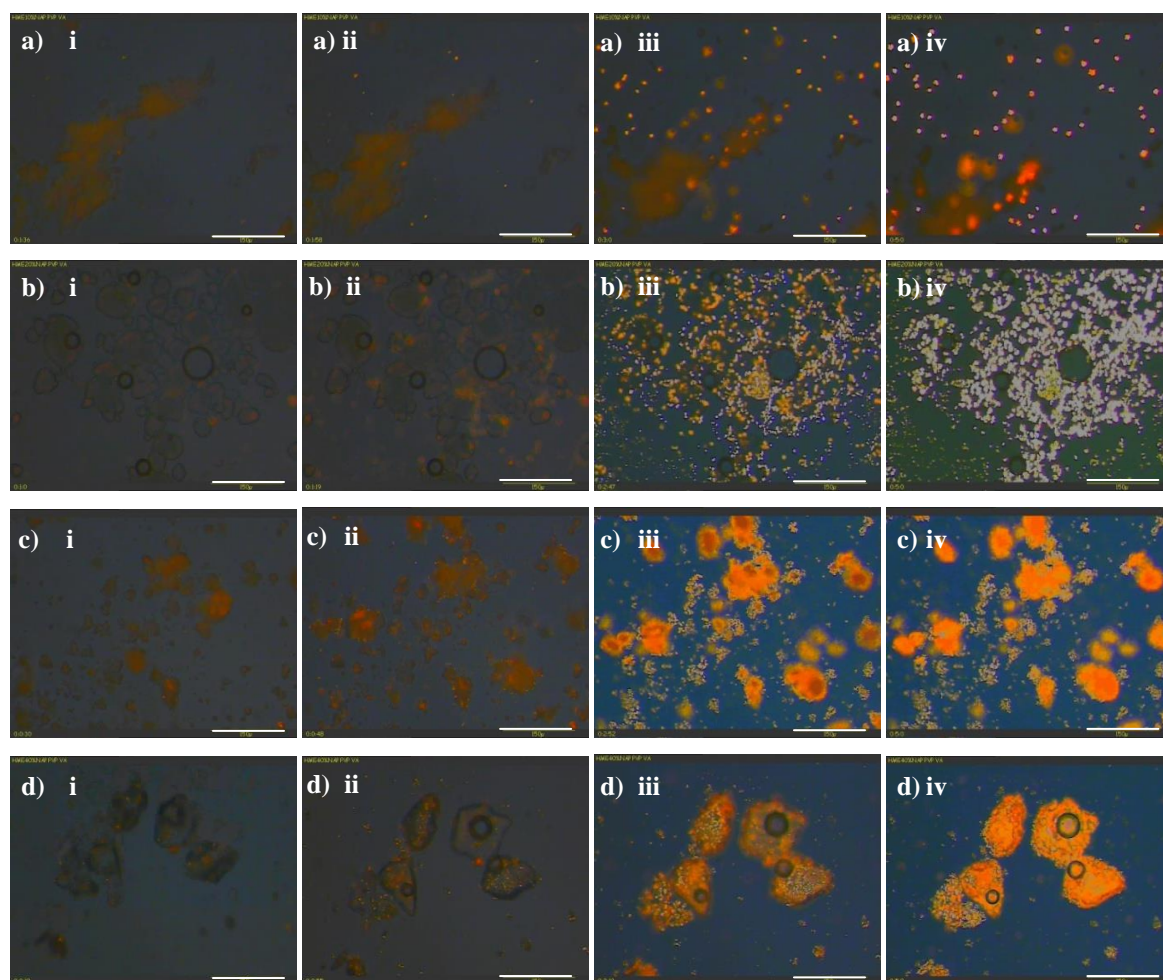


Figure 6.11: Hot stage microscopy examination of HME a) 10%, b) 20%, c) 30% and d) 40% of NAP PVPVA 6:4 upon contact with 0.1M HCl at room temperature. Left to right of each row shows the change in appearance of the ground extrudates upon contact with dissolution medium at various time point, a) i =96s, a) ii=118s, a) iii = 3min, a) iv = 5 min, b) i =60s, b) ii=79s, b) iii = 3min, b) iv = 5 min, c) i =45s, c) ii=48s, c) iii = 3min, c) iv = 5 min, d) i =10s, d) ii=55s, d) iii = 3min, d) iv = 5 min. All the captured images are under magnification of 20x (the white scale bar at right bottom corner indicates 150 μm)

Based on Figure 6.11, birefringence of the recrystallized NAP was clearly noted in all the HME 10-40% NAP-PVPVA 6:4 samples. The refracted birefringence of the wetted HME 10-40% NAP-PVPVA 6:4 particles became more intense with time due to the continuous recrystallization (from left to right in Figure 6.11). By comparing different NAP loadings, 10% loading of NAP revealed the smallest sizes and the least birefringence of the particles (Figure 6.11 (a) to (d)). The birefringence and size of the recrystallized particles increased accordingly with drug loading 40% ($\approx 300 \mu\text{m}$) > 30% ($\approx 100 \mu\text{m}$) > 20% ($\approx 50 \mu\text{m}$) > 10% ($< 10 \mu\text{m}$) of HME NAP-PVPVA 6:4 which was consistent with the results from the laser diffraction technique with the exception of the 10% formulation. This was due to the different hydrodynamic surrounding in the cuvette of the laser diffraction experiment.

Table 6.6 summarises the onset time of birefringence when the HME 10-40% NAP-PVPVA 6:4 were exposed to their dissolution medium. The onset time in revealing birefringence was in the trend of 40% < 30% < 20% and < 10% HME NAP-PVPVA 6:4 which implied the trend of

recrystallization in the reverse, i.e. 40% > 30% > 20% and >10% upon contact with dissolution medium.

Table 6.6: onset time of birefringence upon contact with dissolution medium as recorded via HSM

HME NAP loading PVPVA 6:4 system (%)	Onset time of birefringence (seconds)
10	118
20	79
30	45
40	10

To summarise, higher NAP loading in HME PVPVA 6:4 indicated higher tendencies of agglomeration and recrystallization which could be a possible factor in reducing the dissolution rate of NAP in HME system, although these effects of NAP loading was hardly seen in PM systems.

6.3.2.2. Dissolution study of HME 30% NAP using different MW of PVPs carriers

There is some contradiction regarding the impact of MW on dissolution performance of SD in the available literature. On one hand, dissolution rate of SD was shown to inversely proportional to the MW of carrier (Tantishaiyakul et al., 1999, Doherty and York, 1987). On the other hand, other studies have shown that dissolution rate of SD of poorly soluble drug was directly proportional to the MW of the carrier (Kapsi and Ayres, 2001). Therefore, the effect of different MW of PVPs carriers in dissolution performance of SD was further investigated in this chapter. Figure 6.12 shows the dissolution profiles of HME 30% NAP in different PVPs carriers.

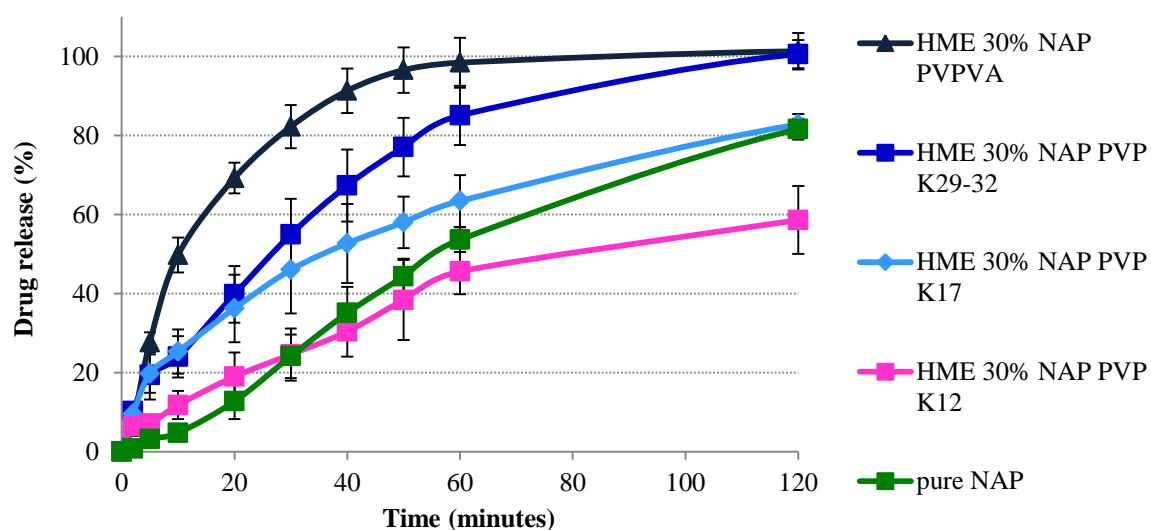


Figure 6.12: Dissolution profiles of HME 30% NAP with different PVPs carriers (PVP K12, PVP K17, PVP K29-32, PVPVA 6:4) in 0.1M HCl at 37 °C.

According to Figure 6.12, it was found that high MW PVP homopolymer carriers, i.e. PVP K29-32 give rise to higher dissolution rate of HME NAP as compared to the low MW PVP, i.e. PVP K12. In dissolution profile of HME NAP-PVP K12, only 45% of the NAP was released after 60 minutes of the dissolution process. The result shows the higher dissolution rate of HME NAP SD in higher MW carrier systems, which was in agreement with Kapsi et al., 2001 where the author found a considerably improved in dissolution of drug with increasing MW of PEG. However, this result is in contrast to the better wetting of PVP K12 than the PVP K17 and PVP K29-32 system that was deduced from Table 6.5. Thus, the low release rate of NAP in the low MW PVPs of HME system may be associated to the low viscous hindrance of the low MW PVPs in their solution, which causes an inability to prevent the agglomeration and recrystallization during the dissolution process.

Furthermore, the similar K-values of PVPVA and PVP K29-32 indicate their similar viscosities, which might imply their similar ability in hindering the possible limiting steps of agglomeration and recrystallization during the dissolution process. However, this is not the case, because HME 30% NAP-PVPVA 6:4 system revealed a higher dissolution rate than the HME 30% NAP-PVP K29-32. 100% NAP release was achieved after 60 minutes of dissolution of HME 30% NAP-PVPVA 6:4 system. Thus, the viscous hindrance of the polymer carriers might not be the sole governing factor in the dissolution performance of HME NAP-PVPs. This phenomenon will be further investigated in the coming sections.

6.3.2.2.1. Surface properties of HME and PM of NAP in different PVP polymers

It is worth paying attention to the dissolution profiles difference between the HME and their PM systems. To simplify the comparison, Figure 6.13 relates the initial dissolution rate of HME 30% NAP-PVPs and PM 30% NAP-PVPs according to their different MW of PVPs.

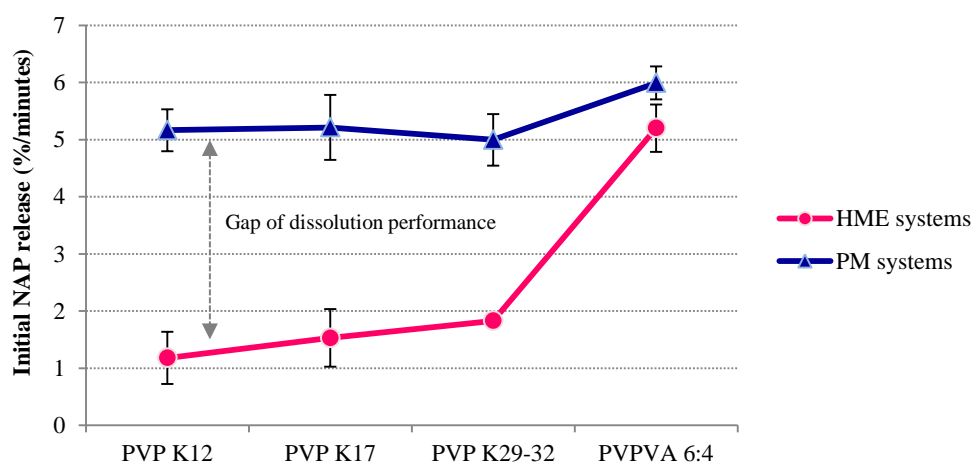


Figure 6.13: The comparison of initial dissolution rate (at linear release of NAP in the first 10 minutes) between HME and PM system of NAP in different PVPs carriers system

There are gaps to dissolution performance between the PM and HME systems of different PVPs as shown by the arrow in Figure 6.13 which were noted to decrease with the increase in MW of the PVPs carrier. These gaps of dissolution performances may be related to the potential drawback of reduced wetting in HME systems as compared to their corresponding PM system which has been concluded in Chapter 5. Hence, the comparison of surface properties between the PM and HME systems were investigated by interfacial tension of the solid phase to the 0.1M HCl (abbreviated as solid system / 0.1M HCl) calculated from the contact angle data (not shown) as described in Chapter 6.2.6. Table 6.7 lists the values of interfacial tension for the HME NAP-PVPs / 0.1M HCl and the difference of interfacial energies between the PM / 0.1M HCl and HME / 0.1M HCl.

Table 6.7: Interfacial tensions of different HME NAP-PVPs system between their solid phase and 0.1 M HCl

NAP	Interfacial tension between the formulation systems and 0.1M HCl, γ_{sl} (mJ/m ²)		
	PM	HME	$\Delta \gamma_{sl}$
NAP	26.98740738	-	-
Binary system	PM	HME	$\Delta \gamma_{sl}$
NAP PVPVA 6:4	9.46	13.40	3.94
NAP PVP K12	8.29	20.28	11.99
NAP PVP K17	10.36	15.40	5.04
NAP PVP K29-32	14.52	15.22	0.7

It is worth emphasizing the interfacial energy presented in Table 6.7 might not be the exact interfacial energy of the powder solid with its dissolution medium as these values were calculated from the contact angle experiments that were performed on surface of compressed tablets. However, relative values of these systems are useful to understand the relative wettability of these systems upon dissolution.

Based on interfacial tension values, γ_{sl} in Table 6.7, PM NAP-PVP K12 / 0.1M HCl exhibited the highest extent of interfacial tension reduction as compared to NAP / 0.1M HCl. This means that the PM of NAP-PVP K12 system possessed the highest increase in wettability among the different polymer types. However, the same binary NAP-PVP K12 system in its HME / medium showed the lowest reduction in interfacial tension among the HME different carrier / 0.1 M HCl. This indicated the highest wettability deterioration in the binary NAP-PVP K12 system after formulating into the HME system (Chibowski and Perea-Carpio, 2002). The differences of interfacial tension between the PM and HME was in the rank of PVP K12 > PVP K17 > PVPVA 6:4 and > PVP K29-32 which indicates the rank of wettability reduction of the HME systems.

Polymer orientation with its hydrophilic moieties facing the surface of the solid might responsible to the reduced contact angle of the PM in comparison to the HME system which has its polymer

coordination restricted due to API-polymer interaction (Dahlberg, 2010). Following this hypothesis, the highest interfacial tension in HME NAP-low MW PVP system shall indicate the highest interaction between the NAP and the lower MW PVP of HME system as compared to other carrier system. However, the intensity of interaction between the NAP and different MW PVPs polymers in the ATR-FTIR study was not convincing in drawing this conclusion (data not shown). Thus, this might serve as a ramification for future study.

6.3.2.2.2. Agglomeration

During the dissolution process of HME NAP different MW PVPs, big particles were also noted in dissolution medium. The changes in the sizes of these particles were analysed by using laser diffraction particle size analyser. Figure 6.14 displays the changes of particle sizes during dissolution experiments of HME 30% NAP of different MW PVPs for up to 1 hour detected by laser diffraction analysis.

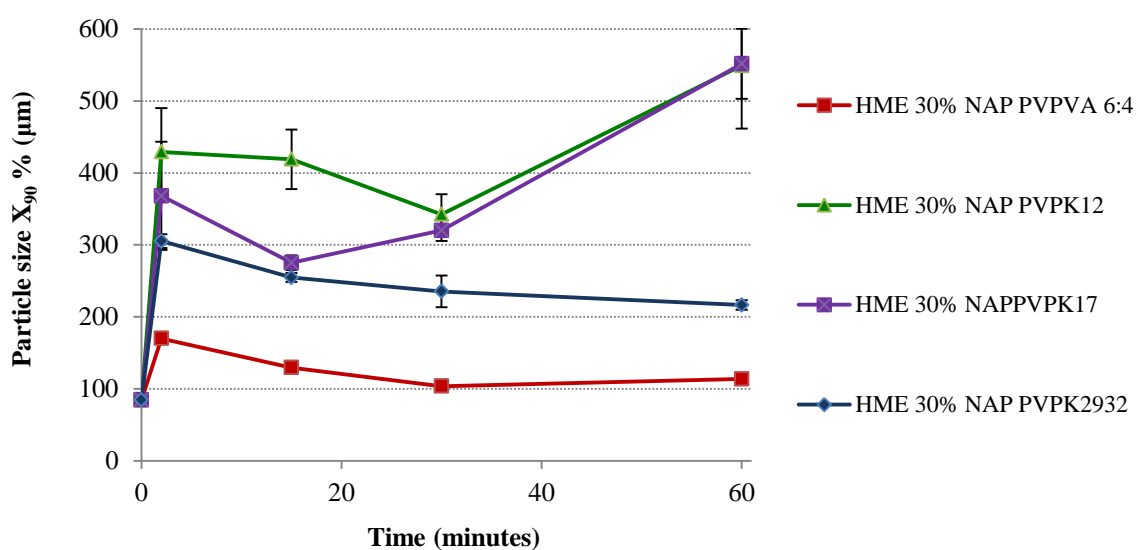


Figure 6.14: Particle size changes of formulation during dissolution experiment.

A dramatic increase in particle size of HME NAP-carriers was noted in all the dissolution experiment of HME system (Figure 6.14). Bigger size of particles were detected in the dissolution medium of HME 30% NAP with lower MW carrier which showing the trend of PVP K12 > PVP K17 > PVP K29-32 and > PVPVA 6:4. This might be due to their higher surface energy of HME 30% NAP with lower MW carrier systems that lead to the agglomeration via hydrophobic forces in order to reduce their energy level (Sievens-Figueroa et al., 2012).

6.3.2.2.3. Recrystallization

The recrystallization of NAP in HME NAP-different PVPs systems upon contact with the dissolution medium was also studied by using HSM. Figure 6.15 shows the images of the ground extrudates after 48 seconds of medium contact.

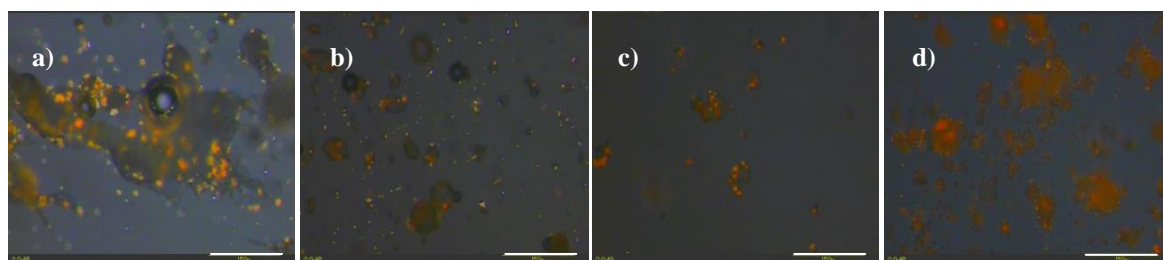


Figure 6.15: Microscopic images of HME 30%NAP with a) PVP K12, b) PVP K17, c) PVP K29-32, and d) PVPVA 6:4 after addition of 0.1M HCl at 48 seconds. All the captured images are under magnification of 20x (white horizontal line at right bottom corner indicated 150 μ m)

Based on Figure 6.15, PVP K12 reflected the highest intensity of birefringence after 48 seconds of medium contact (Figure 6.15 (a)). This is followed by PVP K17, K29-32 and PVPVA 6:4. The times taken in reflecting their birefringence were tabulated in Table 6.8.

Table 6.8: Onset time of birefringence base on HSM studies of HME 30% NAP-PVPs systems

HME NAP-carrier system (63-106 μ m)	Time revealing birefringence (seconds)
PVP K12	22
PVP K17	32
PVP K29-32	34
PVPVA 6:4	45

Based on Table 6.8, the earliest onset of birefringence was recorded for HME NAP-PVP K12 carriers system, i.e. at 22 seconds, followed by PVP K17 > PVP K29-32 > PVPVA 6:4 (Table 6.8). Thus, the recrystallization trend of HME NAP different carriers is PVP K12 > PVP K17 > PVP K29-32 and > PVPVA 6:4. This trend is inversely related to the dissolution rate of HME NAP PVPs SD system as shown in Figure 6.12. Therefore, it is suggested that the slow dissolution rate of HME NAP-PVPs SD could also be ascribed to the fast recrystallization of NAP. This is particularly occurred in the low MW PVPs carrier due to their limited ability in recrystallization inhibition of the particles during the dissolution process.

6.3.2.3. Dissolution studies of HME 30% NAP-PVPVA 6:4-2% and 10% Tween 80

Previous sections have identified the agglomeration and recrystallization of HME formulations during dissolution process as being the limiting steps in dissolution enhancement of HME NAP PVP formulations. To counterbalance these limiting steps, incorporation of a surfactant into the extrudate was attempted. This was performed in order to reduce the driving force of agglomeration and recrystallization of the particles (de Waard et al., 2008) as well as to increase the wetting effect of the HME system during dissolution process.

The freshly prepared HME 30% NAP-PVPVA 6:4-surfactant shows halo pattern in XRPD and no detected melting peak associated with the melting point of crystalline NAP in their DSC thermograms (Appendix V). This suggested the amorphous nature of the HME 30% NAP-PVPVA 6:4-surfactant samples. To test the dissolution behaviour of HME 30% NAP-PVPVA 6:4-Tween 80 system, dissolution experiment in the 0.1M HCl was performed. Figure 6.16 compares the dissolution profiles among PM binary 30% NAP-PVPVA 6:4, PM ternary system (NAP-PVPVA 6:4-Tween 80), HME 30% NAP-PVPVA 6:4 and HME 30% NAP-PVPVA 6:4 -Tween 80 system.

According to Figure 6.16, dissolution profiles of HME 30% NAP-PVPVA 6:4 -10% Tween 80 and HME 30% NAP-PVPVA 6:4 -2% Tween 80 have shown an improved the dissolution rates of NAP as compared to the HME NAP-PVPVA 6:4 system without surfactant. 100% and 90% of NAP were released after 30 minutes dissolution of HME 30% NAP-PVPVA 6:4 -10% Tween 80 and HME 30% NAP-PVPVA 6:4 -2% Tween 80, respectively (blue and red lines, respectively in Figure 6.16).

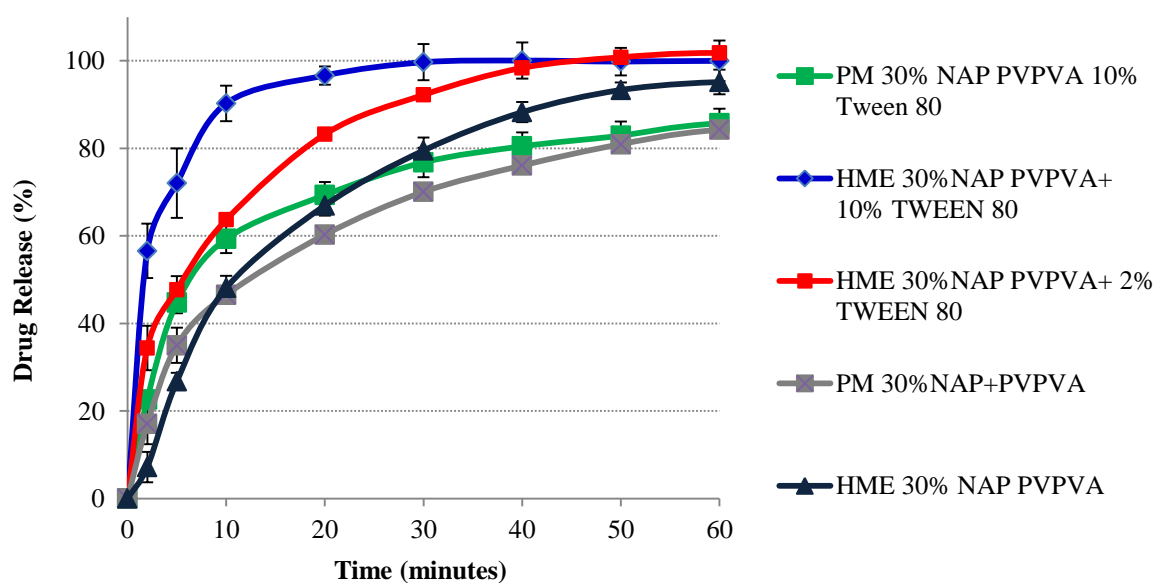


Figure 6.16: Dissolution profiles of PM NAP PVPVA 6:4, PM NAP PVPVA 6:4-Tween 80, HME NAP-PVPVA 6:4, and HME NAP-PVPVA 6:4 -Tween 80 in 0.1M HCl at 37 °C.

The increase dissolution rate of the HME NAP-PVPVA 6:4- surfactant system as a result of micelle solubilisation effect of the NAP by the Tween 80 was excluded as the concentration of tween 80 was lower than its CMC in the dissolution medium (Sjokvist et al., 1992, Ghebremeskel et al., 2007). This can be further confirmed by the limited increase in dissolution rate of the PM NAP-PVPVA 6:4-Tween 80 ternary systems (green line in Figure 6.16). Therefore, the increased dissolution rate of NAP in the HME-surfactant extrudate might be mainly attributed to the reduced agglomeration and recrystallization of particles in the presence of Tween 80 during the dissolution process. These agglomeration and recrystallization of particles will be further confirmed in Chapter 6.3.2.3.1 and 6.3.2.3.2, respectively.

6.3.2.3.1. Agglomeration

The effect of Tween 80 in the agglomeration of the HME-Tween 80 particles during the dissolution process was accessed using laser diffraction. Figure 6.17 and Table 6.9 compare the cumulative curves of particle size distribution of the aggregates within the dissolution bath.

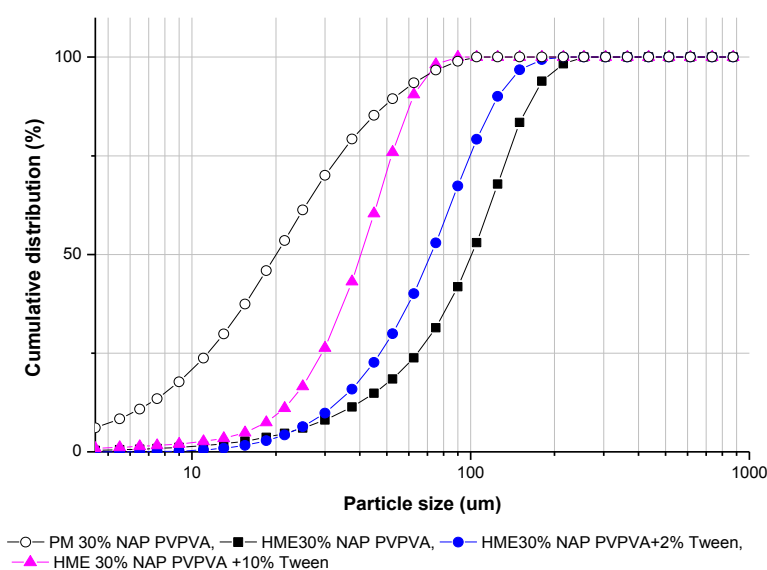


Figure 6.17: Cumulative curves of particle size analysis of PM and HME SD of NAP PVPVA 6:4 and HME NAP-PVPVA 6:4-Tween 80 systems after 2 minutes of dissolution

Table 6.9: Particle size distribution of formulation after 2 minutes of dissolution experiment

Formulations	D _{10%}	D _{50%}	D _{90%}	Span
PM 30% NAP-PVPVA 6:4	6.31 ± 0.147	20.01 ± 0.168	54.51 ± 2.372	2.409
HME 30% NAP-PVPVA 6:4	34.57 ± 0.730	101.03 ± 3.539	170.1 ± 14.427	1.342
HME 30% NAP-PVPVA 6:4 +2% Tw	30.26 ± 0.044	72.71 ± 0.399	128.78 ± 3.553	1.355
HME 30% NAP-PVPVA 6:4 +10% Tw	20.87 ± 0.704	40.86 ± 1.240	65.01 ± 3.129	1.080

Larger particles were also noted in the dissolution experiment HME NAP-PVPVA 6:4-surfactant systems which indicating agglomeration of the particles to a certain extent in these systems. After 2 minutes of dissolution process, the average particle size noted in the dissolution vessel was $101.03 \pm 3.539 \mu\text{m}$ for the HME system without surfactant. This number was reduced to $72.71 \pm 0.399 \mu\text{m}$ and $40.86 \pm 1.240 \mu\text{m}$, respectively, when 2% and 10% of Tween 80 were incorporated into the HME NAP-PVPVA 6:4 systems. Thus it is deduced that the addition of surfactant in the extrudate formulation has effectively reduced the agglomeration of the dissolving particle.

It is worth paying attention to the comparison of particle size between the PM and the HME system without surfactant (Figure 6.17). Although, HME system displayed a much bigger particle size than its corresponding PM system, however both systems revealed superimposable dissolution profiles as shown in Figure 6.16. This infers the possible dissolution advantages of amorphous in HME NAP PVPVA 6:4 during the dissolution process of which will be further examined in Chapter 6.3.3.

6.3.2.3.2. Recrystallization

Since addition of surfactant was reported to potentially reduce recrystallization of API (de Waard et al., 2008). In this section, the onset of recrystallization of NAP was accessed using HSM. Figure 6.18 indicates images captured from the HME 30% NAP-PVPVA 6:4-Tween 80 upon medium contact.

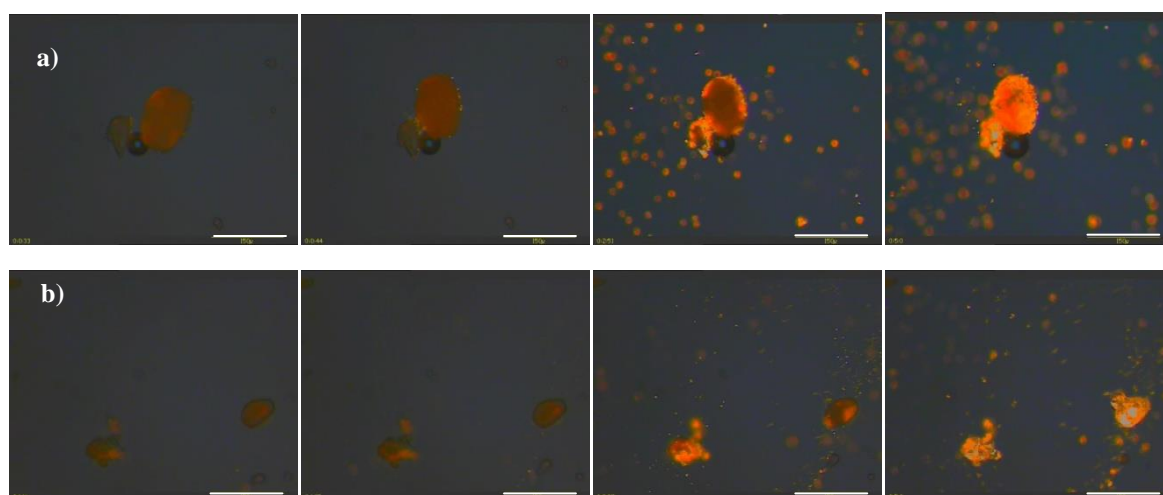


Figure 6.18: Hot stage microscopic observations of a) HME 30%NAP PVPVA +2% Tween 80 , b) HME 30%NAP PVPVA +10% Tween 80 upon contact with 2 drops of 0.1M HCl. Images in the corresponding row from left to right indicated the time increase of the sample contact with 0.1 M HCl up to 5 minutes. All the captured images are under magnification of 20x (white horizontal line at right bottom corner indicated 150 μm)

HME formulation of 30% w/w NAP-PVPVA 6:4 without surfactant shows birefringence of NAP crystal after 45 seconds of medium contact (images not shown). Similarly, HME 30% NAP-PVPVA 6:4-2% Tween 80 formulation revealed birefringence of the particle after 45 seconds of medium contact (Figure 6.18 (a)). Given the similar onset time of birefringence (based on HSM) were seen between HME 30% NAP-PVPVA 6:4-2% Tween 80 and HME 30% NAP-PVPVA 6:4 without surfactant, the former system revealed a faster dissolution rate of NAP (Figure 6.16). Thus, it is suggested that the faster release of NAP in HME 30% NAP-PVPVA 6:4-2% Tween 80 is mainly ascribed to the reduced agglomeration of this system during the dissolution process (as indicated from the particle size analysis of Figure 6.17 and Table 6.9).

Based on HSM images in Figure 6.18, a prolonged onset time of birefringence (≈ 85 seconds) was recorded for HME 30% NAP-PVPVA 6:4-10% Tween 80 formulations (Figure 6.18 (b)). This observation supports the enhanced dissolution rate of NAP in the HME 30% NAP-PVPVA 6:4-10% Tween 80 as shown in Figure 6.16, which suggested that the increase dissolution rate of NAP is also attributed to the slower recrystallization of NAP during dissolution.

To summarise, the addition of Tween 80 to the HME extrudates of NAP-PVPVA 6:4 has improved the dissolution rate of the HME NAP-PVPVA 6:4 system by reduce the recrystallization, agglomeration and increase dispersibility of the system while dissolution process.

6.3.3. Dissolution study of partially crystalline NAP-PVPVA 6:4 system

Previous sections (Figure 6.7 and 6.12) show the dissolution profile of fully amorphous HME NAP-PVPs system being slower than its crystalline counterpart, particularly for HME 30% NAP-PVP K12 system. Thus, the dissolution advantage of amorphous system is questionable. To further investigate this, the dissolution advantages of amorphous state of the HME NAP-PVPVA 6:4 system right after processing was explored.

To do this, dissolution behaviour of a control system which possess a partially crystalline NAP in PVPVA 6:4 was assessed and compared its dissolution performance to the HME fully amorphous system. The partially crystalline formulation (IM 30% NAP-PVPVA 6:4) was prepared by injection moulding with temperature lower than the melting of NAP i.e. at 130 °C. Figure 6.19 compares the dissolution profiles of the freshly prepared HME fully amorphous NAP-PVPVA 6:4 and partially amorphous NAP-PVPVA 6:4 systems as compared to their corresponding PM system.

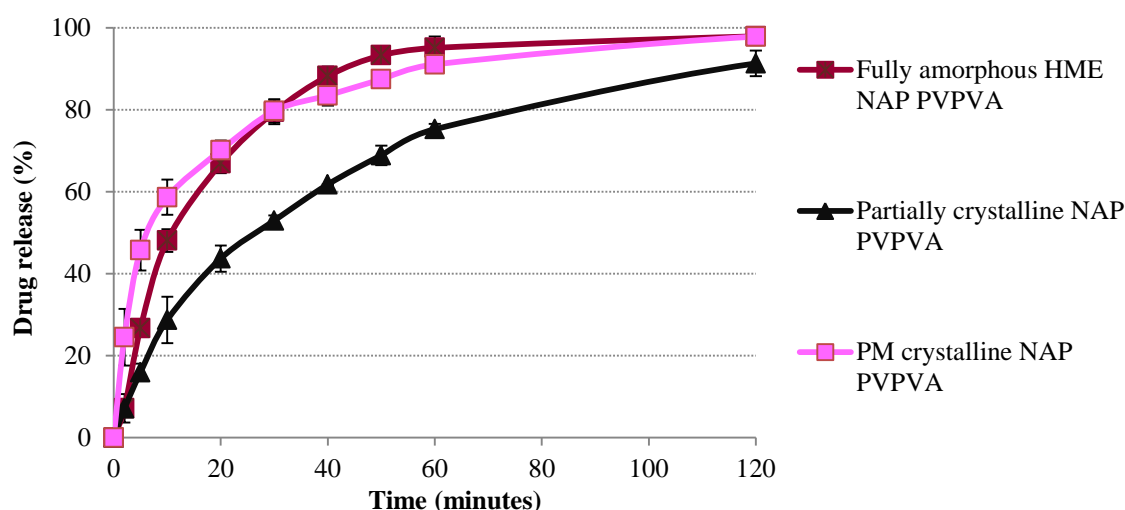


Figure 6.19: Dissolution profiles of the freshly prepared fully amorphous HME NAP PVPVA 6:4, partially amorphous NAP PVPVA 6:4 systems and the corresponding PM systems in 0.1 M HCl at 37 °C.

From Figure 6.19, a decreased in dissolution rate of NAP was noted in the partially crystalline NAP PVPVA 6:4 (black line) as compare to the fully amorphous HME NAP-PVPVA 6:4 (red line). This data clearly showed that the presence of crystalline material did slow down the release rate of NAP which confirmed the importance of the amorphous nature of poorly soluble drugs in a freshly prepared HME SD. However, when the dissolution profile of the partially crystalline NAP-PVPVA 6:4 was compared to the PM, a reduced rate of NAP release was also observed despite the higher crystallinity of NAP in the PM NAP-PVPVA 6:4 system (pink line). This might be attributed to a more extensive agglomeration and recrystallization of the partially crystalline system as compared to the PM and the fully amorphous HME system. Furthermore, the pre-existing NAP crystalline material in the partially crystalline systemt may serve as the crystal seeds that drive the agglomeration and recrystallization of the highly energetic amorphous fraction of the particles.

To summarise, the amorphous form of an API did play a significant role in dissolution enhancement of poorly soluble drug. However, dissolution advantages of the amorphous state could be potentially affected by agglomeration and recrystallization process of the amorphous particles, which might be extensive in a partially crystalline system.

6.4. Discussion

As shown in Chapter 5, dissolution performance of the HME PVP-based systems is highly dependent on type of API as the amorphous form of the API determines its amorphous advantage in SD while dissolution process. However, detail understanding on the other possible factors in affecting the dissolution performance of a SD is also essential for the production of a successful SD as far as immediate release dosage form is concerned.

In this study, several factors of influencing the dissolution performance of SD have been identified. These include the solubilizing and wetting effects of the polymer carrier, amorphous dispersed systems, and solution mediated process such as agglomeration and recrystallization. Among all the previously mentioned factors, there is no sole determinant for dissolution of a particular substance. Often the resultant dissolution profiles reveal the interplay of several mechanisms.

6.4.1. Dissolution process of PM

Based on the dissolution studies of PM NAP-PVPVA 6:4 system, dissolution rate of the crystalline NAP could be enhanced via increase wetting, solubilising of NAP by the addition of hydrophilic polymers. In this context, the wetting effect of polymer onto NAP is more prominent in PVPVA 6:4 and PVP K12 than in PVP K17 and PVP K29-32 carriers due to the reduced surface tension of the polymer solutions of the former. On the other hand, the solubilising effect on NAP was shown to be pronounced in PVP K17 and PVP K29-32 which have led to the similar dissolution profiles of NAP in all the PM NAP-different PVP polymers. Dissolution of the PM system will be further discussed in comparison to the dissolution behaviour of its HME system. At the end of this discussion, a comparison between the dissolution mechanism of PM and HME will be provided.

6.4.2. Different drug loadings of HME NAP-PVPVA 6:4

The study of different NAP loading has shown that low loading of NAP lead to higher dissolution rate of NAP. This is due to the higher proportion of the polymer with its higher viscosity that were created surrounding NAP particles which could reduce the recrystallization and agglomeration of NAP during the dissolution process.

Besides, 30% of NAP was found to be the critical loading of API that leads to a faster dissolution rate of HME system in comparison to the corresponding PM. This observation has also been reported in a study of SD with alkyl p-aminobenzoates (PABA) using polyethylene glycol as the carrier, where 50% of PABA was the critical API loading that led to no additional advantages in the dissolution increment of the SD system (Saers and Craig, 1992). In this study, the critical loading of NAP was found to be highly dependent to the extent of solution mediated phase transformation such as agglomeration and recrystallization of API during dissolution. The agglomeration tendency is mainly attributed to the hydrophobic force which increases with the higher loading of NAP. As a result, intense recrystallization of NAP in the highly agglomerated particle could also occur. This may be pronounced especially in API with high crystallization tendency such as NAP in this study (Baird et al., 2010).

6.4.3. Different carriers

In this study, PM of NAP in different PVPs showed similar dissolution profiles. However, HME of NAP in different PVPs revealed a trend of NAP release rate. The dissolution rate was highest in NAP-PVPVA 6:4 > followed by NAP-PVP K2932 > NAP-PVP K17 > NAP-PVP K12. This trend is closely related to the viscosity (indicated by K-values) of the carriers used. Higher MW of PVPs develops a higher resistance against recrystallization and agglomeration which was shown by the lower birefringence and particle size in HME NAP high MW carrier systems (Yagi et al., 1996, Mokarram et al., 2010b). Hence, in HME system, high dissolution rate of the homopolymer PVP is not favourable for the dissolution process of HME NAP SD, as the highly soluble polymer will dissolve quickly and leave the poorly soluble NAP dispersed in the dissolution medium for its solution mediated phase transformation such as extensive agglomeration and recrystallization.

Besides, the hydrophobic vinyl-acetate group in PVPVA 6:4 has rendered the more surface active properties of PVPVA 6:4 as compared to the homopolymer PVPs. This is evidenced by the lower surface tension of PVPVA 6:4 solution as compared to the homopolymer solutions. Thus, HME systems of PVPVA 6:4 was shown to have lowest interfacial tension between the solid phase (HME) and the PVPVA 6:4 medium phase, thereby gave rise to the highest dissolution rate of HME NAP PVPVA 6:4 amongst all the HME NAP SDs. This result was in contrast to a published paper in comparing the dissolution performance of HME ketoconazole-PVP K17 and ketoconazole-PVPVA 6:4. In that paper, the PVP K17 was showed to be better than PVPVA 6:4 in stabilizing the supersaturated ketoconazole created from the SD (Kanaujia et al., 2010). This might be due to the low crystallization tendency of the ketoconazole as compared to the high recrystallization tendency of NAP that was employed in the current investigation (Baird et al., 2010, Tajarobi et al., 2011a).

Furthermore, the hydrophobicity of vinyl acetate group in PVPVA 6:4 polymer could also enables its adsorption on the hydrophobic surfaces and sites of newly recrystallized growing unit of the poorly soluble API, which subsequently delayed the potential of nucleation and recrystallization process (Ilevbare et al., 2012b). Thus, it is suggested that certain extent of hydrophobicity in the polymer carrier such as PVPVA 6:4 is beneficial for crystallization inhibition and optimal dissolution rate enhancement of an amorphous SD.

6.4.4. The effect of Tween 80 in the HME extrudates on dissolution behaviour of HME NAP-PVPVA 6:4-surfactant system

To reduce the solution mediated phase transformation (agglomeration and recrystallization) during the dissolution of the SD system, surfactant was incorporated into the HME extrudate. It was found that the incorporation of surfactant into the HME SD did not only ease the processing condition (Fernandez et al., 1989, Ghebremeskel et al., 2007, Ghebremeskel et al., 2006, Soontravanich and Scamehorn, 2010), but also maintain the dissolution performance of SD. In this context, instead of having the superimposable dissolution profiles between the PM and HME, dissolution rate of NAP in HME 30% NAP-PVPVA 6:4-Tween 80 was found to be faster than its PM system (Figure 6.16). According to Fernandez et al.(1989) the incorporation of Tween 20 or 80 can allow the higher loading of API in a SD for a carrier controlled dissolution mechanism (Fernandez et al., 1989). This agreed to our results as the increased dissolution rate of NAP in HME 30% NAP-PVPVA 6:4-Tween 80 implying that the critical loading of NAP has shifted to a higher loading, at least > 30% loading of NAP after the addition of Tween 80 in the HME extrudate SD.

Besides, the increased dissolution rate of NAP after incorporation of Tween 80 in the HME extrudates of this study shows agreement to the studies carried out by Ghebremeskel et al., 2007 and Ghebremeskel et al., 2008. In those studies, increased dissolution rate of poorly soluble API after the incorporation of Tween 80 into its SD was also noted as long as the concentration of the surfactant is below its CMC value during dissolution process. The author suggested that surfactant acts via microenvironment modulation by enhancing the apparent solubility of the API molecules at dissolving front of the particle which in turn reduce the degree of supersaturation of the API and the driving force for nucleation and crystallization process. Similar observations of increased dissolution rate were also noted in a study of fenofibrate sugar-based SD after the addition of SLS (de Waard et al., 2008). In that study, the author suggested that effective prevention of API crystallization during dissolution process was noted with the incorporation of SLS in the SD formulation. Conversely, the prevention of API crystallization during dissolution was not significant when the SLS was added physically (de Waard et al., 2008). This observation is in parallel to the result obtained from this study as PM ternary NAP-PVPVA 6:4-Tween 80 did not reveal a similar dissolution advantages as could be seen in HME NAP-PVPVA 6:4-Tween 80 (Figure 6.16) when these profile were compared to the dissolution performance of the corresponding HME system without Tween 80.

The surfactant is also playing a role in the prevention of aggregation and agglomeration of drug particles (Swanepoel et al., 2000) as could be seen by the increase dissolution rate of HME NAP-PVPVA 6:4-2% Tween 80 despite the similar onset of recrystallization with HME NAP-PVPVA 6:4 without surfactant (Chapter 6.3.2.3.2 and Figure 6.18). Besides, the increase dissolution of

HME NAP-PVPVA 6:4-2% Tween 80 as compared to HME NAP-PVPVA 6:4 without surfactant could also be due to the change of crystal defect density by surfactant while recrystallization of particles during the dissolution process (Kumar et al., 2008). In this case, surfactant act via step pinning the recrystallization of the API during dissolution process which alter the growth kinetic and dislocate the API molecule in crystal growing process (Qiu et al., 2004). This could cause a change in hillock and crystal shapes which may potentially give rise to better dissolution properties as shown in the dissolution study of the HME NAP-PVPVA 6:4-surfactant formulations despite the detection of crystal traces in these systems during dissolution process (Qiu et al., 2004).

6.4.5. Pathway of dissolution mechanisms in a physical mixture and HME solid dispersion

Combining the results obtained from the dissolution studies of PM and HME NAP-PVP carriers system, it was found that hydrophilic PVPs carrier play a different roles in dissolution process of PM and HME SD systems. Figure 6.20 shows the different pathways taken by a PVP-based PM and HME of a poorly soluble system.

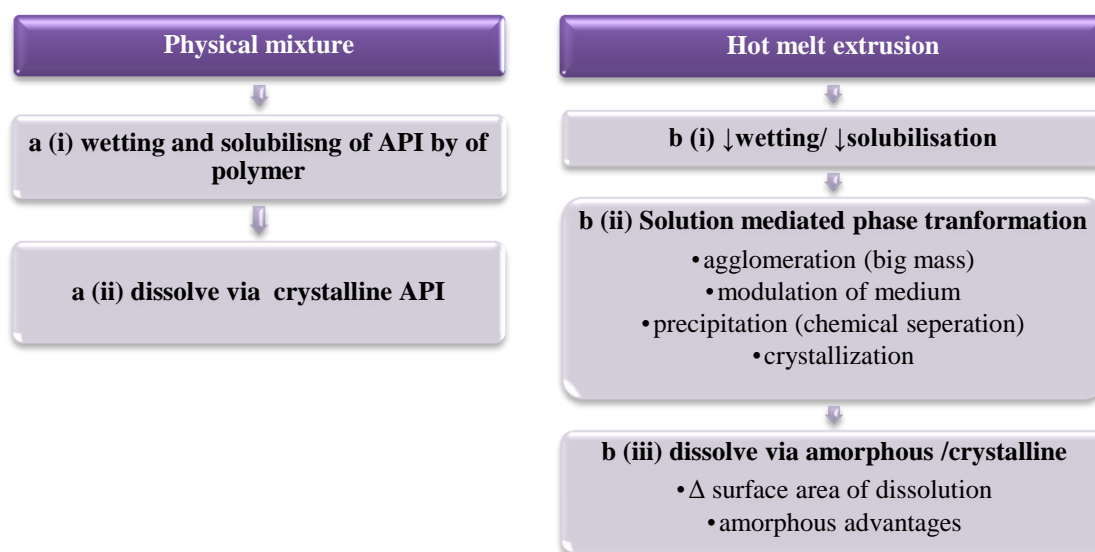


Figure 6.20: Dissolution mechanisms of PM and HME of PVP-based poorly soluble APIs

According to Figure 6.20 a (i), the role of the hydrophilic PVP polymer in PM is merely a wetting and solubilizing agent. However, these roles of the PVP were weakened in HME SD system (Figure 6.20 b (i)) as compared to their PM system. This is due to reduced wettability of this system as could be seen by the higher interfacial energy of the HME system as compare to its PM system (Table 6.7).

Based on the dissolution mechanism as presented in Figure 6.20, there is a distinct step of dissolution (Figure 6.20 b (ii)) involving only the dissolution mechanism of HME PVP-based system but not in the PM, i.e. the step of solution mediated phase transformation. This is the limiting step of dissolution performance of SD, as additional roles of the polymer is required if an immediate release of API is desired. The role of polymer in this step is associated to the effective interruption of the solution mediated phase transformations, i.e. ability in reduce agglomeration, precipitation and recrystallization of the dissolving system. Therefore, the key of dissolution enhancement in SD as compared to its PM is laid in the effective prevention of the solution mediated phase transformations in step (b) ii (Figure 6.20).

The subsequent stages (Figure 6.20 (a (ii)) and (b (iii))) of the dissolution process are highly dependent on the previous steps. Based on the dissolution pathway of HME in Figure 6.20, if an API remains amorphous state devoid any solid state transformation, the enhanced dissolution rate could be retained. In contrast, if the API recrystallize and agglomerate, the resulting dissolution profile would be highly depend on the total surface area of the dissolving surface which could be either dissolve in a similar rate to its PM or slower than that when its total surface area has reduced dramatically due to extensive agglomeration.

6.5. Conclusion

The results obtained in this study suggested that dissolution performance of HME NAP-PVP-based is highly drug loading dependent whereby higher loading of NAP revealed a higher agglomeration and recrystallization tendency. Besides, recrystallization of the poorly soluble NAP during dissolution of the HME NAP-PVPs systems is also closely related to the hydrophobic-hydrophilicity balance, proportion and MW of the polymeric carrier used.

PM and HME NAP PVPs-based systems underwent different pathways of dissolution. The extra solution mediated phase transformations step involving the dissolution of HME NAP products requires the prudent selection of carrier incorporated in this system. Among the tested PVP carriers in this study, PVPVA 6:4 was recognised to be the best carrier for dissolution performance of SD as it revealed lowest extent of solution mediated phase transformations of the studied SD system. In this respect, the solution mediated phase transformations (agglomeration and recrystallization) could be also reduced via incorporation of non-ionic surfactant into the HME formulation which could subsequently maintain the solubility advantage of the amorphous API system. This is an important step in maintaining the effectiveness of solid dispersion for dissolution enhancement.

Chapter 7. Concluding Remarks and Recommendations for Future Work

7.1. Conclusion

Overall, this thesis provides an understanding of the development of PVP-based amorphous solid dispersions prepared using HME processing method, with three main focuses, i.e. manufacturing, physical stability, and performance of formulations.

Chapter 3 investigated the feasibility of using PVP in the HME manufacturing of an interacting API (i.e. PCM) and non-interacting API (i.e. CAF). The first objective of the thesis was addressed in this chapter, where the use of PVP in HME was described to be feasible by applying the phenomenon of ‘melting point depression’. The melting temperatures of the tested APIs were reduced in the presence of PVP polymers which allowed the extrusion process to be carried out at a temperature below the T_g of PVP or T_m of the API. This is particularly useful for API that has a relatively high melting temperature when the extrusion temperature could not be raised above its melting point in the production of the amorphous dispersion, due to the concern over PVP degradation. This lowering of the softening point not only resolves the issues of PVP degradation, but also reduces the risk of the decomposition of the thermolabile API. In addition, the presence of the API plasticised the PVP and hence eases the extrusion process.

Miscibility of API and PVP has reported to be important in the production of amorphous solid dispersions. This could be predicted by using Hansen solubility parameter. In this study, differences in the Hansen solubility parameters ($\Delta\delta$) between drug and polymer were found to be useful in predicting the miscibility of the drug and polymer, in turn leading to a homogeneous amorphous dispersion. In this respect, $\Delta\delta$ of less than 7 MPa^{1/2} indicates miscibility of the two components, whereas the components are not miscible when the $\Delta\delta$ is more than 10 MPa^{1/2} (Forster et al., 2001c). As shown in Chapter 3, extruding the interacting PCM and PVP (which showing a $\Delta\delta$ of less than 7 MPa^{1/2}, miscible) produced fully amorphous dispersion up to 40% and 50% loading of the PCM in PVPVA 6:4 and PVP K29-32 carrier system, respectively. Conversely, extrusion of the non-interacting API, i.e. CAF with PVP ($\Delta\delta > 8$ MPa^{1/2}, limited miscibility) led to the production of a partially crystalline SD. Therefore, in order to produce a fully amorphous HME PVP-based solid dispersion at temperatures lower than the T_m of an API, a miscible API, which was interacting one with respect to PVP carrier, is preferred.

Nonetheless, as shown in Chapter 3, the extrusion of interacting API with PVP polymers at temperatures lower than the T_g of the PVP polymers showed an increase in the torque value over the extrusion time. This implies rheopectic behaviour, i.e. non-Newtonian fluid flow of the molten extrudate. In contrast, shear thinning was observed in the extrusion of non-interacting API with PVP where torque value reduced with time. This parameter is expected to impact on the physical stability of HME SD system which will be further explained in the next paragraphs.

The second area of investigation in thesis is to understand the physical stability of HME PVP-based solid dispersions. Chapter 4 presented the physical stabilities of the interacting API i.e. PCM in HME PVP-based solid dispersions. All extruded systems were found to be highly humidity dependent. The moisture absorbed in the sample has plasticised the SD and caused a certain degree of phase separation in the HME SD system which is the cause of physical instability.

As shown in Chapter 4, hydrogen bonding between the drug and polymer is a critical factor in physical stabilisation of PVP-based dispersion prepared using HME. This is evident in the comparison of recrystallization behaviour between homo-polymer PVP K29-32 and copolymer PVPVA 6:4 carriers for the aged HME PCM extrudates at different PCM loadings. At 50% drug loading, PCM dispersion in PVPVA 6:4 recrystallized faster than in PVP K29-32 SD despite lower water content in the former. This is caused by the insufficiency of proton acceptors that form hydrogen bonds with PCM molecules in the copolymer PVPVA 6:4 as compared to that in the homopolymer PVP. However, at low PCM loadings, i.e. 30%, PVPVA 6:4 carrier systems attained a superior stabilization effect. This was attributed to the optimum drug-polymer interaction as there are sufficient proton acceptors in PVPVA 6:4 that interact with PCM molecule, giving no surplus of free PCM available for the recrystallization process. Hence, it is suggested that the drug loading of an API should be kept below the theoretical limit of its hydrogen interaction with the PVP polymer in order to produce a physically stable HME SD system.

HME systems with a high molecular weight PVP appeared to recrystallize faster than its corresponding composition prepared with lower molecular weights of PVP. This difference correlated well to the torque profiles recorded during the HME preparation process (Chapter 3). The torque value recorded during HME process is a measure of viscosity of the extruded molten. A high torque value implies difficulty in mixing between the drug and polymer. This may minimise the drug-polymer interactions which have been identified to be one of the main factors in maintaining the physical stability of HME PVP-based SDs. However, in order to establish a clearer relationship between the torque and drug-polymer interaction, more extensive studies are needed.

Another specific objective of Chapter 4 is the determination of the critical storage conditions associated with stabilising the HME PVP-based SD. The result of this study suggested that HME PVP-based SD achieved a better stability profile in storage condition with elevated temperature

(i.e. 40 °C) than that with higher humidity (22% RH to 75% RH). Under very humid storage conditions (> 53% RH), the aged extudates underwent physical transformation, changing from solid state (at room temperature) to the rubbery state due to extensive moisture sorption as presented in Chapter 4. This transformation is not favoured as it can affect the performance, particularly in terms of dissolution. Thus, packaging may be a critical step in maintaining a good physical stability of an HME PVP-based solid dispersion.

As discussed in Chapter 1.6, a number of papers have demonstrated the unpredictable trend of dissolution performance for SD system by showing a slower release rate than their corresponding PM systems (Moneghini et al., 1998, Verheyen et al., 2002, van Drooge et al., 2004, Margarit et al., 1994). It was also found in this study that not all the amorphous solid dispersion systems could guarantee a higher dissolution rate of the BCS Class II API as compared to their PM. This is highly dependent on properties of both the API and carrier which were identified in Chapters 5 and 6, respectively.

Chapter 5 of this thesis presented the dissolution behaviours of poorly soluble APIs after the formulation of HME PVPVA based SD which include, ketoprofen (KTP), naproxen (NAP), indomethacin (INDO) and olanzapine (OZP). Based on these studies, factors contributing to the production of an effective SD were identified. These factors include, theoretical ‘solubility advantages’ of amorphous APIs, solubilising capacity of the polymer carrier and wettability of the SD system which promote agglomeration and recrystallization of the SD system during dissolution. These factors are discussed in more details in the subsequent sections.

‘Solubility advantages’ of amorphous APIs

The dissolution performance of a SD is highly drug dependent. Results in Chapter 5 showed that ‘solubility advantages’ ratio of amorphous API calculated from Hoffman equation (Equation 5.1) is the best indicator in formulating a successful solid dispersion, as far as the dissolution enhancement of the poorly soluble API is concerned. This ratio reflects the Gibbs free energy difference between the two solid forms i.e. amorphous form and its crystalline state which dictates whether formulating a solid dispersion is worthwhile. As presented in Chapter 5, a higher ‘solubility advantages’ of OZP gave rise to a dissolution enhancement in its HME OZP PVPVA system. However, lower ‘solubility advantages’ of KTP and NAP lead to only a limited increment in dissolution rates of NAP-PVPVA and KTP-PVPVA systems respectively.

Solubilisation of API in its carrier solution

Based on the classical Noyes Whitney Equation (2.2), the solubility of an API in a dissolution medium can affect its dissolution process. In this study, the solubilisation effect of the carrier on the API (using concentrated PVPVA 6:4 solutions) was found to be more significant to the dissolution performance of the HME system rather than PM system.

As shown in Chapter 5, the high degree of solubility enhancement of OZP in the 10% w/v PVPVA 6:4 polymer solution is one of the contributing factors of the dissolution rate enhancement of HME systems. During the early phase of the dissolution process, a high PVPVA 6:4 concentration is expected to be at the dissolving front of the HME particle. At this early phase, the readily dissolvable amorphous form of API in its HME SD system can immediately initiate the carrier solubilisation effect upon dissolution process which subsequently drives the dissolution of the HME system. This is provided that no other confounding events (such as recrystallization of API) come into play during the dissolution process. However, the increase of dissolution rate was not observed in the PM system. This was largely due to the need for crystal bond breakage of the crystalline OZP in the PM before the effect of carrier solubilisation could exert its influence on the dissolution process. Consequently, it is reasonable to suggest that the strength of a crystalline structure of poorly soluble API is a limiting factor for the dissolution process of its PM system.

Wetting and agglomeration of SD

In this study, the dissolution process was also found to be surface based phenomenon. Often, the presence of a hydrophilic polymer is expected to increase wettability of a system. This was verified for both PM and HME of the API-polymer systems in comparison to their pure API system as presented in Chapter 5.

However, when the wettability was compared between the PM and HME of 30% APIs-PVPVA 6:4 system, the wettability of the HME systems was lower than their corresponding PM systems as indicated by the increase in the contact angle. When a PM system is introduced into a dissolution medium, the polymer carriers can orientate and dissolve into the medium easily. This subsequently increases the wettability of poorly soluble API in by its dissolved carrier. On the other hand, drug-polymer interactions in the HME 30% API-PVPVA 6:4 SD system reduced conformation of the polymer carrier. This has weakened the interaction of the hydrophilic polymer with the dissolution medium which eventually lowered its wettability. Nevertheless, the extruded OZP-PVPVA 6:4 system was an exception which revealed a similar wettability to its PM system, reflecting the originally low wettability enhancement of OZP on contact with the PVPVA 6:4 solution. Thus, any wettability effects of the polymer in the HME system might not be significant.

Low wettability in the HME system suggested strong hydrophobicity with high free energy on its surface. During the hydrodynamic dissolution process, particle collision with their high surface free energy may cause particle aggregation owing to the reduction of their surface-to-volume ratio in reaching the more stable state. This eventually causes agglomeration of the dissolved particles due to the hydrophobic forces on their surfaces as shown in the dissolution process of extruded APIs-PVPVA 6:4 (Chapter 5). This is evident by the growing of particle to a size larger than the initial controlled size range as presented in Chapter 5. Following agglomeration of the dissolving system, its effective surface area exposed to the dissolution medium is reduced hence slowing down the overall dissolution rate.

Recrystallization of API during dissolution

In Chapter 5, recrystallization was clearly observed on the surface of HME particles collected from the dissolution vessel during dissolution. The relative recrystallization tendency of different HME API-PVPVA 6:4 systems did not show a clear trend in dictating their degree of dissolution enhancement in comparison to their PM systems. This was due to the different sensitivity of the amorphous APIs to under the exposure to the dissolution medium and hence different recrystallization behaviours of the APIs that cause their different influences on dissolution enhancement of their HME as compare to their PM systems. However, the recrystallization effect of the API during dissolution process was apparent when focusing on a single API in different carriers or compositions as shown in Chapter 6 which will be further discussed in the subsequent paragraphs.

Chapter 6 of this thesis focused on the dissolution study of formulations with a single API, i.e. NAP. The influences of NAP loading, molecular weight (MW) of PVP carriers and surfactant on the identified dissolution rate limiting processes (i.e. agglomeration and recrystallization of APIs, which were identified in Chapter 5) were studied.

Effect of drug loading

In Chapter 6, the effect of different NAP loadings on dissolution process of HME NAP-PVPVA 6:4 system was investigated. During dissolution process, the dissolution rate limiting processes, i.e. agglomeration and recrystallization were significant especially at high drug loadings. This was due to the higher loading of the hydrophobic API on the surface of the dissolved systems at this loading. The intensity in occurrence of the observed dissolution rate limiting processes causes a

critical drug loading limit of NAP in the HME system that leads to its dissolution advantages over the corresponding PM system. When this critical drug loading limit is exceeded, such as for 30% NAP-PVPVA 6:4, there will be no dissolution enhancement of the HME SD as compared to its PM.

As shown in Chapter 5, naproxen is considered to be a poorly soluble drug with a relatively low 'solubility advantages' of its amorphous state. Thus, these advantages may easily overcome by the minor extent of the dissolution rate limiting process, i.e. agglomeration and recrystallization of HME NAP-PVPVA 6:4 system as shown in its dissolution performances in Chapter 6.

Effect of PVP carrier systems

In the same chapter (chapter 6), the influence of carrier system on dissolution performance of the HME 30% NAP-PVPs-based dispersions was also investigated. In different PVP carrier systems, the relative wettability difference between the PM and HME system might also be different. This was shown in Chapter 6 through examining the interfacial properties of PM and HME of 30% NAP-PVPs in different carrier systems. In this case, a low MW PVP carrier showed a high wettability in the PM system but a low wettability in its HME system. However, this difference in wettability was relatively small in the system with high MW carriers. The reasons behind these differences require further investigations.

Among the tested polymer carriers, PVPVA 6:4 copolymer was proposed as the best candidate for the dissolution performance of HME PVP-based solid dispersion, despite the relatively lower hydrophilic nature of PVPVA 6:4 as compared to the tested homopolymers. The less hydrophilic nature of PVPVA 6:4 (as compared to PVP) has led to its slower dissolution rate which remained its presence at the vicinity of the dissolving amorphous API for a longer period. This promotes the carrier solubilising capacity and ability of PVPVA 6:4 in minimising the extensive agglomeration and recrystallization of the amorphous API via a physical hindrance effect. In addition, the hydrophilic-hydrophobic balance of PVPVA 6:4 has led to its surface active nature, which lowers the agglomeration and recrystallization of its HME system during dissolution. This is another contributing factor for the better dissolution performance of PVPVA 6:4-based HME system as compared to the homopolymeric carriers.

On the other hand, the hydrophilic homopolymer PVP of HME system dissolved quickly. Consequently, the API molecules were isolated which caused extensive agglomeration and recrystallization during dissolution. This is particularly pronounced in low MW carriers of PVP as compared to the high MW PVP. The physical hindrance effect in low MW PVP of HME systems is relatively low, thus the agglomeration and recrystallization may not be effectively reduced as

compared to that of high MW PVP. It is evident in Chapter 6 that the dissolution rate of HME NAP system is lower in the low MW PVP carrier alongside to their higher extent of agglomeration and recrystallization.

Addition of surfactant to the extrudate composition

De Waard et al. (2008) has suggested the addition of a non-ionic surfactant into composition of SD at a concentration below the CMC in order to increase dissolution rate of a SD system (de Waard et al., 2008). In Chapter 6, incorporation of Tween 80 (a non-ionic surfactant) into the composition of NAP PVPVA 6:4 extrudates significantly enhanced the dissolution rate. This could be explained by the reduction of agglomeration and recrystallization during the dissolution process of the PVPVA 6:4-surfactant extrudates. The concentration of surfactant added was below its CMC in the dissolution medium, thus the solubilising effect of the surfactant is expected to be low. However, a transient solubilising effect might be apparent at dissolving front of the HME system which reduces the hydrophobic forces of agglomeration; consequently, this may lead to the reduction in extent of recrystallization and agglomeration as presented in Chapter 6.

Role of amorphous or crystalline states

Chapter 6 also highlighted the roles of amorphicity and crystallinity of NAP in dissolution performance of an immediate release solid dispersion. The importance of amorphicity was confirmed by a reduction in dissolution rate of a partially crystalline NAP-PVPVA system.

Surprisingly, the release of the partially amorphous NAP PVPVA was slower than the PM system with NAP in the fully crystalline form. This implies that the advantage of amorphicity in both the fully and partially amorphous system is not fully apparent as would have been anticipated. This may be due to secondary processes such as agglomeration and recrystallization that negate the advantages of amorphicity during the dissolution process. Therefore, one can conclude that the loss in crystallinity of NAP might be beneficial in aiming for the dissolution enhancement of HME solid dispersion as compared to its PM system but it is not always the case.

The last objective of this thesis was to propose a possible framework of dissolution mechanisms for HME PVP based SD in accordance with the observations in Chapter 5 and 6. In order to visualise the dissolution process, Figure 7.1 illustrates a wetted HME SD particle once it has contacted the dissolution medium. As seen in Figure 7.1, three phases of the particle are identified, i.e. dissolving phase, rubbery phase and un-wetted glassy phase.

When HME SD particles are introduced into a dissolution medium, hydrophilic polymer in the system absorbs a considerable amount of water. At the core, the un-wetted area remains in glassy state. Between the wetted surface and the core of particle, there is an area of rubbery state of the dissolving system as a result of water ingress and exert its plasticization effect. In this area, polymer reptation (thermal motion of a long macromolecule (Dahlberg, 2010)) occurs which increases the local mobility of the SD system. Thus, if the trapped domains of API (from solid dispersion system) obtain sufficient mobility and are close to each other, phase separation can occur. Recrystallization can potentially happen depending on the crystallization tendency and solubility of API in the polymer carrier.

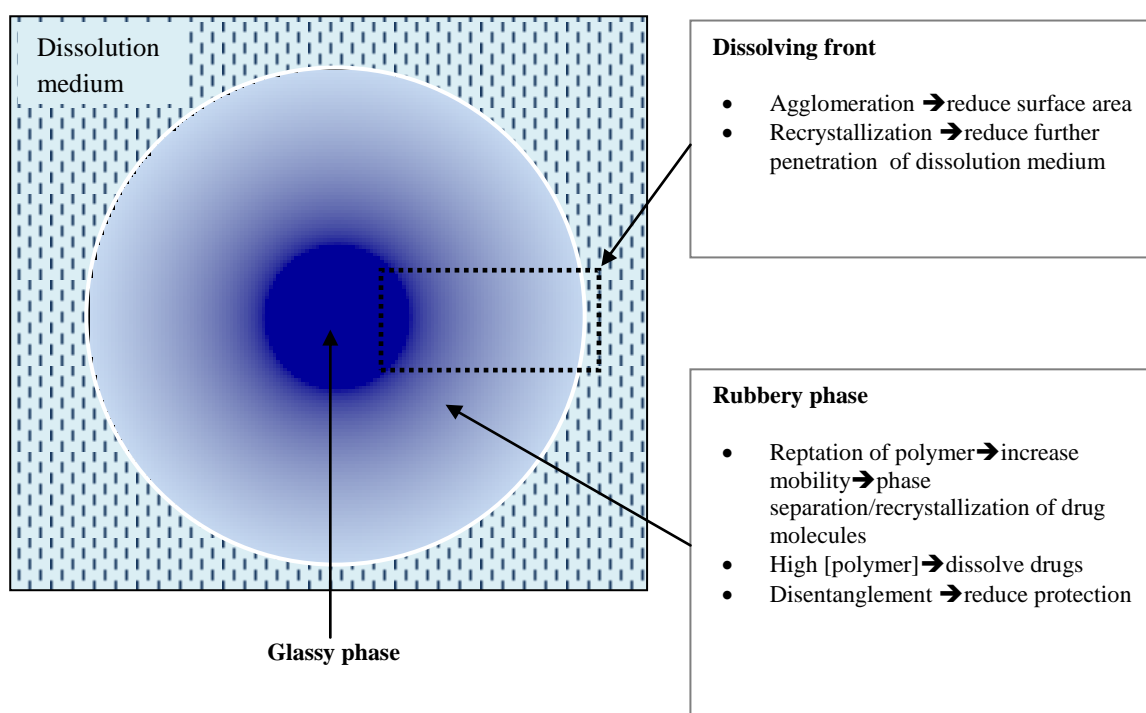


Figure 7.1: Schematic of a wetted particle of HME poorly soluble drug PVP-based solid dispersion when it is in contact with dissolution medium

At the dissolving front, polymer will dissolve at a rate depending on its hydrophilicity. Figure 7.2 is a schematic of a proposed dissolution mechanism of HME PVP-based solid dispersion system at its dissolving front (dashed box in Figure 7.1) according to the results and observations in Chapter 5 and 6.

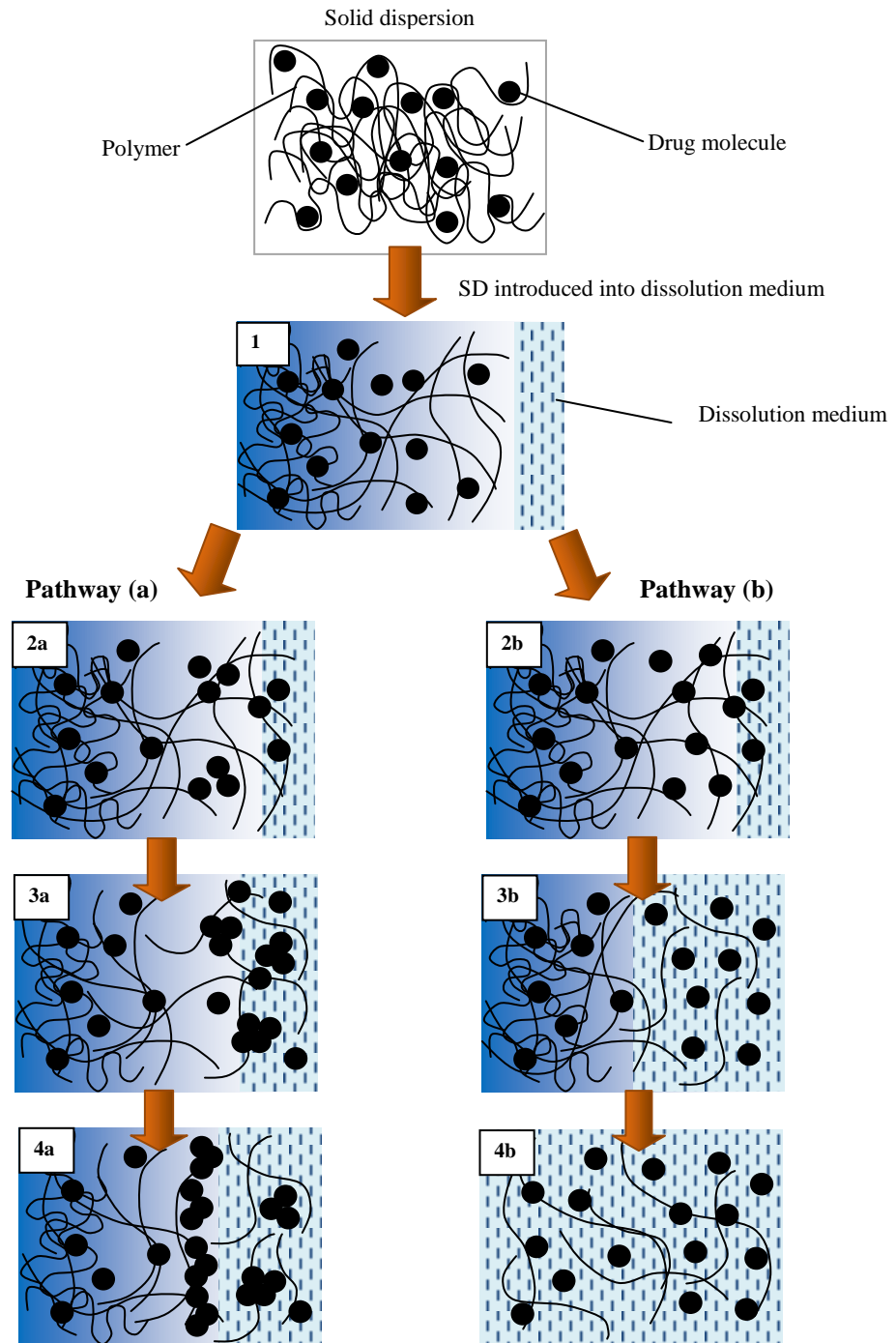


Figure 7.2: A schematic of the proposed dissolution mechanism of HME PVP-based solid dispersion system based on this study. The spheres represent drug domains and the curved lines represent the polymer. Pathway (a) on the left indicates dissolution process of a system with low ‘solubility advantages’ of its amorphous API: 2a shows the occurrence of agglomeration or phase separation, 3a shows the decrease in the effective surface area for dissolution as a result of agglomeration and 4a shows a new barrier formed as a result of continuous recrystallization and agglomeration process which give rise to a hydrophobic layer at the dissolving front of the solid dispersion. Pathway (b) on the right illustrates the dissolution process of a system with high ‘solubility advantage’ of its amorphous API: 2b shows that the drug domains are ready to dissolve once the carrier is dissolved, 3b shows the stable drug molecule in the midst of medium and polymer without agglomeration or crystallization and at 4b, system has completely dissolved.

Assuming the amorphous API is molecularly dispersed in the HME PVP-based solid dispersion, Figure 7.2 shows the homogeneously dispersed drug molecules in the polymer carrier. During the dissolution process, the surface of the solid dispersion particle is wetted by the dissolution medium. The wetting of the SD causes polymer swelling and reptation as mentioned in Figure 7.2 (1). Following reptation and swelling, two possible pathways could be taken, i.e. pathway (a) or pathway (b).

Pathway (a)

Pathway (a) will be taken if the hydrophobic API of interest possesses a low ‘solubility advantage’ in its amorphous state. Due to high energy state and hydrophobicity of amorphous API, there is a high tendency in drug agglomeration and phase separation as shown in Figure 7.2, pathway 2 (a). Besides, this pathway may be also promoted by a high loading of hydrophobic API.

After attaining a certain extent of the polymer dissolution, drug molecules are mostly stranded alone and agglomeration occurs as shown in pathway 3 (a). Agglomeration of the drug domain will lead to recrystallization of the API. At this point, the role of carrier is of utmost importance in solubilising the existing crystalline API and inhibiting further recrystallization of the API.

Pathway 4 (a) in Figure 7.2 shows the continuous crystallization process at the outer surface or the dissolving front of the SD. After a period of dissolution, the properties of dissolving front are altered where it is predominately covered with the hydrophobic recrystallized drug. This newly formed layer can prevent further penetration of the dissolution medium into the core of the SD particle and thus slow down the overall API release. Besides, the highly hydrophobic nature of the recrystallized API may promote further agglomeration of the dissolving particles via its hydrophobic forces and lead to a reduction in effective surface area for dissolution. In this context, a dissolution enhancement effect could be achieved if ‘solubility advantage’ of the amorphous API predominate over the reduced effective surface area for dissolution process. Otherwise, a reduction in dissolution would be noted due to the agglomeration and recrystallization of API, generating a less soluble solid form. This effect is significant in API with a high crystallization tendency.

Pathway (b)

Pathway (b) mainly occurs in API with high ‘solubility advantage’ of its amorphous state and low crystallization tendency. A high ‘solubility advantage’ of an API implies a relatively low hydrophobicity of its amorphous state which reduces the agglomeration as indicated in Figure 7.2 pathway 2 (b), hence, the domains of drug are separated from each other. For a drug with low

crystallization tendency, once the carrier has disentangled, the amorphous drug domains are ready to dissolve again as seen in Figure 7.2 pathway 3 (b). Thus, a fast dissolving polymer which is usually a hydrophilic and low MW polymer will lead to a faster API release of this system.

Application of the dissolution mechanisms

Dissolution mechanism presented in Figure 7.2 has revealed the reasons for an inconsistent benefit observed in solid dispersion system of different APIs in comparison to their corresponding PM. The mechanism infers the significance of ‘solubility advantages’ and recrystallization tendency of amorphous API in determining the dissolution enhancement of HME SD system as compared to the PM system.

Furthermore, the two possible dissolution pathways proposed in Figure 7.2 have resolved the doubt of inconsistent influence of polymer MW on the dissolution rate of solid dispersion as discussed in section 1.6.1.3 of Chapter 1. For a relatively stable amorphous API with its low tendency to crystallise, low MW polymer would promote drug release profoundly due to a higher disentanglement concentration (polymer concentration at which individual or small clusters of the matrix are dissociated from the system (Tajarobi et al., 2011b)) of the matrix system as compared to high MW polymers. In addition to wetting or solubilisation, no other role of the carrier was required in performing the enhanced dissolution of amorphous API. Conversely, for a highly unstable amorphous API (i.e. NAP in this study), high MW polymer is preferred due to its ability to exert steric hindrance in inhibiting molecular mobility that leads to recrystallization. As mentioned before, if amorphous API possesses only a very minor ‘solubility advantages’ its dissolution enhancement effect will be easily compromised by a minor extent of recrystallization and agglomeration.

According to the proposed mechanism in Figure 7.2, pathway (a), polymer carrier in HME PVP-based SD is found to have an additional role in dissolution process of API as compared to its PM. Unlike PM, carrier in solid dispersion is expected to maintain the high solubility state and dispersion of API molecules, limiting agglomeration and recrystallization. But only wetting and solubilising effects are anticipated as main factors affecting carrier in PM as far as an immediate release dosage form is concerned. This explains the unexpected dissolution performances of SD in comparison to their corresponding PM system as previously reviewed in the literature in Chapter 1.6.1.1.

To conclude, the use of PVP and PVPVA 6:4 polymers is feasible in HME application in which interacting API is preferred for the extrudability and production of fully amorphous solid dispersion. Physical stability of these HME PVP-based SD is highly dependent on the hydrogen bond interactions between the drug and polymer. Besides, HME PVPs-based SD should be kept dry at a temperature lower than the T_g of product in order to maintain a good long term stability. A proposal has been suggested for better understanding the dissolution performance of HME PVP-based which outlines an underlying dissolution mechanism of HME PVP-based solid dispersions, based on the properties of both the API and polymer carrier.

7.2. Recommendations for future works

Based on the results obtained in this project, it would be interesting to explore the following research areas in the future.

As processing parameter of torque was found to have an impact on the physical stability of solid dispersion, the relationship between the processing torque of HME SD, physical stability and its final dissolution performance should be further analysed. Investigation of the other processing parameters may contribute to the optimisation of the formulation design. For instance, the relationship of molten residence time in the hot barrel and the physical stability of the product could be investigated.

The characterisation of the PVP-based extrudates in Chapter 3 suggested the existence of trapped moisture in the extrudates. This may well have some impact on the physical stability of the corresponding products. A study of different moisture contents of the same polymer before feeding may serve as good approach to further understanding the physical stabilisation of HME based dispersion. Furthermore, many APIs have shown polymorphism in their crystalline state, thus the extrusion of these APIs at temperatures near to the polymorphic transformation temperature might potentially affect the physical stabilisation of the drugs.

Hydrogen bond interaction between the drug and polymer was shown to be a critical factor in preventing the recrystallization process of HME PVP-based SD. This interaction is suggested to be pertinent to the dissolution performance of HME PVP-based systems which were shown to reduce with an increase in recrystallization of API during the dissolution process. Thus, a further study in this area is required to complement the hypothesis of drug-polymer interactions in modifying the dissolution performance of HME PVP-based SD systems.

In this study, dissolution performance of the HME system is shown to be a surface based phenomenon. In this regards, PVPVA 6:4 was revealed to be a better carrier in dissolution rate enhancement of solid dispersion due to its surface active properties with the presence of the hydrophobic portion of vinyl-acetate. Thus the investigation of different ratio of the pyrrolidone and the vinyl-acetate might be able to further confirm this hypothesis. Besides, the addition of surfactant was found to assist in dissolution performance of HME SD by reducing the extent of recrystallization. However, according to literature (Kumar et al., 2008, Swanepoel et al., 2000), the incorporation of surfactant was reported to increase recrystallization as well as inhibit recrystallization. Thus more study could be concentrated on the use of difference surfactants its effect on the mode of recrystallization and dissolution performance of HME SD system.

Moreover, it would be interesting to study the alteration in dissolution performance of the aged HME PVP-based systems after storing under extreme storage conditions such as high humidity and elevated temperature. In particular, the change in the secondary rate limiting process (as explained in Chapter 5), i.e. agglomeration and recrystallization during dissolution process of the aged HME PVP-based system should be investigated. It may be hypothesized that relaxation of the SD system under these storage conditions leads to different tendencies of recrystallization and agglomeration.

Overall, the ‘solubility advantage’ of amorphous API was found to be a critical factor in determining dissolution performance of solid dispersion. This parameter should be further investigated to extended number of APIs in assessing a clear relationship to their dissolution performance. By studying this aspect, a cut-off point of the ‘solubility advantage’ of amorphous APIs in relation to their secondary dissolution rate limiting step such as agglomeration (due to hydrophobicity) and recrystallization tendency could be established. This could provide a guide to the formulator in API and carrier selection so as to secure the investment of formulating a solid dispersion for commercial use.

References

- ABRAHAMSSON, B. & LENNERNÄS, H. 2009. Application of the Biopharmaceutics Classification System Now and in the Future. *Drug Bioavailability*. Wiley-VCH Verlag GmbH & Co. KGaA. Pages 521-558.
- AIRAKSINEN, S., KARJALAINEN, M., SHEVCHENKO, A., WESTERMARCK, S., LEPPÄNEN, E., RANTANEN, J. & YLIRUUSI, J. 2005. Role of water in the physical stability of solid dosage formulations. *Journal of Pharmaceutical Sciences*, 94, 2147-2165.
- AITKEN-NICHOL, C., ZHANG, F. & MCGINITY, J. W. 1996. Hot Melt Extrusion of Acrylic Films. *Pharmaceutical Research*, 13, 804-808.
- AL-ZOUBI, N., KOUNDOURELLIS, J. E. & MALAMATARIS, S. 2002. FT-IR and Raman spectroscopic methods for identification and quantitation of orthorhombic and monoclinic paracetamol in powder mixes. *Journal of Pharmaceutical and Biomedical Analysis*, 29, 459-467.
- ALBERS, J., ALLES, R., MATTHÉE, K., KNOP, K., NAHRUP, J. S. & KLEINEBUDDE, P. 2009. Mechanism of drug release from polymethacrylate-based extrudates and milled strands prepared by hot-melt extrusion. *European Journal of Pharmaceutics and Biopharmaceutics*, 71, 387-394.
- ALONZO, D., ZHANG, G., ZHOU, D., GAO, Y. & TAYLOR, L. 2010. Understanding the Behavior of Amorphous Pharmaceutical Systems during Dissolution. *Pharmaceutical Research*, 27, 608-618.
- ALSARRA, I., HAMED, A., ALANAZI, F. & NEAU, S. 2011. Rheological and mucoadhesive characterization of poly(vinylpyrrolidone) hydrogels designed for nasal mucosal drug delivery. *Archives of Pharmacal Research*, 34, 573-582.
- ANDREWS, G. P., ABUDIAK, O. A. & JONES, D. S. 2010. Physicochemical characterization of hot melt extruded bicalutamide-polyvinylpyrrolidone solid dispersions. *Journal of Pharmaceutical Sciences*, 99, 1322-1335.
- ANDREWS, G. P., JONES, D. S., DIAK, O. A., MCCOY, C. P., WATTS, A. B. & MCGINITY, J. W. 2008. The manufacture and characterisation of hot-melt extruded enteric tablets. *European Journal of Pharmaceutics and Biopharmaceutics*, 69, 264-273.
- ANGELL, C. A. 1995. Formation of Glasses from Liquids and Biopolymers. *American Association for the Advancement of Science*, 267, 1924-1935.
- ASHLAND. 2012. Plasdone™ K povidones and Plasdone™ S-630 : Properties for Spray Dried and Melt-Extruded Solid Dispersions.
- ASO, Y., YOSHIOKA, S. & KOJIMA, S. 2004. Molecular mobility-based estimation of the crystallization rates of amorphous nifedipine and phenobarbital in poly(vinylpyrrolidone) solid dispersions. *Journal of Pharmaceutical Sciences*, 93, 384-391.
- AULTON, M. E. 2007. Dissolution and Solubility. In: AULTON, M. E. (ed.) *Aulton's Pharmaceutics: The Design and Manufacture of Medicines*. Elsevier Limited.
- AZARMI, S., ROA, W. & LÖBENBERG, R. 2007. Current perspectives in dissolution testing of conventional and novel dosage forms. *International Journal of Pharmaceutics*, 328, 12-21.

- BAIRD, J. A., VAN EERDENBRUGH, B. & TAYLOR, L. S. 2010. A classification system to assess the crystallization tendency of organic molecules from undercooled melts. *Journal of Pharmaceutical Sciences*, 99, 3787-3806.
- BALANI, P. N., WONG, S. Y., NG, W. K., WIDJAJA, E., TAN, R. B. H. & CHAN, S. Y. 2010. Influence of polymer content on stabilizing milled amorphous salbutamol sulphate. *International Journal of Pharmaceutics*, 391, 125-136.
- BANDYOPADHYAY, R., SELBO, J., AMIDON, G. E. & HAWLEY, M. 2005. Application of powder X-ray diffraction in studying the compaction behavior of bulk pharmaceutical powders. *Journal of Pharmaceutical Sciences*, 94, 2520-2530.
- BAUMGARTNER, S. A., LAHAJNAR, G., SEPE, A. & KRISTL, J. 2005. Quantitative evaluation of polymer concentration profile during swelling of hydrophilic matrix tablets using ¹H NMR and MRI methods. *European Journal of Pharmaceutics and Biopharmaceutics*, 59, 299-306.
- BERGGREN, J. & ALDERBORN, G. 2004. Long-term stabilisation potential of poly(vinylpyrrolidone) for amorphous lactose in spray-dried composites. *European Journal of Pharmaceutical Sciences*, 21, 209-215.
- BETTINETTI, G. & MURA, P. 1994. Dissolution Properties of Naproxen in Combinations with Polyvinylpyrrolidone. *Drug Development and Industrial Pharmacy*, 20, 1353-1366.
- BHADESHIA, H. K. D. H. 2002. Differential Scanning Calorimetry. *Material Science & Metallurgy*. University of Cambridge.
- BHARDWAJ, R. M., PRICE, L. S., PRICE, S. L., REUTZEL-EDENS, S. M., MILLER, G. J., OSWALD, I. D. H., JOHNSTON, B. F. & FLORENCE, A. J. 2013. Exploring the Experimental and Computed Crystal Energy Landscape of Olanzapine. *Crystal Growth & Design*, 13, 1602-1617.
- BISWAL, S., SAHOO, J. & MURTHY, P. N. 2009. Physicochemical Properties of Solid Dispersions of Gliclazide in Polyvinylpyrrolidone K90. *AAPS PharmSciTech*, 10, 329-334.
- BOLTEN, D. & TÜRK, M. 2011. Experimental Study on the Surface Tension, Density, and Viscosity of Aqueous Poly(vinylpyrrolidone) Solutions. *Journal of Chemical & Engineering Data*, 56, 582-588.
- BRABANDER, C. D., MOOTER, G. V. D., VERVAET, C. & REMON, J. P. 2002. Characterization of ibuprofen as a nontraditional plasticizer of ethyl cellulose. *Journal of Pharmaceutical Sciences*, 91, 1678-1685.
- BRABANDER, C. D., VERVAET, C., BORTEL, L. V. & REMON, J.-P. 2004. Bioavailability of ibuprofen from hot-melt extruded mini-matrices. *International Journal of Pharmaceutics*, 271, 77-84.
- BREITENBACH, J. 2002. Melt extrusion: from process to drug delivery technology. *European Journal of Pharmaceutics and Biopharmaceutics*, 54, 107-117.
- BREITENBACH, J. & MÄGERLEIN, M. 2007. Melt-Extruded Molecular Dispersions. In: ISAAC GHEBRE-SELASSIE, C. M. (ed.) *Pharmaceutical Extrusion Technology*. New York: Informa Healthcare, 133, 245-260. ISBN: 0-8247-4050-5.
- BRITISH PHARMACOPOEIA COMMISSION 2012. British Pharmacopoeia. London.

- BRUCE, C., FEGELY, K. A., RAJABI-SIAHBOOMI, A. R. & MCGINITY, J. W. 2007. Crystal growth formation in melt extrudates. *International Journal of Pharmaceutics*, 341, 162-172.
- BRUCE, C. D., FEGELY, K. A., RAJABI-SIAHBOOMI, A. R. & MCGINITY, J. W. 2010. The influence of heterogeneous nucleation on the surface crystallization of guaifenesin from melt extrudates containing Eudragit® L10055 or Acryl-EZE®. *European Journal of Pharmaceutics and Biopharmaceutics*, 75, 71-78.
- BRUCE, L. D., SHAH, N. H., WASEEM MALICK, A., INFELD, M. H. & MCGINITY, J. W. 2005. Properties of hot-melt extruded tablet formulations for the colonic delivery of 5-aminosalicylic acid. *European Journal of Pharmaceutics and Biopharmaceutics*, 59, 85-97.
- BUCKTON, G., BULPETT, R. & VERMA, N. 1991. Surface analysis of pharmaceutical powders: X-ray photoelectron spectroscopy (XPS) related to powder wettability. *International Journal of Pharmaceutics*, 72, 157-162.
- BÜHLER, V. 2005. Soluble polyvinylpyrrolidone (Povidone). *Polyvinylpyrrolidone Excipients for Pharmaceutics*.
- C.CASE, C. 2007. Melt Pelletization. In: ISAAC GHEBRE-SELASSIE, C. M. (ed.) *Pharmaceutical Extrusion Technology*. New York: Informa Healthcare, 133, 171-182. ISBN: 0-8247-4050-5.
- CALLAHAN, J. C., CLEARY, G. W., ELEFANT, M., KAPLAN, G., KENSLER, T. & NASH, R. A. 1982. Equilibrium Moisture Content of Pharmaceutical Excipients. *Drug Development and Industrial Pharmacy*, 8, 355-369.
- CAMPBELL, K., CRAIG, D. & MCNALLY, T. 2010. Ibuprofen-loaded poly(ϵ -caprolactone) layered silicate nanocomposites prepared by hot melt extrusion. *Journal of Materials Science: Materials in Medicine*, 21, 2307-2316.
- CAMPBELL, K., CRAIG, D. Q. M. & MCNALLY, T. 2008. Poly(ethylene glycol) layered silicate nanocomposites for retarded drug release prepared by hot-melt extrusion. *International Journal of Pharmaceutics*, 363, 126-131.
- CAMPBELL, K., QI, S., CRAIG, D. Q. M. & MCNALLY, T. 2009. Paracetamol-loaded poly(ϵ -caprolactone) layered silicate nanocomposites prepared using hot-melt extrusion. *Journal of Pharmaceutical Sciences*, 98, 4831-4843.
- CASSIDY, C. M., TUNNEY, M. M., CALDWELL, D. L., ANDREWS, G. P. & DONNELLY, R. F. 2011. Development of Novel Oral Formulations Prepared via Hot Melt Extrusion for Targeted Delivery of Photosensitizer to the Colon. *Photochemistry and Photobiology*, 87, 867-876.
- CHAWLA, G. & BANSAL, A. 2008. Improved dissolution of a poorly water soluble drug in solid dispersions with polymeric and non-polymeric hydrophilic additives. *Acta Pharmaceutica* 58, 257-274.
- CHENG, L., LEI, L. & GUO, S. 2010. In vitro and in vivo evaluation of praziquantel loaded implants based on PEG/PCL blends. *International Journal of Pharmaceutics*, 387, 129-138.
- CHIBOWSKI, E. & PEREA-CARPIO, R. 2002. Problems of contact angle and solid surface free energy determination. *Advances in Colloid and Interface Science*, 98, 245-264.

- CHOKSHI, R. J., SANDHU, H. K., IYER, R. M., SHAH, N. H., MALICK, A. W. & ZIA, H. 2005. Characterization of physico-mechanical properties of indomethacin and polymers to assess their suitability for hot-melt extrusion processes as a means to manufacture solid dispersion/solution. *Journal of Pharmaceutical Sciences*, 94, 2463-2474.
- CHOKSHI, R. J., ZIA, H., SANDHU, H. K., SHAH, N. H. & MALICK, W. A. 2007. Improving the Dissolution Rate of Poorly Water Soluble Drug by Solid Dispersion and Solid Solution—Pros and Cons. *Drug Delivery*, 45, 33-45.
- CORRIGAN, O. I. 1985. Mechanisms of Dissolution of Fast Release Solid Dispersions. *Drug Development and Industrial Pharmacy*, 11, 697-724.
- CORTI, G., MAESTRELLI, F., CIRRI, M., MURA, P. & ZERROUK, N. 2008. Dissolution and Permeation Properties of Naproxen From Solid-State Systems With Chitosan. *Drug Delivery*, 15, 303-312.
- COUCHMAN, P. R. & KARASZ, F. E. 1978. A Classical Thermodynamic Discussion of the Effect of Composition on Glass-Transition Temperatures. *Macromolecules*, 11, 117-119.
- CRAIG, D. Q. M. 2002. The mechanisms of drug release from solid dispersions in water-soluble polymers. *International Journal of Pharmaceutics*, 231, 131-144.
- CRAIG, D. Q. M. & READING, M. (eds.) 2007. *Thermal Analysis of Pharmaceuticals*, New York: CRC Press Taylor & Francis Group.
- CRAIG, D. Q. M., ROYALL, P. G., KETT, V. L. & HOPTON, M. L. 1999. The relevance of the amorphous state to pharmaceutical dosage forms: glassy drugs and freeze dried systems. *International Journal of Pharmaceutics*, 179, 179-207.
- CROWLEY, K. J. & ZOGRAFI, G. 2002. Cryogenic grinding of indomethacin polymorphs and solvates: Assessment of amorphous phase formation and amorphous phase physical stability. *Journal of Pharmaceutical Sciences*, 91, 492-507.
- CROWLEY, M. M., FREDERSDORF, A., SCHROEDER, B., KUCERA, S., PRODDUTURI, S., REPKA, M. A. & MCGINITY, J. W. 2004a. The influence of guaifenesin and ketoprofen on the properties of hot-melt extruded polyethylene oxide films. *European Journal of Pharmaceutical Sciences*, 22, 409-418.
- CROWLEY, M. M., SCHROEDER, B., FREDERSDORF, A., OBARA, S., TALARICO, M., KUCERA, S. & MCGINITY, J. W. 2004b. Physicochemical properties and mechanism of drug release from ethyl cellulose matrix tablets prepared by direct compression and hot-melt extrusion. *International Journal of Pharmaceutics*, 269, 509-522.
- CROWLEY, M. M., ZHANG, F., KOLENG, J. J. & MCGINITY, J. W. 2002b. Stability of polyethylene oxide in matrix tablets prepared by hot-melt extrusion. *Biomaterials*, 23, 4241-4248.
- CROWLEY, M. M., ZHANG, F., REPKA, M. A., THUMMA, S., UPADHYE, S. B., BATTU, S. K., MCGINITY, J. W. & MARTIN, C. 2007. Pharmaceutical applications of hot-melt extrusion: part I. *Drug Dev Ind Pharm*, 33, 909-26.
- DABBAGH, M. A. & TAGHIPOUR, B. 2007. Investigation of Solid Dispersion Technique in Improvement of Physicochemical Characteristics of Ibuprofen Powder. *Journal of Iranian Association of Pharmaceutical Scientists*, 3, 69-76.

- DAHLBERG, C. 2010. *Drugs and polymers in dissolving solid dispersions: NMR imaging and spectroscopy* PhD Doctoral YKI, Ytkemiska institutet AB
- DAHLBERG, C., MILLQVIST-FUREBY, A. & SCHULEIT, M. 2008. Surface composition and contact angle relationships for differently prepared solid dispersions. *European Journal of Pharmaceutics and Biopharmaceutics*, 70, 478-485.
- DE BRABANDER, C., VERVAET, C., FIERMANS, L. & REMON, J. P. 2000. Matrix mini-tablets based on starch/microcrystalline wax mixtures. *International Journal of Pharmaceutics*, 199, 195-203.
- DE BRABANDER, C., VERVAET, C. & REMON, J. P. 2003. Development and evaluation of sustained release mini-matrices prepared via hot melt extrusion. *Journal of Controlled Release*, 89, 235-247.
- DE VILLIERS, M. M., WURSTER, D. E., VAN DER WATT, J. G. & KETKAR, A. 1998. X-Ray powder diffraction determination of the relative amount of crystalline acetaminophen in solid dispersions with polyvinylpyrrolidone. *International Journal of Pharmaceutics*, 163, 219-224.
- DE WAARD, H., HINRICHS, W. L. J., VISSER, M. R., BOLOGNA, C. & FRIJLINK, H. W. 2008. Unexpected differences in dissolution behavior of tablets prepared from solid dispersions with a surfactant physically mixed or incorporated. *International Journal of Pharmaceutics*, 349, 66-73.
- DEROLLEZ, P., CORREIA, N. T., DANÈDE, F., CAPET, F., AFFOUARD, F., LEFEBVRE, J. & DESCAMPS, M. 2005. *Ab initio* structure determination of the high-temperature phase of anhydrous caffeine by X-ray powder diffraction. *Acta Crystallographica* Volume 61, 329-334
- DESCAMPS, M., CORREIA, N. L. T., DEROLLEZ, P., DANENE, F. & CAPET, F. D. R. 2005a. Plastic and Glassy Crystal States of Caffeine. *The Journal of Physical Chemistry*, 109, 16092-16098.
- DESCAMPS, M., CORREIA, N. T., DEROLLEZ, P., DANENE, F. & CAPET, F. 2005b. Plastic and Glassy Crystal States of Caffeine. *J. Phys. Chem., B*, 16092-16098.
- DESCAMPS, M., WILLART, J. F., DUDOGNON, E. & CARON, V. 2007. Transformation of pharmaceutical compounds upon milling and comilling: The role of Tg. *Journal of Pharmaceutical Sciences*, 96, 1398-1407.
- DI MAIO, E., MALI, R. & IANNACE, S. 2010. Investigation of Thermoplasticity of Zein and Kafirin Proteins: Mixing Process and Mechanical Properties. *Journal of Polymers and the Environment*, 18, 626-633.
- DI MARTINO, P., CONFLANT, P., DRACHE, M., HUVENNE, J. P. & GUYOT-HERMANN, A. M. 1997. Preparation and physical characterization of forms II and III of paracetamol. *Journal of Thermal Analysis and Calorimetry*, 48, 447-458.
- DI MARTINO, P., GUYOT-HERMANN, A. M., CONFLANT, P., DRACHE, M. & GUYOT, J. C. 1996. A new pure paracetamol for direct compression: The orthorhombic form. *International Journal of Pharmaceutics*, 128, 1-8.
- DI MARTINO, P., JOIRIS, E., GOBETTO, R., MASIC, A., PALMIERI, G. F. & MARTELLI, S. 2004. Ketoprofen-poly(vinylpyrrolidone) physical interaction. *Journal of Crystal Growth*, 265, 302-308.

- DI MARTINO, P., PALMIERI, G. F. & MARTELLI, S. 2000. Molecular Mobility of the Paracetamol Amorphous Form. *Chem Pharm Bull*, 48, 1105-1108.
- DINUNZIO, J. C., BROUGH, C., HUGHEY, J. R., MILLER, D. A., WILLIAMS III, R. O. & MCGINITY, J. W. 2009. Fusion production of solid dispersions containing a heat-sensitive active ingredient by hot melt extrusion and Kinetisol® dispersing. *European Journal of Pharmaceutics and Biopharmaceutics*, 74, 340-351.
- DJURIS, J., NIKOLAKAKIS, I., IBRIC, S., DJURIC, Z. & KACHRIMANIS, K. 2013a. Preparation of carbamazepine–Soluplus® solid dispersions by hot-melt extrusion, and prediction of drug–polymer miscibility by thermodynamic model fitting. *European Journal of Pharmaceutics and Biopharmaceutics*, 84,, 228-237.
- DJURIS, J., NIKOLAKAKIS, I., IBRIC, S., DJURIC, Z. & KACHRIMANIS, K. 2013b. Preparation of carbamazepine–Soluplus® solid dispersions by hot-melt extrusion, and prediction of drug–polymer miscibility by thermodynamic model fitting. *European Journal of Pharmaceutics and Biopharmaceutics*, 84, 228-237.
- DOETSCH, W. 2007. Material Handling and Feeder Technology. In: ISAAC GHEBRE-SELASSIE, C. M. (ed.) *Pharmaceutical Extrusion Technology*. New York: Informa Healthcare, 133, 111-134. ISBN: 0-8247-4050-5.
- DOHERTY, C. & YORK, P. 1987. Mechanisms of dissolution of frusemide/PVP solid dispersions. *International Journal of Pharmaceutics*, 34, 197-205.
- DONG, Z., CHATTERJI, A., SANDHU, H., CHOI, D. S., CHOKSHI, H. & SHAH, N. 2008b. Evaluation of solid state properties of solid dispersions prepared by hot-melt extrusion and solvent co-precipitation. *International Journal of Pharmaceutics*, 355, 141-149.
- DONG, Z. & CHOI, D. 2008a. Hydroxypropyl Methylcellulose Acetate Succinate: Potential Drug–Excipient Incompatibility. *AAPS PharmSciTech*, 9, 991-997.
- DREIBLATT, A. 2007a. Process Design. In: ISAAC GHEBRE-SELASSIE, C. M. (ed.) *pharmaceutical extrusion technology*. New York: Informa healthcare, 133, 153-181. ISBN: 0-8247-4050-5.
- DU, X., MACNAUGHTAN, B. & MITCHELL, J. R. 2011. Quantification of amorphous content in starch granules. *Food Chemistry*, 127, 188-191.
- EL-BADRY, M. & FATHY, M. 2006. Enhancement of the Dissolution and Permeation Rates of Meloxicam by Formation of Its Freeze-dried Solid Dispersions in Polyvinylpyrrolidone K-30. *Drug Development and Industrial Pharmacy*, 32, 141-150.
- EL-BADRY, M., FETIH, G. & FATHY, M. 2009. Improvement of solubility and dissolution rate of indomethacin by solid dispersions in Gelucire 50/13 and PEG4000. *Saudi Pharmaceutical Journal*, 17, 217-225.
- ELAMIN, A. A., AHLNECK, C., ALDERBORN, G. & NYSTRÖM, C. 1994. Increased metastable solubility of milled griseofulvin, depending on the formation of a disordered surface structure. *International Journal of Pharmaceutics*, 111, 159-170.
- EPPLE, M., CAMMENGA, H. K., SARGE, S. M., DIEDRICH, R. & BALEK, V. 1995. The phase transformation of caffeine: investigation by dynamic X-ray diffraction and emanation thermal analysis. *Thermochimica Acta*, 250, 29-39.

- FAHR, A. & LIU, X. 2007. Drug delivery strategies for poorly water-soluble drugs. *Expert Opinion on Drug Delivery*, 4, 403-416.
- FDA. 1997. Guidance for Industry: Dissolution Testing for Immediate Release Solid Oral Dosage Forms.
- FERNANDEZ, J., VILA-JATO, J. L., BLANCO, J. & FORD, J. L. 1989. Some Properties of Diazepam-Polyethylene Glycol 6000 Solid Dispersions and their Modification in the Presence of Stearic Acid of Polysorbate 80. *Drug Development and Industrial Pharmacy*, 15, 2491-2513.
- FORSTER, A., HEMPENSTALL, J. & RADES, T. 2001b. Characterization of glass solutions of poorly water-soluble drugs produced by melt extrusion with hydrophilic amorphous polymers. *Journal of Pharmacy and Pharmacology*, 53, 303-315.
- FORSTER, A., HEMPENSTALL, J., TUCKER, I. & RADES, T. 2001a. The Potential of Small-Scale Fusion Experiments and the Gordon-Taylor Equation to Predict the Suitability of Drug/Polymer Blends for Melt Extrusion. *Drug Development and Industrial Pharmacy*, 27, 549-560.
- FORSTER, A., HEMPENSTALL, J., TUCKER, I. & RADES, T. 2001c. Selection of excipients for melt extrusion with two poorly water-soluble drugs by solubility parameter calculation and thermal analysis. *International Journal of Pharmaceutics*, 226, 147-161.
- FREITAS, M. R. D., ROLIM, L. A., SOARES, M. F. D. L. R., ROLIM-NETO, P. J., ALBUQUERQUE, M. M. D. & SOARES-SOBRINHO, J. L. 2012. Inclusion complex of methyl- β -cyclodextrin and olanzapine as potential drug delivery system for schizophrenia. *Carbohydrate Polymer*, 89, 1095-1100.
- FUKUDA, M., PEPPAS, N. A. & MCGINITY, J. W. 2006a. Floating hot-melt extruded tablets for gastroretentive controlled drug release system. *Journal of Controlled Release*, 115, 121-129.
- FUKUDA, M., PEPPAS, N. A. & MCGINITY, J. W. 2006b. Properties of sustained release hot-melt extruded tablets containing chitosan and xanthan gum. *International Journal of Pharmaceutics*, 310, 90-100.
- GANGOPADHYAY, R. 2008. Exploring rheological properties of aqueous polyaniline-PVP dispersion. *Journal of Polymer Science Part B: Polymer Physics*, 46, 2443-2455.
- GAO, Y. & OLSEN, K. W. 2013. Molecular Dynamics of Drug Crystal Dissolution: Simulation of Acetaminophen Form I in Water. *Molecular Pharmaceutics*, 10, 905-917.
- GAREKANI, H. A., SADEGHI, F. & GHAZI, A. 2003. Increasing the Aqueous Solubility of Acetaminophen in the Presence of Polyvinylpyrrolidone and Investigation of the Mechanisms Involved. *Drug Dev Ind Pharm*, 29, 173-179.
- GASHI, Z., CENSI, R., MALAJ, L., GOBETTO, R., MOZZICAFREDDO, M., ANGELETTI, M., MASIC, A. & DI MARTINO, P. 2009. Differences in the interaction between aryl propionic acid derivatives and poly(vinylpyrrolidone) K30: A multi-methodological approach. *Journal of Pharmaceutical Sciences*, 98, 4216-4228.
- GHALANBOR, Z., KÖRBER, M. & BODMEIER, R. 2010. Improved Lysozyme Stability and Release Properties of Poly(lactide-co-glycolide) Implants Prepared by Hot-Melt Extrusion. *Pharmaceutical Research*, 27, 371-379.

- GHEBREMESKEL, A., VEMAVARAPU, C. & LODAYA, M. 2006. Use of Surfactants as Plasticizers in Preparing Solid Dispersions of Poorly Soluble API: Stability Testing of Selected Solid Dispersions. *Pharmaceutical Research*, 23, 1928-1936.
- GHEBREMESKEL, A. N., VEMAVARAPU, C. & LODAYA, M. 2007. Use of surfactants as plasticizers in preparing solid dispersions of poorly soluble API: Selection of polymer-surfactant combinations using solubility parameters and testing the processability. *International Journal of Pharmaceutics*, 328, 119-129.
- GILL, P. S., SAUERBRUNN, S. R. & READING, M. 1993. Modulated differential scanning calorimetry. *Journal of thermal analysis*, 40, 931-939.
- GONG, X. F., SHING, K. S. & CHANG, W. V. 1989. Effect of composition dependent Flory interaction parameter χ on polymer adsorption theory. *Polymer Bulletin*, 22, 71-78.
- GORDON, M. & TAYLOR, J. S. 1952. Ideal copolymers and the second-order transitions of synthetic rubbers. i. non-crystalline copolymers. *Journal of Applied Chemistry*, 2, 493-500.
- GRAESER, K. A., PATTERSON, J. E. & RADES, T. 2009a. Applying Thermodynamic and Kinetic Parameters to Predict the Physical Stability of Two Differently Prepared Amorphous Forms of Simvastatin. *Current Drug Delivery*, 374-382
- GRAESER, K. A., PATTERSON, J. E., ZEITLER, J. A., GORDON, K. C. & RADES, T. 2009. Correlating thermodynamic and kinetic parameters with amorphous stability. *European Journal of Pharmaceutical Sciences*, 37, 492-498.
- GRECO, K. & BOGNER, R. 2010. Crystallization of Amorphous Indomethacin during Dissolution: Effect of Processing and Annealing. *Molecular Pharmaceutics*, 7, 1406-1418.
- GRISEDAL, L. C., JAMIESON, M. J., BELTON, P. S., BARKER, S. A. & M. CRAIG, D. Q. 2011. Characterization and quantification of amorphous material in milled and spray-dried salbutamol sulfate: A comparison of thermal, spectroscopic, and water vapor sorption approaches. *Journal of Pharmaceutical Sciences*, 100, 3114-3129.
- GUNS, S., DEREYMAKER, A., KAYAERT, P., MATHOT, V., MARTENS, J. & MOOTER, G. 2011. Comparison Between Hot-Melt Extrusion and Spray-Drying for Manufacturing Solid Dispersions of the Graft Copolymer of Ethylene Glycol and Vinylalcohol. *Pharmaceutical Research*, 28, 673-682.
- GUPTA, M. K., TSENG, Y.-C., GOLDMAN, D. & BOGNER, R. H. 2002. Hydrogen Bonding with Absorbent during Storage Governs Drug Dissolution from Solid-Dispersion Granules. *Pharmaceutical Research*, 19, 1663-1671.
- HALLBRUCKER, A., MAYER, E. & JOHARI, G. P. 1989. Glass-liquid transition and the enthalpy of devitrification of annealed vapor-deposited amorphous solid water: a comparison with hyperquenched glassy water. *The Journal of Physical Chemistry*, 93, 4986-4990.
- HANCOCK, B. & ZOGRAFI, G. 1994. The Relationship Between the Glass Transition Temperature and the Water Content of Amorphous Pharmaceutical Solids. *Pharmaceutical Research*, 11, 471-477.
- HANCOCK, B. C., CARLSON, G. T., LADIPO, D. D., LANGDON, B. A. & MULLARNEY, M. P. 2002. Comparison of the mechanical properties of the crystalline and amorphous forms of a drug substance. *International Journal of Pharmaceutics*, 241, 73-85.

- HANCOCK, B. C. & PARKS, M. 2000. What is the True Solubility Advantage for Amorphous Pharmaceuticals? *Pharmaceutical Research*, 17, 397-404.
- HANCOCK, B. C., SHAMBLIN, S. L. & ZOGRAFI, G. 1995. Molecular Mobility of Amorphous Pharmaceutical Solids Below Their Glass Transition Temperatures. *Pharmaceutical Research*, 12, 799-806.
- HANCOCK, B. C. & ZOGRAFI, G. 1997. Characteristics and significance of the amorphous state in pharmaceutical systems. *Journal of Pharmaceutical Sciences*, 86, 1-12.
- HELJO, V., NORDBERG, A., TENHO, M., VIRTANEN, T., JOUPPILA, K., SALONEN, J., MAUNU, S. & JUPPO, A. 2012. The Effect of Water Plasticization on the Molecular Mobility and Crystallization Tendency of Amorphous Disaccharides. *Pharmaceutical Research*, 29, 2684-2697.
- HERRMANN, S. 2007. *Lipidic Implants for Pharmaceutical Proteins: Mechanisms of Release and Development of Extruded Devices*. PhD, Ludwig-Maximilians-Universität München.
- HILTON, J. E. & SUMMERS, M. P. 1986. The effect of wetting agents on the dissolution of indomethacin solid dispersion systems. *International Journal of Pharmaceutics*, 31, 157-164.
- HOFFMAN, J. D. 1958. Thermodynamic Driving Force in Nucleation and Growth Processes. *The Journal of Chemical Physics*, 29, 1192-1193.
- HORIBA SCIENTIFIC. 2013. *Laser Diffraction Technology* [Online].
- HUANG, Q. R. & WANG, C. H. 1996. Surface laser light scattering studies of the air/poly(N-vinyl-2-pyrrolidone)-water solution interface. *Journal of Chemical Physics*, 105, 6546.
- HÜLSMANN, S., BACKENFELD, T., KEITEL, S. & BODMEIER, R. 2000. Melt extrusion - an alternative method for enhancing the dissolution rate of 17[β]-estradiol hemihydrate. *European Journal of Pharmaceutics and Biopharmaceutics*, 49, 237-242.
- HÖRTER, D. & DRESSMAN, J. B. 2001. Influence of physicochemical properties on dissolution of drugs in the gastrointestinal tract. *Advanced Drug Delivery Reviews*, 46, 75-87.
- ILEVBARE, G. A., LIU, H., EDGAR, K. J. & TAYLOR, L. S. 2012a. Effect of Binary Additive Combinations on Solution Crystal Growth of the Poorly Water-Soluble Drug, Ritonavir. *Crystal Growth & Design*, 12, 6050-6060.
- ILEVBARE, G. A., LIU, H., EDGAR, K. J. & TAYLOR, L. S. 2012b. Understanding Polymer Properties Important for Crystal Growth Inhibition-Impact of Chemically Diverse Polymers on Solution Crystal Growth of Ritonavir. *Crystal Growth & Design*, 12, 3133-3143.
- IMMERGUT, E. H. & MARK, H. F. 1965. Principles of Plasticization. *Plasticization and Plasticizer Processes*, 48, 1-26.
- ISP PHARMACEUTICALS. 2007. Plasdone ® Povidone Performance Enhancing Products for Pharmaceuticals. *Product Guide* [Online].
- IVANOV, I. T. & TSOKEVA, Z. 2009. Effect of chirality on PVP/drug interaction within binary physical mixtures of ibuprofen, ketoprofen, and naproxen: A DSC study. *Chirality*, 21, 719-727.

- IVANOVA, B. B. 2005. Monoclinic and orthorhombic polymorphs of paracetamol--solid state linear dichroic infrared spectral analysis. *Journal of Molecular Structure*, 738, 233-238.
- JACHOWICZ, R., RNBERG, E. N., PIESCZEK, B., KLUCZYKOWSKA, B. & MACIEJEWSKA, A. 2000. Solid dispersion of ketoprofen in pellets. *International Journal of Pharmaceutics*, 206, 13-21.
- JANSSENS, S., ANNÉ, M., ROMBAUT, P. & VAN DEN MOOTER, G. 2009. Spray drying from complex solvent systems broadens the applicability of Kollicoat IR as a carrier in the formulation of solid dispersions. *European Journal of Pharmaceutical Sciences*, 37, 241-248.
- JANSSENS, S. & VAN DEN MOOTER, G. 2009. Review: physical chemistry of solid dispersions. *Journal of Pharmacy and Pharmacology*, 61, 1571-1586.
- JIJUN, F., LISHUANG, X., XIAOGUANG, T., MIN, S., MINGMING, Z., HAIBING, H. & XING, T. 2010. The inhibition effect of high storage temperature on the recrystallization rate during dissolution of nimodipine–Kollidon VA64 solid dispersions (NM–SD) prepared by hot-melt extrusion. *Journal of Pharmaceutical Sciences*, 100, 1643-1647.
- JØRGENSEN, A. C. & TORSTENSON, A. S. 2008. Humid Storage Conditions Increase the Dissolution Rate of Diazepam from Solid Dispersions Prepared by Melt Agglomeration. *Pharmaceutical Development and Technology*, 13, 187-195.
- KALIVODA, A., FISCHBACH, M. & KLEINEBUDDE, P. 2012a. Application of mixtures of polymeric carriers for dissolution enhancement of fenofibrate using hot melt extrusion. *International Journal of Pharmaceutics*.
- KALIVODA, A., FISCHBACH, M. & KLEINEBUDDE, P. 2012b. Application of mixtures of polymeric carriers for dissolution enhancement of oxeglitazar using hot-melt extrusion. *International Journal of Pharmaceutics*, 439, 145-156.
- KANAUJIA, P., LAU, G., NG, W. K., WIDJAJA, E., HANEFELD, A., FISCHBACH, M., MAIO, M. & TAN, R. B. H. 2010. Nanoparticle formation and growth during in vitro dissolution of ketoconazole solid dispersion. *Journal of Pharmaceutical Sciences*, 100, 2876-2885.
- KANG, J., GU, H., ZHONG, L., HU, Y. & LIU, F. 2011. The pH dependent Raman spectroscopic study of caffeine. *Spectrochimica Acta Part A: Molecular and Biomolecular Spectroscopy*, 78, 757-762.
- KAPSI, S. G. & AYRES, J. W. 2001. Processing factors in development of solid solution formulation of itraconazole for enhancement of drug dissolution and bioavailability. *International Journal of Pharmaceutics*, 229, 193-203.
- KARAVAS, E., GEORGARAKIS, E., SIGALAS, M. P., AVGOUSTAKIS, K. & BIKIARIS, D. 2007. Investigation of the release mechanism of a sparingly water-soluble drug from solid dispersions in hydrophilic carriers based on physical state of drug, particle size distribution and drug-polymer interactions. *European Journal of Pharmaceutics and Biopharmaceutics*, 66, 334-347.
- KARAVAS, E., KTISTIS, G., XENAKIS, A. & GEORGARAKIS, E. 2006. Effect of hydrogen bonding interactions on the release mechanism of felodipine from nanodispersions with polyvinylpyrrolidone. *European Journal of Pharmaceutics and Biopharmaceutics*, 63, 103-114.

- KASIM, N. A., WHITEHOUSE, M., RAMACHANDRAN, C., BERMEJO, M., LENNERNÄS, H., HUSSAIN, A. S., JUNGINGER, H. E., STAVCHANSKY, S. A., MIDHA, K. K., SHAH, V. P. & AMIDON, G. L. 2003. Molecular Properties of WHO Essential Drugs and Provisional Biopharmaceutical Classification. *Molecular Pharmaceutics*, 1, 85-96.
- KAWAKAMI, K., USUI, T. & HATTORI, M. 2012. Understanding the glass-forming ability of active pharmaceutical ingredients for designing supersaturating dosage forms. *Journal of Pharmaceutical Sciences*, 101, 3239-3248.
- KE, P., HASEGAWA, S., AL-OBAIDI, H. & BUCKTON, G. 2012. Investigation of preparation methods on surface/bulk structural relaxation and glass fragility of amorphous solid dispersions. *International Journal of Pharmaceutics*, 422, 170-178.
- KELEB, E. I., VERMEIRE, A., VERVAET, C. & REMON, J. P. 2001. Cold extrusion as a continuous single-step granulation and tableting process. *European Journal of Pharmaceutics and Biopharmaceutics*, 52, 359-368.
- KESTUR, U. S., IVANESIVIC, I., ALONZO, D. E. & TAYLOR, L. S. 2012. Influence of particle size on the crystallization kinetics of amorphous felodipine powders. *Powder Technology*, 236, 197-204.
- KHOUGAZ, K. & CLAS, S.-D. 2000. Crystallization inhibition in solid dispersions of MK-0591 and poly(vinylpyrrolidone) polymers. *Journal of Pharmaceutical Sciences*, 89, 1325-1334.
- KIBBE, A. 2002. Povidone. In: ROWE, R. C., SHESKEY, P. J. & WELLER, P. J. (eds.) *Handbook of Pharmaceutical Excipients*. Sixth Edition ed. Chicago London: Science and Practice. ISBN 978 0 85369 792 3 (UK).
- KINDERMANN, C., MATTHÉE, K., STROHMEYER, J., SIEVERT, F. & BREITKREUTZ, J. 2011. Tailor-made release triggering from hot-melt extruded complexes of basic polyelectrolyte and poorly water-soluble drugs. *European Journal of Pharmaceutics and Biopharmaceutics*, 79, 372-381.
- KISHI, Y. & MATSUOKA, M. 2010. Phenomena and Kinetics of Solid-State Polymorphic Transition of Caffeine. *Crystal Growth & Design*, 10, 2916-2920.
- KLEIN, C. E., CHIU, Y.-L., AWNI, W., ZHU, T., HEUSER, R. S., DOAN, T., BREITENBACH, J., MORRIS, J. B., BRUN, S. C. & HANNA, G. J. 2007. The Tablet Formulation of Lopinavir/Ritonavir Provides Similar Bioavailability to the Soft-Gelatin Capsule Formulation With Less Pharmacokinetic Variability and Diminished Food Effect. *JAIDS Journal of Acquired Immune Deficiency Syndromes*, 44, 401-410
- KOLTER, K., KARL, M. & GRYCZKE, A. 2012. Introduction to Solid Dispersions. *Hot Melt Extrusion with BASF Pharma Polymers: Extrusion Compendium 2nd Revised and Enlarged Edition*. The Chemical Company BASF.
- KOLTER, K., KARL, M., S, N. & ROTTMANN, N. (eds.) 2010. *Hot Melt Extrusion with BASF Pharma Polymer*, BASF SE Ludwigshafen: BASF The Chemical Company.
- KRISHNAMOORTHY, V., NAGALINGAM, A., PRASAD, V. P. R., PARAMESHWARAN, S., GEORGE, N. & KALIYAN, P. 2011. Characterization of Olanzapine -Solid Dispersions. *Iranian Journal of Pharmaceutical Research*, 10, 13-24.
- KRISHNAMOORTHY, V., SUCHANDRASEN & PRASAD, V. P. R. 2012. Physicochemical characterization and in vitro dissolution behavior of olanzapine-mannitol solid dispersions. *Brazilian Journal of Pharmaceutical Sciences*, 48, 243-255.

- KULKARNI, P. K., DIXIT, M., KUMAR, Y. S., KINI, A. G. & JOHRI, A. 2010. Preparation and evaluation of Ketoprofen beads by melt solidification technique. *Der Pharmacia Sinica*, 1, 31-43.
- KUMAR, S., CHAWLA, G. & BANSAL, A. K. 2008. Role of Additives like Polymers and Surfactants in the Crystallization of Mebendazole. *YAKUGAKU ZASSHI*, 128, 281-289.
- KÖRNER, A., LARSSON, A., PICULELL, L. & WITTGREN, B. 2005. Molecular Information on the Dissolution of Polydisperse Polymers: Mixtures of Long and Short Poly(ethylene oxide). *The Journal of Physical Chemistry*, 109, 11530-11537.
- LACEY, A., PRICE, D. & READING, M. 2006. Theory and Practice of Modulated Temperature Differential Scanning Calorimetry. In: READING, M. & HOURSTON, D. (eds.) *Modulated Temperature Differential Scanning Calorimetry*. Springer Netherlands.
- LAKSHMAN, J. P., CAO, Y., KOWALSKI, J. & SERAJUDDIN, A. T. M. 2008. Application of Melt Extrusion in the Development of a Physically and Chemically Stable High-Energy Amorphous Solid Dispersion of a Poorly Water-Soluble Drug. *Molecular Pharmaceutics*, 5, 994-1002.
- LAM, C. N. C., WU, R., LI, D., HAIR, M. L. & NEUMANN, A. W. 2002. Study of the advancing and receding contact angles: liquid sorption as a cause of contact angle hysteresis. *Advances in Colloid and Interface Science*, 96, 169-191.
- LARRABEE, J. A. & CHOI, S. 1993. Fourier transform infrared spectroscopy. In: RIORDAN, J. F. & BERT, L. V. (eds.) *Methods in Enzymology*. Vol 226, New York: Metallobiochemistry Part C, pp 289-305.
- LEFORT, R., DE GUSSEME, A., WILLART, J. F., DANÈDE, F. & DESCAMPS, M. 2004. Solid state NMR and DSC methods for quantifying the amorphous content in solid dosage forms: an application to ball-milling of trehalose. *International Journal of Pharmaceutics*, 280, 209-219.
- LEHTO, V.-P. & LAINE, E. 1998. A kinetic study of polymorphic transition of anhydrous caffeine with microcalorimeter. *Thermochimica Acta*, 317, 47-58.
- LEMIEUX, M., GOSSELIN, P. & MATEESCU, M. A. 2010. Influence of Drying Procedure and of Low Degree of Substitution on the Structural and Drug Release Properties of Carboxymethyl Starch. *AAPS PharmSciTech*, 11, 775-785.
- LEUNER, C. & DRESSMAN, J. 2000. Improving drug solubility for oral delivery using solid dispersions. *European Journal of Pharmaceutics and Biopharmaceutics*, 50, 47-60.
- LIU, H., WANG, P., ZHANG, X., SHEN, F. & GOGOS, C. G. 2009. Effects of extrusion process parameters on the dissolution behavior of indomethacin in Eudragit® E PO solid dispersions. *International Journal of Pharmaceutics*, 383, 161-169.
- LIU, H., WANG, P., ZHANG, X., SHEN, F. & GOGOS, C. G. 2010. Effects of extrusion process parameters on the dissolution behavior of indomethacin in Eudragit® E PO solid dispersions. *International Journal of Pharmaceutics*, 383, 161-169.
- LIU, J., ZHANG, F. & MCGINITY, J. W. 2001. Properties of lipophilic matrix tablets containing phenylpropranolamine hydrochloride prepared by hot-melt extrusion. *European Journal of Pharmaceutics and Biopharmaceutics*, 52, 181-190.

- LUKER, K. 2007. Single-Screw Extrusion and Screw Design. *In: ISAAC GHEBRE-SELASSIE, C. M. (ed.) Pharmaceutical Extrusion Technology*. New York: Informa Healthcare, 133, 39-68. ISBN: 0-8247-4050-5.
- LYONS, J. G., BLACKIE, P. & HIGGINBOTHAM, C. L. 2008. The significance of variation in extrusion speeds and temperatures on a PEO/PCL blend based matrix for oral drug delivery. *International Journal of Pharmaceutics*, 351, 201-208.
- LYONS, J. G., HALLINAN, M., KENNEDY, J. E., DEVINE, D. M., GEEVER, L. M., BLACKIE, P. & HIGGINBOTHAM, C. L. 2007a. Preparation of monolithic matrices for oral drug delivery using a supercritical fluid assisted hot melt extrusion process. *International Journal of Pharmaceutics*, 329, 62-71.
- LYONS, J. G., HOLEHONNUR, H., DEVINE, D. M., KENNEDY, J. E., GEEVER, L. M., BLACKIE, P. & HIGGINBOTHAM, C. L. 2007b. The incorporation of an organically modified layered silicate in monolithic polymeric matrices produced using hot melt extrusion. *Materials Chemistry and Physics*, 103, 419-426.
- MALAJ, L., CENSI, R., MOZZICAFREDDO, M., PELLEGRINO, L., ANGELETTI, M., GOBETTO, R. & DI MARTINO, P. 2010. Influence of relative humidity on the interaction between different aryl propionic acid derivatives and poly(vinylpyrrolidone) K30: Evaluation of the effect on drug bioavailability. *International Journal of Pharmaceutics*, 398, 61-72.
- MANIRUZZAMAN, M., MORGAN, D. J., MENDHAM, A. P., PANG, J., SNOWDEN, M. J. & DOUROUMIS, D. 2013. Drug-polymer intermolecular interactions in hot-melt extruded solid dispersions. *International Journal of Pharmaceutics*, 443, 199-208.
- MARGARIT, M. A. V., RODRÁ-GUEZ, I. S. C. & CERESO, A. 1994. Physical characteristics and dissolution kinetics of solid dispersions of ketoprofen and polyethylene glycol 6000. *International Journal of Pharmaceutics*, 108, 101-107.
- MARSAC, P., LI, T. & TAYLOR, L. 2009. Estimation of Drug-Polymer Miscibility and Solubility in Amorphous Solid Dispersions Using Experimentally Determined Interaction Parameters. *Pharmaceutical Research*, 26, 139-151.
- MARSAC, P., SHAMBLIN, S. & TAYLOR, L. 2006. Theoretical and Practical Approaches for Prediction of Drug-Polymer Miscibility and Solubility. *Pharmaceutical Research*, 23, 2417-2426.
- MARTIN, S. T. 2007. Rheology and Torque *In: ISAAC GHEBRE-SELASSIE, C. M. (ed.) Pharmaceutical Extrusion Technology*. New York: Informa Healthcare, 133, 135-151. ISBN: 0-8247-4050-5.
- MATSUMOTO, T. & ZOGRAFI, G. 1999. Physical Properties of Solid Molecular Dispersions of Indomethacin with Poly(vinylpyrrolidone) and Poly(vinylpyrrolidone-co-vinyl-acetate) in Relation to Indomethacin Crystallization. *Pharmaceutical Research*, 16, 1722-1728.
- MCGINITY, J. W., REPKA, M. A., KOLENG, J. J. & ZHANG, F. 2006. Hot-Melt Extrusion Technology. *Encyclopedia of Pharmaceutical Technology: Third Edition, 2004 - 2020*.
- MCGINITY, J. W. & ZHANG, F. 2007. Melt-extruded Controlled-Release Dosage Forms. *In: ISAAC GHEBRE-SELASSIE, C. M. (ed.) Pharmaceutical Extrusion Technology*. New York: Informa healthcare, 100, 183-208.

- MEHUYS, E., REMON, J.-P. & VERVAET, C. 2005a. Production of enteric capsules by means of hot-melt extrusion. *European Journal of Pharmaceutical Sciences*, 24, 207-212.
- MEHUYS, E., REMON, J. P., KORST, A., VAN BORTEL, L., MOLS, R., AUGUSTIJNS, P., PORTER, C. & VERVAET, C. 2005b. Human bioavailability of propranolol from a matrix-in-cylinder system with a HPMC-Gelucire® core. *Journal of Controlled Release*, 107, 523-536.
- MEHUYS, E., VERVAET, C., GIELEN, I., VAN BREE, H. & REMON, J. P. 2004b. In vitro and in vivo evaluation of a matrix-in-cylinder system for sustained drug delivery. *Journal of Controlled Release*, 96, 261-271.
- MEHUYS, E., VERVAET, C. & REMON, J. P. 2004a. Hot-melt extruded ethylcellulose cylinders containing a HPMC-Gelucire® core for sustained drug delivery. *Journal of Controlled Release*, 94, 273-280.
- MIDIDODDI, P. K. & REPKA, M. A. 2007. Characterization of hot-melt extruded drug delivery systems for onychomycosis. *European Journal of Pharmaceutics and Biopharmaceutics*, 66, 95-105.
- MILLER-CHOU, B. A. & KOENIG, J. L. 2003. A review of polymer dissolution. *Progress in Polymer Science*, 28, 1223-1270.
- MILLER, D., DINUNZIO, J., YANG, W., MCGINITY, J. & WILLIAMS, R. 2008b. Targeted Intestinal Delivery of Supersaturated Itraconazole for Improved Oral Absorption. *Pharmaceutical Research*, 25, 1450-1459.
- MILLER, D. A., DINUNZIO, J. C., YANG, W., MCGINITY, J. W. & WILLIAMS, R. O. 2008a. Enhanced In Vivo Absorption of Itraconazole via Stabilization of Supersaturation Following Acidic-to-Neutral pH Transition. *Drug Development and Industrial Pharmacy*, 34, 890 - 902.
- MILLER, D. A., MCCONVILLE, J. T., YANG, W., III, R. O. W. & MCGINITY, J. W. 2007. Hot-melt extrusion for enhanced delivery of drug particles. *Journal of Pharmaceutical Sciences*, 96, 361-376.
- MOKARRAM, A. R., ZADEH, A. K., KESHAVARZ, M. & AHMADI, B. M. 2010a. Preparation and in-vitro evaluation of indomethacin nanoparticles. *DARU Journal of Pharmaceutical Sciences*, 18, 185-192.
- MOKARRAM, A. R., ZADEH, A. K., KESHAVARZ, M., AHMADI, A. & MOHTAT, B. 2010b. Preparation and in-vitro evaluation of indomethacin nanoparticles. *DARU Journal of Pharmaceutical Sciences*, 18, 185-192.
- MOLLAN, M. 2007. Historical Overview In: ISAAC GHEBRE-SELASSIE, C. M. (ed.) *Pharmaceutical Extrusion Technology*. New York: Informa healthcare, 133, 135-151. ISBN: 0-8247-4050-5.
- MONEGHINI, M., CARCANO, A., ZINGONE, G. & PERISSUTTI, B. 1998. Studies in dissolution enhancement of atenolol. Part I. *International Journal of Pharmaceutics*, 175, 177-183.
- MOOTER, G. V. D., WUYTS, M., BLATON, N., BUSSON, R., GROBET, P., AUGUSTIJNS, P. & KINGET, R. 2001. Physical stabilisation of amorphous ketoconazole in solid dispersions with polyvinylpyrrolidone K25. *European Journal of Pharmaceutical Sciences*, 12, 261-269.

- MOURA RAMOS, J. J., CORREIA, N. L. T., DIOGO, H. N. P. & DESCAMPS, M. 2006. Dielectric Study of the Slow Motional Processes in the Polymorphic States of Anhydrous Caffeine. *The Journal of Physical Chemistry B*, 110, 8268-8273.
- MOYNIHAN, C. T., MACEDO, P. B., MONTROSE, C. J., GUPTA, P. K., DEBOLT, M. A., DILL, J. F., DOM, B. E., DRAKE, P. W., EASTEAL, A. J., ELTERMAN, P. B., MOELLER, R. P., SASABE, H. & WILDER, J. A. 1976. STRUCTURAL RELAXATION IN VITREOUS MATERIALS*. *Annals of the New York Academy of Sciences*, 279, 15-35.
- MUNJAL, M., ELSOHLY, M. & REPKA, M. 2006. Chemical stabilization of a Δ^9 -tetrahydrocannabinol prodrug in polymeric matrix systems produced by a hot-melt method: Role of microenvironment pH. *AAPS PharmSciTech*, 7, E114-E125.
- MURA, P., BETTINETTI, G., MELANI, F. & MANDERIOLI, A. 1995. Interaction between naproxen and chemically modified β -cyclodextrins in the liquid and solid state. *European Journal of Pharmaceutical Sciences*, 3, 347-355.
- MURA, P., FAUCCI, M. T., MAESTRELLI, F., FURLANETTO, S. & PINZAUTI, S. 2002. Characterization of physicochemical properties of naproxen systems with amorphous β -cyclodextrin-epichlorohydrin polymers. *Journal of Pharmaceutical and Biomedical Analysis*, 29, 1015-1024.
- MURA, P., ZERROUK, N., MENNINI, N., MAESTRELLI, F. & CHEMTOB, C. 2003. Development and characterization of naproxen-chitosan solid systems with improved drug dissolution properties. *European Journal of Pharmaceutical Sciences*, 19, 67-75.
- NAGAPUDI, K. & JONA, J. 2008. Amorphous Active Pharmaceutical Ingredients in Preclinical Studies: Preparation, Characterization, and Formulation. *Current Bioactive Compounds*, 4, 213-224.
- NAIR, R., NYAMWEYA, N., GÖNEN, S., MARTÍNEZ-MIRANDA, L. J. & HOAG, S. W. 2001. Influence of various drugs on the glass transition temperature of poly(vinylpyrrolidone): a thermodynamic and spectroscopic investigation. *International Journal of Pharmaceutics*, 225, 83-96.
- NAKAMICHI, K., NAKANO, T., YASUURA, H., IZUMI, S. & KAWASHIMA, Y. 2002. The role of the kneading paddle and the effects of screw revolution speed and water content on the preparation of solid dispersions using a twin-screw extruder. *International Journal of Pharmaceutics*, 241, 203-211.
- NAKAMICHI, K., NAKANO, T., YASUURA, H., IZUMI, S. & KAWASHIMA, Y. 2003. Stabilization of sodium guaiazulene sulfonate in granules for tableting prepared using a twin-screw extruder. *European Journal of Pharmaceutics and Biopharmaceutics*, 56, 347-354.
- NAKAMICHI, K., YASUURA, H., FUKUI, H., OKA, M. & IZUMI, S. 2001. Evaluation of a floating dosage form of nifedipine hydrochloride and hydroxypropylmethylcellulose acetate succinate prepared using a twin-screw extruder. *International Journal of Pharmaceutics*, 218, 103-112.
- NDINDAYINO, F., HENRIST, D., KIEKENS, F., VAN DEN MOOTER, G., VERVAET, C. & REMON, J. P. 2002a. Direct compression properties of melt-extruded isomalt. *International Journal of Pharmaceutics*, 235, 149-157.

- NDINDAYINO, F., VERVAET, C., VAN DEN MOOTER, G. & REMON, J. P. 2002b. Direct compression and moulding properties of co-extruded isomalt/drug mixtures. *International Journal of Pharmaceutics*, 235, 159-168.
- NOKHODCHI, A., JAVADZADEH, Y., SIAHI-SHADBAD, M. R. & BARZEGAR-JALALI, M. 2005. The Effect of Type and Concentration of Vehicles on the Dissolution Rate of a Poorly Soluble Drug (indomethacin) from Liquisolid Compacts. *J Pharm Pharmaceut Sci* 8, 18-25.
- NOYES, A. A. & WHITNEY, W. R. 1897. THE RATE OF SOLUTION OF SOLID SUBSTANCES IN THEIR OWN SOLUTIONS. *Journal of the American Chemical Society*, 19, 930-934.
- OBERG, K. A. & FINK, A. L. 1998. A New Attenuated Total Reflectance Fourier Transform Infrared Spectroscopy Method for the Study of Proteins in Solution. *ANALYTICAL BIOCHEMISTRY*, 256, 92-106.
- ODACI, E., BILEN, H., HACIMUFTUOGLU, A., KELES, O. N., CAN, I. & BILICI, M. (eds.) 2009. *Long-term treatments with low and high-dose olanzapine changed hepatocyte numbers in rats.*
- OJOVAN, M. I. & LEE, W. E. 2005. Fragility of oxide melts as a thermodynamic parameter. *Physics and Chemistry of Glasses*, 46, 7-11.
- ÖZGÜNEY, I., SHUWISITKUL, D. & BODMEIER, R. 2009. Development and characterization of extended release Kollidon® SR mini-matrices prepared by hot-melt extrusion. *European Journal of Pharmaceutics and Biopharmaceutics*, 73, 140-145.
- PATIL, S., SHERIKAR, A. & SUJIT PATIL, A. P. 2010. Improvement of physicochemical characteristics and dissolution profile of poorly water soluble drug: ketoprofen by solid dispersion technique *International Journal of Res. Pharmaceutical Sci*, 1, 450-453.
- PATTERSON, J. E., JAMES, M. B., FORSTER, A. H., LANCASTER, R. W., BUTLER, J. M. & RADES, T. 2005. The influence of thermal and mechanical preparative techniques on the amorphous state of four poorly soluble compounds. *Journal of Pharmaceutical Sciences*, 94, 1998-2012.
- PATTERSON, J. E., JAMES, M. B., FORSTER, A. H. & RADES, T. 2008. Melt Extrusion and Spray Drying of Carbamazepine and Dipyridamole with Polyvinylpyrrolidone/Vinyl Acetate Copolymers. *Drug Development and Industrial Pharmacy*, 34, 95-106.
- PAUDEL, A. & MOOTER, G. 2012. Influence of Solvent Composition on the Miscibility and Physical Stability of Naproxen/PVP K 25 Solid Dispersions Prepared by Cosolvent Spray-Drying. *Pharmaceutical Research*, 29, 251-270.
- PAUDEL, A. & VAN DEN MOOTER, G. 2011. Influence of Solvent Composition on the Miscibility and Physical Stability of Naproxen/PVP K 25 Solid Dispersions Prepared by Cosolvent Spray-Drying. *Pharmaceutical Research*, 29, 251-270.
- PENICHE, C., ZALDÍVAR, D., PAZOS, M., PÁZ, S., BULAY, A. & ROMÁN, J. S. 1993. Study of the thermal degradation of poly(N-vinyl-2-pyrrolidone) by thermogravimetry-FTIR. *Journal of Applied Polymer Science*, 50, 485-493.
- PERISSUTTI, B., NEWTON, J. M., PODCZECK, F. & RUBESSA, F. 2002. Preparation of extruded carbamazepine and PEG 4000 as a potential rapid release dosage form. *European Journal of Pharmaceutics and Biopharmaceutics*, 53, 125-132.

- PINAL, R. 2008. Entropy of Mixing and the Glass Transition of Amorphous Mixtures. *Entropy*, 10, 207-223.
- PINTO, S. S. & DIOGO, H. P. 2006. Thermochemical study of two anhydrous polymorphs of caffeine. *The Journal of Chemical Thermodynamics*, 38, 1515-1522.
- PRODDUTURI, S., MANEK, R. V., KOLLING, W. M., STODGHILL, S. P. & REPKA, M. A. 2005. Solid-state stability and characterization of hot-melt extruded poly(ethylene oxide) films. *Journal of Pharmaceutical Sciences*, 94, 2232-2245.
- PRODDUTURI, S., URMAN, K., OTAIGBE, J. & REPKA, M. 2007. Stabilization of hot-melt extrusion formulations containing solid solutions using polymer blends. *AAPS PharmSciTech*, 8, E152-E161.
- QI, S., AVALLE, P., SAKLATVALA, R. & CRAIG, D. Q. M. 2008a. An investigation into the effects of thermal history on the crystallisation behaviour of amorphous paracetamol. *European Journal of Pharmaceutics and Biopharmaceutics*, 69, 364-371.
- QI, S., BELTON, P., NOLLENBERGER, K., CLAYDEN, N., READING, M. & CRAIG, D. 2010. Characterisation and Prediction of Phase Separation in Hot-Melt Extruded Solid Dispersions: A Thermal, Microscopic and NMR Relaxometry Study. *Pharmaceutical Research*, 27, 1869-1883.
- QI, S., GRYCZKE, A., BELTON, P. & CRAIG, D. Q. M. 2008b. Characterisation of solid dispersions of paracetamol and EUDRAGIT® E prepared by hot-melt extrusion using thermal, microthermal and spectroscopic analysis. *International Journal of Pharmaceutics*, 354, 158-167.
- QIU, S. R., WIERZBICKI, A., ORME, C. A., CODY, A. M., HOYER, J. R., NANCOLLAS, G. H., ZEPEDA, S. & DE YOREO, J. J. 2004. Molecular modulation of calcium oxalate crystallization by osteopontin and citrate. *Proceedings of the National Academy of Sciences of the United States of America*, 101, 1811-1815.
- QUINTAVALLE, U., VOINOVICH, D., PERISSUTTI, B., SERDOZ, F., GRASSI, G., DAL COL, A. & GRASSI, M. 2008. Preparation of sustained release co-extrudates by hot-melt extrusion and mathematical modelling of in vitro/in vivo drug release profiles. *European Journal of Pharmaceutical Sciences*, 33, 282-293.
- RADL, S., TRITTHART, T. & KHINAST, J. G. 2010. A novel design for hot-melt extrusion pelletizers. *Chemical Engineering Science*, 65, 1976-1988.
- RAWLINSON, C. F., WILLIAMS, A. C., TIMMINS, P. & GRIMSEY, I. 2007. Polymer-mediated disruption of drug crystallinity. *International Journal of Pharmaceutics*, 336, 42-48.
- REITZ, C. & KLEINEBUDDE, P. 2007a. Influence of thermal and thermo-mechanical treatment. *Journal of Thermal Analysis and Calorimetry*, 89, 669-673.
- REITZ, C. & KLEINEBUDDE, P. 2007b. Solid lipid extrusion of sustained release dosage forms. *European Journal of Pharmaceutics and Biopharmaceutics*, 67, 440-448.
- REPKA, M. A., GERDING, T. G., REPKA, S. L. & MCGINITY, J. W. 1999. Influence of plasticizers and drugs on the physical-mechanical properties of hydroxypropylcellulose films prepared by hot melt extrusion. *Drug Dev Ind Pharm*, 25, 625-633.

- REPKA, M. A. & MCGINITY, J. W. 2000. Influence of Vitamin E TPGS on the properties of hydrophilic films produced by hot-melt extrusion. *International Journal of Pharmaceutics*, 202, 63-70.
- REPKA, M. A., PRODDUTURI, S. & STODGHILL, S. P. 2003. Production and Characterization of Hot-Melt Extruded Films Containing Clotrimazole. *Drug Development and Industrial Pharmacy*, 29, 757-765.
- REUTZEL-EDENS, S. M., BUSH, J. K., MAGEE, P. A., STEPHENSON, G. A. & BYRN, S. R. 2003. Anhydrates and Hydrates of Olanzapine: Crystallization, Solid-State Characterization, and Structural Relationships. *Crystal Growth & Design*, 3, 897-907.
- RICHARDSON, S. 1970. The die swell phenomenon. *Rheologica Acta*, 9, 193-199.
- RINA CHOKSHI, H. Z. 2004 Hot-Melt Extrusion Technique: A Review. *Iranian Journal of Pharmaceutical Research*, 3, 3-16.
- ROTHEN-WEINHOLD, A., BESSEGHIR, K., VUARIDEL, E., SUBLET, E., OUDRY, N., KUBEL, F. & GURNY, R. 1999. Injection-molding versus extrusion as manufacturing technique for the preparation of biodegradable implants. *European Journal of Pharmaceutics and Biopharmaceutics*, 48, 113-121.
- RUAN, L.-P., YU, B.-Y., FU, G.-M. & ZHU, D.-N. 2005. Improving the solubility of ampelopsin by solid dispersions and inclusion complexes. *Journal of Pharmaceutical and Biomedical Analysis*, 38, 457-464.
- RUMONDOR, A. C. F., MARSAC, P. J., STANFORD, L. A. & TAYLOR, L. S. 2009. Phase Behavior of Poly(vinylpyrrolidone) Containing Amorphous Solid Dispersions in the Presence of Moisture. *Molecular Pharmaceutics*, 6, 1492-1505.
- S.CRAIG DYAR, M. M., ISSAC GHEBRE-SELLASSIE 2007. Melt Extruded Particulate Dispersion. In: ISAAC GHEBRE-SELASSIE, C. M. (ed.) *Pharmaceutical Extrusion Technology*. New York: Infroma Healthcare, 133, 261-276. ISBN: 0-8247-4050-5.
- SAERS, E. S. K. & CRAIG, D. Q. M. 1992. An investigation into the mechanisms of dissolution of alkyl p-aminobenzoates from polyethylene glycol solid dispersions. *International Journal of Pharmaceutics*, 83, 211-219.
- SALEKI-GERHARDT, A., AHLNECK, C. & ZOGRAFI, G. 1994. Assessment of disorder in crystalline solids. *International Journal of Pharmaceutics*, 101, 237-247.
- SARODE, A. L., SANDHU, H., SHAH, N., MALICK, W. & ZIA, H. 2013. Hot melt extrusion (HME) for amorphous solid dispersions: Predictive tools for processing and impact of drug-polymer interactions on supersaturation. *European Journal of Pharmaceutical Sciences*, 48, 371-384.
- SATHIGARI, S. K., RADHAKRISHNAN, V. K., DAVIS, V. A., PARSONS, D. L. & BABU, R. J. 2012. Amorphous-state characterization of efavirenz-polymer hot-melt extrusion systems for dissolution enhancement. *Journal of Pharmaceutical Sciences*, 101, 3456-3464.
- SCHACHTER, D. M., XIONG, J. & TIROL, G. C. 2004. Solid state NMR perspective of drug-polymer solid solutions: a model system based on poly(ethylene oxide). *International Journal of Pharmaceutics*, 281, 89-101.

- SCHILLING, S. U., BRUCE, C. D., SHAH, N. H., MALICK, A. W. & MCGINITY, J. W. 2008. Citric acid monohydrate as a release-modifying agent in melt extruded matrix tablets. *International Journal of Pharmaceutics*, 361, 158-168.
- SCHILLING, S. U., SHAH, N. H., WASEEM MALICK, A. & MCGINITY, J. W. 2010. Properties of melt extruded enteric matrix pellets. *European Journal of Pharmaceutics and Biopharmaceutics*, 74, 352-361.
- SCHULZE, S. & WINTER, G. 2009. Lipid extrudates as novel sustained release systems for pharmaceutical proteins. *Journal of Controlled Release*, 134, 177-185.
- SCINTAG INC 1999. Chapter 7 Basics of X-ray Diffraction. *Providing Solution To Your Diffraction Needs*, 7.1-7.24.
- SEKIGUCHI, K. & OBI, N. 1961. Studies on absorption of eutectic mixtures. I. A comparison of the behavior of eutectic mixtures of sulphathiazole and that of ordinary sulphathiazole in man. . *Chem Pharm Bull*, 9, 866-872.
- SEKIKAWA, H., NAKANO, M. & ARITA, T. 1978. Inhibitory Effect of Polyvinylpyrrolidone on the Crystallization of Drugs. *Chem.Pharm.Bull*, 26, 118-126.
- SHAH, S., MADDINENI, S., LU, J. & REPKA, M. A. 2012. Melt extrusion with poorly soluble drugs. *International Journal of Pharmaceutics*, DOI:10.1016/j.ijpharm.2012.11.001.
- SHAKHTSHNEIDER, T., DANÈDE, F., CAPET, F., WILLART, J., DESCAMPS, M., MYZ, S., BOLDYREVA, E. & BOLDYREV, V. 2007a. Grinding of drugs with pharmaceutical excipients at cryogenic temperatures. *Journal of Thermal Analysis and Calorimetry*, 89, 699-707.
- SHAKHTSHNEIDER, T., DANÈDE, F., CAPET, F., WILLART, J., DESCAMPS, M., PACCOU, L., SUROV, E., BOLDYREVA, E. & BOLDYREV, V. 2007b. Grinding of drugs with pharmaceutical excipients at cryogenic temperatures. *Journal of Thermal Analysis and Calorimetry*, 89, 709-715.
- SHAMBLIN, S. L., TAYLOR, L. S. & ZOGRAFI, G. 1998. Mixing behavior of colyophilized binary systems. *Journal of Pharmaceutical Sciences*, 87, 694-701.
- SHENG, J. J., KASIM, N. A., CHANDRASEKHARAN, R. & AMIDON, G. L. 2006. Solubilization and dissolution of insoluble weak acid, ketoprofen: Effects of pH combined with surfactant. *European Journal of Pharmaceutical Sciences*, 29, 306-314.
- SHERMAN HSU C.P. 1997. Infrared Spectroscopy. In: F.A. SETTLE (ed.) *Handbook of Instrumental Techniques for Analytical Chemistry*. Englewood Cliffs, NJ: Prentice-Hall.
- SHIM, S.-Y., JI, C.-W., SAH, H., PARK, E.-S. & LEE, B.-J. 2006. Characterization of itraconazole semisolid dosage forms prepared by hot melt technique. *Archives of Pharmacal Research*, 29, 1055-1060.
- SIEPMANN, J. & PEPPAS, N. A. 2001. Modeling of drug release from delivery systems based on hydroxypropyl methylcellulose (HPMC). *Advanced Drug Delivery Reviews*, 48, 139-157.
- SIEVENS-FIGUEROA, L., BHAKAY, A., JEREZ-ROZO, J. I., PANDYA, N., ROMAÑACH, R. J., MICHNIAK-KOHN, B., IQBAL, Z., BILGILI, E. & DAVÉ, R. N. 2012. Preparation and characterization of hydroxypropyl methyl cellulose films containing stable BCS Class II drug nanoparticles for pharmaceutical applications. *International Journal of Pharmaceutics*, 423, 496-508.

- SIVERT, A., BÉRARD, V. & ANDRÈS, C. 2009. New binary solid dispersion of indomethacin with surfactant polymer: From physical characterization to in vitro dissolution enhancement. *Journal of Pharmaceutical Sciences*, 99, 1399-1413.
- SIX, K., BERGHMANS, H., LEUNER, C., DRESSMAN, J., VAN WERDE, K., MULLENS, J., BENOIST, L., THIMON, M., MEUBLAT, L., VERRECK, G., PEETERS, J., BREWSTER, M. & VAN DEN MOOTER, G. 2003a. Characterization of Solid Dispersions of Itraconazole and Hydroxypropylmethylcellulose Prepared by Melt Extrusion, Part II. *Pharmaceutical Research*, 20, 1047-1054.
- SIX, K., DAEMS, T., DE HOON, J., VAN HECKEN, A., DEPRE, M., BOUCHE, M.-P., PRINSEN, P., VERRECK, G., PEETERS, J., BREWSTER, M. E. & VAN DEN MOOTER, G. 2005. Clinical study of solid dispersions of itraconazole prepared by hot-stage extrusion. *European Journal of Pharmaceutical Sciences*, 24, 179-186.
- SIX, K., LEUNER, C., DRESSMAN, J., VERRECK, G., PEETERS, J., BLATON, N., AUGUSTIJNS, P., KINGET, R. & VAN DEN MOOTER, G. 2002. Thermal Properties of Hot-Stage Extrudates of Itraconazole and Eudragit E100. Phase separation and polymorphism. *Journal of Thermal Analysis and Calorimetry*, 68, 591-601.
- SIX, K., MURPHY, J., WEUTS, I., CRAIG, D. Q. M., VERRECK, G., PEETERS, J., BREWSTER, M. & VAN DEN MOOTER, G. 2003. Identification of Phase Separation in Solid Dispersions of Itraconazole and Eudragit® E100 Using Microthermal Analysis. *Pharmaceutical Research*, 20, 135-138.
- SIX, K., VERRECK, G., PEETERS, J., BREWSTER, M. & MOOTER, G. V. D. 2004. Increased physical stability and improved dissolution properties of itraconazole, a class II drug, by solid dispersions that combine fast- and slow-dissolving polymers. *Journal of Pharmaceutical Sciences*, 93, 124-131.
- SJOKVIST, E., NYSTROM, C., ALDEN, M. & CARAM-LELHAM, N. 1992. Physicochemical aspects of drug release. XIV. The effects of some ionic and non-ionic surfactants on properties of a sparingly soluble drug in solid dispersions. *International Journal of Pharmaceutics*, 79, 123-133.
- SOONTRAVANICH, S. & SCAMEHORN, J. 2010. Use of a Nonionic Surfactant to Inhibit Precipitation of Anionic Surfactants by Calcium. *Journal of Surfactants and Detergents*, 13, 13-18.
- STEWART, P. J. & ZHAO, F.-Y. 2005. Understanding agglomeration of indomethacin during the dissolution of micronised indomethacin mixtures through dissolution and de-agglomeration modeling approaches. *European Journal of Pharmaceutics and Biopharmaceutics*, 59, 315-323.
- STUART J.KAPP, P. A. P. 2007. Controls and Instrumentation. In: ISAAC GHEBRE-SELASSIE, C. M. (ed.) *Pharmaceutical Extrusion Technology*. New York: Informa Healthcare, 133, 361-382. ISBN: 0-8247-4050-5.
- SUGA, H. 2000. PROSPECTS OF MATERIALS SCIENCE From crystalline to amorphous solids. *Journal of Thermal Analysis and Calorimetry*, 60, 957-974.
- SUGANO, K., OKAZAKI, A., SUGIMOTO, S., TAVORNVIPAS, S., OMURA, A. & MANO, T. 2007. Solubility and Dissolution Profile Assessment in Drug Discovery. *Drug Metabolism and Pharmacokinetics*, 22, 225-254.

- SWANEPOEL, E., LIEBENBERG, W., DE VILLIERS, M. M. & DEKKER, T. G. 2000. Dissolution Properties of Piroxicam Powders and Capsules as a Function of Particle Size and the Agglomeration of Powders. *Drug Development and Industrial Pharmacy*, 26, 1067-1076.
- SZAKONYI, G. & ZELKÓ, R. 2012. The effect of water on the solid state characteristics of pharmaceutical excipients: Molecular mechanisms, measurement techniques, and quality aspects of final dosage form. *Int J Pharm Investig*, 2, 18-25.
- TAJAROBI, F., ABRAHMSÉN-ALAMI, S. & LARSSON, A. 2011a. Dissolution rate enhancement of parabens in PEG solid dispersions and its influence on the release from hydrophilic matrix tablets. *J Pharm Sci*, 100, 275-83.
- TAJAROBI, F., LARSSON, A., MATIC, H. & ABRAHMSÉN-ALAMI, S. 2011b. The influence of crystallization inhibition of HPMC and HPMCAS on model substance dissolution and release in swellable matrix tablets. *European Journal of Pharmaceutics and Biopharmaceutics*, 78, 125-133.
- TAMAKI, M., SUMIE, Y., YUKIO, A. & SHIGEO, K. 2004. Ability of polyvinylpyrrolidone and polyacrylic acid to inhibit the crystallization of amorphous acetaminophen. *Journal of Pharmaceutical Sciences*, 93, 2710-2717.
- TANG, X. & PIKAL, M. 2004. Design of Freeze-Drying Processes for Pharmaceuticals: Practical Advice. *Pharmaceutical Research*, 21, 191-200.
- TANTISHAIYAKUL, V., KAEWNOPPARAT, N. & INGKATAWORNWONG, S. 1996. Properties of solid dispersions of piroxicam in polyvinylpyrrolidone K-30. *International Journal of Pharmaceutics*, 143, 59-66.
- TANTISHAIYAKUL, V., KAEWNOPPARAT, N. & INGKATAWORNWONG, S. 1999. Properties of solid dispersions of piroxicam in polyvinylpyrrolidone. *International Journal of Pharmaceutics*, 181, 143-151.
- TAVANA, H. & NEUMANN, A. W. 2007. Recent progress in the determination of solid surface tensions from contact angles. *Advances in Colloid and Interface Science*, 132, 1-32.
- TAYLOR, L. S. & ZOGRAFI, G. 1997. Spectroscopic Characterization of Interactions Between PVP and Indomethacin in Amorphous Molecular Dispersions. *Pharmaceutical Research*, 14, 1691-1698.
- THUMMA, S., ELSOHLY, M. A., ZHANG, S.-Q., GUL, W. & REPKA, M. A. 2008b. Influence of plasticizers on the stability and release of a prodrug of Δ^9 -tetrahydrocannabinol incorporated in poly (ethylene oxide) matrices. *European Journal of Pharmaceutics and Biopharmaceutics*, 70, 605-614.
- THUMMA, S., MAJUMDAR, S., ELSOHLY, M., GUL, W. & REPKA, M. 2008a. Preformulation Studies of a Prodrug of Δ^9 -Tetrahydrocannabinol. *AAPS PharmSciTech*, 9, 982-990.
- THUMMA, S., MAJUMDAR, S., ELSOHLY, M. A., GUL, W. & REPKA, M. A. 2008c. Chemical stability and bioadhesive properties of an ester prodrug of [Delta]9-tetrahydrocannabinol in poly(ethylene oxide) matrices: Effect of formulation additives. *International Journal of Pharmaceutics*, 362, 126-132.
- THYBO, P., HOVGAARD, L., LINDELÅ, V. J. D., BRASK, A. & ANDERSEN, S. 2008a. Scaling Up the Spray Drying Process from Pilot to Production Scale Using an Atomized Droplet Size Criterion. *Pharmaceutical Research*, 25, 1610-1620.

- THYBO, P., HOVGAARD, L., LINDELØV, J., BRASK, A. & ANDERSEN, S. 2008b. Scaling Up the Spray Drying Process from Pilot to Production Scale Using an Atomized Droplet Size Criterion. *Pharmaceutical Research*, 25, 1610-1620.
- THYBO, P., KRISTENSEN, J. & HOVGAARD, L. 2007. Characterization and Physical Stability of Tolfenamic Acid-PVP K30 Solid Dispersions. *Pharmaceutical Development and Technology*, 12, 43-53.
- TIAN, Y., BOOTH, J., MEEHAN, E., JONES, D. S., LI, S. & ANDREWS, G. P. 2012. Construction of Drug-Polymer Thermodynamic Phase Diagrams Using Flory-Huggins Interaction Theory: Identifying the Relevance of Temperature and Drug Weight Fraction to Phase Separation within Solid Dispersions. *Molecular Pharmaceutics*, 10, 236-248.
- TINKE, A. P., CARNICER, A., GOVOREANU, R., SCHELTJENS, G., LAUWERYSSEN, L., MERTENS, N., VANHOUTTE, K. & BREWSTER, M. E. 2008. Particle shape and orientation in laser diffraction and static image analysis size distribution analysis of micrometer sized rectangular particles. *Powder Technology*, 186, 154-167.
- TINKE, A. P., VANHOUTTE, K., VANHOUTTE, F., DE SMET, M. & DE WINTER, H. 2005. Laser diffraction and image analysis as a supportive analytical tool in the pharmaceutical development of immediate release direct compression formulations. *International Journal of Pharmaceutics*, 297, 80-88.
- TRASI, N. S. & TAYLOR, L. S. 2012. Effect of Additives on Crystal Growth and Nucleation of Amorphous Flutamide. *Crystal Growth & Design*, 12, 3221-3230.
- TREY, S. M., WICKS, D. A., MIDIDODDI, P. K. & REPKA, M. A. 2007. Delivery of Itraconazole from Extruded HPC Films. *Drug Development and Industrial Pharmacy*, 33, 727-735.
- TRUONG, V., BHANDARI, B. R., HOWES, T. & ADHIKARI, B. P. 2002. Analytical model for the prediction of glass transition temperature of food systems *Amorphous Food and Pharmaceutical Systems* United Kingdom Royal Society of Chemistry, pages 30-47, ISBN : 978-0-85404-866-3.
- TÜRK, M. & BOLTEN, D. 2010. Formation of submicron poorly water-soluble drugs by rapid expansion of supercritical solution (RESS): Results for Naproxen. *The Journal of Supercritical Fluids*, 55, 778-785.
- UNGA, J., MATSSON, P. & MAHLIN, D. 2010. Understanding polymer-lipid solid dispersions-- The properties of incorporated lipids govern the crystallisation behaviour of PEG. *International Journal of Pharmaceutics*, 386, 61-70.
- VAN DEN BRANDE, J., WEUTS, I., VERRECK, G., PEETERS, J., BREWSTER, M. & VAN DEN MOOTER, G. 2004. DSC analysis of the anti-HIV agent loviride as a preformulation tool in the development of hot-melt extrudates. *Journal of Thermal Analysis and Calorimetry*, 77, 523-530.
- VAN DEN MOOTER, G., WUYTS, M., BLATON, N., BUSSON, R., GROBET, P., AUGUSTIJS, P. & KINGET, R. 2001. Physical stabilisation of amorphous ketoconazole in solid dispersions with polyvinylpyrrolidone K25. *European Journal of Pharmaceutical Sciences*, 12, 261-269.
- VAN DROOGE, D. J., HINRICHS, W. L. J. & FRIJLINK, H. W. 2004. Anomalous dissolution behaviour of tablets prepared from sugar glass-based solid dispersions. *Journal of Controlled Release*, 97, 441-452.

- VAN EERDENBRUGH, B. & TAYLOR, L. 2012. Molecular Weight Effects on the Miscibility Behavior of Dextran and Maltodextrin with Poly(vinylpyrrolidone). *Pharmaceutical Research*, 29, 2754-2765.
- VAN KREVELEN, D. W. & TE NIJENHUIS, K. 2009. Properties of polymers. *Chapter 7*. Fourth Edition ed. Oxford, UK: Elsevier Scientific Publication. ISBN: 978-0-08-054819-7.
- VAN LAARHOVEN, H., VEURINK, J., KRUF, M.-A. & VROMANS, H. 2004. Influence of Spline Stress on Release Properties of a Coaxial Controlled Release Device Based on EVA Polymers. *Pharmaceutical Research*, 21, 1811-1817.
- VASANTHAVADA, M., TONG, W.-Q., JOSHI, Y. & KISLALIOGLU, M. S. 2004. Phase Behavior of Amorphous Molecular Dispersions I: Determination of the Degree and Mechanism of Solid Solubility. *Pharmaceutical Research*, 21, 1598-1606.
- VASANTHAVADA, M., TONG, W.-Q., JOSHI, Y. & KISLALIOGLU, M. S. 2005. Phase Behavior of Amorphous Molecular Dispersions II: Role of Hydrogen Bonding in Solid Solubility and Phase Separation Kinetics. *Pharmaceutical Research*, 22, 440-448.
- VASCONCELOS, T., SARMENTO, B. & COSTA, P. 2007. Solid dispersions as strategy to improve oral bioavailability of poor water soluble drugs. *Drug Discovery Today*, 12, 1068-1075.
- VERHEYEN, S., BLATON, N., KINGET, R. & VAN DEN MOOTER, G. 2002. Mechanism of increased dissolution of diazepam and temazepam from polyethylene glycol 6000 solid dispersions. *International Journal of Pharmaceutics*, 249, 45-58.
- VERHOEVEN, E., DE BEER, T. R. M., SCHACHT, E., VAN DEN MOOTER, G., REMON, J. P. & VERVAET, C. 2009a. Influence of polyethylene glycol/polyethylene oxide on the release characteristics of sustained-release ethylcellulose mini-matrices produced by hot-melt extrusion: in vitro and in vivo evaluations. *European Journal of Pharmaceutics and Biopharmaceutics*, 72, 463-470.
- VERHOEVEN, E., DE BEER, T. R. M., VAN DEN MOOTER, G., REMON, J. P. & VERVAET, C. 2008. Influence of formulation and process parameters on the release characteristics of ethylcellulose sustained-release mini-matrices produced by hot-melt extrusion. *European Journal of Pharmaceutics and Biopharmaceutics*, 69, 312-319.
- VERHOEVEN, E., SIEPMANN, F., DE BEER, T. R. M., VAN LOO, D., VAN DEN MOOTER, G., REMON, J. P., SIEPMANN, J. & VERVAET, C. 2009b. Modeling drug release from hot-melt extruded mini-matrices with constant and non-constant diffusivities. *European Journal of Pharmaceutics and Biopharmaceutics*, 73, 292-301.
- VERHOEVEN, E., VERVAET, C. & REMON, J. P. 2006. Xanthan gum to tailor drug release of sustained-release ethylcellulose mini-matrices prepared via hot-melt extrusion: in vitro and in vivo evaluation. *European Journal of Pharmaceutics and Biopharmaceutics*, 63, 320-330.
- VERRECK, G., DECORTE, A., HEYMANS, K., ADRIAENSEN, J., CLEEREN, D., JACOBS, A., LIU, D., TOMASKO, D., ARIEN, A., PEETERS, J., ROMBAUT, P., VAN DEN MOOTER, G. & BREWSTER, M. E. 2005. The effect of pressurized carbon dioxide as a temporary plasticizer and foaming agent on the hot stage extrusion process and extrudate properties of solid dispersions of itraconazole with PVP-VA 64. *European Journal of Pharmaceutical Sciences*, 26, 349-358.

- VERRECK, G., DECORTE, A., HEYMANS, K., ADRIAENSEN, J., LIU, D., TOMASKO, D., ARIEN, A., PEETERS, J., VAN DEN MOOTER, G. & BREWSTER, M. E. 2006a. Hot stage extrusion of p-amino salicylic acid with EC using CO₂ as a temporary plasticizer. *International Journal of Pharmaceutics*, 327, 45-50.
- VERRECK, G., DECORTE, A., LI, H., TOMASKO, D., ARIEN, A., PEETERS, J., ROMBAUT, P., VAN DEN MOOTER, G. & BREWSTER, M. E. 2006b. The effect of pressurized carbon dioxide as a plasticizer and foaming agent on the hot melt extrusion process and extrudate properties of pharmaceutical polymers. *The Journal of Supercritical Fluids*, 38, 383-391.
- VERRECK, G., VANDECROUYS, R., CONDE, V. D., BAERT, L., PEETERS, J. & BREWSTER, M. E. 2004. The use of three different solid dispersion formulations - melt extrusion, film-coated beads, and a glass thermoplastic system - to improve the bioavailability of a novel microsomal triglyceride transfer protein inhibitor. *Journal of Pharmaceutical Sciences*, 93, 1217-1228.
- VRETTOS, J. S. & MEUSE, C. W. 2009. Infrared techniques for quantifying protein structural stability. *Analytical Biochemistry*, 390, 14-20.
- WANG, S.-L., LIN, S.-Y. & WEI, Y.-S. 2002. Transformation of Metastable Forms of Acetaminophen Studied by Thermal Fourier Transform Infrared (FT-IR) Microspectroscopy. *Chemical & Pharmaceutical Bulletin*, 50, 153-156.
- WEGIEL, L. A., MAUER, L. J., EDGAR, K. J. & TAYLOR, L. S. 2013. Crystallization of amorphous solid dispersions of resveratrol during preparation and storage—Impact of different polymers. *Journal of Pharmaceutical Sciences*, 102, 171-184.
- WELTON, J. E. (ed.) 1984. *SEM Petrology Atlas*, Oklahoma: The American Association of Petroleum Geologists.
- WHITEHEAD, L., FELL, J. T., COLLETT, J. H., SHARMA, H. L. & SMITH, A. M. 1998. Floating dosage forms: an in vivo study demonstrating prolonged gastric retention. *Journal of Controlled Release*, 55, 3-12.
- WILLART, J. F. & DESCAMPS, M. 2008. Solid State Amorphization of Pharmaceuticals. *Molecular Pharmaceutics*, 5, 905-920.
- WILLIAMS, A. C., TIMMINS, P., LU, M. & FORBES, R. T. 2005. Disorder and dissolution enhancement: Deposition of ibuprofen on to insoluble polymers. *European Journal of Pharmaceutical Sciences*, 26, 288-294.
- WINDBERGS, M., GUERES, S., STRACHAN, C. & KLEINEBUDDE, P. 2010. Two-Step Solid Lipid Extrusion as a Process to Modify Dissolution Behavior. *AAPS PharmSciTech*, 11, 2-8.
- WINDBERGS, M., STRACHAN, C. & KLEINEBUDDE, P. 2009a. Investigating the Principles of Recrystallization from Glyceride Melts. *AAPS PharmSciTech*, 10, 1224-1233.
- WINDBERGS, M., STRACHAN, C. J. & KLEINEBUDDE, P. 2009b. Understanding the solid-state behaviour of triglyceride solid lipid extrudates and its influence on dissolution. *European Journal of Pharmaceutics and Biopharmaceutics*, 71, 80-87.
- WITT, C., MÄDER, K. & KISSEL, T. 2000. The degradation, swelling and erosion properties of biodegradable implants prepared by extrusion or compression moulding of poly(lactide-co-glycolide) and ABA triblock copolymers. *Biomaterials*, 21, 931-938.

- WOJNAROWSKA, Z., GRZYBOWSKA, K., ADRJANOWICZ, K., KAMINSKI, K., PALUCH, M., HAWELEK, L., WRZALIK, R., DULSKI, M., SAWICKI, W., MAZGALSKI, J., TUKALSKA, A. & BIEG, T. 2010. Study of the Amorphous Glibenclamide Drug: Analysis of the Molecular Dynamics of Quenched and Cryomilled Material. *Molecular Pharmaceutics*, 7, 1692-1707.
- WU, C. & MCGINITY, J. W. 1999. Non-traditional plasticization of polymeric films. *International Journal of Pharmaceutics*, 177, 15-27.
- WU, C. & MCGINITY, J. W. 2003. Influence of methylparaben as a solid-state plasticizer on the physicochemical properties of Eudragit® RS PO hot-melt extrudates. *European Journal of Pharmaceutics and Biopharmaceutics*, 56, 95-100.
- WU, K., LI, J., WANG, W. & WINSTEAD, D. A. 2009. Formation and characterization of solid dispersions of piroxicam and polyvinylpyrrolidone using spray drying and precipitation with compressed antisolvent. *Journal of Pharmaceutical Sciences*, 98, 2422-2431.
- WU, T. & YU, L. 2006. Origin of Enhanced Crystal Growth Kinetics near T_g Probed with Indomethacin Polymorphs. *The Journal of Physical Chemistry B*, 110, 15694-15699.
- YADAV, V. & YADAV, A. 2009. Enhancement of solubility and dissolution rate of indomethacin with different polymers by compaction process. *International Journal of ChemTech Research*, 1, 1072-1078.
- YAGI, N., TERASHIMA, Y., KENMOTSU, H., SEKIKAWA, H. & TAKADA, M. 1996. Dissolution Behavior of ProbucoI from Solid Dispersion Systems of ProbucoI-Polyvinylpyrrolidone. *Chemical & pharmaceutical bulletin* 44, 241-244.
- YAN, Y.-D., SUNG, J. H., KIM, K. K., KIM, D. W., KIM, J. O., LEE, B.-J., YONG, C. S. & CHOI, H.-G. 2012. Novel valsartan-loaded solid dispersion with enhanced bioavailability and no crystalline changes. *International Journal of Pharmaceutics*, 422, 202-210.
- YANG, J., GREY, K. & DONEY, J. 2010a. An improved kinetics approach to describe the physical stability of amorphous solid dispersions. *International Journal of Pharmaceutics*, 384, 24-31.
- YANG, M., WANG, P., HUANG, C.-Y., KU, M. S., LIU, H. & GOGOS, C. 2010b. Solid dispersion of acetaminophen and poly(ethylene oxide) prepared by hot-melt mixing. *International Journal of Pharmaceutics*, 395, 53-61.
- YANG, R., WANG, Y., ZHENG, X., MENG, J. & TANG, X. 2008. Preparation and Evaluation of Ketoprofen Hot-Melt Extruded Enteric and Sustained-Release Tablets. *Drug Development and Industrial Pharmacy*, 34, 83-89.
- YOSHIOKA, M., HANCOCK, B. C. & ZOGRAFI, G. 1995. Inhibition of indomethacin crystallization in poly(vinylpyrrolidone) coprecipitates. *Journal of Pharmaceutical Sciences*, 84, 983-986.
- YOUNG, C. R., DIETZSCH, C., CEREIA, M., FARRELL, T., FEGELY, K. A., RAJABI-SIAHBOOMI, A. & MCGINITY, J. W. 2005. Physicochemical characterization and mechanisms of release of theophylline from melt-extruded dosage forms based on a methacrylic acid copolymer. *International Journal of Pharmaceutics*, 301, 112-120.
- YOUNG, T. 1804. *An Essay on the Cohesion of Fluids*, London, Philosophical Transactions, Vol 95, Page 65-87. doi: 10.1098/rstl.1805.0005

- YU, L. 2001. Amorphous pharmaceutical solids: preparation, characterization and stabilization. *Advanced Drug Delivery Reviews*, 48, 27-42.
- ZAHEDI, P. & LEE, P. I. 2007. Solid molecular dispersions of poorly water-soluble drugs in poly(2-hydroxyethyl methacrylate) hydrogels. *European Journal of Pharmaceutical and Biopharmaceutics*, 65, 320-328.
- ŻENKIEWICZ, M. 2007. Methods for the calculation of surface free energy of solids. *Journal of Achievements in Materials and Manufacturing Engineering*, 24, 137-145.
- ZHANG, F. & MCGINITY, J. W. 2000. Properties of Hot-Melt Extruded Theophylline Tablets Containing Poly(Vinyl Acetate). *Drug Development and Industrial Pharmacy*, 26, 931 - 942.
- ZHAO, M. 2010. *The Development of Spray Dried Solid Dispersion Systems for the Formulation of Low Tg and Low Solubility Drugs*. PhD, University of East Anglia.
- ZHAO, Y., INBAR, P., CHOKSHI, H. P., MALICK, A. W. & CHOI, D. S. 2011. Prediction of the thermal phase diagram of amorphous solid dispersions by flory–huggins theory. *Journal of Pharmaceutical Sciences*, 100, 3196-3207.
- ZHENG, X., YANG, R., TANG, X. & ZHENG, L. 2007a. Part I: Characterization of Solid Dispersions of Nimodipine Prepared by Hot-melt Extrusion. *Drug Development and Industrial Pharmacy*, 33, 791 - 802.
- ZHENG, X., YANG, R., ZHANG, Y., WANG, Z., TANG, X. & ZHENG, L. 2007b. Part II: Bioavailability in Beagle Dogs of Nimodipine Solid Dispersions Prepared by Hot-Melt Extrusion. *Drug Development and Industrial Pharmacy*, 33, 783-789.
- ZHU, Y., SHAH, N. H., MALICK, A. W., INFELD, M. H. & MCGINITY, J. W. 2002. Solid-state plasticization of an acrylic polymer with chlorpheniramine maleate and triethyl citrate. *International Journal of Pharmaceutics*, 241, 301-310.
- ZHU, Y., SHAH, N. H., WASEEM MALICK, A., INFELD, M. H. & MCGINITY, J. W. 2006. Controlled Release of a Poorly Water-Soluble Drug from Hot-Melt Extrudates Containing Acrylic Polymers. *Drug Development and Industrial Pharmacy*, 32, 569-583.

Appendices

Appendix I: Calibration curve of PCM crystallinity based on diffracted peak of XRPD

Calibration curves were constructed according to the intensity of the two sharp peaks at 23.4 and 24.5° 2 θ Bragg diffraction peaks from XRPD diffractograms of physical mixture of PCM and polymer with known crystalline percentage as suggested in a previous literature (de Villiers et al., 1998). Detail of the parameter could be found in Chapter 2.4.5. Figure (i) shows the obtained calibration curves with $R^2 = 0.9817$ and $R^2 = 0.9898$, respectively for PCM-PVP and PCM-PVPVA 6:4 systems ranged from 10 -100% w/w of PCM loading.

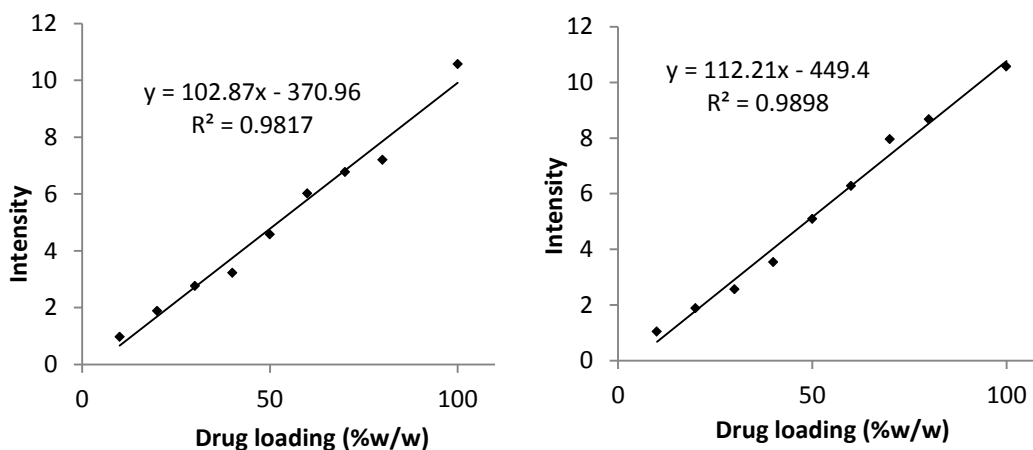


Figure (i): Calibration curves based on physical mixture of 10-80% w/w PCM-carriers system a) PVP K29-32, b) PVPVA 6:4

Appendix II: Validation of ATR-FTIR method in tracking crystalline content of PCM in HME PCM PVPs-based solid dispersions

To validate the use of ATR-FTIR as an analytical tool for the quantification of Form I PCM as developed in Chapter 4, section 4.3.1, crystallinity estimation of partially crystalline HME PVP-based products measured by different analytical methods were compared with the crystallinity detected from the developed ATR-FITR method.

To do this, hot melt extruded products with excess of crystalline content were prepared, in order to enable the crystal detection by using all the employed methods (XRPD, DSC and ATR-FTIR). With that, HME extrudates with 55% to 70% of PCM in PVP K29-32 and 45% to 60% of PCM in PVPVA were extruded at 120 °C 5 minutes residence time. Crystallinity of these products was accessed by ATR-FTIR using Equation 4.6 (Chapter 4, section 4.3.1), XRPD, and DSC.

Verification by XRPD

The partially crystalline HME products were scanned by using XRPD and their degree of crystallinity was approximated using the calibration curves presented in Figure (i). Figure (ii) demonstrated the XRPD diffraction spectra of the partially crystalline HME products of 45 to 60% PCM loading of HME PCM PVPVA 6:4 and 55 to 70% PCM loading of HME PCM PVP K29-32 systems. These results indicated the consistent increment of diffraction peaks intensity with higher loading of PCM. The percentage of crystallinity in each formulation could be found in Table (i), which will be further discussed in the later section for overall comparison.

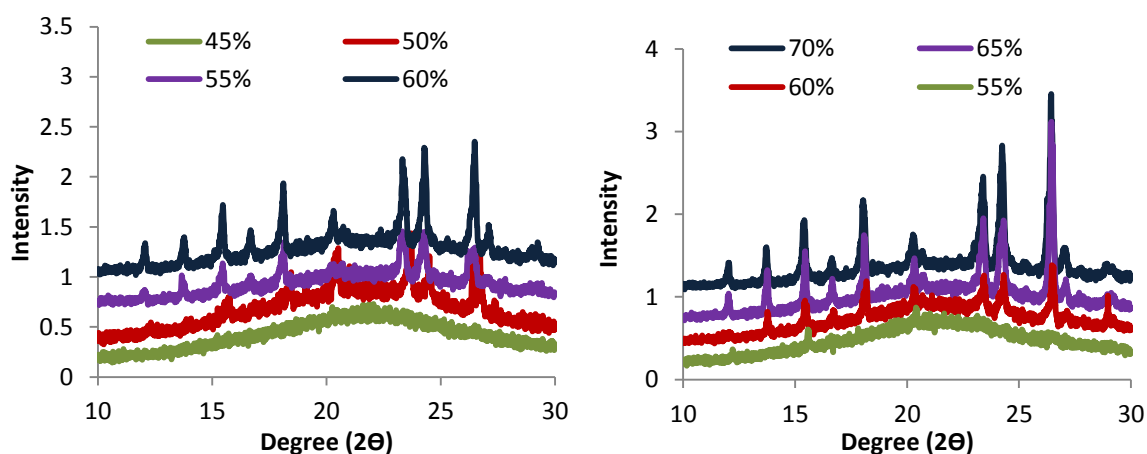


Figure (ii): Verification of crystallinity of partially crystalline HME products a) 45% - 60% PVPVA carriers system, b) 55% -70% PVP K29-32 carrier systems

Verification by DSC

Besides, the partially crystalline HME products were also scanned in DSC. The issue of crystalline material dissolution into the polymer carrier during heating scan of DSC was reported. On this basis, standard DSC melting enthalpy method (10 °C per minute) was employed to minimise the dissolution effect. The ratio of the enthalpy melting of the partially crystalline HME product to the melting enthalpy of pure PCM was taken as the degree of crystallinity.

Alternatively, the heat capacity method could also be used to estimate crystallinity of product (Qi et al., 2010). In this method, amorphous content was assumed to be linearly proportional to the heat capacity value. The reversing heat capacity signal was used to remove the effects of the endothermic relaxation processes occurring simultaneously. The changes in C_p values before and after complete melting were taken to calculate the content of crystalline material (Figure iii).

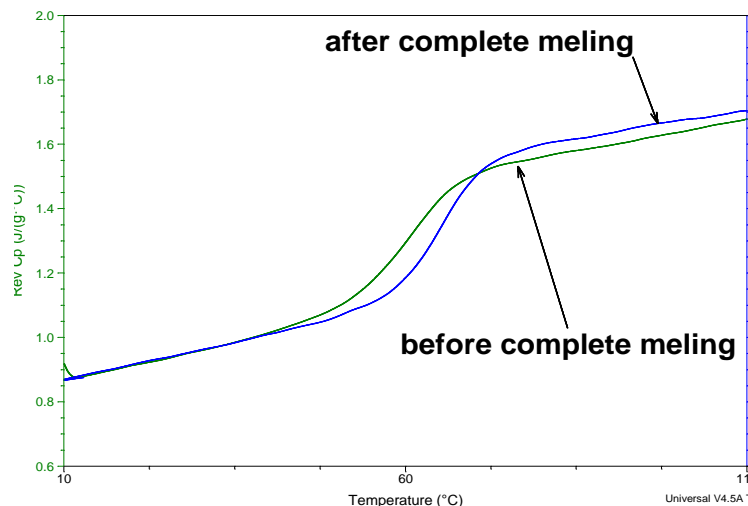


Figure (iii): MTDSC traces of reversing heat capacity of HME 55% PCM PVP K29-32. Green lines represent the first cycle of the heating scan and blue line representing the second cycle of the heating scan after complete melting of the existing crystalline material during the first heating cycle.

Generally, the C_p value of an amorphous material is higher than the crystalline counterpart at temperature above T_g . If the fresh samples are totally amorphous, there should be no changes in C_p value in first heating cycle, cooling cycle and reheating cycle. Instead, if crystals exist in the fresh samples; C_p value of the first cycle should be lower than the C_p in cooling and reheating cycle. It is attributed to the melted crystal above melting point that contributed to the higher heat capacity at cooling and reheating scans (Qi et al., 2010).

The total heat capacity of the sample can be expressed as Equation II-I,

$$C_p^{total}(T) = \phi C_p^{drug}(T) + (1 - \phi) C_p^{polymer}(T) \quad (II-I)$$

Heat capacity contributed by the drug component could be detailed in Equation (II-II):

$$C_p^{drug} = x C_p^{amorphous}(T) + (1 - x) C_p^{crystalline}(T) \quad (II - II)$$

By combining the Equation 4.7 and 4.8, heat capacity of the samples can be expressed using Equation (II-III):

$$C_p^{total}(T) = \phi [x C_p^{amorphous}(T) + (1 - x) C_p^{crystalline}(T)] + (1 - \phi) C_p^{polymer}(T) \quad (II-III)$$

Heating upon melting, all the initial crystal content disappears. Thus, the heat capacity during the cooling cycle could be expressed as Equation (II-IV):

$$C_p^{total}(T) = \phi C_p^{amorphous}(T) + (1 - \phi) C_p^{polymer}(T) \quad (II - IV)$$

Therefore, the changes of heat capacity between the first and cooling / reheating cycles can be solved into Equation (II-V) by using equations above:

$$\Delta C_p^{heat-cool}(T) = \phi(1 - x)[C_p^{amorphous}(T) - C_p^{crystalline}(T)] \quad (II - V)$$

where $C_p^{total}, C_p^{drug}, C_p^{polymer}$ are total heat capacity, heat capacity of the drug and polymer respectively at temperature T, and $C_p^{amorphous}$ and $C_p^{crystalline}$ are the heat capacity of the amorphous and crystalline of the drug at temperature, T; ϕ is the weight fraction of the drug in the extrudate and x is the weight fraction of amorphous drug in the total amount of drug in extrudate.

In the current studies, partially crystalline HME PCM PVPs systems were scanned in MT DSC at 2°C per minutes with modulation of ± 0.318 °C, 60 seconds. To avoid the influence of water content in Cp values of the scanned extrudate, Cp value at temperature 110 °C (higher than 100 °C) was chosen for the calculation of crystallinity using heat capacity method. The quantified crystalline content were tabulated in Table (i) for overall comparison.

Table (i) summarises the percentage of crystalline material in the partially crystalline HME PCM PVP K29-32 or PVPVA 6:4 products using different analytical methods. According to the obtained crystallinity, there are good agreements among the percentage of crystallinity detected from these methods.

Table (i): Comparison of crystallinity (the average of n=3) of PCM in partially HME PCM PVPs-based SD systems estimated by using different methods

HME Drug Loading (%)	XRPD (%crystal)	ATR-FTIR (%crystal)	DSC Cp (% crystal)	DSC Tm (% crystal)
PVP K29-32				
55%	2.75	3.71	4.75	4.7
60%	13.72	15.44	15.19	14.33
65%	21.96	27.48	24.41	21.3
70%	29.25	33.42	29.34	24.82
PVPVA 6:4				
45%	0	2.09	2.33	2.59
50%	10.528	10.86	10.86	8.25
55%	13.149	19.77	20.63	13.59
60%	20.973	28.05	28.08	19.64

Figure (iv) compares the percentage of crystallinity in HME 55 to 70 % PCM PVP K29-32 and HME 45%- 60% PCM PVPVA 6:4 estimated using ATR-FTIR, XRPD, DSC heat capacity and melting methods. XRPD and DSC melting methods consistently revealed a lower crystallinity content as compared to ATR-FTIR methods and DSC heat capacity method. However, cross validation indicated that the results showed less than 5% deviation from each method. This result is in agreement with Grisedale et al., 2011.

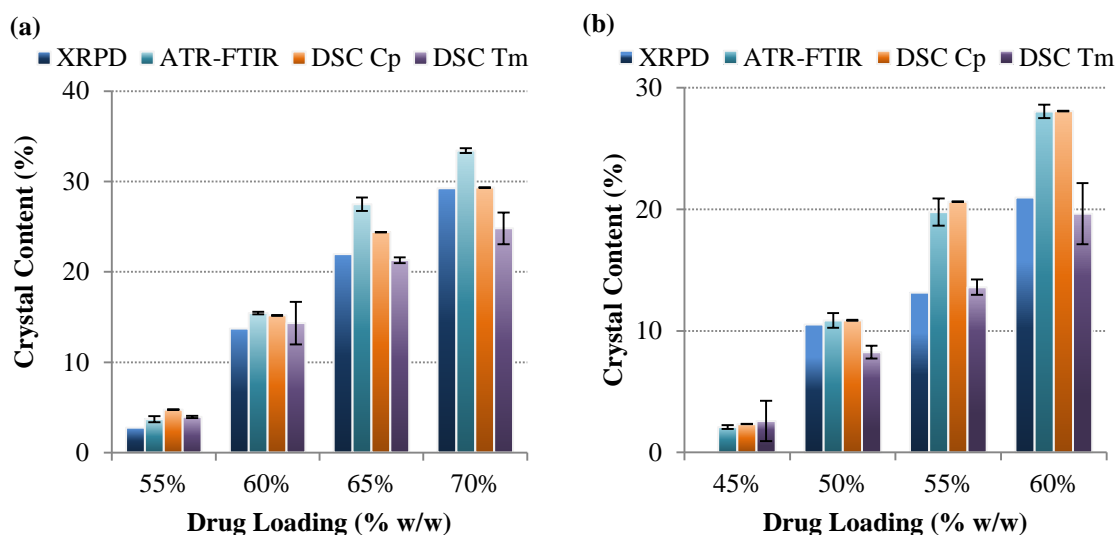


Figure (iv) : Comparison of crystallinity of (a) HME PCM-PVP K29-32 and (b) HME PCM-PVPVA 6:4 estimated using different methods

XRPD was reported to be much less sensitive in comparison with DSC (Nagapudi and Jona, 2008), in which crystals are undetectable if the amount of crystals was $< 10\%$ (Saleki-Gerhardt et al., 1994). In the current study, it was found that the sensitivity for XRPD for Form I PCM detection was $\geq 3\%$ w/w via scanning the low crystal content of PM PCM-PVP. Based on the results in Table (i), crystal contents detected by using DSC heat capacity method and ATR-FTIR are generally higher than that by using XRPD method. Thus, in this study, XRPD was found to be less sensitive in detecting the HME PCM-PVP based SD systems. In DSC, there is a high potential of interference of different thermal events in the DSC heating scans, hence, data interpretation using this method may be complex.

On the other hand, ATR-FTIR method is a sensitive method where lower detection limit of PCM in PM was found to be $< 1\%$ via scanning the PMs of low PCM loading. Thus, ATR-FTIR is an appropriate method for tracking the recrystallization process of SD due to the reliable crystallinity prediction, good sensitivity, fast data acquisition and simple sample preparation of this approach.

Appendix III : Dissolution of crystalline PCM during heating scan of DSC

As presented in Chapter 4, the result of ATR-FTIR was not coherent to the DSC data as the former indicated the presence of crystalline material and the later did not show any detectable crystalline material even in the sample that was stored in an accelerated humidity conditions, 75% RH. This could be arisen dissolution of the existing crystalline materials into the polymer during the DSC heating scan.

To further confirm the dissolution of PCM in polymer upon heating in DSC, an aged HME samples with high percentage of crystal was taken to scan in ATR-FTIR with variation by controlling the temperature of the ATR accessory at 2 °C per minutes from 30 - 200 °C. Upon gradual heating of the aged sample in ATR-FTIR scanning, relative intensity change of 807 cm⁻¹ (the characteristic peak) in its spectrum may indicates the change in amount of Form I crystal in the scanned sample. In this measurement, the aged HME 40% PCM PVPVA 6:4 after 3 months in 75%RH was selected. Figure (v) shows the temperature variation (at 2°C per minutes from 30-200°C) of ATR-FTIR spectra for aged HME PCM PVPVA 6:4 after 3 months storage in 75% RH

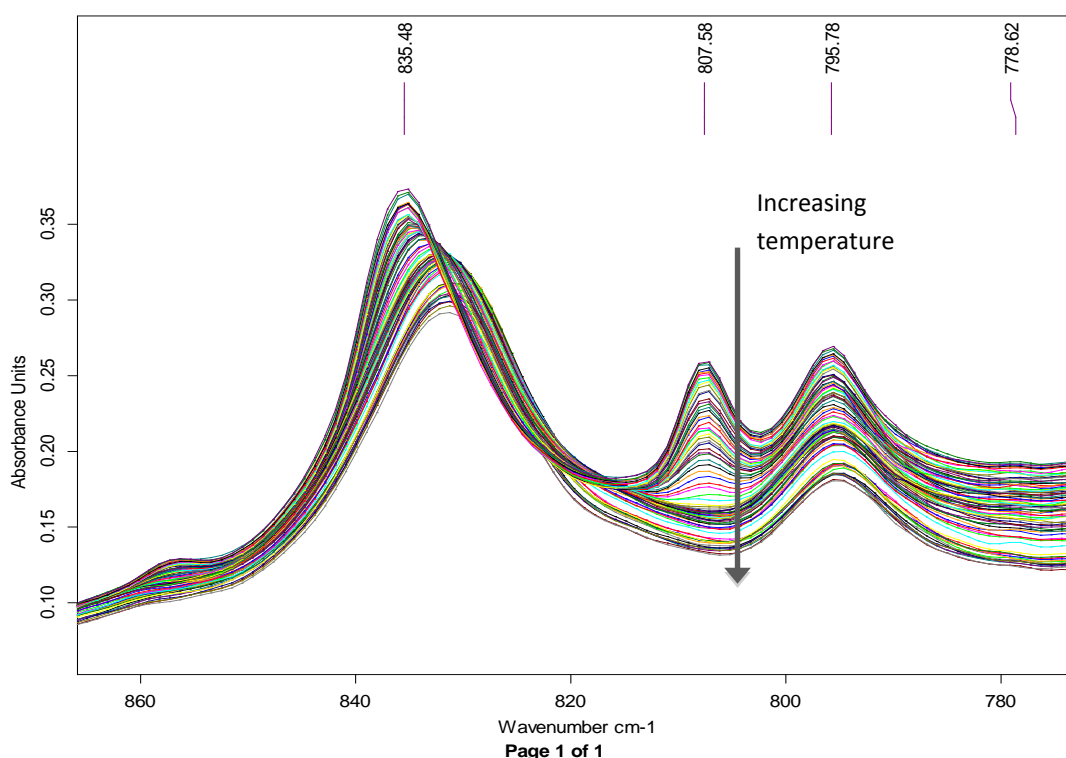


Figure (v) : FTIR-ATR spectra of aged HME PCM PVPVA 6:4 (after 3 months storage in 75% RH) scanning at 2°C per minutes from 30-200°C which corresponded to the ATR-FTIR spectra from top to bottom.

According to Figure (v), the intensity of the diagnostic wavenumber of 807 cm⁻¹ was decreasing with the increase of heating temperature. This indicated the gradual disappearance of the Form I PCM upon heating. This relative intensity change may be closely correlated to the undetectable crystalline material upon heating in DSC measurement.

Figure (vi) display the overlay profiles of DSC thermograms and the profile of relative intensity of $807\text{ cm}^{-1}/797\text{ cm}^{-1}$ of the aged HME PCM PVPVA 6:4 in the same heating scan rate.

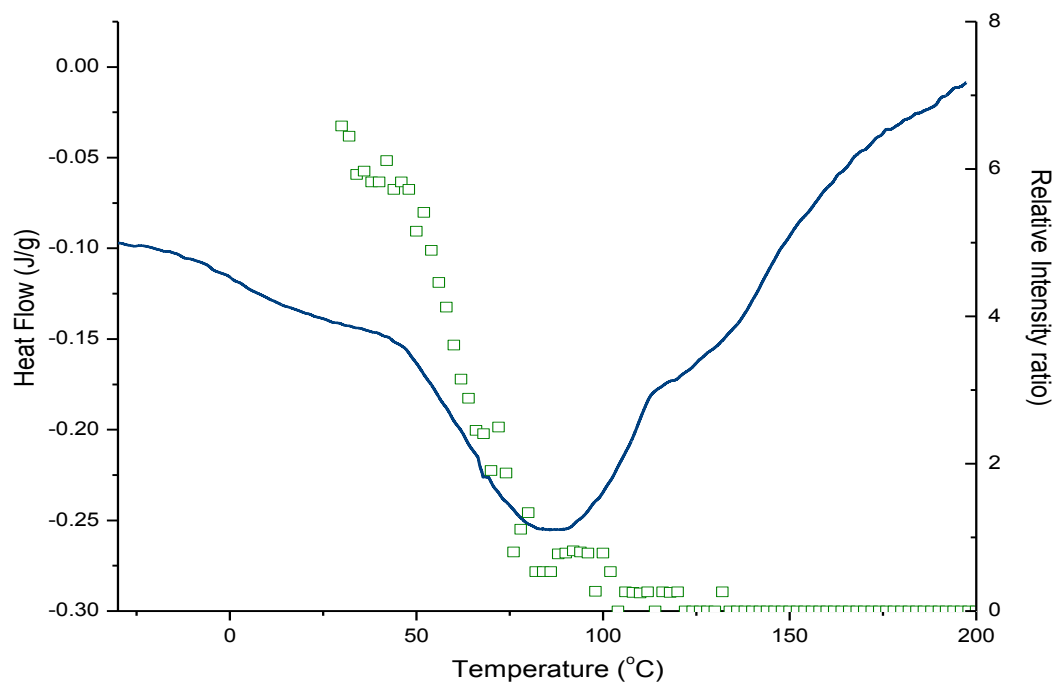
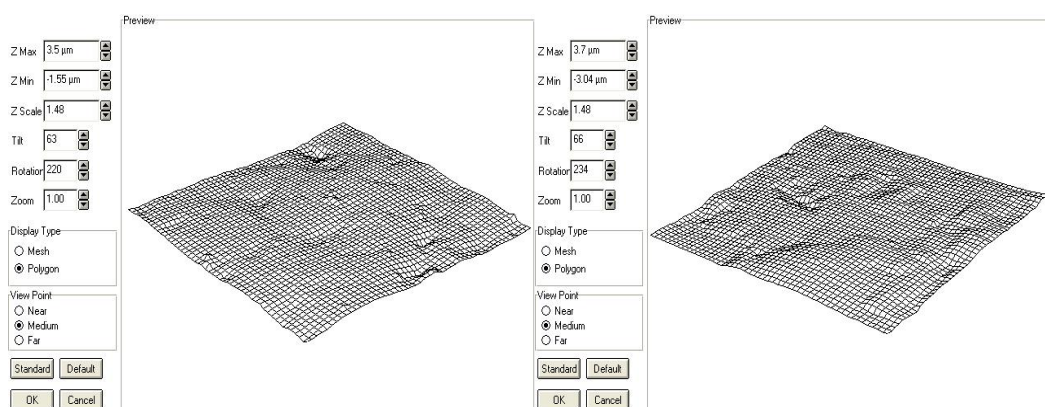


Figure (vi) The Overlay profiles of DSC thermograms and the profile of relative intensity of $807\text{ cm}^{-1}/797\text{ cm}^{-1}$ for aged HME 50% PCM PVPVA 6:4 in the same heating scan rate

Base on Figure (v), relative intensity of the characteristic peak of the aged sample were decreasing with heating. Approaching $100\text{ }^{\circ}\text{C}$, relative intensity of the characteristic peak was approaching to zero, which indicated the disappearance of the crystalline material upon heating. This might be ascribed to the dissolution process of the crystalline into the polymer system while heating. The disappearance of the characteristic peaks were apparent in between the temperature of $50\text{ }^{\circ}\text{C}$ to $100\text{ }^{\circ}\text{C}$ which is coincide to the temperature of moisture evaporation as indicated from the corresponding DSC thermogram. Thus, it is suggested that the water detachment from the sample has leads to a high solubilisation of the existing crystal in the polymer via drug polymer interaction. From Figure (vi), relative peak intensity of the characteristic peak was zero at any possible melting temperature of the crystalline PCM (circa $148\text{ }^{\circ}\text{C}$ for depressed melting of Form I PCM in the presence of PVPVA 6:4 based on Chapter 3, circa $158\text{ }^{\circ}\text{C}$ and $169\text{ }^{\circ}\text{C}$ for Form II and Form I PCM, respectively) which indicated complete dissolution of the crystalline material at this temperature. Therefore, the dissolution of the existing crystal while heating is the main reason for the undetectable melting endotherm in DSC thermogram of the aged samples.

Appendix IV: Analysis of surface of HME API-PVPVA systems for contact angle measurement

In order to effectively compare the surface roughness of the compacted tablets that were used for the contact angle measurement in Chapter 5.2.6.4, Atomic Force Microscope (AFM) was used to map the surfaces. Figures (vii) reveals the example topography of the examined surfaces for both the compacted physical mixture and hot melt extruded product. In this case, the z variations of the piezoelectric scanner were deemed in providing the roughness information. These magnitudes were presented in Table (ii). According to Table (ii) the generated surfaces were comparable with standard deviation of $< 0.86 \mu\text{m}$. This suggested the validity of the results in reflecting wetting properties of the solid dispersion.



Figures (vii) : AFM images of sruface roughness of compacted tablet of PM and HME formulations

Table (ii): Z is the Surface roughness information of the generated flat surface by IR press.

API	Physical mixture		Hot melt extrusion	
	Z_{max} (μm)	Z_{min} (μm)	Z_{max} (μm)	Z_{min} (μm)
Ketoprofen	3.13	-1.33	3.44	-2.08
Naproxen	4.12	-2.76	4.55	-0.40
Indomethacin	3.50	-2.13	4.33	-1.69
Olanzapine	3.50	-1.55	3.70	-3.04

Appendix V : Amorphous nature of HME NAP-PVPVA-Tween 80 systems

DSC thermograms of HME NAP-PVPVA-Tween 80 revealed apparent reduction in glass transition temperatures. T_g was lowered slightly in formulation with 2% added Tween 80, more intense reduction is noted in formulation with 10% w/w added of Tween 80 (Figure (x)). No apparent melting endotherm was detected which indicated the absent of detectable crystalline naproxen.

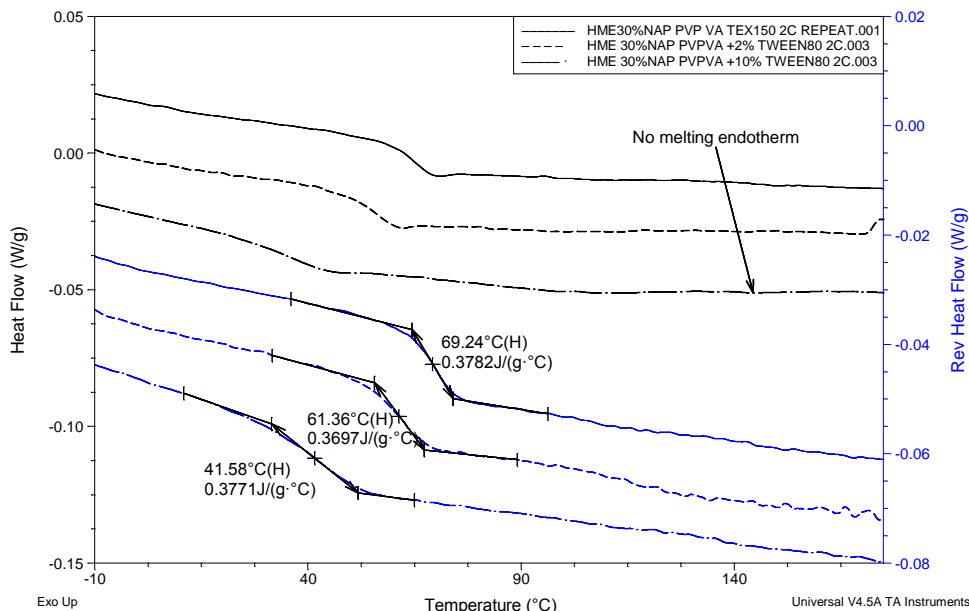


Figure (x) : DSC thermogram of HME 30% NAP PVPVA, HME 30% NAP PVPVA+2% Tween 80 and HME 30% NAP PVPVA + 10% Tween 80

The amorphous nature of HME 30% NAP-PVPVA-Tween 80 was further confirmed by the XRPD diffractograms as presented below.

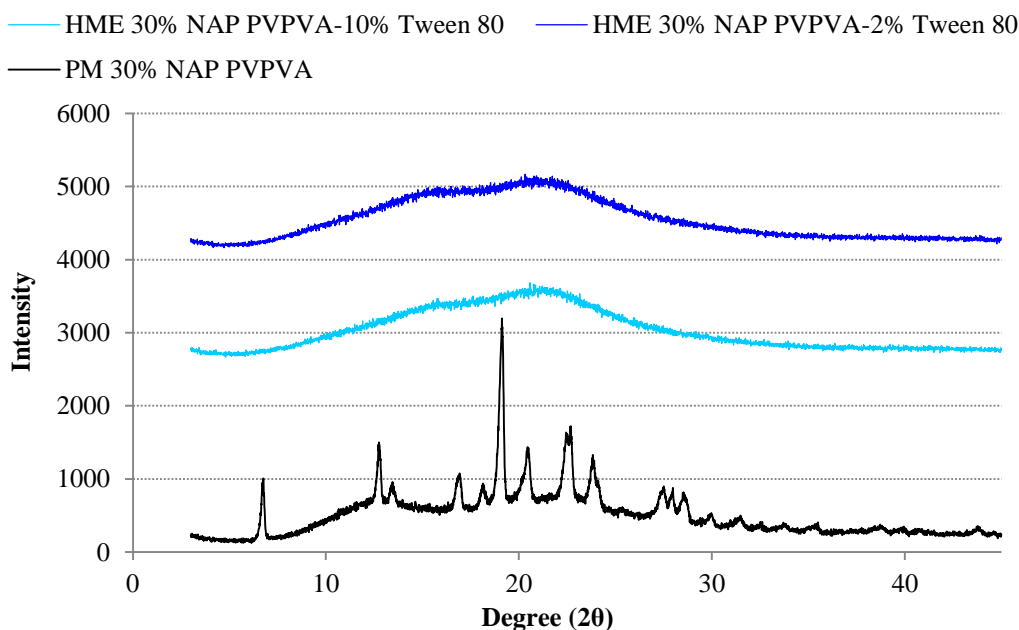


Figure (xi) : XRPD diffractograms of HME 30% NAP-PVPVA-Tween 80 in comparison to PM 30 NAP-PVPVA

Publications

CHAN, S. Y., QI, S. & CRAIG, D. Q. M. An Investigation into Drug-Polymer Interactions for Stability Enhancement of Hot Melt Extrusion Systems. APS PharmSci 2011, 2011a 31 August - 2 September 2011; East Midlands Conference Centre, University of Nottingham. APS PharmSci 2011.

CHAN, S. Y., QI, S. & CRAIG, D. Q. M. 2011b. An Investigation into Drug-Polymer Interactions for Stability Enhancement of Hot Melt Extrusion Systems. Oral presentation at APS PharmSci 2012. 31 August - 2 September 2011; East Midlands Conference Centre, University of Nottingham: APS PharmSci 2011.

CHAN, S. Y., QI, S. & CRAIG, D. Q. M. Enhanced dissolution of hot melt extruded naproxen-PVPVA 6:4 solid dispersions containing a non-ionic surfactant. APS Amorphous IV: Hot melt extrusion and powder technology in pharmaceutical industry, 2012a 12th - 13th June 2012, Medway Campus - The School of Science in the University of Greenwich, UK. The Academy of Pharmaceutical Sciences.

CHAN, S. Y., QI, S. & CRAIG, D. Q. M. Enhanced dissolution of Naproxen using Hot Melt Extruded Polyvinylpyrrolidone Vinyl Acetate Formulations. APS PharmSci 2012, 2012b 12 -14th September 2012; East Midlands Conference Centre, University of Nottingham. APS PharmSci 2012.

CHAN, S. Y., QI, S., KHAN, N. A. K. & CRAIG, D. Q. M. An Investigation into the Recrystallization Behavior of Paracetamol (Acetaminophen) in Hot Melt Extruded Solid Dispersions. Poster presentation at 2011 AAPS Annual Meeting and Exposition 2011c October 23–27, 2011; Washington, D.C Poster W4258.

CHAN, S. Y., QI, S., KHAN, N. A. K. & CRAIG, D. Q. M. Quantification of Crystallinity in Amorphous Paracetamol and Solid Dispersions of Paracetamol in Polyvinylpyrrolidone using High Speed Differential Scanning Calorimetry and Attenuated Reflectance-Fourier Transform Infrared Spectroscopy. Poster presentation at the 2011 AAPS Annual Meeting and Exposition, 2011d October 23–27, 2011; Washington, D.C. Poster W4259.

"The foot feels the foot when it feels the ground."

~Buddha~